

Manganese and Nickel Complexes as Catalysts for Aromatic Oxidation

Novel Methodologies for Non-Noble Metal Catalysis



Eduard Masferrer Rius

Manganese and Nickel Complexes as Catalysts for Aromatic Oxidation

Novel Methodologies for Non-Noble Metal Catalysis

Mangaan- en nikkelcomplexen als katalysatoren voor aromatische oxidatie

Nieuwe methoden voor katalyse met niet-edelmetalen

(met een samenvatting in het Nederlands)

Proefschrift

ter verkrijging van de graad van doctor aan de Universiteit Utrecht
op gezag van de rector magnificus, prof.dr. H.R.B.M. Kummeling,
ingevolge het besluit van het college voor promoties
in het openbaar te verdedigen
op woensdag 13 juli 2022 des middags te 2.15 uur

door

Eduard Masferrer Rius

geboren op 20 augustus 1993 te Arbúcies (Girona), Spanje

Promotor:

Prof. dr. R.J.M. Klein Gebbink

This thesis was accomplished with financial support through the NoNoMeCat project (675020-MSCA-ITN-2015-ETN).

Manganese and Nickel Complexes as Catalysts for Aromatic Oxidation

Novel Methodologies for Non-Noble Metal Catalysis

A vosaltres, que ja no hi sou.

Per cada petita part que em vau deixar.

Masferrer Rius, Eduard

Manganese and Nickel Complexes as Catalysts for Aromatic Oxidation

Novel Methodologies for Non-Noble Metal Catalysis

ISBN: 978-94-6458-369-4

The work described in this PhD thesis was carried out at the Organic Chemistry and Catalysis group, Debye Institute for Nanomaterials Science, Faculty of Science, Utrecht University, Utrecht, The Netherlands

Front Cover: In a minimalist design the Dom Tower of Utrecht is represented. In addition to be the tallest church tower in The Netherlands, it has also become a shape that reminds me of home. When one looks at the cover, the Dom is viewed at a certain distance, with a perspective that I would not have acquired without all experiences shared in Utrecht.

Cover Design: Eila Serrano Hervás

Print: Ridderprint | www.ridderprint.nl.

Table of Contents

Chapter 1	Non-Noble Metal Aromatic Oxidation Catalysis: from Metalloenzymes to Synthetic Complexes	7
Chapter 2	On the Ability of Nickel Complexes Derived from Tripodal Aminopyridine Ligands to Catalyze Arene Hydroxylations	75
Chapter 3	Aromatic C–H Hydroxylation Reactions with Hydrogen Peroxide Catalyzed by Bulky Manganese Complexes	97
Chapter 4	Electronic and Steric Ligand Effects on Catalytic Arene Oxidation by Aminopyridine-based Manganese Complexes	131
Chapter 5	Exploration of Highly Electron-Rich Manganese Complexes in Enantioselective Oxidation Catalysis; a Focus on Enantioselective Benzylic Oxidation	163
Chapter 6	An Experimental and Computational Study on Tetradentate Imidazole-based Manganese Complexes for Oxidation Catalysis	197
Appendices		
	Appendix A: Supplementary Information to Chapter 2	219
	Appendix B: Supplementary Information to Chapter 3	222
	Appendix C: Supplementary Information to Chapter 4	230
	Appendix D: Supplementary Information to Chapter 5	233
	Appendix E: Supplementary Information to Chapter 6	241

Summary	243
Samenvatting	251
Acknowledgements	259
About the Author	266
List of Publications	267

Chapter 1

Non-Noble Metal Aromatic Oxidation Catalysis: from Metalloenzymes to Synthetic Complexes

Abstract

The development of selective aromatic oxidation catalysts based on non-noble metals has emerged over the last decades, mainly due to the importance of phenol products as intermediates for the generation of pharmaceuticals or functional polymers. In nature, metalloenzymes can perform a wide variety of oxidative processes using molecular oxygen, including arene oxidations, however, the implementation of such enzymes in the chemical industry remains challenging. In this context, chemists have tried to mimic nature and design synthetic non-noble metal catalysts inspired by these enzymes. This introduction chapter aims at providing a general overview on aromatic oxidation reactions catalyzed by metalloenzymes as well as synthetic first-row transition-metal complexes as homogeneous catalysts. The enzymes and complexes discussed in this chapter have been classified on the basis of the transition-metal ion present in their active site, *i.e.*, iron, copper, nickel, and manganese. The main points of discussion focus on enzyme structure and function, catalyst design, mechanism of operation in terms of oxidant activation and substrate oxidation, and substrate scope. At the end of the chapter, the aim and scope of this thesis is outlined.

1.1 Overview of Arene Oxidations

1.1.1 Relevance and Challenges

Oxidations of organic compounds are essential reactions that are widely studied in academia as well as in the chemical industry.^{1,2} The interest in these reactions is based on the fact that oxygenated organic molecules can be used as intermediates to produce different classes of chemicals, as well as end products. Since the last decades, improvements have been made in the development of different catalytic oxidation systems, however, in most cases the selective oxidation of the organic substrate represents a critical challenge. Of more recent interest are C–H oxidations that can be applied for late-stage functionalization and in which C–H bonds are basically considered as functional groups.³⁻⁷

A particular area of interest has been the direct oxygenation of aromatic compounds to the corresponding phenol products (Figure 1), which has been a challenging class of reactions for decades. Indeed, the direct hydroxylation of benzene to phenol using molecular oxygen as a benign oxidant has been known as one of the “10 challenges for catalysis”.^{8,9} Phenols are essential intermediates in the generation of a broad range of products, like pharmaceuticals or functional polymers, which make them highly desired.^{6,10-12} However, the direct transformation of an aromatic C–H bond into a hydroxyl functionality, such as in benzene oxidation, is difficult because of poor substrate reactivity (an aromatic C–H bond has a high bond dissociation energy of about 112 kcal·mol⁻¹).¹³ To overcome this challenge, the generation of highly reactive and selective oxygen species is necessary. However, often phenol products are more easily oxidized than non-oxidized aromatic compounds, causing a chemoselectivity issue. Generally, the oxidation of phenols to the corresponding catechols, hydroquinones or benzoquinones is well documented, particularly in oxidations catalyzed by metalloporphyrins (Figure 1).¹⁴⁻¹⁸ Besides, a lack of discrimination between different oxidation sites produces a regioselectivity issue, especially when alkylbenzenes are used, where oxidation at the weaker and activated (benzylic) aliphatic C(sp³)–H bonds is thermodynamically preferred over oxidation at the aromatic ring.

Generally, the field of homogeneous catalysis has been dominated by noble metal complexes, which are based on elements that are generally considered toxic for humans and the environment, and are associated with high costs due to their low availability in the earth crust.¹⁹ In this context, non-noble metal complexes have appeared as attractive catalysts, particularly in oxidation catalysis. Within this field, chemists have typically looked at nature for inspiration. A widely applied approach has been the development of synthetic catalytic systems that can mimic the active site and functionality of metalloenzymes to carry out oxidative processes. A well-known inspiration example are iron-containing metalloenzymes that are able to activate molecular oxygen.²⁰⁻²⁶ However, other kinds of metalloenzymes containing copper, nickel or

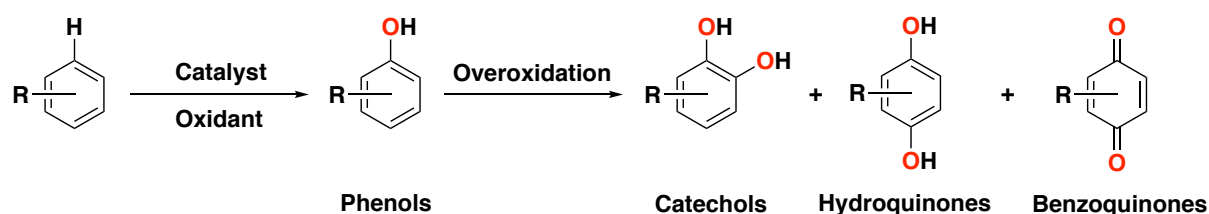


Figure 1. Direct hydroxylation of aromatic substrates to the corresponding phenol products, and overoxidation to catechols, hydroquinones or benzoquinones products.

manganese have also been investigated in this field.^{22,25,27-32} Generally, the active site is the only area of the enzyme that is being mimicked in such bioinspired complexes. A downside of this design strategy is that these synthetic complexes generally display poor selectivities, whereas the natural counterparts show outstanding selectivities due to their highly elaborated structure, including the second coordination sphere around the active site.^{22,33} Thus, a lot of efforts have been devoted to the understanding of the geometric and electronic structure/function correlations between the synthetic and their enzyme ‘molds’.^{34,35}

In the current chapter, we provide an overview on homogeneous, non-noble metal catalysis for aromatic oxidation reactions. Several reviews can be found in literature regarding heterogeneous catalytic systems for oxidation chemistry, also detailing arene oxidation reactivity.³⁶⁻³⁸ Of note, a review on heterogeneous catalysts for the direct hydroxylation of benzene to phenol, with a special focus on mesoporous transition metal-based catalysts, was very recently published.³⁹ The present overview on homogeneous catalysts systems specifically targets catalytic systems capable of performing the direct hydroxylation of an aromatic substrate using a metal-based oxidant and avoiding the use of unselective hydroxyl radicals generated via Fenton-type processes. We have classified this chapter on basis of the transition-metal that is used in catalysis, *i.e.*, iron, copper, nickel, and manganese. First, we introduce the most important families of metalloenzymes capable of catalyzing aromatic oxidation reactions, followed by a description of the development of synthetic bioinspired transition-metal complexes for arene oxidation. Special attention is given to complexes based on aminopyridine ligands, which have been extensively used and investigated in general in the field of homogeneous oxidation chemistry.⁴⁰ Initially, we will review enzymes and complexes based on iron and copper, since these are the two metals that chemists have employed most in the field of oxidation chemistry, in particular for aromatic oxidation. In the second part, nickel- and manganese-based complexes will be covered. Although less examples for arene oxidation are known using these metals, the experimental chapters in this thesis will focus on the development of arene oxidation catalysts based on these metals. At this point, it is important to mention that complexes containing other first-row transition metals, such as cobalt or vanadium, have also been proven to be active for aromatic oxidation. For further information

on these complexes and their catalytic activity, the reader is referred to a number of selected examples.⁴¹⁻⁴⁶

1.1.2 Hydroxyl Radicals vs Metal-based Oxidants

Fenton-type chemistry has been known and studied in detail for quite some time.⁴⁷⁻⁴⁹ Overall, this chemistry consists of the reaction between an iron(II) salt and H_2O_2 to generate an oxidized iron(III) species and hydroxyl radicals.⁵⁰⁻⁵² The oxidation of aromatic substrates, such as benzene and benzene derivatives, by Fenton-type chemistry using H_2O_2 as oxidant has been investigated and is well-understood, and studies have shown that hydroxyl radicals are added rapidly to the aromatic ring.⁵³⁻⁵⁶ After addition of the hydroxyl radical to the benzene ring, the reaction can proceed either by dimerization of the hydroxycyclohexadienyl radical and dehydration to form biphenyl, or alternatively by oxidation to generate phenol (Figure 2). Other oxidants, such as *tert*-butylhydroperoxide (TBHP), can also engage in a Fenton-type process, generating free-diffusing *tert*-butoxy and *tert*-butylperoxy radicals that can engage in hydrogen abstraction reactions with aliphatic C–H bonds.⁵⁷⁻⁵⁹ However, TBHP activation does not produce hydroxyl radicals, and *tert*-butoxy radicals, unlike hydroxyl radicals, do not add to aromatic rings.⁶⁰ For this reason, the effectiveness of using TBHP in arene hydroxylation reactions has been used as an evidence against the involvement of hydroxyl radicals, and consequently in favor of the involvement of metal-based oxidants.⁶¹

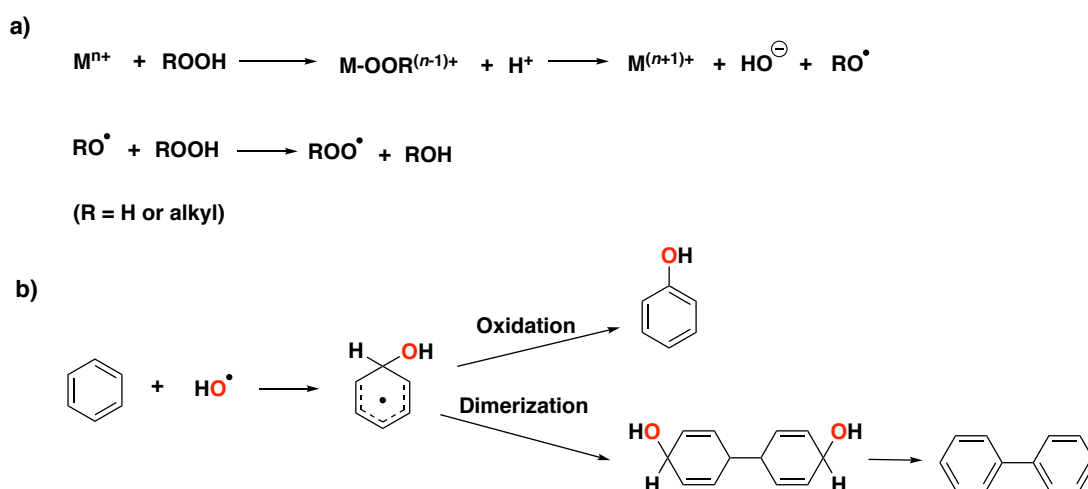


Figure 2. a) Generation of free diffusing oxygen-centered radicals via initial Fenton reaction. b) Hydroxylation of benzene by addition of hydroxyl radicals to generate phenol and biphenyl.

In 1954, another process involving hydroxyl radicals was reported, known as the Udenfriend system.⁶²⁻⁶⁴ This consists of a mixture of an iron(II) salt with EDTA (EDTA = ethylenediaminetetraacetic acid) and ascorbic acid under an oxygen atmosphere, which is able

to generate hydroxyl radicals that can attack aromatic substrates in the same way as described for Fenton-type chemistry. A system using iron(II) salts and tetrahydropterins as reducing agents has also been reported to be efficient for the hydroxylation of aromatic compounds using dioxygen as oxidant. In this particular case, hydroxylation of electron-rich arenes, such as anisole, phenetole, toluene and ethylbenzene is possible, favoring *meta*-hydroxylation in all cases.⁶⁵ Overall, free-diffusing oxygen-centered radicals are known to provide low catalytic efficiencies and selectivities, leading to side products through lateral site chain oxidation for alkylbenzene substrates.^{55, 56, 66, 67} For this reason, over the past years research efforts have focused on the development of catalytic systems that make use of metal-based oxidants rather than hydroxyl radicals, so that higher selectivities and efficiencies for aromatic oxidations can be achieved.

1.2 Iron in Biological and Synthetic Systems

1.2.1 Iron-containing Metalloenzymes

Iron is one of most often found transition-metals in the active sites of metalloenzymes. Numerous iron-containing enzymes are known to be able to activate oxygen to perform oxidative processes. Among these enzymes, we can distinguish two groups based on the active site structure: heme and non-heme containing enzymes (Figure 3). The first group has been well investigated and their chemistry is well understood.

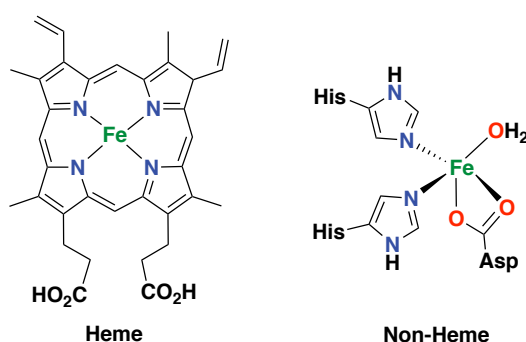


Figure 3. Schematic diagram of the typical heme prosthetic group (iron protoporphyrin IX) found in the active site of heme enzymes (left),^{69, 70} and of the 2-His-1-carboxylate facial triad active site found in the mononuclear non-heme enzyme naphthalene dioxygenase (NDO; right).^{26, 34, 76, 82}

The main feature of this group of enzymes is the prosthetic heme group that bears the iron center in their active site.^{26, 68-72} Within this group we can distinguish heme-containing enzymes like cytochrome P450's, peroxidases, nitric oxide synthases, chloroperoxidases, heme oxygenases, or indoleamine 2,3-dioxygenase and tryptophan 2,3-dioxygenase. Non-heme enzymes, on the other hand, can be classified in mononuclear and dinuclear depending on the

number of iron atoms in their active site.^{23, 34, 73} Within the former type, different types of mononuclear active sites have been identified. One very common active site features an iron center bound to two histidine ligands and one carboxylate ligand in a facial manner; this structural feature is known as the “2-His-1-carboxylate facial triad”.^{23, 24, 35, 74-79} One remarkable example of this last family of enzymes are Rieske oxygenases, which can perform the *syn*-dihydroxylation of aromatic substrates, among other substrate oxidations, with high levels of regio- and stereospecificity.^{24, 80, 81} In the following sections, some of the most important iron-containing metalloenzymes able to perform aromatic oxidation reactions are discussed, in terms of the structure of their active site and their catalytic oxidation capabilities.

1.2.1.1 Cytochrome P450

Cytochromes (CYP) are ubiquitous in all life forms, going from bacteria to humans. Within this family, cytochrome P450 is one of the most important classes of iron enzymes found in nature that metabolize atmospheric dioxygen in an oxygenase catalytic cycle, and a lot of details on the mechanism of dioxygen activation for this enzyme family are known. Overall, this class of iron enzymes takes part in several processes, ranging from the detoxification of xenobiotic compounds to drug metabolism and the biosynthesis of steroids.^{69, 83-86}

Among the different oxidative processes, cytochrome P450 is best known for its monooxygenation capability, *i.e.*, the insertion of an oxygen atom from molecular oxygen into an organic compound. Among these reactions are aromatic oxidations, as well as arene and alkene epoxidations, and the oxygenation of heteroatoms. Because of the catalytic capabilities of cytochrome P450 enzymes, a lot of research efforts have been devoted to the investigation of cytochrome P450 variants as catalysts for site-selective and enantioselective C–H hydroxylation reactions in the past decades.⁸⁷⁻⁹⁰ Several studies have shown the coordination chemistry of the active site of cytochrome P450's in detail, which nowadays has been well established based on several X-ray crystal structures.^{69, 91-96} It is based on a ferric iron center coordinated to four nitrogen atoms (protoporphyrin IX) and a cysteinyl sulfur atom; this last residue occupies an axial position at the metal center, whereas the other axial position contains a hydroxide ligand or a water molecule.^{68, 97, 98} The mechanism of operation of cytochrome P450's starts with the ferric compound accepting an electron to form the respective ferrous state of the enzyme. Next, reaction with molecular oxygen produces an Fe(III)-OOH species that undergoes O–O bond cleavage to generate the real active oxidant, which is a high-valent Fe(IV)-oxo porphyrin π radical cation complex, also known as Compound I (CpdI) (Figure 4a).^{14, 84, 99-102} For the oxidation of aliphatic C–H bonds, this last species transfers the oxo group to the substrate following a two-step process, known as the “oxygen rebound” mechanism.^{86, 103, 104} First, a hydrogen atom abstraction takes place from the substrate to the oxo group, and secondly, a fast rebound to the substrate carbon radical by the hydroxyl group occurs.

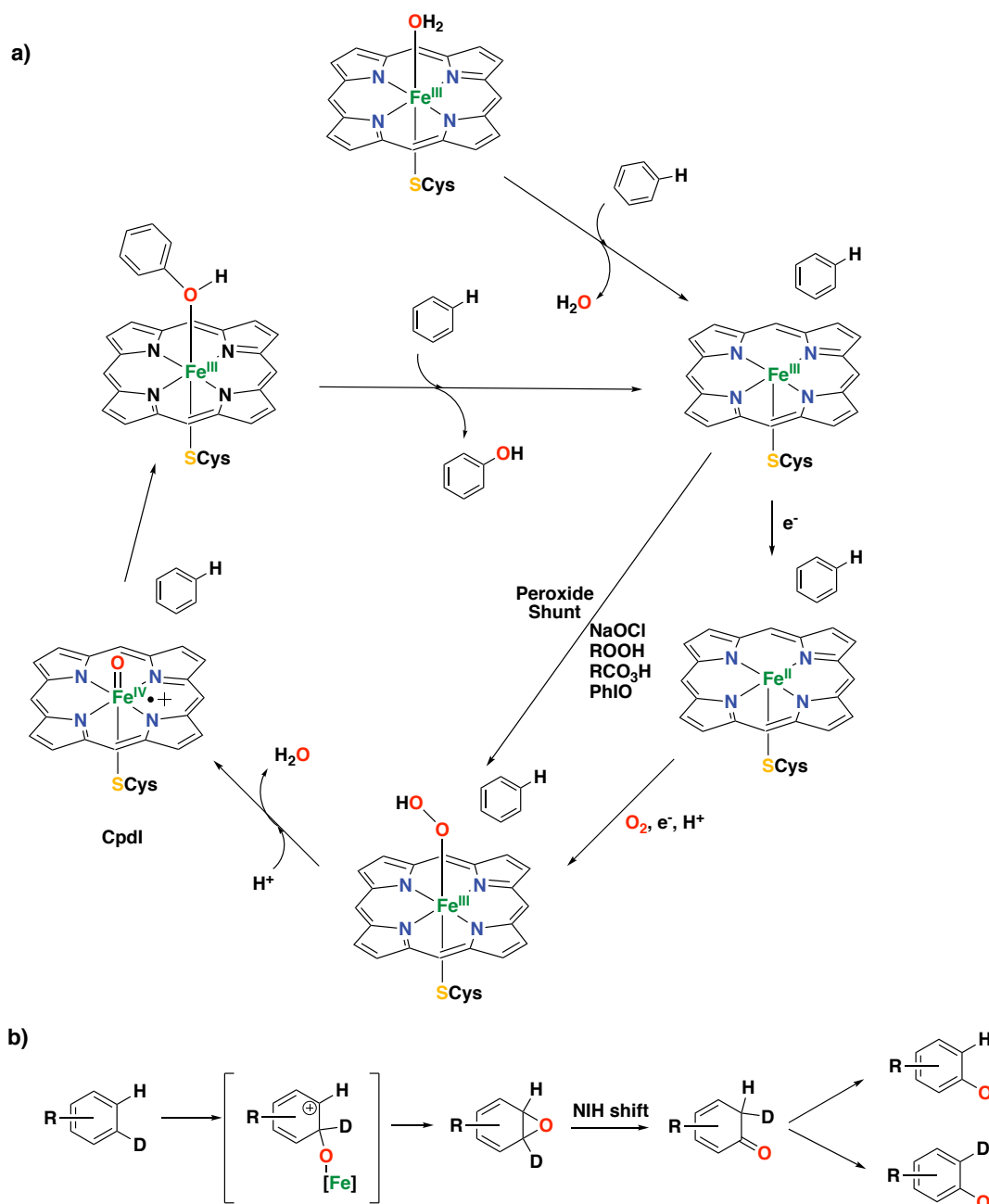


Figure 4. a) Established catalytic cycle for arene oxidation catalyzed by cytochrome P450.^{68, 93, 107-109} b) Oxidation of deuterated aromatic compounds catalyzed by cytochrome P450, illustrating the “NIH shift” process.^{106, 107}

In contrast, oxidation of aromatic substrates with CpdI proceeds via the oxidation of a π -bond, generating arene oxides, that transform to an unstable ketone intermediate via heterolytic cleavage of the epoxide followed by migration of a hydride ion (known as “NIH shift”).¹⁰⁵⁻¹⁰⁷ The last step is the tautomerization of the ketone compound to generate the final phenol product (Figure 4b).^{107, 108} Worth mentioning is the use of hydro- and alkylperoxides, sodium hypochlorite, iodosobenzene or peracids, which allow the conversion of the resting state directly to the high-valent iron-oxo species; this cycle is known as the “peroxide shunt”.⁶⁸

1.2.1.2 Rieske Oxygenases

Rieske oxygenases are a family of bacterial enzymes based on a non-heme iron center, with the metal facially coordinated to two histidine residues and one carboxylate residue (Figure 5b).⁷⁷ This class of enzymes have been well-studied, and they have been found to be effective in several oxidative reactions, such as selective C–H hydroxylations and stereoselective *syn*-dihydroxylations of arenes and alkenes.^{80, 110, 111} Basically, the reactions performed by this class of enzymes are involved in the biodegradation of aromatic compounds.^{24, 76, 80, 81} Rieske oxygenases are based on a reductase and an oxygenase component.¹¹² The first one is a Rieske-type dinuclear iron cluster that mediates the electron transfer from NAD(P)H to the oxygenase component. The latter is characterized by an octahedral mononuclear non-heme iron(II) that can perform the activation of dioxygen to oxidize a hydrocarbon substrate.^{113, 114}

One particular member of this family of enzymes is naphthalene-1,2-dioxygenase (NDO), which was crystallographically characterized in 1998.¹¹⁰⁻¹¹² The proposed catalytic cycle for the *syn*-dihydroxylation of naphthalene consists of the reaction of dioxygen and an electron with the iron center to generate an Fe(III)-peroxo intermediate.^{77, 111, 115, 116}

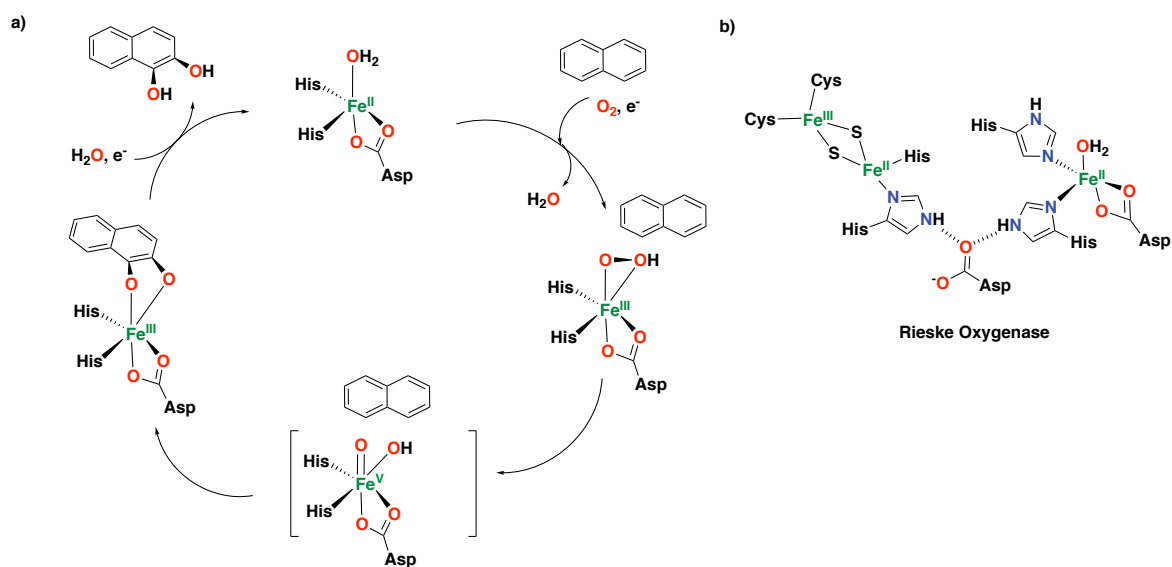


Figure 5. a) Proposed catalytic cycle for the oxidation of naphthalene catalyzed by Rieske dioxygenases, involving the generation of an Fe(V)(O)(OH) species. b) Active site of Naphthalene 1,2-dioxygenase (NDO), showing the Rieske [2Fe:2S] cluster (reductase component) and the catalytic iron center (oxygenase component).¹¹²

The cycle follows with the heterolytic cleavage of the O–O bond of the peroxo intermediate to generate what is proposed to be an Fe(V)(O)(OH) species, responsible for the oxidation of the substrate to form the *syn*-diol product (Figure 5a).^{23, 76, 117, 118} Overall, the mechanism proposed for Rieske oxygenases resembles that of cytochrome P450 regarding the activation of dioxygen

via a heterolytic O–O bond cleavage step. Besides, NDO can also perform the reaction in the presence of hydrogen peroxide via a “peroxide shunt”.¹¹⁹

1.2.1.3 Bacterial Multicomponent Monooxygenases

Bacterial multicomponent monooxygenases (BMMs) are a family of non-heme iron enzymes that comprise a carboxylate-bridged diiron core in the active site.¹²⁰⁻¹²² Such enzymes catalyze the oxidation of various hydrocarbons, such as alkanes, alkenes and aromatic compounds.¹²³⁻¹²⁶ Within this family we can distinguish several classes of multicomponent monooxygenases, such as soluble methane monooxygenases (sMMOs), toluene/*o*-xylene monooxygenases (ToMOs) and phenol hydroxylases (PHs).¹²⁷⁻¹²⁹ Among these, sMMO is the only enzyme that can catalyze the difficult conversion of methane to methanol, which is one of the most challenging reactions found in nature¹²³, whereas ToMO performs the hydroxylation of aromatics and alkenes^{125, 130}, and PH hydroxylates aromatic compounds (Figure 6, left).¹²⁹ The hydroxylation of toluene by ToMO occurs through the generation of an epoxide and a subsequent NIH shift that forms *p*-cresol in 95% yield (*o*- and *m*-cresols are formed in ~4% yield).^{107, 120, 131}

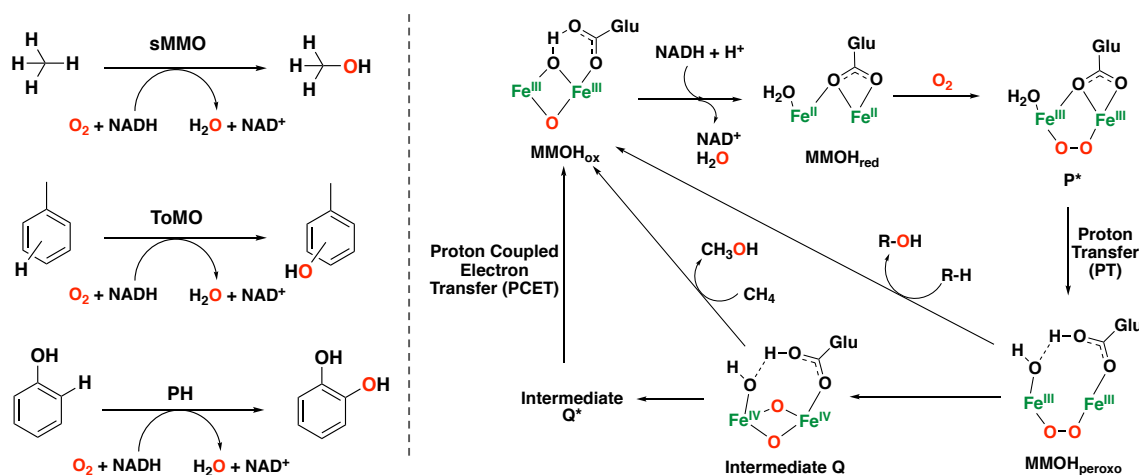


Figure 6. Left: Hydroxylation reactions catalyzed by some of the most representative bacterial multicomponent monooxygenases.^{14, 120} Right: Catalytic mechanism of sMMO for dioxygen activation and substrate oxidation, involving the MMOH_{ox} , MMOH_{red} , intermediate P^* , $\text{MMOH}_{\text{peroxo}}$ and intermediate Q species.^{14, 120, 133}

One of the most studied catalytic cycles is the one of sMMO for methane hydroxylation (Figure 6, right). In addition, sMMO has been shown to be capable of oxidizing benzene to phenol.¹³² Initially, the oxidized diiron(III) species (MMOH_{ox}) is activated by two-electron reduction to a diiron(II) species (MMOH_{red}). Then, the reaction with dioxygen forms peroxy intermediate P^* (via a superoxo species). Intermediate P^* then converts into $\text{MMOH}_{\text{peroxo}}$ through a proton

transfer, which can decay to MMOH_{ox} via oxidation of electrophilic substrates, or convert to diiron(IV) intermediate **Q** by homolytic cleavage of the O–O bond, which is able to hydroxylate methane. In the absence of methane, intermediate **Q** decays to intermediate **Q*** and then to MMOH_{ox} .^{14, 120, 123, 133-137}

The mechanism of ToMO and PH has also been investigated in detail, but it is less well understood compared to that of sMMO. Overall, these classes of bacterial multicomponent monooxygenases show a very similar diiron active site, which may imply a similar mechanism regarding the activation of dioxygen generating peroxodiiron(III) and **Q**-type species.^{128, 138} Nevertheless, an unprecedented peroxodiiron(III) species has been elucidated for ToMO and no evidences of **Q**-type intermediates are known yet, suggesting that the mechanism may differ from that described for sMMO. The general mechanism for dioxygen activation and substrate oxidation has been proposed to proceed through an electrophilic attack by a peroxodiiron(III) intermediate on the arene, to form an arene epoxide that ultimately leads to the aromatic oxidized product bound to the diiron(III) core (see Figure 7 for representative scheme of phenol oxidation).¹³⁹

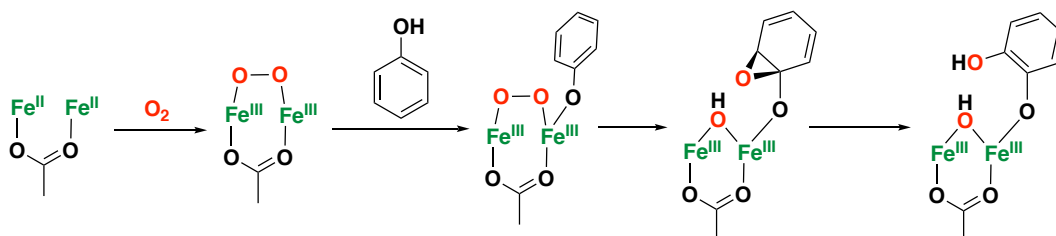


Figure 7. Schematic representation of the mechanism of PH for dioxygen activation and phenol hydroxylation. A similar mechanism is postulated for toluene hydroxylation, however, substrate orientation is controlled by residues of the active site rather than by coordination to the diiron core.¹³⁹

1.2.1.4 Pterin-Dependent Aromatic Amino Acid Hydroxylases

Aryl amino acid hydroxylases, or also known as pterin-dependent oxygenases, are a class of enzymes that utilize tetrahydrobiopterin (BH_4) as a two-electron cofactor. Within this family, we can distinguish phenylalanine (PheOH), tyrosine (TyrOH) and tryptophan hydroxylases (TrpOH), which perform the hydroxylation of phenylalanine, tyrosine and tryptophan, respectively (Figure 8).^{23, 34, 140-144} In addition, pterin-dependent hydroxylases can also perform epoxidations and benzylic hydroxylation reactions, in a similar way as the reactivity observed for cytochrome P450 enzymes.^{68, 142}

A general mechanism has been proposed regarding of oxygen activation and substrate oxidation by these enzymes (Figure 9). Initially, tetrahydrobiopterin (BH_4) reacts with dioxygen to form a hydroperoxydihydropterin intermediate that reacts with the iron(II) center of the

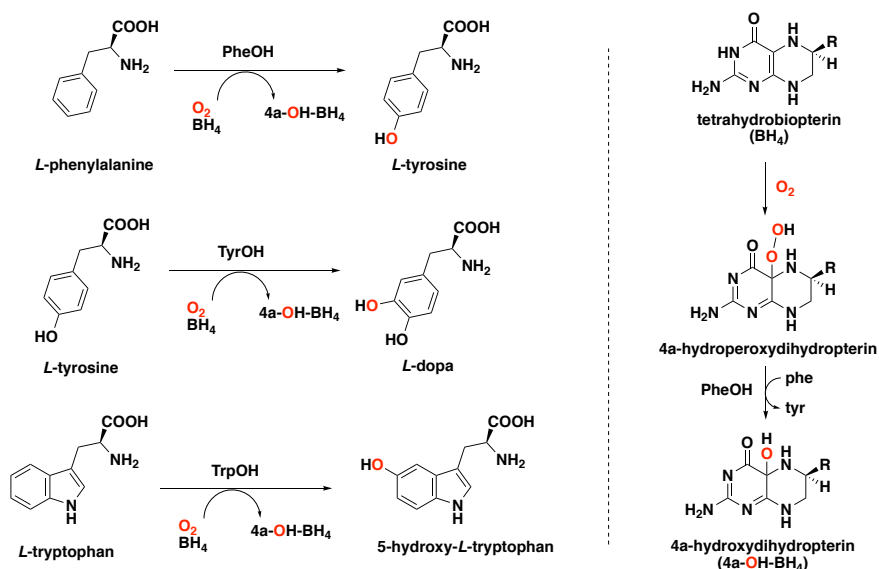


Figure 8. Left: Arene hydroxylation reactions catalyzed by pterin-dependent amino acid hydroxylases. Right: Reaction of the tetrahydropterin cofactor with dioxygen in the presence of aryl amino acid hydroxylases.

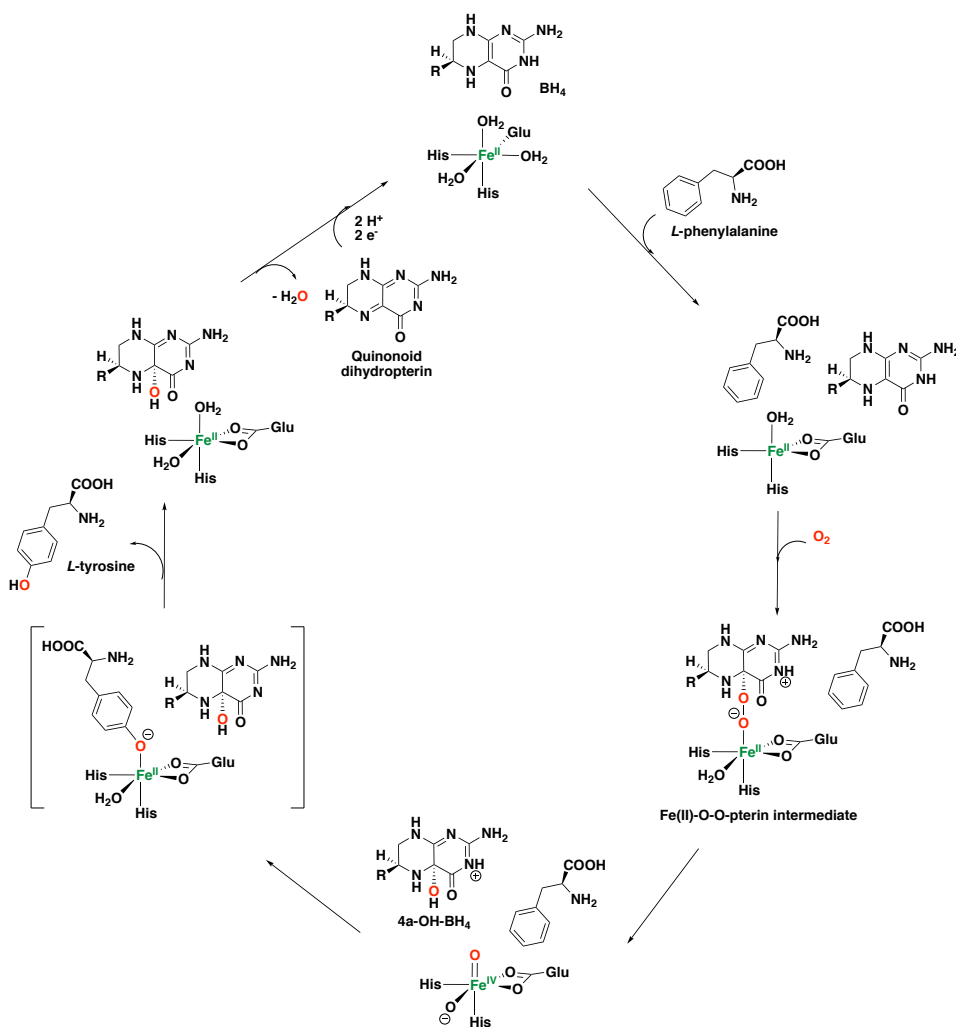


Figure 9. Proposed catalytic mechanism for phenylalanine hydroxylases (PheOH).^{23, 34}

active site of the enzyme to generate an Fe(II)–O–O–pterin intermediate.^{34, 140, 142, 145} Alternatively, the direct reaction of dioxygen with the iron center to form an Fe(III)–peroxo complex may take place, which then reacts with the tetrahydrobiopterin compound.^{143, 146-148} Subsequently, heterolytic cleavage of the O–O bond takes place to form a hydroxydihydropterin compound and an Fe(IV) oxo species responsible for the arene hydroxylation reaction. Several studies using labelled dioxygen have corroborate this last step because of the incorporation of labelled oxygen into both the amino acid and the hydroxydihydropterin product.¹⁴⁹⁻¹⁵¹ Once the hydroxylated amino acid is formed, the resting state of the enzyme is restored, and the oxidized tetrahydrobiopterin undergoes dehydration to generate a quinonoid dihydropterin. This latter compound is reduced by an external reductase to regenerate the tetrahydrobiopterin and start a new catalytic turnover.¹⁴⁵ Computational studies have also been performed to investigate the mechanism of pterin-dependent aromatic amino acid hydroxylases.^{152, 153}

1.2.2 Synthetic Iron Systems

Most of the synthetic iron complexes reported for aromatic oxidation are supported by polydentate N-based donor ligands and make use of the environmentally benign 2e⁻ oxidant H₂O₂. Overall, these systems have been extensively studied for the oxidation of inert C(sp³)–H and C=C bonds, whereas aromatic oxidations using these complexes has mostly been studied in recent years. The mechanism of action of these bioinspired non-heme iron complexes has been extensively studied and is proposed to proceed through the involvement of highly stereoselective, high oxidation-state metal-based oxidants.^{26, 154-159}

1.2.2.1 Iron-Based Systems and Oxidation Mechanism

The first example of a stereospecific hydrocarbon hydroxylation reaction catalyzed by a bioinspired non-heme iron complex was reported by Que and co-workers in 1997 using Fe(II) complex **8** supported by the tpa ligand (tpa = tris(2-pyridylmethyl)amine) with H₂O₂ as the oxidant (see Figure 14b for the structure of complex **8**).¹⁶⁰ The results shown in this study, based on the ratio of alcohol/ketone (A/K) products in the oxidation of cyclohexane (A/K > 5), retention of configuration in specific oxidation reactions (such as the oxidation of *cis*-1,2-dimethylcyclohexane), regioselectivity in the oxidation of tertiary C–H bonds over secondary C–H bonds (adamantane oxidation), and kinetic isotope effect (KIE) experiments, pointed towards a metal-based species as the active oxidant. Besides, the idea of a metal-based oxidant was also proposed in other studies using different aminopyridine ligands based on the tpa ligand scaffold.¹⁶¹

Generally, this type of iron catalysts is supported by tetradentate aminopyridine ligands, with the ligands being either tripodal or linear. Different geometries around the metal center can be

adopted in the case of linear tetradentate aminopyridine ligands, such as for the bpmcn ligand (bpmcn = *N,N'*-dimethyl-*N,N'*-bis(2-picoly)cyclohexane-*trans*-1,2-diamine). On the one hand, complexes with two *cis* positions open for coordination can form, whereas on the other hand, the two open coordination sites can be *trans* to each other. For the *cis* topologies, two configurations are possible, namely *cis-α* and *cis-β*, and different reactivities have been found depending on the specific geometry that the complex may adopt (Figure 10).^{82, 157, 162-166}

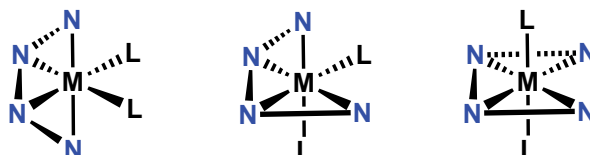


Figure 10. Different topologies for complexes with linear tetradentate aminopyridine ligands. L is an open coordination site.

A lot of debate has emerged regarding the mechanism of activation of H_2O_2 by non-heme iron complexes that are able to perform hydroxylation reaction. Nonetheless, a general mechanistic pathway has been elucidated for iron complexes supported by strong-field tetradentate aminopyridine ligands with two *cis* open sites. This pathway proposes the generation of an Fe(V)(O)(OH) species generated via the O–O bond cleavage of an Fe(III)(OOH) intermediate with the help of a proton provided by a water molecule, reminiscent of the mechanism of Rieske dioxygenases (Figure 11).^{26, 156-158, 167, 168}

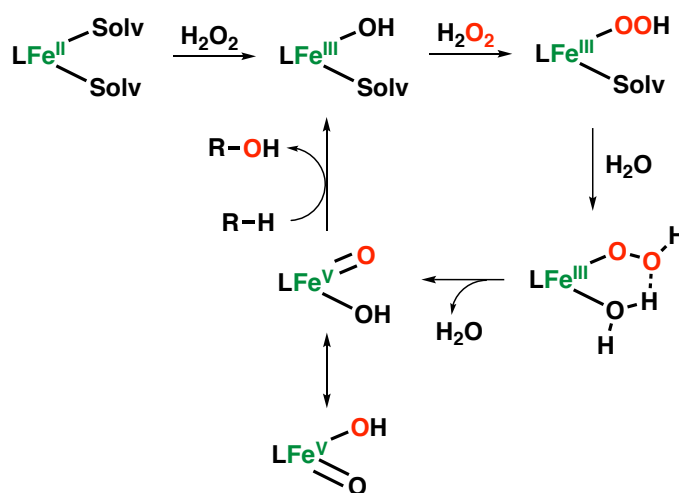


Figure 11. Water-assisted mechanism proposed for the generation of an Fe(V)(O)(OH) species in hydroxylation reactions catalyzed by non-heme iron complexes supported by strong-field tetradentate aminopyridine ligands with two *cis* open sites.

This pathway has been called the “water assisted mechanism”, and several studies on olefin epoxidation and *syn*-dihydroxylation reactions have pointed out the involvement of Fe(V)(O)(OH) species as the electrophilic oxidant responsible for the oxidation reactions by

these kind of complexes.¹⁶⁹⁻¹⁷¹ Indeed, several pieces of evidence that demonstrate the existence of these high-valent iron oxo-hydroxo species have been reported in recent years.¹⁷²⁻¹⁷⁵

Another very important aspect of this chemistry was the introduction of carboxylic acid additives, which act as co-ligands binding to the metal center and modulating the reactivity of the complexes towards H_2O_2 . For the first time in 2001, Jacobsen and co-workers introduced the use of acetic acid in combination with an iron complex supported by the bpmen ligand (bpmen = *N,N'*-dimethyl-*N,N'*-bis(2-picolyl)ethylenediamine) and H_2O_2 , which enhanced the catalytic activity of the iron system in the epoxidation of olefins.¹⁷⁶ Later, White and co-workers demonstrated the same beneficial effect of carboxylic acids in aliphatic C–H bond oxidations.¹⁷⁷

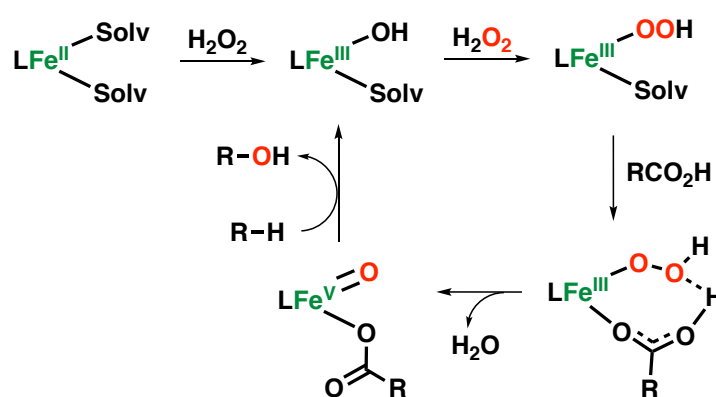


Figure 12. Carboxylic acid-assisted mechanism proposed for the generation of an Fe(V)(O)(OCOR) species in the hydroxylation reaction catalyzed by non-heme iron complexes supported by strong-field tetradentate aminopyridine ligands with two cis open sites.

This remarkable study showed for the first time that an iron complex supported by the robust bpbp ligand (bpbp = *N,N'*-bis(2-pyridylmethyl)-2,2'-bipyrrrolidine) can perform C–H oxidations in synthetically useful yields and, in addition, is able to discriminate between different C–H bonds within a complex substrate molecule.^{178, 179} Various mechanistic studies have been carried out to elucidate the effect of the carboxylic acid in the activation of H_2O_2 , and have led to a proposed mechanistic pathway now known as the “carboxylic acid assisted mechanism” (Figure 12).^{26, 57, 82, 156-158, 167, 168, 180} In this pathway, an Fe(V)(O)(OCOR) intermediate is postulated as the active species, which forms through the heterolytic cleavage of the O–O bond of an Fe(III)(OOH) intermediate with the help of the carboxylic acid instead of a water molecule. Overall, the use of a carboxylic acid as additive and co-ligand in aliphatic and aromatic oxidations, as well as epoxidation reactions, has been found to generate catalytic systems with higher activities in most of the cases.

1.2.2.2 Iron-catalyzed Arene Oxidation

As discussed previously, bioinspired non-heme iron complexes have been widely investigated in the field of aliphatic C(sp³)-H oxidation and alkene epoxidation reactions, whereas catalytic arene oxidations with such complexes have remained challenging until recently.¹⁸¹ Initial reports on aromatic oxidation reactions using iron are based on the incorporation of an aromatic ring into the ligand structure of the complex and therefore represent examples of intramolecular arene hydroxylation reactions. Even though these examples do not represent catalytic systems, their study has allowed for further insight into the mechanism of these reactions. In 1993, Morooka and co-workers described the hydroxylation of a series of trispyrazolylborate-based ferric bis-phenoxo complexes (**1**, **2** and **3**) to form catecholato complexes using *m*CPBA as the oxidant, resulting in a system that acts as a functional model for tyrosine hydroxylase.¹⁸² Reaction of the Fe(III) complexes with 1 equiv. of *m*CPBA resulted in the formation of the corresponding catechol in quantitative yields, and a proposed reaction mechanism includes the formation of an acylperoxo intermediate (Figure 13a). However, attempts to detect the (acylperoxo)-phenoxo intermediate were unsuccessful. Later, Fontecave and co-workers reported on diiron complexes that act as models for methane monooxygenase, based on an ethylenediamine tetraacetic acid (EDTA) derived ligand bearing two electron-rich phenyl groups.^{183, 184} Complex **4** is able to react with aqueous H₂O₂, which leads to the *ortho*-hydroxylation of one of the phenyl groups of the ligand, generating a monomeric iron species (Figure 13b). This intramolecular reaction also proceeds in the presence of dioxygen and excess ascorbate as a reductant, while alkylhydroperoxides, sodium hypochlorite and *m*CPBA do not oxidize the diiron complex. Similar iron complexes supported by the *N,N'*-bis(pyridin-2-ylmethyl)-*N,N'*-bis(3,4,5-trimethoxybenzyl)ethane-1,2-diamine ligand ([Fe(II)(L)X₂], **5** and **6**) were reported to react with aqueous H₂O₂ leading to *ortho*-hydroxylation of one of the substituted phenyl moieties of the ligand as well (Figure 13c).¹⁸⁵ However, for complex **6**, in which the chloride ligands have been exchanged by acetonitrile solvent molecules, the organic ligand does not undergo aromatic hydroxylation, but instead N-dealkylation of the ligand was observed. In addition, this complex showed activity for epoxidation reactions and hydroxylation of alkanes.¹⁸⁵ For complex **5** it was proposed that the hydroxylation reaction proceeds through the reaction with H₂O₂ via an outer-sphere electron transfer to generate hydroxyl radicals that add to the aromatic ring of the ligand. In contrast, complex **6** is proposed to generate iron peroxo and oxo complexes because of the more labile sites of this complex, which allows for an inner-sphere reaction of H₂O₂ with the metal center.¹⁸⁵

In 1999, Que and co-workers reported on iron complex **7** based on a modified tpa ligand containing a pendant phenyl group, Fe(6-Ph-tpa)(NCCH₃)₂(ClO₄)₂ (6-Ph-tpa = bis(2-pyridylmethyl)-6-phenyl-2-pyridylmethylamine), that is capable of performing an

intramolecular hydroxylation of the phenyl group of the ligand to form an Fe(III)-phenolate species (Figure 14a).¹⁸⁶ Reaction of complex **7** with TBHP at low temperature afforded a transient blue species formulated as Fe(III)(OObu)(6-Ph-tpa) that decays over 4 h at $-60\text{ }^{\circ}\text{C}$ to give the final iron complex bearing the hydroxylated ligand.¹⁸⁶

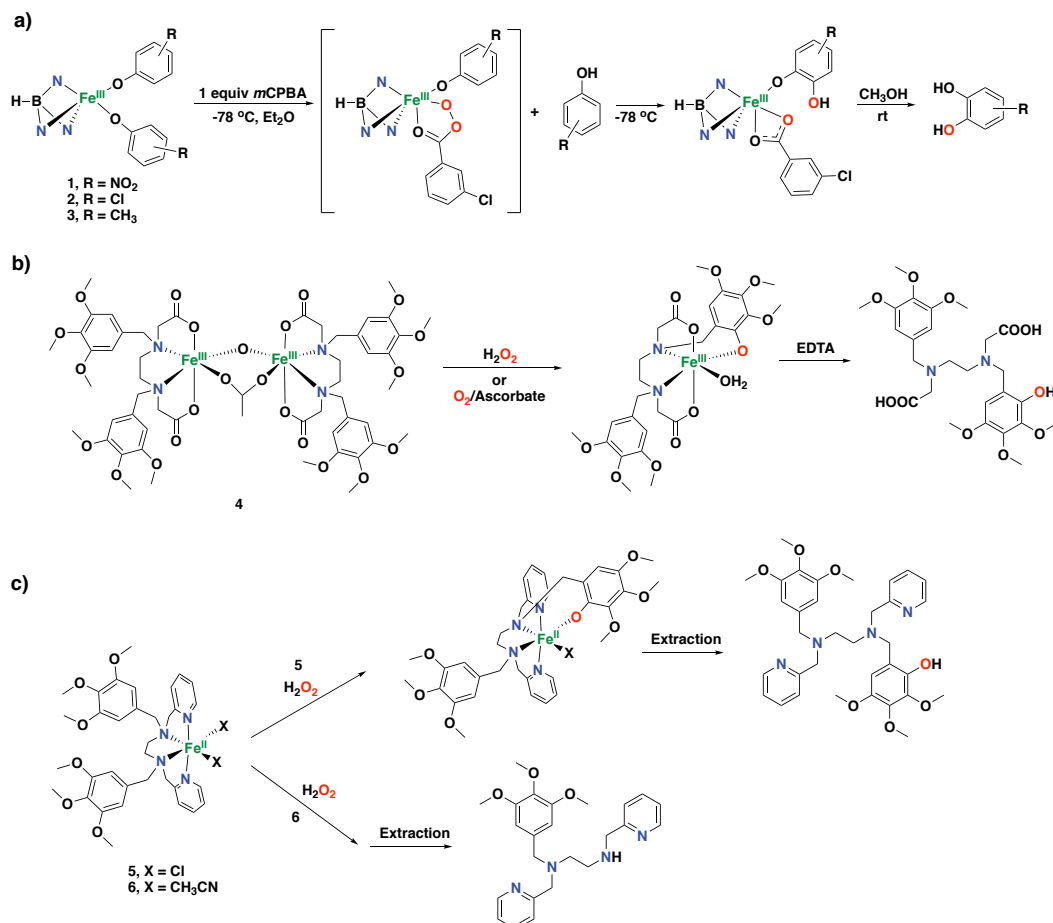


Figure 13. Early examples of iron complexes capable of intramolecular aromatic hydroxylation of the organic ligand.

Indirect evidence suggested the involvement of an Fe(IV) oxo species as the active oxidant in this reaction. Complex **7** also performs the *ortho*-hydroxylation of the ligand phenyl ring efficiently and selectively by reaction with iodosobenzene.¹⁸⁷ The same reactivity with TBHP was also demonstrated for other iron complexes with modified versions of the 6-Ph-tpa ligand.¹⁸⁸ In 2005, it was shown that the parent iron complex **8** supported by the tpa ligand is capable of oxidizing ligated perbenzoic acids through the self-hydroxylation of the aromatic ring forming iron(III)-salicylate complexes (Figure 14b).¹⁸⁹

Iron complex **9** supported by the linear tetradentate bpmn ligand was also found to perform the *ortho*- and *ipso*-hydroxylation of benzoic acids to afford salicylates and phenolates, respectively (Figure 14c).^{190, 191} Later on, hydroxylation of externally added aromatic substrates

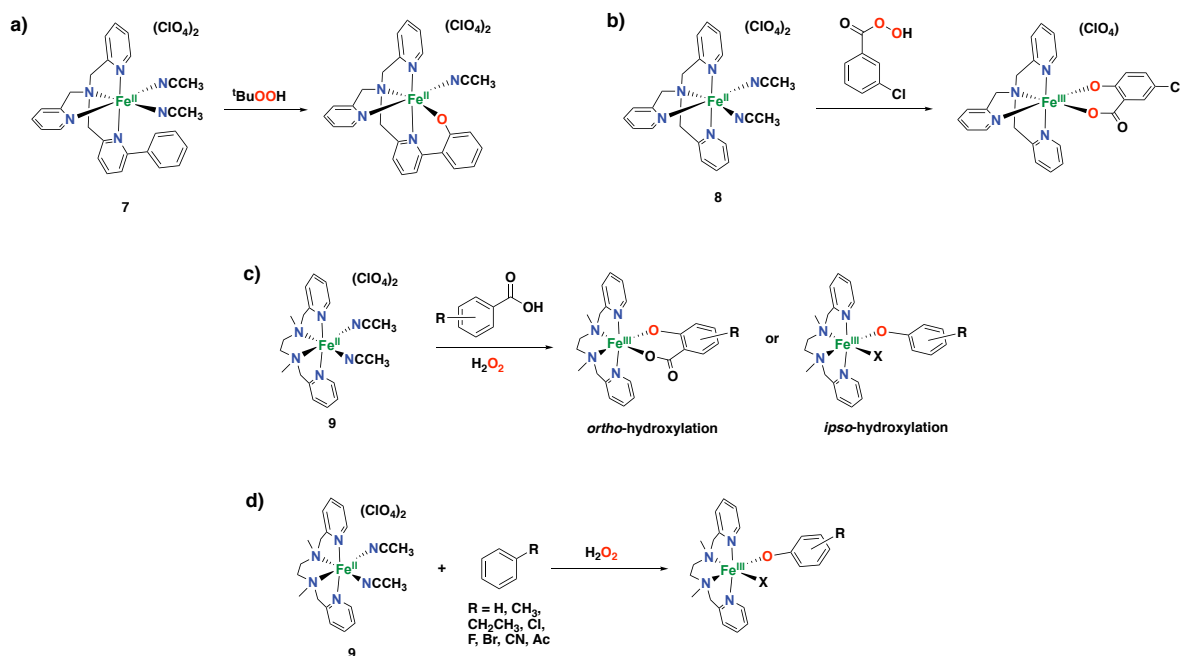


Figure 14. Iron(II) complexes capable of performing arene hydroxylation reactions with different oxidants, generating phenolate or salicylate species.

without directing groups was found to be effective using iron complex **9** in combination with H_2O_2 as oxidant, although strong coordination of the generated phenolates to the resulting iron(III) center prevented efficient catalysis, *i.e.* **9** performs up to 1.4 turn-overs (Figure 14d).¹⁹²

A lot of efforts have been devoted to the investigation of the active oxidant responsible of the arene hydroxylation reaction using these iron complexes. Whereas for some an Fe(IV)-oxo species generated via the homolysis of the O–O bond has been postulated as the oxidant responsible for the oxidation reaction,^{186, 188} an Fe(V)-oxo species has been proposed as an alternative active species in other cases.^{154, 159, 189, 191-193}

Computational studies have also been performed to provide mechanistic insight in the *ortho*-hydroxylation of aromatic compounds by non-heme iron complexes. Particularly, DFT calculations have clearly shown that Fe(III)-hydroperoxo species are sluggish oxidants, whereas the heterolytic cleavage of the former species to generate a transient Fe(V)-oxo oxidant has been postulated as a plausible reaction mechanism on arene oxidations.¹⁹⁴ Moreover, some studies have demonstrated that Fe(IV)-oxo species are inactive in the hydroxylation of externally added aromatic substrates.^{192, 195-197}

Nam and co-workers provided further insight in the capabilities and reaction mechanisms of the oxidation of aromatic substrates by non-heme iron(IV)-oxo complexes.¹⁹⁸ Iron complexes containing Bn-tpen and N4Py ligands (Bn-tpen = *N*-benzyl-*N,N',N'*-tris(2-pyridylmethyl)ethane-1,2-diamine and N4Py = *N,N*-bis(2-pyridylmethyl)-*N*-bis(2-

pyridyl)methylamine) were considered in these studies. Experimental data, such as a large and negative Hammett p value and an inverse C–H/C–D KIE effect, together with computational investigations indicated that arene hydroxylation by these iron(IV)-oxo complex does not occur via a hydrogen atom abstraction, but instead proceeds through an electrophilic aromatic substitution pathway. Oxidation of anthracene as the substrate produced the anthraquinone as the product, which is generated via the reaction of two metal oxo complexes as has been described previously for the generation of quinone compounds.¹⁵⁻¹⁷ Worth mentioning is that these non-heme iron(IV)-oxo complexes do not perform the hydroxylation of benzene or naphthalene, which highlights the low reactivity of bioinspired iron(IV)-oxo species in arene hydroxylation reactions.¹⁹⁸

In 2002, Mansuy and co-workers described a non-heme iron complex supported by the TPAA ligand (TPAA = tris-[*N*-2-pyridylmethyl]-2-aminoethyl]amine), which is effective in the hydroxylation of aromatic compounds using H₂O₂ as oxidant, whereas this complex shows poor catalytic activity for olefin epoxidation and alkane hydroxylation (see Figure 15a for the structure of the TPAA ligand).¹⁹⁹ Overall, this complex shows up to 10 turnovers for the oxidation of anisole (53% yield based on the oxidant), but shows poor activities for the oxidation of less electron-rich substrates, such as benzene or chlorobenzene.¹⁹⁹ Non-heme iron complexes with tetradentate and pentadentate aminopyridine ligands, namely L₄³, L₅² and L₅³ (Figure 15a), have shown comparable arene hydroxylation capabilities in combination with H₂O₂. In addition, for most of these iron complexes it has been demonstrated that the addition of an appropriate reducing agent, such as hydroquinones, thiophenol or tetrahydropterins, dramatically enhances the yields of the hydroxylation aromatic products (up to 69% yield for anisole oxidation based on the oxidant catalyzed by iron complex based on the L₅² ligand, *i.e.* TON = 13.8).²⁰⁰

A more recent study on the non-heme iron complexes containing the TPEN (TPEN = *N,N,N',N'*-tetrakis-(2-pyridylmethyl)ethane-1,2-diamine) and L₆²4E ligands has shown activity for the hydroxylation of electron-rich anisole, as well as for benzene and chlorobenzene. In particular, the former complex performed best in the presence of 1-naphthol as reducing agent, with a yield up to 86% for anisole oxidation (TON = 17.2), whereas the latter complex performed best employing thiophenol as reducing agent, with a yield up to 38% for anisole oxidation (TON = 7.6).²⁰¹ Worth mentioning is that these systems make use of substrate-excess conditions, providing high product selectivities, however, with low substrate conversions.

Bianchi and co-workers described a method for the selective hydroxylation of benzene to phenol catalyzed by an iron complex using H₂O₂ as benign oxidant and trifluoroacetic acid as co-catalyst in a biphasic system.²⁰² The study investigated a series of bidentate N,N-, N,O- and

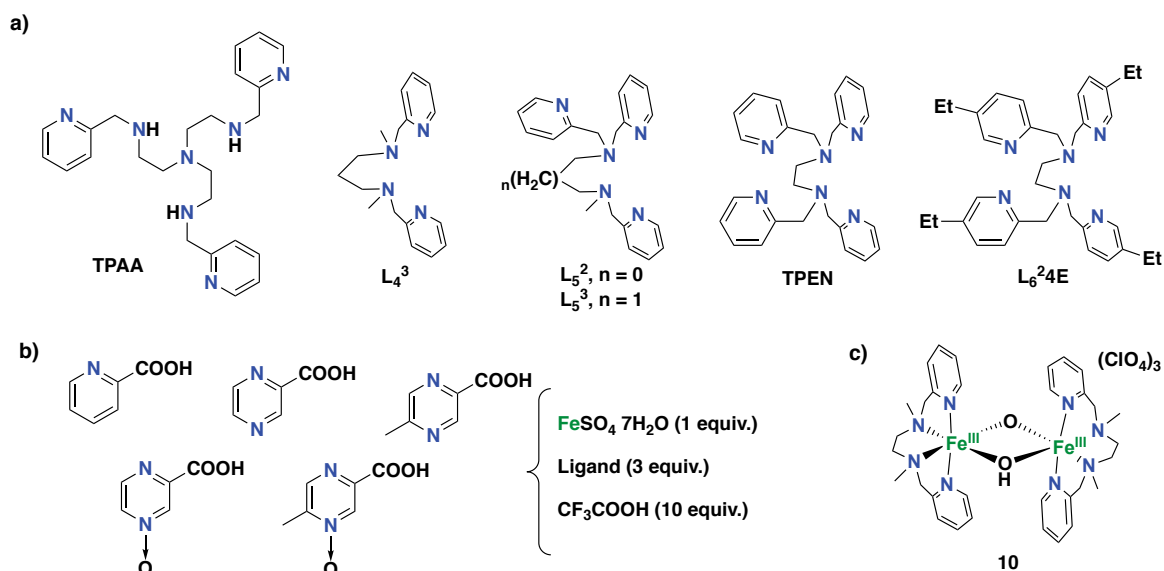


Figure 15. a) Aminopyridine ligands studied in iron-mediated arene hydroxylation reactions under substrate-excess conditions in the presence of a reductant.¹⁹⁹⁻²⁰¹ b) Three-component system for the hydroxylation of aromatics using a biphasic reaction medium under substrate-excess conditions.²⁰²⁻²⁰⁴ c) Example of a diiron complex that mimics the reactivity of toluene monooxygenases.²⁰⁵

O,O-based ligands, finding that the most efficient catalyst system was obtained by using 5-carboxy-2-methylpyrazine-*N*-oxide as ligand (see Figure 15b for ligand structures). The system was used under substrate-excess conditions, providing poor benzene conversions, while H₂O₂ conversion was 94%. Selectivity for the phenol product was 85% based on benzene conversion. Remarkably, the use of a biphasic system (mixture of water, acetonitrile, and aromatic substrate) allowed easy recovery and recycling of the catalyst. Later, the same authors reported on the use of a similar system, using pyrazine-3-carboxylic acid *N*-oxide as the ligand (Figure 15b), for the direct hydroxylation of a series of aromatic substrates to the corresponding phenol products.²⁰³ The authors highlight the low selectivity obtained for the oxidation of electron-rich arenes, as well as possible competition for hydroxylation of the lateral alkyl chain in the case of alkylbenzenes. Finally, another study showed how small modifications in the structure of the ligand used in this biphasic system can produce significant differences in activities for the oxidation of benzene and toluene; the system using pyrazine-3-carboxylic acid *N*-oxide as the ligand being the most efficient for the synthesis of phenols.²⁰⁴

Biswas and co-workers have also described an iron system for the hydroxylation of aromatic C–H bonds under substrate-excess conditions.²⁰⁵ This system consists of diiron(III) complex **10** supported by the bpmen ligand (Figure 15c), that is able to carry out the hydroxylation of benzene and alkylbenzenes with high selectivities, albeit with very low turnover numbers. The addition of acetic acid was found to produce a small increase in phenol yields. For alkylbenzene oxidations, products deriving from the hydroxylation of the lateral alkyl chain were also

observed. On the basis of its dinuclear nature, this system mimics the activity of toluene monooxygenase and methane monooxygenase.

In 2014, Kühn and co-workers reported iron complex **11** capable of hydroxylating aromatic substrates to the corresponding phenol products under catalytic conditions, with equimolar amounts of substrate/oxidant or excess of the oxidant.²⁰⁶ This particular catalyst is based on a chelating di-pyridyl-di-NHC ligand (NHC = N-heterocyclic carbene; Figure 16).

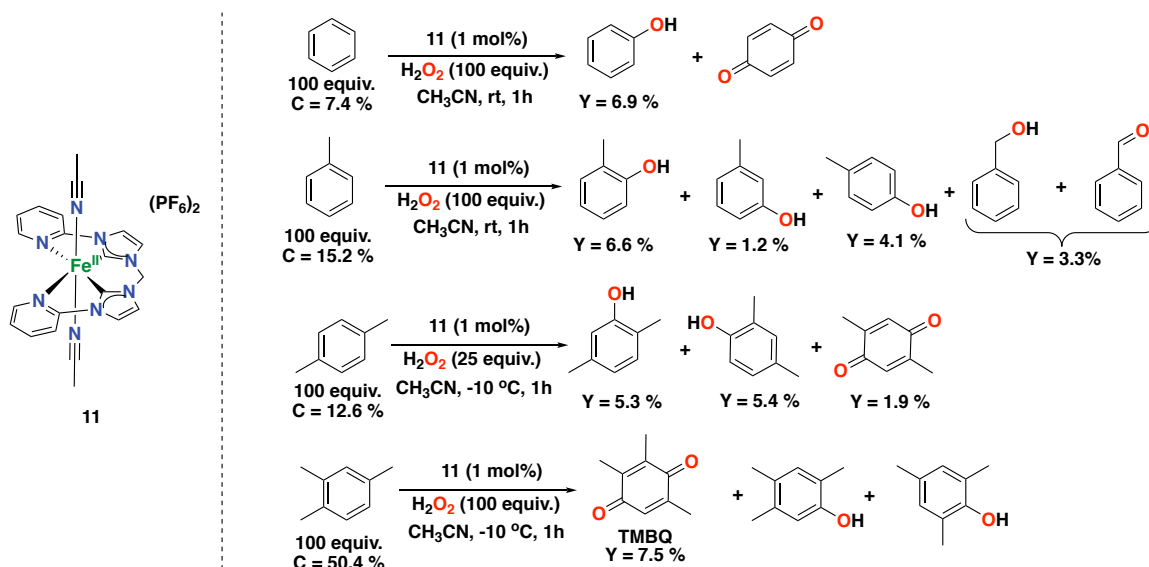


Figure 16. Reaction products of the catalytic oxidation of benzene and benzene derivatives catalyzed by NHC-based iron complex **11** with H_2O_2 as the oxidant.^{206, 210} C: substrate conversion. Y: product yield.

The difference of this complex compared to other complexes typically used in oxidation chemistry is that the iron center is coordinated in part by NHC-based carbon donors.²⁰⁷ NHCs are considered as good σ -donors and, therefore, the authors anticipated that the corresponding complex would exhibit high kinetic stability towards oxidation conditions.^{208, 209} Complex **11** is able to oxidize benzene to phenol using equimolar amounts of H_2O_2 and substrate, albeit in low conversion (7.4%) and phenol yield (6.9%, *i.e.* TON = 6.9), but with high selectivity (94%). The major by-product in this reaction is *para*-benzoquinone. The involvement of hydroxyl radicals in this catalytic system was discarded since no formation of biphenyl was observed. Based on an experimental inverse C–H/C–D KIE of 0.9, the authors have postulated a mechanism that involves an sp^2 -to- sp^3 hybridization change during the attack of a putative high-valent iron-oxo to the aromatic ring forming a σ -complex. Complex **11** is capable of hydroxylating methyl substituted arene substrates as well, such as toluene, *p*-xylene and pseudocumene (Figure 16). Mixtures of phenol products were observed together with some alkyl side chain oxidation products in some cases, overall showing a high selectivity for arene oxidation over benzylic oxidation reactions (up to 11.9% total yield for aromatic oxidation of toluene, and up to 12.6% total yield for *p*-xylene oxidation). A so-called NIH-shift for a methyl

group was observed for the current system in the oxidation of *p*-xylene, which resembles the same process observed for arene oxidations catalyzed by cytochrome P450 or pterin-dependent aromatic amino acid hydroxylases. The system was also tested for the oxidation of pseudocumene, affording trimethylbenzoquinone (TMBQ) in 7.5% yield (a valuable chemical for vitamin E synthesis).^{206,210}

In 2016, Silva and co-workers reported on the reactivity of a series of iron complexes (**12-17**) based on acetylacetonate and Schiff base ligands in the direct hydroxylation of benzene to phenol with H₂O₂ (Figure 17a).⁴² Within this study it was found that the complex based on a N₄-donor Schiff base ligand shows the highest activity and selectivity for the hydroxylation of benzene under substrate-limiting conditions, with 65% conversion and 98% phenol selectivity, generating *para*-benzoquinone as overoxidized side-product.⁴² This system has shown some of the highest conversions and phenol selectivities ever reported for arene hydroxylation using iron catalysts with H₂O₂ as oxidant.

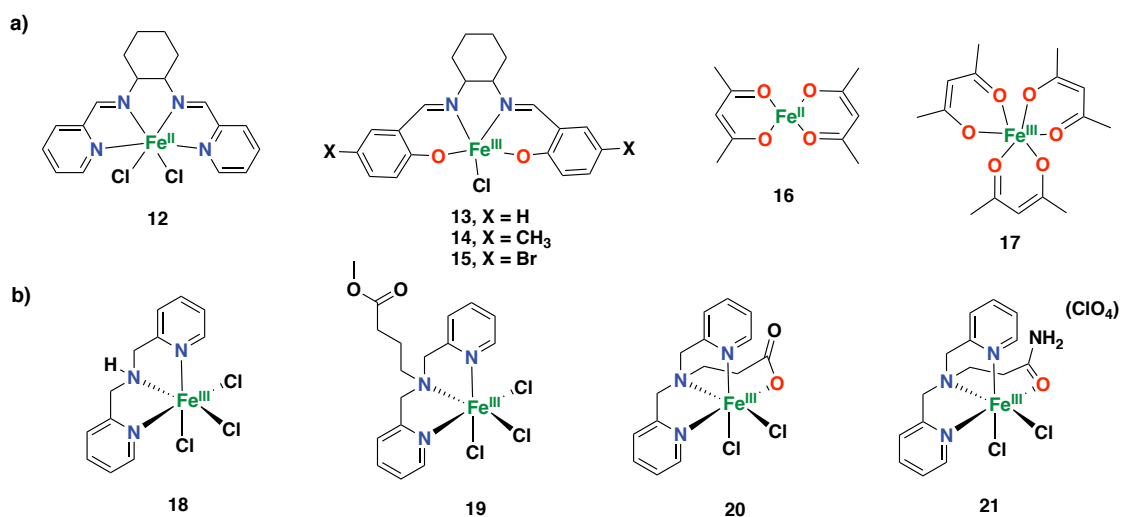


Figure 17. a) Iron complexes supported by acetylacetonate and Schiff base ligands tested for the direct aromatic hydroxylation of benzene to phenol with H₂O₂.⁴² b) Iron(III) complexes tested for the hydroxylation of toluene with H₂O₂ as oxidant.²¹¹

A later study by Antunes et al. describes the reactivity of a series of iron(III) complexes (**18-21**) based on the BMPA and similar ligands as catalysts for the hydroxylation of toluene with H₂O₂ as oxidant (BMPA = bis-(2-pyridylmethyl)amine; Figure 17b).²¹¹ All complexes tested in this study showed reactivity for the oxidation of toluene, generating mixtures of phenol products (*ortho*-, *meta*- and *para*-isomers), as well as products deriving from lateral alkyl chain oxidation (benzaldehyde and benzyl alcohol). Complex **18** based on the BMPA ligand showed the higher yields of all catalysts tested in this study, with a 30% total product yield for the oxidation of toluene at 50 °C after 24 h.²¹¹

Despite the extensively investigation of non-heme iron complexes based on aminopyridine ligands, studies have also shown the effectiveness of imine-based non-heme iron complexes for different oxidative processes.²¹² A remarkable example in the field of arene oxidations catalyzed by imine-based iron complexes was recently reported by Di Stefano and co-workers using iminopyridine iron(II) complex **22**, prepared in situ by self-assembly of commercial starting materials (iron(II) triflate, 2-picolyamine and 2-picolylaldehyde), and H₂O₂ as oxidant under mild reaction conditions (Figure 18).²¹³

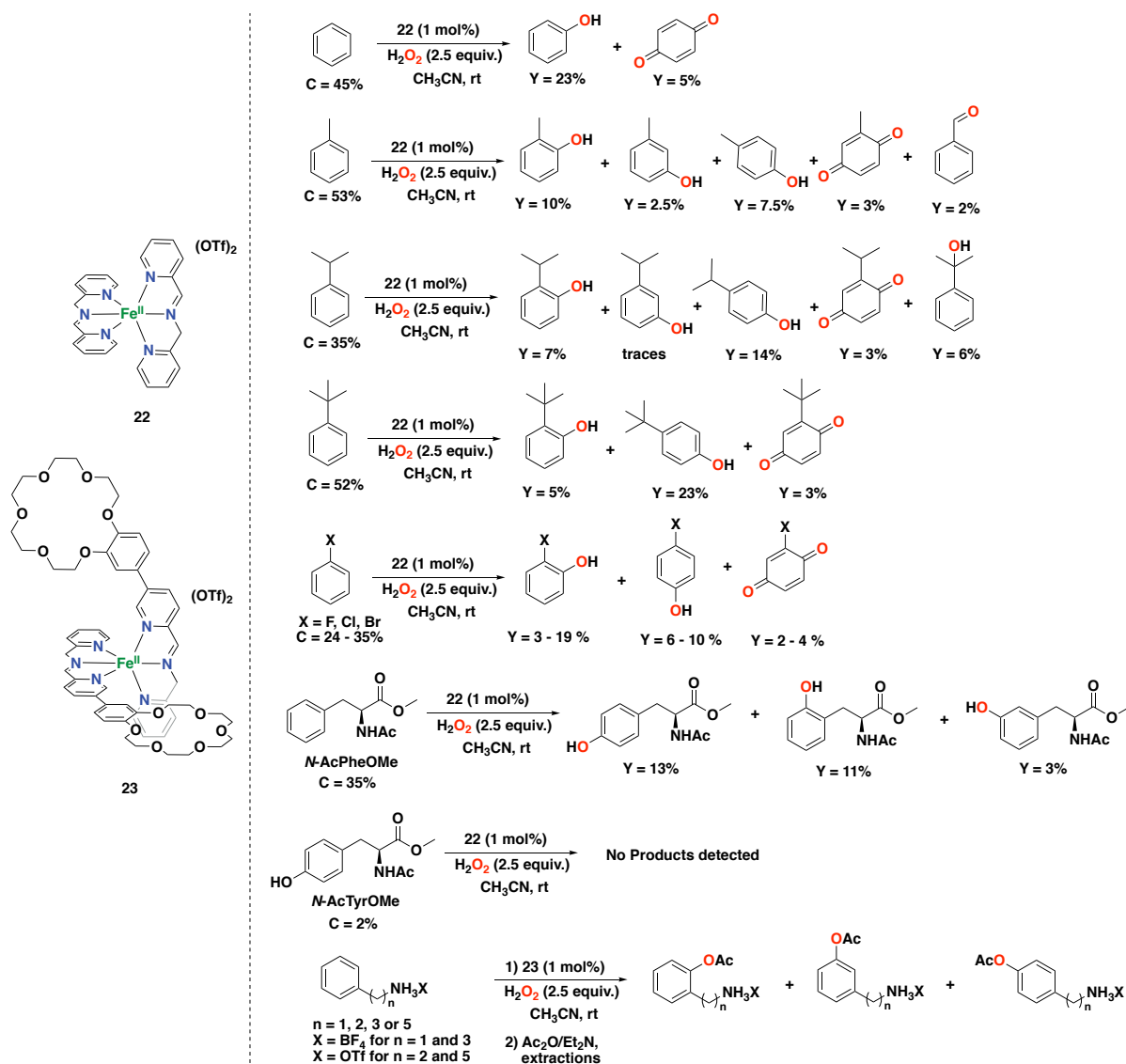


Figure 18. Reaction products of the catalytic oxidation of benzene, benzene derivatives and aromatic amino acids catalyzed by iminopyridine iron(II) complexes **22** and **23** with H₂O₂ as oxidant.²¹³⁻²¹⁵ C: substrate conversion. Y: product yield.

The authors found that complex **22** is capable of oxidizing benzene in 23% phenol yield after 90 min of reaction time, generating benzoquinone as overoxidized by-product in only 5% yield. The oxidation of benzene was also effective on a 0.5 g scale, generating phenol in 26% yield.

A metal-based reaction was postulated as a plausible mechanism for this system since no biphenyl product was detected, suggesting that oxygen-centered radicals are likely not involved. Besides, oxidation of benzene derivatives was also performed with this iminopyridine iron system. Oxidation of phenol afforded *para*-benzoquinone in 13% yield exclusively. Oxidation of toluene afforded the corresponding cresol products (mixture of *ortho*-, *meta*- and *para*-isomers) in a total yield of 20%, as well as overoxidized methyl-*p*-benzoquinone in 3% yield and alkyl chain oxidation product benzaldehyde in 2% yield. Oxidation of ethylbenzene provided products deriving from hydroxylation at the aromatic ring as well as from alkyl side chain oxidation, albeit in smaller amounts. However, when cumene was considered, which bears a more encumbered isopropyl substituent with a weak tertiary benzylic C–H bond, the yield for the alkyl side chain oxidation alcohol product increased (6% yield). Hydroxylation of *tert*-butylbenzene was also proven to be effective, generating phenols in a total yield of 28%, with *tert*-butyl-*p*-benzoquinone by-product in only 3% yield. For all alkylbenzenes tested, mixtures of *ortho* and *para*-phenols were obtained, whereas *meta*-phenols formed in small amounts, suggesting that an electrophilic aromatic substitution-type of mechanism is operative for this catalytic system. Oxidation of halobenzenes was also effective, exclusively generating *ortho*- and *para*-phenols, together with quinone by-products. The electron-rich substrate anisole was oxidized in 21% total yield, providing a mixture of *ortho*-phenol, *para*-phenol and benzoquinone. This product profile agrees with the fact that electron-donating groups favor the oxidation by electrophilic oxidants. On the contrary, electron-withdrawing substituents suppress the reactivity of the catalyst towards the aromatic ring.

Iron complex **22** has also been found to be effective for the oxidation of several aliphatic C–H bonds,²¹⁶ as well as alcohol oxidation to ketones.²¹⁷ Noteworthy is that benzylic alcohols are oxidized in low yields due to competitive arene hydroxylation, showing that the **22**/H₂O₂ catalytic system has a preference for oxidizing aromatic over aliphatic sites. Moreover, the oxidation of monocyclic and polycyclic aromatic systems showed a clear chemoselectivity for aromatic over aliphatic side chain oxidation. However, for more activated polycyclic substrates with lower BDEs of the benzylic C–H bond, the chemoselectivity decreased.²¹⁸

A mechanism for H₂O₂ activation and substrate oxidation by complex **22** has been proposed to include decoordination of one of the pyridine donor arms.^{213, 219} Initially, the starting Fe(II) complex is oxidized to an Fe(III) intermediate, after which detachment of one of the pyridine arms of the ligand allows the complex to react with H₂O₂ to generate an Fe(III) hydroperoxo species (Figure 19). Further generation of the active species is still a matter of debate, but generation of a high-valent Fe(V) oxo species is proposed to be unlikely since imine-based ligands usually favor low oxidation states of the metal center.²¹⁹

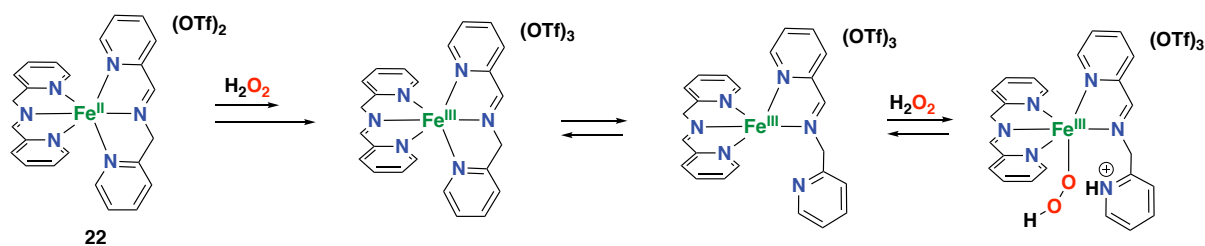


Figure 19. Proposed mechanism for H₂O₂ activation with iminopyridine iron(II) complex **22**.²¹⁹

Complex **22** was also shown to be capable of oxidizing an aromatic amino acid derivative with H₂O₂. Particularly, the oxidation of a protected phenylalanine (*N*-AcPheOMe) yields the corresponding tyrosine (*N*-AcTyrOMe) as the main product (13% yield), together with the two isomeric phenolic derivatives in 14% total yield (Figure 18).²¹⁴ Interestingly, no formation of products deriving from benzylic hydroxylation were observed. An important point to highlight is that **22** does not seem to suffer from irreversible phenolate binding to the iron center, which generally avoids catalytic turnover by catalyst inhibition, as found for several examples presented in this review.

More recently, Di Stefano and co-workers designed a modified version of iminopyridine iron(II) complex **22**, by decorating the ligand with crown-ether moieties. Complex **23** catalyzes the oxidation of aromatic compounds endowed with an alkylammonium anchoring group with H₂O₂ with a moderate activity (up to 31% total yield) and selectivity for hydroxylation of the *meta* over the *ortho* site (up to 1.5 for *meta/ortho* ratio; Figure 18).²¹⁵ The selectivity observed was proposed to be guided by the steric bulk provided by the crown-ether moieties of the ligand, with minor contribution from substrate recognition.

In 2018, Talsi and co-workers described iron complex **24** based on a bpbp type ligand as catalyst for the hydroxylation of aromatics with H₂O₂ or peracetic acid as oxidants and a carboxylic acid as co-ligand (Figure 20).²²⁰ Particularly, iron complex **24** is based on a diferric core, which was previously found to be effective in other oxidative processes, such as alkane hydroxylations and alkene epoxidation reactions.²²¹⁻²²³ Complex **24** was found to be also effective in the oxidation of different aromatic substrates, such as benzene and mono- and dialkylbenzenes (Figure 21). With 0.62 mol% of catalyst loading, 4 equiv. aqueous H₂O₂ and 10 equiv. acetic acid, a total TON of 12.6 in benzene oxidation was achieved, forming hydroquinone (TON = 11.4) as the major, overoxidized product, next to phenol as a minor product (TON = 1.2). For the oxidation of toluene, cresols were obtained in only 1.9 turnovers as a mixture of *ortho*- and *para*-phenols, whereas the major products were the corresponding methylhydroquinone (TON = 8.2) and 4-(hydroxymethyl)phenol (TON = 4.9). Products deriving exclusively from the oxidation of the alkyl side chain were also obtained. Oxidation of other alkylbenzene derivatives provided similar results, with the corresponding

hydroquinones as the major product (Figure 21). Overall, overoxidized products and poor selectivities for the oxidation of the aromatic ring were obtained, resulting in mixtures of products in which oxidation has taken place on aromatic as well as aliphatic positions.²²⁰

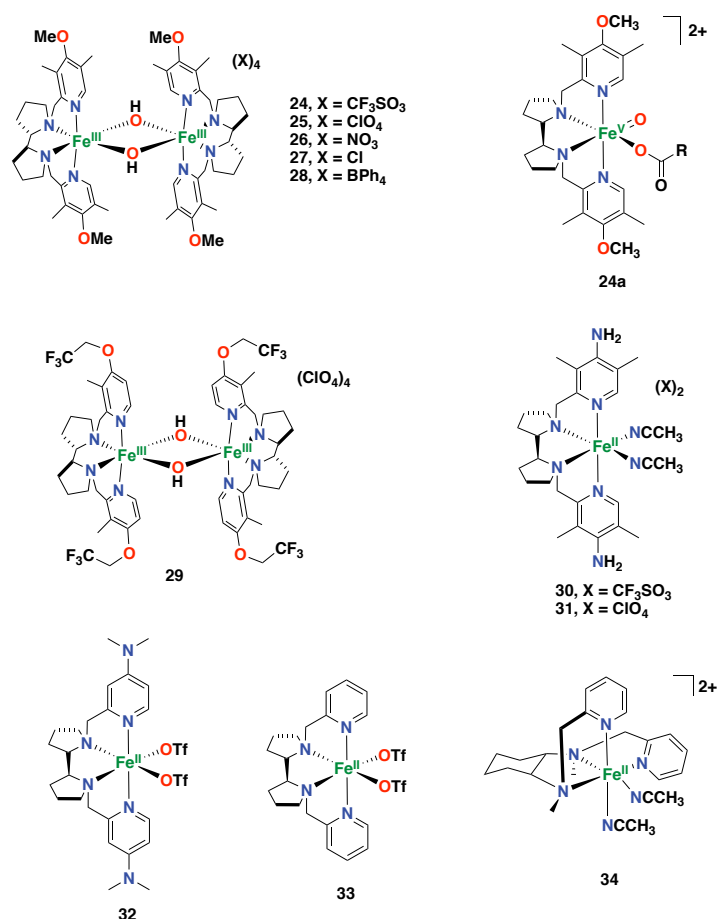


Figure 20. Structures of iron complexes supported by tetradentate aminopyridine ligands that catalyze aromatic oxidation using H₂O₂.

Regarding the active oxidant responsible for the arene hydroxylation reaction, the mechanism was proposed to proceed through Fe(V)-oxo species **24a**, which is formed as a monomeric species upon the reaction of dimeric complex **24** with H₂O₂ and the carboxylic acid additive at low temperatures.^{221, 222, 224} This assignment was based on characteristic EPR parameters, which were similar to those for previously reported non-heme Fe(V)-oxo species.^{225, 226}

Subsequently, Bryliakov and co-workers explored a series of related iron complexes **24-33** based on (substituted) bpbp ligands and containing different counter anions for the oxidation of alkylbenzenes.²²⁷ Among the different counter anions tested, it was found that complex **24**, containing triflate ions, performed the best, with the highest efficiency and selectivity for the oxidation of *o*-xylene. Complex **25**, with perchlorate counter anions, showed a slightly lower catalytic activity, whereas complexes **26-28**, with other counteranions, performed less

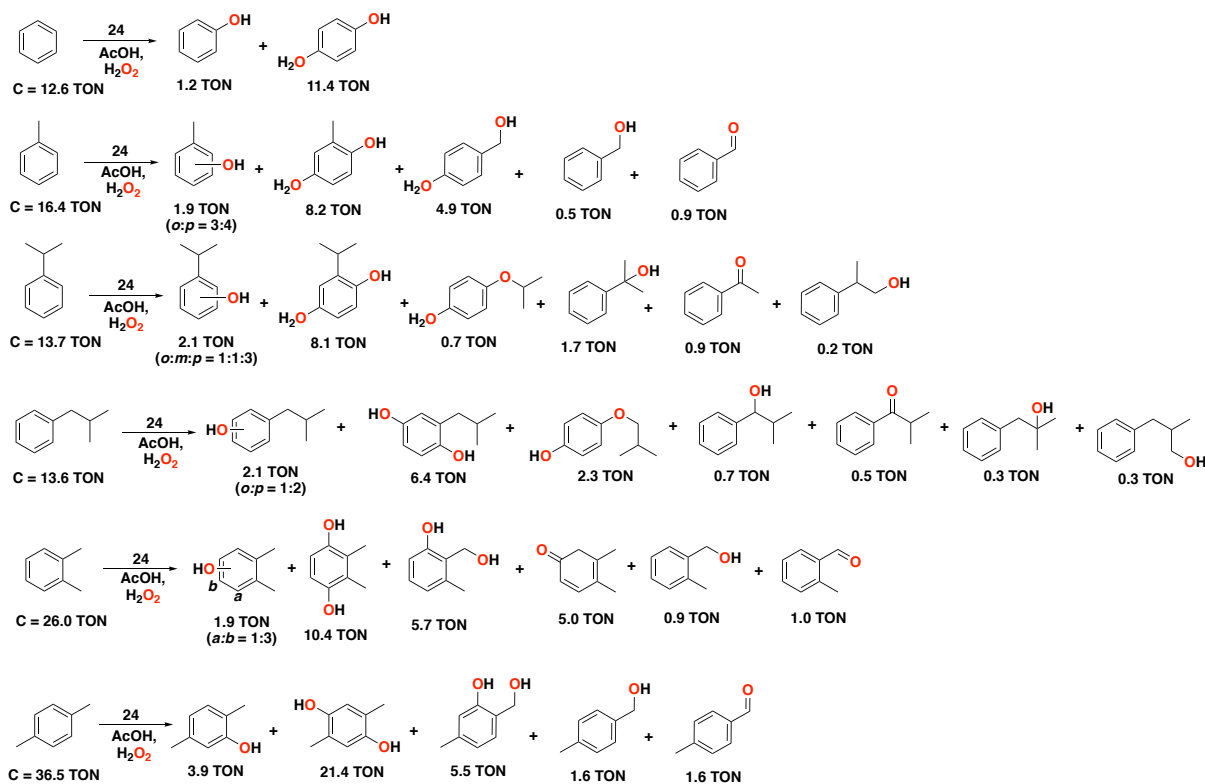


Figure 21. Reaction products of the catalytic oxidation of benzene and benzene derivatives catalyzed by diferric complex **24** as catalyst with H_2O_2 as oxidant and AcOH as carboxylic acid additive. Reaction conditions: complex **24** (0.62 mol% cat. / 1.24 μmol Fe), substrate (100 μmol), H_2O_2 (400 μmol), AcOH (1000 μmol) in CH_3CN at 0 °C for 1.5 h. See the corresponding reference for further details on the oxidation of other alkylbenzene substrates.²²⁰

efficiently for arene oxidation. Importantly, all these iron complexes are active in aromatic oxidation, but show low selectivities, as shown by the formation of considerable amounts of mixed aromatic/aliphatic double oxygenation products.

Among the series of iron complexes tested in this study, it was found that the mononuclear, non-substituted bpbp complex **33** (1.24 mol%) performed best for the oxidation of several aromatic substrates with H_2O_2 (4 equiv.), employing acetic acid (10 equiv.) as additive (Figure 22).²²⁷ Complex **33** is capable of oxidizing benzene, providing hydroquinone as the major product (TON = 9.6), together with small amounts of phenol (TON = 2.2). For toluene oxidation, the hydroquinone was again generated as the main product (TON = 11.1), together with small amounts of cresol products (TON = 2.9). Products in which oxidation has taken place at the benzylic position were also observed in considerable amounts. Oxidation of other alkylbenzene substrates, including mono and dialkylbenzenes, was also performed. Of interest is the oxidation of *p*-xylene, in which a high conversion (TON = 51.5) and yield for the hydroquinone product (TON = 30.3) was observed. Overall, hydroquinone products were

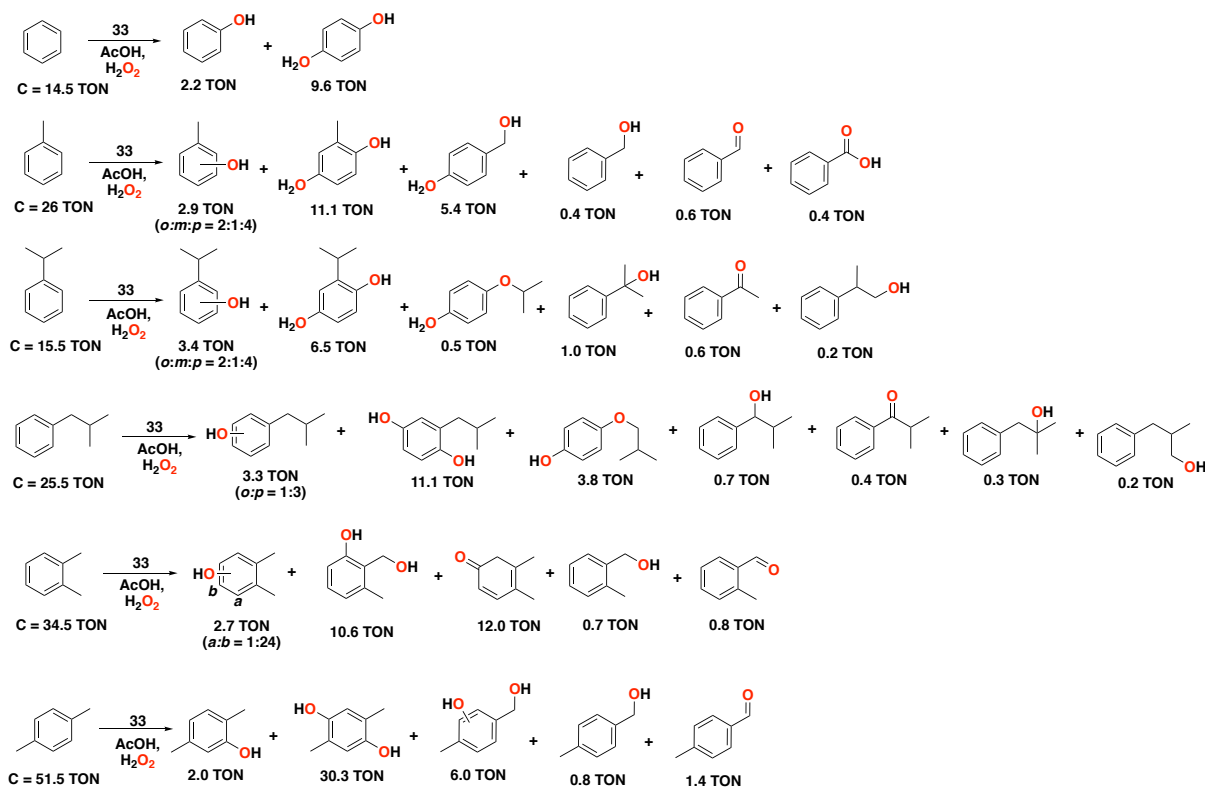


Figure 22. Reaction products of the catalytic oxidation of benzene and benzene derivatives catalyzed by complex **33** as catalyst with H_2O_2 as oxidant and AcOH as carboxylic acid additive. Reaction conditions: complex **33** ($1.24 \mu\text{mol Fe}$), substrate ($100 \mu\text{mol}$), H_2O_2 ($400 \mu\text{mol}$), AcOH ($1000 \mu\text{mol}$) in CH_3CN at 0°C for 1.5 h. See the corresponding reference for further details on the oxidation of other alkylbenzene substrates.²²⁷

obtained as the main product, with small amounts of phenol products and benzylic oxidation products, in a similar way as observed for complex **24** (compare Figure 21 and Figure 22).

The authors also tested other mononuclear iron complexes based on the parent bpbp ligand and comprising differently substituted pyridine rings, but these were found to perform less efficiently compared to parent complex **33**. For instance, the use of mononuclear complexes **30** and **31**, containing an amino group at the pyridine ring instead of a methoxy group, did not improve the reactivity in the oxidation of *o*-xylene with respect to that of complex **24** or **33**. A similar reactivity was also found when the diferric trifluoroethoxy iron complex **29** was employed, whereas complex **32**, bearing dimethylamino substituents, was less efficient. Finally, complex **8**, containing the parent tripodal tpa ligand, was also tested in this same study, also showing poor catalytic activity.

An exploration of different carboxylic acid additives in the aromatic oxidation of *m*-xylene catalyzed by complex **33** revealed that 2-ethylhexanoic acid provided the best results among a series of different linear and branched carboxylic acids tested.²²⁸ Using optimized conditions,

i.e. complex **33** (1.24 mol%), with 2-ethylhexanoic acid additive (10 equiv.) and H₂O₂ (4 equiv.), the oxidation of a series of aromatic substrates was performed (Figure 23).

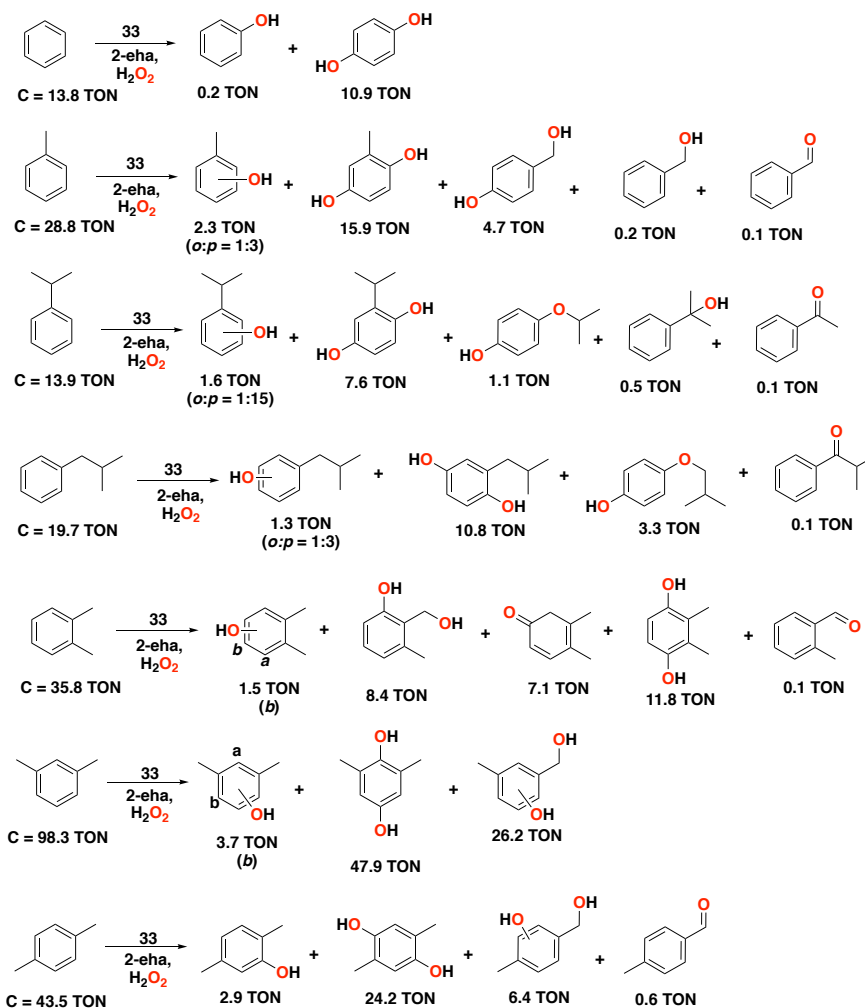


Figure 23. Reaction products of the catalytic oxidation of benzene and benzene derivatives catalyzed by complex **33** with H₂O₂ as oxidant and 2-eha as carboxylic acid additive. Reaction conditions: complex **33** (1.24 μmol Fe), substrate (100 μmol), H₂O₂ (400 μmol), 2-eha (1000 μmol) in CH₃CN at 0 °C for 1.5 h. See the corresponding reference for further details on the oxidation of other alkylbenzene substrates.²²⁸ 2-eha = 2-ethylhexanoic acid.

Benzene was oxidized to hydroquinone (TON = 10.9), with small amounts of phenol product being formed (TON = 0.2). For the oxidation of toluene, the corresponding hydroquinone was formed in 15.9 turnovers, with small amounts of phenol products and products deriving from oxidation at the aliphatic side chain. Catalytic oxidation of a series of mono and dialkylbenzene substrates gave similar results to those obtained when acetic acid was employed, however, yields for the oxidized products were slightly higher when 2-ethylhexanoic acid was used (compare Figure 22 and Figure 23). Interestingly, *m*-xylene was oxidized with a conversion of 98.3 turnovers using these conditions, providing the corresponding hydroquinone in up to 47.9 turnovers.

In an independent study, Que and co-workers tested the reactivity of iron complex **34** ($[\text{Fe}(\beta\text{-bpmcn})(\text{CH}_3\text{CN})_2]^{2+}$) in the oxidation of benzene (Figure 20), which was found to perform several catalytic turnovers to generate phenol in the presence of $\text{Sc}(\text{OTf})_3$ or HClO_4 additives.²²⁹ Generally, it has been established that iron complex **34** is a sluggish oxidation catalyst with H_2O_2 as the oxidant.¹⁶⁵ Nevertheless, it was found that by adding a strong Lewis acid like $\text{Sc}(\text{OTf})_3$ or a Brønsted acid like HClO_4 , a highly electrophilic oxidant is formed that is able to carry out 4 catalytic turnovers in the hydroxylation of benzene to phenol at -40°C . The authors have proposed that an interaction between Sc^{3+} and the iron-oxo oxidant or its iron-hydroperoxo precursor occurs, in a similar way as it has been proposed in other studies for related iron complexes.²³⁰⁻²³⁴ In another study, Que and co-workers showed that activation of the non-heme iron-hydroperoxo species generated with the **34**/ H_2O_2 system can also be accomplished using $\text{Fe}^{\text{III}}(\text{OTf})_3$ as a Lewis acid, leading to the formation of the iron(V)-oxo oxidant.²³⁵ This system was found to be slightly more active in the hydroxylation of benzene to phenol, affording up to 5.4 turnovers. This finding is of interest since it provided insight into the role of a second iron center, which can be related to the activity of diiron active sites found in metalloenzymes, such as in sMMOs.

Finally in 2021, Han and co-workers reported on an iron complex supported by the L-cystine-derived BCPOM ligand and its activity in the arene hydroxylation reaction with H_2O_2 as oxidant (Figure 24).²³⁶

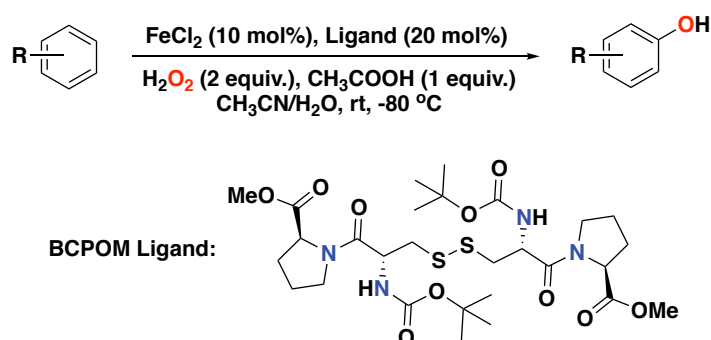


Figure 24. Arene oxidation reaction catalyzed by FeCl_2 , the L-cystine-derived BCPOM ligand and H_2O_2 as oxidant.

The selectivity of this system is excellent, with good yields, and a compatibility with a broad number of substrates. For instance, for the oxidation of protected anilines, oxidation takes place at the *para*-position with respect to the amide substituent with up to 68% isolated product yield. Oxidation of arenes containing methyl, dimethyl or isopropyl substituents were also tested and afforded the phenol products in up to 70% isolated yield. The BCPOM-based system is also active in the oxidation of strongly electron-deficient arene substrates, including aryl ketones

and aldehydes. Of note, the system makes use of 10 mol% of FeCl₂ as the metal salt precursor and 20 mol% of ligand.

1.3 Copper in Biological and Synthetic Systems

1.3.1 Copper-containing Metalloenzymes

Copper-containing enzymes also play an important role in biological oxidation chemistry and, accordingly, are a big source of inspiration in the area of homogeneous oxidation catalysis.^{22, 25, 27} Copper enzymes can be classified by the number of copper centers in their active site; either one copper center (mononuclear)²³⁷ or two or more copper centers (di- or polynuclear).^{27, 238} Examples that stand out among this class of copper-containing metalloenzymes are galactose oxidase (*i.e.* radical copper oxidases that use copper(II)-tyrosyl radical intermediates), amine oxidase, dopamine β -monooxygenase and peptidylglycine α -hydroxylating monooxygenase (*i.e.* enzymes that involve monocopper-oxygen species as intermediates during catalysis), and tyrosinase and catechol oxidases (*i.e.* enzymes that contain dicopper(I) active sites).

1.3.1.1 Tyrosinase and Catechol Oxidases

In this section we briefly discuss copper-containing metalloenzymes capable of performing the oxidation of aromatic substrates. Tyrosinase and catechol oxidases are well-known copper-containing metalloenzymes that catalyze the two-electron oxidation of catechols to *o*-quinones.²³⁹ The difference is that tyrosinase oxidases can also perform the *o*-hydroxylation of phenols to catechols, along with the further oxidation to *o*-quinones.^{240, 241} This reactivity is of importance in melanin biosynthesis.

The active site of tyrosinase comprises a dinuclear copper(I) center in which each metal center is coordinated to three histidine residues (catechol oxidases and haemocyanin share a similar active site).²⁴² Reaction with O₂ forms a (peroxo)dicopper(II) species in which oxygen is bound in a side-on bridging (μ - η^2 : η^2) binding mode.²⁴³ The overall catalytic cycle for phenol oxidation by tyrosinase (phenolase cycle) to generate a quinone product is depicted in Figure 25.^{14, 107, 238, 240, 241} The *deoxy* species can bind O₂ to form the *oxy* intermediate, as stated above. Then, the phenol substrate (in its phenolate form) coordinates to the *oxy* intermediate to only one of the copper centers and *ortho*-hydroxylation occurs to generate an *o*-catecholate dianion that binds in single bridging mode to both copper centers and in a bidentate fashion to only one of the copper centers. Subsequently, a two-electron oxidation yields the final *o*-quinone, thereby restoring the *deoxy* species. An additional catalytic cycle involves the oxidation of external catechol substrates to form *o*-quinones (diphenolase activity; not shown).

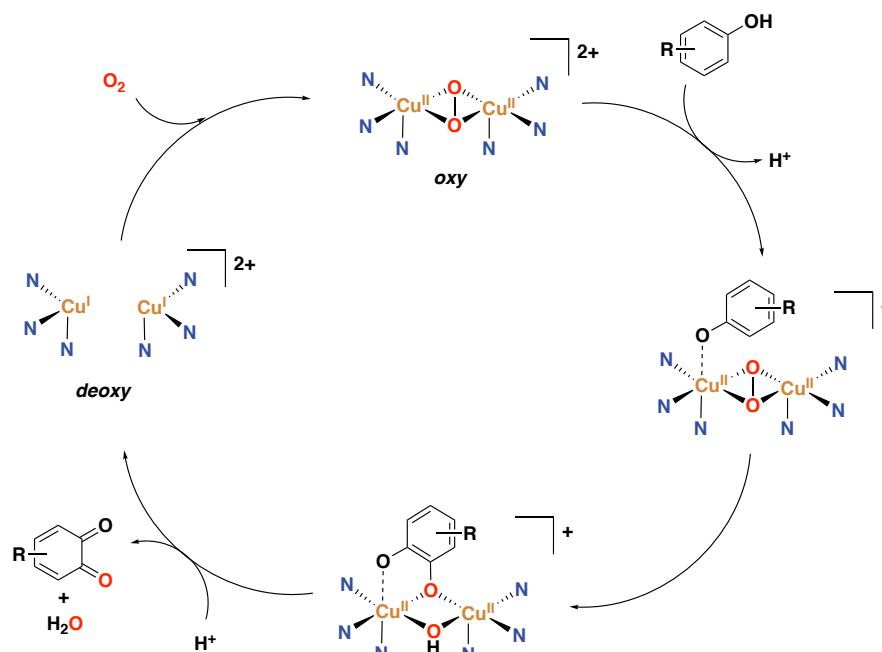


Figure 25. Oxidation of monophenols to o-quinones catalyzed by tyrosinase oxidase.^{14, 107, 240, 241, 244}

1.3.2 Synthetic Copper Systems

Inspired by copper-containing metalloenzymes, chemists have tried to copy their interesting activity and selectivity by mimicking their active sites. Accordingly, various studies have reported on the synthesis of bioinspired model complexes for these copper-containing metalloenzymes. In general, the ligands used in these models contain nitrogen atom donors to reproduce the histidine environment around the catalytic active site of the metalloenzyme. Within this context, these studies have mainly employed pyridines, secondary and tertiary amines, and benzimidazole donor groups.

Within this field, Karlin with co-workers have published numerous examples of copper complexes capable of performing oxidation processes related to the reactions catalyzed by tyrosinase oxidase.²⁴⁵⁻²⁵³ Generally, the ligands used in their studies contain a *meta*-xylyl linker, which allows for the proper orientation of the two copper centers to react with external reagents in a cooperative manner. Earlier examples are based on dinuclear copper(I) complexes of the general structure presented in Figure 26 for complex **35**, bearing two aminopyridine moieties bridged by a *m*-xylyl linker, which react with O₂ to form intermediate species **36** that contains a side-on (μ - η^2 : η^2) coordinated peroxo ligand. Intermediate **36** is responsible for the intramolecular hydroxylation of the aromatic ring in the *m*-xylyl linker of the ligand to afford compound **37**.^{245-247, 251}

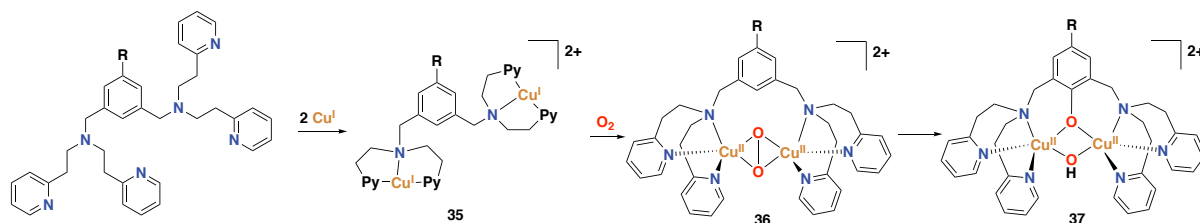


Figure 26. Representative synthetic copper complex **35** inspired by tyrosinase oxidase, reported by Karlin et al.²⁴⁵⁻²⁴⁷ Upon complexation of copper to the dinucleating aminopyridine ligand, reaction with dioxygen leads to a side-on ($\mu\text{-}\eta^2\text{:}\eta^2$) peroxo copper intermediate that can perform an intramolecular aromatic hydroxylation. Py = pyridine; R = H, MeO, ^tBu, F, CN, NO₂.

Other dicopper model complexes have also been found to react with dioxygen, to subsequently display arene hydroxylation reactivity (Figure 27). For instance, a dicopper complex supported by triazacyclononan-based ligands bridged by *m*-xylyl groups reacts with dioxygen at $-80\text{ }^\circ\text{C}$ to form species **38** with a ($\mu\text{-}\eta^2\text{:}\eta^2$) peroxo moiety that could be spectroscopically traced by means of UV-Vis and resonance Raman. Such species are subsequently able to hydroxylate the bridging arene group of the ligand.²⁵⁴ A dicopper complex supported by the 1,3-bis{[3-(*N,N*-dimethyl)propyl]iminomethyl}benzene ligand also reacts with dioxygen to afford a Cu₂O₂ species that performs arene hydroxylation of the ligand to afford compound **39**, which was isolated and characterized by X-ray crystallography.²⁵⁵ In a similar way, a dicopper complex ligated to a dinucleating hexaaza macrocycle is capable of performing intramolecular arene hydroxylation of the ligand to yield compound **40**.²⁵⁶ Casella and co-workers reported a synthetic dicopper complex derived from ligand L-66 (L-66 = α,α' -bis{bis[2-(1'-methyl-2'-benzimidazolyl)ethyl]amino}-*m*-xylene), which for the first time, performed the intermolecular hydroxylation of phenols, therefore displaying similar reactivity as found for tyrosinase oxidase.²⁵⁷ Reaction of the dicopper(I) complex with dioxygen was shown by low temperature UV-Vis and resonance Raman to generate intermediate **41** with a highly reminiscent structure to that of prototypical intermediate **36**. Species **41** is able to hydroxylate external phenol substrates, such as the *o*-hydroxylation of 4-carbomethoxyphenolate to the catecholate product (about 40% yield with respect to intermediate **41**) and the oxidation of 3,5-di-*tert*-butyl-catechol to the corresponding quinone (the formation of the product was demonstrated by low temperature UV-Vis).²⁵⁷ Later, related benzimidazole-based copper-oxygen intermediates, such as **42**, were also found to react with external phenols to form quinones at different temperatures.²⁵⁸

Mononuclear copper complexes have also been used to generate Cu₂O₂ intermediates that can mimic the activity of tyrosinase.²⁵⁹⁻²⁶² For instance, Itoh and co-workers reported the synthesis of a side-on ($\mu\text{-}\eta^2\text{:}\eta^2$) peroxo complex **43**, supported by the *N,N*-bis[2-(2-pyridyl)-ethyl]- α,α -dideuteriobenzylamine ligand. This complex is able to perform the intermolecular

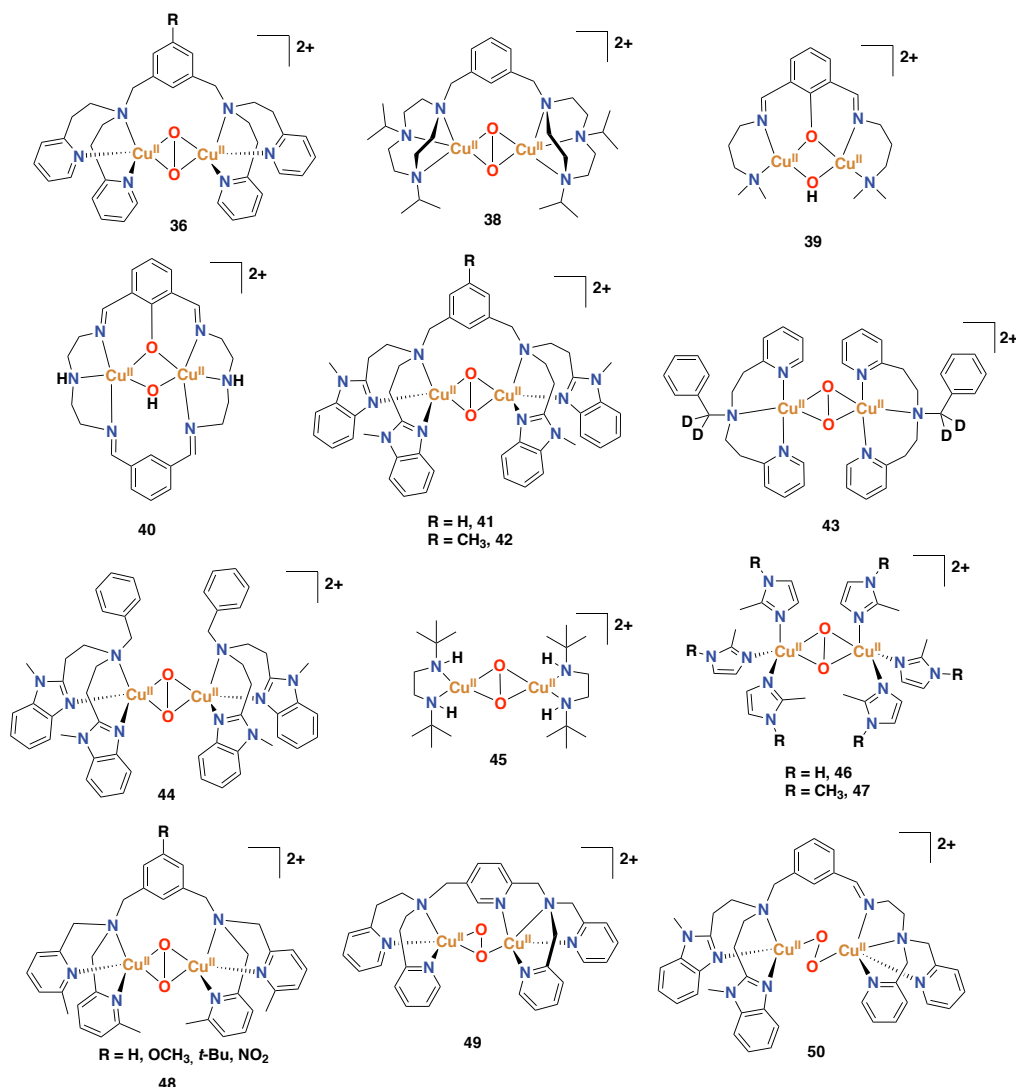


Figure 27. Selected examples of dicopper(II) dioxygen complexes (supported by mono- and dinucleating ligands, as well as non-symmetrical dinucleating ligands) that mimic the activity of tyrosinase.^{254-262, 264, 266-269}

hydroxylation of lithium salts of phenols ($p\text{-X-C}_6\text{H}_4\text{-OLi}$; X = Cl, Me and CO_2Me) to generate the corresponding catechols with up to 90% isolated yield in a stoichiometric reaction.²⁵⁹ Another mononuclear copper complex supported by N,N -bis(2-(N -methylbenzimidazol-2-yl)ethyl)benzylamine has also been found to react with dioxygen to generate a binuclear ($\mu\text{-}\eta^2\text{:}\eta^2$) peroxo complex **44**, that can perform the o -hydroxylation of externally added phenols.²⁶⁰ Next, ($\mu\text{-}\eta^2\text{:}\eta^2$) peroxo dicopper complexes supported by bidentate ligands have also been reported. For instance, complex **45** (supported by a bidentate secondary diamine ligand) was synthesized from the reaction of its corresponding mononuclear copper(I) complex with dioxygen, and its reactivity with phenolates to yield catechols and quinone products was described.^{261, 262} The mechanism through which complex **45** reacts with phenolate substrates works in the presence of dioxygen has been shown to involve the formation of a

bis(μ -oxo)dicopper(III) intermediate prior to the aromatic hydroxylation step (vide infra; Figure 28b).²⁶³ (μ - η^2 : η^2) Peroxo dicopper(II) complexes **46** and **47** supported by monodentate imidazole ligands have also been reported and their reactivity has been explored towards the hydroxylation of exogenous phenolic substrates to afford catechols in good stoichiometric yields at -125 °C, representing more recent examples of bioinspired copper complexes based on the active site of tyrosinase enzyme.²⁶⁴ Along the same line, mononuclear copper complex supported by imine-based ligand containing pyrazole groups have been reported, and their reaction with dioxygen has been proposed to generate a side-on (μ - η^2 : η^2) bound dicopper species that can react with 2,4-di-*tert*-butyl-phenolate (DTBP-H) to generate 3,5-di-*tert*-butyl-*o*-quinone (DTBQ).²⁶⁵ Suzuki and co-workers have reported on side-on (μ - η^2 : η^2)-peroxo dicopper(II) complex **48** supported by H-L-H-type ligands (H-L-H = 1,3-bis-[bis(6-methyl-2-pyridylmethyl)aminomethyl]benzene). This species is very similar to species **36** previously reported by Karlin and co-workers, and not only performs the aromatic ligand hydroxylation of the *m*-xylyl linker but also performs the intermolecular epoxidation of styrene and hydroxylation of THF.²⁶⁹

Unsymmetrical dinucleating ligands have also been employed in the field of synthetic copper-oxygen chemistry. For instance, Itoh and co-workers reported on a dicopper complex supported by an asymmetric pentapyridine dinucleating ligand.²⁶⁷ Upon reaction with dioxygen, they postulated that dicopper(II) species **49** with an unprecedented (μ - η^1 : η^2) binding mode is formed, by comparison of its UV-Vis spectra and resonance Raman features with that of well-characterized (μ - η^1 : η^1)-peroxo dicopper(II) and (μ - η^2 : η^2)-peroxo dicopper(II) complexes. Later, Costas and co-workers reported on a non-symmetrical dicopper(I) complex supported by a non-symmetric dinucleating ligand, which upon reaction with dioxygen generates (μ - η^1 : η^1) peroxo dicopper(II) complex **50**.²⁶⁸ The reactivity of this species was studied by means of experimental and computational methods, and it was found to perform the *ortho* hydroxylation of externally added sodium *p*-chlorophenolate to form *p*-chlorocatechol in 39% yield with respect to **50**.

Generally, a side-on (μ - η^2 : η^2) coordination mode of the O₂-ligand in these kind of Cu:O₂ complexes has been proposed to be the responsible for the hydroxylation reaction. However, an equilibrium has been demonstrated to exist between the side-on (μ - η^2 : η^2) peroxo dicopper species and a bis(μ -oxo)dicopper(III) species, in which the later can be formed upon cleavage of the O–O bond.²⁷⁰⁻²⁷³ Accordingly, the capability of bis(μ -oxo)dicopper(III) species to perform aromatic hydroxylation reactions was scrutinized, and indeed, for some cases this reactivity has been demonstrated.^{241, 256, 263, 266, 270, 271, 274, 275} For example, Tolman and co-workers made use of a mononuclear copper(I) complex containing a bidentate pyridine/amine ligand with a pendant phenyl group, which upon reaction with dioxygen formed bis(μ -oxo)

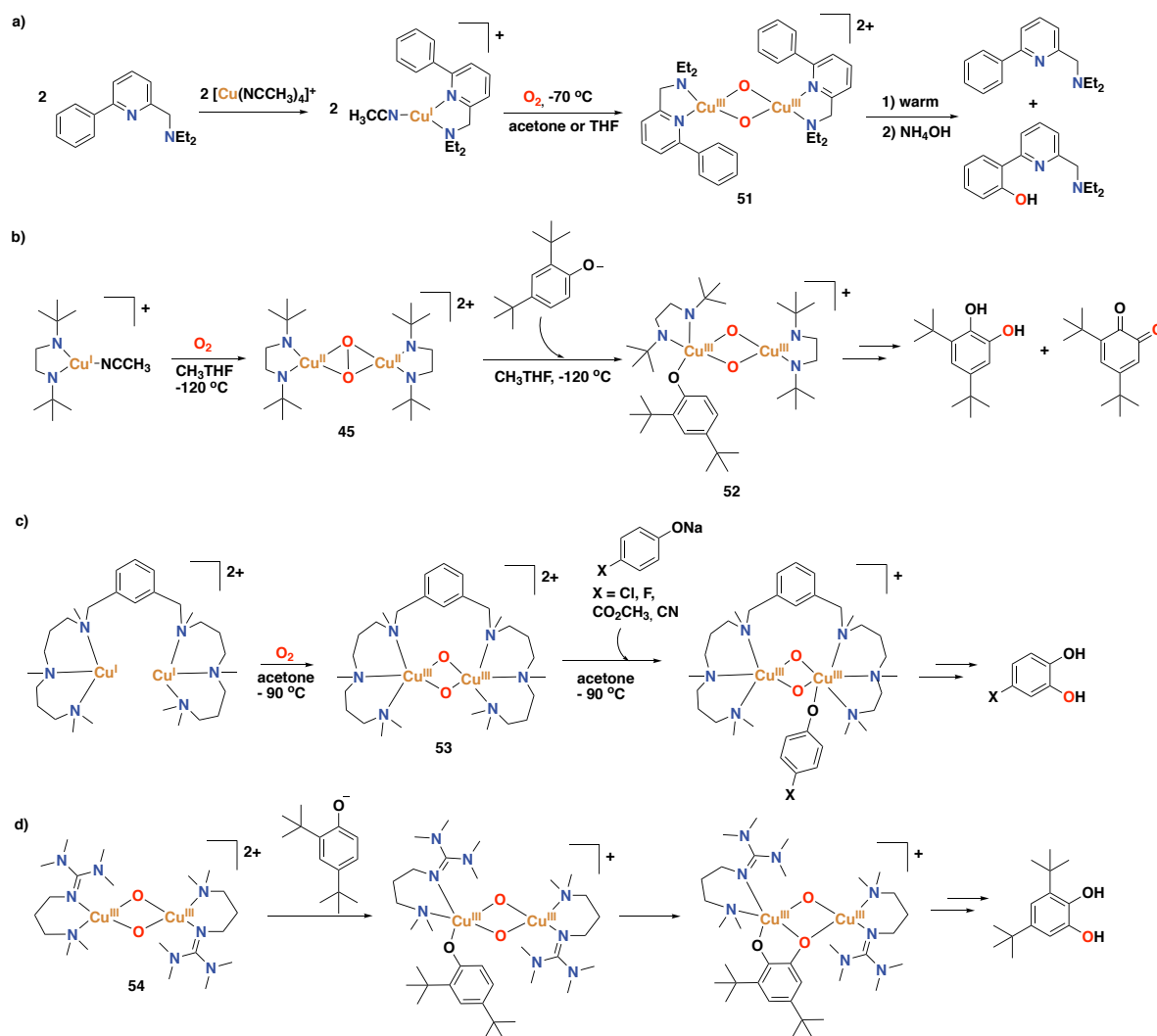


Figure 28. a) Synthesis of a copper(I) complex that performs the hydroxylation of an arene of the ligand upon reaction with dioxygen through bis(μ -oxo)dicopper(III) intermediate **51**.²⁷⁵ b) Mechanism of phenolate oxidation by a mononuclear copper(I) complex, involving formation of intermediates **45** and **52**.²⁶³ c) Mechanism of phenolate oxidation by a dinuclear copper(I) complex, involving bis(μ -oxo)dicopper(III) intermediate **53**.²⁶⁶ d) Reaction of bis(μ -oxo)dicopper(III) complex **54** with phenolates to afford catechol products.²⁷⁶

dicopper(III) species **51** that can perform the intramolecular aromatic hydroxylation of a phenyl group (Figure 28a).²⁷⁵ Stack and co-workers have studied the reactivity of (μ - η^2 : η^2)-peroxo dicopper(II) complex **45** towards phenols, and they could demonstrate that upon addition of the substrate at -120 °C a bis(μ -oxo)dicopper(III)-phenolate complex **52** formed prior to the hydroxylation step (Figure 28b).²⁶³ This intermediate was characterized by UV-Vis, resonance Raman, and Cu K-edge X-ray absorption spectroscopy. Later, Costas and co-workers reported a dicopper(I) complex containing a tertiary N-methylated hexaaza ligand with a bridging *m*-xylyl linker, which generates bis(μ -oxo)dicopper(III) species **53** upon reaction with dioxygen at -90 °C. Intermediate **53** is able to bind and hydroxylate phenolates, and indeed the authors

were able to trap and spectroscopically characterize the species that results from the reaction of sodium *p*-chlorophenolate with species **53** and that precedes phenolate hydroxylation. The 4-chlorocatechol product was formed in 67% yield with respect to the initial dicopper(I) complex.²⁶⁶ Stack and co-workers reported another bis(μ -oxo)dicopper(III) species (**54**) supported by a permethylated-amine-guanidine ligand based on the 1,3-propanediamine backbone that is able to perform the *ortho*-hydroxylation of phenolates to afford catechol products.²⁷⁶

Mononuclear oxygenated copper complexes, such as end-on bound superoxo copper(II) species or copper(II)-alkylperoxide complexes, have also been shown to perform aromatic oxidation reactivity (Figure 29a and b).²⁷⁷ For instance, copper(II) complexes **55** supported by tridentate bis[(pyridin-2-yl)methyl]benzylamine ligands containing *m*-substituted phenyl substituents at the 6th position of each pyridine group were reported to react with H₂O₂ in acetone to form 2-hydroxy-2-hydroperoxypropane species **56**. The latter intermediate undergoes an aromatic ligand hydroxylation reaction to afford copper(II)-phenolate complex **57** (Figure 29a).²⁷⁸ This reaction pathway has been studied by means of spectroscopic and kinetic analysis and an electrophilic aromatic substitution mechanism has been proposed.²⁷⁹ A carbonyl copper complex, supported by an electron-rich tripodal tetradentate aminopyridine ligand based on the tpa scaffold, was reported to react with dioxygen to generate end-on bound superoxo copper(II) compound **58**. The reactivity of the latter complex was tested for the oxidation of phenol substrates, leading to decomposition of complex **58** to generate a phenoxyl radical in 40% yield, together with the generation of 1,4-benzoquinone (24% yield) and arylhydroperoxide (Figure 29c).²⁴⁹ Thus, the reactivity of complex **58** was not exclusively towards aromatic oxidation. Another study reported on the reactivity of a similar end-on superoxo copper(II) complex (**59**), supported by the TMG₃tren ligand (TMG₃tren = tris(2-(*N*-tetramethylguanidyl)ethyl)amine), towards external phenol substrates (Figure 29d).²⁵⁰ Complex **59** could be characterized by means of X-ray crystallography, providing structural evidence for the existence of an end-on superoxo copper(II) species.²⁸⁰ Reaction with phenol substrates showed products in which aromatic oxidation had occurred, in a similar way as the reactivity previously found for complex **58**. Upon reaction of complex **59** with 4-MeO-2,6-*t*Bu₂-phenol, 1,4-benzoquinone was formed in 22% yield, together with the stabilized phenoxyl radical (37% yield) and the arylhydroperoxide product. Interestingly, for the generation of the 1,4-benzoquinone product the displacement of a methoxy group has taken place. Reaction with 2,6-*t*Bu₂-phenol and 2,4,6-*t*Bu₃-phenol lead to formation of the benzoquinone product in 33% and 35% yield, respectively. Finally, reaction with 3,5-*t*Bu₂-catechol lead to the corresponding benzoquinone product in 20% yield (Figure 29d). From all reactions of complex **59** with phenols, a hydroxylated copper(II) alkoxide complex in which a methyl group on the ligand has been hydroxylated was detected.²⁵⁰ Later on, a new end-on bound superoxo copper(II)

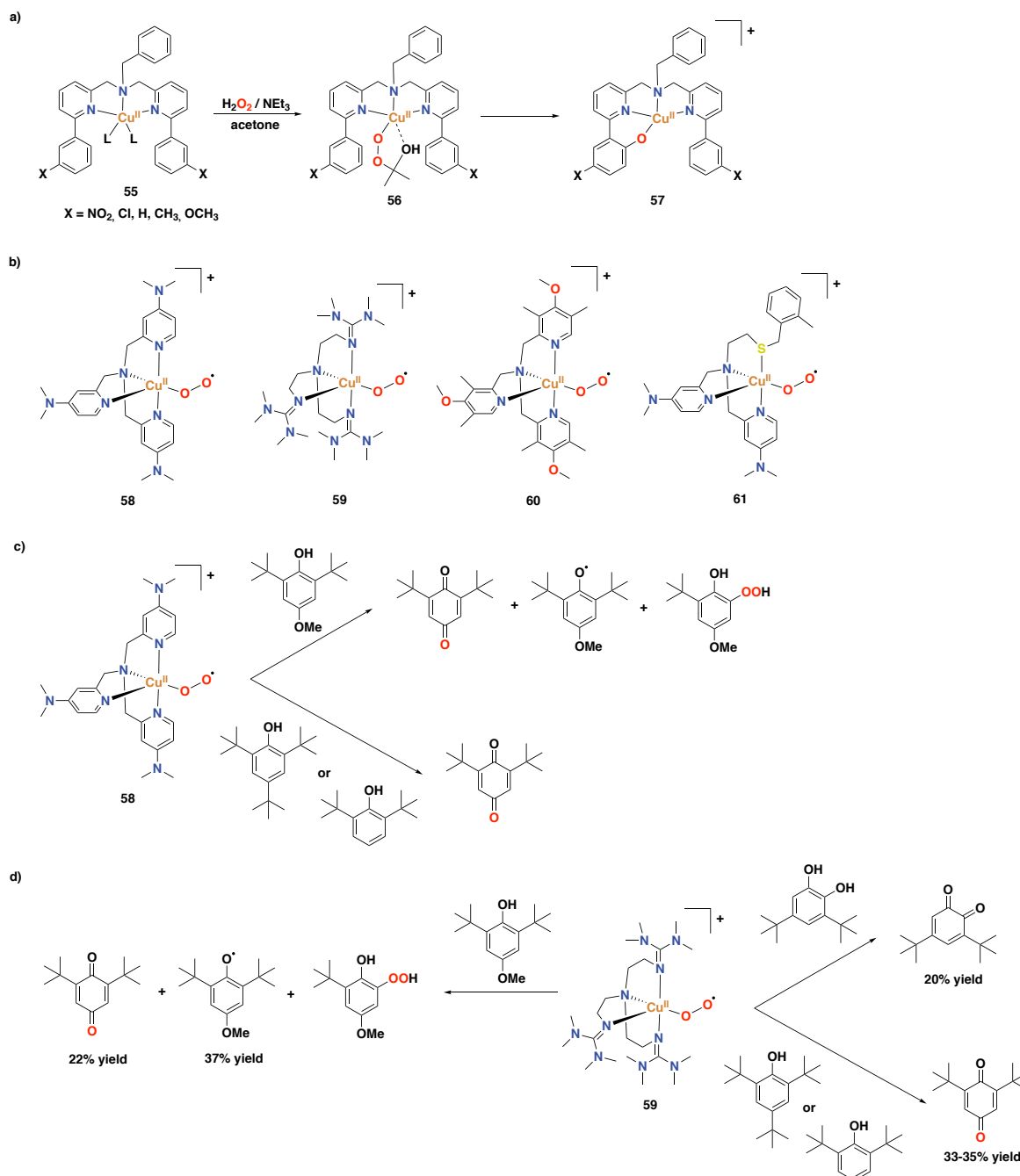


Figure 29. a) Aromatic hydroxylation reactivity of a mononuclear copper(II)-alkylperoxo complex.^{278, 279} b) Selected end-on bound superoxo copper(II) complexes.^{249, 250, 252, 253} c) Reactivity of complex **58** towards phenol substrates.²⁴⁹ d) Reactivity of complex **59** towards phenol substrates.²⁵⁰

complex (**60**) supported by another electron-rich aminopyridine ligand containing dimethylmethoxy substituents on each pyridine ring was reported, and its reactivity towards *para*-substituted 2,6-di-*tert*-butyl-phenols was shown to afford 2,6-di-*tert*-butyl-1,4-benzoquinone in up to 50% yield.²⁵² Much more recently, copper(II)-superoxo species **61** in which the metal center is coordinated to two pyridyl groups, one tertiary amine and one

thioether donor was also described to perform the oxidation of 2,6-di-*tert*-butyl-4-methoxyphenol to 2,6-di-*tert*-butyl-1,4-benzoquinone.²⁵³

All the examples reported until that point were based on stoichiometric reactions. However, in recent years, examples of catalytic copper systems have been developed, and their catalytic activity has been demonstrated towards the oxidation of aromatic substrates.²⁸¹⁻²⁸⁵ Generally, chemists have tried to develop systems that generate metal-based oxidants to perform aromatic hydroxylation reactions, whereas systems that generate hydroxyl radicals through Fenton-type processes were aimed to be avoided because of their non-selective oxidation chemistry (*vide supra*). However, some examples have shown that hydroperoxyl radicals generated through Fenton-type processes can perform the aromatic oxidation of benzene to phenol in high activities and selectivities. For instance, Karlin, Fukuzumi and co-workers reported on a system based on a mononuclear copper complex supported by the tpa ligand, which reacts with H₂O₂ to generate hydroperoxyl radicals and performs the oxidation of benzene to phenol.²⁸⁶ Particularly, they demonstrated that by incorporating the copper complex into mesoporous silica-alumina (Al-MCM-41), they could enhance the activity of the system, reaching up to 4320 turnovers for phenol formation.²⁸⁶

A study reported by Pérez and co-workers showed that catalytic amounts of copper complexes supported by trispyrazolylborate type ligands can perform the direct oxidation of aromatic C–H bonds with H₂O₂ under acid-free conditions (Figure 30, complex **62** for general structure).²⁸¹ Particularly, they tested the system for the oxidation of benzene to phenol (and 1,4-benzoquinone as a overoxidized product), showing conversions within the range of 14 - 30%, and selectivities towards phenol of 67 - 85%. In addition, oxidation of anthracene to 9,10-anthraquinone (98% isolated yield), and 2-ethylanthracene to 2-ethyl-9,10-anthraquinone (98% isolated yield) occurred successfully. In a follow-up study, the same authors reported on a mechanistic investigation, combining experimental and DFT studies, in which they demonstrated that these copper systems perform the aromatic hydroxylation through a copper-oxyl species.²⁸² Moreover, they proposed that hydroxylation occurs through two competing pathways, either via an electrophilic aromatic substitution pathway in which the copper-oxyl species acts as the electrophile, or via a rebound mechanism in which the hydrogen on the substrate is abstracted by the copper-oxyl species prior to C–O bond formation.²⁸²

Liu and co-workers reported a catalyst based on dicopper(II) complex **63** supported by two 2-(((1-methyl-1H-imidazol-2-yl)methyl)(pyridin-2-ylmethyl)amino)methyl)phenol ligands (Figure 30), that can perform the direct hydroxylation of benzene to phenol using H₂O₂ as oxidant, with up to 11.9% phenol yield and 79.3 turnovers.²⁸³

Later on, Kodera and co-workers developed dicopper(II) complex **64** based on the bis(tpa) ligand (6-hpa). This complex was reported to catalyze the selective hydroxylation of benzene to phenol using H_2O_2 reaching a turnover number higher than 12,000 after 40 h for phenol formation in CH_3CN at 50°C , and with a turnover frequency $[\text{mol phenol}\cdot(\text{mol catalyst})^{-1}\cdot\text{h}^{-1}]$ of 1010.²⁸⁴ Noteworthy, these are the highest values reported until now for benzene hydroxylation with H_2O_2 catalyzed by a homogeneous catalyst.

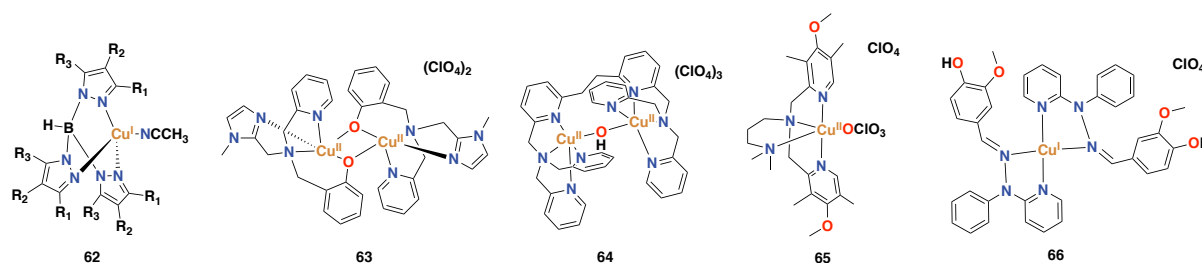


Figure 30. Synthetic copper complexes that display catalytic activity for the hydroxylation of aromatic substrates through a metal-based mechanism.^{281, 283-285, 287}

With regard to the mechanism for H_2O_2 activation and benzene hydroxylation, the authors proposed that upon addition of 1 equiv. of H_2O_2 in the presence of Et_3N at -40°C , an end-on *trans*-peroxodicopper(II) (Cu_2O_2) complex is formed (Figure 31). Then, in the presence of excess amounts of H_2O_2 , Cu_2O_2 decomposes to form hydroperoxocopper(II) complex (CuO_2H)₂. This latter complex is proposed to release H_2O reversibly with the assistance of H_2O to give a copper-bound oxyl and peroxy radical, which is stabilized by hydrogen-bonding interactions with H_2O . Then, the copper-oxyl radical is proposed to react with benzene in the rate-limiting step through an electrophilic aromatic oxidation mechanism to form phenol.²⁸⁴

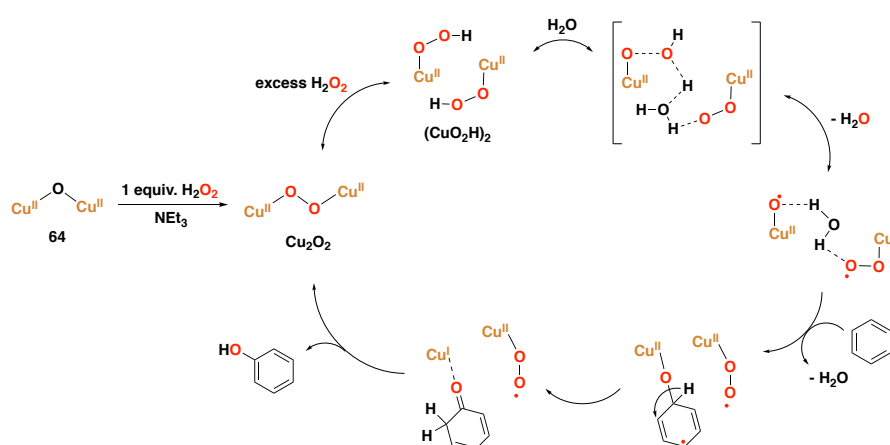


Figure 31. Proposed mechanism for the activation of H_2O_2 and hydroxylation of benzene to phenol catalyzed by complex **64** supported by the 6-hpa ligand.²⁸⁴

Recently, Mayilmurugan and co-workers have described a set of copper(II) complexes based on tripodal tetradentate aminopyridine ligands, and have reported that complex **65** containing

an electron-rich pyridine is the best for the aromatic hydroxylation of benzene with H_2O_2 , affording phenol in 37% yield and with 98% selectivity.²⁸⁵ The authors proposed that oxidation of benzene occurs, most likely, through the generation of a copper(II) hydroperoxo intermediate (Figure 32), and evidence for such species has been obtained using vibrational and electronic spectra, as well as ESI mass spectrometry.

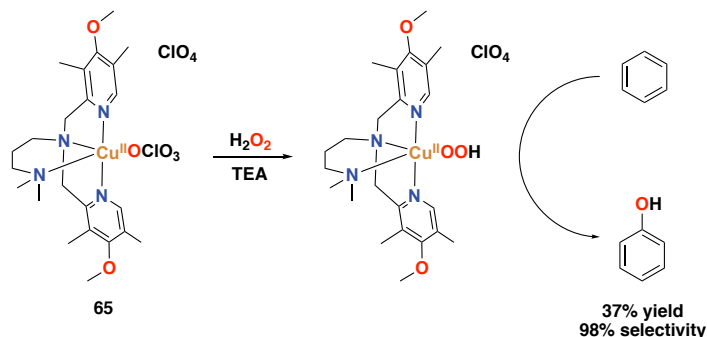


Figure 32. Proposed mechanism for benzene hydroxylation catalyzed by complex **61** through a copper(II) hydroperoxo species.²⁸⁵ TEA = triethylamine.

Mayilmurugan, Ghosh and co-workers also reported on catalyst **66**, in which copper(I) is supported by bidentate nitrogen ligands (Figure 30), that can perform the direct hydroxylation of benzene to phenol in 29% yield, with the benzoquinone by-product being generated in <1% yield.²⁸⁷ The authors also reported on the effectiveness of using this catalyst for the oxidation of toluene, which afforded *p*-cresol and *o*-cresol in 37% yield and benzaldehyde in 21% yield, showing a selectivity for aromatic oxidation of 42%.

1.4 Nickel in Biological and Synthetic Systems

1.4.1 Nickel-containing Metalloenzymes

Despite being less studied in the literature compared to iron and copper-containing metalloenzymes, several nickel enzymes are known to be involved in a number of different oxidation processes. Examples include glyoxalase I, quercetin 2,4-dioxygenase, acireductone dioxygenase, urease, superoxide dismutase, [NiFe]-hydrogenase, carbon monoxide dehydrogenase, acetyl-coenzyme A synthase/decarbonylase, methyl-coenzyme M reductase, and lactate racemase.²⁸⁸ Among these nickel-based metalloenzymes, none of them is capable of performing arene hydroxylation, in contrast to what is known for iron- or copper-based Rieske oxygenases, pterin-dependent oxygenases, tyrosinase oxidases, and others. Despite this fact, several synthetic nickel-oxygen species have been identified and reported to be capable of performing aromatic and alkane oxidation, as well as epoxidation reactions.²⁸⁹ Because of that, chemists have also studied biological oxidation reactions proceeding in nickel-containing

metalloenzymes, with a special interest in (putative) reactive nickel-superoxo, -peroxo and -oxo intermediates involved in these enzymatic oxidations. As an example, we briefly discuss nickel superoxide dismutases in this section, in terms of their catalytic active site, their mechanism of action, and the nickel-oxygen intermediates involved.

1.4.1.1 Nickel Superoxide Dismutase

Superoxide dismutases (SOD) are a class of metalloenzymes that protect cells from toxic products of aerobic metabolism. These nickel-containing metalloenzymes regulate the formation of superoxide by converting superoxide into hydrogen peroxide and molecular oxygen.³¹ It was in 1996 that this class of NiSOD was found in *Streptomyces* and cyanobacteria.³⁰

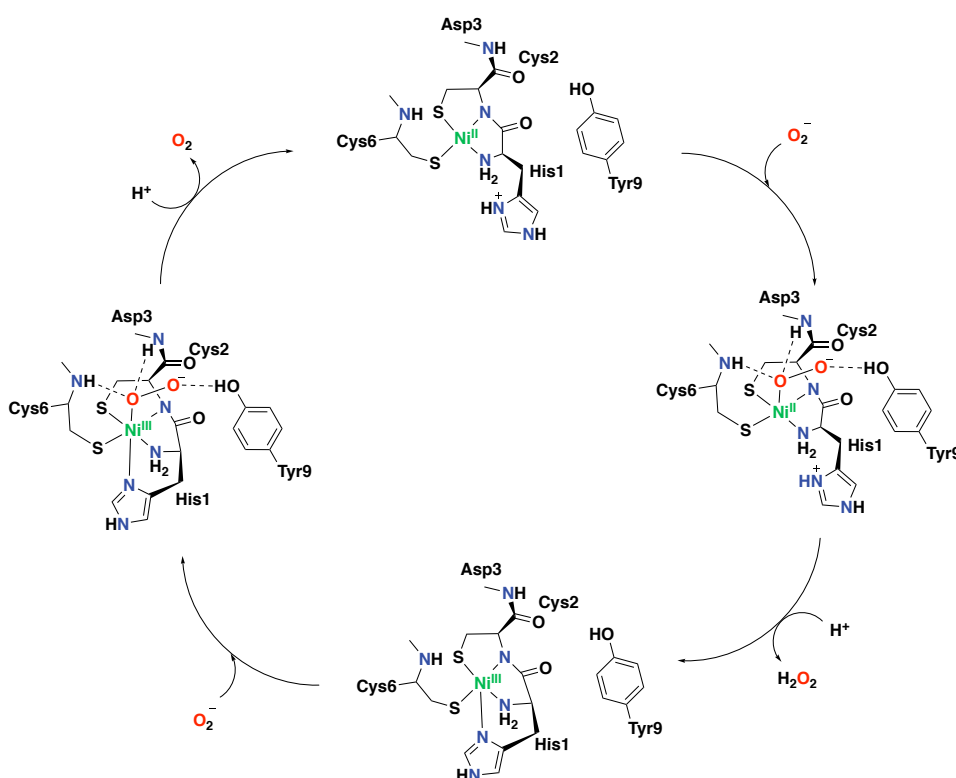


Figure 33. Catalytic cycle of nickel superoxide dismutase (NiSOD).³¹

The active site of NiSOD comprises a Ni(II) atom bound to two sulphide donors (from Cys2 and Cys6) and two nitrogen donors (the N-terminal amine of His1 and the backbone amide of Cys2) in an undistorted square planar geometry (Figure 33).³¹ In the first step of the catalytic cycle, a superoxide anion binds to the nickel center, forming a superoxo-nickel(II) intermediate. The ligated oxygen atom in this intermediate is stabilized by hydrogen bonding with two backbone amide moieties (Asp3 and Cys6). Additional stabilization is caused by hydrogen bonding of the non-ligated oxygen atom with the oxygen atom of Tyr9. Electron transfer from

Ni(II) to the superoxide, coupled with a proton transfer from Asp3, Cys6 or Tyr9 (and not from His1 since it is located on the wrong side of the nickel ion), forms hydrogen peroxide as product and generates a Ni(III) species. The Ni(III) intermediate has a five-coordinate square pyramidal geometry due to a second binding with His1. Then, a second superoxide molecule binds to Ni(III), forming a superoxo-nickel(III) species, followed by electron transfer from superoxide to Ni(III), to form molecular oxygen and regenerate the original Ni(II) four-coordinated intermediate.

1.4.2 Synthetic Aromatic Oxidation Systems based on Nickel

An early study reported by Kimura and co-workers in 1984 described a nickel(II) compound supported by a macrocyclic polyamine that is able to activate dioxygen and oxidize aromatic substrates to generate hydroxylated products.²⁹⁰ This study represents an early example of nickel-based systems that model biological monooxygenases in the selective hydroxylation of aromatic substrates.

More recently, Suzuki and co-workers reported on the development of bis(μ -oxo)dinickel(III) complexes supported by H-L-H-type ligands (H-L-H = 1,3-bis-[bis(6-methyl-2-pyridylmethyl)aminomethyl]benzene), in which different substituents were introduced onto the xylyl linker of the ligand.²⁹¹ This study was a follow-up on the exploration of copper complexes based on the same type of ligands performed by the same authors (Figure 27, complex **48** for general structure).²⁶⁹ Whereas the nickel complexes reacted with H₂O₂ to generate a bis(μ -oxo)dinickel(III) species, the copper counterparts reacted with dioxygen to form a (μ - η^2 : η^2)-peroxo dicopper(II) complex. Both species have been demonstrated to undergo arene hydroxylation of the xylyl linker.^{269,291}

As a follow-up of the study on copper(II) complexes containing tridentate bis[(pyridin-2-yl)methyl]benzylamine ligands carrying *m*-substituted 6-phenyl rings on each pyridine group, in which intramolecular aromatic ligand hydroxylation occurred (see Figure 29a), Itoh and co-workers extended their investigation to the corresponding nickel complexes.²⁹² In this particular study, the authors synthesized and characterized a series of nickel(II) complexes supported by tridentate ligands that contain different substituents at the *meta* position of the phenyl substituents (OCH₃, CH₃, H, Cl, NO₂) (Figure 34, complex **63** for general structure). These complexes were found to react with H₂O₂ in acetone to form bis(μ -oxo)dinickel(III) intermediate **64**. This species decomposes to form (μ -phenoxo)(μ -hydroxo)dinickel(II) species **65** in which one of the phenyl groups on the ligand has been hydroxylated. This aromatic hydroxylation reaction was proposed to proceed through an electrophilic aromatic substitution mechanism. Finally, mononuclear nickel(II) complex **66** is formed, containing the hydroxylated ligand, together with a (μ -hydroxo)dinickel(II) species. Complex **66** was characterized by ESI-

MS and X-ray crystallographic analysis (see Figure 34).²⁹² Worthy of note is that the mechanism of action proposed for these nickel(II) complexes differs from the one proposed for the analogues copper(II) complexes. For the former complexes a bis(μ -oxo)dinickel(III) species seems to be involved, whereas for the latter complexes a 2-hydroxy-2-hydroperoxypropane adduct is generated (see Figure 29a and Figure 34 for comparison).^{278, 279, 292}

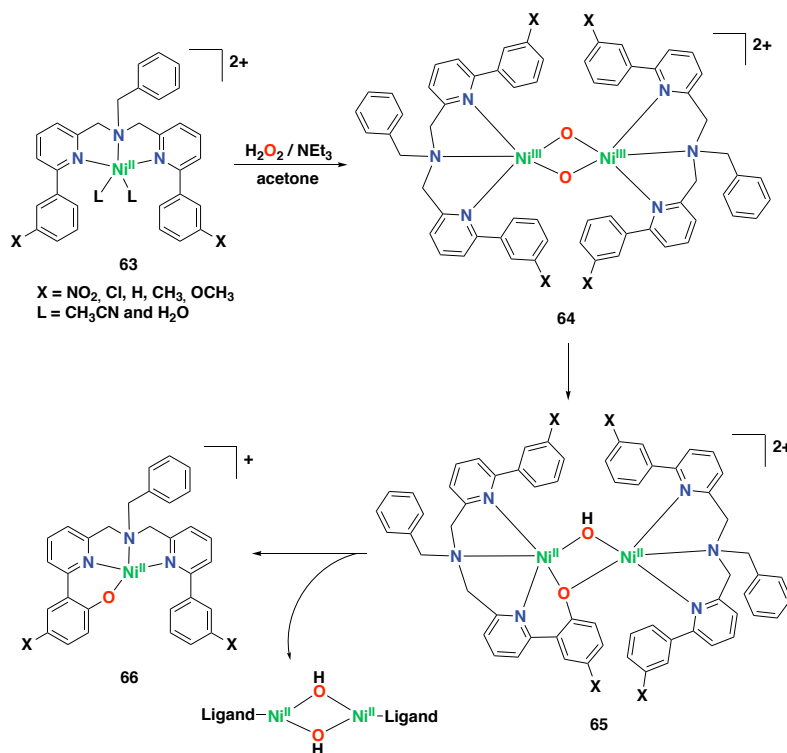


Figure 34. Reaction of nickel(II) complex **63** with H_2O_2 and triethylamine at low temperature to yield bis(μ -oxo)dinickel(III) intermediate **64** that can hydroxylate a phenyl ring of one of the ligands through the formation of intermediate **65**.²⁹²

Itoh and co-workers have also investigated nickel complexes derived from tpa ligands bearing with one, two or three aryl substituents.²⁹³ Particularly, they found that nickel complexes with two (**67**) or three aryl substituents react with H_2O_2 to afford bis(μ -oxo)dinickel(III) species (like complex **68**) at low temperatures (Figure 35), in contrast to what was observed for the nickel complexes derived from tpa ligands bearing fewer aryl rings, which hardly react with the oxidant. Bis(μ -oxo)dinickel(III) species (like complex **68**) were detected using UV-Vis and resonance Raman, and its features compared with other known bis(μ -oxo)dinickel(III) intermediates.²⁹⁴⁻²⁹⁹ Interestingly, it was reported that the former complexes can undergo intramolecular aromatic hydroxylation of the aminopyridine ligand to afford mononuclear nickel species **69** in which one aryl ring on the ligand has been hydroxylated and binds to the metal center.²⁹³ Remarkably, complex **67** was found to be capable of hydroxylating externally added benzene substrates at 60 °C, although phenol was only obtained in 3% yield. The authors

described that the extremely low yield can be attributed to the competition between intermolecular and intramolecular reactions.

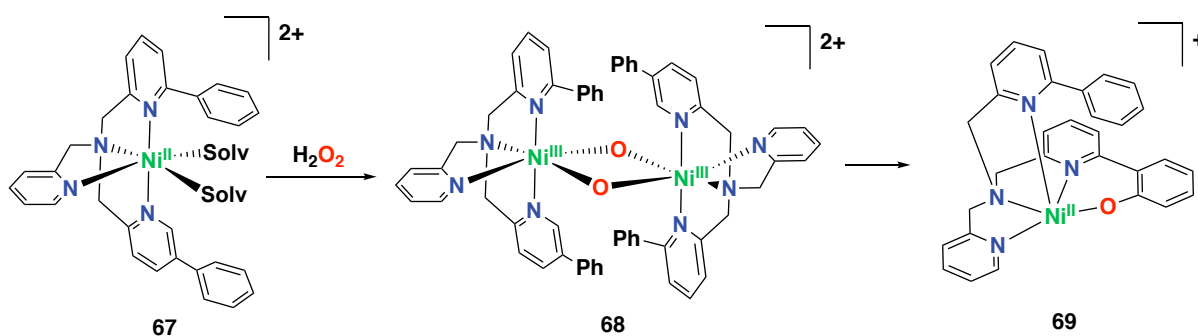


Figure 35. Formation of a bis(μ -oxo)dinickel(III) intermediate and intramolecular arene hydroxylation of the ligand.^{293, 300}

In 2015, the same group reported an interesting study in which they described the catalytic ability of nickel(II) complexes as homogeneous catalysts for the direct hydroxylation of benzene to phenol employing H₂O₂ as oxidant.³⁰⁰ In these catalytic reactions the substrate is mixed with H₂O₂ in the presence of a catalytic amount of the nickel complex (10 mol% catalyst loading) and triethylamine. The best catalyst in this study proved to be nickel complex **70**, supported by the tepa ligand (tepa = tris[2-(pyridine-2-yl)ethyl]amine), which provided 21% phenol yield based on the amount of substrate and small amounts of overoxidized products. The same complex was also used for the oxidation of the alkylbenzene substrates toluene, ethylbenzene, and cumene. Interestingly, the selectivity for aromatic oxidation was up to 90% for these substrates. Nevertheless, reactions do not exceed two turnovers per nickel. In an independent experiment, the authors reported high turnover numbers using extremely low concentrations of the nickel complex and very long reaction times (TON = 749 after 216 h). Based on an experimental kinetic isotope effect, the authors excluded the involvement of hydroxyl radicals in these reactions and postulated a metal-based mechanism. In addition, it was proposed that the aromatic hydroxylation occurs via an electrophilic aromatic substitution mechanism and through the formation of a bis(μ -oxo)dinickel(III) intermediate.³⁰⁰ However, no experimental evidence was provided for the involvement of such an active oxidant. Recently, Itoh and co-workers reported on the synthesis and characterization of a bis(μ -oxo)dinickel(III) complex bearing a similar ligand, exhibiting hydrogen abstraction and oxygenation reactivity towards external substrates, but no aromatic oxidation reactivity was described.³⁰¹

Recently, Mayilmurugan and co-workers reported on related nickel(II) complexes supported by tetradentate aminopyridine ligands for the direct hydroxylation of benzene and toluene to the corresponding phenol products with H₂O₂ as oxidant (Figure 37).³⁰² Interestingly, oxidation

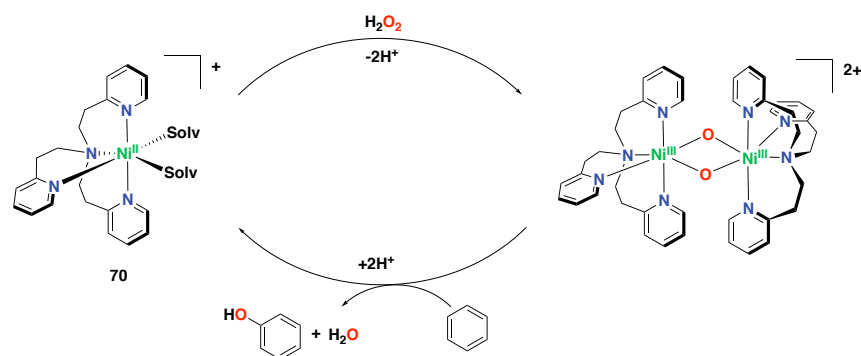


Figure 36. Proposed catalytic mechanism for the direct hydroxylation of benzene to phenol catalyzed by nickel(II) complex **70** supported by a tripodal tetradentate aminopyridine ligand, and involving a bis(μ -oxo)dinickel(III) intermediate.³⁰⁰

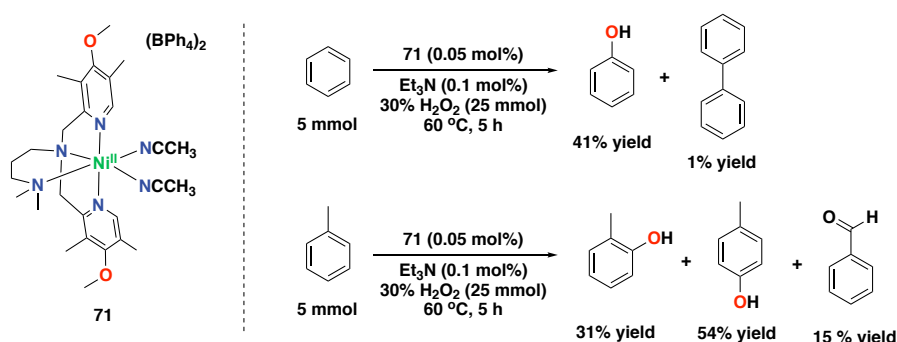


Figure 37. Reaction products of the catalytic oxidation of benzene and toluene catalyzed by nickel(II) complex **71** with H₂O₂ as oxidant and triethylamine as additive.

did not occur when phenol was used as substrate, thus preventing overoxidation to hydroquinone or benzoquinone products. By employing nickel(II) complex **71** bearing an electron-rich ligand (0.05 mol% catalyst loading), the authors reported up to 41% phenol yield and 820 turnovers. Aromatic hydroxylation was proposed to occur through the formation of a bis(μ -oxo)dinickel(III) intermediate, in a similar way as in the mechanism proposed by Itoh and co-workers (Figure 36).³⁰²

1.5 Manganese in Biological and Synthetic Systems

1.5.1 Manganese-containing Metalloenzymes

Manganese, in a similar way as iron, is a non-toxic, inexpensive and earth abundant first-row transition metal. So far, no manganese-containing enzymes are known to perform aromatic oxidation in nature. Nevertheless, manganese plays an important role in the oxygen-evolving complex (OEC) in photosystem II (PS II). PS II is an enzyme present in the thylakoid membranes of oxygenic photosynthetic organisms. Particularly, it is in the oxygen-evolving

complex (OEC) where the oxidation of water to dioxygen occurs.^{303, 304} Several X-ray crystal structure determinations have been successfully achieved for PS II, thus allowing for a better understanding of the structure geometry and components involved in the oxidation reaction.³⁰⁵ The OEC consists of an oxo-bridged structure containing four Mn atoms and one Ca atom, linked via three di- μ -oxo and one mono- μ -oxo-bridged Mn–Mn interactions and the Ca cofactor is linked by single-O bridging to two Mn centers.³⁰⁶

1.5.2 Synthetic Manganese Systems

Due to the advantages of manganese (*i.e.* earth abundant, non-toxic and cheap), in the last years researchers have focused on the exploration of the reactivity of synthetic manganese-based complexes. This element has several available oxidation states (–3 to +7), consequently resulting in a great variety of reactivities for manganese-containing coordination complexes.^{307, 308} For instance, complexes in which the manganese center has a low oxidation state can perform chemistry similar to main group elements, whereas high oxidation manganese complexes can perform oxidation chemistry. Along this vein, manganese complexes have been widely studied in various catalytic oxidation reactions, such as (asymmetric) epoxidation reactions³⁰⁹ and (enantioselective) aliphatic C–H oxidation^{310, 311}, whereas only few examples are known for aromatic oxidation reactions.

Nam and co-workers reported on manganese(II) complex **72** (Figure 38) bearing the Bn-TPEN ligand (Bn-TPEN = *N*-benzyl-*N,N',N'*-tris(2-pyridylmethyl)-1,2-diaminoethane), which upon reaction with iodosylbenzene forms a manganese(IV)-oxo complex that is active in the oxidation of naphthalene, among other types of oxidation reactions.³¹² Nonetheless, no efficient catalytic turnover numbers were achieved.

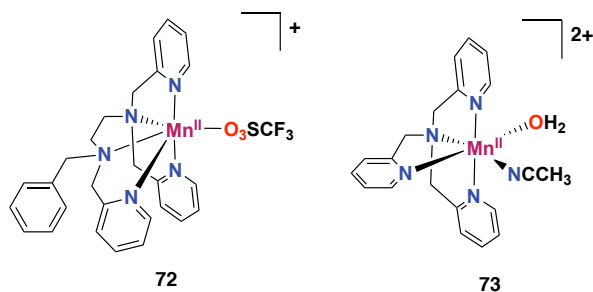


Figure 38. Synthetic manganese complexes that display aromatic oxidation reactivity. Complex **73** is incorporated into a mesoporous silica-alumina (Al-MCM-41).^{312, 313}

In 2015 Fukuzumi and co-workers described the remarkably selective hydroxylation of benzene derivatives to phenols with H₂O₂ employing manganese-tpa complex **73** incorporated into mesoporous silica-alumina (Al-MCM-41).³¹³ The selectivity obtained for phenol formation was excellent and the authors showed the importance of the incorporation of the complex into the

solid support, which prevents the formation of bis(μ -oxo)dimanganese(III,IV) species that are catalytically much less active.

1.6 Aim and Scope of this Thesis

The general aim of the research described in this thesis is focused on the direct conversion of aryl, and to lesser extent alkyl, C–H bonds into the corresponding C–OH functionality, which represents a highly important transformation in both academia and industry. The strategy used in this thesis to accomplish such transformations relies on the development of transition metal complexes as homogeneous catalysts. In addition, the focal point of the current thesis aims at the transition from the use of noble metal catalysts to catalysts based on first-row transition metals, which is of special interest since the latter ones are more abundant and affordable, and usually less toxic. Particularly, in this thesis we have explored complexes based on nickel and manganese as the metal center, since these elements have been less explored in the field of arene oxidation compared to iron and copper. Moreover, the thesis focusses on the use of the environmentally benign oxidant hydrogen peroxide, which only generates water and dioxygen as by-products.

As the first experimental chapter in this thesis, **Chapter 2** investigates molecular nickel(II) complexes supported by tripodal tetradentate aminopyridine ligands as catalysts for the direct hydroxylation of benzene to phenol with H_2O_2 as oxidant. Particularly, the reactivity of several nickel complexes bearing modified aminopyridine ligands is presented, and their activities have been compared to the work reported by Itoh and co-workers.³⁰⁰ In addition, the effectiveness of several commercially available nickel(II) salts in the oxidation of aromatic substrates with a fluorinated alcohol solvent and H_2O_2 is explored.

Chapter 3 and **Chapter 4** of this thesis focus on the exploration of bioinspired manganese(II) complexes bearing linear tetradentate aminopyridine ligands as catalysts for the direct hydroxylation of aromatic substrates to the corresponding phenol products employing H_2O_2 as oxidant. In **Chapter 3** we envisioned that the introduction of bulky *tris*-(isopropyl)silyl groups into the ligand of the complex might prevent catalyst inhibition through phenolate-binding to the manganese center, and might consequently enhance catalytic turnover. The exploration of such bulky complexes towards arene oxidation is presented in this chapter, along with a mechanistic study to better understand how aromatic oxidation is brought about by these complexes.

Next, **Chapter 4** describes a follow-up investigation on the exploration of manganese(II) complexes for arene oxidation, and an evaluation of the sensitivity of the reactions described in

Chapter 3 to electronic and steric effects is presented. A set of complexes bearing different pyridine donors are presented, and their reactivity towards alkylbenzenes is explored. In addition, we show a comparison between the reactivity of C_2 -symmetric and C_1 -symmetric manganese complexes, as well as the design of new manganese complexes that combine electron-rich and bulky pyridines. In addition, particular attention is focused on the product profile of these oxidation reactions (aromatic vs. benzylic oxidation).

Inspired by the findings on chemoselectivity described in Chapter 4, enantioselective benzylic oxidation reactions catalyzed by manganese complexes with H_2O_2 as oxidant are explored in **Chapter 5**. New highly electron-rich manganese(II) complexes bearing 4-pyrrolidinopyridine moieties are presented, and their reactivity towards oxidation of alkylbenzenes is shown and compared with the state-of-the-art homogeneous catalysts. This chapter also describes the use of some of newly developed Mn-complexes in asymmetric epoxidation reactions.

Finally, **Chapter 6** of this thesis describes a novel family of tetradentate amino-imidazole ligands that comprise bulky diphenylimidazole donor moieties. This study mainly focuses on experimental attempts to complex this new family of ligands to manganese, and is complemented with a computational study. In doing so, C_2 -symmetric complexes bearing the new ligands are compared with C_1 -symmetric complexes. At the end, exploration of the imidazole-based complexes towards oxidation of aromatic substrates is presented.

1.7 References

1. Arakawa, H.; Aresta, M.; Armor, J. N.; Barteau, M. A.; Beckman, E. J.; Bell, A. T.; Bercaw, J. E.; Creutz, C.; Dinjus, E.; Dixon, D. A.; Domen, K.; DuBois, D. L.; Eckert, J.; Fujita, E.; Gibson, D. H.; Goddard, W. A.; Goodman, D. W.; Keller, J.; Kubas, G. J.; Kung, H. H.; Lyons, J. E.; Manzer, L. E.; Marks, T. J.; Morokuma, K.; Nicholas, K. M.; Periana, R.; Que, L.; Rostrup-Nielson, J.; Sachtler, W. M. H.; Schmidt, L. D.; Sen, A.; Somorjai, G. A.; Stair, P. C.; Stults, B. R.; Tumas, W., Catalysis Research of Relevance to Carbon Management: Progress, Challenges, and Opportunities. *Chem. Rev.* **2001**, *101* (4), 953-996.
2. Punniyamurthy, T.; Velusamy, S.; Iqbal, J., Recent Advances in Transition Metal Catalyzed Oxidation of Organic Substrates with Molecular Oxygen. *Chem. Rev.* **2005**, *105* (6), 2329-2363.
3. White, M. C.; Zhao, J., Aliphatic C–H Oxidations for Late-Stage Functionalization. *J. Am. Chem. Soc.* **2018**, *140* (43), 13988-14009.
4. Hong, B.; Luo, T.; Lei, X., Late-Stage Diversification of Natural Products. *ACS Cent. Sci.* **2020**, *6* (5), 622-635.
5. Feng, K.; Quevedo, R. E.; Kohrt, J. T.; Oderinde, M. S.; Reilly, U.; White, M. C., Late-stage oxidative C(sp³)–H methylation. *Nature* **2020**, *580* (7805), 621-627.

6. Genovino, J.; Sames, D.; Hamann, L. G.; Touré, B. B., Accessing Drug Metabolites via Transition-Metal Catalyzed C–H Oxidation: The Liver as Synthetic Inspiration. *Angew. Chem. Int. Ed.* **2016**, *55* (46), 14218-14238.
7. Börgel, J.; Tanwar, L.; Berger, F.; Ritter, T., Late-stage aromatic C–H oxygenation. *J. Am. Chem. Soc.* **2018**, *140* (47), 16026-16031.
8. Haggin, J., Chemists seek greater recognition for catalysis. *Chem. Eng. News*, **1993**, *71* (22).
9. Cornils, B.; Herrmann, W. A., Concepts in homogeneous catalysis: the industrial view. *J. Catal.* **2003**, *216* (1-2), 23-31.
10. Weber, M.; Weber, M.; Kleine-Boymann, M., In *Ullmann's Encyclopedia of Industrial Chemistry*, Wiley-VCH: Weinheim, Germany, 2004; pp 503-519.
11. Fukuzumi, S.; Ohkubo, K., One-Step Selective Hydroxylation of Benzene to Phenol. *Asian J. Org. Chem.* **2015**, *4* (9), 836-845.
12. Sheldon, R. A.; Kochi, J. K., In *Metal-Catalyzed Oxidations of Organic Compounds*, Academic Press, New York, 1981; pp 315-339.
13. Luo, Y.-R., *Comprehensive Handbook of Chemical Bond Energies*. CRC Press: Boca Raton, FL, 2007.
14. Lewis, J. C.; Coelho, P. S.; Arnold, F. H., Enzymatic functionalization of carbon–hydrogen bonds. *Chem. Soc. Rev.* **2011**, *40* (4), 2003-2021.
15. Song, R.; Sorokin, A.; Bernadou, J.; Meunier, B., Metalloporphyrin-catalyzed oxidation of 2-methylnaphthalene to vitamin K3 and 6-methyl-1,4-naphthoquinone by potassium monopersulfate in aqueous solution. *J. Org. Chem.* **1997**, *62* (3), 673-678.
16. Sorokin, A.; Meunier, B., Oxidation of polycyclic aromatic hydrocarbons catalyzed by iron tetrasulfophthalocyanine FePcS: inverse isotope effects and oxygen labeling studies. *Eur. J. Inorg. Chem.* **1998**, *1998* (9), 1269-1281.
17. Higuchi, T.; Satake, C.; Hirobe, M., Selective quinone formation by oxidation of aromatics with heteroaromatic N-oxides catalyzed by ruthenium porphyrins. *J. Am. Chem. Soc.* **1995**, *117* (34), 8879-8880.
18. Khavasi, H. R.; Davarani, S. S. H.; Safari, N., Remarkable solvent effect on the yield and specificity of oxidation of naphthalene catalyzed by iron(III) porphyrins. *J. Mol. Catal. A: Chem.* **2002**, *188* (1-2), 115-122.
19. Klein Gebbink, R. J. M.; Moret, M.-E., *Non-Noble Metal Catalysis: Molecular Approaches and Reactions*. John Wiley & Sons: 2019.
20. Wallar, B. J.; Lipscomb, J. D., Dioxygen activation by enzymes containing binuclear non-heme iron clusters. *Chem. Rev.* **1996**, *96* (7), 2625-2658.
21. Que Jr, L.; Ho, R. Y., Dioxygen activation by enzymes with mononuclear non-heme iron active sites. *Chem. Rev.* **1996**, *96* (7), 2607-2624.
22. Holm, R. H.; Kennepohl, P.; Solomon, E. I., Structural and functional aspects of metal sites in biology. *Chem. Rev.* **1996**, *96* (7), 2239-2314.
23. Costas, M.; Mehn, M. P.; Jensen, M. P.; Que, L., Dioxygen activation at mononuclear nonheme iron active sites: enzymes, models, and intermediates. *Chem. Rev.* **2004**, *104* (2), 939-986.

24. Bruijninx, P. C.; van Koten, G.; Klein Gebbink, R. J. M., Mononuclear non-heme iron enzymes with the 2-His-1-carboxylate facial triad: recent developments in enzymology and modeling studies. *Chem. Soc. Rev.* **2008**, *37* (12), 2716-2744.
25. Que, L.; Tolman, W. B., Biologically inspired oxidation catalysis. *Nature* **2008**, *455* (7211), 333-340.
26. Guo, M.; Corona, T.; Ray, K.; Nam, W., Heme and nonheme high-valent iron and manganese oxo cores in biological and abiological oxidation reactions. *ACS Cent. Sci.* **2019**, *5* (1), 13-28.
27. Solomon, E. I.; Chen, P.; Metz, M.; Lee, S. K.; Palmer, A. E., Oxygen binding, activation, and reduction to water by copper proteins. *Angew. Chem. Int. Ed.* **2001**, *40* (24), 4570-4590.
28. Pecoraro, V. L.; Baldwin, M. J.; Gelasco, A., Interaction of manganese with dioxygen and its reduced derivatives. *Chem. Rev.* **1994**, *94* (3), 807-826.
29. Law, N. A.; Caudle, M. T.; Pecoraro, V. L., Manganese redox enzymes and model systems: properties, structures, and reactivity. In *Adv. Inorg. Chem.*, Elsevier: 1998; Vol. 46, pp 305-440.
30. Youn, H.-D.; Kim, E.-J.; Roe, J.-H.; HAH, Y. C.; KANG, S.-O., A novel nickel-containing superoxide dismutase from *Streptomyces* spp. *Biochem. J.* **1996**, *318* (3), 889-896.
31. Barondeau, D. P.; Kassmann, C. J.; Bruns, C. K.; Tainer, J. A.; Getzoff, E. D., Nickel superoxide dismutase structure and mechanism. *Biochemistry* **2004**, *43* (25), 8038-8047.
32. Ragsdale, S. W., Nickel-based enzyme systems. *J. Biol. Chem.* **2009**, *284* (28), 18571-18575.
33. Kirby, A. J.; Hollfelder, F., *From enzyme models to model enzymes*. Royal Society of Chemistry: 2009.
34. Solomon, E. I.; Brunold, T. C.; Davis, M. I.; Kemsley, J. N.; Lee, S.-K.; Lehnert, N.; Neese, F.; Skulan, A. J.; Yang, Y.-S.; Zhou, J., Geometric and electronic structure/function correlations in non-heme iron enzymes. *Chem. Rev.* **2000**, *100* (1), 235-350.
35. Neidig, M. L.; Solomon, E. I., Structure–function correlations in oxygen activating non-heme iron enzymes. *Chem. Commun.* **2005**, (47), 5843-5863.
36. Matsumoto, K.; Tachikawa, S.; Hashimoto, N.; Nakano, R.; Yoshida, M.; Shindo, M., Aerobic C–H Oxidation of Arenes Using a Recyclable, Heterogeneous Rhodium Catalyst. *J. Org. Chem.* **2017**, *82* (8), 4305-4316.
37. Santoro, S.; Kozhushkov, S. I.; Ackermann, L.; Vaccaro, L., Heterogeneous catalytic approaches in C–H activation reactions. *Green Chem.* **2016**, *18* (12), 3471-3493.
38. Reay, A. J.; Fairlamb, I. J., Catalytic C–H bond functionalisation chemistry: the case for quasi-heterogeneous catalysis. *Chem. Commun.* **2015**, *51* (91), 16289-16307.
39. Rahmani, N.; Amiri, A.; Ziarani, G. M.; Badiei, A., Review of some transition metal-based mesoporous catalysts for the direct hydroxylation of benzene to phenol (DHBP). *Mol. Catal.* **2021**, *515*, 111873.
40. Vicens, L.; Olivo, G.; Costas, M., Rational Design of Bioinspired Catalysts for Selective Oxidations. *ACS Catal.* **2020**, *10* (15), 8611-8631.
41. Bailey, C. L.; Drago, R. S., Utilization of O₂ for the specific oxidation of organic substrates with cobalt(II) catalysts. *Coord. Chem. Rev.* **1987**, *79* (3), 321-332.

42. Carneiro, L.; Silva, A. R., Selective direct hydroxylation of benzene to phenol with hydrogen peroxide by iron and vanadyl based homogeneous and heterogeneous catalysts. *Catal. Sci. Technol.* **2016**, *6* (22), 8166-8176.
43. Han, J. W.; Jung, J.; Lee, Y.-M.; Nam, W.; Fukuzumi, S., Photocatalytic oxidation of benzene to phenol using dioxygen as an oxygen source and water as an electron source in the presence of a cobalt catalyst. *Chem. Sci.* **2017**, *8* (10), 7119-7125.
44. Anandababu, K.; Muthuramalingam, S.; Velusamy, M.; Mayilmurugan, R., Single-step benzene hydroxylation by cobalt(II) catalysts via a cobalt(III)-hydroperoxo intermediate. *Catal. Sci. Technol.* **2020**, *10* (8), 2540-2548.
45. Lemke, K.; Ehrich, H.; Lohse, U.; Berndt, H.; Jähnisch, K., Selective hydroxylation of benzene to phenol over supported vanadium oxide catalysts. *Appl. Catal. A: Gen.* **2003**, *243* (1), 41-51.
46. Zhang, J.; Tang, Y.; Li, G.; Hu, C., Room temperature direct oxidation of benzene to phenol using hydrogen peroxide in the presence of vanadium-substituted heteropolymolybdates. *Appl. Catal. A: Gen.* **2005**, *278* (2), 251-261.
47. Fenton, H., LXXIII.—Oxidation of tartaric acid in presence of iron. *J. Chem. Soc., Trans.* **1894**, *65*, 899-910.
48. Haber, F.; Weiss, J., Ueber die Katalyse des Hydroperoxydes. *Naturwissenschaften* **1932**, *20* (51), 948-950.
49. Haber, F.; Weiss, J., The catalytic decomposition of hydrogen peroxide by iron salts. *Proc. R. Soc. London A Math. Phys. Sci.* **1934**, *147* (861), 332-351.
50. Walling, C., Intermediates in the reactions of Fenton type reagents. *Acc. Chem. Res.* **1998**, *31* (4), 155-157.
51. MacFaul, P. A.; Wayner, D.; Ingold, K., A radical account of “oxygenated Fenton chemistry”. *Acc. Chem. Res.* **1998**, *31* (4), 159-162.
52. Goldstein, S.; Meyerstein, D., Comments on the mechanism of the “Fenton-like” reaction. *Acc. Chem. Res.* **1999**, *32* (7), 547-550.
53. Merz, J.; Waters, W., 511. The oxidation of aromatic compounds by means of the free hydroxyl radical. *J. Chem. Soc.* **1949**, 2427-2433.
54. Smith, J. L.; Norman, R., 539. Hydroxylation. Part I. The oxidation of benzene and toluene by Fenton's reagent. *J. Chem. Soc.* **1963**, 2897-2905.
55. Walling, C.; Johnson, R. A., Fenton's reagent. V. Hydroxylation and side-chain cleavage of aromatics. *J. Am. Chem. Soc.* **1975**, *97* (2), 363-367.
56. Kurata, T.; Watanabe, Y.; Katoh, M.; Sawaki, Y., Mechanism of aromatic hydroxylation in the Fenton and related reactions. One-electron oxidation and the NIH shift. *J. Am. Chem. Soc.* **1988**, *110* (22), 7472-7478.
57. Cussó, O.; Garcia-Bosch, I.; Ribas, X.; Lloret-Fillol, J.; Costas, M., Asymmetric epoxidation with H₂O₂ by manipulating the electronic properties of non-heme iron catalysts. *J. Am. Chem. Soc.* **2013**, *135* (39), 14871-14878.
58. MacFaul, P. A.; Ingold, K.; Wayner, D.; Que, L., A Putative Monooxygenase Mimic Which Functions via Well-Disguised Free Radical Chemistry1. *J. Am. Chem. Soc.* **1997**, *119* (44), 10594-10598.

59. Ingold, K. U.; MacFaul, P. A., *Biomimetic oxidations catalyzed by transition metal complexes*. Meunier, B., Ed.; Imperial College Press: London, 2000; p 45.
60. Hiatt, R.; Clipsham, J.; Visser, T., The induced decomposition of tert-butyl hydroperoxide. *Can. J. Chem.* **1964**, *42* (12), 2754-2757.
61. Masferrer-Rius, E.; Borrell, M.; Lutz, M.; Costas, M.; Klein Gebbink, R. J. M., Aromatic C–H Hydroxylation Reactions with Hydrogen Peroxide Catalyzed by Bulky Manganese Complexes. *Adv. Synth. Catal.* **2021**.
62. Udenfriend, S.; Clark, C. T.; Axelrod, J.; Brodie, B. B., Ascorbic acid in aromatic hydroxylation. *J. Biol. Chem.* **1954**, *208*, 731-738.
63. Brodie, B. B.; Axelrod, J.; Shore, P. A.; Udenfriend, S., Ascorbic acid in aromatic hydroxylation II. Products formed by reaction of substrates with ascorbic acid, ferrous ion, and oxygen. *J. Biol. Chem.* **1954**, *208* (2), 741-750.
64. Slavik, R.; Peters, J.-U.; Giger, R.; Bürkler, M.; Bald, E., Synthesis of potential drug metabolites by a modified Udenfriend reaction. *Tetrahedron Lett.* **2011**, *52* (7), 749-752.
65. Mathieu, D.; Bartoli, J. F.; Battioni, P.; Mansuy, D., Monooxygenation of aromatic compounds by dioxygen with bioinspired systems using non-heme iron catalysts and tetrahydropterins: comparison with other reducing agents and interesting regioselectivity favouring meta-hydroxylation. *Tetrahedron* **2004**, *60* (17), 3855-3862.
66. Metelitsa, D. I., Mechanisms of the hydroxylation of aromatic compounds. *Russ. Chem. Rev.* **1971**, *40* (7), 563.
67. Kunai, A.; Hata, S.; Ito, S.; Sasaki, K., The role of oxygen in the hydroxylation reaction of benzene with Fenton's reagent. Oxygen 18 tracer study. *J. Am. Chem. Soc.* **1986**, *108* (19), 6012-6016.
68. Sono, M.; Roach, M. P.; Coulter, E. D.; Dawson, J. H., Heme-containing oxygenases. *Chem. Rev.* **1996**, *96* (7), 2841-2888.
69. Meunier, B.; De Visser, S. P.; Shaik, S., Mechanism of oxidation reactions catalyzed by cytochrome P450 enzymes. *Chem. Rev.* **2004**, *104* (9), 3947-3980.
70. Poulos, T. L., Heme enzyme structure and function. *Chem. Rev.* **2014**, *114* (7), 3919-3962.
71. De Montellano, P. R. O., *Cytochrome P450: Structure, Mechanism, and Biochemistry*. 3rd ed.; Kluwer Academic/Plenum Publishers: New York, 2005.
72. Meunier, B., *Biomimetic Oxidations Catalyzed by Transition Metal Complexes*. Imperial College Press: London: 2000; pp 171-214.
73. Tshuva, E. Y.; Lippard, S. J., Synthetic models for non-heme carboxylate-bridged diiron metalloproteins: strategies and tactics. *Chem. Rev.* **2004**, *104* (2), 987-1012.
74. Hegg, E. L.; Jr, L. Q., The 2-His-1-carboxylate facial triad—an emerging structural motif in mononuclear non-heme iron(II) enzymes. *Eur. J. Biochem.* **1997**, *250* (3), 625-629.
75. Que, L., One motif—many different reactions. *Nat. Struct. Biol.* **2000**, *7* (3), 182-184.
76. Abu-Omar, M. M.; Loaiza, A.; Hontzeas, N., Reaction mechanisms of mononuclear non-heme iron oxygenases. *Chem. Rev.* **2005**, *105* (6), 2227-2252.

77. Koehntop, K. D.; Emerson, J. P.; Que, L., The 2-His-1-carboxylate facial triad: a versatile platform for dioxygen activation by mononuclear non-heme iron(II) enzymes. *J. Biol. Inorg. Chem.* **2005**, *10* (2), 87-93.
78. Kryatov, S. V.; Rybak-Akimova, E. V.; Schindler, S., Kinetics and mechanisms of formation and reactivity of non-heme iron oxygen intermediates. *Chem. Rev.* **2005**, *105* (6), 2175-2226.
79. Kovaleva, E. G.; Lipscomb, J. D., Versatility of biological non-heme Fe(II) centers in oxygen activation reactions. *Nat. Chem. Biol.* **2008**, *4* (3), 186.
80. Gibson, D.; Resnick, S.; Lee, K.; Brand, J.; Torok, D.; Wackett, L.; Schocken, M.; Haigler, B., Desaturation, dioxygenation, and monooxygenation reactions catalyzed by naphthalene dioxygenase from *Pseudomonas* sp. strain 9816-4. *J. Bacteriol.* **1995**, *177* (10), 2615-2621.
81. Wolfe, M. D.; Parales, J. V.; Gibson, D. T.; Lipscomb, J. D., Single Turnover Chemistry and Regulation of O₂ Activation by the Oxygenase Component of Naphthalene 1,2-Dioxygenase. *J. Biol. Chem.* **2001**, *276* (3), 1945-1953.
82. Cussó, O.; Ribas, X.; Costas, M., Biologically inspired non-heme iron-catalysts for asymmetric epoxidation; design principles and perspectives. *Chem. Commun.* **2015**, *51* (76), 14285-14298.
83. Denisov, I. G.; Makris, T. M.; Sligar, S. G.; Schlichting, I., Structure and chemistry of cytochrome P450. *Chem. Rev.* **2005**, *105* (6), 2253-2278.
84. Ortiz de Montellano, P. R., Hydrocarbon hydroxylation by cytochrome P450 enzymes. *Chem. Rev.* **2010**, *110* (2), 932-948.
85. Meunier, B.; Bernadou, J., Active iron-oxo and iron-peroxo species in cytochromes P450 and peroxidases; oxo-hydroxo tautomerism with water-soluble metalloporphyrins. In *Metal-Oxo and Metal-Peroxo Species in Catalytic Oxidations*, Springer: 2000; pp 1-35.
86. De Montellano, P. R. O., Cytochrome P450: Structure, Mechanism, and Biochemistry. 3rd ed.; Springler ed.: New York: 2005; pp 1-42.
87. Kille, S.; Zilly, F. E.; Acevedo, J. P.; Reetz, M. T., Regio- and stereoselectivity of P450-catalysed hydroxylation of steroids controlled by laboratory evolution. *Nat. Chem.* **2011**, *3* (9), 738.
88. Narayan, A. R.; Jiménez-Osés, G.; Liu, P.; Negretti, S.; Zhao, W.; Gilbert, M. M.; Ramabhadran, R. O.; Yang, Y.-F.; Furan, L. R.; Li, Z.; Podust, L. M.; Montgomery, J.; Houk, K. N.; Sherman, D. H., Enzymatic hydroxylation of an unactivated methylene C-H bond guided by molecular dynamics simulations. *Nat. Chem.* **2015**, *7* (8), 653.
89. Roiban, G. D.; Agudo, R.; Reetz, M. T., Cytochrome P450 Catalyzed Oxidative Hydroxylation of Achiral Organic Compounds with Simultaneous Creation of Two Chirality Centers in a Single C-H Activation Step. *Angew. Chem. Int. Ed.* **2014**, *53* (33), 8659-8663.
90. Zhang, K.; Shafer, B. M.; Demars, M. D.; Stern, H. A.; Fasan, R., Controlled oxidation of remote sp³ C-H bonds in artemisinin via P450 catalysts with fine-tuned regio- and stereoselectivity. *J. Am. Chem. Soc.* **2012**, *134* (45), 18695-18704.
91. Poulos, T. L.; Finzel, B.; Gunsalus, I.; Wagner, G. C.; Kraut, J., The 2.6-Å crystal structure of *Pseudomonas putida* cytochrome P-450. *J. Biol. Chem.* **1985**, *260* (30), 16122-16130.
92. Li, H.; Narasimhulu, S.; Havran, L. M.; Winkler, J. D.; Poulos, T. L., Crystal structure of cytochrome P450cam complexed with its catalytic product, 5-exo-hydroxycamphor. *J. Am. Chem. Soc.* **1995**, *117* (23), 6297-6299.

93. Schlichting, I.; Berendzen, J.; Chu, K.; Stock, A. M.; Maves, S. A.; Benson, D. E.; Sweet, R. M.; Ringe, D.; Petsko, G. A.; Sligar, S. G., The catalytic pathway of cytochrome P450cam at atomic resolution. *Science* **2000**, *287* (5458), 1615-1622.
94. Yano, J. K.; Wester, M. R.; Schoch, G. A.; Griffin, K. J.; Stout, C. D.; Johnson, E. F., The structure of human microsomal cytochrome P450 3A4 determined by X-ray crystallography to 2.05-Å resolution. *J. Biol. Chem.* **2004**, *279* (37), 38091-38094.
95. Kells, P. M.; Ouellet, H.; Santos-Aberturas, J.; Aparicio, J. F.; Podust, L. M., Structure of cytochrome P450 PimD suggests epoxidation of the polyene macrolide pimaricin occurs via a hydroperoxoferric intermediate. *Chem. Biol.* **2010**, *17* (8), 841-851.
96. Shah, M. B.; Jang, H.-H.; Zhang, Q.; Stout, C. D.; Halpert, J. R., X-ray crystal structure of the cytochrome P450 2B4 active site mutant F297A in complex with clopidogrel: insights into compensatory rearrangements of the binding pocket. *Arch. Biochem. Biophys.* **2013**, *530* (2), 64-72.
97. Dawson, J. H.; Sono, M., Cytochrome P-450 and chloroperoxidase: thiolate-ligated heme enzymes. Spectroscopic determination of their active-site structures and mechanistic implications of thiolate ligation. *Chem. Rev.* **1987**, *87* (5), 1255-1276.
98. Mueller, E. J.; Loida, P. J.; Sligar, S. G., Twenty-five Years of P450 cam Research. In *Cytochrome P450*, Springer: 1995; pp 83-124.
99. King, N. K.; Winfield, M., Oxygen uptake and evolution by iron porphyrin enzymes. *Aust. J. Chem.* **1959**, *12* (1), 47-64.
100. Dunford, H.; Stillman, J., Structure and functional properties of peroxidases and catalases. *Coord. Chem. Rev.* **1976**, *19*, 187-251.
101. Meunier, B.; Bernadou, J., Metal-oxo species in P450 enzymes and biomimetic models. Oxo-hydroxo tautomerism with water-soluble metalloporphyrins. *Top. Catal.* **2002**, *21* (1-3), 47-54.
102. Rittle, J.; Green, M. T., Cytochrome P450 compound I: capture, characterization, and C-H bond activation kinetics. *Science* **2010**, *330* (6006), 933-937.
103. Groves, J. T.; McClusky, G. A., Aliphatic hydroxylation via oxygen rebound. Oxygen transfer catalyzed by iron. *J. Am. Chem. Soc.* **1976**, *98* (3), 859-861.
104. Groves, J. T.; McClusky, G. A.; White, R. E.; Coon, M. J., Aliphatic hydroxylation by highly purified liver microsomal cytochrome P-450. Evidence for a carbon radical intermediate. *Biochem. Biophys. Res. Commun.* **1978**, *81*, 154.
105. Daly, J.; Jerina, D.; Witkop, B., Arene oxides and the NIH shift: the metabolism, toxicity and carcinogenicity of aromatic compounds. *Experientia* **1972**, *28* (10), 1129-1149.
106. Guroff, G.; Daly, J. W.; Jerina, D. M.; Renson, J.; Witkop, B.; Udenfriend, S., Hydroxylation-induced migration: the NIH shift. *Science* **1967**, *157* (3796), 1524-1530.
107. Ullrich, R.; Hofrichter, M., Enzymatic hydroxylation of aromatic compounds. *Cell. Mol. Life Sci.* **2007**, *64* (3), 271-293.
108. de Montellano, P. R. O.; de Voss, J. J., Substrate oxidation by cytochrome P450 enzymes. In *Cytochrome P450 - Structure, Mechanism and Biochemistry*, 3rd ed. Kluwer Academic/Plenum Publishers, New York: 2005; pp 183-245.

109. Groves, J. T., High-valent iron in chemical and biological oxidations. *J. Inorg. Biochem.* **2006**, *100* (4), 434-447.
110. Barry, S. M.; Challis, G. L., Mechanism and catalytic diversity of Rieske non-heme iron-dependent oxygenases. *ACS Catal.* **2013**, *3* (10), 2362-2370.
111. Karlsson, A.; Parales, J. V.; Parales, R. E.; Gibson, D. T.; Eklund, H.; Ramaswamy, S., Crystal structure of naphthalene dioxygenase: side-on binding of dioxygen to iron. *Science* **2003**, *299* (5609), 1039-1042.
112. Kauppi, B.; Lee, K.; Carredano, E.; Parales, R. E.; Gibson, D. T.; Eklund, H.; Ramaswamy, S., Structure of an aromatic-ring-hydroxylating dioxygenase–naphthalene 1,2-dioxygenase. *Structure* **1998**, *6* (5), 571-586.
113. Parales, R. E.; Parales, J. V.; Gibson, D. T., Aspartate 205 in the catalytic domain of naphthalene dioxygenase is essential for activity. *J. Bacteriol.* **1999**, *181* (6), 1831-1837.
114. Perry, C.; De Los Santos, E. L.; Alkhalaf, L. M.; Challis, G. L., Rieske non-heme iron-dependent oxygenases catalyse diverse reactions in natural product biosynthesis. *Nat. Prod. Rep.* **2018**, *35* (7), 622-632.
115. Martins, B. M.; Svetlitchnaia, T.; Dobbek, H., 2-Oxoquinoline 8-monooxygenase oxygenase component: active site modulation by Rieske-[2Fe-2S] center oxidation/reduction. *Structure* **2005**, *13* (5), 817-824.
116. Hsueh, K.-L.; Westler, W. M.; Markley, J. L., NMR investigations of the Rieske protein from *Thermus thermophilus* support a coupled proton and electron transfer mechanism. *J. Am. Chem. Soc.* **2010**, *132* (23), 7908-7918.
117. Wolfe, M. D.; Altier, D. J.; Stubna, A.; Popescu, C. V.; Münck, E.; Lipscomb, J. D., Benzoate 1,2-dioxygenase from *Pseudomonas putida*: single turnover kinetics and regulation of a two-component Rieske dioxygenase. *Biochemistry* **2002**, *41* (30), 9611-9626.
118. Bugg, T. D.; Ramaswamy, S., Non-heme iron-dependent dioxygenases: unravelling catalytic mechanisms for complex enzymatic oxidations. *Curr. Op. Chem. Biol.* **2008**, *12* (2), 134-140.
119. Wolfe, M. D.; Lipscomb, J. D., Hydrogen peroxide-coupled *cis*-diol formation catalyzed by naphthalene 1,2-dioxygenase. *J. Biol. Chem.* **2003**, *278* (2), 829-835.
120. Lippard, S. J., Hydroxylation of C–H bonds at carboxylate-bridged diiron centres. *Philos. Trans. R. Soc. London, Ser. A*, **2005**, *363* (1829), 861-877.
121. Rosenzweig, A. C.; Frederick, C. A.; Lippard, S. J., Crystal structure of a bacterial non-haem iron hydroxylase that catalyses the biological oxidation of methane. *Nature* **1993**, *366* (6455), 537-543.
122. Que Jr, L.; True, A. E., Dinuclear iron-and manganese-oxo sites in biology. *Prog. Inorg. Chem.* **1990**, 97-200.
123. Merckx, M.; Kopp, D. A.; Sazinsky, M. H.; Blazyk, J. L.; Müller, J.; Lippard, S. J., Dioxygen activation and methane hydroxylation by soluble methane monooxygenase: a tale of two irons and three proteins. *Angew. Chem. Int. Ed.* **2001**, *40* (15), 2782-2807.
124. Notomista, E.; Lahm, A.; Di Donato, A.; Tramontano, A., Evolution of bacterial and archaeal multicomponent monooxygenases. *J. Mol. Evol.* **2003**, *56* (4), 435-445.
125. Leahy, J. G.; Batchelor, P. J.; Morcomb, S. M., Evolution of the soluble diiron monooxygenases. *FEMS Microbiol. Rev.* **2003**, *27* (4), 449-479.

126. Green, J.; Dalton, H., Substrate specificity of soluble methane monooxygenase. Mechanistic implications. *J. Biol. Chem.* **1989**, *264* (30), 17698-17703.
127. Siewert, I.; Limberg, C., Low-Molecular-Weight Analogues of the Soluble Methane Monooxygenase (sMMO): From the Structural Mimicking of Resting States and Intermediates to Functional Models. *Chem. Eur. J.* **2009**, *15* (40), 10316-10328.
128. Sazinsky, M. H.; Bard, J.; Di Donato, A.; Lippard, S. J., Crystal Structure of the Toluene/o-Xylene Monooxygenase Hydroxylase from *Pseudomonas stutzeri* OX1. *J. Biol. Chem.* **2004**, *279* (29), 30600-30610.
129. Sazinsky, M. H.; Dunten, P. W.; McCormick, M. S.; DiDonato, A.; Lippard, S. J., X-ray Structure of a Hydroxylase Regulatory Protein Complex from a Hydrocarbon-Oxidizing Multicomponent Monooxygenase, *Pseudomonas* sp. OX1 Phenol Hydroxylase. *Biochemistry* **2006**, *45* (51), 15392-15404.
130. Chauhan, S.; Barbieri, P.; Wood, T. K., Oxidation of trichloroethylene, 1,1-dichloroethylene, and chloroform by toluene/o-xylene monooxygenase from *Pseudomonas stutzeri* OX1. *Appl. Environ. Microbiol.* **1998**, *64* (8), 3023-3024.
131. Mitchell, K. H.; Rogge, C. E.; Gierahn, T.; Fox, B. G., Insight into the mechanism of aromatic hydroxylation by toluene 4-monooxygenase by use of specifically deuterated toluene and p-xylene. *Proc. Natl. Acad. Sci.* **2003**, *100* (7), 3784-3789.
132. Colby, J.; Stirling, D. I.; Dalton, H., The soluble methane mono-oxygenase of *Methylococcus capsulatus* (Bath). Its ability to oxygenate n-alkanes, n-alkenes, ethers, and alicyclic, aromatic and heterocyclic compounds. *Biochem. J.* **1977**, *165* (2), 395-402.
133. Friedle, S.; Reisner, E.; Lippard, S. J., Current challenges of modeling diiron enzyme active sites for dioxygen activation by biomimetic synthetic complexes. *Chem. Soc. Rev.* **2010**, *39* (8), 2768-2779.
134. Kovaleva, E.; Neibergall, M.; Chakrabarty, S.; Lipscomb, J. D., Finding intermediates in the O₂ activation pathways of non-heme iron oxygenases. *Acc. Chem. Res.* **2007**, *40* (7), 475-483.
135. Tinberg, C. E.; Lippard, S. J., Revisiting the mechanism of dioxygen activation in soluble methane monooxygenase from *M. capsulatus* (Bath): evidence for a multi-step, proton-dependent reaction pathway. *Biochemistry* **2009**, *48* (51), 12145-12158.
136. Valentine, A. M.; Stahl, S. S.; Lippard, S. J., Mechanistic studies of the reaction of reduced methane monooxygenase hydroxylase with dioxygen and substrates. *J. Am. Chem. Soc.* **1999**, *121* (16), 3876-3887.
137. Beauvais, L. G.; Lippard, S. J., Reactions of the peroxo intermediate of soluble methane monooxygenase hydroxylase with ethers. *J. Am. Chem. Soc.* **2005**, *127* (20), 7370-7378.
138. Song, W. J.; Lippard, S. J., Mechanistic studies of reactions of peroxodiiron(III) intermediates in T201 variants of toluene/o-xylene monooxygenase hydroxylase. *Biochemistry* **2011**, *50* (23), 5391-5399.
139. Murray, L. J.; Naik, S. G.; Ortillo, D. O.; García-Serres, R.; Lee, J. K.; Huynh, B. H.; Lippard, S. J., Characterization of the arene-oxidizing intermediate in ToMOH as a diiron(III) species. *J. Am. Chem. Soc.* **2007**, *129* (46), 14500-14510.
140. Kappock, T. J.; Caradonna, J. P., Pterin-dependent amino acid hydroxylases. *Chem. Rev.* **1996**, *96* (7), 2659-2756.
141. Flatmark, T.; Stevens, R. C., Structural insight into the aromatic amino acid hydroxylases and their disease-related mutant forms. *Chem. Rev.* **1999**, *99* (8), 2137-2160.

142. Fitzpatrick, P. F., Tetrahydropterin-dependent amino acid hydroxylases. *Annu. Rev. Biochem.* **1999**, *68* (1), 355-381.
143. Klinman, J. P., Life as aerobes: are there simple rules for activation of dioxygen by enzymes? *J. Biol. Inorg. Chem.* **2001**, *6* (1), 1-13.
144. Nagatsu, T.; Levitt, M.; Udenfriend, S., Tyrosine hydroxylase the initial step in norepinephrine biosynthesis. *J. Biol. Chem.* **1964**, *239* (9), 2910-2917.
145. Davis, M. D.; Kaufman, S., Evidence for the formation of the 4a-carbinolamine during the tyrosine-dependent oxidation of tetrahydrobiopterin by rat liver phenylalanine hydroxylase. *J. Biol. Chem.* **1989**, *264* (15), 8585-8596.
146. Francisco, W. A.; Tian, G.; Fitzpatrick, P. F.; Klinman, J. P., Oxygen-18 kinetic isotope effect studies of the tyrosine hydroxylase reaction: Evidence of rate limiting oxygen activation. *J. Am. Chem. Soc.* **1998**, *120* (17), 4057-4062.
147. Bassan, A.; Blomberg, M. R.; Siegbahn, P. E., Mechanism of Dioxygen Cleavage in Tetrahydrobiopterin-Dependent Amino Acid Hydroxylases. *Chem. Eur. J.* **2003**, *9* (1), 106-115.
148. Kemsley, J. N.; Wasinger, E. C.; Datta, S.; Mitić, N.; Acharya, T.; Hedman, B.; Caradonna, J. P.; Hodgson, K. O.; Solomon, E. I., Spectroscopic and Kinetic Studies of PKU Inducing Mutants of Phenylalanine Hydroxylase: Arg158Gln and Glu280Lys. *J. Am. Chem. Soc.* **2003**, *125* (19), 5677-5686.
149. Dix, T. A.; Bollag, G. E.; Domanico, P.; Benkovic, S. J., Phenylalanine hydroxylase: absolute configuration and source of oxygen of the 4a-hydroxytetrahydropterin species. *Biochemistry* **1985**, *24* (12), 2955-2958.
150. Daly, J.; Levitt, M.; Guroff, G.; Udenfriend, S., Isotope studies on the mechanism of action of adrenal tyrosine hydroxylase. *Arch. Biochem. Biophys.* **1968**, *126* (2), 593-598.
151. Siegmund, H.-U.; Kaufman, S., Hydroxylation of 4-methylphenylalanine by rat liver phenylalanine hydroxylase. *J. Biol. Chem.* **1991**, *266* (5), 2903-2910.
152. Olsson, E.; Martinez, A.; Teigen, K.; Jensen, V. R., Formation of the Iron–Oxo Hydroxylating Species in the Catalytic Cycle of Aromatic Amino Acid Hydroxylases. *Chem. Eur. J.* **2011**, *17* (13), 3746-3758.
153. Olsson, E.; Martinez, A.; Teigen, K.; Jensen, V. R., Substrate Hydroxylation by the Oxido–Iron Intermediate in Aromatic Amino Acid Hydroxylases: A DFT Mechanistic Study. *Eur. J. Inorg. Chem.* **2011**, *2011* (17), 2720-2732.
154. Kal, S.; Xu, S.; Que Jr, L., Bio-inspired Nonheme Iron Oxidation Catalysis: Involvement of Oxoiron(V) Oxidants in Cleaving Strong C–H Bonds. *Angew. Chem. Int. Ed.* **2020**, *59* (19), 7332-7349.
155. Bryliakov, K. P.; Talsi, E. P., Active sites and mechanisms of bioinspired oxidation with H₂O₂, catalyzed by non-heme Fe and related Mn complexes. *Coord. Chem. Rev.* **2014**, *276*, 73-96.
156. Oloo, W. N.; Que Jr, L., Bioinspired Nonheme Iron Catalysts for C–H and C=C Bond Oxidation: Insights into the Nature of the Metal-Based Oxidants. *Acc. Chem. Res.* **2015**, *48* (9), 2612-2621.
157. Olivo, G.; Cussó, O.; Costas, M., Biologically inspired C–H and C=C oxidations with hydrogen peroxide catalyzed by iron coordination complexes. *Chem. Asian J.* **2016**, *11* (22), 3148-3158.
158. Olivo, G.; Cussó, O.; Borrell, M.; Costas, M., Oxidation of alkane and alkene moieties with biologically inspired nonheme iron catalysts and hydrogen peroxide: from free radicals to stereoselective transformations. *J. Biol. Inorg. Chem.* **2017**, *22* (2-3), 425-452.

159. Lyakin, O. Y.; Bryliakov, K. P.; Talsi, E. P., Non-heme oxoiron(V) intermediates in chemo-, regio- and stereoselective oxidation of organic substrates. *Coord. Chem. Rev.* **2019**, *384*, 126-139.
160. Kim, C.; Chen, K.; Kim, J.; Que, L., Stereospecific alkane hydroxylation with H₂O₂ catalyzed by an iron(II)–tris(2-pyridylmethyl)amine complex. *J. Am. Chem. Soc.* **1997**, *119* (25), 5964-5965.
161. Chen, K.; Que, L., Stereospecific alkane hydroxylation by non-heme iron catalysts: mechanistic evidence for an Fe^VO active species. *J. Am. Chem. Soc.* **2001**, *123* (26), 6327-6337.
162. Aldrich-Wright, J. R.; Vagg, R. S.; Williams, P. A., Design of chiral picen-based metal complexes for molecular recognition of α -aminoacids and nucleic acids. *Coord. Chem. Rev.* **1997**, *166*, 361-389.
163. Knof, U.; von Zelewsky, A., Predetermined chirality at metal centers. *Angew. Chem. Int. Ed.* **1999**, *38* (3), 302-322.
164. Ng, C.; Sabat, M.; Fraser, C. L., Metal complexes with cis α topology from stereoselective quadridentate ligands with amine, pyridine, and quinoline donor groups. *Inorg. Chem.* **1999**, *38* (24), 5545-5556.
165. Costas, M.; Que, J., Lawrence, Ligand topology tuning of iron-catalyzed hydrocarbon oxidations. *Angew. Chem. Int. Ed.* **2002**, *41* (12), 2179-2181.
166. Lee, D.; Park, H., Ligand Taxonomy for Bioinorganic Modeling of Dioxygen-Activating Non-Heme Iron Enzymes. *Chem. Eur. J.* **2020**, *26* (27), 5916-5926.
167. Gamba, I.; Codolà, Z.; Lloret-Fillol, J.; Costas, M., Making and breaking of the O–O bond at iron complexes. *Coord. Chem. Rev.* **2017**, *334*, 2-24.
168. Dantignana, V.; Company, A.; Costas, M., Oxoiron(V) Complexes of Relevance in Oxidation Catalysis of Organic Substrates. *Isr. J. Chem.* **2020**, *60* (10-11), 1004-1018.
169. Borrell, M.; Costas, M., Mechanistically driven development of an iron catalyst for selective syn-dihydroxylation of alkenes with aqueous hydrogen peroxide. *J. Am. Chem. Soc.* **2017**, *139* (36), 12821-12829.
170. Chen, K.; Costas, M.; Kim, J.; Tipton, A. K.; Que, L., Olefin cis-dihydroxylation versus epoxidation by non-heme iron catalysts: two faces of an Fe^{III}–OOH coin. *J. Am. Chem. Soc.* **2002**, *124* (12), 3026-3035.
171. Borrell, M.; Costas, M., Greening oxidation catalysis: iron catalyzed alkene syn-dihydroxylation with aqueous hydrogen peroxide in green solvents. *ACS Sustainable Chem. Eng.* **2018**, *6* (7), 8410-8416.
172. Prat, I.; Mathieson, J. S.; Güell, M.; Ribas, X.; Luis, J. M.; Cronin, L.; Costas, M., Observation of Fe(V)=O using variable-temperature mass spectrometry and its enzyme-like C–H and C=C oxidation reactions. *Nat. Chem.* **2011**, *3* (10), 788.
173. Hitomi, Y.; Arakawa, K.; Funabiki, T.; Kodera, M., An Iron(III)–Monoamidate Complex Catalyst for Selective Hydroxylation of Alkane C–H Bonds with Hydrogen Peroxide. *Angew. Chem. Int. Ed.* **2012**, *51* (14), 3448-3452.
174. Xu, S.; Veach, J. J.; Oloo, W. N.; Peters, K. C.; Wang, J.; Perry, R. H.; Que, L., Detection of a transient Fe^V(O)(OH) species involved in olefin oxidation by a bio-inspired non-haem iron catalyst. *Chem. Commun.* **2018**, *54* (63), 8701-8704.
175. Borrell, M.; Andris, E.; Navrátil, R.; Roithová, J.; Costas, M., Characterized cis-Fe^V(O)(OH) intermediate mimics enzymatic oxidations in the gas phase. *Nat. Commun.* **2019**, *10* (1), 1-9.

176. White, M. C.; Doyle, A. G.; Jacobsen, E. N., A synthetically useful, self-assembling MMO mimic system for catalytic alkene epoxidation with aqueous H₂O₂. *J. Am. Chem. Soc.* **2001**, *123* (29), 7194-7195.
177. Chen, M. S.; White, M. C., A predictably selective aliphatic C–H oxidation reaction for complex molecule synthesis. *Science* **2007**, *318* (5851), 783-787.
178. Chen, M. S.; White, M. C., Combined effects on selectivity in Fe-catalyzed methylene oxidation. *Science* **2010**, *327* (5965), 566-571.
179. White, M. C., Adding aliphatic C–H bond oxidations to synthesis. *Science* **2012**, *335* (6070), 807-809.
180. Mas-Ballesté, R.; Que, L., Iron-catalyzed olefin epoxidation in the presence of acetic acid: insights into the nature of the metal-based oxidant. *J. Am. Chem. Soc.* **2007**, *129* (51), 15964-15972.
181. Lyakin, O. Y.; Talsi, E. P., Direct C–H Oxidation of Aromatic Substrates in the Presence of Biomimetic Iron Complexes. In *Frontiers of Green Catalytic Selective Oxidations*, Springer: 2019; pp 253-276.
182. Kitajima, N.; Ito, M.; Fukui, H.; Morooka, Y., A reaction mimic of tyrosine hydroxylase: hydroxylation of a phenoxo ferric complex to a catecholato complex with *m*CPBA. *J. Am. Chem. Soc.* **1993**, *115* (20), 9335-9336.
183. Ménage, S.; Galey, J. B.; Hussler, G.; Seité, M.; Fontecave, M., Aromatic Hydroxylation by H₂O₂ and O₂ Catalyzed by a μ -Oxo Diiron(III) Complex. *Angew. Chem. Int. Ed.* **1996**, *35* (20), 2353-2355.
184. Ménage, S.; Galey, J.-B.; Dumats, J.; Hussler, G.; Seité, M.; Luneau, I. G.; Chottard, G.; Fontecave, M., O₂ activation and aromatic hydroxylation performed by diiron complexes. *J. Am. Chem. Soc.* **1998**, *120* (51), 13370-13382.
185. Mekmouche, Y.; Ménage, S.; Toia-Duboc, C.; Fontecave, M.; Galey, J. B.; Lebrun, C.; Pécaut, J., H₂O₂-Dependent Fe-Catalyzed Oxidations: Control of the Active Species. *Angew. Chem. Int. Ed.* **2001**, *40* (5), 949-952.
186. Lange, S. J.; Miyake, H.; Que, L., Evidence for a nonheme Fe(IV)=O species in the intramolecular hydroxylation of a phenyl moiety. *J. Am. Chem. Soc.* **1999**, *121* (26), 6330-6331.
187. Jensen, M. P.; Mehn, M. P.; Que Jr, L., Intramolecular Aromatic Amination through Iron-Mediated Nitrene Transfer. *Angew. Chem. Int. Ed.* **2003**, *42* (36), 4357-4360.
188. Jensen, M. P.; Lange, S. J.; Mehn, M. P.; Que, E. L.; Que, L., Biomimetic Aryl Hydroxylation Derived from Alkyl Hydroperoxide at a Nonheme Iron Center. Evidence for an Fe^{IV}=O Oxidant. *J. Am. Chem. Soc.* **2003**, *125* (8), 2113-2128.
189. Oh, N. Y.; Seo, M. S.; Lim, M. H.; Consugar, M. B.; Park, M. J.; Rohde, J.-U.; Han, J.; Kim, K. M.; Kim, J.; Que Jr, L., Self-hydroxylation of perbenzoic acids at a nonheme iron(II) center. *Chem. Commun.* **2005**, (45), 5644-5646.
190. Taktak, S.; Flook, M.; Foxman, B. M.; Que Jr, L.; Rybak-Akimova, E. V., *ortho*-Hydroxylation of benzoic acids with hydrogen peroxide at a non-heme iron center. *Chem. Commun.* **2005**, (42), 5301-5303.
191. Makhlynets, O. V.; Das, P.; Taktak, S.; Flook, M.; Mas-Ballesté, R.; Rybak-Akimova, E. V.; Que Jr, L., Iron-Promoted *ortho*-and/or *ipso*-Hydroxylation of Benzoic Acids with H₂O₂. *Chem. Eur. J.* **2009**, *15* (47), 13171-13180.
192. Makhlynets, O. V.; Rybak-Akimova, E. V., Aromatic Hydroxylation at a Non-Heme Iron Center: Observed Intermediates and Insights into the Nature of the Active Species. *Chem. Eur. J.* **2010**, *16* (47), 13995-14006.

193. Makhlynets, O. V.; Oloo, W. N.; Moroz, Y. S.; Belaya, I. G.; Palluccio, T. D.; Filatov, A. S.; Müller, P.; Cranswick, M. A.; Que, L.; Rybak-Akimova, E. V., H₂O₂ activation with biomimetic non-haem iron complexes and AcOH: connecting the g = 2.7 EPR signal with a visible chromophore. *Chem. Commun.* **2014**, 50 (6), 645-648.
194. Ansari, A.; Kaushik, A.; Rajaraman, G., Mechanistic Insights on the ortho-Hydroxylation of Aromatic Compounds by Non-heme Iron Complex: A Computational Case Study on the Comparative Oxidative Ability of Ferric-Hydroperoxo and High-Valent Fe^{IV}=O and Fe^V=O Intermediates. *J. Am. Chem. Soc.* **2013**, 135 (11), 4235-4249.
195. Ségaud, N.; Rebilly, J.-N.; Sénéchal-David, K.; Guillot, R.; Billon, L.; Baltaze, J.-P.; Farjon, J.; Reinaud, O.; Banse, F. d. r., Iron Coordination Chemistry with New Ligands Containing Triazole and Pyridine Moieties. Comparison of the Coordination Ability of the N-Donors. *Inorg. Chem.* **2013**, 52 (2), 691-700.
196. Martinho, M.; Banse, F.; Bartoli, J.-F.; Mattioli, T. A.; Battioni, P.; Horner, O.; Bourcier, S.; Girerd, J.-J., New example of a non-heme mononuclear iron(IV) oxo complex. Spectroscopic data and oxidation activity. *Inorg. Chem.* **2005**, 44 (25), 9592-9596.
197. Rebilly, J. N.; Zhang, W.; Herrero, C.; Dridi, H.; Sénéchal-David, K.; Guillot, R.; Banse, F., Hydroxylation of aromatics by H₂O₂ catalyzed by mononuclear non-heme iron complexes: Role of triazole hemilability in substrate-induced bifurcation of the H₂O₂ activation mechanism. *Chem. Eur. J.* **2020**, 26, 659-668.
198. de Visser, S. P.; Oh, K.; Han, A.-R.; Nam, W., Combined Experimental and Theoretical Study on Aromatic Hydroxylation by Mononuclear Nonheme Iron(IV)-Oxo Complexes. *Inorg. Chem.* **2007**, 46 (11), 4632-4641.
199. Bartoli, J.-F.; Lambert, F.; Morgenstern-Badarau, I.; Battioni, P.; Mansuy, D., Unusual efficiency of a non-heme iron complex as catalyst for the hydroxylation of aromatic compounds by hydrogen peroxide: comparison with iron porphyrins. *C. R. Chimie* **2002**, 5 (4), 263-266.
200. Balland, V.; Mathieu, D.; Pons-Y-Moll, N.; Bartoli, J. F.; Banse, F.; Battioni, P.; Girerd, J.-J.; Mansuy, D., Non-heme iron polyazadentate complexes as catalysts for oxidations by H₂O₂: particular efficiency in aromatic hydroxylations and beneficial effects of a reducing agent. *J. Mol. Catal. A: Chem.* **2004**, 215 (1-2), 81-87.
201. Thibon, A.; Bartoli, J.-F.; Guillot, R.; Sainton, J.; Martinho, M.; Mansuy, D.; Banse, F., Non-heme iron polyazadentate complexes as catalysts for aromatic hydroxylation by H₂O₂: Particular efficiency of tetrakis(2-pyridylmethyl)ethylenediamine-iron(II) complexes. *J. Mol. Catal. A* **2008**, 287 (1-2), 115-120.
202. Bianchi, D.; Bortolo, R.; Tassinari, R.; Ricci, M.; Vignola, R., A novel iron-based catalyst for the biphasic oxidation of benzene to phenol with hydrogen peroxide. *Angew. Chem. Int. Ed.* **2000**, 39 (23), 4321-4323.
203. Bianchi, D.; Bertoli, M.; Tassinari, R.; Ricci, M.; Vignola, R., Direct synthesis of phenols by iron-catalyzed biphasic oxidation of aromatic hydrocarbons with hydrogen peroxide. *J. Mol. Catal. A: Chem.* **2003**, 200 (1-2), 111-116.
204. Bianchi, D.; Bertoli, M.; Tassinari, R.; Ricci, M.; Vignola, R., Ligand effect on the iron-catalysed biphasic oxidation of aromatic hydrocarbons by hydrogen peroxide. *J. Mol. Catal. A: Chem.* **2003**, 204, 419-424.
205. Kejriwal, A.; Bandyopadhyay, P.; Biswas, A. N., Aromatic hydroxylation using an oxo-bridged diiron(III) complex: a bio-inspired functional model of toluene monooxygenases. *Dalton Trans.* **2015**, 44 (39), 17261-17267.

206. Raba, A.; Cokoja, M.; Herrmann, W. A.; Kühn, F. E., Catalytic hydroxylation of benzene and toluene by an iron complex bearing a chelating di-pyridyl-di-NHC ligand. *Chem. Commun.* **2014**, 50 (78), 11454-11457.
207. Raba, A.; Cokoja, M.; Ewald, S.; Riener, K.; Herdtweck, E.; Pöthig, A.; Herrmann, W. A.; Kühn, F. E., Synthesis and Characterization of Novel Iron(II) Complexes with Tetradentate Bis(N-heterocyclic carbene)-Bis(pyridine)(NCCN) Ligands. *Organometallics* **2012**, 31 (7), 2793-2800.
208. Rogers, M. M.; Stahl, S. S., N-Heterocyclic carbenes as ligands for high-oxidation-state metal complexes and oxidation catalysis. In *N-Heterocyclic Carbenes in Transition Metal Catalysis*, Springer: 2006; pp 21-46.
209. Strassner, T., The role of NHC ligands in oxidation catalysis. In *Organometallic Oxidation Catalysis*, Springer: 2006; pp 125-148.
210. Lindhorst, A. C.; Schütz, J.; Netscher, T.; Bonrath, W.; Kühn, F. E., Catalytic oxidation of aromatic hydrocarbons by a molecular iron-NHC complex. *Catal. Sci. Technol.* **2017**, 7 (9), 1902-1911.
211. Silva, G. C.; Carvalho, N. M.; Horn Jr, A.; Lachter, E. R.; Antunes, O. A., Oxidation of aromatic compounds by hydrogen peroxide catalyzed by mononuclear iron(III) complexes. *J. Mol. Catal. A: Chem.* **2017**, 426, 564-571.
212. Olivo, G.; Lanzalunga, O.; Di Stefano, S., Non-Heme Imine-Based Iron Complexes as Catalysts for Oxidative Processes. *Adv. Synth. Catal.* **2016**, 358 (6), 843-863.
213. Capocasa, G.; Olivo, G.; Barbieri, A.; Lanzalunga, O.; Di Stefano, S., Direct hydroxylation of benzene and aromatics with H₂O₂ catalyzed by a self-assembled iron complex: evidence for a metal-based mechanism. *Catal. Sci. Technol.* **2017**, 7 (23), 5677-5686.
214. Ticconi, B.; Colcerasa, A.; Di Stefano, S.; Lanzalunga, O.; Lapi, A.; Mazzonna, M.; Olivo, G., Oxidative functionalization of aliphatic and aromatic amino acid derivatives with H₂O₂ catalyzed by a nonheme imine based iron complex. *RSC Adv.* **2018**, 8 (34), 19144-19151.
215. Capocasa, G.; Di Berto Mancini, M.; Fratello, F.; Lanzalunga, O.; Olivo, G.; Di Stefano, S., Easy Synthesis of a Self-Assembled Imine-Based Iron(II) Complex Endowed with Crown-Ether Receptors. *Eur. J. Org. Chem.* **2020**, 23, 3390-3397.
216. Olivo, G.; Arancio, G.; Mandolini, L.; Lanzalunga, O.; Di Stefano, S., Hydrocarbon oxidation catalyzed by a cheap nonheme imine-based iron(II) complex. *Catal. Sci. Technol.* **2014**, 4 (9), 2900-2903.
217. Olivo, G.; Giosia, S.; Barbieri, A.; Lanzalunga, O.; Di Stefano, S., Alcohol oxidation with H₂O₂ catalyzed by a cheap and promptly available imine based iron complex. *Org. Biomol. Chem.* **2016**, 14 (45), 10630-10635.
218. Ticconi, B.; Capocasa, G.; Cerrato, A.; Di Stefano, S.; Lapi, A.; Marincioni, B.; Olivo, G.; Lanzalunga, O., Insight into the chemoselective aromatic vs. side-chain hydroxylation of alkylaromatics with H₂O₂ catalyzed by a non-heme imine-based iron complex. *Catal. Sci. Technol.* **2021**, 11 (1), 171-178.
219. Olivo, G.; Nardi, M.; Vidal, D.; Barbieri, A.; Lapi, A.; Gómez, L.; Lanzalunga, O.; Costas, M.; Di Stefano, S., C-H Bond Oxidation Catalyzed by an Imine-Based Iron Complex: A Mechanistic Insight. *Inorg. Chem.* **2015**, 54 (21), 10141-10152.
220. Lyakin, O. Y.; Zima, A. M.; Tkachenko, N. V.; Bryliakov, K. P.; Talsi, E. P., Direct Evaluation of the Reactivity of Nonheme Iron(V)-Oxo Intermediates toward Arenes. *ACS Catal.* **2018**, 8 (6), 5255-5260.

221. Lyakin, O. Y.; Zima, A. M.; Samsonenko, D. G.; Bryliakov, K. P.; Talsi, E. P., EPR Spectroscopic Detection of the Elusive $\text{Fe}^{\text{V}}=\text{O}$ Intermediates in Selective Catalytic Oxofunctionalizations of Hydrocarbons Mediated by Biomimetic Ferric Complexes. *ACS Catal.* **2015**, *5* (5), 2702-2707.
222. Zima, A. M.; Lyakin, O. Y.; Ottenbacher, R. V.; Bryliakov, K. P.; Talsi, E. P., Dramatic effect of carboxylic acid on the electronic structure of the active species in $\text{Fe}(\text{PDP})$ -catalyzed asymmetric epoxidation. *ACS Catal.* **2016**, *6* (8), 5399-5404.
223. Zima, A. M.; Lyakin, O. Y.; Ottenbacher, R. V.; Bryliakov, K. P.; Talsi, E. P., Iron-catalyzed enantioselective epoxidations with various oxidants: Evidence for different active species and epoxidation mechanisms. *ACS Catal.* **2017**, *7* (1), 60-69.
224. Zima, A. M.; Lyakin, O. Y.; Lubov, D. P.; Bryliakov, K. P.; Talsi, E. P., Aromatic C–H oxidation by non-heme iron(V)-oxo intermediates bearing aminopyridine ligands. *J. Mol. Catal.* **2020**, *483*, 110708.
225. Van Heuvelen, K. M.; Fiedler, A. T.; Shan, X.; De Hont, R. F.; Meier, K. K.; Bominaar, E. L.; Münck, E.; Que, L., One-electron oxidation of an oxoiron(IV) complex to form an $[\text{O}=\text{Fe}^{\text{V}}=\text{NR}]^+$ center. *Proc. Natl. Acad. Sci. U.S.A.* **2012**, *109* (30), 11933-11938.
226. Serrano-Plana, J.; Oloo, W. N.; Acosta-Rueda, L.; Meier, K. K.; Verdejo, B.; García-España, E.; Basallote, M. G.; Münck, E.; Que Jr, L.; Company, A.; Costas, M., Trapping a Highly Reactive Nonheme Iron Intermediate That Oxygenates Strong C–H Bonds with Stereoretention. *J. Am. Chem. Soc.* **2015**, *137* (50), 15833-15842.
227. Tkachenko, N. V.; Ottenbacher, R. V.; Lyakin, O. Y.; Zima, A. M.; Samsonenko, D. G.; Talsi, E. P.; Bryliakov, K. P., Highly Efficient Aromatic C–H Oxidation with H_2O_2 in the Presence of Iron Complexes of the PDP Family. *ChemCatChem* **2018**, *10* (18), 4052-4057.
228. Tkachenko, N. V.; Lyakin, O. Y.; Zima, A. M.; Talsi, E. P.; Bryliakov, K. P., Effect of different carboxylic acids on the aromatic hydroxylation with H_2O_2 in the presence of an iron aminopyridine complex. *J. Organomet. Chem.* **2018**, *871*, 130-134.
229. Kal, S.; Draksharapu, A.; Que Jr, L., Sc^{3+} (or HClO_4) Activation of a Nonheme $\text{Fe}^{\text{III}}\text{-OOH}$ Intermediate for the Rapid Hydroxylation of Cyclohexane and Benzene. *J. Am. Chem. Soc.* **2018**, *140* (17), 5798-5804.
230. Li, F.; Van Heuvelen, K. M.; Meier, K. K.; Münck, E.; Que Jr, L., Sc^{3+} -triggered oxoiron(IV) formation from O_2 and its non-heme iron(II) precursor via a Sc^{3+} -peroxo- Fe^{3+} intermediate. *J. Am. Chem. Soc.* **2013**, *135* (28), 10198-10201.
231. Lee, Y.-M.; Bang, S.; Kim, Y. M.; Cho, J.; Hong, S.; Nomura, T.; Ogura, T.; Troeppner, O.; Ivanović-Burmazović, I.; Sarangi, R., A mononuclear nonheme iron(III)-peroxo complex binding redox-inactive metal ions. *Chem. Sci.* **2013**, *4* (10), 3917-3923.
232. Zhang, J.; Wei, W.-J.; Lu, X.; Yang, H.; Chen, Z.; Liao, R.-Z.; Yin, G., Nonredox metal ions promoted olefin epoxidation by iron(II) complexes with H_2O_2 : DFT calculations reveal multiple channels for oxygen transfer. *Inorg. Chem.* **2017**, *56* (24), 15138-15149.
233. Nodzevska, A.; Watkinson, M., Remarkable increase in the rate of the catalytic epoxidation of electron deficient styrenes through the addition of $\text{Sc}(\text{OTf})_3$ to the MnTMTACN catalyst. *Chem. Commun.* **2018**, *54* (12), 1461-1464.
234. Chatterjee, S.; Paine, T. K., Olefin *cis*-Dihydroxylation and Aliphatic C–H Bond Oxygenation by a Dioxygen-Derived Electrophilic Iron–Oxygen Oxidant. *Angew. Chem. Int. Ed.* **2015**, *54*, 9338-9342.

235. Kal, S.; Que Jr, L., Activation of a Non-Heme Fe^{III}-OOH by a Second Fe^{III} to Hydroxylate Strong C–H Bonds: Possible Implications for Soluble Methane Monooxygenase. *Angew. Chem. Int. Ed.* **2019**, *58* (25), 8484-8488.
236. Cheng, L.; Wang, H.; Cai, H.; Zhang, J.; Gong, X.; Han, W., Iron-catalyzed arene C–H hydroxylation. *Science* **2021**, *374* (6563), 77-81.
237. Klinman, J. P., Mechanisms whereby mononuclear copper proteins functionalize organic substrates. *Chem. Rev.* **1996**, *96* (7), 2541-2562.
238. Fontecave, M.; Pierre, J.-L., Oxidations by copper metalloenzymes and some biomimetic approaches. *Coord. Chem. Rev.* **1998**, *170* (1), 125-140.
239. Klabunde, T.; Eicken, C.; Sacchettini, J. C.; Krebs, B., Crystal structure of a plant catechol oxidase containing a dicopper center. *Nat. Struct. Mol. Biol.* **1998**, *5* (12), 1084-1090.
240. Solomon, E. I.; Sundaram, U. M.; Machonkin, T. E., Multicopper oxidases and oxygenases. *Chem. Rev.* **1996**, *96* (7), 2563-2606.
241. Rolff, M.; Schottenheim, J.; Decker, H.; Tucek, F., Copper–O₂ reactivity of tyrosinase models towards external monophenolic substrates: molecular mechanism and comparison with the enzyme. *Chem. Soc. Rev.* **2011**, *40* (7), 4077-4098.
242. Decker, H.; Schweikardt, T.; Tucek, F., The first crystal structure of tyrosinase: all questions answered? *Angew. Chem. Int. Ed.* **2006**, *45* (28), 4546-4550.
243. Matoba, Y.; Kumagai, T.; Yamamoto, A.; Yoshitsu, H.; Sugiyama, M., Crystallographic evidence that the dinuclear copper center of tyrosinase is flexible during catalysis. *J. Biol. Chem.* **2006**, *281* (13), 8981-8990.
244. Serrano-Plana, J.; Garcia-Bosch, I.; Company, A.; Costas, M., Structural and reactivity models for copper oxygenases: cooperative effects and novel reactivities. *Acc. Chem. Res.* **2015**, *48* (8), 2397-2406.
245. Karlin, K. D.; Hayes, J. C.; Gultneh, Y.; Cruse, R. W.; McKown, J. W.; Hutchinson, J. P.; Zubieta, J., Copper-mediated hydroxylation of an arene: model system for the action of copper monooxygenases. Structures of a binuclear copper(I) complex and its oxygenated product. *J. Am. Chem. Soc.* **1984**, *106* (7), 2121-2128.
246. Karlin, K. D.; Nasir, M. S.; Cohen, B. I.; Cruse, R. W.; Kaderli, S.; Zuberbuehler, A. D., Reversible dioxygen binding and aromatic hydroxylation in O₂-reactions with substituted xylyl dinuclear copper(I) complexes: syntheses and low-temperature kinetic/thermodynamic and spectroscopic investigations of a copper monooxygenase model system. *J. Am. Chem. Soc.* **1994**, *116* (4), 1324-1336.
247. Pidcock, E.; Obias, H. V.; Zhang, C. X.; Karlin, K. D.; Solomon, E. I., Investigation of the reactive oxygen intermediate in an arene hydroxylation reaction performed by xylyl-bridged binuclear copper complexes. *J. Am. Chem. Soc.* **1998**, *120* (31), 7841-7847.
248. Becker, M.; Schindler, S.; Karlin, K. D.; Kaden, T. A.; Kaderli, S.; Palanché, T.; Zuberbühler, A. D., Intramolecular ligand hydroxylation: Mechanistic high-pressure studies on the reaction of a dinuclear copper(I) complex with dioxygen. *Inorg. Chem.* **1999**, *38* (9), 1989-1995.
249. Maiti, D.; Fry, H. C.; Woertink, J. S.; Vance, M. A.; Solomon, E. I.; Karlin, K. D., A 1: 1 copper–dioxygen adduct is an end-on bound superoxo copper(II) complex which undergoes oxygenation reactions with phenols. *J. Am. Chem. Soc.* **2007**, *129* (2), 264-265.

250. Maiti, D.; Lee, D. H.; Gaoutchenova, K.; Würtele, C.; Holthausen, M. C.; Narducci Sarjeant, A. A.; Sundermeyer, J.; Schindler, S.; Karlin, K. D., Reactions of a Copper(II) Superoxo Complex Lead to C–H and O–H Substrate Oxygenation: Modeling Copper-Monooxygenase C–H Hydroxylation. *Angew. Chem. Int. Ed.* **2008**, *47*, 82-85.
251. Karlin, K. D.; Zhang, C. X.; Rheingold, A. L.; Galliker, B.; Kaderli, S.; Zuberbühler, A. D., Reversible dioxygen binding and arene hydroxylation reactions: Kinetic and thermodynamic studies involving ligand electronic and structural variations. *Inorganica Chim. Acta* **2012**, *389*, 138-150.
252. Lee, J. Y.; Peterson, R. L.; Ohkubo, K.; Garcia-Bosch, I.; Himes, R. A.; Woertink, J.; Moore, C. D.; Solomon, E. I.; Fukuzumi, S.; Karlin, K. D., Mechanistic insights into the oxidation of substituted phenols via hydrogen atom abstraction by a cupric-superoxo complex. *J. Am. Chem. Soc.* **2014**, *136* (28), 9925-9937.
253. Kim, S.; Lee, J. Y.; Cowley, R. E.; Ginsbach, J. W.; Siegler, M. A.; Solomon, E. I.; Karlin, K. D., A N₃S(thioether)-ligated Cu^{II}-superoxo with enhanced reactivity. *J. Am. Chem. Soc.* **2015**, *137* (8), 2796-2799.
254. Mahapatra, S.; Kaderli, S.; Llobet, A.; Neuhold, Y.-M.; Palanché, T.; Halfen, J. A.; Young, V. G.; Kaden, T. A.; Que, L.; Zuberbühler, A. D.; Tolman, W. B., Binucleating ligand structural effects on (μ-peroxo)- and bis(μ-oxo) dicopper complex formation and decay: Competition between arene hydroxylation and aliphatic C–H bond activation. *Inorg. Chem.* **1997**, *36* (27), 6343-6356.
255. Sander, O.; Henß, A.; Näther, C.; Würtele, C.; Holthausen, M. C.; Schindler, S.; Tuczek, F., Aromatic Hydroxylation in a Copper Bis(imine) Complex Mediated by a μ-η²:η² Peroxo Dicopper Core: A Mechanistic Scenario. *Chem. Eur. J.* **2008**, *14* (31), 9714-9729.
256. Menif, R.; Martell, A. E.; Squattrito, P. J.; Clearfield, A., New hexaaza macrocyclic binucleating ligands. Oxygen insertion with a dicopper(I) Schiff base macrocyclic complex. *Inorg. Chem.* **1990**, *29* (23), 4723-4729.
257. Santagostini, L.; Gullotti, M.; Monzani, E.; Casella, L.; Dillinger, R.; Tuczek, F., Reversible dioxygen binding and phenol oxygenation in a tyrosinase model system. *Chem. Eur. J.* **2000**, *6* (3), 519-522.
258. Palavicini, S.; Granata, A.; Monzani, E.; Casella, L., Hydroxylation of phenolic compounds by a peroxodicopper(II) complex: Further insight into the mechanism of tyrosinase. *J. Am. Chem. Soc.* **2005**, *127* (51), 18031-18036.
259. Itoh, S.; Kumei, H.; Taki, M.; Nagatomo, S.; Kitagawa, T.; Fukuzumi, S., Oxygenation of phenols to catechols by a (μ-η²:η²-peroxo) dicopper(II) complex: mechanistic insight into the phenolase activity of tyrosinase. *J. Am. Chem. Soc.* **2001**, *123* (27), 6708-6709.
260. Battaini, G.; De Carolis, M.; Monzani, E.; Tuczek, F.; Casella, L., The phenol *ortho*-oxygenation by mononuclear copper(I) complexes requires a dinuclear μ-η²:η²-peroxodicopper(II) complex rather than mononuclear CuO₂ species. *Chem. Commun.* **2003**, (6), 726-727.
261. Mirica, L. M.; Vance, M.; Rudd, D. J.; Hedman, B.; Hodgson, K. O.; Solomon, E. I.; Stack, T., A Stabilized μ-η²:η² Peroxodicopper(II) Complex with a Secondary Diamine Ligand and Its Tyrosinase-like Reactivity. *J. Am. Chem. Soc.* **2002**, *124* (32), 9332-9333.
262. Mirica, L. M.; Rudd, D. J.; Vance, M. A.; Solomon, E. I.; Hodgson, K. O.; Hedman, B.; Stack, T. D. P., μ-η²:η²-Peroxodicopper(II) complex with a secondary diamine ligand: a functional model of tyrosinase. *J. Am. Chem. Soc.* **2006**, *128* (8), 2654-2665.
263. Mirica, L. M.; Vance, M.; Rudd, D. J.; Hedman, B.; Hodgson, K. O.; Solomon, E. I.; Stack, T. D. P., Tyrosinase reactivity in a model complex: an alternative hydroxylation mechanism. *Science* **2005**, *308* (5730), 1890-1892.

264. Citek, C.; Lyons, C. T.; Wasinger, E. C.; Stack, T. D. P., Self-assembly of the oxy-tyrosinase core and the fundamental components of phenolic hydroxylation. *Nat. Chem.* **2012**, *4* (4), 317-322.
265. Hamann, J. N.; Tucek, F., New catalytic model systems of tyrosinase: fine tuning of the reactivity with pyrazole-based N-donor ligands. *Chem. Commun.* **2014**, *50* (18), 2298-2300.
266. Company, A.; Palavicini, S.; Garcia-Bosch, I.; Mas-Ballesté, R.; Que Jr, L.; Rybak-Akimova, E. V.; Casella, L.; Ribas, X.; Costas, M., Tyrosinase-Like Reactivity in a $\text{Cu}^{\text{III}}_2(\mu\text{-O})_2$ Species. *Chem. Eur. J.* **2008**, *14* (12), 3535-3538.
267. Tachi, Y.; Aita, K.; Teramae, S.; Tani, F.; Naruta, Y.; Fukuzumi, S.; Itoh, S., Dicopper–Dioxygen Complex Supported by Asymmetric Pentapyridine Dinucleating Ligand. *Inorg. Chem.* **2004**, *43* (15), 4558-4560.
268. Garcia-Bosch, I.; Company, A.; Frisch, J. R.; Torrent-Sucarrat, M.; Cardellach, M.; Gamba, I.; Güell, M.; Casella, L.; Que Jr, L.; Ribas, X.; Luis, J. M.; Costas, M., O_2 Activation and Selective Phenolate ortho Hydroxylation by an Unsymmetric Dicopper $\mu\text{-}\eta^1\text{:}\eta^1\text{-Peroxido}$ Complex. *Angew. Chem. Int. Ed.* **2010**, *49*, 2406–2409.
269. Matsumoto, T.; Furutachi, H.; Kobino, M.; Tomii, M.; Nagatomo, S.; Tosha, T.; Osako, T.; Fujinami, S.; Itoh, S.; Kitagawa, T.; Suzuki, M., Intramolecular arene hydroxylation versus intermolecular olefin epoxidation by ($\mu\text{-}\eta^2\text{:}\eta^2\text{-peroxo}$)dicopper(II) complex supported by dinucleating ligand. *J. Am. Chem. Soc.* **2006**, *128* (12), 3874-3875.
270. Mirica, L. M.; Ottenwaelder, X.; Stack, T. D. P., Structure and spectroscopy of copper–dioxygen complexes. *Chem. Rev.* **2004**, *104* (2), 1013-1046.
271. Lewis, E. A.; Tolman, W. B., Reactivity of dioxygen–copper systems. *Chem. Rev.* **2004**, *104* (2), 1047-1076.
272. Halfen, J. A.; Mahapatra, S.; Wilkinson, E. C.; Kaderli, S.; Young Jr, V. G.; Que Jr, L.; Zuberbühler, A. D.; Tolman, W. B., Reversible cleavage and formation of the dioxygen O–O bond within a dicopper complex. *Science* **1996**, 1397-1400.
273. Tolman, W. B., Making and breaking the dioxygen O–O bond: New insights from studies of synthetic copper complexes. *Acc. Chem. Res.* **1997**, *30* (6), 227-237.
274. Op't Holt, B. T.; Vance, M. A.; Mirica, L. M.; Heppner, D. E.; Stack, T. D. P.; Solomon, E. I., Reaction coordinate of a functional model of tyrosinase: spectroscopic and computational characterization. *J. Am. Chem. Soc.* **2009**, *131* (18), 6421-6438.
275. Holland, P. L.; Rodgers, K. R.; Tolman, W. B., Is the Bis($\mu\text{-oxo}$)dicopper Core Capable of Hydroxylating an Arene? *Angew. Chem. Int. Ed.* **1999**, *38* (8), 1139-1142.
276. Herres-Pawlis, S.; Verma, P.; Haase, R.; Kang, P.; Lyons, C. T.; Wasinger, E. C.; Flörke, U.; Henkel, G.; Stack, T. D. P., Phenolate hydroxylation in a bis($\mu\text{-oxo}$)dicopper(III) complex: lessons from the guanidine/amine series. *J. Am. Chem. Soc.* **2009**, *131* (3), 1154-1169.
277. Itoh, S., Developing mononuclear copper–active-oxygen complexes relevant to reactive intermediates of biological oxidation reactions. *Acc. Chem. Res.* **2015**, *48* (7), 2066-2074.
278. Kunishita, A.; Teraoka, J.; Scanlon, J. D.; Matsumoto, T.; Suzuki, M.; Cramer, C. J.; Itoh, S., Aromatic Hydroxylation Reactivity of a Mononuclear $\text{Cu}(\text{II})$ –Alkylperoxo Complex. *J. Am. Chem. Soc.* **2007**, *129* (23), 7248-7249.

279. Kunishita, A.; Scanlon, J. D.; Ishimaru, H.; Honda, K.; Ogura, T.; Suzuki, M.; Cramer, C. J.; Itoh, S., Reactions of copper(II)-H₂O₂ adducts supported by tridentate bis(2-pyridylmethyl)amine ligands: Sensitivity to solvent and variations in ligand substitution. *Inorg. Chem.* **2008**, *47* (18), 8222-8232.
280. Würtele, C.; Gaoutchenova, E.; Harms, K.; Holthausen, M. C.; Sundermeyer, J.; Schindler, S., Crystallographic characterization of a synthetic 1:1 end-on copper dioxygen adduct complex. *Angew. Chem. Int. Ed.* **2006**, *45* (23), 3867-3869.
281. Conde, A.; Diaz-Requejo, M. M.; Pérez, P. J., Direct, copper-catalyzed oxidation of aromatic C–H bonds with hydrogen peroxide under acid-free conditions. *Chem. Commun.* **2011**, *47* (28), 8154-8156.
282. Vilella, L.; Conde, A.; Balcells, D.; Díaz-Requejo, M. M.; Lledós, A.; Pérez, P. J., A competing, dual mechanism for catalytic direct benzene hydroxylation from combined experimental-DFT studies. *Chem. Sci.* **2017**, *8* (12), 8373-8383.
283. Wu, L.; Zhong, W.; Xu, B.; Wei, Z.; Liu, X., Synthesis and characterization of copper(II) complexes with multidentate ligands as catalysts for the direct hydroxylation of benzene to phenol. *Dalton Trans.* **2015**, *44* (17), 8013-8020.
284. Tsuji, T.; Zaoputra, A. A.; Hitomi, Y.; Mieda, K.; Ogura, T.; Shiota, Y.; Yoshizawa, K.; Sato, H.; Kodera, M., Specific enhancement of catalytic activity by a dicopper core: selective hydroxylation of benzene to phenol with hydrogen peroxide. *Angew. Chem. Int. Ed.* **2017**, *56* (27), 7779-7782.
285. Muthuramalingam, S.; Anandababu, K.; Velusamy, M.; Mayilmurugan, R., Benzene Hydroxylation by Bioinspired Copper(II) Complexes: Coordination Geometry versus Reactivity. *Inorg. Chem.* **2020**, *59* (9), 5918-5928.
286. Yamada, M.; Karlin, K. D.; Fukuzumi, S., One-step selective hydroxylation of benzene to phenol with hydrogen peroxide catalysed by copper complexes incorporated into mesoporous silica–alumina. *Chem. Sci.* **2016**, *7* (4), 2856-2863.
287. Kumari, S.; Muthuramalingam, S.; Dhara, A. K.; Singh, U.; Mayilmurugan, R.; Ghosh, K., Cu(I) complexes obtained via spontaneous reduction of Cu(II) complexes supported by designed bidentate ligands: bioinspired Cu(I) based catalysts for aromatic hydroxylation. *Dalton Trans.* **2020**, *49* (39), 13829-13839.
288. Boer, J. L.; Mulrooney, S. B.; Hausinger, R. P., Nickel-dependent metalloenzymes. *Arch. Biochem. Biophys.* **2014**, *544*, 142-152.
289. Corona, T.; Company, A., Spectroscopically characterized synthetic mononuclear nickel–oxygen species. *Chem. Eur. J.* **2016**, *22* (38), 13422-13429.
290. Kimura, E.; Machida, R., A mono-oxygenase model for selective aromatic hydroxylation with nickel(II)-macrocyclic polyamines. *J. Chem. Soc. Chem. Commun.* **1984**, (8), 499-500.
291. Honda, K.; Cho, J.; Matsumoto, T.; Roh, J.; Furutachi, H.; Tosha, T.; Kubo, M.; Fujinami, S.; Ogura, T.; Kitagawa, T.; Suzuki, M., Oxidation Reactivity of Bis(μ -oxo) Dinickel(III) Complexes: Arene Hydroxylation of the Supporting Ligand. *Angew. Chem. Int. Ed.* **2009**, *48* (18), 3304-3307.
292. Kunishita, A.; Doi, Y.; Kubo, M.; Ogura, T.; Sugimoto, H.; Itoh, S., Ni(II)/H₂O₂ reactivity in bis[(pyridin-2-yl)methyl]amine tridentate ligand system. Aromatic hydroxylation reaction by bis(μ -oxo)dinickel(III) complex. *Inorg. Chem.* **2009**, *48* (11), 4997-5004.
293. Tano, T.; Doi, Y.; Inosako, M.; Kunishita, A.; Kubo, M.; Ishimaru, H.; Ogura, T.; Sugimoto, H.; Itoh, S., Nickel(II) Complexes of tpa Ligands with 6-Phenyl Substituents (Phntpa). Structure and H₂O₂-Reactivity. *Bull. Chem. Soc. Jpn.* **2010**, *83* (5), 530-538.

294. Hikichi, S.; Yoshizawa, M.; Sasakura, Y.; Akita, M.; Moro-oka, Y., First Synthesis and Structural Characterization of Dinuclear M(III) Bis(μ -oxo) Complexes of Nickel and Cobalt with Hydrotris(pyrazolyl)borate Ligand. *J. Am. Chem. Soc.* **1998**, *120* (40), 10567-10568.
295. Itoh, S.; Bandoh, H.; Nagatomo, S.; Kitagawa, T.; Fukuzumi, S., Aliphatic hydroxylation by a bis(μ -oxo)dinickel(III) complex. *J. Am. Chem. Soc.* **1999**, *121* (38), 8945-8946.
296. Shiren, K.; Ogo, S.; Fujinami, S.; Hayashi, H.; Suzuki, M.; Uehara, A.; Watanabe, Y.; Moro-oka, Y., Synthesis, Structures, and Properties of Bis(μ -oxo)nickel(III) and Bis(μ -superoxo)nickel(II) Complexes: An Unusual Conversion of a Ni^{III}₂(μ -O)₂ Core into a Ni^{II}₂(μ -OO)₂ Core by H₂O₂ and Oxygenation of Ligand. *J. Am. Chem. Soc.* **2000**, *122* (2), 254-262.
297. Mandimutsira, B. S.; Yamarik, J. L.; Brunold, T. C.; Gu, W.; Cramer, S. P.; Riordan, C. G., Dioxygen activation by a nickel thioether complex: Characterization of a Ni^{III}₂(μ -O)₂ Core. *J. Am. Chem. Soc.* **2001**, *123* (37), 9194-9195.
298. Itoh, S.; Bandoh, H.; Nakagawa, M.; Nagatomo, S.; Kitagawa, T.; Karlin, K. D.; Fukuzumi, S., Formation, Characterization, and Reactivity of Bis(μ -oxo)dinickel(III) Complexes Supported by A Series of Bis[2-(2-pyridyl)ethyl]amine Ligands. *J. Am. Chem. Soc.* **2001**, *123* (45), 11168-11178.
299. Schenker, R.; Mandimutsira, B. S.; Riordan, C. G.; Brunold, T. C., Spectroscopic and Computational Studies on [(PhTtBu)₂Ni₂(μ -O)₂]: Nature of the Bis- μ -oxo (Ni³⁺)₂ "Diamond" Core. *J. Am. Chem. Soc.* **2002**, *124* (46), 13842-13855.
300. Morimoto, Y.; Bunno, S.; Fujieda, N.; Sugimoto, H.; Itoh, S., Direct hydroxylation of benzene to phenol using hydrogen peroxide catalyzed by nickel complexes supported by pyridylalkylamine ligands. *J. Am. Chem. Soc.* **2015**, *137* (18), 5867-5870.
301. Morimoto, Y.; Takagi, Y.; Saito, T.; Ohta, T.; Ogura, T.; Tohnai, N.; Nakano, M.; Itoh, S., A Bis(μ -oxido)dinickel(III) Complex with a Triplet Ground State. *Angew. Chem. Int. Ed.* **2018**, *57* (26), 7640-7643.
302. Muthuramalingam, S.; Anandababu, K.; Velusamy, M.; Mayilmurugan, R., One step phenol synthesis from benzene catalysed by nickel(II) complexes. *Catal. Sci. Technol.* **2019**, *9* (21), 5991-6001.
303. McEvoy, J. P.; Brudvig, G. W., Water-splitting chemistry of photosystem II. *Chem. Rev.* **2006**, *106* (11), 4455-4483.
304. Cady, C. W.; Crabtree, R. H.; Brudvig, G. W., Functional models for the oxygen-evolving complex of photosystem II. *Coord. Chem. Rev.* **2008**, *252* (3-4), 444-455.
305. Umena, Y.; Kawakami, K.; Shen, J.-R.; Kamiya, N., Crystal structure of oxygen-evolving photosystem II at a resolution of 1.9 Å. *Nature* **2011**, *473* (7345), 55-60.
306. Cinco, R. M.; McFarlane Holman, K. L.; Robblee, J. H.; Yano, J.; Pizarro, S. A.; Bellacchio, E.; Sauer, K.; Yachandra, V. K., Calcium EXAFS establishes the Mn-Ca cluster in the oxygen-evolving complex of photosystem II. *Biochemistry* **2002**, *41* (43), 12928-12933.
307. Cahiez, G.; Duplais, C.; Buendia, J., Chemistry of organomanganese(II) compounds. *Chem. Rev.* **2009**, *109* (3), 1434-1476.
308. Carney, J. R.; Dillon, B. R.; Thomas, S. P., Recent advances of manganese catalysis for organic synthesis. *Eur. J. Org. Chem.* **2016**, *2016* (23), 3912-3929.
309. Philip, R. M.; Radhika, S.; Abdulla, C. A.; Anilkumar, G., Recent Trends and Prospects in Homogeneous Manganese-Catalysed Epoxidation. *Adv. Synth. Catal.* **2021**, *363* (5), 1272-1289.

310. Chen, J.; Jiang, Z.; Fukuzumi, S.; Nam, W.; Wang, B., Artificial nonheme iron and manganese oxygenases for enantioselective olefin epoxidation and alkane hydroxylation reactions. *Coord. Chem. Rev.* **2020**, *421*, 213443.

311. Sun, W.; Sun, Q., Bioinspired manganese and iron complexes for enantioselective oxidation reactions: ligand design, catalytic activity, and beyond. *Acc. Chem. Res.* **2019**, *52* (8), 2370-2381.

312. Wu, X.; Seo, M. S.; Davis, K. M.; Lee, Y.-M.; Chen, J.; Cho, K.-B.; Pushkar, Y. N.; Nam, W., A highly reactive mononuclear non-heme manganese(IV)–Oxo complex that can activate the strong C–H bonds of alkanes. *J. Am. Chem. Soc.* **2011**, *133* (50), 20088-20091.

313. Aratani, Y.; Yamada, Y.; Fukuzumi, S., Selective hydroxylation of benzene derivatives and alkanes with hydrogen peroxide catalysed by a manganese complex incorporated into mesoporous silica–alumina. *Chem. Commun.* **2015**, *51* (22), 4662-4665.

Chapter 2

On the Ability of Nickel Complexes Derived from Tripodal Aminopyridine Ligands to Catalyze Arene Hydroxylations

Abstract

The development of catalysts for the selective hydroxylation of aromatic C–H bonds is an essential challenge in current chemical research. The accomplishment of this goal requires the discovery of powerful metal-based oxidizing species capable of hydroxylating inert aromatic bonds in a selective manner, avoiding the generation of non-selective oxygen-centered radicals. Herein we show an investigation on the ability of nickel(II) complexes supported by tripodal tetradentate aminopyridine ligands to catalyze the direct hydroxylation of benzene to phenol with H₂O₂ as oxidant. We have found that modifications on the ligand structure of the nickel complex do not translate into different reactivity, which differs from previous findings for nickel-based arene hydroxylations. Besides, several nickel(II) salts have been found to be effective in the oxidation of aromatic C–H bonds. The use of fluorinated alcohols as solvent has been found to result in an increase in phenol yield; however, showing no more than two turn-overs per nickel. These findings raise questions on the nature of the oxidizing species responsible for the arene hydroxylation reaction.

This chapter is based on:

Masferrer-Rius, E.; Hopman, R. M.; van der Kleij, J.; Lutz, M.; Klein Gebbink, R. J. M. *CHIMIA*, **2020**, *74*, 489-494

2.1 Introduction

Oxidations of organic compounds are essential reactions and have been intensively studied in academia as well as in the chemical industry.^{1,2} Interest is born from the fact that oxygenated organic molecules can further be used to produce different classes of chemicals. Nowadays, many improvements have been made in the development of different oxidation catalysts; however, the selective oxidation of organic substrates, such as aromatic compounds, still represents a critical challenge in modern chemical research.

Phenols are essential intermediates in the generation of a broad range of products, like pharmaceuticals and polymers.³⁻⁶ Currently, the industrial production of phenol from benzene is carried out via the cumene process, which overall suffers from low efficiencies in product yield.⁷ The direct introduction of a hydroxyl functionality through activation of an aromatic C–H bond is difficult because of the high stability of aromatic compounds and the high bond dissociation energy of an aromatic C–H bond (112 kcal mol⁻¹).⁸ To overcome this challenge, the generation of highly reactive and selective metal-oxygen species is necessary. However, often phenol products are more easily to be oxidized than non-oxidized aromatic compounds, causing a chemoselectivity issue. Besides, a lack of discrimination between different oxidation sites results in a regioselectivity issue, especially when substituted benzenes are used in which the oxidation of benzylic C–H bonds is preferred over oxidation at the aromatic ring.

On the one hand, hydroxyl radicals, as well as hydroperoxyl radicals, are well known to oxidize aromatic compounds; however, poor selectivity is usually observed due to the non-discriminative reactivity of oxygen-centered radicals.^{9, 10} On the other hand, metal-based oxidants are known to lead to more selective hydroxylation reactions.¹¹ Along this line, some progress has been made for the direct hydroxylation of benzene to phenol using H₂O₂ as the benign oxidant catalyzed by homogeneous catalysts (Figure 1), also providing some mechanistic insights.¹²⁻¹⁹

Over the last years, much interest has been devoted to the study of bioinspired iron complexes, which are minimalistic models of natural oxygenase enzymes.²⁰ These systems have been extensively studied for the oxidation of aliphatic C–H groups and epoxidation reactions with H₂O₂,²¹ whereas hydroxylation of aromatic compounds has remained challenging since the last years. The main problem is that the phenol products bind irreversibly to the iron center, which prevents catalytic turnover.²²⁻²⁴ For instance, several studies on the use of iron complexes supported by the tpa and bpmen aminopyridine ligands (tpa = tris(2-pyridylmethyl)amine) and bpmen = *N,N'*-dimethyl-*N,N'*-bis(2-picolyl)ethylenediamine) showed that these complexes were capable of oxidizing aromatic C–H bonds, but do not allow for catalytic turnover.²²⁻²⁴

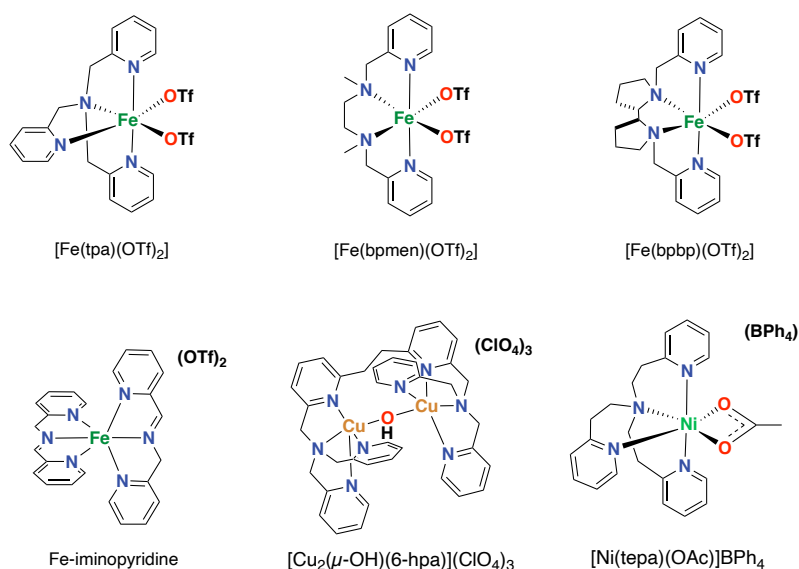


Figure 1. Examples of metal complexes previously used in catalytic arene hydroxylation reactions with H_2O_2 .

Recently, a series of iron complexes supported by the bppb type ligands (bppb = *N,N'*-bis(2-pyridylmethyl)-2,2'-bipyrrolidine) were found to be active for the hydroxylation of aromatic substrates with H_2O_2 , but with poor selectivities due to the generation of overoxidation products.¹²⁻¹⁴ Non-heme imine-based iron complexes have also been investigated in the field of hydroxylation reactions.²⁵ For instance, an iminopyridine iron(II) complex prepared in situ by self-assembly of commercially starting materials was found to be active for the hydroxylation of aromatic rings using H_2O_2 as the oxidant, likely through a metal-based electrophilic aromatic substitution mechanism.¹⁵

Other first-row transition metals have also been shown to be capable of performing arene hydroxylation reactions with H_2O_2 as benign oxidant. Koderá and co-workers reported a dinuclear copper complex stabilized by the 6-hpa ligand (6-hpa = 1,2-bis{2-[bis(2-pyridylmethyl)aminomethyl]-6-pyridyl}ethane) for the selective hydroxylation of benzene to phenol with H_2O_2 , showing high activity for phenol formation.¹⁶ Another remarkable example is the selective hydroxylation of benzene catalyzed by a $[\text{Ni}(\text{tepa})(\text{OAc})]\text{BPh}_4$ (tepa = tris(2-pyridylethyl)amine) / H_2O_2 system, which was reported to work through a metal-based mechanism, affording a maximum of 749 turnover numbers in 216 h at 60 °C for phenol production when using an 10000-fold excess of benzene with respect to the catalyst.¹⁸ The authors found that among a series of nickel complexes supported by tripodal tetradentate aminopyridine ligands, the one supported by the tepa ligand is able to chemoselectively catalyze the hydroxylation of benzene and alkylbenzenes at high H_2O_2 loadings, without the formation of substantial amounts of over-oxidized products.¹⁸ Remarkably though, when this complex was used in catalysis in 10 mol% loading with respect to the benzene substrate only 21% phenol

(2.1 turnovers per nickel) was formed in 5 h reaction time at 60 °C. Based on the previous work from Itoh and co-workers, another recently reported study shows improved nickel-based catalysts for the selective oxidation of benzene to phenol through modifications of aminopyridine ligands by introduction of electron-rich pyridines, affording phenol with up to 820 turnover numbers in 5 h at 60 °C using 0.05 mol% loading of catalyst.¹⁹

Many efforts have focused on the development of highly selective catalyst system for phenol formation. These studies parallel the development of catalysts for the selective hydroxylation of aliphatic C–H bonds to the corresponding alcohols, avoiding the generation of overoxidized ketone products. In an effort to get more selective catalysts, several of the latter studies have described the use of fluorinated alcohol solvents, *i.e.* 2,2,2-trifluoroethanol (TFE) or 1,1,1,3,3,3-hexafluoro-2-propanol (HFIP), in hydroxylation reactions; showing improved selectivities for the first-formed hydroxylation product and avoiding overoxidation reactions.²⁶⁻

30

Inspired by previous studies on arene hydroxylation catalyzed by nickel complexes,^{18,19} we studied the effect of different tripodal aminopyridine ligands for the direct hydroxylation of benzene to phenol with H₂O₂ by nickel under mild reaction conditions. Our findings show that the use of different tripodal tetradentate aminopyridine ligand designs in the nickel complexes does not lead to a different reactivity in arene hydroxylation reactions, showing that this type of ligands does not play an important role in catalysis. Besides, we show that the oxidation of benzene can be achieved using simple nickel salts with high chemoselectivity. The effect of solvents, such as fluorinated alcohols, is found to produce and enhance activity for phenol formation, highlighting the use of this kind of solvents on oxidation processes. On basis of these results, we discuss some mechanistic considerations for arene hydroxylations using molecular nickel complexes derived from aminopyridine ligands.

2.2 Results and Discussion

2.2.1 Aminopyridine Ligands and Nickel Complexes

For our study, we have investigated several nickel complexes supported by aminopyridine ligands as arene hydroxylation catalysts with H₂O₂ as the benign oxidant under mild reaction conditions (Figure 2). Our aim was to investigate if small modifications in the structure of the aminopyridine ligand would influence the reactivity of the complexes in arene hydroxylation reactions.

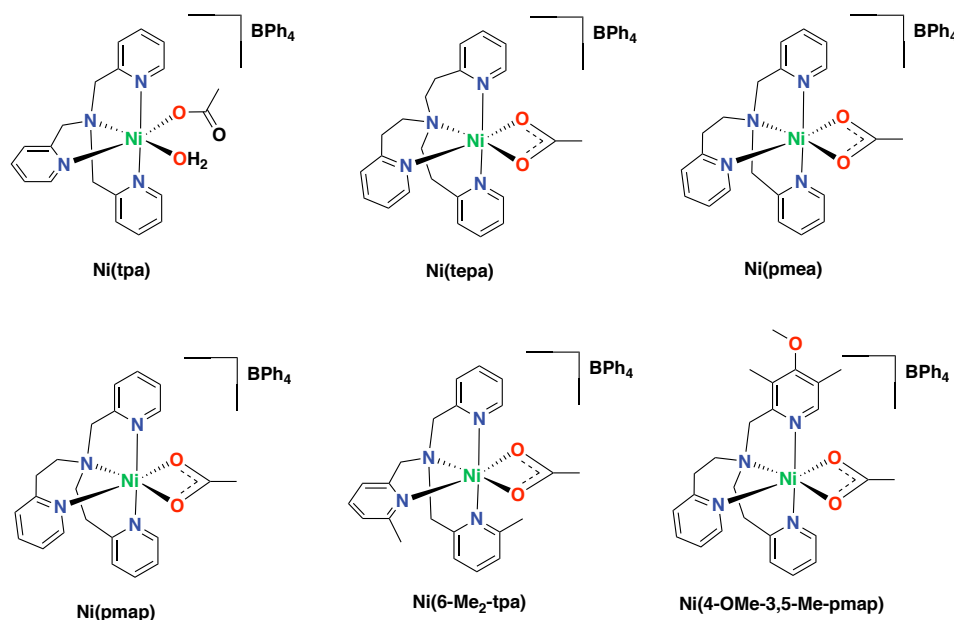


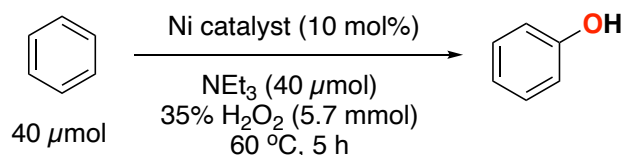
Figure 2. Nickel(II) complexes supported by tripodal tetradentate aminopyridine ligands employed in this Chapter.

Based on the work of Itoh and co-workers,¹⁸ we focused on the use of tripodal tetradentate aminopyridine ligands, playing with the length of the arms. First, we synthesized the parent tpa ligand, containing three methylene arms, and the tepa ligand, which contains three ethylene arms. Of interest was also the pmea ligand (pmea = (2-(2-pyridylethyl))bis(2-pyridylmethyl)amine), and the pmap ligand (pmap = bis(2-(2-pyridylethyl))-2-pyridylmethylamine). Finally, we envisioned an enhancement on efficiency towards aromatic C–H oxidations by introducing electron-donating substituents into some of the pyridines, such as the 6-Me₂-tpa and 4-OMe-3,5-Me-pmap ligands (6-Me₂-tpa = bis(6-methyl-2-pyridylmethyl)(2-pyridylmethyl)amine, and 4-OMe-3,5-Me-pmap = bis(2-(2-pyridylethyl))-(4-methoxy-3,5-dimethyl)-2-pyridylmethylamine). The benefit of such electron-rich pyridine donors has been shown for several C–H and C=C oxidation reactions with non-heme iron and manganese complexes,^{31–34} as well as for arene hydroxylation reactions with nickel complexes.¹⁹

The corresponding nickel complexes were synthesized by mixing the nickel acetate tetrahydrate and the different aminopyridine ligands; subsequent addition of sodium tetraphenylborate lead to precipitate of the final complex. Several of the complexes were analyzed by X-ray crystal structure, showing a mononuclear nickel(II) species exhibiting a distorted octahedral geometry. Details of the synthesis and characterization of the ligands and complexes can be found in the experimental section.

2.2.2 Screening of Complexes

Next, we have focused on the oxidation of benzene as model substrate to selectively screen for aromatic oxidation (Scheme 1). Catalytic experiments were carried out using 40 μmol of benzene, 40 μmol of triethylamine as a base, and 5.7 mmol of H_2O_2 (142 equiv.) in acetonitrile as solvent, with 10 mol% of catalyst; following the initial conditions described by Itoh.¹⁸



Scheme 1. Catalytic hydroxylation of benzene to phenol catalyzed by nickel(II) complexes with H_2O_2 under mild reaction conditions.

Reactions were run under air, at 60 $^\circ\text{C}$, for 5 h using a closed reaction vessel. Crude mixtures were analyzed by GC, detecting mainly phenol as oxidized product, whereas formation of *para*-benzoquinone as an over-oxidized by-product was not observed. Thus, all complexes tested show chemoselectivity for phenol formation, as was reported previously for similar Ni/ H_2O_2 systems.^{18, 19} Furthermore, biphenyl was detected after analysis of the crude mixtures. The formation of biphenyl seems to originate from the tetraphenylborate counterion of the complex, since it is known that biphenyl can form through radical decomposition of tetraphenylborate.^{35, 36} Similar oxidation experiments without benzene substrate afford biphenyl as well, corroborating that benzene is not the source for biphenyl formation. Interestingly, acetamide was detected as the main product in the crude reaction mixtures. Acetamide may form through the oxidation of triethylamine, which can be oxidized in the presence of H_2O_2 .^{37, 38} However, the amounts of acetamide obtained were higher than the amount of triethylamine used, suggesting that the acetonitrile solvent is hydrated to acetamide under our experimental conditions.

Overall, these first catalytic experiments using acetonitrile as solvent provided poor phenol yields, ranging from 9.0 to 10.5 % (Table 1). These findings compare quite well with the initial experiments performed by Itoh and co-workers, for which they reported 2 turnover numbers for the oxidation of benzene catalyzed by **Ni(tepa)** under the same experimental conditions.¹⁸ Not only do our results represent a single turn-over per nickel, the differences in phenol yields between the different complexes lie within the experimental error of our GC analysis. Accordingly, these results indicate no particular complex in the series of complexes tested catalyzes benzene hydroxylation more effectively than another complex. Our results might even indicate that the aminopyridine ligand plays no important role in performing the oxidation reaction. A control experiment without any complex as catalyst showed that no phenol product

formation occurs in the absence of a nickel complex. Thus, we can confidently conclude that a nickel complex is involved in the oxidation reaction.

Table 1. Direct hydroxylation of benzene to phenol employing Ni(II) complexes in acetonitrile.

Entry	Catalyst	Phenol Yield [%]
1	Ni(tpa)	9.6
2	Ni(tepa)	9.9
3	Ni(pmea)	9.7
4	Ni(pmap)	9.0
5	Ni(6-Me₂-tpa)	10.5
6	-	n.d.

n.d. = non-detected. ^aReaction conditions: benzene (40 μ mol), H₂O₂ (5.7 mmol), Ni complex (4 μ mol), and NEt₃ (40 μ mol) at 60 °C for 5 h in CH₃CN.

2.2.3 Different Reaction Solvents

Since the phenol yields were low, we decided to screen different solvents for the hydroxylation of benzene with the **Ni(tepa)** catalyst (Table 2). With acetonitrile, we could detect 4.7% phenol yield after 2.5 h, which increased to 9.9 % when the reaction was run for 5 h (Table 2, entries 1 and 2). Next, fluorinated alcohols were tested, which have been reported to be suitable solvents in different hydroxylation reactions.²⁶⁻³⁰ TFE provided 7.6% phenol formation after 2.5 h, which slightly increase to 8% when the reaction was run for 5 h (Table 2, entries 3 and 4). Another fluorinated alcohol, HFIP, was also tested as solvent providing an enhanced activity, with 11.8 and 15.3% phenol yield after 2.5 and 5 h of reaction time, respectively. Methanol afforded poor phenol formation (3.8% yield), whereas acetone did not provide any phenol product (Table 2, entries 7 and 8); showing that these two solvents are not suitable to perform arene hydroxylation reactions with nickel complexes.

From these results, we concluded that the fluorinated alcohol HFIP is the best solvent to perform the oxidation of benzene to phenol catalyzed by the **Ni(tepa)** complex. Next, we tried higher amounts of H₂O₂, which did not afford an increase in phenol formation (Table 2, entry 9). We also envisioned an increase on catalytic activity by delivering the H₂O₂ slowly during the catalysis, as it has been shown for other C–H hydroxylation reactions using that oxidant.^{39, 40} However, no improvement was observed, and phenol was formed in a much lower yield, highlighting that the disproportionation of H₂O₂ is not product-limiting, probably due to the high-excess conditions (Table 2, entry 10).

Table 2. Screening of solvents for the direct hydroxylation of benzene to phenol catalyzed by **Ni(tepa)**.^a

Entry	Solvent	Reaction Time [h]	Phenol Yield [%]
1	CH ₃ CN	2.5	4.7
2	CH ₃ CN	5	9.9
3	TFE	2.5	7.6
4	TFE	5	8.0
5	HFIP	2.5	11.8
6	HFIP	5	15.3
7	CH ₃ OH	5	3.8
8	(CH ₃) ₂ CO	5	n.d.
9 ^b	HFIP	5	14.8
10 ^c	HFIP	2.5	7.2

^aReaction conditions: benzene (40 μ mol), H₂O₂ (5.7 mmol), Ni complex (4 μ mol), and NEt₃ (40 μ mol) at 60 °C. ^b500 equivalents of H₂O₂ were used. ^cH₂O₂ was added slowly within 1 h with the use of a syringe pump. n.d. = non-detected.

As it is shown in Table 3, we also screened all nickel complexes for catalysis in the HFIP solvent. Overall, we observed that for all complexes phenol yields increase when HFIP is used as the solvent compared to the use of acetonitrile, as was initially shown for the **Ni(tepa)** complex. While this observation highlights the use of a fluorinated alcohol solvent in arene hydroxylation catalysis by nickel(II) complexes, the overall yields still represent an average 1.5 turn-over number per nickel. In addition, no distinctive differences in catalytic efficiencies are observed between the different complexes. Even the nickel complexes **Ni(6-Me₂-tpa)** and **Ni(4-OMe-3,5-Me-pmap)** supported by electron-rich tripodal ligands did not afford substantial changes in reactivity (Table 3, entries 5 and 6). Control experiment with HFIP as solvent show us that reaction does not work without the presence of any catalyst (Table 3, entry 7). Even though a solvent screening did result in some increase in catalytic efficiency, small differences in product yields attainable with the current, yet limited, set of tripodal tetradentate aminopyridine ligands in our view does not allow for a rationalized ligand modification toward improve catalyst efficiency.

Interestingly, the simple salts nickel nitrate hexahydrate and nickel chloride hexahydrate lead to 6.7 and 3.0% phenol yield, respectively, using our current conditions (Table 3, entries 8 and 9). However, the hydroxylation reaction did not work when nickel acetate tetrahydrate was used (Table 3, entry 10). Remarkably, these results show that aromatic C–H oxidations can be done using some simple commercial nickel(II) salts with high chemoselectivity, albeit in low efficiencies.

Table 3. Direct hydroxylation of benzene to phenol employing Ni(II) complexes in HFIP.

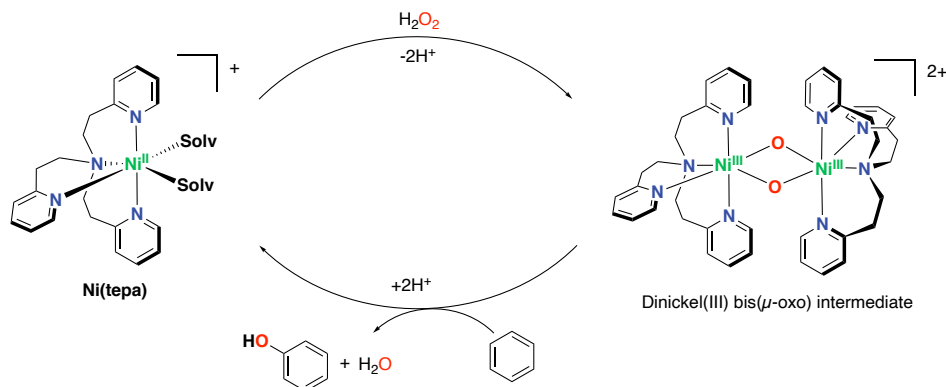
Entry	Catalyst	Phenol Yield [%]
1	Ni(tpa)	14.9
2	Ni(tepa)	15.3
3	Ni(pmea)	14.6
4	Ni(pmap)	16.4
5	Ni(6-Me₂-tpa)	15.0
6	Ni(4-OMe-3,5-Me-pmap)	17.4
7	-	n.d.
8	Ni(NO ₃) ₂ ·6H ₂ O	6.7
9	NiCl ₂ ·6H ₂ O	3.0
10	Ni(CH ₃ CO ₂) ₂ ·4H ₂ O	n.d.

n.d. = non-detected. ^aReaction conditions: benzene (40 μmol), H₂O₂ (5.7 mmol), Ni complex (4 μmol), and NEt₃ (40 μmol) at 60 °C for 5 h in HFIP.

2.2.4 Mechanistic Considerations

Finally, our efforts have been devoted to the understanding of the mechanism of the aromatic hydroxylation catalyzed by nickel complexes. In previous studies by Itoh and co-workers with the **Ni(tepa)** complex, it has been proposed that oxidation of benzene proceeds through a metal-based mechanism in which, after activation of H₂O₂, a dinickel(III) bis(μ -oxo) species is formed as the active oxidant (Scheme 2).¹⁸ However, no direct evidence for the involvement of such species has been shown. A recent work by Mayilmurugan and co-workers on arene hydroxylations catalyzed by nickel complexes supported by similar tripodal tetradentate aminopyridine ligands, postulate the same dinuclear nickel species as the real oxidant responsible for the oxidation of the aromatic ring. Only recently, Itoh and co-workers have shown an example of a dinickel(III) bis(μ -oxo) species with the dpema ligand (dpema = *N,N*-di-[2-pyridine-2-yl]ethyl)methylamine) displaying oxygenation reactivity towards external hydrocarbon substrates, however, no reactivity of such species towards external aromatics was reported.⁴¹

Here, we considered the role of triethylamine as a base, and how this component could affect catalysis. In these oxidation reactions triethylamine is thought to activate H₂O₂ and facilitate its reaction with the mononuclear nickel complex. Aqueous H₂O₂ solutions are acidic (pK_a of H₂O₂ = 11.62);⁴² therefore, the presence of a base in the catalytic reactions could help in the activation of H₂O₂ by deprotonating it. Indeed, we carried out some catalytic experiments using **Ni(tepa)** in acetonitrile without triethylamine, where we could observe a slight decrease in phenol



Scheme 2. Proposed catalytic mechanism for the direct hydroxylation of benzene to phenol with nickel(II) complexes based on previous studies.¹⁸

formation (6.9% yield) in comparison with experiments using the base (compare with Table 1, entry 2); indicating the positive role of the amine in activating the oxidant.

However, the fluorinated solvent HFIP is rather acidic (pK_a of HFIP = 9.3)⁴³ and could consequently affect the role of triethylamine (pK_a for the conjugate acid = 10.75)⁴⁴ in the deprotonation of H_2O_2 . Carrying out a catalytic reaction with **Ni(pmea)** in HFIP and in the absence of triethylamine as a base gave a 15.4% phenol yield, which is similar to the yield obtained when triethylamine was employed (14.6%, see Table 3.). Thus, this observation made us conclude that triethylamine does not have an essential role in aromatic oxidations catalyzed by nickel complexes when HFIP is used as a solvent. Indeed, this fluorinated alcohol itself is known to activate H_2O_2 , as has been showed in some selective oxidation reactions such as the epoxidation of alkenes.⁴⁵

Overall, we believe that the reaction might proceed through a metal-based mechanism, since high chemoselectivity for the formation of phenol is observed. Generation of overoxidized products, such as hydroquinones or benzoquinones, easily occurs when oxygen-centered radicals are involved in catalysis.⁴⁶⁻⁴⁹ However, such products have not been observed in the current and in previous studies using aminopyridine-based nickel complexes.

On the other hand, we believe that deactivation of the catalyst occurs during catalysis, which prevents efficient turnover numbers. To further investigate catalyst stability, we have studied the formation of phenol over time using the **Ni(tepa)** complex with H_2O_2 , triethylamine and acetonitrile as the solvent, which showed that the phenol yield increases in the first few hours of reaction, to then come to a stop. Reaction analysis after 5 h provided us with 10% phenol yield, which remained the same for the next 24 h. Addition of an extra portion of catalyst and allowing the reaction to run for another 5 h resulted in an increase in phenol yield to 32%. Besides, attempts to obtain high turnover numbers by reproducing the same conditions described by Itoh and co-workers did not afford results that are consistent with the ones reported

in the literature.¹⁸ Therefore, our results clearly differ from those reported by Itoh and co-workers, in which they describe up to 749 turnover numbers for phenol formation after 216 h of reaction time using the **Ni(tepa)** catalyst with H₂O₂, triethylamine and acetonitrile.¹⁸

2.3 Conclusions

We have presented a study on the effect of changes in the tripodal tetradentate aminopyridine ligand in nickel complexes used for the direct one-step hydroxylation of benzene to phenol in combination with H₂O₂ as benign oxidant under mild reaction conditions. Our results show that these modifications in the ligand structure do not translate into different activities in phenol formation, which differs from previous studies on nickel-based arene hydroxylations using similar tetradentate aminopyridine ligands.^{18, 19} Remarkably, the oxidation of benzene could also be achieved using nickel(II) salts without the use of sophisticated ligand designs and using a fluorinated alcohol solvent, which seemed to improve phenol yields for the nickel complexes. The phenol yields obtained with the salts is significantly lower than with the complexes. The product selectivity obtained throughout our study, with no formation of catechols, hydroquinones or benzoquinones, points towards a metal-based mechanism, with no involvement of oxygen-centered radicals.

Our studies do corroborate the earlier findings of Itoh *et al.* concerning the catalytic performance of the nickel complexes at high catalyst loadings. Yet, attempts to reproduce the high-turnover numbers achieved at low catalyst loadings were not successful. Together with the findings that catalytic performance is rather insensitive towards ligand structure variation and that simple nickel salts also are able to form phenol, the molecular nature of the catalyst involved in benzene hydroxylation by the nickel complexes can be questioned. Other than the involvement of a dinickel(III) bis(μ -oxo) species proposed earlier,^{18, 19} we believe that some kind of decomposition of the nickel complexes occurs under the experimental conditions, possibly leading to the formation of nickel-based nanoparticles that are involved in catalysis. Our future efforts will therefore be focused on identifying the actual nature of the hydroxylation catalyst and on the development of more active and stable catalyst systems based on nickel that allow for the high-turnover direct hydroxylation of benzene to phenol.

2.4 Experimental Section

2.4.1 General Remarks

Air- and moisture-sensitive reactions were performed under an inert nitrogen atmosphere using standard Schlenk line and glovebox techniques. All catalytic oxidation reactions were run under air with no precautions taken to exclude moisture. The solvents diethyl ether and acetonitrile were purified using

an MBraun MB SPS-800 solvent purification system. Tetrahydrofuran and methanol were dried with sodium and magnesium turnings, respectively, and distilled under nitrogen prior to use.

All other reagents and reaction products were obtained commercially from Across, Aldrich, Scharlab or Fluorochem, and used without further purification. Column chromatography was performed using Merck silica gel (60-200 mesh). ^1H and ^{13}C NMR spectra were recorded with a 400 MHz Varian spectrometer at 25 °C, chemical shifts (δ) are given in ppm referenced to the residual solvent peak. IR spectra were recorded with a Perkin-Elmer Spectrum One FTIR spectrometer. ESI-MS measurements were recorded with a Walters LCT Premier XE KE317 machine. GC analyses were performed on a Perkin-Elmer Clarus 500 Gas Chromatograph equipped with a PE Elite-5 column ((30m x 0.23 mm x 0.25 μm), (50% phenyl)-(50% methyl)polysiloxane) and a flame-ionization detector. X-ray diffraction analysis was carried out on a Bruker Kappa ApexII diffractometer.

CCDC 1998049-1998051 contain the supplementary crystallographic data for this chapter. These data can be obtained free of charge from The Cambridge Crystallographic Data Centre via www.ccdc.cam.ac.uk/structures.

Appendix A contains the supplementary information of this Chapter, which includes ^1H -NMR spectra for each ligand employed.

2.4.2 Synthesis of Ligands and Nickel Complexes

2.4.2.1 Synthesis of Pyridine Synthons

***N,N*-bis(2-(2-pyridyl)ethyl)hydroxylamine:** The compound was synthesized following a similar procedure as described in the literature.^{50, 51} To a stirring suspension of hydroxylamine hydrochloride (1.02 g, 14.7 mmol) in DMF (2 mL) was added 2-vinylpyridine (3.2 mL, 3.1 g, 29.7 mmol) dropwise. The resulting clear yellow solution was left to stir for 1 day. The resulting reaction mixture was basified with saturated aqueous NaHCO_3 , after which the organics were extracted using CH_2Cl_2 (3 x 10 mL). Organics were combined and dried over MgSO_4 , after which the drying agent was filtered off and solvents were removed under reduced pressure. The desired product was obtained as a white solid in 48% yield (1.7 g, 7.1 mmol). ^1H NMR (400 MHz, CDCl_3) δ 8.47 (dt, 2 H), 7.54 (td, 2H), 7.12 (d, 2H), 7.08 (t, 2H), 3.09 (s, 8H).

***N,N*-bis(2-(2-pyridyl)ethyl)amine:** The compound was synthesized following a similar procedure as described in the literature.^{50, 51} Zn-powder (2.17 g, 33.2 mmol) was added to a stirring solution of *N,N*-bis(2-(2-pyridyl)ethyl)hydroxylamine (1.72 g, 7.1 mmol) in 2N aqueous HCl (15 mL). The reaction mixture was heated to 85 °C for 22 hours. After the mixture was cooled down to rt, the pH was adjusted to 10 using an aqueous 4M K_2CO_3 solution. The resulting mixture was extracted with CH_2Cl_2 (3 x 30 mL), the organics were combined, dried over MgSO_4 and the drying agent was filtered off. The solvents were evaporated under reduced pressure, resulting in a yellow oil in 98% yield (1.58 g, 7.0 mmol). ^1H NMR (400 MHz, CDCl_3) δ 8.41 (d, 2H), 7.48 (td, 2H), 7.06 (d, 2H), 7.01 (td, 2H), 2.98 (t, 4H), 2.90 (t, 4H), 2.03 (s, 1H).

2.4.2.2 Synthesis of Tripodal Tetradentate Aminopyridine Ligands

Tris(2-pyridyl)methylamine (tpa) The ligand was synthesized following the same procedure as described by Wang and co-workers.⁵² The desired ligand was obtained as a yellowish solid (52% yield). Spectral properties of the product agree with the literature data. ^1H NMR (400 MHz, CD_3CN): δ 8.47 (d, 3 H), 7.70 (t, 3 H), 7.59 (d, 3 H), 7.18 (t, 3 H), 3.81 (s, 6 H).

Tris[2-(pyridin-2-yl)ethyl]amine (tepa). The ligand was synthesized following a similar procedure as described by Réglie and co-workers.⁵³ 2-vinylpyridine was purified using a plug of silica before using it. A mixture of (2-pyridyl)ethylamine (0.37 g, 3 mmol) and 2-vinylpyridine (0.95 g, 9 mmol), with acetic acid (0.19 g, 3.2 mmol) in 5 mL of methanol was refluxed for 42 h. After that time, the resulting red-brown mixture was cooled and stirred with 30 mL of 15% NaOH and then extracted with CH₂Cl₂ (4 x 10 mL) to remove the product from the aqueous phase. The organic phase was dried over MgSO₄ and filtered through a coarse frit. The solvent was removed by rotary evaporation, leaving a brown oil that was chromatographed on alumina neutral using a 99/1 (v/v) mixture of ethyl acetate/methanol as eluent. The purified product was obtained as a slightly viscous yellow oil (50% yield). ¹H NMR (400 MHz, CD₃CN): δ 8.46 (d, 3 H), 7.56 (t, 3 H), 7.12 (t, 2 H), 7.07 (d, 6 H), 2.91 (m, 6 H), 2.82 (m, 6 H). ¹³C NMR (CD₃CN): δ 161.93, 150.03, 137.00, 124.25, 121.98, 54.54, 36.64. HRMS (FAB⁺): *m/z* 333.1995 [M + H]⁺, calcd for C₂₁H₂₄N₄H 333.2079.

(2-(2-pyridylethyl))bis(2-pyridylmethyl)amine (pmea). The ligand was synthesized following a modified procedure described by Colbran and co-workers.⁵⁴ 2-vinylpyridine was purified passing through a plug of silica before using it. 2-vinylpyridine (3.56 g, 33.75 mmol), bis(2-pyridylmethyl)amine (2.24 g, 11.25 mmol) and acetic acid (0.72 g, 12.05 mmol) in H₂O / CH₃OH (10 mL / 2.5 mL) were heated at reflux for 45 h. 20% aqueous NaOH solution (2 mL) was added to the clear dark red solution causing two layers to separate. The mixture was extracted with CH₂Cl₂ (3 x 20 mL), the extracts dried over MgSO₄, filtered, and the chloroform removed under rotary evaporation. The obtained brown-orange oil was purified using column chromatography with basic alumina using CH₂Cl₂ as eluent and CH₃OH in 1-20%. The pure pmea ligand was obtained as an orange oil (1.8 g, 53% yield). ¹H NMR (400 MHz, CDCl₃): δ 8.51 (d, 2H), 8.48 (d, 1H), 7.60-7.53 (m, 3H), 7.35 (d, 2H), 7.13-7.08 (m, 4H), 3.89 (s, 4H), 3.07-2.97 (m, 4H). ¹³C NMR (100 MHz, CDCl₃): δ 160.65, 159.89, 149.26, 149.05, 136.48, 136.27, 123.52, 122.93, 122.01, 121.21, 60.39, 54.59, 36.14. ATR-IR: ν [cm⁻¹]: 3052, 3008, 2928, 2818, 1588, 1568, 1473, 1432, 1362, 1148, 1123, 1048, 994, 756, 615. HRMS (FAB⁺): *m/z* 305.1700 [M + H]⁺, calcd for C₁₉H₂₀N₄ 305.1766.

Bis(2-(2-pyridylethyl))-2-pyridylmethylamine (pmap). The ligand was synthesized following a modified procedure described by Colbran and co-workers.⁵⁴ *N,N*-bis(2-(2-pyridyl)ethyl)amine (0.27 g, 1.5 mmol) was combined with sodium triacetoxyborohydride (0.38 g, 1.8 mmol), 2-pyridinecarbaldehyde (0.14 mL, 1.5 mmol) and 1,2-dichloroethane (6.6 mL). Under N₂-atmosphere, the reaction was stirred for 36 hours affording a yellow liquid, which over the course of a day turned green. The green solution was washed with a saturated aqueous NaHCO₃ solution (2 times). The organic phase was dried over MgSO₄, filtered, and extracted with CH₂Cl₂, which was then removed under reduced pressure affording a green/orange oil. The obtained oil was purified using column chromatography with neutral alumina using CH₂Cl₂/CH₃OH (99/1). The pure pmap ligand was obtained as a brown/orange oil (0.13 g, 28% yield). ¹H NMR (400 MHz, CDCl₃): δ 8.49 (d, 3 H), 7.55-7.47 (m, 3 H), 7.13-7.04 (m, 6 H), 3.88 (s, 2 H), 3.01-2.96 (m, 8 H). ATR-IR: ν [cm⁻¹]: 2929, 1589, 1432, 1120. HRMS (FAB⁺): *m/z* 319.192; [M + H]⁺, calcd for C₂₀H₂₂N₄ 319.189.

Bis(6-methyl-2-pyridylmethyl)(2-pyridylmethyl)amine (6-Me₂-tpa) The ligand was synthesized following the same procedure as described by Schindler and co-workers.⁵⁵ The desired ligand was obtained as a light-yellow solid (2.8 g, 88%). Spectral properties of the product agree with the literature data. ¹H NMR (400 MHz, CDCl₃): δ 8.50 (d, 1H), 7.64-7.57 (m, 2H), 7.52 (t, 2H), 7.40 (d, 2H), 7.11 (t, 1H), 6.96 (d, 2H), 3.87 (s, 2H), 3.84 (s, 4H), 2.50 (s, 6H). ¹³C NMR (100 MHz, CDCl₃): δ 159.78, 159.03, 157.70, 149.10, 136.73, 136.47, 122.92, 121.99, 121.51, 119.67, 60.42, 60.24, 24.50. ATR-IR:

ν [cm^{-1}]: 3069, 3006, 2932, 2817, 1589, 1575, 1463, 1434, 1446, 1368, 1233, 1161, 1120, 1088, 982, 799, 793, 766, 758.

Bis(2-(2-pyridylethyl)-(4-methoxy-3,5-dimethyl)-2-pyridylmethylamine (4-OMe-3,5-Me-pmap).

A solution of 2-chloromethyl-4-methoxy-3,5-dimethylpyridine hydrochloride (1 g, 4.5 mmols) in deionized water (5 mL) was cooled to 0 °C in an ice bath. To this solution was added, with stirring, NaOH (180 mg, 4.5 mmols). To this mixture was then added a solution of *N,N*-bis(2-(2-pyridyl)ethylamine (1 g, 4.5 mmols) in CH_2Cl_2 (5 mL). The mixture was then allowed to warm to rt and stirred for 2 days. The crude mixture was then extracted with CH_2Cl_2 , and the organic phase was dried with MgSO_4 , filtered, and dried under reduced pressure. The resulting oil was purified by column chromatography on silica (CH_2Cl_2 : CH_3OH : NEt_3 in 9:1:0.1 was used as eluent) to yield a brownish solid. (0.89 g, 54 %). ^1H NMR (400 MHz, CDCl_3): δ 8.41 (d, 2 H), 8.10 (s, 1 H), 7.47 (t, 2 H), 7.03-6.98 (m, 4 H), 3.78 (s, 2 H), 3.65 (s, 3 H), 2.97-2.90 (m, 8 H), 2.18 (s, 3 H), 1.99 (s, 3 H). ^{13}C NMR (100 MHz, CDCl_3): δ 164.03, 160.78, 157.16, 149.05, 149.04, 148.19, 148.16, 136.18, 136.13, 126.52, 125.13, 123.29, 120.99, 59.86, 53.70, 45.92, 35.33, 13.31, 13.27, 10.60, 10.58, 9.17, 9.14.

2.4.2.3 Synthesis of Nickel Complexes

Ni(tpa): The complex was synthesized following a reported procedure described by Itoh and co-workers.⁵⁶ The desired complex was obtained as purple crystals in 25% yield. Spectral properties of the product agree with the literature data. ATR-IR: ν [cm^{-1}]: 1604.58, 1557.75, 1416.87 (COO⁻), 730.89, 705.23 (BPh₄⁻). HRMS (FAB⁺): m/z 407.1003 [M-BPh₄-H₂O]⁺, calcd for C₂₀H₂₁N₄NiO₂ 407.1018.

Ni(tepa): The complex was synthesized following a reported procedure described Itoh and co-workers.⁵⁷ The desired complex was obtained as a pale blue precipitate in 83% yield. Spectral properties of the product agree with the literature data. ATR-IR: ν [cm^{-1}]: 1536, 1456 (OAc⁻), 733, 707 (BPh₄⁻). HRMS (FAB⁺): m/z 449.1340 [M – BPh₄]⁺, calcd for C₂₃H₂₇N₄NiO₂ 449.1487.

Ni(pmea): The complex was synthesized following a modified procedure described by Itoh and co-workers.⁵⁷ A solution of Ni^{II}(OAc)₂ 4H₂O (62.3 mg, 0.25 mmol) in 5 mL of methanol was added to a solution of the pmea (76.1 mg, 0.25 mmol) ligand in 5 mL methanol. The solution was stirred for 2 h at room temperature. NaBPh₄ (86.2 mg, 0.25 mmol) was added to the solution. The mixture was stirred for 1 h at room temperature. The purple precipitate was collected, washed with methanol, and dried (129.5 mg, 70%). Single crystals were obtained by crystallization by liquid-liquid diffusion using CH_2Cl_2 and cyclohexane. ATR-IR: ν [cm^{-1}]: 3055, 3035, 2982, 1605, 1533, 1479, 1442, 1423, 1305, 1266, 1025, 766, 730, 703, 677, 612. HRMS (FAB⁺): m/z 421.1046 [M – BPh₄]⁺, calcd for C₂₁H₂₃N₄NiO₂ 421.1175.

Ni(pmap): The complex was synthesized following a modified procedure described by Itoh and co-workers.⁵⁷ A solution of Ni^{II}(OAc)₂ 4H₂O (0.1047 g, 0.42 mmol) in 5 mL methanol was added to a solution of pmap (0.13 g, 0.42 mmol) ligand in 5 mL methanol. The solution was stirred for 2 h at rt. NaBPh₄ (0.144 g, 0.42 mmol) was added to the solution. The mixture was stirred for 1 h at room temperature. The purple precipitate was collected, washed with methanol, and dried (120.2 mg, 64%). Single crystals were obtained by crystallization by liquid-liquid diffusion using CH_2Cl_2 and cyclohexane. ATR-IR: ν [cm^{-1}]: 3571, 3054, 1880, 1606, 1540, 1444, 733, 707. HRMS (FAB⁺): m/z 435.1158 [M – BPh₄]⁺, calcd for C₂₂H₂₅N₄NiO₂ 435.1331.

Ni(6-Me₂-tpa): The complex was synthesized following a modified procedure described by Itoh and co-workers.⁵⁷ A solution of Ni^{II}(OAc)₂ 4H₂O (62.3 mg, 0.25 mmol) in 5 mL methanol was added to a solution of 6-Me₂-tpa (79.3 mg, 0.25 mmol) ligand in 5 mL methanol. The solution was stirred for 2 h

at rt. NaBPh₄ (86.2 mg, 0.25 mmol) was added to the solution. The mixture was stirred for 1 h at room temperature. The violet precipitate was collected, washed with methanol, and dried (120.2 mg, 64%). Single crystals were obtained by crystallization by liquid-liquid diffusion using CH₂Cl₂ and cyclohexane. ATR-IR: ν [cm⁻¹]: 3056, 3032, 3002, 1606, 1579, 1542, 1478, 1467, 1448, 1426, 1165, 1099, 788, 765, 742, 707, 675, 607. HRMS (FAB⁺): m/z 435.1204 [M – BPh₄]⁺, calcd for C₂₂H₂₄N₄NiO₂ 435.1331.

Ni(4-OMe-3,5-Me-pmap): The complex was synthesized following a modified procedure described by Itoh and co-workers.⁵⁷ A methanol solution (5 mL) of Ni^{II}(OAc)₂·4H₂O (62.3 mg, 0.25 mmol) was added to a methanol solution (5 mL) of the corresponding ligand (94.13 mg, 0.25 mmol) with stirring at room temperature. Color of the solution turned to violet. After stirring for 2 h, NaBPh₄ (86 mg, 0.25 mmol) was added to the mixture to give a purple precipitate, which was collected by filtration, washed with methanol, and dried (120.3 mg, 54.4 %). ATR-IR: ν [cm⁻¹]: 3055, 3040, 2998, 2981, 2920, 2870, 1578, 1570, 1606, 1538, 1478, 1455, 1445, 1402, 1385, 1361, 771, 749, 733, 703.

2.4.3 X-Ray Crystal Structure Determination of Ni Complexes

2.4.3.1 X-Ray Crystal Structure Determination of Ni(pmea)

[C₂₁H₂₃N₄NiO₂](C₂₄H₂₀B), Fw = 741.35, purple plate, 0.51 × 0.30 × 0.05 mm³, monoclinic, P2₁/n (no. 14), a = 13.4449(6), b = 15.3074(10), c = 18.2233(9) Å, β = 90.482(3) °, V = 3750.3(3) Å³, Z = 4, D_x = 1.313 g/cm³, μ = 0.56 mm⁻¹. The diffraction experiment was performed on a Bruker Kappa ApexII diffractometer with sealed tube and Triumph monochromator (λ = 0.71073 Å) at a temperature of 150(2) K up to a resolution of $(\sin \theta/\lambda)_{\max}$ = 0.65 Å⁻¹. The Eval15 software⁵⁸ was used for the intensity integration. A large anisotropic mosaicity⁵⁹ about $hkl=(1,0,1)$ was used for the prediction of the reflection profiles. A numerical absorption correction and scaling was performed with SADABS⁶⁰ (correction range 0.76-1.00). A total of 76642 reflections was measured, 8637 reflections were unique (R_{int} = 0.047), 6876 reflections were observed [$I > 2\sigma(I)$]. The structure shown in Figure 3 was solved with Patterson superposition methods using SHELXT.⁶¹

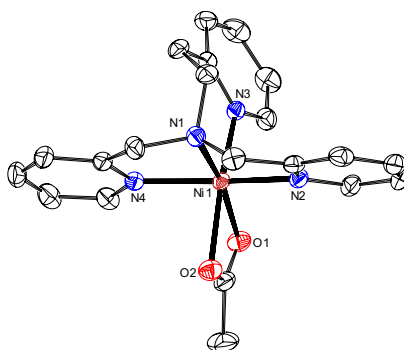


Figure 3. Displacement ellipsoid plot of the cation of Ni(pmea) (50% probability level). Hydrogen atoms and non-coordinated BPh₄ anion are omitted for clarity.

Structure refinement was performed with SHELXL-2016⁶² on F² of all reflections. Non-hydrogen atoms were refined freely with anisotropic displacement parameters. Hydrogen atoms were introduced in calculated positions and refined with a riding model. 479 Parameters were refined with no restraints. R1/wR2 [$I > 2\sigma(I)$]: 0.0333 / 0.0825. R1/wR2 [all refl.]: 0.0492 / 0.0904. S = 1.041. Residual electron

density between -0.51 and $0.51 \text{ e}/\text{\AA}^3$. Geometry calculations and checking for higher symmetry was performed with the PLATON program.⁶³

2.4.3.2 X-Ray Crystal Structure Determination of Ni(pmap)

$[\text{C}_{22}\text{H}_{25}\text{N}_4\text{NiO}_2](\text{C}_{24}\text{H}_{20}\text{B}) + \text{disordered solvent}$, $F_w = 755.38^{[*]}$, purple plate, $0.40 \times 0.25 \times 0.04 \text{ mm}^3$, triclinic, $P\bar{1}$ (no. 2), $a = 11.1742(3)$, $b = 12.4629(3)$, $c = 15.8917(4) \text{ \AA}$, $\alpha = 74.394(1)$, $\beta = 88.801(1)$, $\gamma = 71.060(1)^\circ$, $V = 2010.78(8) \text{ \AA}^3$, $Z = 2$, $D_x = 1.248 \text{ g/cm}^{3[*]}$, $\mu = 0.53 \text{ mm}^{-1[*]}$. The diffraction experiment was performed on a Bruker Kappa ApexII diffractometer with sealed tube and Triumph monochromator ($\lambda = 0.71073 \text{ \AA}$) at a temperature of $150(2) \text{ K}$ up to a resolution of $(\sin \theta/\lambda)_{\text{max}} = 0.65 \text{ \AA}^{-1}$. The Eval15 software⁵⁸ was used for the intensity integration. A multiscan absorption correction and scaling was performed with SADABS⁶⁰ (correction range 0.66-0.75). A total of 46938 reflections was measured, 9240 reflections were unique ($R_{\text{int}} = 0.034$), 7636 reflections were observed [$I > 2\sigma(I)$]. The structure shown in Figure 4 was solved with Patterson superposition methods using SHELXT.⁶¹ Structure refinement was performed with SHELXL-2016⁶² on F^2 of all reflections. The crystal structure contains large voids ($146 \text{ \AA}^3/\text{unit cell}$) filled with severely disordered cyclohexane/ CH_2Cl_2 molecules. Their contribution to the structure factors was secured by the SQUEEZE algorithm⁶⁴ resulting in 46 electrons / unit cell. The *pmap* ligand was refined with a disorder model involving two coordination modes (Figure S2). The major disorder form (82.0(3) % occupancy) was refined with anisotropic displacement parameters. The nitrogen atoms of the minor disorder component (18.0(3) % occupancy) were constrained to the major form. The carbon atoms of the minor disorder component were refined with isotropic displacement parameters. Hydrogen atoms were introduced in calculated positions and refined with a riding model. 581 Parameters were refined with 88 restraints (distances, angles and molecular flatness in modelling the disorder). $R1/wR2 [I > 2\sigma(I)]: 0.0334 / 0.0788$. $R1/wR2 [\text{all refl.}]: 0.0451 / 0.0831$. $S = 1.027$. Residual electron density between -0.32 and $0.37 \text{ e}/\text{\AA}^3$. Geometry calculations and checking for higher symmetry was performed with the PLATON program.⁶³

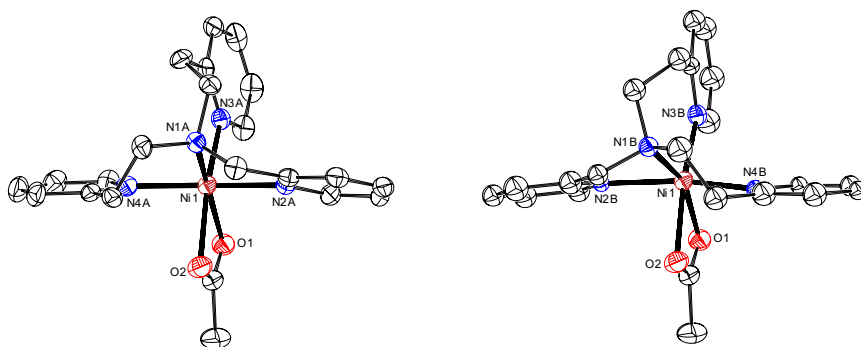


Figure 4. Displacement ellipsoid plot of the cation of **Ni(pmap)** (50% probability level). The major disorder form (82.0(3) % occupancy) is drawn on the left, the minor form (18.0(3) % occupancy) on the right. Carbon atoms of the minor disorder form were refined with isotropic displacement parameters. Hydrogen atoms,

* Derived values do not contain the contribution of the disordered solvent molecules.

non-coordinated BPh₄ anion and severely disordered cyclohexane/CH₂Cl₂ solvent molecules are omitted for clarity.

2.4.3.3 X-Ray Crystal Structure Determination of Ni(6-Me₂-tpa)

[C₂₂H₂₅N₄NiO₂](C₂₄H₂₀B), Fw = 755.38, purple plate, 0.51 × 0.48 × 0.08 mm³, monoclinic, P2₁/n (no. 14), a = 18.4021(7), b = 10.0723(5), c = 21.3918(8) Å, β = 91.333(2) °, V = 3963.9(3) Å³, Z = 4, D_x = 1.266 g/cm³, μ = 0.53 mm⁻¹. The diffraction experiment was performed on a Bruker Kappa ApexII diffractometer with sealed tube and Triumph monochromator (λ = 0.71073 Å) at a temperature of 150(2) K up to a resolution of (sin θ/λ)_{max} = 0.65 Å⁻¹. The Eval15 software⁵⁸ was used for the intensity integration. A numerical absorption correction and scaling was performed with SADABS⁶⁰ (correction range 0.82-0.97). A total of 87732 reflections was measured, 9094 reflections were unique (R_{int} = 0.047), 7865 reflections were observed [I > 2σ(I)]. The structure shown in Figure 5 was solved with Patterson superposition methods using SHELXT.⁶¹ Structure refinement was performed with SHELXL-2016⁶² on F² of all reflections. Non-hydrogen atoms were refined freely with anisotropic displacement parameters. All hydrogen atoms were located in difference Fourier maps and refined with a riding model. 490 Parameters were refined with no restraints. R1/wR2 [I > 2σ(I)]: 0.0351 / 0.0938. R1/wR2 [all refl.]: 0.0419 / 0.0974. S = 1.028. Residual electron density between -0.31 and 0.81 e/Å³. Geometry calculations and checking for higher symmetry was performed with the PLATON program.⁶³

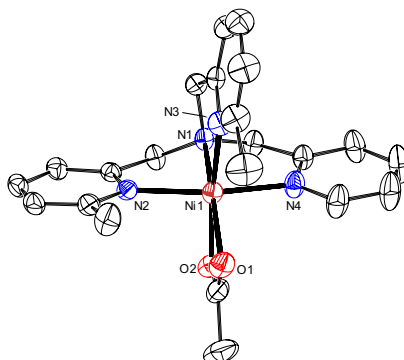


Figure 5. Displacement ellipsoid plot of the cation of Ni(6-Me₂-tpa) (50% probability level). Hydrogen atoms and non-coordinated BPh₄ anion are omitted for clarity.

2.4.4 Reaction Protocol for Catalytic Studies

2.4.4.1 General Procedure for Catalytic Hydroxylation Reaction.

In a pressurized reaction vessel, the nickel complex (4 μmol, 10 mol%) was dissolved in 1 mL of the corresponding solvent. Then, triethylamine (0.2 mL of stock solution 0.2 M, 40 μmol) and benzene (0.4 mL of stock solution 0.1 M, 40 μmol) were added. Aqueous commercial solution of hydrogen peroxide (0.5 mL of 35% aqueous H₂O₂, 5.7 mmol) was added directly under constant stirring, which was stirred for 5 h at 60 °C. After the catalytic reaction, the crude mixture was cooled to rt using an ice bath and nitrobenzene was added as internal standard (20 μmols). Then, the nickel catalyst was removed by column chromatography on silica, and then magnesium sulfate was added to remove the water from the solution. The reaction mixture was analyzed by GC analysis. Reported analysis data represent the outcome of at least two independent catalysis experiments. All peaks of interest were identified by comparison of the retention times and co-injection with the authentic samples. The products were

quantified by comparison against a known amount of internal standard using a calibration curve consisting of a plot of mole ratio (moles of organic compound/moles of internal standard) versus area ratio (area of organic compound/area of internal standard).

Author Contribution

E.M-R. and R.K.G devised the project and designed experiments. E.M-R. performed the experiments. R.M.H. and J.K. performed the synthesis of some aminopyridine ligands and nickel complexes. M.L. performed X-ray analysis. E.M-R. wrote the Chapter and R.K.G. provided comments on the experiments and Chapter content.

2.5 References

1. Arakawa, H.; Aresta, M.; Armor, J. N.; Barteau, M. A.; Beckman, E. J.; Bell, A. T.; Bercaw, J. E.; Creutz, C.; Dinjus, E.; Dixon, D. A.; Domen, K.; DuBois, D. L.; Eckert, J.; Fujita, E.; Gibson, D. H.; Goddard, W. A.; Goodman, D. W.; Keller, J.; Kubas, G. J.; Kung, H. H.; Lyons, J. E.; Manzer, L. E.; Marks, T. J.; Morokuma, K.; Nicholas, K. M.; Periana, R.; Que, L.; Rostrup-Nielson, J.; Sachtler, W. M. H.; Schmidt, L. D.; Sen, A.; Somorjai, G. A.; Stair, P. C.; Stults, B. R.; Tumas, W., Catalysis Research of Relevance to Carbon Management: Progress, Challenges, and Opportunities. *Chem. Rev.* **2001**, *101* (4), 953-996.
2. Punniyamurthy, T.; Velusamy, S.; Iqbal, J., Recent Advances in Transition Metal Catalyzed Oxidation of Organic Substrates with Molecular Oxygen. *Chem. Rev.* **2005**, *105* (6), 2329-2363.
3. Weber, M.; Weber, M.; Kleine-Boymann, M., In *Ullmann's Encyclopedia of Industrial Chemistry*, Wiley-VCH: Weinheim, Germany, 2004; pp 503-519.
4. Fukuzumi, S.; Ohkubo, K., One-Step Selective Hydroxylation of Benzene to Phenol. *Asian J. Org. Chem.* **2015**, *4* (9), 836-845.
5. Genovino, J.; Sames, D.; Hamann, L. G.; Touré, B. B., Accessing Drug Metabolites via Transition-Metal Catalyzed C–H Oxidation: The Liver as Synthetic Inspiration. *Angew. Chem. Int. Ed.* **2016**, *55* (46), 14218-14238.
6. Sheldon, R. A.; Kochi, J. K., In *Metal-Catalyzed Oxidations of Organic Compounds*, Academic Press, New York, 1981; pp 315-339.
7. Schmidt, R. J., Industrial catalytic processes—phenol production. *Appl. Catal. A.* **2005**, *280* (1), 89-103.
8. Luo, Y.-R., *Comprehensive Handbook of Chemical Bond Energies*. CRC Press: Boca Raton, FL, 2007.
9. Yuan, C.; Liang, Y.; Hernandez, T.; Berriochoa, A.; Houk, K. N.; Siegel, D., Metal-free oxidation of aromatic carbon–hydrogen bonds through a reverse-rebound mechanism. *Nature* **2013**, *499* (7457), 192-196.
10. Hage, J. P.; Llobet, A.; Sawyer, D. T., Aromatic hydroxylation by fenton reagents {Reactive intermediate $[L_x^+ Fe^{III}OOH (BH^+)]$, not free hydroxyl radical (HO•)}. *Bioorganic Med. Chem.* **1995**, *3* (10), 1383-1388.
11. Costas, M.; Chen, K.; Que Jr, L., Biomimetic nonheme iron catalysts for alkane hydroxylation. *Coord. Chem. Rev.* **2000**, *200*, 517-544.

12. Lyakin, O. Y.; Zima, A. M.; Tkachenko, N. V.; Bryliakov, K. P.; Talsi, E. P., Direct Evaluation of the Reactivity of Nonheme Iron(V)–Oxo Intermediates toward Arenes. *ACS Catal.* **2018**, *8* (6), 5255-5260.
13. Tkachenko, N. V.; Ottenbacher, R. V.; Lyakin, O. Y.; Zima, A. M.; Samsonenko, D. G.; Talsi, E. P.; Bryliakov, K. P., Highly Efficient Aromatic C–H Oxidation with H₂O₂ in the Presence of Iron Complexes of the PDP Family. *ChemCatChem* **2018**, *10* (18), 4052-4057.
14. Zima, A. M.; Lyakin, O. Y.; Lubov, D. P.; Bryliakov, K. P.; Talsi, E. P., Aromatic C–H oxidation by non-heme iron(V)-oxo intermediates bearing aminopyridine ligands. *Mol. Catal.* **2020**, *483*, 110708.
15. Capocasa, G.; Olivo, G.; Barbieri, A.; Lanzalunga, O.; Di Stefano, S., Direct hydroxylation of benzene and aromatics with H₂O₂ catalyzed by a self-assembled iron complex: evidence for a metal-based mechanism. *Catal. Sci. Technol.* **2017**, *7* (23), 5677-5686.
16. Tsuji, T.; Zaoputra, A. A.; Hitomi, Y.; Mieda, K.; Ogura, T.; Shiota, Y.; Yoshizawa, K.; Sato, H.; Kodera, M., Specific Enhancement of Catalytic Activity by a Dicopper Core: Selective Hydroxylation of Benzene to Phenol with Hydrogen Peroxide. *Angew. Chem. Int. Ed.* **2017**, *129* (27), 7887-7890.
17. Muthuramalingam, S.; Anandababu, K.; Velusamy, M.; Mayilmurugan, R., Benzene Hydroxylation by Bioinspired Copper(II) Complexes: Coordination Geometry versus Reactivity. *Inorg. Chem.* **2020**, *59* (9), 5918-5928.
18. Morimoto, Y.; Bunno, S.; Fujieda, N.; Sugimoto, H.; Itoh, S., Direct hydroxylation of benzene to phenol using hydrogen peroxide catalyzed by nickel complexes supported by pyridylalkylamine ligands. *J. Am. Chem. Soc.* **2015**, *137* (18), 5867-5870.
19. Muthuramalingam, S.; Anandababu, K.; Velusamy, M.; Mayilmurugan, R., One step phenol synthesis from benzene catalysed by nickel(II) complexes. *Catal. Sci. Technol.* **2019**, *9* (21), 5991-6001.
20. Que Jr, L.; Tolman, W. B., Biologically inspired oxidation catalysis. *Nature* **2008**, *455* (7211), 333.
21. Olivo, G.; Cussó, O.; Costas, M., Biologically Inspired C–H and C=C Oxidations with Hydrogen Peroxide Catalyzed by Iron Coordination Complexes. *Chem. Asian J.* **2016**, *11* (22), 3148-3158.
22. Oh, N. Y.; Seo, M. S.; Lim, M. H.; Consugar, M. B.; Park, M. J.; Rohde, J.-U.; Han, J.; Kim, K. M.; Kim, J.; Que Jr, L., Self-hydroxylation of perbenzoic acids at a nonheme iron(II) center. *Chem. Commun.* **2005**, (45), 5644-5646.
23. Taktak, S.; Flook, M.; Foxman, B. M.; Que Jr, L.; Rybak-Akimova, E. V., *ortho*-Hydroxylation of benzoic acids with hydrogen peroxide at a non-heme iron center. *Chem. Commun.* **2005**, (42), 5301-5303.
24. Makhlynets, O. V.; Rybak-Akimova, E. V., Aromatic Hydroxylation at a Non-Heme Iron Center: Observed Intermediates and Insights into the Nature of the Active Species. *Chem. Eur. J.* **2010**, *16* (47), 13995-14006.
25. Olivo, G.; Lanzalunga, O.; Di Stefano, S., Non-Heme Imine-Based Iron Complexes as Catalysts for Oxidative Processes. *Adv. Synth. Catal.* **2016**, *358* (6), 843-863.
26. Dantignana, V.; Milan, M.; Cussó, O.; Company, A.; Bietti, M.; Costas, M., Chemoselective Aliphatic C–H Bond Oxidation Enabled by Polarity Reversal. *ACS Cent. Sci.* **2017**, *3* (12), 1350-1358.
27. Ottenbacher, R. V.; Talsi, E. P.; Rybalova, T. V.; Bryliakov, K. P., Enantioselective Benzylic Hydroxylation of Arylalkanes with H₂O₂ in Fluorinated Alcohols in the Presence of Chiral Mn Aminopyridine Complexes. *ChemCatChem* **2018**, *10* (22), 5323-5330.

28. Wang, D.; Shuler, W. G.; Pierce, C. J.; Hilinski, M. K., An iminium salt organocatalyst for selective aliphatic C–H hydroxylation. *Org. Lett.* **2016**, *18* (15), 3826-3829.
29. Gaster, E.; Kozuch, S.; Pappo, D., Selective Aerobic Oxidation of Methylarenes to Benzaldehydes Catalyzed by N-Hydroxyphthalimide and Cobalt(II) Acetate in Hexafluoropropan-2-ol. *Angew. Chem. Int. Ed.* **2017**, *56* (21), 5912-5915.
30. Adams, A. M.; Du Bois, J., Organocatalytic C–H hydroxylation with Oxone® enabled by an aqueous fluoroalcohol solvent system. *Chem. Sci.* **2014**, *5* (2), 656-659.
31. Cussó, O.; Garcia-Bosch, I.; Ribas, X.; Lloret-Fillol, J.; Costas, M., Asymmetric epoxidation with H₂O₂ by manipulating the electronic properties of non-heme iron catalysts. *J. Am. Chem. Soc.* **2013**, *135* (39), 14871-14878.
32. Cussó, O.; Cianfanelli, M.; Ribas, X.; Klein Gebbink, R. J. M.; Costas, M., Iron catalyzed highly enantioselective epoxidation of cyclic aliphatic enones with aqueous H₂O₂. *J. Am. Chem. Soc.* **2016**, *138* (8), 2732-2738.
33. Cussó, O.; Garcia-Bosch, I.; Font, D.; Ribas, X.; Lloret-Fillol, J.; Costas, M., Highly stereoselective epoxidation with H₂O₂ catalyzed by electron-rich aminopyridine manganese catalysts. *Org. Lett.* **2013**, *15* (24), 6158-6161.
34. Milan, M.; Carboni, G.; Salamone, M.; Costas, M.; Bietti, M., Tuning Selectivity in Aliphatic C–H Bond Oxidation of N-Alkylamides and Phthalimides Catalyzed by Manganese Complexes. *ACS Catal.* **2017**, *7* (9), 5903-5911.
35. Mlondo, S. N.; O'Brien, P.; Thomas, P. J.; Helliwell, M.; Raftery, J.; Procter, D. J., Methanolysis of tetraphenylborate (BPh₄) as a reaction unit in halotris (2,4-pentadecanato) complexes of Zr(IV) and Hf (IV). *Chem. Commun.* **2008**, (21), 2456-2458.
36. Grisdale, P. J.; Williams, J. L.; Glogowski, M.; Babb, B., Boron photochemistry. Possible role of bridged intermediates in the photolysis of borate complexes. *J. Org. Chem.* **1971**, *36* (4), 544-549.
37. Ross, S. D., The rate of oxidation of thiodiglycol and triethylamine by hydrogen peroxide. *J. Am. Chem. Soc.* **1946**, *68* (8), 1484-1485.
38. Gee, J.; Williamson, R., Kinetics of hydrogen peroxide oxidation of alkyl dimethyl amines. *J. Am. Oil Chem. Soc.* **1997**, *74* (1), 65-67.
39. Chen, M. S.; White, M. C., A predictably selective aliphatic C–H oxidation reaction for complex molecule synthesis. *Science* **2007**, *318* (5851), 783-787.
40. Suzuki, K.; Oldenburg, P. D.; Que Jr, L., Iron-Catalyzed Asymmetric Olefin *cis*-Dihydroxylation with 97% Enantiomeric Excess. *Angew. Chem. Int. Ed.* **2008**, *47* (10), 1887-1889.
41. Morimoto, Y.; Takagi, Y.; Saito, T.; Ohta, T.; Ogura, T.; Tohnai, N.; Nakano, M.; Itoh, S., A Bis(μ -oxido)dinickel(III) Complex with a Triplet Ground State. *Angew. Chem. Int. Ed.* **2018**, *57* (26), 7640-7643.
42. Lide, D. R., *Handbook of Chemistry and Physics*. CRC Press, Boca Raton, FL: 2005.
43. Filler, R.; Schure, R. M., Highly acidic perhalogenated alcohols. A new synthesis of perfluoro-tert-butyl alcohol. *J. Org. Chem.* **1967**, *32* (4), 1217-1219.
44. Riddick, J.; Bunger, W.; Sakano, T., In *Techniques of Chemistry* 4th ed., Volume II. Organic Solvents. New York, NY: John Wiley and Sons, 1985; p 638.

45. Neimann, K.; Neumann, R., Electrophilic activation of hydrogen peroxide: selective oxidation reactions in perfluorinated alcohol solvents. *Org. Lett.* **2000**, *2* (18), 2861-2863.
46. Metelitsa, D. I., Mechanisms of the hydroxylation of aromatic compounds. *Russ. Chem. Rev.* **1971**, *40* (7), 563.
47. Walling, C.; Johnson, R. A., Fenton's reagent. V. Hydroxylation and side-chain cleavage of aromatics. *J. Am. Chem. Soc.* **1975**, *97* (2), 363-367.
48. Kunai, A.; Hata, S.; Ito, S.; Sasaki, K., The role of oxygen in the hydroxylation reaction of benzene with Fenton's reagent. Oxygen 18 tracer study. *J. Am. Chem. Soc.* **1986**, *108* (19), 6012-6016.
49. Kurata, T.; Watanabe, Y.; Katoh, M.; Sawaki, Y., Mechanism of aromatic hydroxylation in the Fenton and related reactions. One-electron oxidation and the NIH shift. *J. Am. Chem. Soc.* **1988**, *110* (22), 7472-7478.
50. Leaver, S. A.; Palaniandavar, M.; Kilner, C. A.; Halcrow, M. A., A new synthesis of bis(2-(pyrid-2-yl)ethyl)amine (L^H) from bis(2-(pyrid-2-yl)ethyl)hydroxylamine (L^{OH}), and the copper-dependent reduction of L^{OH} to L^H . *Dalton Trans.* **2003**, (22), 4224-4225.
51. Li, H.-Y.; Chen, C.-Y.; Cheng, H.-T.; Chu, Y.-H., Exploiting 1,2,3-triazolium ionic liquids for synthesis of tryptanthrin and chemoselective extraction of copper(II) ions and histidine-containing peptides. *Molecules* **2016**, *21* (10), 1355.
52. Wang, J.; Li, C.; Zhou, Q.; Wang, W.; Hou, Y.; Zhang, B.; Wang, X., Photocatalytic hydrogen evolution by Cu (II) complexes. *Dalton Trans.* **2016**, *45* (13), 5439-5443.
53. Alilou, E.; Hallaoui, A.; Ghadraoui, E.; Giorgi, M.; Pierrot, M.; Reglier, M., Two TEPA-Copper(II) Complexes {TEPA is Tris[2-(2-pyridyl)ethyl]amine}. *Acta Crystallogr. C* **1997**, *53* (5), 559-562.
54. Lonnon, D. G.; Craig, D. C.; Colbran, S. B., Rhodium, palladium and platinum complexes of tris(pyridylalkyl)amine and tris(benzimidazolylmethyl)amine N_4 -tripodal ligands. *Dalton Trans.* **2006**, (31), 3785-3797.
55. Kisslinger, S.; Kelm, H.; Zheng, S.; Beitat, A.; Würtele, C.; Wortmann, R.; Bonnet, S.; Herres-Pawlis, S.; Krüger, H. J.; Schindler, S., Synthesis and Characterization of Iron(II) Thiocyanate Complexes with Derivatives of the Tris(pyridine-2-ylmethyl)amine (tmpa) Ligand. *Z. Anorg. Allg. Chem* **2012**, *638* (12-13), 2069-2077.
56. Nagataki, T.; Tachi, Y.; Itoh, S., Ni^{II} (TPA) as an efficient catalyst for alkane hydroxylation with *m*-CPBA. *Chem. Commun.* **2006**, (38), 4016-4018.
57. Nagataki, T.; Ishii, K.; Tachi, Y.; Itoh, S., Ligand effects on Ni^{II} -catalysed alkane-hydroxylation with *m*-CPBA. *Dalton Trans.* **2007**, (11), 1120-1128.
58. Schreurs, A. M.; Xian, X.; Kroon-Batenburg, L. M., EVAL15: a diffraction data integration method based on ab initio predicted profiles. *J. Appl. Cryst.* **2010**, *43* (1), 70-82.
59. Duisenberg, A. J., Diffractometry and reflection profiles of anisotropic mosaic and split crystals. *Acta Cryst.* **1983**, *A39* (2), 211-216.
60. Sheldrick, G. M., (2014). SADABS. Universität of Göttingen, Germany.
61. Sheldrick, G. M., SHELXT-Integrated space-group and crystal-structure determination. *Acta Cryst.* **2015**, *A71* (1), 3-8.

62. Sheldrick, G. M., Crystal structure refinement with SHELXL. *Acta Cryst.* **2015**, *C71* (1), 3-8.
63. Spek, A. L., Structure validation in chemical crystallography. *Acta Cryst.* **2009**, *D65* (2), 148-155.
64. Spek, A. L., PLATON SQUEEZE: a tool for the calculation of the disordered solvent contribution to the calculated structure factors. *Acta Cryst.* **2015**, *C71* (1), 9-18.

Chapter 3

Aromatic C–H Hydroxylation Reactions with Hydrogen Peroxide Catalyzed by Bulky Manganese Complexes

Abstract

The oxidation of aromatic substrates to phenols with H₂O₂ as a benign oxidant remains an ongoing challenge in synthetic chemistry. Herein, we successfully achieved to catalyze aromatic C–H bond oxidations using a series of biologically inspired manganese catalysts in fluorinated alcohol solvents. While introduction of bulky substituents into the ligand structure of the catalyst favors aromatic C–H oxidations in alkylbenzenes, oxidation occurs at the benzylic position with ligands bearing electron-rich substituents. Therefore, the nature of the ligand is key in controlling the chemoselectivity of these Mn-catalyzed C–H oxidations. We show that introduction of bulky groups into the ligand prevents catalyst inhibition through phenolate-binding, consequently providing higher catalytic turnover numbers for phenol formation. Furthermore, employing halogenated carboxylic acids in the presence of bulky catalysts provides enhanced catalytic activities, which can be attributed to their low pK_a's that reduces catalyst inhibition by phenolate protonation as well as to their electron-withdrawing character that makes the manganese oxo species a more electrophilic oxidant. Moreover, to the best of our knowledge, the new system can accomplish the oxidation of alkylbenzenes with the highest yields so far reported for homogeneous arene hydroxylation catalysts. Overall our data provide a proof-of-concept of how Mn(II)/H₂O₂/RCO₂H oxidation systems are easily tunable by means of the solvent, carboxylic acid additive, and steric demand of the ligand. The chemo- and site-selectivity patterns of the current system, a negligible KIE, the observation of an NIH-shift, and the effectiveness of using ^tBuOOH as oxidant overall suggest that hydroxylation of aromatic C–H bonds proceeds through a metal-based mechanism, with no significant involvement of hydroxyl radicals, and via an arene oxide intermediate.

This chapter is based on:

Masferrer-Rius, E.; Borrell, M.; Lutz, M.; Costas, M.; Klein Gebbink, R. J. M. *Adv. Synth. Catal.* **2021**, *363*, 3783-3795

3.1 Introduction

Oxidations of organic compounds are essential reactions widely studied in academia as well as in the chemical industry. The interest mainly arises by the fact that the oxygenated organic molecules can be further used to produce different classes of valuable chemicals, such as pharmaceuticals. Despite many research efforts, the selective oxidation of organic substrates still represents a critical challenge in synthetic chemistry. For instance, the direct one-step hydroxylation of aromatic molecules to the corresponding phenols could provide easy access to relevant building blocks for more complex molecules, thereby becoming a highly desired reaction.

To date, several bioinspired iron and manganese complexes have been shown to perform aliphatic C–H oxidations¹⁻²¹ as well as olefin oxidation reactions²²⁻³⁵, whereas hydroxylation of aromatic compounds has remained an ongoing issue since recent years.³⁶⁻⁵⁴ In earlier studies, an iron complex supported by the tpa ligand (tpa = tris(2-pyridylmethyl)amine) was found to be capable of stoichiometrically oxidizing ligated perbenzoic acids through the self-hydroxylation of the aromatic ring, forming iron(III)-salicylate complexes.³⁶ Also, an iron complex based on the bpmen ligand (bpmen = *N,N'*-dimethyl-*N,N'*-bis(2-picolyl)ethylenediamine) showed activity for the hydroxylation of aromatic compounds using H₂O₂, although strong coordination of phenolates to the iron(III) center prevented efficient catalysis.^{37, 39} An iron complex supported by a *N*-heterocyclic carbene ligand has been shown to be capable of hydroxylating benzene and alkylbenzenes with H₂O₂ as well, albeit at low conversions and yields for phenol products, and with the formation of benzylic oxidized products from alkylbenzene substrates.^{40, 43} Recent research progress indicates that iron complexes supported by bpbp-type ligands (bpbp = *N,N'*-bis(2-pyridylmethyl)-2,2'-bipyrrrolidine) can hydroxylate aromatic substrates with H₂O₂.^{44, 45, 50} However, overoxidation products and modest selectivities for oxidation of the aromatic ring were observed, resulting in mixtures of products in which oxidation has taken place on aromatic as well as aliphatic positions. A manganese complex supported by the Bn-TPEN ligand (Bn-TPEN = *N*-benzyl-*N,N,N'*-tris(2-pyridylmethyl)-1,2-diaminoethane) has been found to oxidize naphthalene, among other substrates, with iodosylbenzene as oxidant.⁵¹ However, efficient catalytic turnover numbers (TON) were not achieved. Later, a manganese tpa complex incorporated into mesoporous silica-alumina was described to be active in the selective hydroxylation of benzene derivatives with H₂O₂.⁵² Interestingly, incorporation of the complex into the mesoporous support was necessary to get useful catalytic activities. Very recently, intramolecular aromatic hydroxylation, as well as intermolecular hydroxylation of benzene to phenol, has been demonstrated with an iron complex based on the Bn-TPEN ligand through O–O bond heterolysis of an Fe(III)–OOH species to form an Fe(V)=O oxidant.⁴⁹

Other transition-metal complexes have also been developed as homogeneous catalysts for aromatic C–H oxidations with H_2O_2 as the oxidant.^{55–61} Itoh *et al.* demonstrated the catalytic ability of a nickel complex supported by a tripodal tetradentate aminopyridine ligand in the direct hydroxylation of aromatics using a significant excess of oxidant (Figure 1).⁵⁵ High TONs were only achieved using extremely low concentration of catalyst under long reaction times; yet, absolute yields of phenol products do not exceed 7.5%. Remarkably though, when the complex was used at 10 mol% loading with respect to the substrate, 21% phenol yield was formed (2 turnovers per nickel).^{55, 62} Later, Kodera *et al.* described a dinuclear copper complex as catalyst for the hydroxylation of aromatics, showing good selectivities for phenol products (Figure 1).⁵⁶ Again, an elevated TON (12,550) was obtained under low catalyst concentration, with phenol yields up to 21% for benzene oxidation. Di Stefano *et al.* reported an iminopyridine iron complex capable of oxidizing aromatic substrates, as well as aromatic amino acids, under mild reaction conditions (Figure 1).^{42, 63} However, for all these examples, aromatic oxidation of alkylbenzenes is effectively accompanied by benzylic hydroxylation. In addition, recently reported nickel, copper and cobalt complexes supported by aminopyridine ligands accomplished the oxidation of benzene to phenol in improved yields (29–41%) (Figure 1).^{59–61}

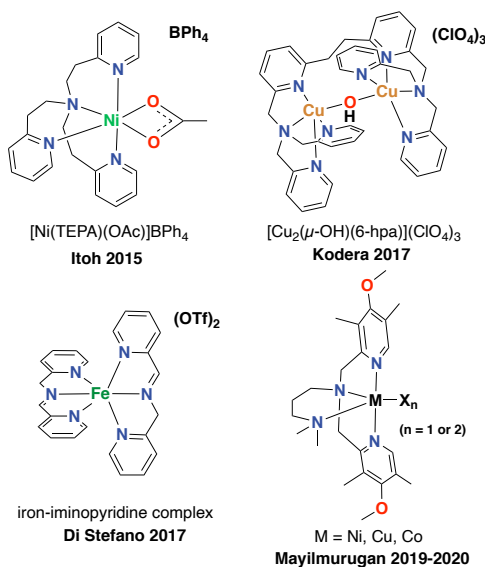


Figure 1. Examples of metal complexes previously employed in aromatic C–H hydroxylation reactions with H_2O_2 .

Previously, we have shown that bulky iron complexes with *tris*-(isopropyl)silyl (tips) moieties catalyze the site-selective oxidation of alkyl C–H bonds with H_2O_2 , affording high product yields and enhanced preferential oxidation of secondary over tertiary C–H bonds.⁹ Likewise, manganese complexes supported by aminopyridine ligands catalyze chemo- and enantioselective aliphatic C–H oxidation with H_2O_2 .^{6, 10, 11, 15–18, 20, 64–67} Recently, White *et al.* reported that a bulky manganese complex with pendant *o*- CF_3 -substituted aryl rings can oxidize

methylene groups in the presence of aromatic functionalities.²¹ The authors also report non-productive aromatic substrate oxidation as a side-reaction. Finally, fluorinated alcohols have recently been shown to be suitable solvents for oxidation chemistry, preserving the first-formed alcohol products and, thus, reducing overoxidation reactions.^{15, 64, 68-73}

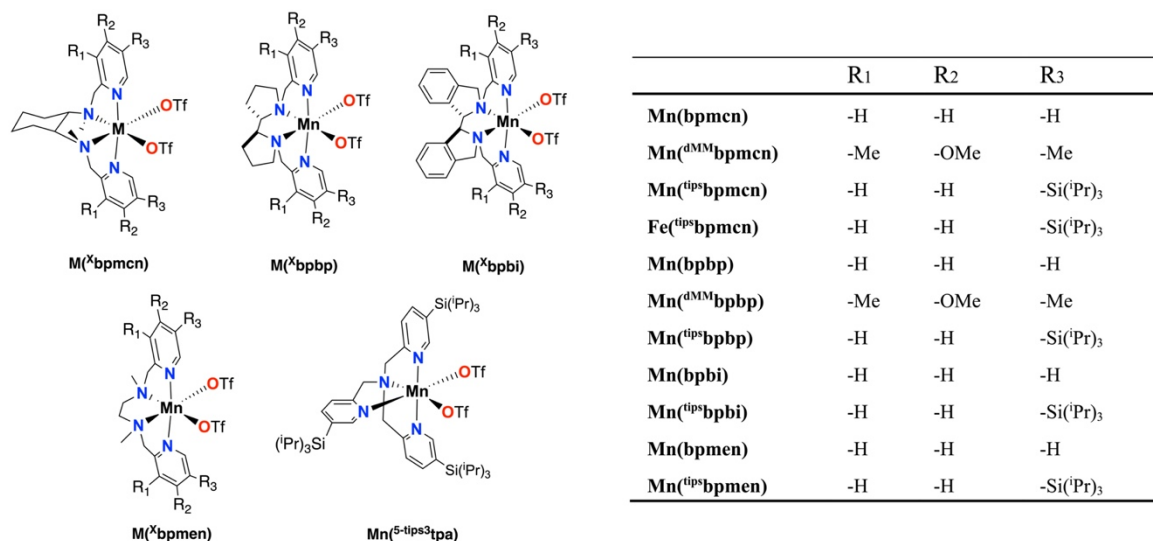
Herein, we focus on the use of bioinspired manganese complexes for the oxidation of aromatic substrates. We demonstrate that the application of bulky Mn catalysts in the presence of fluorinated alcohol solvents favors the oxidation at the aromatic ring over the oxidation of benzylic positions, providing an improved route to produce phenols. On the basis of previous literature examples which propose that product inhibition through metal-phenolate binding prevents catalytic turnover in aromatic oxidation reactions, we rationalized that the presence of bulky tips groups in position 5 of the pyridine rings may help in preventing product inhibition. Our study also shows that the yields of the aromatic reactions are further improved by using halogenated carboxylic acids as additives, which in part can be attributed to their lower pK_a 's which reduces product inhibition through a favorable acid-base equilibrium between the acetic acid and the (substituted) phenol products. Overall, our study has resulted in the development of a highly selective manganese-based catalyst system that performs arene hydroxylation reactions with H_2O_2 as a benign oxidant with improved yields of (substituted) phenol products with respect to the previously described homogeneous catalysts.

3.2 Results and Discussion

3.2.1 Aliphatic vs Aromatic C–H Oxidation

For our study we have investigated complexes of the type $[M(OTf)_2(L)]$ based on the bpmcn, bpbp, bpbi and bpmn ligand families (Scheme 1) (bpmcn = *N,N'*-dimethyl-*N,N'*-bis(2-picolyl)-cyclohexane-*trans*-1,2-diamine, bpbi = *N,N'*-bis(2-picolyl)-2,2'-bis-isoindoline). We have included manganese complexes containing electron-rich, as well as bulky pyridines.

Initially, we focused our attention on the hydroxylation of propylbenzene as substrate using 1 mol% of **Mn**(^{tips}**bpmcn**), **Mn**(^{dMM}**bpmcn**), or **Mn**(**bpmcn**) as catalyst (Table 1). Catalytic oxidation reactions were carried out by mixing the Mn(II) catalyst and AcOH (2 equiv.) into a solution of propylbenzene (1 equiv.) in TFE (TFE = 2,2,2-trifluoroethanol) at 0 °C. A sub-stoichiometric amount of aqueous H_2O_2 (0.5 equiv., 35% w/w solution) was added dropwise through a syringe pump over a period of 30 min. Interestingly, chemoselectivity was found to be largely dependent on the catalyst used. The bulky manganese complex **Mn**(^{tips}**bpmcn**) favors the oxidation at the aromatic ring, providing the *para*-phenol as the major product, together



Scheme 1. Manganese and iron complexes employed in this chapter.

with *ortho*-phenol and propyl-*p*-benzoquinone as minor products. Some 1-phenyl-1-propanol was also detected as minor product in this case, showing a ratio of aromatic:aliphatic oxidation of 7.3:1. In contrast, when the electron-rich catalyst **Mn(^{dMM}bpmcn)** was used the chemoselectivity changed completely, and preference for the oxidation at the benzylic position was observed with a ratio of aromatic:aliphatic oxidation products of 1:13.5. This observation is in agreement with previous reports on the use of electron-rich manganese complexes for asymmetric benzylic oxidations, where no aromatic oxidation products were detected.^{15, 64, 73}

Table 1. Oxidation of propylbenzene in TFE with different manganese catalysts.

Catalyst	r.s.m ^a	<i>p</i> -Phenol ^b	<i>o</i> -Phenol ^b	Quinone ^b	Alcohol ^b	Ketone ^b	MB ^c	Ratio ^d
Mn(^{tips}bpmcn)	68	9 (18)	1 (3)	2 (8)	2 (4)	n.d.	88	7.3:1
Mn(^{dMM}bpmcn)	65	1 (2)	n.d.	n.d.	12 (23)	1 (4)	85	1:13.5
Mn(bpmcn)	72	3 (6)	1 (2)	3 (11)	4 (9)	n.d.	89	2.1:1

^aRemaining starting material (r.s.m) in %. ^bYields in % with respect to substrate determined by GC against an internal standard. In parenthesis yields in % with respect to H₂O₂. Yields are calculated considering that 2 equiv. of H₂O₂ are necessary for the formation of the ketone and quinone products. ^cMass balance (MB) was calculated considering remaining starting material and all products formed, plus a percentage of substrate loss calculated with blank experiments (an average of 6% of substrate is lost): MB = (r.s.m %) + (Product Yields %) + (Substrate loss). ^dRatio (aromatic:aliphatic) = n(*p*-phenol) + n(*o*-phenol) + n(quinone) / n(alcohol) + n(ketone). n.d. = non-detected.

With the parent **Mn(bpmcn)** complex, we observed both oxidation at the aromatic ring as well as at the benzylic position in a ratio of 2.1:1, respectively, showing a slight preference for aromatic oxidation.

Worthy of note are the blue colors that progressively form in the reaction mixtures after starting the addition of H₂O₂ to the reaction mixture containing the substrate and the catalyst (**Mn(tipsbpmcn)** or **Mn(bpmcn)**). We hypothesize that these colors are charge transfer bands arising from phenolate binding to the Mn center, which in turn inhibits the catalyst and prevents further catalytic turnover.⁷⁴⁻⁷⁸ Consistent with this hypothesis, ESI-MS analysis of a mixture of **Mn(tipsbpmcn)** (1 mol%), *tert*-butylbenzene (1 equiv), AcOH (2 equiv) and H₂O₂ (1 equiv) at 0 °C in TFE showed a main peak at $m/z = 493.8060$, which corresponds to the formation of a complex ion composed of a **Mn(tipsbpmcn)** fragment and a coupled bis(phenolate) fragment ($[\text{Mn}(\text{tipsbpmcn})(\text{C}_6\text{H}_3\text{OC}(\text{CH}_3)_3)_2]^{2+}$, calcd m/z 493.8064). Importantly, the blue color was observed immediately after the start of H₂O₂ addition in the case of **Mn(bpmcn)**, whereas for the reaction with **Mn(tipsbpmcn)** the blue color appears later in the course of the reaction. These observations lead us to believe that the bulky tips groups help in preventing phenolate binding, and thus, allow for higher catalytic turnover numbers. A control experiment without an aromatic substrate did not show the appearance of the blue colors described above.

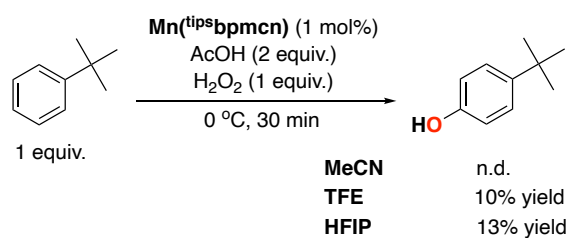
Comparing our result on arene hydroxylation catalyzed by **Mn(tipsbpmcn)** with previous literature examples, such as the systems described by Itoh⁵⁵ and Kodera⁵⁶, we can conclude that the current system performs the hydroxylation of an alkylbenzene with yields commensurate to state of the art homogeneous catalysts, at a relatively low catalyst loading. Furthermore, the nature of the ligand in the current system seems key for diverting the chemoselectivity of the catalyst from oxidation of the more activated benzylic position to the hydroxylation of the aromatic ring, showing a catalyst dependent selectivity. Yet, overall the reactions shown in Table 1 suffer from moderate conversions and yields, but do show reasonable mass balances. Noteworthy is that blank experiments without catalyst showed that a certain amount of substrate is lost during the reaction and analysis protocol (~6 %). This loss was taken into account to calculate the mass balances in Table 1.

3.2.2 Screening of Catalysts

Based on these results, we selected bulky manganese complexes with different amine backbones for further screening for the oxidation of aromatic C–H bonds (Scheme 1). A bulky iron complex, **Fe(tipsbpmcn)**, was also included in our study. The parent complexes without any substituents on the pyridines were considered as well. For all cases, the metal center adopts a C₂-symmetric *cis*- α topology, with the two pyridines *trans* to each other. A new manganese

complex supported by a bulky tripodal tetradentate ligand based on the tpa motif ($^{5\text{-tips}^3\text{tpa}}$)³⁴ was also included.

Tert-butylbenzene was used as a model substrate since it lacks benzylic C–H bonds to selectively screen for activity in aromatic oxidation. Using stoichiometric amounts of H₂O₂, crude mixtures were analyzed by GC, detecting mainly 4-*tert*-butylphenol as the oxidized product, next to unreacted substrate. Interestingly, no *ortho*-hydroxylation product was observed, which is in contrast to, *e.g.*, the oxidation of *tert*-butylbenzene catalyzed by an iminopyridine Fe(II) complex.⁴² In general, poor mass balances were observed for these reactions. We believe that a side reaction might happen, leading to overoxidized by-products, which we have not been able to identify yet. However, interest was focused here on the formation of the phenol product. First, a screening of different solvents was done (Scheme 2).



Scheme 2. Oxidation of *tert*-butylbenzene in different solvent.

Next to TFE, HFIP (HFIP = 1,1,1,3,3,3-hexafluoro-2-propanol) was found to be an appropriate solvent as well, allowing similar phenol formation as TFE. Interestingly, acetonitrile is not a suitable solvent, showing no formation of the desired phenol product. The positive effect of using fluorinated alcohol solvents may be attributed to their strong hydrogen donor ability, which decreases the nucleophilicity of the phenol, thereby allowing higher catalytic turnover numbers by hampering product inhibition. These findings inspired us to use manganese complexes in the presence of fluorinated alcohol solvents in further investigations.

Next, we proceeded to screen the different complexes shown in Scheme 1 using TFE (Table 2). Overall, complexes bearing bulky, tips-appended ligands exhibited a better catalytic activity, showing higher conversion and phenol production compared to their parent complexes. Maximum yields for the 4-*tert*-butylphenol product were obtained using **Mn(tipsbpmcn)**, **Mn(tipsbpbi)**, and **Mn(tipsbpmen)** (Table 2, entry 2, 7 and 9), whereas the other complexes show good conversions but lower yields. The current findings suggest the relevance of steric effects in aromatic hydroxylation reactions, whereas electronic effects may play a less important role. We believe that product inhibition in complexes with bulky ligands occurs to a lower extent in comparison to complexes with non-bulky ligands. Besides, iron complex **Fe(tipsbpmcn)**, supported by a bulky bpmcn ligand, provided a poor yield (Table 2, entry 3). Iron complexes

Table 2. Oxidation of *tert*-butylbenzene with H₂O₂ catalyzed by different manganese and iron complexes as catalysts.^a

Reaction scheme: *tert*-butylbenzene (1 equiv.) reacts with cat (1 mol%), AcOH (2 equiv.), and H₂O₂ (1 equiv.) in TFE at 0 °C for 30 min to produce 4-*tert*-butylphenol.

Entry	cat. (1.0 mol%)	4- <i>tert</i> -butylphenol yield (%) ^b	Conv. (%) ^b
1	Mn(bpmcn)	2	28
2	Mn(^{tips}bpmcn)	9	30
3	Fe(^{tips}bpmcn)	2	27
4	Mn(bpbp)	1	28
5	Mn(^{tips}bpbp)	4	38
6	Mn(bpbi)	2	35
7	Mn(^{tips}bpbi)	8	41
8	Mn(bpmen)	2	26
9	Mn(^{tips}bpmen)	9	43
10	Mn(^{dMM}bpbp)	1	30
11	Mn(^{5-tips}3tpa)	1	25
12	Mn(OTf)₂	n.d.	6
13	-	n.d.	10

^aReaction conditions: Mn-cat. : H₂O₂ : substrate : HOAc = 1 : 100 : 100 : 200, in TFE at 0°C. ^bConversion and yields determined from crude reaction mixtures by GC. n.d. = non-detected.

with N4 ligands have been reported as catalysts for aromatic oxidation by Bryliakov and co-workers.^{45, 46} Yet, we believe that product inhibition in these catalysts through phenolate-ironcoordination is more prominent than with our manganese complexes, which translates in much low catalytic efficiency for the iron catalysts. Accordingly, we focused our study exclusively on the use of manganese complexes as catalysts. Complex **Mn(^{5-tips}3tpa)**, which bears a sterically encumbered tripodal tetradentate aminopyridine ligand based on the tpa scaffold, also provided a poor 4-*tert*-butylphenol yield (Table 2, entry 11); indicating that the use of linear tetradentate aminopyridine ligands with a *cis-α* topology seems preferred over the use of tripodal ligands. Manganese triflate was also tested as catalyst, showing no reaction.

Catalyst **Mn(^{tips}bpmcn)** was then chosen for further reaction optimization (Table 3) since it showed the better selectivity for phenol production. Different reaction temperatures, reaction times, catalyst loadings, equiv. of H₂O₂ and additives were tested. However, at this point yields for phenol product were still modest (up to 15 % yield).

Table 3. Optimization of reaction conditions for the oxidation of *tert*-butylbenzene using catalyst $\text{Mn}(\text{t}^{\text{ips}}\text{bpmcn})$.^a

Entry	Catalyst loading (mol%)	Solvent	H ₂ O ₂ (equiv)	Reaction time (min.)	temp. (°C)	Conversion (%) ^b	Yield Phenol (%) ^b
1	1	TFE	1	30	0	29.8	9.1
2	1	TFE	1	30	-30	55.2	12.8
3 ^c	1	TFE	1	30	-30	52.8	10.9
4 ^d	1	TFE	1	30	-30	0	n.d.
5	1	TFE	3	30	-30	58.7	2.9
6	1	TFE	5	30	-30	72.8	2.9
7 ^e	1	TFE	1	30	-30	53.1	14.2
8 ^e	1	TFE	1	30	-30	26.6	7.4
9 ^e	0.5	TFE	1	30	-30	52.9	12.9
10 ^e	2	TFE	1	30	-30	56.1	14.6
11 ^e	1	TFE	1	60	-30	53.1	15.1

^aReaction conditions: Mn-cat. : H₂O₂ : substrate : HOAc = 1 : 100 : 100 : 200, 0°C, oxidant added by syringe pump over 30 minutes. Total reaction volume of 2 mL. ^bConversion and yields determined from crude reaction mixtures by GC. ^cTriflic acid was used as additive (0.1 mol%). ^dSc(OTf)₃ was used as additive (5 equiv). ^eTotal reaction volume of 2 mL instead of 0.5 mL. n.d. = non-detected.

3.2.3 Carboxylic Acid Additives

Carboxylic acids have been investigated in detail as additives in H₂O₂-mediated oxidation catalysis. We found that very low phenol product formation was observed when the oxidation of *tert*-butylbenzene was run without the addition of any carboxylic acid, showing that this additive is crucial for reactivity (Table 4, entry 1). As previously discussed in the literature catalysis might proceed through a “carboxylic acid-assisted” pathway, in which the acid helps in the heterolytic cleavage of the O–O bond of a Mn(III) hydroperoxo intermediate to form a Mn(V) oxo species, responsible for the oxidation of the aromatic substrate.^{13, 79–82} Alternatively, the acid could also help in C–H bond activation, as in acetate-assisted C–H activation with palladium.^{83–85} Since introduction of bulky substituents in the ligand has been found to be a key feature in order to obtain catalytic turnover, several bulkier carboxylic acids were tested. Carboxylic acids with longer alkyl chains, *i.e.* propionic acid and butyric acid, showed low phenol formation compared to acetic acid (Table 4, entries 3 and 4). When bulkier carboxylic acids such as isobutyric acid, pivalic acid, and 2-ethylhexanoic acid were tested, yields for the

Table 4. Oxidation of *tert*-butylbenzene in HFIP using different carboxylic acids.^a

Entry	Carboxylic acid	4- <i>tert</i> -butylphenol yield (%) ^b
1	-	4
2	Acetic acid	13
3	Propionic acid	6
4	Butyric acid	6
5	Isobutyric acid	3
6	Pivalic acid	1
7	2-ethylhexanoic acid	5
8	Chloroacetic acid	26
9	Dichloroacetic acid	29
10	Trichloroacetic acid	2
11	Fluoroacetic acid	26
12	Difluoroacetic acid	21
13	Trifluoroacetic acid	n.d.
14	Iodoacetic acid	6
15	<i>N,N</i> -dimethylglycine	2
16	2-nitrobenzoic acid	23
17	3-nitrobenzoic acid	25

^aReaction conditions: **Mn**(^{tip}**bp**m^{cn}) : H₂O₂ : substrate : RCO₂H = 1 : 100 : 100 : 200, in HFIP at 0 °C.
^bConversion and yields determined from crude reaction mixtures by GC. n.d. = non-detected.

desired oxidized product also decreased (Table 4, entries 5, 6 and 7). Therefore, our findings show that the introduction of bulk into the carboxylic acid additive decreases product formation. Similar trends were observed when either HFIP or TFE were used as solvent (Table 5).

Next, we considered the use of halogenated carboxylic acids, which have been used previously in oxidation reactions.^{21, 67, 86} Interestingly, we have found that chloroacetic acid, dichloroacetic acid, fluoroacetic acid, and difluoroacetic acid afford a significant increase in yield for the desired phenol product, with up to 29% 4-*tert*-butylphenol yield (Table 4, entry 9). The reason of this improvement could be related to the pK_a of the carboxylic acids, which varies significantly within the series of tested aliphatic carboxylic acids. The role of the lower pK_a of these carboxylic acids in arene hydroxylation reactions could be twofold. First, it keeps the phenol products protonated, which hampers catalyst deactivation by phenolate binding. Second, the electron-withdrawing character of these acids makes the proposed Mn(V) oxo species more electrophilic, which may result in a more reactive oxidant towards arenes. The use of nitrobenzoic acids also lead to increased phenol formation compared to the use of acetic

acid. However, in these cases side-product formation through arene hydroxylation of the nitrobenzoic acid was observed. In the presence of halogenated carboxylic acids higher catalytic activities were achieved in HFIP compared to TFE (Table 4 and 5).

Table 5. Oxidation of *tert*-butylbenzene in TFE using different carboxylic acids.^a

Entry	Carboxylic acid	Conversion (%) ^b	Yield Phenol (%) ^b
1	-	6.8	n.d.
2	Formic acid	20.5	8.2
3	Acetic acid	53.1	14.2
4	Propionic acid	45.2	7.1
5	Butyric acid	52.5	6.1
6	2,2-Dimethylbutyric acid	46.2	2.8
7	3,3-Dimethylbutyric acid	37.5	3.6
8	2-Ethylhexanoic acid	41.8	4.0
9	Isobutyric acid	48.1	4.1
10	Pivalic acid	50.7	3.5
11	Chloroacetic acid	53.9	23.5
12	Dichloroacetic acid	52.1	24.7
13 ^c	Trichloroacetic acid	5.2	n.d.
14 ^c	Trifluoroacetic acid	8.8	0.8
15 ^d	4-nitrobenzoic acid	34.0	7.5

^aReaction conditions: Mn-cat. : H₂O₂ : substrate : HOAc = 1 : 100 : 100 : 200, in TFE at -30 °C, oxidant added by syringe pump over 30 minutes. Total reaction volume of 2 mL. ^bConversion and yields determined from crude reaction mixtures by GC. ^cReaction mixture remained colorless. ^d4-nitrobenzoic acid was not completely soluble in the reaction mixture. n.d. = non-detected.

Increasing the acidity has a positive effect, going from acetic acid (pK_a = 4.76) to 3-nitrobenzoic acid (pK_a = 3.46), chloroacetic acid (pK_a = 2.87), fluoroacetic acid (pK_a = 2.59), 2-nitrobenzoic acid (pK_a = 2.17) and dichloroacetic acid (pK_a = 1.35) (Figure 2).⁸⁷ However, the use of trichloroacetic acid (pK_a = 0.66) or trifluoroacetic acid (pK_a = 0.52) lead to a dramatic decrease in catalytic activity, which might be due to protonation of the amine moieties of the ligand. Iodoacetic acid (pK_a = 3.18) provided good conversion but a poor phenol yield, which could be explained by the weaker C-halogen bond that may lead to side reactions (Table 4, entry 14). N,N-dimethylglycine was also not a suitable additive, showing poor yield for the desired phenol product, as well as low substrate conversion (Table 4, entry 15). Thus, we can conclude that sterics on the carboxylic acid additive are not good for the arene hydroxylation reaction, and that there is an optimum pK_a of the acid additive.

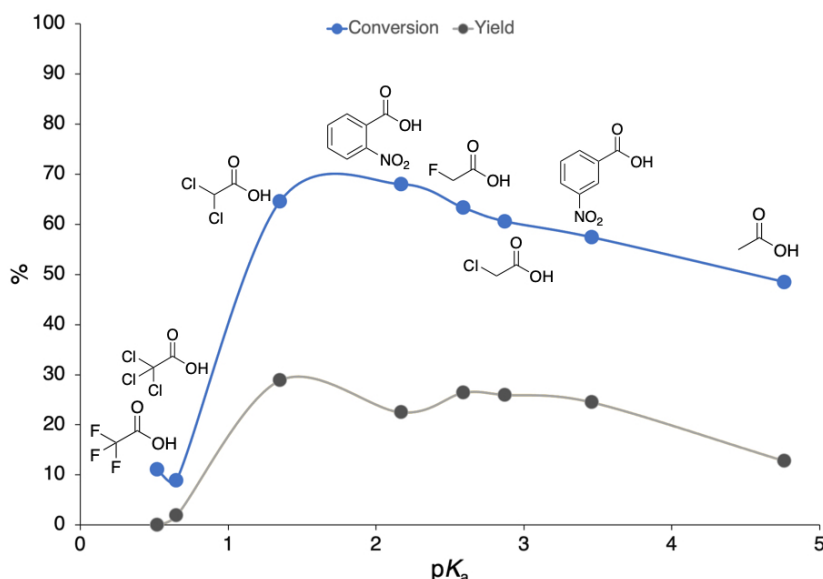


Figure 2. Effect of pK_a of the carboxylic acid additive on the hydroxylation of *tert*-butylbenzene. Reaction conditions: **Mn**(^{tips}**bpmcn**) : H₂O₂ : substrate : RCO₂H = 1 : 100 : 100 : 200, in HFIP at 0 °C.

While it may be initially regarded as a modest value, the 29% yield obtained for 4-*tert*-butylphenol in a completely site selective manner is remarkable when compared with literature precedents; a recently reported iminopyridine Fe(II) catalyst has been shown to be capable of oxidizing *tert*-butylbenzene to 4-*tert*-butylphenol in 23% yield, together with the *ortho*-phenol and benzoquinone as minor products, which at that time were the highest numbers reported for *tert*-butylbenzene oxidation.⁴²

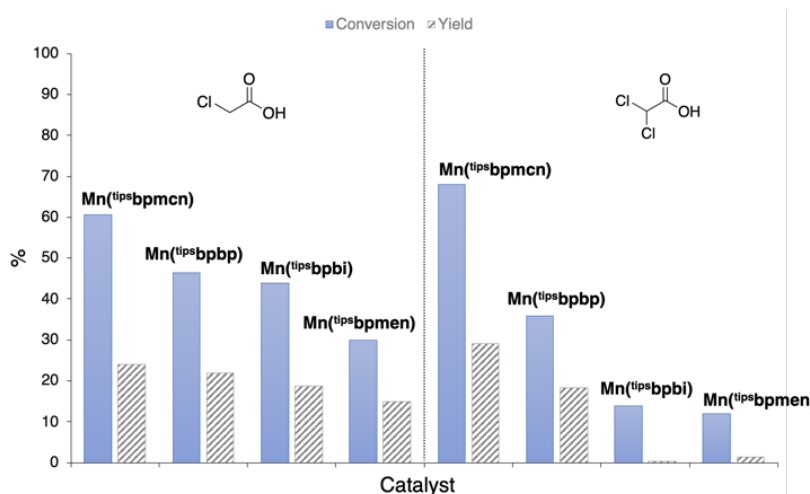
Further investigations on the effect of halogenated carboxylic acids showed that the conversion and yield do not drastically change between 0.5 to 8 equiv. of acid when **Mn**(^{tips}**bpmcn**) is used as catalyst (Table 6). This allows catalysis to be performed at a much lower carboxylic acid loading.

Next, bulky manganese complexes with different amine backbones in the ligand structure were tested in the aromatic hydroxylation of *tert*-butylbenzene using optimized chloro- and dichloroacetic acid loadings (Figure 3). The use of chloroacetic acid afforded similar efficiencies for the four catalysts tested, **Mn**(^{tips}**bpmcn**) being the one that showed better conversion and yield. For dichloroacetic acid, we observed that **Mn**(^{tips}**bpmcn**) and **Mn**(^{tips}**bpbp**) performed best, with **Mn**(^{tips}**bpmcn**) showing significantly higher conversion and yield. In contrast, **Mn**(^{tips}**bpbi**) and **Mn**(^{tips}**bpmen**) showed very poor results when using dichloroacetic acid. A similar reactivity trend was observed when TFE was used as solvent (Figure 4). Therefore, we can conclude that the amine backbone in the ligand structure of the manganese complexes has a considerable impact on catalytic activity. Besides, we believe that

Table 6. Effect of different equivalents of dichloroacetic acid in aromatic C–H oxidation of *tert*-butylbenzene.^a

Entry	Equiv. of Cl ₂ CHCO ₂ H	Conversion (%) ^b	Yield Phenol (%) ^b
1	0	19.1	3.9
2	0.5	68.0	29.2
3	1	69.0	29.7
4	2	64.6	28.9
5	4	66.1	30.3
6	6	69.2	30.0
7	8	66.9	29.4
8	10	36.7	19.1
9	15	39.4	20.1

^aReaction conditions: Mn-cat. : H₂O₂ : substrate = 1 : 100 : 100, in HFIP at 0°C, oxidant added by syringe pump over 30 minutes. Total reaction volume of 2 mL. ^bConversion and yields determined from crude reaction mixtures by GC.

**Figure 3.** Effect of different amine ligand backbones on the Mn-catalyzed hydroxylation of *tert*-butylbenzene in HFIP. Reaction conditions: Mn-cat.: H₂O₂ : substrate : RCO₂H = 1 : 100 : 100 : 50, in HFIP at 0 °C.

the simpler ethylene diamine backbone is less stable under acidic conditions, since with dichloroacetic acid as additive a poor 4-*tert*-butylphenol yield is afforded. Consistent with this hypothesis, this complex is more efficient under low carboxylic acid loadings; hydroxylation of *tert*-butylbenzene with Mn(II)psbpmen leads to only 6% 4-*tert*-butylphenol yield when 2 equivalents of chloroacetic acid are used, whereas 15% yield is obtained with 0.5 equiv. of the acid.

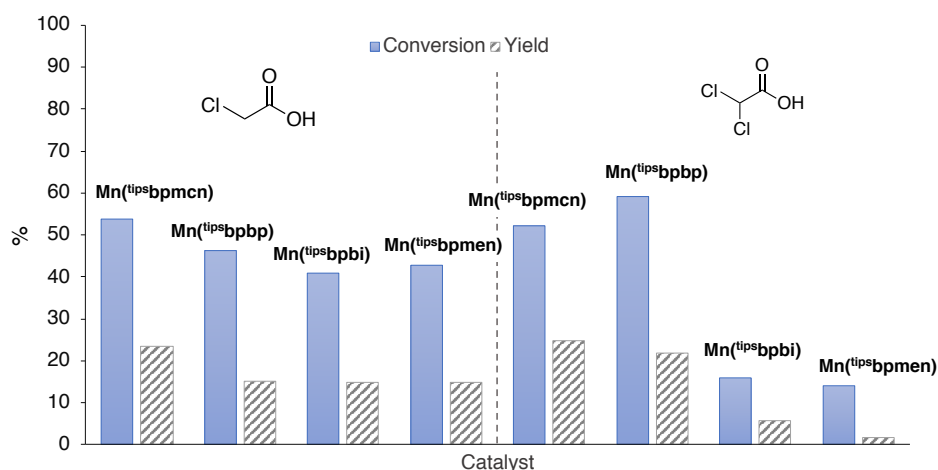


Figure 4. Effect of different amine ligand backbones on the Mn-catalyzed hydroxylation of tert-butylbenzene in TFE. Reaction conditions: Mn-cat.: H₂O₂ : substrate : RCO₂H = 1 : 100 : 100 : 50, in TFE at 0 °C.

Table 7. Investigation of dichloroacetic acid as additive with different manganese complexes.

Entry	Catalyst	r.s.m (%) ^a	<i>p</i> -Phenol ^b	<i>o</i> -Phenol ^b	Quinone ^b	Alcohol ^b	MB ^c
1	Mn(tipsbpmcn)	68	14 (28)	4 (9)	1 (3)	Traces	92
2	Mn(dMMbpmcn)	90	3 (6)	2 (3)	Traces	Traces	>99
3	Mn(bpmcn)	85	5 (10)	2 (5)	Traces	Traces	97

^aRemaining starting material. ^bYields with respect to substrate determined by GC against an internal standard. In parenthesis yields respect to H₂O₂. Yields are calculated considering that 2 equiv of H₂O₂ are necessary for the formation of the quinone product. Yields for propyl-*p*-benzoquinone were calculated with the response factor of methyl-*p*-benzoquinone. ^cMass balance was calculated considering remaining starting material and all products formed, plus a percentage of substrate loss calculated from blank experiments (an average of 5% of substrate is lost): MB = (r.s.m %) + (Product Yields %) + (Substrate loss).

Finally, we have further investigated the role of the halogenated carboxylic acid additives by examining the use of dichloroacetic acid with different manganese complexes for the hydroxylation of propylbenzene, this time at a low H₂O₂ loading (Table 7). Our earlier findings showed that for **Mn(tipsbpmcn)** the use of dichloroacetic acid provides an enhanced catalytic activity compared to the use of AcOH (compare Tables 1 and 7). On the other hand, for the electron-rich complex **Mn(dMMbpmcn)** a complete change in chemoselectivity from aliphatic to aromatic hydroxylation was observed when switching to dichloroacetic acid, albeit at low

yields (compare Tables 1 and 7). For the parent complex **Mn(bpmcn)** an increased activity for aromatic hydroxylation was observed when dichloroacetic acid was employed instead of AcOH. Remarkably, traces of 1-phenyl-1-propanol were detected for all these catalysts when dichloroacetic acid was employed, revealing that the use of a halogenated carboxylic acid increases the selectivity towards the oxidation of aromatic C–H bonds for these complexes in a general sense, avoiding the generation of products originating from oxidation at a more activated benzylic position.

3.2.4 Substrate Scope

Aromatic C–H hydroxylation of different substrates has been explored under the optimized experimental conditions using the manganese complex **Mn(^{tips}bpmcn)** (Table 8). In general, our current Mn(II)/H₂O₂/Cl₂CHCOOH catalytic system affords higher yields and substantially improved selectivities for aromatic over aliphatic C–H oxidation.

At first, we considered benzene as substrate, which leads to phenol in a remarkable yield of 32%, along with *para*-benzoquinone in 7% yield (Table 8, entry 1). Interestingly, when phenol was used as the substrate, 13% yield of *para*-benzoquinone was observed; showing that the primary oxidation product in benzene hydroxylation can indeed engage in a second oxidation step (Table 8, entry 2). Next, we extended our study to the oxidation of alkylbenzenes. Oxidized products were obtained in remarkable total product yields ranging from 29 to 37%, with the *para*-phenol as the main product in all cases, which is reminiscent to reactions proceeding via an electrophilic aromatic substitution type of mechanism. Toluene was oxidized to *para*-cresol in 22% yield, together with *ortho*-cresol and methyl-*para*-benzoquinone in 8 and 1% yield, respectively (Table 8, entry 3). Recent studies on aromatic oxidations have shown other complexes to be capable of oxidizing the aromatic ring of toluene as well, however, showing significant amounts of aliphatic oxidation towards benzyl alcohol or benzaldehyde products.^{42, 55, 56, 59, 60} Remarkably, **Mn(^{tips}bpmcn)** shows an excellent selectivity for oxidation of the aromatic ring over the aliphatic site chain. Oxidation of other alkylbenzene derivatives with more reactive benzylic C–H bonds was also explored. Ethylbenzene provided 4-ethylphenol as the major product in 26% yield, along with 2-ethylphenol and ethyl-*para*-benzoquinone in 8 and 2% yield, respectively (Table 8, entry 4). For the oxidation of propylbenzene, we observed 4-propylphenol, 2-propylphenol and propyl-*para*-benzoquinone in 24, 8, and 2% yield, respectively (Table 8, entry 5). Cumene was also considered, which bears a more encumbered isopropyl substituent with a weak 3^o benzylic C–H bond. 4-Isopropylphenol and 2-isopropylphenol were obtained in 30 and 5% yield, respectively. Minor amounts of isopropyl-*para*-benzoquinone were also detected in 2% yield (Table 8, entry 6). To the best of our knowledge, hydroxylation of this group of alkylbenzene substrates catalyzed by the current

system provides the highest yields reported to date with homogeneous catalysts. Remarkably, only traces of benzylic oxidation products were detected in these reactions, suggesting that the current catalytic system is selective for aromatic hydroxylation reactions. A cautious note must be introduced at this point because some of these compounds show the lowest mass balance of all substrates tested in this study, which raises the possibility that benzylic oxidation products are also formed but overoxidized to non-detected products. Important to note is that no formation of ketone products was observed, *i.e.* secondary oxidation of initial benzylic alcohol products does not seem to take place. Blank experiments without catalyst were done to calculate the amount of substrate loss during the reactions, and were used to calculate the mass balances in Table 8.

We observed a correlation between the bulk of the lateral alkyl chain in the aromatic substrate and the product profile. Our results clearly show that increasing the bulk of the substituents on the substrate translates into a decreased formation of *ortho*-phenol product, which is likely due to steric effects of both the catalyst and the substrate. The amounts of *ortho*-phenol were similar for toluene, ethylbenzene, and propylbenzene. However, when a bulkier

Table 8. Product analysis in the oxidation of benzene and its derivatives catalyzed by $\text{Mn}(\text{t}^{\text{ips}}\text{bpmcn})^{\text{a}}$


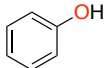
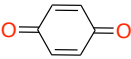
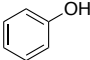
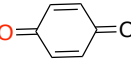
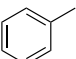
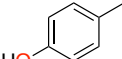
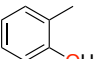
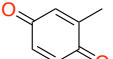
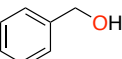
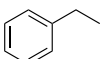
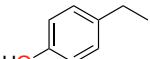
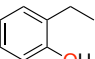
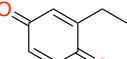
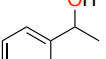
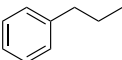
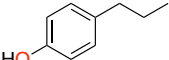
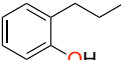
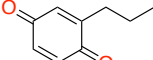
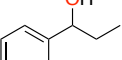
Entry	Substrate (r.s.m %) ^b	<i>p</i> -Phenol (%) ^c	<i>o</i> -Phenol (%) ^c	Quinone (%) ^c	Benzylic oxidation (%) ^d	Mass balance (%) ^e
1	 44	 32	–	 7	–	88
2	 70	–	–	 13	–	86
3	 49	 22	 8	 1	 traces	80
4	 34	 26	 8	 2	 traces	71
5	 45	 24	 8	 2	 traces	81

Table 8 (continued)

6						75
	38	30	5	2	traces	
7			–	–	–	66
	32	29				
8					–	72
	45	8	14	5		
9				–	–	94 ^f
	84	6	4			
10		–	–	–	–	> 99 ^f
	> 99					

^aReaction conditions: **Mn**(^{tip}**s****bpmcn**) : H₂O₂ : substrate : Cl₂CHCOOH = 1 : 100 : 100 : 50, in HFIP at 0 °C for 30 min. ^bRemaining starting material (r.s.m.) determined from crude reaction mixtures by GC. ^cProduct yields determined from crude reaction mixtures by GC. ^dBenzaldehyde or ketone products were not detected. ^eMass balance was calculated considering remaining starting material and all products formed, plus a percentage of substrate loss calculated from blank experiments: MB = (r.s.m %) + (Product Yields %) + (Substrate loss %). ^fPercentage of substrate loss was not calculated.

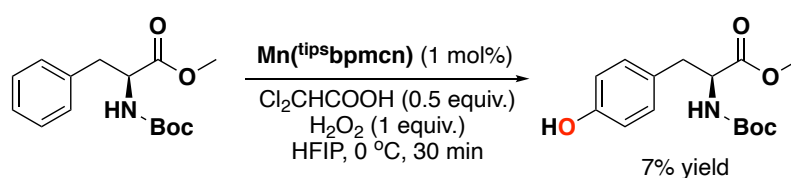
substrate, such as in cumene, was used, the yield for the *ortho*-phenol decreased. More remarkably is the oxidation of *tert*-butylbenzene, where no *ortho*-phenol product was detected at all, *i.e.* 4-*tert*-butylphenol was detected as the only product in 29% yield (Table 8, entry 7). The current data contrasts with the oxidation of cumene catalyzed by a Ni(II) complex supported by an aminopyridine ligand, where mixtures of *ortho*-, *meta*- and *para*-phenols were obtained together with benzylic oxidized products; albeit in very low yields.⁵⁵ Thus, our data indicate the importance of steric catalyst effects to dictate the regioselectivity of the hydroxylation reaction.

Using bromobenzene as substrate, 2-bromophenol and 4-bromophenol were obtained in 14 and 8% yield, respectively. 2-Bromo-1,4-benzoquinone was also detected in 5% yield (Table 8, entry 8). The formation of *ortho* and *para* phenols is in agreement with classical aromatic substitution reactions, halogen and alkyl substituents being *ortho* and *para* directing groups. However, of importance is the different selectivity observed for bromobenzene compared to

the alkylbenzene substrates; where the *ortho*-phenol was obtained as the main oxidized product in the former case, the *para*-phenol was the major product in the latter case.

An electron-donating substituent was expected to enhance the reactivity of the arene substrate in our system. Nonetheless, anisole showed a poor reactivity, with 4-methoxyphenol and 2-methoxyphenol being produced in only 6 and 4% yield, respectively (Table 8, entry 9). No benzoquinone was detected in this case. For benzonitrile, bearing an electron-withdrawing cyano group, no oxidized products were detected (Table 8, entry 10). While the cyano group could deactivate the aromatic ring towards electrophiles, the coordinating ability of the methoxy and cyano groups in anisole and benzonitrile might also interfere with catalysis. We also believe that the poor catalytic activity for anisole may be due to strong binding of the first formed hydroxylated product to the metal center (indicated by a strong color change to purple). Indeed, competitive experiments using equimolar amounts of anisole and *tert*-butylbenzene show only 2 % 4-*tert*-butylphenol yield, demonstrating catalyst deactivation in the presence of anisole.

Amino acid substrates are particularly interesting because of their biological significance and their molecular complexity, containing different types of C–H bonds. We therefore examined the catalytic hydroxylation of phenylalanine. Our idea was to extrapolate the reactivity that we have observed using simple aromatic substrates to the oxidation of more complex molecules. Interestingly, we found that oxidation at the *para*-position of the aromatic ring of a protected phenylalanine yields the corresponding tyrosine as the main product in 7% yield, which represents 7 catalytic turn-overs per Mn (Scheme 3). The hydroxylation of phenylalanine might be further optimized by variation of reaction conditions and protecting groups.

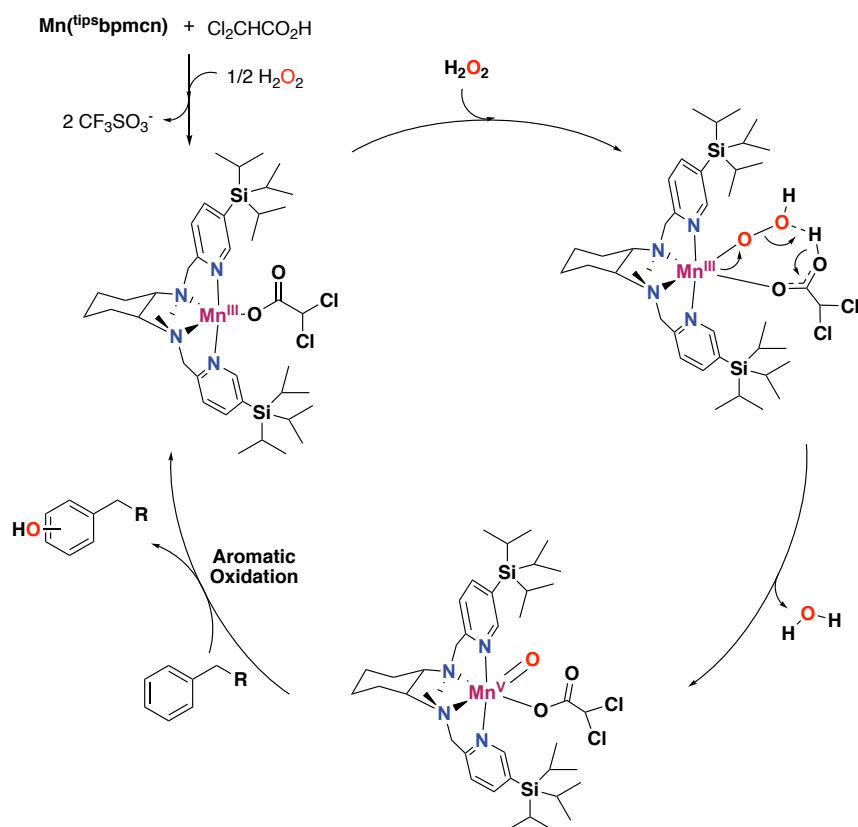


Scheme 3. Aromatic C–H hydroxylation of a natural product.

3.2.5 Mechanistic Considerations

Finally, our efforts have been devoted to the understanding of the mechanism of the aromatic hydroxylation reaction. Generally, activation of H_2O_2 by manganese or iron complexes supported by aminopyridine ligands leads to electrophilic oxidants.^{8, 26, 28, 79, 80} It is proposed that the starting Mn(II) complex is first oxidized to a Mn(III) hydroperoxo species, which then converts to a Mn(V) oxo complex through O–O bond heterolysis,^{13, 79, 80} this last step being assisted by the carboxylic acid additive (Scheme 4). We propose that the aromatic

hydroxylation reaction occurs via a similar oxidizing species, without the involvement of oxygen-centered radicals. It is well-known that free radicals, such as hydroxyl radicals generated via a Fenton process, can perform the oxidation of aromatic C–H bonds, but show low efficiencies and selectivities.⁸⁸⁻⁹¹ The involvement of such radicals would lead to side products through lateral site chain oxidation in alkylbenzene derivatives, because these oxygen-centered radicals are unable to differentiate between C–H bonds of different strengths.^{42, 92} In addition, hydroxylation of alkylbenzenes via hydroxyl radicals give a specific distribution of *ortho*-, *meta*- and *para*-phenol isomers.⁹³ Several of our observations speak against the involvement of hydroxyl radicals in our aromatic hydroxylation reaction, and point towards a metal-based oxidation mechanism.



Scheme 4. Proposed mechanistic cycle based on the carboxylic acid assisted O–O cleavage of non-heme Fe and Mn complexes.^{8, 13, 26, 94, 95}

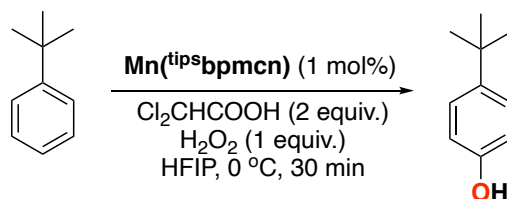
Our catalysis experiments show that oxidation of electron-rich benzene derivatives leads to the formation of *para* and *ortho* phenol products, with no formation of the *meta* isomer. This clearly contrasts with other catalysts capable of performing arene hydroxylation, such as the systems reported by Itoh⁵⁵, Bryliakov⁴⁵ and Di Stefano⁴², where mixtures of *ortho*-, *meta*- and *para*-phenols were observed; and thus, suggests that the current reaction undergoes through a more selective species. In contrast, when switching to electron-poor substrates, no aromatic hydroxylation reaction takes place with the current system. These observations agree with the

proposal of an electrophilic manganese-oxo species, with a reactivity sensitive to the electronic nature of the substrate.

Previous studies have shown that the oxidation of toluene with hydroxyl radicals afford cresols with a distribution of 71 : 9 : 20 for *ortho* : *meta* : *para* isomers.⁹³ The current Chapter has shown that the bulky **Mn**(^{tip}**sbpmcn**) catalyst is capable of oxidizing toluene with high selectivity, affording a ratio of 27 : 0 : 73 for the *ortho*-, *meta*- and *para*-cresols, respectively. Therefore, our data clearly show a distinct distribution of isomers compared with the reaction involving hydroxyl radicals, and consequently point towards the involvement of a metal-based mechanism.

To get further insight in the mechanism, we considered performing the hydroxylation reaction with another oxidant than H₂O₂. Remarkably, we found that catalytic hydroxylation of *tert*-butylbenzene by **Mn**(^{tip}**sbpmcn**) in fluorinated alcohol solvents can also be accomplished employing ^tBuOOH as oxidant, generating 4-*tert*-butylphenol as the oxidized product in 9% yield. It is known that oxidations with ^tBuOOH can proceed through a Fenton-type process, generating free-diffusing *tert*-butoxy and *tert*-butylperoxy radicals that can engage in hydrogen abstraction reactions with aliphatic C–H bonds.^{26, 96, 97} However, ^tBuOOH activation does not produce hydroxyl radicals, and *tert*-butoxy radicals, unlike hydroxyl radicals, do not add to aromatic rings.⁹⁸ Another evidence against the involvement of hydroxyl radicals is that the aromatic hydroxylation reactions catalyzed by **Mn**(^{tip}**sbpmcn**) are not affected by the presence, or absence, of air. Independent experiments carried out under air and under a nitrogen atmosphere showed similar efficiencies for the generation of 4-*tert*-butylphenol (Table 9). In contrast, a significant impact of air on product yields is observed when oxidations are mediated by oxygen-centered radicals.^{42, 90, 91, 99}

Next, we carried out a kinetic isotope effect (KIE) experiment using a 1:1 mixture of benzene and perdeuterated benzene as substrate and **Mn**(^{tip}**sbpmcn**) as catalyst. From the ratio of phenol to phenol-*d*₅, a KIE value of 0.97 ± 0.06 was determined for this reaction. This value rules out Fenton-type processes, for which a KIE of 1.7 has been reported.¹⁰⁰ Overall, our combined data suggest that aromatic hydroxylation reactions catalyzed by **Mn**(^{tip}**sbpmcn**) occur through a metal-based mechanism, with no significant involvement of hydroxyl radicals. Besides, the high bond dissociation energy of aromatic C–H's discard a HAT initiated process. Instead, the data is consistent with an aromatic hydroxylation mechanism via electrophilic attack of the high valent metal oxo on the aromatic ring. As a first option, the KIE value found in this study is compatible with the formation of a Wheland type of intermediate found in an electrophilic aromatic substitution mechanism. Alternatively, an initial arene epoxidation reaction conducted by the high valent manganese-oxo species, followed by an acid catalyzed re-aromatization to

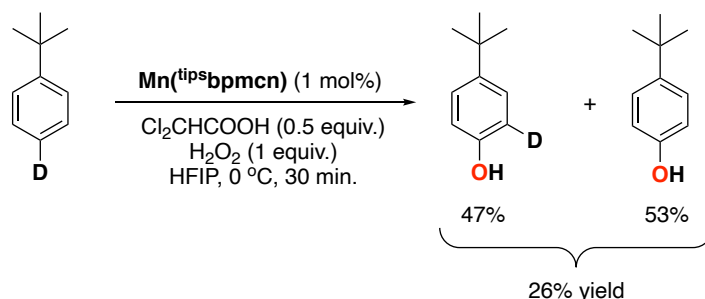
Table 9. Investigation on the presence or absence of atmospheric oxygen in the oxidation of *tert*-butylbenzene.^a

Entry	Conditions	Conversion (%) ^b	Yield Phenol (%) ^b
1	Under air	65	29
2	Under N ₂	59	26

^aReaction conditions: Mn-cat. : H₂O₂ : substrate = 1 : 100 : 100, in HFIP at 0 °C, oxidant added by syringe pump over 30 minutes. Total reaction volume of 2 mL. ^bConversion and yields determined from crude reaction mixtures by GC.

form the corresponding phenol could also be a plausible mechanism.¹⁰¹ Both proposed processes show a negligible KIE, which is consistent with a change in hybridization from sp² to sp³ of the aromatic carbon where the oxidation takes place.^{42, 102}

To get further insight into the arene hydroxylation mechanism, we performed a catalytic experiment using 1-*tert*-butyl-4-deuterobenzene to probe the occurrence of an NIH shift (Scheme 5). This characteristic feature of arene hydroxylation reactions based on the migration of a substituent from the formal hydroxylation site to an adjacent carbon position can indicate the involvement of an arene oxide as a reaction intermediate.¹⁰³⁻¹⁰⁷ Based on our previous experiments, we know that hydroxylation of *tert*-butylbenzene only occurs at the *para*-position of the benzene ring.

**Scheme 5.** Deuterium labeling study.

Combined GC and GC-MS analysis of the reaction with 1-*tert*-butyl-4-deuterobenzene indeed showed the exclusive formation of *para*-phenol products (26%), with a 4-*tert*-butyl-2-deuterophenol and 4-*tert*-butylphenol ratio of 47/53, indicating that an NIH-shift takes place during the reaction. On basis of this observation, we suggest that the aromatic hydroxylation

reaction most likely occurs through an arene epoxidation mechanism, involving the generation of a cyclohexadienone intermediate after arene oxide formation.

We propose that the use of an electron-deficient acid can make the metal oxo species more electrophilic, as well as reducing catalyst inhibition by phenolates protonation. These effects, together with a sterically demanding aminopyridine ligand, translate into an oxidizing agent reactive towards the *para*-position of the aromatic ring instead of the (benzylic) aliphatic C–H bonds. Overall, we believe that there is a synergy between the carboxylic acid and the manganese complex, as was recently also shown for methylene and tertiary C–H oxidation catalyzed by other manganese complexes with chloroacetic acid as additive.^{21, 67, 108} Further investigations into the exact role of halogenated carboxylic acids are required to understand how chemoselectivity is governed in these aromatic hydroxylation reactions.

3.3 Conclusions

We have presented a new catalytic procedure for the direct one-step hydroxylation of aromatic C–H bonds to the corresponding phenol products using manganese complexes in combination with H₂O₂. Pivotal to our findings is the use of sterically encumbered tetradentate aminopyridine ligands in combination with a halogenated carboxylic acid additive and a fluorinated alcohol solvent. We have shown that complexes with bulky ligands perform better in arene oxidations by preventing coordination of the phenolate products to the manganese center. Remarkably, the use of bulky manganese complexes favors aromatic oxidation over (benzylic) aliphatic C–H bond oxidation, whereas electron-rich manganese complexes selectively oxidize the weaker benzylic C–H bonds, demonstrating a dependency of the chemoselectivity on the catalyst. A synthetically relevant property of the current Mn system is that oxidation of a broad range of aromatic substrates can be accomplished. Notable is the oxidation of monoalkylbenzenes using **Mn**(^{tip}**sbpmcn**) as the catalyst, which to our knowledge provide the highest phenol product yields reported to date for homogeneous catalysts. The overall product profiles of this system, in combination with a negligible KIE effect and the effectiveness of using ^tBuOOH as oxidant, overall point towards a metal-based mechanism, with no significant involvement of oxygen-centered radicals. Besides, the observation of a NIH shift indicates that aromatic oxidation with the current system is likely to occur via an arene epoxidation pathway.

Future efforts will be focused on the understanding of the factors that govern product selectivity, as well as of possible catalyst deactivation pathways that lead to the still moderate product yields observed in this study. Additional investigations of the current catalytic system will also focus on a further insight in the overall modest mass balances obtained. Overall, our

current findings represent a next step in the design of molecular catalysts for the selective oxidation of aromatic substrates, and provide a stepping stone for the further development of selective oxidation catalysts based on manganese.

3.4 Experimental Section

3.4.1 General Remarks

The synthesis of manganese and iron complexes and other air- and moisture-sensitive reactions was performed under an inert nitrogen atmosphere using standard Schlenk line and glovebox techniques. All catalytic oxidation reactions were run under air with no precautions taken to exclude moisture. The solvents diethyl ether and acetonitrile were purified using an MBraun MB SPS-800 solvent purification system. Tetrahydrofuran and methanol were dried with sodium and magnesium turnings, respectively, and distilled under nitrogen prior to use. Ligands *S,S*-bpmcn¹⁰⁹, *R,R*-*tips*bpmcn¹¹⁰, *S,S*-*tips*bpmcn¹¹⁰, *S,S*-bpbp¹¹¹, *S,S'*-*tips*bpbp¹¹⁰, *S,S*-bpb¹¹², *S,S'*-*tips*bpb¹¹², bpmen¹¹³, ⁵-*tips*tpa³⁴, (*S,S*)-^{dMM}bpmcn²⁶ and (*S,S*)-^{dMM}bpbp²⁶ were synthesized according to literature procedures. Mn(OTf)₂ was bought from Sigma-Aldrich. Manganese complexes **Mn(bpmcn)**¹¹⁴, **Mn(*tips*bpmcn)**¹¹, **Fe(*tips*bpmcn)**¹¹⁰, **Mn(bpbp)**⁶⁵, **Mn(*tips*bpbp)**¹¹, **Mn(bpb¹¹²)**¹¹⁵, **Mn(bpmen)**¹¹⁴, **Mn(^{dMM}bpmcn)**¹¹⁶ and **Mn(^{dMM}bpbp)**²⁵ were synthesized according to literature procedures.

Tert-butylbenzene, benzene, ethylbenzene, propylbenzene, cumene, bromobenzene, anisole and benzonitrile were filtered through a plug of alumina before being used in catalysis. Toluene was taken from an MBraun MB SPS-800 solvent purification system. All other reagents and reaction products were obtained commercially and used without further purification. Column chromatography was performed using Merck silica gel (60-200 mesh). ¹H, ¹³C, and ¹⁹F NMR spectra were recorded with a 400 MHz Varian spectrometer at 25°C, chemical shifts (δ) are given in ppm referenced to the residual solvent peak. IR spectra were recorded with a Perkin-Elmer Spectrum One FTIR spectrometer. ESI-MS spectra were recorded with an Advion expression compact mass. High resolution mass spectrometry (HRMS) was performed on a Bruker MicrOTOF-Q^{II} (Q-TOF) instrument with a quadrupole analyzer. GC analyses were performed on a Perkin-Elmer Clarus 500 Gas Chromatograph equipped with a PE Elite-5 column ((30m x 0.32 mm x 0.25 μm), (5% phenyl)-(95% methyl)polysiloxane) and a flame-ionization detector. X-ray diffraction analysis was carried out using two different diffractometers: Bruker Kappa ApexII and Bruker D8 QUEST ECO.

Appendix B contains the supplementary information of this Chapter, which includes MS-data of the investigation on catalyst inhibition, ¹H-NMR spectra for the newly synthesized ligands and substrates, and representative GC chromatographs of the catalytic reactions.

3.4.2 Synthesis of Ligands, Manganese Complexes and Substrates

3.4.2.1 Synthesis of Ligands

***tips*bpmen.** NaOH (205.4 mg, 5.14 mmol) was added to a round-bottom flask charged with a stir bar and *tips*PyCH₂Cl (400 mg, 1.41 mmol) dissolved in CH₂Cl₂ (2 mL) and H₂O (2 mL). Subsequently, a solution containing *N,N*-dimethylethylenediamine (56.6 mg, 0.64 mmol) was added. The combined mixture was vigorously stirred overnight at room temperature. At this point, the organic phase was separated and the aqueous phase was extracted with CH₂Cl₂ (3 times). The combined organic extracts were dried over MgSO₄ and the solvent was eliminated under vacuum. The obtained oil was purified by silica column

(petroleum ether:EtOAc 9:1 at first, then CH₂Cl₂:CH₃OH:NH₃ 90:9:1) to provide the desired ligand as a light yellow-white solid (60% yield). ¹H NMR (400 MHz, CDCl₃) δ 8.60 (s, 2H), 7.73 (dd, *J* = 7.7, 1.8 Hz, 2H), 7.41 (d, *J* = 7.7 Hz, 2H), 3.68 (s, 4H), 2.68 (s, 4H), 2.29 (s, 6H), 1.45 – 1.34 (m, 6H), 1.07 (d, *J* = 7.4 Hz, 36H). ¹³C NMR (100 MHz, CDCl₃) δ 159.06, 154.96, 143.61, 128.02, 122.68, 64.10, 55.60, 43.03, 18.57, 10.76.

3.4.2.2 Synthesis of Manganese Complexes

Mn(^{tips}bpmen): Under a nitrogen atmosphere in a glovebox, a solution of ^{tips}bpmen (128.5 mg, 0.22 mmol) in THF (2 mL) was added to a vigorously stirred solution of Mn(OTf)₂ (72.6 mg, 0.21 mmol) in THF (2 mL) at room temperature. The reaction mixture was stirred at rt overnight, providing a white precipitate. The precipitate was allowed to settle and the supernatant was removed. The remaining precipitate was washed with diethyl ether twice, then dissolved in CH₂Cl₂. The resulting solution contained some black impurities, which were removed *via* filtration through a filter paper. Subsequently, crystallization by slow vapor diffusion of diethyl ether into the CH₂Cl₂ solution afforded, in a few days, the desired complex as a white powder in 53% yield. ESI-MS calcd. *m/z* for C₃₄H₆₅MnN₄O₂Si₂ ([Mn(L)(OH)₂+H]⁺): 672.4, found 671.9. FT-IR (ATR) ν , cm⁻¹: 2947-2868 (C–H)_{sp3}, 1591, 1460, 1312, 1233, 1212, 1171, 1032, 982, 881, 697, 681, 636, 566, 512.

Mn(^{tips}bpbi): This complex was prepared in an analogous manner to the [Mn(OTf)₂(^{tips}bpmen)] complex, starting from (*S,S*)-^{tips}bpbi ligand and Mn(OTf)₂. The desired complex was obtained as white crystals in 42% yield. ESI-MS calcd. *m/z* for C₄₆H₆₉MnN₄O₂Si₂ ([Mn(L)(OH)₂+H]⁺): 820.4, found 819.9. FT-IR (ATR) ν , cm⁻¹: 2944-2866 (C–H)_{sp3}, 1594, 1456, 1312, 1215, 1160, 1037, 995, 960, 881, 865, 766, 726, 693, 637, 568, 514. Elemental Analysis (%) for C₄₈H₆₆F₆MnN₄O₆S₂Si₂ (MW = 1084.30 g/mol). Calculated C: 53.17, H: 6.14, N: 5.16; obtained C: 52.85, H: 5.61, N: 5.12. See section 3.4.3.1 for X-ray crystal structure.

Mn(^{5-tips3}tpa): This complex was prepared in an analogous manner to the [Mn(OTf)₂(^{tips}bpmen)] complex, starting with ^{5-tips3}tpa ligand and Mn(OTf)₂. The desired complex was obtained as white crystals. HRMS (ESI-TOF): *m/z* calculated for C₄₆H₇₈F₃MnN₄O₃SSi₃, [M-OTf]⁺ 962.4435, Found 962.4423. Elemental Analysis (%) for C₄₇H₇₈F₆MnN₄O₆S₂Si₃ (MW = 1112.47 g/mol). Calculated C: 50.74, H: 7.07, N: 5.04; obtained C: 50.53, H: 7.04, N: 5.28. See section 3.4.3.2 for X-ray crystal structure.

3.4.2.3 Synthesis of substrates

***tert*-butylbenzene-4-*d*₁.** 1-Bromo-4-*tert*-butylbenzene (5 mmol, 0.87 mL) was dissolved in 15 mL of anhydrous diethyl ether under inert atmosphere and cooled to –78 °C in an acetone/dry ice bath. Then 2.1 equiv of *t*BuLi (1.9 M in pentane, 5.8 mL, 11 mmol) were added dropwise over 15 min, and the reaction mixture was let stir for 1 h. Then, the temperature was raised up to 0 °C and D₂O (1 mL) was added dropwise. The reaction mixture was let stir for 30 min. At this point, the reaction was quenched by addition of more water and extracted with diethyl ether (3 x 20 mL). The combined organic layers were dried over MgSO₄, concentrated on a rotatory evaporator and dried under reduced pressure to yield the desired compound (0.56 g, 4.13 mmol, 83% yield) as a colorless liquid. ¹H NMR (400 MHz, CDCl₃) δ 7.42 (d, *J* = 7.0 Hz, 2H), 7.32 (d, *J* = 7.0 Hz, 2H), 1.35 (s, 9H). Spectral properties of the products agree with the literature data.¹¹⁷

3.4.3 X-Ray Crystal Structure Determination of Mn(^{tips}bpbi)

$C_{48}H_{66}F_6MnN_4O_6S_2Si_2 \cdot C_4H_{10}O$, Fw = 1158.40, colourless plate, $0.38 \times 0.19 \times 0.08$ mm³, orthorhombic, $P2_12_12_1$ (no. 19), $a = 13.6943(2)$, $b = 14.3549(3)$, $c = 30.9303(7)$ Å, $V = 6080.3(2)$ Å³, $Z = 4$, $D_x = 1.265$ g/cm³, $\mu = 0.39$ mm⁻¹. The diffraction experiment was performed on a Bruker Kappa ApexII diffractometer with sealed tube and Triumph monochromator ($\lambda = 0.71073$ Å) at a temperature of 150(2) K up to a resolution of $(\sin \theta/\lambda)_{\max} = 0.65$ Å⁻¹. The Eval15 software¹¹⁸ was used for the intensity integration. A multiscan absorption correction and scaling was performed with SADABS¹¹⁹ (correction range 0.68-0.75). A total of 108068 reflections was measured, 13972 reflections were unique ($R_{\text{int}} = 0.058$), 10924 reflections were observed [$I > 2\sigma(I)$]. The structure was solved with Patterson superposition methods using SHELXT.¹²⁰ Structure refinement was performed with SHELXL-2018¹²¹ on F^2 of all reflections. Non-hydrogen atoms were refined freely with anisotropic displacement parameters. All hydrogen atoms were introduced in calculated positions and refined with a riding model. One isopropyl group was refined with a disorder model. 702 Parameters were refined with 242 restraints (distances and angles of the isopropyl groups, displacement parameters of the disordered atoms). $R1/wR2$ [$I > 2\sigma(I)$]: 0.0413 / 0.0897. $R1/wR2$ [all refl.]: 0.0614 / 0.0971. $S = 1.043$. Flack parameter¹²² $x = 0.015(6)$. Residual electron density between -0.26 and 0.35 e/Å³. Geometry calculations and checking for higher symmetry was performed with the PLATON program.¹²³

3.4.4 Reaction Protocol for Catalytic Studies

3.4.4.1 General Procedure for Catalytic Hydroxylation Reaction

A 3 mL or 20 mL vial was charged with: substrate (1 equiv.) and the indicated loading of catalyst and corresponding solvent (0.5 mL or 2 mL). The carboxylic acid was added with indicated loading. The vial was cooled on an ice bath or acetonitrile/dry ice bath, depending on the desired temperature, with stirring. Subsequently, a solution of H₂O₂ in the corresponding solvent (indicated loading, diluted from a 35% H₂O₂ aqueous solution) was delivered by syringe pump over 30 min. After the oxidant addition, the resulting mixture was brought to room temperature, and at this point, a 0.8 M biphenyl solution in CH₃CN (0.5 equiv) was added as internal standard. The solution was filtered through a Celite®, silica and alumina plug, which was subsequently rinsed with 2 x 1 mL EtOAc. Then the sample was submitted to GC analysis to determine the mass balance, the conversion, and relative ratio of products by comparison with authentic samples. Yields for ethyl-*p*-benzoquinone, propyl-*p*-benzoquinone and isopropyl-*p*-benzoquinone were calculated with the response factor of methyl-*p*-benzoquinone.

3.4.4.2 Determination of Kinetic Deuterium Isotope Effect

Benzene (0.2 mmol), benzene-*d*₆ (0.2 mmol), and dichloroacetic acid (0.1 mmol) were added into a solution of Mn(^{tips}bpmen) (2 μmol) in HFIP (2 mL). Subsequently, a solution of H₂O₂ (0.2 mmol, diluted from a 35% H₂O₂ aqueous solution) was added during a period of 30 min under constant stirring. The mixture was stirred for 30 minutes at 0 °C. After the oxidant addition, the resulting mixture was brought to room temperature, and the complex was removed by column chromatography with silica, which was subsequently rinsed with 2 x 1 mL EtOAc. Product distribution was determined by GC-MS. The kinetic isotope effect (KIE) was measured taking into account the abundances for ions with $m/z = 94$ and 99 for the phenol peak.

Author Contributions

E.M-R., M.C. and R.K.G. devised the project and designed experiments. E.M-R. performed the experiments and analyzed the data. M.B. analyzed data. M.L. performed X-ray analysis. E.M-R. wrote the Chapter and M.C. and R.K.G provided comments on the experiments and Chapter content.

3.5 References

1. Costas, M.; Chen, K.; Que Jr, L., Biomimetic nonheme iron catalysts for alkane hydroxylation. *Coord. Chem. Rev.* **2000**, *200*, 517-544.
2. Chen, M. S.; White, M. C., A predictably selective aliphatic C–H oxidation reaction for complex molecule synthesis. *Science* **2007**, *318* (5851), 783-787.
3. Nam, W., High-valent iron(IV)–oxo complexes of heme and non-heme ligands in oxygenation reactions. *Acc. Chem. Res.* **2007**, *40* (7), 522-531.
4. Gormisky, P. E.; White, M. C., Catalyst-controlled aliphatic C–H oxidations with a predictive model for site-selectivity. *J. Am. Chem. Soc.* **2013**, *135* (38), 14052-14055.
5. Ottenbacher, R. V.; Talsi, E. P.; Bryliakov, K. P., Mechanism of selective C–H hydroxylation mediated by manganese aminopyridine enzyme models. *ACS Catal.* **2014**, *5* (1), 39-44.
6. Shen, D.; Miao, C.; Wang, S.; Xia, C.; Sun, W., Efficient benzylic and aliphatic C–H oxidation with selectivity for methylenic sites catalyzed by a bioinspired manganese complex. *Org. Lett.* **2014**, *16* (4), 1108-1111.
7. Oloo, W. N.; Que Jr, L., Bioinspired Nonheme Iron Catalysts for C–H and C=C Bond Oxidation: Insights into the Nature of the Metal-Based Oxidants. *Acc. Chem. Res.* **2015**, *48* (9), 2612-2621.
8. Olivo, G.; Cussó, O.; Costas, M., Biologically Inspired C–H and C=C Oxidations with Hydrogen Peroxide Catalyzed by Iron Coordination Complexes. *Chem. Asian J.* **2016**, *11* (22), 3148-3158.
9. Font, D.; Canta, M.; Milan, M.; Cussó, O.; Ribas, X.; Klein Gebbink, R. J. M.; Costas, M., Readily accessible bulky iron catalysts exhibiting site selectivity in the oxidation of steroidal substrates. *Angew. Chem. Int. Ed.* **2016**, *55* (19), 5776-5779.
10. Milan, M.; Carboni, G.; Salamone, M.; Costas, M.; Bietti, M., Tuning Selectivity in Aliphatic C–H Bond Oxidation of N-Alkylamides and Phthalimides Catalyzed by Manganese Complexes. *ACS Catal.* **2017**, *7* (9), 5903-5911.
11. Milan, M.; Bietti, M.; Costas, M., Highly enantioselective oxidation of nonactivated aliphatic C–H bonds with hydrogen peroxide catalyzed by manganese complexes. *ACS Cent. Sci.* **2017**, *3* (3), 196-204.
12. Chen, J.; Lutz, M.; Milan, M.; Costas, M.; Otte, M.; Klein Gebbink, R. J. M., Non-Heme Iron Catalysts with a Rigid Bis-Isoindoline Backbone and Their Use in Selective Aliphatic C–H Oxidation. *Adv. Synth. Catal.* **2017**, *359*, 2590-2595.
13. Ottenbacher, R. V.; Talsi, E. P.; Bryliakov, K. P., Chiral Manganese Aminopyridine Complexes: the Versatile Catalysts of Chemo- and Stereoselective Oxidations with H₂O₂. *Chem. Rec.* **2018**, *18* (1), 78-90.
14. Milan, M.; Salamone, M.; Costas, M.; Bietti, M., The Quest for Selectivity in Hydrogen Atom Transfer Based Aliphatic C–H Bond Oxygenation. *Acc. Chem. Res.* **2018**, *51* (9), 1984-1995.

15. Ottenbacher, R. V.; Talsi, E. P.; Rybalova, T. V.; Bryliakov, K. P., Enantioselective Benzylic Hydroxylation of Arylalkanes with H₂O₂ in Fluorinated Alcohols in the Presence of Chiral Mn Aminopyridine Complexes. *ChemCatChem* **2018**, *10* (22), 5323-5330.
16. Milan, M.; Bietti, M.; Costas, M., Aliphatic C–H Bond Oxidation with Hydrogen Peroxide Catalyzed by Manganese Complexes: Directing Selectivity through Torsional Effects. *Org. Lett.* **2018**, *20* (9), 2720-2723.
17. Qiu, B.; Xu, D.; Sun, Q.; Miao, C.; Lee, Y.-M.; Li, X.-X.; Nam, W.; Sun, W., Highly Enantioselective Oxidation of Spirocyclic Hydrocarbons by Bioinspired Manganese Catalysts and Hydrogen Peroxide. *ACS Catal.* **2018**, *8* (3), 2479-2487.
18. Wang, W.; Xu, D.; Sun, Q.; Sun, W., Efficient Aliphatic C–H Bond Oxidation Catalyzed by Manganese Complexes with Hydrogen Peroxide. *Chem. Asian J.* **2018**, *13* (17), 2458-2464.
19. White, M. C.; Zhao, J., Aliphatic C–H Oxidations for Late-Stage Functionalization. *J. Am. Chem. Soc.* **2018**, *140* (43), 13988-14009.
20. Qiu, B.; Xu, D.; Sun, Q.; Lin, J.; Sun, W., Manganese-Catalyzed Asymmetric Oxidation of Methylene C–H of Spirocyclic Oxindoles and Dihydroquinolinones with Hydrogen Peroxide. *Org. Lett.* **2019**, *21* (3), 618-622.
21. Zhao, J.; Nanjo, T.; de Lucca Jr, E. C.; White, M. C., Chemoselective methylene oxidation in aromatic molecules. *Nature* **2019**, *11*, 213-221.
22. Wu, M.; Wang, B.; Wang, S.; Xia, C.; Sun, W., Asymmetric Epoxidation of Olefins with Chiral Bioinspired Manganese Complexes. *Org. Lett.* **2009**, *11* (16), 3622-3625.
23. Ottenbacher, R. V.; Bryliakov, K. P.; Talsi, E. P., Non-Heme Manganese Complexes Catalyzed Asymmetric Epoxidation of Olefins by Peracetic Acid and Hydrogen Peroxide. *Adv. Synth. Catal.* **2011**, *353* (6), 885-889.
24. Garcia-Bosch, I.; Gomez, L.; Polo, A.; Ribas, X.; Costas, M., Stereoselective Epoxidation of Alkenes with Hydrogen Peroxide using a Bipyrrolidine-Based Family of Manganese Complexes. *Adv. Synth. Catal.* **2012**, *354* (1), 65-70.
25. Cussó, O.; Garcia-Bosch, I.; Font, D.; Ribas, X.; Lloret-Fillol, J.; Costas, M., Highly stereoselective epoxidation with H₂O₂ catalyzed by electron-rich aminopyridine manganese catalysts. *Org. Lett.* **2013**, *15* (24), 6158-6161.
26. Cussó, O.; Garcia-Bosch, I.; Ribas, X.; Lloret-Fillol, J.; Costas, M., Asymmetric epoxidation with H₂O₂ by manipulating the electronic properties of non-heme iron catalysts. *J. Am. Chem. Soc.* **2013**, *135* (39), 14871-14878.
27. Ottenbacher, R. V.; Samsonenko, D. G.; Talsi, E. P.; Bryliakov, K. P., Highly Enantioselective Bioinspired Epoxidation of Electron-Deficient Olefins with H₂O₂ on Aminopyridine Mn Catalysts. *ACS Catal.* **2014**, *4* (5), 1599-1606.
28. Cussó, O.; Ribas, X.; Costas, M., Biologically inspired non-heme iron-catalysts for asymmetric epoxidation; design principles and perspectives. *Chem. Commun.* **2015**, *51* (76), 14285-14298.
29. Cussó, O.; Cianfanelli, M.; Ribas, X.; Klein Gebbink, R. J. M.; Costas, M., Iron catalyzed highly enantioselective epoxidation of cyclic aliphatic enones with aqueous H₂O₂. *J. Am. Chem. Soc.* **2016**, *138* (8), 2732-2738.

30. Shen, D.; Qiu, B.; Xu, D.; Miao, C.; Xia, C.; Sun, W., Enantioselective Epoxidation of Olefins with H₂O₂ Catalyzed by Bioinspired Aminopyridine Manganese Complexes. *Org. Lett.* **2016**, *18* (3), 372-375.
31. Du, J.; Miao, C.; Xia, C.; Lee, Y.-M.; Nam, W.; Sun, W., Mechanistic Insights into the Enantioselective Epoxidation of Olefins by Bioinspired Manganese Complexes: Role of Carboxylic Acid and Nature of Active Oxidant. *ACS Catal.* **2018**, *8* (5), 4528-4538.
32. Clarasó, C.; Vicens, L.; Polo, A.; Costas, M., Enantioselective Epoxidation of β, β -Disubstituted Enamides with a Manganese Catalyst and Aqueous Hydrogen Peroxide. *Org. Lett.* **2019**, *21*, 2430-2435.
33. Mitra, M.; Cussó, O.; Bhat, S. S.; Sun, M.; Cianfanelli, M.; Costas, M.; Nordlander, E., Highly enantioselective epoxidation of olefins by H₂O₂ catalyzed by a non-heme Fe(II) catalyst of a chiral tetradentate ligand. *Dalton Trans.* **2019**, *48* (18), 6123-6131.
34. Borrell, M.; Costas, M., Mechanistically driven development of an iron catalyst for selective syn-dihydroxylation of alkenes with aqueous hydrogen peroxide. *J. Am. Chem. Soc.* **2017**, *139* (36), 12821-12829.
35. Vicens, L.; Olivo, G.; Costas, M., Rational Design of Bioinspired Catalysts for Selective Oxidations. *ACS Catal.* **2020**, *10* (15), 8611-8631.
36. Oh, N. Y.; Seo, M. S.; Lim, M. H.; Consugar, M. B.; Park, M. J.; Rohde, J.-U.; Han, J.; Kim, K. M.; Kim, J.; Que Jr, L., Self-hydroxylation of perbenzoic acids at a nonheme iron(II) center. *Chem. Commun.* **2005**, (45), 5644-5646.
37. Taktak, S.; Flook, M.; Foxman, B. M.; Que Jr, L.; Rybak-Akimova, E. V., *ortho*-Hydroxylation of benzoic acids with hydrogen peroxide at a non-heme iron center. *Chem. Commun.* **2005**, (42), 5301-5303.
38. Thibon, A.; Bartoli, J.-F.; Guillot, R.; Sainton, J.; Martinho, M.; Mansuy, D.; Banse, F., Non-heme iron polyazadentate complexes as catalysts for aromatic hydroxylation by H₂O₂: Particular efficiency of tetrakis(2-pyridylmethyl)ethylenediamine–iron(II) complexes. *J. Mol. Catal. Chem.* **2008**, *287* (1-2), 115-120.
39. Makhlynets, O. V.; Rybak-Akimova, E. V., Aromatic Hydroxylation at a Non-Heme Iron Center: Observed Intermediates and Insights into the Nature of the Active Species. *Chem. Eur. J.* **2010**, *16* (47), 13995-14006.
40. Raba, A.; Cokoja, M.; Herrmann, W. A.; Kühn, F. E., Catalytic hydroxylation of benzene and toluene by an iron complex bearing a chelating di-pyridyl-di-NHC ligand. *Chem. Commun.* **2014**, *50* (78), 11454-11457.
41. Kejriwal, A.; Bandyopadhyay, P.; Biswas, A. N., Aromatic hydroxylation using an oxo-bridged diiron(III) complex: a bio-inspired functional model of toluene monooxygenases. *Dalton Trans.* **2015**, *44* (39), 17261-17267.
42. Capocasa, G.; Olivo, G.; Barbieri, A.; Lanzalunga, O.; Di Stefano, S., Direct hydroxylation of benzene and aromatics with H₂O₂ catalyzed by a self-assembled iron complex: evidence for a metal-based mechanism. *Catal. Sci. Technol.* **2017**, *7* (23), 5677-5686.
43. Lindhorst, A. C.; Schütz, J.; Netscher, T.; Bonrath, W.; Kühn, F. E., Catalytic oxidation of aromatic hydrocarbons by a molecular iron–NHC complex. *Catal. Sci. Technol.* **2017**, *7* (9), 1902-1911.
44. Lyakin, O. Y.; Zima, A. M.; Tkachenko, N. V.; Bryliakov, K. P.; Talsi, E. P., Direct Evaluation of the Reactivity of Nonheme Iron(V)-Oxo Intermediates Toward Arenes. *ACS Catal.* **2018**, *8* (6), 5255-5260.

45. Tkachenko, N. V.; Ottenbacher, R. V.; Lyakin, O. Y.; Zima, A. M.; Samsonenko, D. G.; Talsi, E. P.; Bryliakov, K. P., Highly Efficient Aromatic C–H Oxidation with H₂O₂ in the Presence of Iron Complexes of the PDP Family. *ChemCatChem* **2018**, *10* (18), 4052-4057.
46. Tkachenko, N. V.; Lyakin, O. Y.; Zima, A. M.; Talsi, E. P.; Bryliakov, K. P., Effect of different carboxylic acids on the aromatic hydroxylation with H₂O₂ in the presence of an iron aminopyridine complex. *J. Organomet. Chem.* **2018**, *871*, 130-134.
47. Kal, S.; Draksharapu, A.; Que Jr, L., Sc³⁺ (or HClO₄) Activation of a Nonheme Fe^{III}-OOH Intermediate for the Rapid Hydroxylation of Cyclohexane and Benzene. *J. Am. Chem. Soc.* **2018**, *140* (17), 5798-5804.
48. Kal, S.; Que Jr, L., Activation of a Non-Heme Fe^{III}-OOH by a Second Fe^{III} to Hydroxylate Strong C–H Bonds: Possible Implications for Soluble Methane Monooxygenase. *Angew. Chem.* **2019**, *58* (25), 8484-8488.
49. Xu, S.; Draksharapu, A.; Rasheed, W.; Que Jr, L., Acid pKa Dependence in O–O Bond Heterolysis of a Nonheme Fe^{III}-OOH Intermediate To Form a Potent Fe^V=O Oxidant with Heme Compound I-Like Reactivity. *J. Am. Chem. Soc.* **2019**, *141* (40), 16093-16107.
50. Zima, A. M.; Lyakin, O. Y.; Lubov, D. P.; Bryliakov, K. P.; Talsi, E. P., Aromatic C–H oxidation by non-heme iron(V)-oxo intermediates bearing aminopyridine ligands. *Mol. Catal.* **2020**, *483*, 110708.
51. Wu, X.; Seo, M. S.; Davis, K. M.; Lee, Y.-M.; Chen, J.; Cho, K.-B.; Pushkar, Y. N.; Nam, W., A Highly Reactive Mononuclear Non-Heme Manganese(IV)-Oxo Complex That Can Activate the Strong C–H Bonds of Alkanes. *J. Am. Chem. Soc.* **2011**, *133* (50), 20088-20091.
52. Aratani, Y.; Yamada, Y.; Fukuzumi, S., Selective hydroxylation of benzene derivatives and alkanes with hydrogen peroxide catalysed by a manganese complex incorporated into mesoporous silica–alumina. *Chem. Commun.* **2015**, *51* (22), 4662-4665.
53. Ottenbacher, R. V.; Talsi, E. P.; Bryliakov, K. P., Recent progress in catalytic oxygenation of aromatic C–H groups with the environmentally benign oxidants H₂O₂ and O₂. *Appl Organomet Chem.* **2020**, *34*, e5900.
54. Fukuzumi, S.; Ohkubo, K., One-Step Selective Hydroxylation of Benzene to Phenol. *Asian J. Org. Chem.* **2015**, *4* (9), 836-845.
55. Morimoto, Y.; Bunno, S.; Fujieda, N.; Sugimoto, H.; Itoh, S., Direct hydroxylation of benzene to phenol using hydrogen peroxide catalyzed by nickel complexes supported by pyridylalkylamine ligands. *J. Am. Chem. Soc.* **2015**, *137* (18), 5867-5870.
56. Tsuji, T.; Zaoputra, A. A.; Hitomi, Y.; Mieda, K.; Ogura, T.; Shiota, Y.; Yoshizawa, K.; Sato, H.; Kodera, M., Specific Enhancement of Catalytic Activity by a Dicopper Core: Selective Hydroxylation of Benzene to Phenol with Hydrogen Peroxide. *Angew. Chem. Int. Ed.* **2017**, *129* (27), 7887-7890.
57. Vilella, L.; Conde, A.; Balcells, D.; Díaz-Requejo, M. M.; Lledós, A.; Pérez, P. J., A competing, dual mechanism for catalytic direct benzene hydroxylation from combined experimental-DFT studies. *Chem. Sci.* **2017**, *8* (12), 8373-8383.
58. Kwong, H. K.; Lo, P. K.; Yiu, S. M.; Hirao, H.; Lau, K. C.; Lau, T. C., Highly Selective and Efficient Ring Hydroxylation of Alkylbenzenes with Hydrogen Peroxide and an Osmium(VI) Nitrido Catalyst. *Angew. Chem. Int. Ed.* **2017**, *56* (40), 12260-12263.
59. Muthuramalingam, S.; Anandababu, K.; Velusamy, M.; Mayilmurugan, R., One step phenol synthesis from benzene catalysed by nickel(II) complexes. *Catal. Sci. Technol.* **2019**, *9* (21), 5991-6001.

60. Muthuramalingam, S.; Anandababu, K.; Velusamy, M.; Mayilmurugan, R., Benzene Hydroxylation by Bioinspired Copper (II) Complexes: Coordination Geometry versus Reactivity. *Inorg. Chem.* **2020**, *59*, 5918-5928.
61. Anandababu, K.; Muthuramalingam, S.; Velusamy, M.; Mayilmurugan, R., Single-step benzene hydroxylation by cobalt(II) catalysts via a cobalt(III)-hydroperoxo intermediate. *Catal. Sci. Technol.* **2020**, *10*, 2540-2548.
62. Masferrer-Rius, E.; Hopman, R. M.; van der Kleij, J.; Lutz, M.; Klein Gebbink, R. J. M., On the Ability of Nickel Complexes Derived from Tripodal Aminopyridine Ligands to Catalyze Arene Hydroxylations. *CHIMIA* **2020**, *74* (6), 489-494.
63. Ticconi, B.; Colcerasa, A.; Di Stefano, S.; Lanzalunga, O.; Lapi, A.; Mazzonna, M.; Olivo, G., Oxidative functionalization of aliphatic and aromatic amino acid derivatives with H₂O₂ catalyzed by a nonheme imine based iron complex. *RSC Adv.* **2018**, *8* (34), 19144-19151.
64. Dantignana, V.; Milan, M.; Cussó, O.; Company, A.; Bietti, M.; Costas, M., Chemoselective Aliphatic C–H Bond Oxidation Enabled by Polarity Reversal. *ACS Cent. Sci.* **2017**, *3* (12), 1350-1358.
65. Ottenbacher, R. V.; Samsonenko, D. G.; Talsi, E. P.; Bryliakov, K. P., Highly Efficient, Regioselective, and Stereospecific Oxidation of Aliphatic C–H Groups with H₂O₂, Catalyzed by Aminopyridine Manganese Complexes. *Org. Lett.* **2012**, *14* (17), 4310-4313.
66. Talsi, E. P.; Samsonenko, D. G.; Ottenbacher, R. V.; Bryliakov, K. P., Highly Enantioselective C–H Oxidation of Arylalkanes with H₂O₂ in the Presence of Chiral Mn-Aminopyridine Complexes. *ChemCatChem* **2017**, *9* (24), 4580-4586.
67. Chambers, R. K.; Zhao, J.; Delaney, C. P.; White, M. C., Chemoselective Tertiary C–H Hydroxylation for Late-Stage Functionalization with Mn(PDP)/Chloroacetic Acid Catalysis. *Adv. Synth. Catal.* **2020**, *362* (2), 417-423.
68. Roberts, B. P., Polarity-reversal catalysis of hydrogen-atom abstraction reactions: concepts and applications in organic chemistry. *Chem. Soc. Rev.* **1999**, *28* (1), 25-35.
69. Wang, D.; Shuler, W. G.; Pierce, C. J.; Hilinski, M. K., An iminium salt organocatalyst for selective aliphatic C–H hydroxylation. *Org. Lett.* **2016**, *18* (15), 3826-3829.
70. Gaster, E.; Kozuch, S.; Pappo, D., Selective Aerobic Oxidation of Methylarenes to Benzaldehydes Catalyzed by N-Hydroxyphthalimide and Cobalt(II) Acetate in Hexafluoropropan-2-ol. *Angew. Chem. Int. Ed.* **2017**, *56* (21), 5912-5915.
71. Adams, A. M.; Du Bois, J., Organocatalytic C–H hydroxylation with Oxone® enabled by an aqueous fluoroalcohol solvent system. *Chem. Sci.* **2014**, *5* (2), 656-659.
72. Borrell, M.; Gil-Caballero, S.; Bietti, M.; Costas, M., Site-selective and product chemoselective aliphatic CH bond hydroxylation of polyhydroxylated substrates. *ACS Catal.* **2020**, *10* (8), 4702-4709.
73. Ottenbacher, R. V.; Talsi, E. P.; Bryliakov, K. P., Highly Enantioselective Undirected Catalytic Hydroxylation of Benzylic CH₂ Groups with H₂O₂. *J. Catal.* **2020**, *390*, 170-177.
74. Neves, A.; Erthal, S. M.; Vencato, I.; Ceccato, A. S.; Mascarenhas, Y. P.; Nascimento, O. R.; Horner, M.; Batista, A. A., Synthesis, crystal structure, electrochemical, and spectroelectrochemical properties of the new manganese(III) complex [Mn^{III}(BBPEN)][PF₆][H₂BBPEN=N,N'-bis(2-hydroxybenzyl)-N,N'-bis(2-methylpyridyl)ethylenediamine]. *Inorg. Chem.* **1992**, *31* (23), 4749-4755.

75. Wada, S.; Mikuriya, M., Synthesis and structural characterization of dinuclear manganese(III) complexes with cyclam-based macrocyclic ligands having Schiff-base pendant arms as chelating agents. *Bull. Chem. Soc. Jpn.* **2008**, *81* (3), 348-357.
76. Mandal, D.; Chatterjee, P. B.; Bhattacharya, S.; Choi, K.-Y.; Clérac, R.; Chaudhury, M., Tetra-, tri-, and mononuclear manganese(II/III) complexes of a phenol-based N₂O₂ capping ligand: use of carboxylates as ancillary ligands in tuning the nuclearity of the complexes. *Inorg. Chem.* **2009**, *48* (5), 1826-1835.
77. Sankaralingam, M.; Palaniandavar, M., Tuning the olefin epoxidation by manganese(III) complexes of bisphenolate ligands: effect of Lewis basicity of ligands on reactivity. *Dalton Trans.* **2014**, *43* (2), 538-550.
78. Mikuriya, M.; Kurahashi, S.; Tomohara, S.; Koyama, Y.; Yoshioka, D.; Mitsuhashi, R.; Sakiyama, H., Synthesis, Crystal Structures, and Magnetic Properties of Mixed-Valent Tetranuclear Complexes with Y-Shaped Mn^{II}₂Mn^{III}₂ Core. *Magnetochemistry* **2019**, *5* (1), 8.
79. Talsi, E. P.; Bryliakov, K. P., Chemo- and stereoselective C–H oxidations and epoxidations/*cis*-dihydroxylations with H₂O₂, catalyzed by non-heme iron and manganese complexes. *Coord. Chem. Rev.* **2012**, *256* (13-14), 1418-1434.
80. Bryliakov, K. P.; Talsi, E. P., Active sites and mechanisms of bioinspired oxidation with H₂O₂, catalyzed by non-heme Fe and related Mn complexes. *Coord. Chem. Rev.* **2014**, *276*, 73-96.
81. Lyakin, O. Y.; Ottenbacher, R. V.; Bryliakov, K. P.; Talsi, E. P., Asymmetric epoxidations with H₂O₂ on Fe and Mn aminopyridine catalysts: probing the nature of active species by combined electron paramagnetic resonance and enantioselectivity study. *ACS Catal.* **2012**, *2* (6), 1196-1202.
82. Ottenbacher, R. V.; Talsi, E. P.; Bryliakov, K. P., Mechanism of selective C–H hydroxylation mediated by manganese aminopyridine enzyme models. *ACS Catal.* **2015**, *5* (1), 39-44.
83. Ryabov, A. D.; Sakodinskaya, I. K.; Yatsimirsky, A. K., Kinetics and mechanism of ortho-palladation of ring-substituted NN-dimethylbenzylamines. *J. Chem. Soc., Dalton Trans.* **1985**, (12), 2629-2638.
84. Lafrance, M.; Gorelsky, S. I.; Fagnou, K., High-yielding palladium-catalyzed intramolecular alkane arylation: reaction development and mechanistic studies. *J. Am. Chem. Soc.* **2007**, *129* (47), 14570-14571.
85. Maleckis, A.; Kampf, J. W.; Sanford, M. S., A Detailed Study of Acetate-Assisted C–H Activation at Palladium(IV) Centers. *J. Am. Chem. Soc.* **2013**, *135* (17), 6618-6625.
86. de Boer, J. W.; Brinksma, J.; Browne, W. R.; Meetsma, A.; Alsters, P. L.; Hage, R.; Feringa, B. L., *Cis*-dihydroxylation and epoxidation of alkenes by [Mn₂O(RCO₂)₂(tmtacn)₂]: tailoring the selectivity of a highly H₂O₂-efficient catalyst. *J. Am. Chem. Soc.* **2005**, *127* (22), 7990-7991.
87. pK_a values were taken from: Haynes, W. M., *Handbook of Chemistry and Physics*. 91st ed.; CRC Press (Taylor and Francis Group): Boca Raton, FL.
88. Metelitsa, D. I., Mechanisms of the hydroxylation of aromatic compounds. *Russ. Chem. Rev.* **1971**, *40* (7), 563.
89. Walling, C.; Johnson, R. A., Fenton's reagent. V. Hydroxylation and side-chain cleavage of aromatics. *J. Am. Chem. Soc.* **1975**, *97* (2), 363-367.
90. Kunai, A.; Hata, S.; Ito, S.; Sasaki, K., The role of oxygen in the hydroxylation reaction of benzene with Fenton's reagent. Oxygen 18 tracer study. *J. Am. Chem. Soc.* **1986**, *108* (19), 6012-6016.

91. Kurata, T.; Watanabe, Y.; Katoh, M.; Sawaki, Y., Mechanism of aromatic hydroxylation in the Fenton and related reactions. One-electron oxidation and the NIH shift. *J. Am. Chem. Soc.* **1988**, *110* (22), 7472-7478.
92. Olivo, G.; Lanzalunga, O.; Di Stefano, S., Non-Heme Imine-Based Iron Complexes as Catalysts for Oxidative Processes. *Adv. Synth. Catal.* **2016**, *358* (6), 843-863.
93. Marusawa, H.; Ichikawa, K.; Narita, N.; Murakami, H.; Ito, K.; Tezuka, T., Hydroxyl radical as a strong electrophilic species. *Bioorg. Med. Chem.* **2002**, *10* (7), 2283-2290.
94. Mas-Ballesté, R.; Que, L., Iron-catalyzed olefin epoxidation in the presence of acetic acid: insights into the nature of the metal-based oxidant. *J. Am. Chem. Soc.* **2007**, *129* (51), 15964-15972.
95. Ottenbacher, R. V.; Talsi, E. P.; Bryliakov, K. P., Direct selective oxidative functionalization of C–H bonds with H₂O₂: Mn-Aminopyridine complexes challenge the dominance of non-heme Fe catalysts. *Molecules* **2016**, *21* (11), 1454.
96. MacFaul, P. A.; Ingold, K.; Wayner, D.; Que, L., A Putative Monooxygenase Mimic Which Functions via Well-Disguised Free Radical Chemistry. *J. Am. Chem. Soc.* **1997**, *119* (44), 10594-10598.
97. Ingold, K. U.; MacFaul, P. A., *Biomimetic oxidations catalyzed by transition metal complexes*. Meunier, B., Ed.; Imperial College Press: London, 2000; p 45.
98. Hiatt, R.; Clipsham, J.; Visser, T., The induced decomposition of tert-butyl hydroperoxide. *Can. J. Chem.* **1964**, *42* (12), 2754-2757.
99. Ito, S.; Mitarai, A.; Hikino, K.; Hiram, M.; Sasaki, K., Deactivation reaction in the hydroxylation of benzene with Fenton's reagent. *J. Org. Chem.* **1992**, *57* (25), 6937-6941.
100. Augusti, R.; Dias, A. O.; Rocha, L. L.; Lago, R. M., Kinetics and mechanism of benzene derivative degradation with Fenton's reagent in aqueous medium studied by MIMS. *The Journal of Physical Chemistry A* **1998**, *102* (52), 10723-10727.
101. Siddiqi, Z.; Wertjes, W. C.; Sarlah, D., Chemical Equivalent of Arene Monooxygenases: Dearomative Synthesis of Arene Oxides and Oxepines. *J. Am. Chem. Soc.* **2020**, *142* (22), 10125-10131.
102. Lowry, T. H.; Richardson, K. S., *Mechanism and Theory in Organic Chemistry*. III edn, Harper & Row Publishers, New York, 1987; p 628.
103. Ortiz de Montellano, P. R., *Cytochrome P450: Structure, Mechanism, and Biochemistry*. 2nd ed. ed.; Ortiz de Montellano, P. R., Ed. Plenum Press, New York: 1995; pp 245-303.
104. Meunier, B.; De Visser, S. P.; Shaik, S., Mechanism of oxidation reactions catalyzed by cytochrome P450 enzymes. *Chem. Rev.* **2004**, *104* (9), 3947-3980.
105. Korzekwa, K. R.; Swinney, D. C.; Trager, W. F., Isotopically labeled chlorobenzenes as probes for the mechanism of cytochrome P-450 catalyzed aromatic hydroxylation. *Biochemistry* **1989**, *28* (23), 9019-9027.
106. de Visser, S. P.; Shaik, S., A proton-shuttle mechanism mediated by the porphyrin in benzene hydroxylation by cytochrome P450 enzymes. *J. Am. Chem. Soc.* **2003**, *125* (24), 7413-7424.
107. Kudrik, E. V.; Sorokin, A. B., N-Bridged Diiron Phthalocyanine Catalyzes Oxidation of Benzene with H₂O₂ via Benzene Oxide with NIH Shift Evidenced by Using 1,3,5-[D₃]Benzene as a Probe. *Chem. Eur. J.* **2008**, *14* (24), 7123-7126.

108. Feng, K.; Quevedo, R. E.; Kohrt, J. T.; Oderinde, M. S.; Reilly, U.; White, M. C., Late-stage oxidative C(sp³)-H methylation. *Nature* **2020**, *580* (7805), 621-627.
109. Esarey, S. L.; Holland, J. C.; Bartlett, B. M., Determining the Fate of a Non-Heme Iron Oxidation Catalyst Under Illumination, Oxygen, and Acid. *Inorg. Chem.* **2016**, *55*, 11040-11049.
110. Font, D.; Canta, M.; Milan, M.; Cussó, O.; Ribas, X.; Klein Gebbink, R. J. M.; Costas, M., Readily accessible bulky iron catalysts exhibiting site selectivity in the oxidation of steroidal substrates. *Angew. Chem. Int. Ed.* **2016**, *55* (19), 5776-5779.
111. S., C. M.; White, M. C., A Predictably Selective Aliphatic C-H Oxidation Reaction for Complex Molecule Synthesis. *Science* **2007**, *318*, 783-787.
112. Chen, J.; Lutz, M.; Milan, M.; Costas, M.; Otte, M.; Klein Gebbink, R. J. M., Non-Heme Iron Catalysts with a Rigid Bis-Isoindoline Backbone and Their Use in Selective Aliphatic C-H Oxidation. *Adv. Synth. Catal.* **2017**, *359*, 2590-2595.
113. Mautner, F. A.; Koikawa, M.; Mikuriya, M.; Harrelson, E. V.; Massoud, S. S., Copper(II)-azido complexes constructed from polypyridyl amine ligands. *Polyhedron* **2013**, *59*, 17-22.
114. Murphy, A.; Dubois, G.; Stack, T. D. P., Efficient Epoxidation of Electron-Deficient Olefins with a Cationic Manganese Complex. *J. Am. Chem. Soc.* **2003**, *125*, 5250-5251.
115. Chen, J.; de Liedekerke Beaufort, M.; Gyurik, L.; Dorresteijn, J.; Otte, M.; Klein Gebbink, R. J. M., Highly efficient epoxidation of vegetable oils catalyzed by a manganese complex with hydrogen peroxide and acetic acid. *Green Chem.* **2019**, *21* (9), 2436-2447.
116. Urbanová, K.; Ramírez-Macías, I.; Martín-Escolano, R.; Rosales, M. J.; Cussó, O.; Serrano, J.; Sánchez-Moreno, M.; Costas, M.; Ribas, X.; Marín, C., Effective Tetradentate Compound Complexes against *Leishmania* spp. that Act on Critical Enzymatic Pathways of These Parasites. *Molecules* **2019**, *24* (1), 134.
117. Patra, T.; Mukherjee, S.; Ma, J.; Strieth-Kalthoff, F.; Glorius, F., Visible-Light-Photosensitized Aryl and Alkyl Decarboxylative Functionalization Reactions. *Angew. Chem. Int. Ed.* **2019**, *58* (31), 10514-10520.
118. Schreurs, A. M.; Xian, X.; Kroon-Batenburg, L. M., EVAL15: a diffraction data integration method based on ab initio predicted profiles. *J. Appl. Crystallogr.* **2010**, *43* (1), 70-82.
119. Sheldrick, B. M., SADABS. **2014**, Universität Göttingen, Germany.
120. Sheldrick, G. M., SHELXT—Integrated space-group and crystal-structure determination. *Acta Cryst.* **2015**, *A71* (1), 3-8.
121. Sheldrick, G. M., Crystal structure refinement with SHELXL. *Acta Cryst.* **2015**, *C71* (1), 3-8.
122. Parsons, S.; Flack, H. D.; Wagner, T., Use of intensity quotients and differences in absolute structure refinement. *Acta Cryst.* **2013**, *B69* (3), 249-259.
123. Spek, A. L., Structure validation in chemical crystallography. *Acta Cryst.* **2009**, *D65* (2), 148-155.

Chapter 4

Electronic and Steric Ligand Effects on Catalytic Arene Oxidation by Aminopyridine-based Manganese Complexes

Abstract

The catalytic activity of a series of bioinspired manganese complexes of the bpmcn ligand family (bpmcn = *N,N'*-dimethyl-*N,N'*-bis(2-picoyl)-cyclohexane-*trans*-1,2-diamine) with different substituents on the pyridine donors, [Mn^{II}(CF₃SO₃)^(X)(^Xbpmcn)] (^X**1**) (X = CF₃, Cl, H, dMM, Me₂N, Pyr, TIPS, Ph(CF₃)₂), has been studied in the oxidation of a monoalkylbenzene with H₂O₂ to evaluate the sensitivity of the reaction to electronic and steric effects. In the presence of the dichloroacetic acid additive, the electron-poor manganese complexes are not active as arene oxidation catalysts, whereas electron-rich manganese complexes afford high substrate conversions, although showing poor selectivity for aromatic hydroxylation. C₂-symmetric bulky ^{TIPS}**1** complex has demonstrated the highest catalytic efficiency and aromatic oxidation selectivity, which is superior to the other bulky complex tested, ^{Ph(CF₃)₂}**1**. An analysis of the two bulky substituents shows that the TIPS group might provide a better encapsulation of the catalytic active site, thus, better preventing product inhibition by phenolate binding to manganese. Moreover, the electron-withdrawing character of the ligand on complex ^{Ph(CF₃)₂}**1** might contribute to its lower aromatic oxidation activity. Along the same line, we have explored the reactivity of two new manganese complexes (**4** and **5**) that combine electron-rich bulky pyridines in arene oxidation and have compared it with the reactivity of our benchmark catalyst ^{TIPS}**1**.

This chapter is based on:

Masferrer-Rius, E.; Cianfanelli, M.; Lutz, M.; Costas, M.; Klein Gebbink, R. J. M. *Manuscript in preparation*

4.1 Introduction

The direct hydroxylation of aromatic substrates to the corresponding phenol products is a very challenging and interesting reaction since phenolic products are essential intermediates in the generation of a broad range of products, like pharmaceuticals and polymers.^{1,2} Amongst other approaches, molecular coordination compounds are investigated for their catalytic propensity to carry out these reactions, with a special focus on the direct oxidation of benzene or alkylbenzenes to the corresponding phenol products.³⁻⁸ Current efforts specifically address the challenges of obtaining good conversions, yields and selectivities for the phenol products, employing benign oxidants such as O₂ and H₂O₂. Nevertheless, to date there are only a few molecular systems that can perform such challenging arene oxidations.⁹⁻²⁵ An additional interest in direct arene hydroxylation is the possible application of such reactions to functionalized substrates, such that late-stage oxidative functionalization of arene moieties becomes possible.

Over the last years, attention has been devoted to the exploration of biologically inspired non-heme iron and manganese complexes based on aminopyridine ligands as arene oxidation catalysts, which are minimalistic models of natural oxygenase enzymes.^{26,27} The use of such complexes as catalysts is of interest from a sustainable perspective, since they are based on an abundant and non-toxic metal, and allow for the use of environmentally benign oxidants, such as H₂O₂. However, most of the reported aromatic oxidations catalyzed by such complexes are stoichiometric and suffer from product inhibition, in which the phenol binds irreversibly to the metal center and prevents further catalytic turnover.²⁸⁻⁴² Bryliakov and co-workers described the use of iron complexes based on bpbp-type ligands (bpbp = *N,N'*-bis(2-pyridylmethyl)-2,2'-bipyrrolidine), which are able to perform a few catalytic turnovers in the oxidation of (substituted) arenes, albeit with modest chemoselectivity and the formation of overoxidation and benzylic alcohol products.⁴³⁻⁴⁶ Kühn and co-workers reported on an iron complex based on an N-heterocyclic carbene ligand that is able to perform aromatic oxidation reactions. Also in this case, conversions and yields for phenol products are relatively low and benzylic alcohol byproducts are formed.^{47,48} Another iron complex supported by an iminopyridine ligand capable of arene hydroxylation was developed by Di Stefano and co-workers, also displaying benzylic hydroxylation as a side reaction.^{14,22}

Despite the extensive research on complexes based on iron, complexes based on other first-row transition metal have also been investigated as arene oxidation catalysts, such as the systems described by Itoh et al.¹² and Mayilmurugan et al.¹⁷, which are both based on nickel supported by aminopyridine ligands. Other reports have described the use of complexes based on copper as catalysts for aromatic oxidation, such as a dicopper complex supported by the 6-hpa (6-hpa = 1,2-bis[2-[bis(2-pyridylmethyl)aminomethyl]-6-pyridyl]ethane) ligand reported by Kodera and co-workers,¹³ and mononuclear copper complexes supported by electron-rich

tetradentate aminopyridine ligands and bidentate iminopyridine ligands described by Mayilmurugan and co-workers.^{19, 20} Pérez and co-workers have also shown that a mononuclear copper complex containing a hydrotrispyrazolylborate ligand is an active arene hydroxylation catalyst using H_2O_2 as the oxidant.^{49, 50}

In Chapter 3 of this thesis, we have reported that a bulky aminopyridine-based manganese complex **TIPS1** bearing triisopropylsilyl (TIPS) moieties at the 5-position of each pyridine ring efficiently catalyzes the hydroxylation of monoalkylbenzene substrates to the corresponding phenol products with aqueous H_2O_2 , employing a halogenated carboxylic acid additive (dichloroacetic acid) in fluorinated alcohol solvents (TFE = 2,2,2-trifluoroethanol or HFIP = 1,1,1,3,3,3-hexafluoro-2-propanol) under mild reaction conditions (Figure 1).²⁴

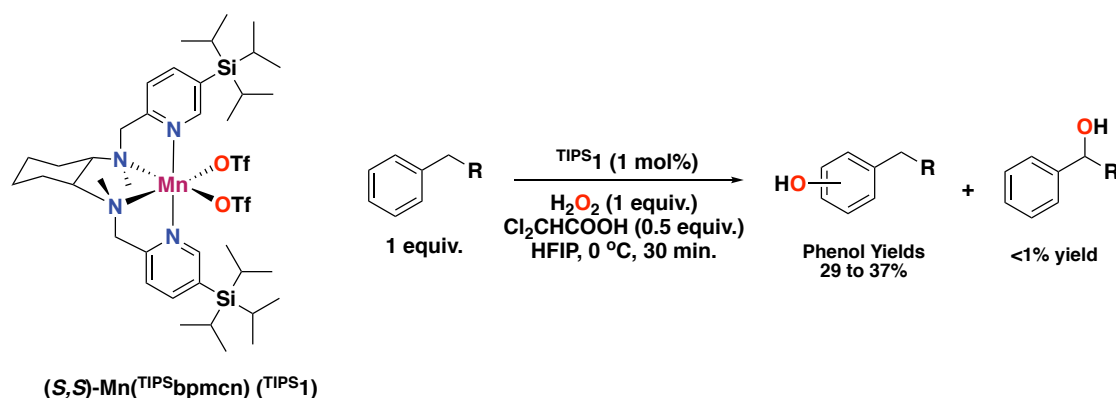


Figure 1. Aromatic C–H hydroxylation reaction with H_2O_2 catalyzed by bulky manganese catalyst **TIPS1**.

A crucial finding was the use of manganese complexes supported by sterically encumbered tetradentate aminopyridine ligands containing TIPS groups, which retarded product inhibition by phenolate binding. The overall product profile, in combination with a negligible KIE and the effectiveness of using $t\text{BuOOH}$ as oxidant, indicate that this complex operates via a metal-based mechanism with no significant involvement of oxygen-centered radicals. In addition, we postulated that the reaction mechanism might proceed via an arene epoxidation pathway due to the observation of an NIH shift.²⁴

Some of the main challenges in the aromatic oxidation of alkylbenzene substrates are the achievement of a good chemoselectivity for the reaction (aromatic vs benzylic oxidation) and the prevention of overoxidation of phenol products to, e.g., catechols, hydroquinones, or benzoquinones. While electron-rich manganese complexes such as **dMM1** (see Figure 2) in combination with acetic acid as additive preferentially oxidize the weaker, benzylic C–H bonds in alkylbenzene substrates, the oxidation of monoalkylbenzene substrates using the **TIPS1**/ H_2O_2 / Cl_2CHCOOH system features excellent chemoselectivity for aromatic oxidation over aliphatic side-chain oxidation.²⁴ The yields obtained for phenol products were the best

reported at the time this work was published (up to 37% total yield based on the substrate as the limiting reagent), with only trace amounts of benzylic alcohol products and benzoquinone being detected (<1% yield). The chemoselectivity observed for this system is higher than that observed for other transition-metal catalysts.^{11-14, 22, 44, 47, 51-53}

Another important aspect of this system is the use of an electron-deficient carboxylic acid additive with a low pK_a value, which considerably enhances the efficiency of the aromatic oxidation compared to the use of aliphatic carboxylic acids. Dichloroacetic acid was selected as the additive of choice and a twofold role in catalysis was proposed. First, the acid additive keeps the phenol products protonated, which avoids product inhibition by phenolate binding to the catalyst. And second, we hypothesize that its electron-withdrawing character makes the electrophilic oxidant, *i.e.* the manganese-oxo species formed after cleavage of the O–O bond of the manganese-hydroperoxo species,⁵⁴⁻⁵⁶ even more electrophilic, which might result in a more reactive oxidant towards arenes.

In this Chapter, we further investigate the electronic and steric properties of the aminopyridine ligand used in the **TIPS1** catalyst. We envision that modification of the electronic properties of the ligand structure of the manganese complex could lead to a further enhancement of catalytic activity. Particularly, we envisioned that electron-withdrawing substituents could enhance the electrophilicity of the manganese-oxo species, and therefore, also improve the efficiency of the complex towards the reaction with arenes. Accordingly, we have explored a series of manganese complexes with different electronic properties by varying the pyridine donors of the ligand, so that we could test their activity in the aromatic oxidation of an alkylbenzene substrate and evaluate the sensitivity of the reaction to electronic effects. Modulation of the electronic properties has been previously investigated for non-heme iron and manganese complexes, however their reactivity has only been explored in aliphatic C(sp³)–H bond oxidation and epoxidation reactions,⁵⁷⁻⁶⁰ whereas it has not yet been explored for aromatic oxidation. Moreover, we are presenting a detailed comparison between steric and electronic ligand effects for the Mn-catalyzed arene oxidation, which highlight that steric effects in a C₂-symmetric manganese complex provide an active system capable of catalytic turnover, whereas electronic effects (electron-donating substituents) seem to enhance reactivity (higher substrate conversions) but result in lower selectivities towards phenol formation. Finally, we have explored the reactivity of manganese complexes (**4** and **5**) that combine electron-rich bulky pyridines in arene oxidation and have compared it with the reactivity of our benchmark catalyst **TIPS1**.

4.2 Results and discussion

4.2.1 Synthesis and characterization of ligands and metal complexes

In order to explore the electronic properties of the manganese catalyst, we have synthesized a set of complexes of the general formula $[\text{Mn}^{\text{II}}(\text{CF}_3\text{SO}_3)(^{\text{X}}\text{bpmcn})]$ (**X1**) ($\text{X} = \text{CF}_3, \text{Cl}, \text{H}, \text{dMM}, \text{Me}_2\text{N}, \text{Pyr}$), with different electron-withdrawing and electron-donating substituents on each of the pyridine moieties (see Figure 2 for structures and Experimental Section for further details). The most electron-poor manganese complex comprises a *para*- CF_3 substituent ($\sigma_{\text{para}} = +0.54$), the most electron-rich ones a *para*- NMe_2 or *para*- $\text{N}(\text{CH}_2)_4$ group ($\sigma_{\text{para}} = -0.83$).⁶¹ Complex **TIPS1** was also considered in this Chapter for comparison purposes. Moreover, another bulky manganese complex containing *ortho*- CF_3 phenyl substituents on each pyridine ring, $[\text{Mn}^{\text{II}}(\text{CF}_3\text{SO}_3)(^{\text{Ph}(\text{CF}_3)_2}\text{bpmcn})]$ (**Ph(CF₃)₂1**), was also prepared in the present Chapter, and its reactivity was compared to **TIPS1**, as well as to the other complexes synthesized in this Chapter. In addition, C_1 -symmetric manganese complexes with different heterocyclic arms have also been considered as potential catalysts for arene hydroxylation in the current Chapter. Accordingly, we have designed a complex that combines a non-substituted pyridine with a bulky pyridine ($[\text{Mn}^{\text{II}}(\text{CF}_3\text{SO}_3)_2(^{\text{H,TIPS}}\text{bpmcn})]$, **2**). Moreover, a complex containing an electron-rich pyridine with a 4-dimethylamino group, and a bulky pyridine ($[\text{Mn}^{\text{II}}(\text{CF}_3\text{SO}_3)_2(^{\text{NMe}_2,\text{TIPS}}\text{bpmcn})]$, **3**) has also been prepared (Figure 2).

C_2 -symmetric ligands were prepared in good yields by the reaction of two equiv. of the corresponding pyridine chloride synthon with one equiv. of the corresponding amine backbone, whereas a different synthetic strategy was used for C_1 -symmetric ligands (details on the preparation of the ligands are collected in the Experimental Section). Ligands were characterized by ^1H NMR and ^{13}C NMR spectroscopy, IR, and high-resolution mass spectrometry (HRMS) (see Experimental Section for further details). Complexation reactions were then performed by the reaction of equimolar amounts of the corresponding ligand with $[\text{Mn}^{\text{II}}(\text{CF}_3\text{SO}_3)_2]$ in dry THF under an inert atmosphere. Evaporation of the solvent under vacuum and recrystallization by slow vapor diffusion of ether into a CH_2Cl_2 solution afforded the desired complexes as crystalline materials in yields ranging from 31 to 78%. Complexes **H1**, **dMM1**, **NMe21**, **Pyr1**, **TIPS1** and **Ph(CF₃)₂1** have been previously characterized by HRMS or X-ray crystallography⁶²⁻⁶⁵, whereas the newly reported complexes **CF₃1**, **Cl1**, **2** and **3** were characterized by HRMS. X-ray structures were determined for **CF₃1** and **Cl1** (*vide infra*). HRMS analysis of **CF₃1** showed a prominent mass peak at m/z 664.0963 corresponding to the $[\text{Mn}^{\text{II}}(\text{CF}_3\text{SO}_3)(^{\text{CF}_3}\text{1})]^+$ ion (calc. 664.0962), and HRMS analysis of complex **Cl1** showed a prominent mass peak at m/z 596.0431 corresponding to the $[\text{Mn}^{\text{II}}(\text{CF}_3\text{SO}_3)(^{\text{Cl}}\text{1})]^+$ ion (calc. 596.0435). Regarding the non-symmetrical manganese complexes, HRMS analysis of **2** showed a prominent mass peak at m/z

684.2548 corresponding to the $[\text{Mn}^{\text{II}}(\text{CF}_3\text{SO}_3)(\mathbf{2})]^+$ ion (calc. 684.2549), and HRMS analysis of **3** showed a prominent mass peak at m/z 727.2965 corresponding to the $[\text{Mn}^{\text{II}}(\text{CF}_3\text{SO}_3)(\mathbf{3})]^+$ ion (calc. 727.2971).

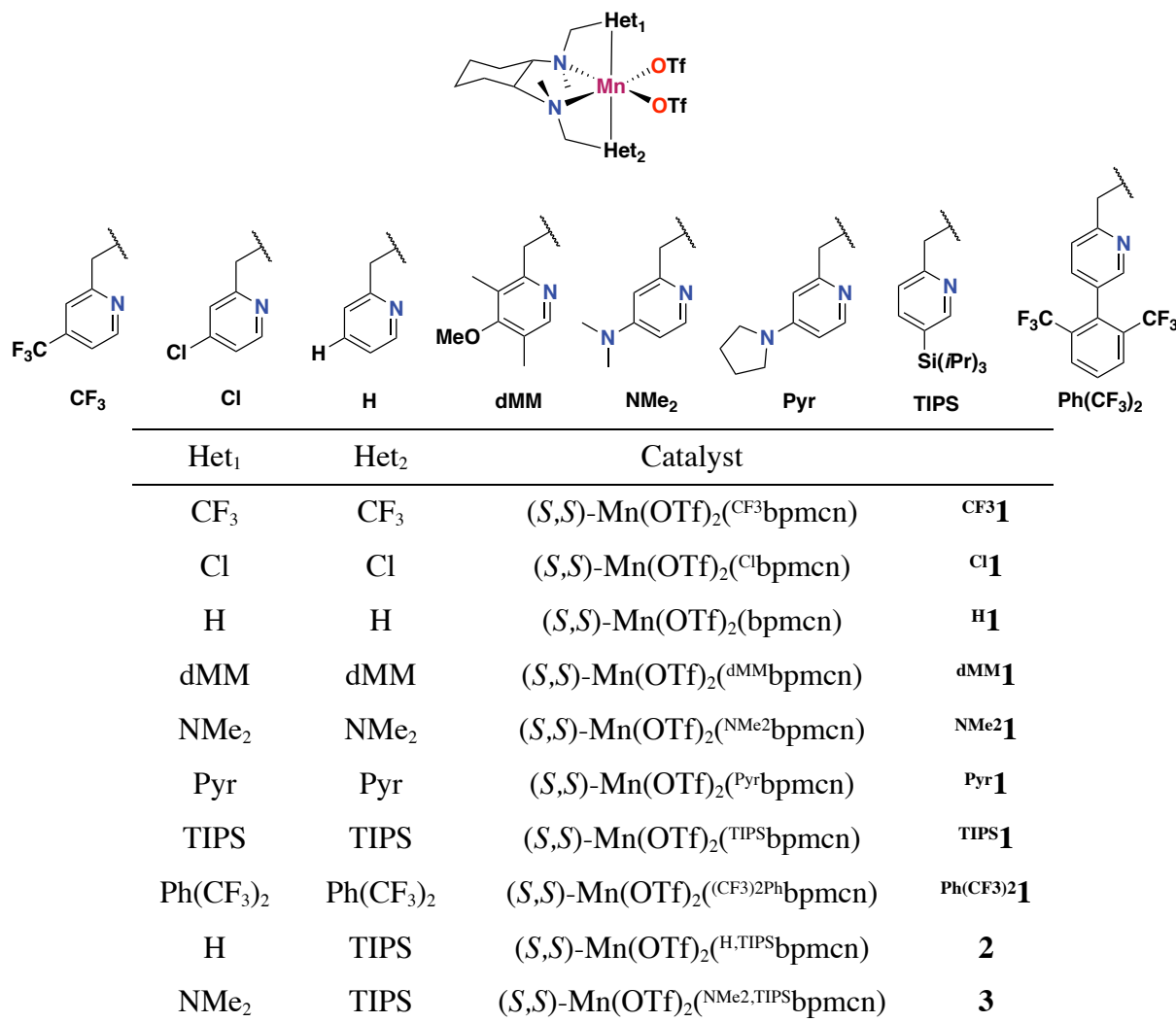


Figure 2. Schematic diagram of the different catalysts employed in this Chapter.

4.2.2 Crystal and molecular structure of complexes ^{CF₃}**1** and ^{Cl}**1**

The solid state structures of complexes ^{CF₃}**1** and ^{Cl}**1** were confirmed by X-ray crystallography, showing that both complexes are enantiopure with an (*S,S*) configuration (Figure 3). A list of the most important bond distances and bond angles of the two new complexes is shown in Table 1 and compared with manganese complex (*R,R*)-^H**1** (enantiopure complex with the opposite (*R,R*) configuration) containing non-substituted pyridine moieties.⁶² Both complexes adopt a *cis-α* conformation with a distorted octahedral coordination geometry in which the triflate anions are in a *cis* orientation. Each pyridine moiety is positioned above and below the plane that contains the manganese center. The mentioned plane also contains the two nitrogens of the *N,N*-cyclohexanediamine backbone and the two oxygen atoms of the triflate anions.

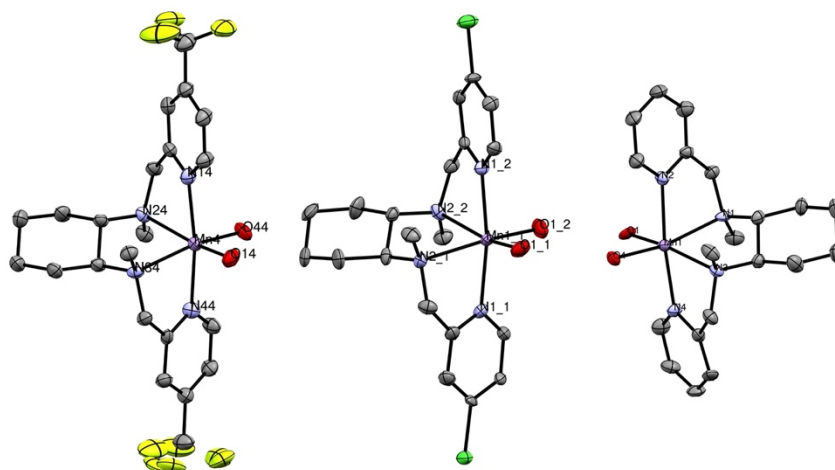


Figure 3. From left to right: ORTEP diagram of the molecular structure of (*S,S*)-[Mn^{II}(CF₃SO₃)₂(CF₃bpmcn)] (CF³**1**), (*S,S*)-[Mn^{II}(CF₃SO₃)₂(Cl^bbpmcn)] (Cl¹) and (*R,R*)-[Mn^{II}(CF₃SO₃)₂(bpmcn)] ((*R,R*)-**H1**), showing the atom numbering scheme. Triflate anions are omitted except for the oxygen atoms directly bound to the metal center, and hydrogen atoms are omitted for clarity. The X-ray structure of complex (*R,R*)-**H1** is taken from a study by Stack and co-workers.⁶²

The Mn–N bond distances of complex CF³**1** range from 2.24 to 2.28 Å and the Mn–O bond distances from 2.14 to 2.15 Å. For complex Cl¹, the Mn–N bond distances range from 2.23 to 2.28 Å and the Mn–O bond distances from 2.14 to 2.16 Å. These values compare quite well with the Mn–N and Mn–O bond distances of complex (*R,R*)-**H1** (see Table 1). Complexes CF³**1** and Cl¹ display a slightly larger O–Mn–O angle (103.8(2)° and 103.8(3)°, respectively) relative to the corresponding angle in complex (*R,R*)-**H1** (98.4(1)°), which indicates that the trifluoromethyl and chloro groups do not introduce significant steric strain in the complex.

Table 1. Selected bond lengths (Å) and angles (°) for manganese complexes CF³**1**, Cl¹ and **H1**.

CF ³ 1		Cl ¹		(<i>R,R</i>)- H1	
Mn4–N24	2.280(4)	Mn1_1–N2_2	2.276(8)	Mn–N1	2.292(5)
Mn4–N34	2.263(5)	Mn1_1–N2_1	2.30(1)	Mn–N3	2.300(5)
Mn4–N14	2.248(4)	Mn1_1–N1_2	2.240(8)	Mn–N2	2.216(5)
Mn4–N44	2.241(4)	Mn1_1–N1_1	2.234(7)	Mn–N4	2.200(4)
Mn4–O44	2.148(4)	Mn1_1–O1_2	2.16(1)	Mn–O1	2.189(4)
Mn4–O14	2.153(4)	Mn1_1–O1_1	2.137(7)	Mn–O4	2.157(4)
N24–Mn–N14	75.4(2)	N2_2–Mn1_1–N1_2	75.9(3)	N1–Mn–N2	75.0(2)
N34–Mn–N44	76.0(2)	N2_1–Mn1_1–N1_1	75.9(3)	N3–Mn–N4	76.1(2)
N14–Mn–N34	98.6(2)	N1_2–Mn1_1–N2_1	96.3(3)	N2–Mn–N3	102.0(2)
N24–Mn–N34	79.9(2)	N2_2–Mn1_1–N2_1	78.4(3)	N1–Mn–N3	78.7(2)
O44–Mn–O14	103.8(2)	O1_2–Mn1_1–O1_1	103.8(3)	O1–Mn–O4	98.4(1)

4.2.3 Screening of C₂-symmetric Mn complexes for aromatic oxidation catalysis

The above-mentioned manganese complexes (see Figure 2) have been screened for their activity in the direct aromatic hydroxylation using propylbenzene as the model substrate (Table 2). Catalytic experiments were carried out following the optimized conditions that we have previously reported.²⁴ The manganese catalyst (1 mol%) and Cl₂CHCOOH (0.5 equiv.) were mixed into a solution of propylbenzene (1 equiv.) in HIFP at 0 °C. Aqueous H₂O₂ (1 equiv., 35% w/w solution) was added dropwise through a syringe pump over a period of 30 min. After work-up, the reaction mixtures were analyzed by GC, detecting 4-propylphenol, 2-propylphenol and propyl-*para*-benzoquinone as aromatic oxidation products, and 1-phenyl-1-propanol and propiophenone as aliphatic (benzylic) oxidation products, next to unreacted substrate.

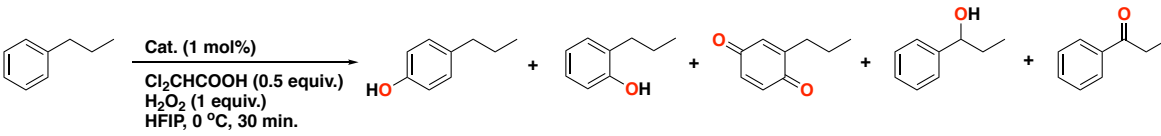
Our initial hypothesis was that electron-poor manganese complexes would enhance the electrophilicity of the manganese-oxo species, and therefore the complex would be more reactive towards an aromatic substrate. However, we found that the manganese complex containing the most electron-withdrawing substituent of the whole series, **CF₃1** ($\sigma_{\text{para}(\text{CF}_3)} = +0.54$)⁶¹, was not active for the oxidation of propylbenzene, showing only trace amounts of *para*-, and *ortho*-phenol products (Table 2, entry 1). In a similar way, the second most electron-poor manganese complex of the series, **Cl1** ($\sigma_{\text{para}(\text{Cl})} = +0.23$),⁶¹ was also found to be a poor aromatic oxidation catalyst, with only 3 and 1% yield for *para*-phenol and *ortho*-phenol, respectively (Table 2, entry 2). In addition, complexes **CF₃1** and **Cl1** show low substrate conversions of 9 and 15%, respectively, indicative of low catalytic activities. These initial results showed us that manganese complexes supported by electron-poor aminopyridine ligands do not provide access to an active catalyst for aromatic oxidation. Even though the reactions operate through different mechanisms, this observation also agrees with previous literature reports on the use of non-heme iron and manganese complexes for aliphatic C(sp³)-H hydroxylation and epoxidation reactions, where electron-poor complexes also showed poor catalytic activities.⁵⁷⁻⁵⁹ We rationalize that the reason of the poor catalytic behavior is related to the ability of the ligand to facilitate the H₂O₂ activation step, for example by stabilizing the high-valent Mn(V)-oxo species. A strongly electron-donating ligand seems necessary for the formation and stabilization of such species. The parent manganese complex with non-substituted pyridine moieties (**H1**), which contains a stronger electron-donating ligand, was found to be a more active catalyst, showing 25% substrate conversion. *Para*-phenol, *ortho*-phenol and benzoquinone were obtained in 8, 3 and 1% yield, respectively (Table 2, entry 3). Moreover, the selectivity of catalyst **H1** was excellent for aromatic oxidation, with only trace

amounts of benzylic alcohol product being detected. In addition, a good mass balance of 89% was obtained with this parent complex.

Next, we moved to the use of electron-rich manganese complexes. On the one hand, complex ^{dMM}**1**, with dimethyl methoxy substituents, afforded similar catalytic activity as the parent complex ^H**1**, with 25% substrate conversion, and 8, 4 and 3% yield for *para*-phenol, *ortho*-phenol and benzoquinone, respectively. Some benzylic alcohol product was also detected in 2% yield (Table 2, entry 4). An excellent mass balance was observed when complex ^{dMM}**1** was employed (94%). On the other hand, complexes with the most electron-donating substituents on the pyridines moieties of the ligand, namely dimethylamino (^{NMe2}**1**) and pyrrolidine (^{Pyr}**1**) groups, afforded a significant increase in catalytic activity, with up to 69% substrate conversion (Table 2, entries 5 and 6). However, the selectivity of the reaction towards phenol products clearly decreased, as these complexes favor aliphatic (benzylic) oxidation towards the alcohol product instead of aromatic oxidation (14 and 16% alcohol yield for ^{NMe2}**1** and ^{Pyr}**1**, respectively). The preferential benzylic hydroxylation reactivity by electron-rich complexes agrees with previous literature.⁶⁶⁻⁷⁰ At the same time, poor mass balances (63 and 65%) were obtained for these electron-rich manganese complexes, which might indicate that a side reaction is going on, probably towards the generation of overoxidized by-products, that we have not been able to detect by GC.

Compared to these complexes, our reported bulky manganese complex ^{TIPS}**1** is the better catalyst in terms of yield and selectivity for phenol formation. *Para*-phenol, *ortho*-phenol and benzoquinone were obtained in 24, 8 and 2% yield, respectively, whereas the benzylic alcohol product was obtained in only 1% yield (Table 2, entry 7). Of note is that complex ^{TIPS}**1** shows only 55% substrate conversion, which is lower than for electron-rich manganese complexes ^{NMe2}**1** and ^{Pyr}**1**, which seems to indicate a lower relative catalytic activity for ^{TIPS}**1**. This observation reflects the importance of designing catalysts that are active in a challenging oxidation reaction like the one we are addressing in this Chapter, but at the same time do not lead to secondary reaction products; *i.e.* overoxidation is prevented. Thus, a fine balance between catalytic activity and selectivity is key in the optimization of such reactions.

Next, we decided to investigate the previously reported bulky manganese complex ^{Ph(CF₃)₂}**1**⁶⁵ in the aromatic oxidation reaction. Complex ^{Ph(CF₃)₂}**1**, with pendant *ortho*-CF₃ phenyl substituents on the 5-position of each pyridine moiety, showed an excellent selectivity for aromatic over aliphatic (benzylic) oxidation, albeit with low conversion (23%) and yields for aromatic oxidation products. Particularly, *para*-phenol and *ortho*-phenol were obtained in 8 and 5% yield, respectively (Table 2, entry 8). We tentatively attribute the difference in reactivity between ^{TIPS}**1** and ^{Ph(CF₃)₂}**1** to the difference in steric bulk of the ligand provided by the triisopropylsilyl (TIPS) and 2,6-(CF₃)₂ phenyl substituents, respectively (*vide infra*). Moreover,

Table 2. Oxidation of propylbenzene using various manganese complexes.


Entry	Cat.	Conv. ^a	Yield 4-propylphenol ^b	Yield 2-propylphenol ^b	Yield BQ ^b	Yield A ^b	Yield K ^b	MB ^c
1	CF3 1	9	<1	<1	n.d.	n.d.	n.d.	93
2	Cl 1	15	3	1	n.d.	n.d.	n.d.	91
3	H 1	25	8	3	1	<1	n.d.	89
4	dMM 1	25	8	4	3	2	n.d.	94
5	NMe2 1	69	10	3	3	14	<1	63
6	Pyr 1	68	10	2	3	16	<1	65
7	TIPS 1	55	24	8	2	1	n.d.	82
8	Ph(CF3) ₂ 1	23	8	5	n.d.	n.d.	n.d.	92

^aSubstrate conversion in %. ^bYields in % with respect to substrate determined by GC against an internal standard. ^cMass balance was calculated considering remaining starting material (100 – conversion %) and all products formed, plus a percentage of substrate loss calculated from blank experiments (an average of 2% of substrate is lost): MB = (100 – conversion %) + (Product Yields %) + (Substrate loss). n.d. = non-detected, BQ = benzoquinone, A = alcohol, K = ketone.

we envision that the different reactivity might be due to the different electronic properties of both ligands, which might impact H₂O₂ activation, as shown previously for electron-poor manganese complexes. The low aromatic oxidation activity observed for complex **Ph(CF₃)₂1** agrees with data reported for a similar manganese complex based on the bis-pyrrolidine backbone by White and co-workers, [Mn^{II}(CF₃SO₃)₂(**Ph(CF₃)₂bpbp**)], for which no aromatic oxidation products were detected in the oxidation of aromatic compounds containing medicinally relevant moieties.⁷¹

4.2.4 Comparison of bulky manganese complexes **TIPS1** and **Ph(CF₃)₂1**

Since bulky manganese complex **TIPS1** shows the better activity and selectivity for aromatic oxidation, we decided to look closer into its structure and compare it to the other bulky manganese complex tested in this Chapter (**Ph(CF₃)₂1**). Of interest was the understanding why the complex containing the TIPS groups shows enhanced phenol yields compared to the one with 2,6-CF₃-phenyl groups. We have previously rationalized that a bulky ligand might help in preventing product inhibition by phenolate binding to the metal center.²⁴ Thus, we would expect that both complexes (**TIPS1** and **Ph(CF₃)₂1**) would show an enhanced aromatic oxidation activity because of the steric bulk provided by their corresponding ligands. However, **Ph(CF₃)₂1** shows a significantly lower aromatic oxidation activity, which suggests that the sterics of the two

complexes are different. Another important aspect to consider is the electronics of both complexes, which has been shown previously to also have an important effect on the overall reactivity. Complex **TIPS1** is supported by a tetradentate aminopyridine ligands with bulky silyl groups, which are electronically neutral substituents. On the other hand, complex **Ph(CF₃)₂1** contains phenyl substituents with CF₃ groups, in which the phenyl substituent might act as an inductively electron-withdrawing group in combination with the electron-withdrawing character of the *o*-CF₃ groups, consequently affecting the overall electronics of the complex. Thus, complex **Ph(CF₃)₂1** could be considered as an electron-poor manganese complex, in a similar way as complexes **CF₃1** and **Cl1**, which would explain its lower aromatic oxidation activity compared to **TIPS1**.

First, we wanted to have a closer look into the different steric bulk provided by the ligands in complexes **TIPS1** and **Ph(CF₃)₂1**. In considering the geometrics of the pyridine substituents in the complexes, we considered the TIPS group as a spherical substituent, and the phenyl group as a planar substituent. This consideration would indicate that the steric bulk provided by the TIPS group might be bigger than that of the phenyl substituent; thus, the TIPS group would provide a better encapsulation of the catalytic active site and, consequently, would better prevent product inhibition (phenolate binding to Mn). To probe this hypothesis, we made an overlay of the molecular structures of the two bulky complexes to analyze possible differences in the accessibility of the catalytic active site. For this comparison, we took the X-ray crystal structure of complexes [Fe(OTf)₂(**TIPS**BPBP)] and complex [Mn(Cl)₂(**Ph(CF₃)₂BPBP**)], since these are the only X-ray structures reported in literature based on the same ligand backbone that contain the desired bulky substituents.^{71, 72} Both structures are based on the bis-pyrrolidine instead of the *N,N*-cyclohexanediamine backbone, however, we have previously reported that complexes based on the bis-pyrrolidine backbone are also active aromatic oxidation catalysts.²⁴ In addition, the former structure is based on iron as the metal center, which is known not to significantly affect the geometry of the complex compared to its manganese analogue.

Indeed, a space-filling representation of the bulky substituents of both complexes, together with an overlay of the complexes (Figure 4a), shows that the TIPS groups occupies a larger space around the catalytic active site. In addition, we have also analyzed the distances between the bulky substituents and the labile sites in each complex (Figure 4b). For complex [Fe(OTf)₂(**TIPS**BPBP)], a distance of 3.68 Å between O2 of the triflate and H2 of one of the methyls of the TIPS group was observed. The distance between H1 of the other TIPS group and O1 is 4.02 Å. Alternatively, in [Mn(Cl)₂(**Ph(CF₃)₂BPBP**)] a distance between the F1 of one of the

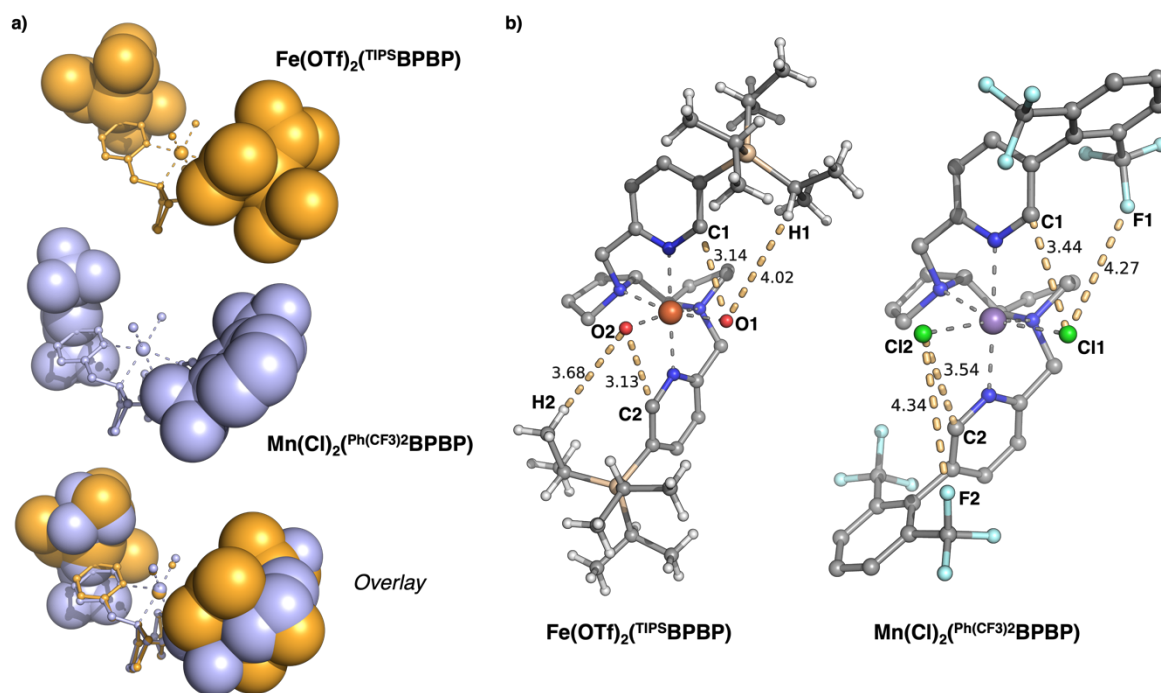


Figure 4. a) Space-filling representations of the bulky substituents on complexes $[\text{Fe}(\text{OTf})_2(\text{TIPSBPBP})]$ (orange) and $[\text{Mn}(\text{Cl})_2(\text{Ph}(\text{CF}_3)_2\text{BPBP})]$ (light-blue), and overlay of both complexes. The fit is based on the metal and its nitrogen coordinating atoms and performed with the PyMOL software. b) Selected bond distances between the bulky substituents and the catalytic active site in X-ray crystal structures of $[\text{Fe}(\text{OTf})_2(\text{TIPSBPBP})]$ ⁷² and $[\text{Mn}(\text{Cl})_2(\text{Ph}(\text{CF}_3)_2\text{BPBP})]$.⁷¹

o-CF₃ phenyl substituents and C11 is 4.27 Å, while the distance between F2 of the other substituent and C12 is 4.34 Å. This comparison also suggests that TIPS groups provide a better encapsulation of the active site, since distances between the substituents and the active site are shorter. We have also looked at the distances between the carbon on position 6 of each of the pyridine rings and the labile sites. For complex $[\text{Fe}(\text{OTf})_2(\text{TIPSBPBP})]$, a distance of 3.14 and 3.13 Å was observed between C1-O1 and C2-O2, respectively. For complex $[\text{Mn}(\text{Cl})_2(\text{Ph}(\text{CF}_3)_2\text{BPBP})]$, distances of 3.44 and 3.54 Å were observed for C1-C11 and C2-C12, respectively. Thus, these latter data also suggest that TIPS groups introduce more steric strain in the complex than 2,6-(CF₃)₂-phenyl substituents.

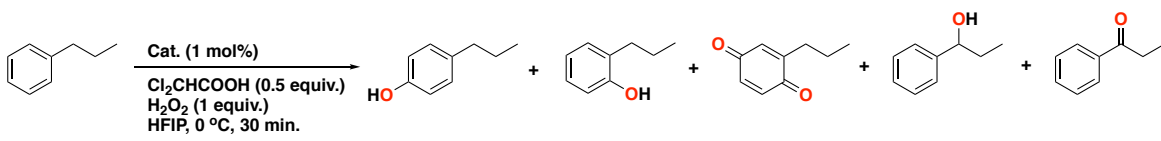
Next, we looked closer into the electronic effects of both ligands in complexes **TIPS1** and **Ph(CF₃)₂1**. As mentioned before, a 2,6-(CF₃)₂-phenyl substituent can be considered as an electron-withdrawing group, whereas a TIPS group has a neutral electronic character. To further investigate this hypothesis, we analyzed complexes **TIPS1** and **Ph(CF₃)₂1** using cyclic voltammetry (CV). These measurements showed that **TIPS1** and **Ph(CF₃)₂1** have different Mn(II)/Mn(III) potentials ($E_{1/2} = 0.64$ V and 0.76 V, respectively). Thus, the first oxidation event for complex **Ph(CF₃)₂1** is observed at a somewhat more positive potential than that of complex **TIPS1**, which is likely due to the electron-withdrawing properties of the 2,6-(CF₃)₂-phenyl substituents.

Accordingly, we hypothesize that the lower aromatic oxidation activity of complex $\text{Ph}(\text{CF}_3)_2\mathbf{1}$ is also affected by the electron-poor character of its ligand, which might lead to a less effective H_2O_2 activation pathway and a less stabilized manganese-oxo species, as was proposed for related electron-poor manganese complexes $\text{CF}_3\mathbf{1}$ and $\text{Cl}\mathbf{1}$.

4.2.5 C_1 -symmetric Mn complexes for arene oxidation

Having found that TIPS-substituted aminopyridines are good ligands for manganese-catalyzed arene oxidation, next we wanted to investigate the activity of C_1 -symmetric manganese complexes containing only one bulky pyridine on the ligand structure of the complex. Particularly, we have considered complex **2**, with one bulky pyridine and a non-substituted pyridine, and complex **3**, with one bulky pyridine and an electron-rich pyridine (see Figure 2). We have selected a dimethylamino substituent for complex **3** since electron-donating groups have been found to provide a more active catalyst (more substrate conversion) than electron-withdrawing substituents.

Complexes **2** and **3** were tested in the oxidation of propylbenzene as substrate using the previous optimized conditions, and their catalytic activity was compared to those of complexes $\text{H}\mathbf{1}$ and $\text{TIPS}\mathbf{1}$ (Table 3). Complex **2** showed aromatic oxidation towards *para*-phenol, *ortho*-phenol and benzoquinone, in 9, 4 and 1% yield, respectively, with 26% substrate conversion (Table 3, entry 1). Benzylic hydroxylation towards the alcohol product was observed in only 1% yield. An excellent mass balance was observed using complex **2** (91%). In a similar way, complex **3** afforded 25% substrate conversion, with 8 and 3% yield of *para*-phenol and *ortho*-phenol, respectively, and only trace amounts of benzoquinone (Table 3, entry 2). Benzylic alcohol product was also detected in 1% yield, together with trace amounts of the overoxidized ketone product. Both complexes **2** and **3** show activities very similar to the ones obtained using the parent manganese complex $\text{H}\mathbf{1}$ (Table 3, entry 3), all of them showing the same substrate conversion (~25%) and high selectivity for aromatic over aliphatic (benzylic) oxidation reaction. However, comparing these results with the ones obtained with $\text{TIPS}\mathbf{1}$, we can clearly see that a complex containing two bulky pyridines is more active, with 55% substrate conversion and with up to 34% total yield for aromatic oxidation (Table 3, entry 4). At the same time, $\text{TIPS}\mathbf{1}$ is also the most selective complex for phenol formation over aliphatic (benzylic) oxidation. Thus, from these experimental results we can conclude that a C_2 -symmetric manganese complex with an aminopyridine ligand bearing two bulky pyridine moieties is preferred over a non-symmetrical complex bearing only one bulky pyridine moiety in its ligand for aromatic hydroxylation towards phenol products; i.e. ligand bulk in a C_2 -symmetric geometry is required to properly prevent product inhibition.

Table 3. Oxidation of propylbenzene using C_1 -symmetric manganese complexes.


Entry	Cat.	Conv. ^a	Yield 4-propylphenol ^b	Yield 2-propylphenol ^b	Yield BQ ^b	Yield A ^b	Yield K ^b	MB ^c
1	2	26	9	4	1	1	n.d.	91
2	3	25	8	3	<1	1	<1	89
3	^H 1	25	8	3	1	<1	n.d.	89
4	^{TIPS} 1	55	24	8	2	1	n.d.	82

^aSubstrate conversion in %. ^bYields in % with respect to substrate determined by GC against an internal standard. ^cMass balance was calculated considering remaining starting material (100 – conversion %) and all products formed, plus a percentage of substrate loss calculated from blank experiments (an average of 2% of substrate is lost): MB = (100 – conversion %) + (Product Yields %) + (Substrate loss). n.d. = non-detected, BQ = benzoquinone, A = alcohol, K = ketone.

4.2.6 Design of manganese complexes containing electron-rich bulky pyridines

Next, we considered C_2 -symmetric manganese complexes **4** and **5**, supported by tetradentate aminopyridine ligands that comprise pyridine moieties in which a bulky substituent is combined with an electron-rich substituent (Figure 5B). On the basis of our previous findings, we were interested to investigate Mn-complexes based on aminopyridine ligands that contain both a bulky TIPS group at position 5 and a dimethylamino group on each pyridine moiety. For the position of the dimethylamino substituent, several options can be considered. The logical option would be to introduce this substituent on position 4 of the pyridine, where it would act as a strongly electron-donating group ($\sigma_{\text{para}} = -0.83$).⁶¹ Alternatively, the dimethylamino group could also be introduced on position 3 of the pyridine, where it would be more remote from the bulky TIPS group, but would act as a weaker electron-donating substituent ($\sigma_{\text{meta}} = -0.16$).⁶¹ Finally, introduction of the dimethylamino group on position 6 of the pyridine ring was not considered, since it would come too close to the catalytic active site.

Accordingly, we have designed ligand **L4** and the corresponding Mn-complex **4**, which is based on the bis-pyrrolidine backbone, and constitutes two pyridine moieties that contain a TIPS group at position 5 and a dimethylamino group at position 3 (Figure 5). We selected the ligand with the bis-pyrrolidine backbone since it was synthetically more feasible than the one containing the *N,N*-dimethylcyclohexanediamine, and also because we have previously shown that manganese complexes based on bpbp-type ligands are also active aromatic oxidation catalysts.²⁴ We have also considered manganese complex **5**, which is based on a ligand with the

dimethylamino group at position 4 of each pyridine ring and the TIPS group at position 5, so that both substituents are in close proximity (Figure 5B).

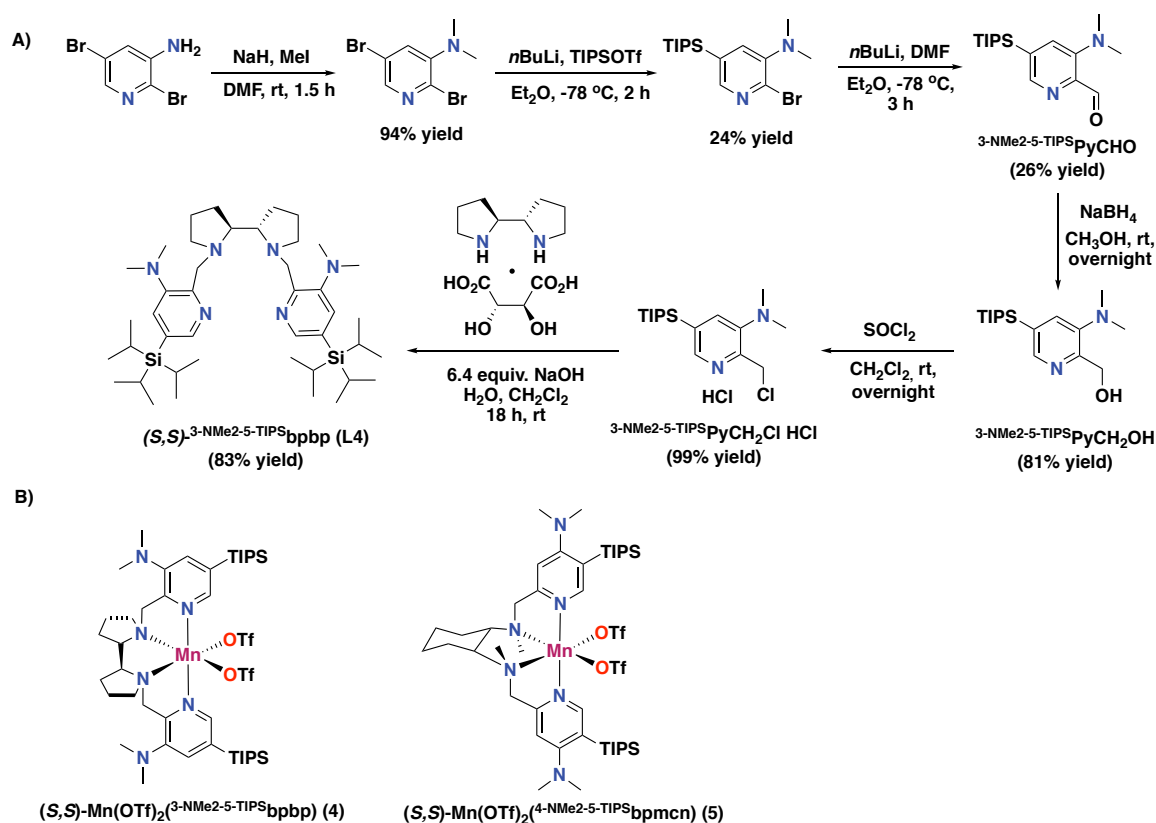


Figure 5. A) Synthesis of tetradentate aminopyridine ligand **L4**. B) Structures of complexes **4** and **5**.

For the synthesis of ligand **L4** it was first necessary to synthesize the pyridine synthon ³-NMe2-5-TIPSPyCH₂Cl·HCl. First, methylation of 3-amino-2,5-dibromopyridine using iodomethane afforded 2,5-dibromo-*N,N*-dimethylpyridin-3-amine in 94% yield. Afterwards, non-selective lithiation of the obtained product give us access to the product with a TIPS group at position 5, although in a low yield of 24%. Next, lithiation on position 2 of the pyridine and reaction with DMF formed aldehyde ³-NMe2-5-TIPSPyCHO in 26% yield. Reduction of the latter afforded the corresponding alcohol ³-NMe2-5-TIPSPyCH₂OH in 81% yield. Finally, reaction of the alcohol with SOCl₂ yielded the desired pyridine synthon ³-NMe2-5-TIPSPyCH₂Cl·HCl in 99% yield. Ligand **L4** could then be prepared by the reaction of two equiv. of the corresponding pyridine synthon ³-NMe2-5-TIPSPyCH₂Cl·HCl with one equiv. of the corresponding amine backbone, affording the desired ligand **L4** in 83% yield (Figure 5A, see Experimental Section for further details). The ligand was characterized by ¹H NMR and ¹³C NMR spectroscopy, and HRMS (see Experimental Section for further details on the characterization). Complex **4** was then obtained in 78% yield by the reaction of equimolar amounts of ligand **L4** with [Mn^{II}(CF₃SO₃)₂] in dry THF under an inert atmosphere. HRMS analysis of **4** showed a prominent mass peak at *m/z* 924.4568 corresponding to the [Mn^{II}(CF₃SO₃)(**L4**)]⁺ ion (calc. 924.4571).

4.2.7 Oxidation activity of complex 4 and 5

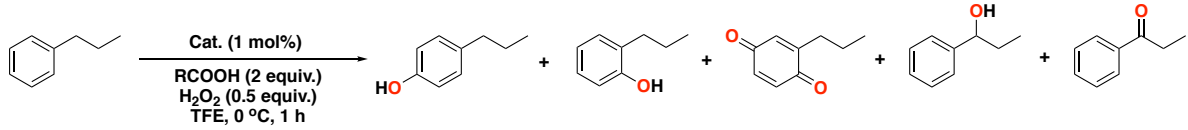
Complexes **4** and **5** were tested in the aromatic hydroxylation of propylbenzene as substrate using aqueous H₂O₂. We investigated these complexes in the presence of dichloroacetic acid or acetic acid, using TFE as fluorinated alcohol solvent, this time at a low H₂O₂ loading of 0.5 equiv. instead of 1.0 equiv. with respect to the substrate (Table 4). Since in previous experiments using electron-rich manganese complexes, such as ^{NMe}**21** and ^{Pyr}**1**, we have observed high substrate conversions with poor mass balances, this time we wanted to prevent possible overoxidation reactions by using a lower H₂O₂ loading.

Surprisingly, none of these complexes were active in the aromatic oxidation of propylbenzene towards phenol products. When complex **4** was tested using dichloroacetic acid as additive, no phenol products were detected at all, and only 1% yield for the benzylic alcohol product was observed with a substrate conversion of 23% (Table 4, entry 1). When the same complex was tested in combination with acetic acid, substrate conversion increases to 31% but affording only trace amounts of *para*-phenol, whereas the yield for the benzylic alcohol product increased to 4% (Table 4, entry 2). The mass balance of these reactions ranged between 73–78%. Next, we tested complex **5** using the same experimental conditions. When complex **5** was used in the presence of dichloroacetic acid, the substrate conversion was low (6%), with 1% yield of *para*-phenol and trace amounts of *ortho*-phenol (Table 4, entry 3). Interestingly, when we switched the additive from dichloroacetic acid to acetic acid, complex **5** preferentially oxidized the weaker benzylic C–H bond to generate the alcohol product in 14% yield and the overoxidized ketone product in 1% yield, whereas the *para*-phenol was still detected in only 1% yield (Table 4, entry 4). The mass balance for this latter reaction was 80%.

Complex **4** was further tested for aromatic oxidations using different carboxylic acid loadings. At this time catalytic reactions were tested using stoichiometric amounts of H₂O₂, with HFIP as solvent (Table 4, entries 5–7). When 0.5 equiv. of dichloroacetic acid additive was used, substrate conversion increased from 23% to 37%, and 2% yield for the benzylic alcohol product was detected as the only product; *i.e.* no aromatic oxidation products were observed (Table 4, entry 5). The poor mass balance observed for this reaction (65%) indicates that overoxidation reactions might be occurring, indicative of the use of a higher H₂O₂ loading. Aromatic oxidation was also not effective when 2 equiv. of acetic acid additive were used in combination with complex **4**, with only trace amounts of *para*-phenol being detected, and 2% yield of the benzylic alcohol product being formed (Table 4, entry 6). However, substrate conversion increases up to 49%, leading to a poor mass balance (53%). Finally, complex **4** was also tested for the oxidation of propylbenzene in the absence of any carboxylic acid additive. An experiment employing complex **4** with 1 equiv. of H₂O₂ in HFIP as solvent afforded the benzylic alcohol product in 9% yield (Table 4, entry 7), and did not lead to a large decline in

catalytic activity (41% conversion). Yet, again no aromatic oxidation products were detected, indicating that complex **4** might not be an active aromatic oxidation catalyst. The mass balance of the latter reaction was again poor (68%).

Table 4. Oxidation of propylbenzene using manganese complexes **4** and **5** at low H₂O₂ loading with different carboxylic acid additives.



Entry	Cat.	Acid	Conv. ^a	Yield 4- propylphe nol ^b	Yield 2- propylphe nol ^b	BQ ^b	A ^b	K ^b	MB ^c
1	4	Cl ₂ CHCO ₂ H	23	n.d.	n.d.	n.d.	1	n.d.	78
2	4	AcOH	31	<1	n.d.	n.d.	4	n.d.	73
3	5	Cl ₂ CHCO ₂ H	6	1	<1	n.d.	n.d.	n.d.	95
4	5	AcOH	36	1	n.d.	n.d.	14	1	80
5 ^{d,e}	4	Cl ₂ CHCO ₂ H	37	n.d.	n.d.	n.d.	2	n.d.	65
6 ^d	4	AcOH	49	<1	n.d.	n.d.	2	n.d.	53
7 ^d	4	-	41	n.d.	n.d.	n.d.	9	<1	68

^aSubstrate conversion in %. ^bYields in % with respect to substrate determined by GC against an internal standard. ^cMass balance was calculated considering remaining starting material (100 – conversion %) and all products formed: MB = (100 – conversion %) + (Product Yields %). ^dReaction performed at 1 equiv. H₂O₂ loading using HFIP for 30 min. of reaction time. ^e0.5 equiv. of acid was employed. n.d. = non-detected, BQ = benzoquinone, A = alcohol, K = ketone.

We envisioned that the overall poor catalytic activity observed with complex **4** and **5** might be caused of steric effects around the dimethylamino group, which affects its orientation with respect to the pyridine ring. We know that the π -orbital of the dimethylamino substituent needs to properly arrange in a co-planar way with the aromatic system of the pyridine to act as an electron-donating group. For complex **4**, the dimethylamino substituent has an alkyl chain in *ortho* position, which could affect its orientation to the pyridine ring, therefore, affecting its electronic properties. In a similar way, the orientation of the dimethylamino group in complex **5** can be affected by the proximity of the bulky TIPS group, which again would affect the electronic properties of the dimethylamino substituent. Overall, we believe that ligands **L4** and **L5** do not provide good catalysts for aromatic oxidation because the combination of a TIPS and a dimethylamino group does not provide a pyridine ring that is overall more electron-rich with respect to a pyridine ring bearing only the TIPS group. Regarding, the slight increase in benzylic alcohol product formation when no carboxylic acid additive was used in combination with

complex **4**, we propose that this could be related to protonation of the dimethylamino group of the ligand to some extent by the carboxylic acid additive, resulting in a change of the electronic properties of the complex. Along the same line, the fluorinated alcohol solvent (TFE) employed in these reactions is a strong H-bond donor that could cause protonation of the dimethylamino group as well, also changing its electronics from an electron-donating to an electron-withdrawing group. Thus, we also envision this as one of the reasons why complexes **4** and **5** do not show catalytic activity.

4.3 Conclusions

In conclusion, the present Chapter illustrates the sensitivity of manganese-catalyzed aromatic oxidations upon modulation of the electronic and steric effects of the supporting aminopyridine ligand. We have reported on a series of manganese complexes containing aminopyridine ligands with different electronic and steric properties by varying the pyridine donors of the ligand, which have been tested for the aromatic oxidation of an alkylbenzene substrate employing a halogenated carboxylic acid additive with aqueous H₂O₂ in fluorinated alcohol solvents. The electron-poor manganese complexes were found to be sluggish oxidants, which was against our initial hypothesis on the use of electron-withdrawing groups to enhance the electrophilicity of the manganese-oxo species. In contrast, electron-rich manganese complexes show higher catalytic activities (high substrate conversions), but low selectivities for aromatic oxidation, yielding a mixture of aromatic and benzylic oxidized products. The detrimental effect of electron-withdrawing substituents might be related to stability issues of the high-valent manganese-oxo species and inefficient H₂O₂ activation, whereas electron-donating groups might help in the stabilization of the metal-oxo species. Finally, the current investigation has shown that the C₂-symmetric complex **TIPS1** can be considered as the best homogeneous catalyst reported to date for the aromatic oxidation of monoalkylbenzenes, as it outperforms all other complexes tested in this Chapter. Our findings also highlight the important role of the steric bulk provided by the TIPS groups to encapsulate the active site of the manganese complex. We have rationalized how the steric bulk of TIPS groups can provide a better encapsulation of the catalytic center in comparison to another bulky complex comprising 2,6-(CF₃)₂-phenyl groups. In addition, the latter group has an electron-withdrawing compared to the TIPS group, which might lead to efficient H₂O₂ activation as observed for other electron-poor complexes. Further investigations are needed to rationalize the chemoselectivity of the reaction upon modulation of the electronic properties of the manganese catalyst, as well as getting a better view on the overall product composition to provide further insight into the mass balance of the reactions.

4.4 Experimental Section

4.4.1 General Remarks

The synthesis of manganese complexes, and other air- and moisture-sensitive reactions, was performed under an inert nitrogen atmosphere using standard Schlenk line and glovebox techniques. All catalytic oxidation reactions were run under air with no precautions taken to exclude moisture. The solvents diethyl ether and acetonitrile were purified using an MBraun MB SPS-800 solvent purification system. Tetrahydrofuran and methanol were dried with sodium and magnesium turnings, respectively, and distilled under nitrogen prior to use. $\text{Mn}(\text{OTf})_2$ was bought from Sigma-Aldrich. All reagents and reaction products were obtained commercially and used without further purification, unless being specify. GC quantification was done by using calibration lines for each compound employing an internal standard. Complex **5** was provided by the group of Costas and its synthesis will be reported in a future publication.

Column chromatography was performed using Merck silica gel (60–200 mesh). ^1H , ^{13}C , and ^{19}F NMR spectra were recorded with a 400 MHz Varian spectrometer at 25 °C, chemical shifts (δ) are given in ppm referenced to the residual solvent peak. IR spectra were recorded with a Perkin-Elmer Spectrum One FTIR spectrometer. HRMS analysis was performed with a 6560 Ion Mobility LC/Q-TOF from Agilent Technologies. GC analyses were performed on a Perkin-Elmer Clarus 500 Gas Chromatograph equipped with a PE Elite-5 column ((30m x 0.32 mm x 0.25 μm), (5% phenyl)-(95% methyl)polysiloxane) and a flame-ionization detector. X-ray diffraction analysis was carried out using a Bruker Kappa ApexII diffractometer.

Appendix C contains the supplementary information of this Chapter, which includes ^1H -NMR spectra for the newly synthesized ligands.

4.4.2 Synthesis of Pyridine Synthons and Ligands

2-Hydroxymethyl-4-trifluoromethylpyridine ($^{\text{CF}_3}\text{PyCH}_2\text{OH}$): The procedure followed is inspired in the method reported by White and co-workers.⁷³ 2-Bromo-4-(trifluoromethyl)pyridine (4 mL, 32.3 mmol, 1 equiv.) was suspended in dry toluene (100 mL) in a Schlenk flask. The suspension was cooled to -78 °C and *n*BuLi (25.1 mL, 40.2 mmol, 1.2 equiv., 1.6 M in hexanes) was added dropwise over 20 min. The color of the solution changed immediately to yellow, and after full addition of *n*BuLi to dark red. The reaction was stirred for 45 min at -78 °C, at which time anhydrous DMF (4.8 mL, 62.3 mmol, 1.9 equiv.) was added dropwise and stirring continued an additional 1 h. The dark solution was warmed to 0 °C and CH_3OH (18 mL) followed by NaBH_4 (4.9 g, 129.5 mmol, 4 equiv.) were added carefully. Stirring was continued for 12 h allowing the reaction to warm to room temperature. The reaction was quenched with H_2O . The resulting layers were separated, and the aqueous layer was extracted with CH_2Cl_2 (3 times). The combined organic layers were dried (MgSO_4), filtered and concentrated to give a crude brown liquid. Purification by flash chromatography on silica eluting with Petroleum Ether/EtOAc (2:1) first, followed by pure EtOAc, afforded the title compound (4.8 g, 27.1 mmol, 84% yield) as an orange liquid. ^1H NMR (400 MHz, CDCl_3) δ 8.74 (d, $J = 5.1$ Hz, 1H), 7.58 – 7.53 (m, 1H), 7.47 – 7.41 (m, 1H), 4.86 (s, 2H), 3.52 (s, 1H); ^{13}C NMR (101 MHz, CDCl_3) δ 161.36, 149.76, 124.22, 121.50, 118.18, 116.49, 64.42; ^{19}F NMR (376 MHz, CDCl_3) δ 64.91; IR (ATR) ν , cm^{-1} : 3294, 2922, 1736, 1614, 1574, 1484, 1410, 1366, 1328, 1243, 1207, 1167, 1130, 1085, 1065, 1002, 886, 841, 739, 667, 607.

2-Chloromethyl-4-trifluoromethylpyridine ($^{CF_3}PyCH_2Cl$): The procedure followed is inspired in the method reported by Klein Gebbink and co-workers.⁷⁴ A solution of $^{CF_3}PyCH_2OH$ (500 mg, 2.82 mmol, 1 equiv.) in dry CH_2Cl_2 (20 mL) was cooled to 0 °C. Thionyl chloride (0.31 mL, 4.23 mmol, 1.5 equiv.) was slowly added. After addition, the resulting mixture was stirred at rt overnight. The reaction was quenched with an aqueous solution of $NaHCO_3$, and the organic layer was collected. The aqueous layer was extracted with CH_2Cl_2 (3 times), and the combined organic layers were dried over $MgSO_4$, filtered and concentrated to give the title compound (275 mg, 1.41 mmol, 50% yield) as a brown liquid. 1H NMR (400 MHz, $CDCl_3$) δ 8.80 – 8.72 (m, 1H), 7.76 – 7.69 (m, 1H), 7.51 – 7.44 (m, 1H), 4.75 (s, 2H); ^{13}C NMR (101 MHz, $CDCl_3$) δ 207.08, 158.31, 150.38, 118.92, 118.69, 45.99, 31.09; ^{19}F NMR (376 MHz, $CDCl_3$) δ 64.88.

(*S,S*)- $^{CF_3}bpmcn$ ($^{CF_3}bpmcn$): The procedure followed is inspired in the method reported by Costas and co-workers.^{58, 65} (*S,S*)-*N,N*-Dimethyl-1,2-cyclohexanediamine (31 mg, 0.22 mmol, 1 equiv.), $^{CF_3}PyCH_2Cl$ (85 mg, 0.44 mmol, 2 equiv.), Na_2CO_3 (186 mg, 1.75 mmol) and TBABr (10 mg, 0.031 mmol) were dissolved in anhydrous CH_3CN (5 mL). The reaction mixture was refluxed overnight under N_2 . At this point, the crude reaction was filtered, and the solvent was evaporated under reduced pressure. Then, a 1 M aqueous solution of NaOH was added, and the organic layer was collected. The aqueous layer was extracted with CH_2Cl_2 (3 times), and the organic layers were combined, dried over $MgSO_4$, filtered, and concentrated to give a crude brown liquid. The crude ligand thus obtained was purified by silica gel chromatography eluting with $CH_2Cl_2:CH_3OH:Et_3N$ (96:3:1) and the collected fractions were combined, washed with saturated $NaHCO_3$ solution, dried over $MgSO_4$, and concentrated in vacuo to provide the title compound (37 mg, 0.08 mmol, 37% yield) as a brown oil. 1H NMR (400 MHz, $CDCl_3$) δ 8.65 (d, $J = 5.1$ Hz, 2H), 7.82 (d, $J = 1.8$ Hz, 2H), 7.32 (dd, $J = 5.2, 1.7$ Hz, 2H), 3.94 (d, $J = 14.8$ Hz, 2H), 3.81 (d, $J = 14.8$ Hz, 2H), 2.68 – 2.60 (m, 2H), 2.30 (s, 6H), 2.03 – 1.96 (m, 2H), 1.81 – 1.76 (m, 2H), 1.28 (t, $J = 10.8$ Hz, 2H), 1.17 (ddd, $J = 10.3, 8.4, 3.4$ Hz, 2H); ^{13}C NMR (101 MHz, $CDCl_3$) δ 163.40, 149.65, 124.40, 121.68, 118.70, 117.38, 64.68, 59.97, 36.97, 25.78, 25.39; ^{19}F NMR (376 MHz, $CDCl_3$) δ 65.10; HRMS: m/z calculated for $C_{22}H_{27}F_6N_4$, $[L+H]^+$ 461.2140, found 461.2155.

2-Chloromethyl-4-chloropyridine ($^{Cl}PyCH_2Cl$): This compound was prepared following a reported procedure.⁷⁵ The desired compound was obtained as a brown liquid in 98% yield. 1H NMR (400 MHz, $CDCl_3$) δ 8.47 (d, $J = 5.3$ Hz, 1H), 7.51 (d, $J = 1.9$ Hz, 1H), 7.27 – 7.23 (m, 1H), 4.64 (s, 2H). Spectral properties of the product agree with the literature data.

(*S,S*)- $^{Cl}bpmcn$ ($^{Cl}bpmcn$): The procedure followed is inspired by a method reported by Costas and co-workers.^{58, 65} (*S,S*)-*N,N*-Dimethyl-1,2-cyclohexanediamine (162 mg, 1.14 mmol, 1 equiv.), $^{Cl}PyCH_2Cl$ (400 mg, 2.5 mmol, 2.2 equiv.), Na_2CO_3 (1.18 g, 11.13 mmol) and TBABr (64 mg, 0.20 mmol) were dissolved in anhydrous CH_3CN (15 mL). The reaction mixture was refluxed overnight under N_2 . At this point, the crude reaction was filtered, and the solvent was evaporated under reduced pressure. Then, a 1 M aqueous solution of NaOH was added, and the organic layer was collected. The aqueous layer was extracted with CH_2Cl_2 (3 times), and the organic layers were combined, dried over $MgSO_4$, filtered and concentrated to give a crude orange-brown oil. The crude ligand thus obtained was purified by silica gel chromatography eluting with $CH_2Cl_2:CH_3OH:Et_3N$ (96:3:1) and the collected fractions were combined, washed with saturated $NaHCO_3$ solution, dried over $MgSO_4$, and concentrated in vacuo to provide the title compound (399 mg, 1.01 mmol, 88% yield) as a yellow solid. 1H NMR (400 MHz, $CDCl_3$) δ 8.38 (d, $J = 5.4$ Hz, 2H), 7.59 (d, $J = 2.2$ Hz, 2H), 7.13 (dd, $J = 5.5, 2.1$ Hz, 2H), 3.88 (d, $J = 14.9$ Hz, 2H), 3.72 (d, $J = 14.9$ Hz, 2H), 2.63 (d, $J = 9.3$ Hz, 2H), 2.29 (s, 6H), 1.98 (d, $J = 12.2$ Hz, 2H), 1.82 – 1.74 (m, 2H), 1.29 – 1.26 (m, 2H), 1.22 – 1.12 (m, 2H); ^{13}C NMR (101 MHz, $CDCl_3$) δ 163.44, 149.71,

144.91, 123.26, 122.37, 64.77, 59.81, 36.99, 25.83, 25.39; IR (ATR) ν , cm^{-1} : 3110, 3069, 3050, 2926, 2878, 2859, 2845, 2817, 2791, 1575, 1554, 1457, 1422, 1379, 1351, 1199, 1062, 1031, 939, 885, 840, 742, 701, 529, 436; HRMS: m/z calculated for $\text{C}_{20}\text{H}_{27}\text{Cl}_2\text{N}_4$, $[\text{L}+\text{H}]^+$ 393.1613, found 393.1616.

(4-Pyrrolidinopyridin-2-yl)methanol ($^{\text{Pyr}}\text{PyCH}_2\text{OH}$): This compound was prepared following a reported procedure.⁷⁶ The desired $^{\text{Pyr}}\text{PyCH}_2\text{OH}$ compound was obtained as a light yellow solid in 84% yield. ^1H NMR (400 MHz, CDCl_3) δ 8.12 (d, $J = 5.8$ Hz, 1H), 6.34 – 6.22 (m, 1H), 4.62 (s, 2H), 3.85 (s, 1H), 3.36 – 3.24 (m, 4H), 2.02 (td, $J = 6.7, 5.8, 2.8$ Hz, 4H). Spectral properties of the product agree with the literature data.

2-Chloromethyl-4-pyrrolidinopyridine hydrochloride ($^{\text{Pyr}}\text{PyCH}_2\text{Cl}\cdot\text{HCl}$): The procedure followed is inspired by a method reported by Costas and co-workers.⁶⁵ A solution of $^{\text{Pyr}}\text{PyCH}_2\text{OH}$ (1.57 g, 8.8 mmol, 1 equiv.) in dry CH_2Cl_2 (60 mL) was cooled to 0 °C. Thionyl chloride (0.96 mL, 13.2 mmol, 1.5 equiv.) was slowly added. After addition, the resulting mixture was stirred at rt overnight. Then, the solvent was removed at reduced pressure to yield the desired product as a brown solid (1.7 g, 7.3 mmol, 83% yield). ^1H NMR (400 MHz, CDCl_3) δ 8.02 (dd, $J = 7.1, 5.9$ Hz, 1H), 6.74 (s, 1H), 6.56 (dd, $J = 6.8, 2.6$ Hz, 1H), 4.94 (s, 2H), 3.62 – 3.46 (m, 4H), 2.57 (s, 1H), 2.22 – 2.09 (m, 4H); ^{13}C NMR (101 MHz, CDCl_3) δ 156.35, 152.72, 149.24, 106.31, 105.71, 47.47, 47.21, 25.42.

(*S,S*)- $^{\text{Pyr}}\text{bpmcn}$: A 20 mL vial was charged with a stir bar, (*S,S*)-*N,N*-Dimethyl-1,2-cyclohexanediamine (1 equiv., 149.4 mg, 1.05 mmol), H_2O (2 mL), and CH_2Cl_2 (5 mL). Solid NaOH pellets (7.5 equiv., 316 mg, 7.9 mmol) were added, followed by $^{\text{Pyr}}\text{PyCH}_2\text{Cl}\cdot\text{HCl}$ (2.04 equiv., 500 mg, 2.14 mmol). After 18 h stirring at room temperature, the reaction mixture was diluted with 1M NaOH. The aqueous layer was extracted with CH_2Cl_2 (3x), and the organic extracts were combined, dried over MgSO_4 , and concentrated in vacuo. The obtained crude ligand was purified by silica gel chromatography eluting with $\text{CH}_2\text{Cl}_2:\text{CH}_3\text{OH}:\text{NH}_4\text{OH}$ (90 : 4.5 : 1.8), and the collected fractions were combined, washed with 1 M NaOH, dried over MgSO_4 , and concentrated in vacuo to provide the desired (*S,S*)- $^{\text{Pyr}}\text{bpmcn}$ ligand as a light-orange solid (367 mg, 0.79 mmol, 76% yield). ^1H NMR (400 MHz, CDCl_3) δ 8.02 (d, $J = 6.0$ Hz, 2H), 6.69 (d, $J = 2.5$ Hz, 2H), 6.28 (dd, $J = 6.0, 2.5$ Hz, 2H), 3.87 (d, $J = 14.1$ Hz, 2H), 3.59 (d, $J = 14.1$ Hz, 2H), 3.20 (s, 8H), 2.70 – 2.68 (m, 2H), 2.34 (s, 6H), 2.03 - 2.00 (m, 2H), 1.94 (s, 8H), 1.80 – 1.77 (m, 2H), 1.30 – 1.17 (m, 4H); ^{13}C NMR (101 MHz, CDCl_3) δ 161.20, 152.41, 148.46, 106.05, 105.45, 64.67, 60.55, 46.87, 36.86, 25.96, 25.60, 25.39; IR (ATR) ν , cm^{-1} : 2965, 2924, 2849, 2781, 1594, 1541, 1496, 1484, 1448, 1384, 1349, 1262, 1242, 1179, 1157, 1052, 1015, 981, 801; HRMS: m/z calculated for $\text{C}_{28}\text{H}_{43}\text{N}_6$, $[\text{M}+\text{H}]^+$ 463.3549, found 463.3543.

1,3-dimethyl-2-(pyridine-2-yl)octahydro-1*H*-benzo[d]imidazole: This compound was prepared following a reported procedure, using (*S,S*)-(+)-*N,N'*-dimethyl-1,2-cyclohexanediamine and picolinaldehyde.⁷⁷ The desired product was obtained as a pale-yellow oil in 48% yield. ^1H NMR (400 MHz, CDCl_3) δ 8.62 – 8.56 (m, 1H), 7.67 (td, $J = 7.6, 1.8$ Hz, 1H), 7.59 – 7.53 (m, 1H), 7.20 (ddd, $J = 7.5, 4.9, 1.3$ Hz, 1H), 4.36 (s, 1H), 2.61 (s, 1H), 2.32 (s, 3H), 2.25 – 2.13 (m, 1H), 2.08 (s, 3H), 2.07 – 2.01 (m, 1H), 2.00 – 1.91 (m, 1H), 1.89 – 1.81 (m, 2H), 1.30 (s, 4H). Spectral properties of the product agree with the literature data.

(*S,S*)-mcp-Py: This compound was prepared following a reported procedure.⁷⁷ The desired product was obtained as a brown oil in 94% yield. ^1H NMR (400 MHz, CDCl_3) δ 8.51 (ddd, $J = 4.9, 1.8, 1.0$ Hz, 1H), 7.66 (td, $J = 7.7, 1.8$ Hz, 1H), 7.39 (d, $J = 7.9$ Hz, 1H), 7.15 (ddd, $J = 7.5, 4.9, 1.2$ Hz, 1H), 3.80 (d, $J = 14.3$ Hz, 1H), 3.60 (d, $J = 14.3$ Hz, 1H), 2.41 (s, 3H), 2.30 (td, $J = 10.3, 4.1$ Hz, 1H), 2.21 (s, 3H), 2.17 – 2.08 (m, 1H), 1.92 (ddt, $J = 7.4, 3.5, 1.4$ Hz, 1H), 1.81 (dq, $J = 7.7, 2.7, 2.2$ Hz, 1H), 1.75 – 1.68 (m,

1H), 1.31 – 1.12 (m, 4H), 1.11 – 0.99 (m, 1H). Spectral properties of the product agree with the literature data.

(*S,S*)-^H-TIPSBpmcn: The procedure followed is inspired by a method reported by Klein Gebbink, Costas and co-workers.⁶⁰ (*S,S*)-mcp-Py (291 mg, 1.25 mmol) were dissolved in CH₂Cl₂ (20 mL) and cooled to 0 °C, and 1.3 equiv. of NaBH(AcO)₃ (344 mg, 1.63 mmol) were added to the reaction mixture, which was stirred for 30 min at 0 °C. ^{TIPSPy}CHO (328 mg, 1.25 mmol) was added at this point, and the crude was stirred at room temperature overnight. It was then extracted with 40 mL of a saturated aqueous NaHCO₃ solution. The aqueous layer was extracted with CH₂Cl₂ (3 times). The combined organic layers were dried over MgSO₄, filtered, and concentrated to give a crude brown liquid. Purification using column chromatography on alumina neutral eluting with CH₂Cl₂/CH₃OH (40:1) afforded the title compound (458 mg, 0.95 mmol, 76% yield) as a light-yellow oil. Basic washing using NaHCO₃, followed by extraction with CH₂Cl₂ was necessary after the column. ¹H NMR (400 MHz, CDCl₃) δ 8.51 (d, *J* = 25.6 Hz, 2H), 7.76 – 7.47 (m, 4H), 7.11 (s, 1H), 4.03 – 3.63 (m, 4H), 2.73 – 2.61 (m, 2H), 2.29 (d, *J* = 5.6 Hz, 6H), 2.05 – 1.92 (m, 2H), 1.76 (s, 2H), 1.39 (p, *J* = 7.5 Hz, 3H), 1.33 (s, 4H), 1.07 (d, *J* = 7.0 Hz, 18H); ¹³C NMR (101 MHz, CDCl₃) δ 161.56, 154.55, 148.76, 143.44, 136.37, 127.19, 123.01, 122.23, 121.69, 77.36, 64.89, 64.66, 60.80, 60.68, 53.56, 36.95, 36.71, 26.20, 26.12, 25.97, 18.59, 10.76; IR (ATR) ν, cm⁻¹: 2929, 2890, 2863, 2789, 1580, 1544, 1462, 1433, 1383, 1343, 1264, 1206, 1144, 1106, 1052, 1026, 1014, 994, 944, 919, 881, 757, 733, 678, 647, 518; HRMS: *m/z* calculated for C₂₈H₄₃N₆, [L+H]⁺ 481.3726, found 481.3723.

1,3-dimethyl-2-(4-triisopropylsilyl-pyridine-2-yl)octahydro-1*H*-benzo[d]imidazole: This compound was prepared following a modified procedure reported by Costas and co-workers.⁷⁷ (*S,S*)-(+)-*N,N'*-Dimethyl-1,2-cyclohexanediamine (0.4 g, 2.8 mmol) was dissolved in 4 mL of anhydrous diethyl ether. ^{TIPSPy}CHO (0.73 g, 2.8 mmol) was added to the solution and the resulting mixture was stirred at rt overnight. The reaction was quenched, by removing solvent, under reduced pressure. The obtained residue was dissolved in methanol, filtered on MgSO₄ and dried under vacuum, giving the desired product as a pale-yellow oil (1.07 g, 2.76 mmol, 99% yield). ¹H NMR (400 MHz, CDCl₃) δ 8.65 (s, 1H), 7.77 (d, *J* = 7.7 Hz, 1H), 7.51 (d, *J* = 7.7 Hz, 1H), 4.33 (s, 1H), 2.69 – 2.60 (m, 1H), 2.35 (s, 3H), 2.23 – 2.17 (m, 1H), 2.10 (s, 3H), 2.06 – 2.04 (m, 1H), 1.98 – 1.94 (m, 1H), 1.86 – 1.83 (m, 2H), 1.43 – 1.35 (m, 3H), 1.35 – 1.26 (m, 4H), 1.07 (d, *J* = 7.5 Hz, 18H); ¹³C NMR (101 MHz, CDCl₃) δ 160.70, 154.65, 143.37, 128.97, 122.59, 91.19, 69.39, 67.55 38.29, 35.36, 29.35, 28.31, 24.67, 24.43, 18.57, 10.78.

mcp-^{TIPSPy}: This compound was prepared following a modified procedure reported by Costas and co-workers.⁷⁷ 1,3-dimethyl-2-(4-triisopropylsilyl-pyridine-2-yl)octahydro-1*H*-benzo[d]imidazole (1.05 g, 2.7 mmol) was dissolved in dry methanol (45 mL) and the solution was cooled at 0 °C. CF₃COOH (1.7 mL, 22.68 mmol) and then NaBH₃CN (0.9 g, 14.31 mmol) were added slowly to the solution at 0 °C. After the addition, the mixture was warmed up to room temperature and stirred overnight. The reaction was then quenched by adding water, and the organic solvent was then removed by rotary evaporator. An aqueous 4 M NaOH solution was then added to the residue, and the mixture was stirred at room temperature for 4 h. Next, extraction with CH₂Cl₂ (3 x) was done. The combined organic fractions were dried on MgSO₄, filtered, and the solvent was removed under reduced pressure to afford the desired product as a brown oil (1.07 g, 2.7 mmol, >99% yield), which was pure enough for the next step. ¹H NMR (400 MHz, CDCl₃) δ 8.55 (s, 1H), 7.75 (dd, *J* = 7.7, 1.8 Hz, 1H), 7.31 (d, *J* = 7.7 Hz, 1H), 3.79 (d, *J* = 14.7 Hz, 1H), 3.49 (d, *J* = 14.7 Hz, 1H), 2.60 – 2.57 (m, 1H), 2.49 (s, 3H), 2.44 – 2.41 (m, 1H), 2.28 (s, 3H), 2.17 – 2.14 (m, 1H), 1.96 – 1.94 (m, 1H), 1.85 – 1.71 (m, 2H), 1.44 – 1.34 (m, 3H), 1.32 – 1.14 (m, 4H), 1.07 (d, *J* = 7.5 Hz, 18H); ¹³C NMR (101 MHz, CDCl₃) δ 160.25, 154.68, 143.67, 127.81,

121.72, 66.64, 60.31, 33.56, 32.96, 30.74, 30.16, 25.30, 24.58, 22.52, 18.43, 10.61; IR (ATR) ν , cm^{-1} : 3318, 2930, 2890, 2863, 2787, 1686, 1580, 1545, 1462, 1383, 1343, 1254, 1199, 1142, 1107, 1056, 1013, 994, 919, 882, 832, 751, 678, 647, 517; HRMS: m/z calculated for $\text{C}_{23}\text{H}_{44}\text{N}_3\text{Si}$, $[\text{L}+\text{H}]^+$ 390.3304, found 390.3309.

(*S,S*)-^{NMe₂,TIPS}bpmcn: The procedure followed is inspired by a method reported by Costas and co-workers.^{58, 65} mcp-TIPSPy (100 mg, 0.257 mmol, 1 equiv.), $\text{Me}_2\text{NPyCH}_2\text{Cl}\cdot\text{HCl}$ (55 mg, 0.267 mmol, 1.04 equiv.), Na_2CO_3 (110 mg, 1.04 mmol) and TBABr (5 mg, 0.02 mmol) were dissolved in anhydrous CH_3CN (15 mL). The reaction mixture was refluxed overnight under N_2 . At this point, the crude reaction was filtered, and the solvent was evaporated under reduced pressure. Then, a 1 M aqueous solution of NaOH was added, and the organic layer was collected. The aqueous layer was extracted with CH_2Cl_2 (3 times), and the organic layers were combined, dried over MgSO_4 , filtered, and concentrated to give a crude oil. The crude ligand thus obtained was purified by chromatography on basic alumina eluting with ethyl acetate : petroleum ether : Et_3N (9 : 1 : 0.1) and the collected fractions were combined, washed with 1 M NaOH solution, dried over MgSO_4 , and concentrated in vacuo to provide the title compound (65 mg, 0.124 mmol, 48% yield) as a brown solid. ^1H NMR (400 MHz, CDCl_3) δ 8.50 (s, 1H), 7.95 (d, $J = 6.3$ Hz, 1H), 7.69 (d, $J = 7.7$ Hz, 1H), 7.55 (d, $J = 7.7$ Hz, 1H), 7.00 (s, 1H), 6.39 (d, $J = 6.3$ Hz, 1H), 4.01 (dd, $J = 14.4, 4.5$ Hz, 2H), 3.79 (dd, $J = 20.6, 14.5$ Hz, 2H), 3.00 (s, 6H), 2.85 – 2.74 (m, 2H), 2.11 – 2.03 (m, 2H), 1.86 – 1.75 (m, 2H), 1.42 – 1.34 (m, 3H), 1.26 – 1.18 (m, 4H), 1.05 (d, $J = 7.5$ Hz, 18H); ^{13}C NMR (101 MHz, CDCl_3) δ 155.72, 154.68, 146.34, 143.77, 128.25, 123.15, 105.98, 105.41, 64.37, 39.58, 37.30, 32.03, 31.54, 30.29, 29.80, 29.76, 29.46, 25.46, 25.42, 22.79, 18.56, 14.22, 10.70.

2,5-Dibromo-*N,N*-dimethylpyridin-3-amine: This compound was prepared following a modified reported procedure.⁷⁸ 2,5-Dibromo-pyridin-3-ylamine (2.52 g, 10 mmol, 1 equiv.) was dissolved in anhydrous DMF (35 mL) at 0 °C, and 60% NaH (1.1 g, 27.5 mmol, 2.75 equiv.) was slowly added. The solution was stirred for 20 min, and MeI (1.43 mL, 23 mmol, 2.3 equiv.) was added dropwise. After 30 min at 0 °C and 1 h at room temperature, the reaction was quenched with water (5 mL). The solvents were removed, and the residue dissolved in water and extracted with Et_2O . The organic layer was washed with water, 0.1 M HCl, saturated NaHCO_3 solution and brine, dried over MgSO_4 , and dried under reduced pressure. Finally, the mineral oil was removed by column chromatography on silica eluting with petroleum ether first, followed by ethyl acetate to yield the desired product as a light-brown solid (2.63 g, 9.4 mmol, 94% yield). ^1H NMR (400 MHz, CDCl_3) δ 8.06 (s, 1H), 7.38 (d, 1H), 2.85 (s, 6H); ^{13}C NMR (101 MHz, CDCl_3) δ 149.98, 143.15, 136.69, 130.27, 119.74, 43.53.

2-Bromo-3-dimethylamino-5-triisopropylsilyl-pyridine: 2,5-Dibromo-*N,N*-dimethyl-pyridine-3-amine (1.27 g, 4.54 mmol) were dissolved in 40 mL of anhydrous diethyl ether under inert atmosphere and cooled to –78 °C in an acetone/dry ice bath. Then 1 equiv. of *n*-BuLi (1.6 M in hexanes, 2.84 mL, 4.54 mmol) were slowly added over 10 min, and the reaction mixture was let stir for 45 min. At that point, 1.1 equiv. of triisopropylsilyl triflate (1.34 mL, 5 mmol) was added slowly at –78 °C and stirred for another hour. Afterwards, the temperature was raised up to –15 °C. At this point, the reaction was quenched with 20 mL of H_2O and extracted with diethyl ether (3 x 30 mL). The combined organic layers were washed with 30 mL of brine, dried over MgSO_4 , concentrated on a rotatory evaporator and purified by silica column chromatography eluting with petroleum ether : ethyl acetate (30:1) to yield the desired product as a yellow solid (390 mg, 1.09 mmol, 24% yield), which was pure enough for the next step (an impurity was still present in the final crude mixture, which corresponds to 3-dimethylamino-2,5-triisopropylsilyl-pyridine). ^1H NMR (400 MHz, CDCl_3) δ 8.01 (s, 1H), 7.33 (s, 1H), 2.81 (s, 6H), 1.42–1.30 (m, 3H), 1.05 (d, $J = 7.5$ Hz, 18 H).

5-Triisopropylsilyl-3-(Dimethylamino)picolinaldehyde (^{3-NMe2-5-TIPS}PyCHO): 2-Bromo-3-dimethylamino-5-triisopropylsilyl-pyridine (438 mg, 1.23 mmol) were dissolved in 10 mL of anhydrous diethyl ether under inert atmosphere and cooled to $-78\text{ }^{\circ}\text{C}$ in an acetone/dry ice bath. Then, 1.1 equiv. of *n*-BuLi (1.6 M in hexanes, 0.85 mL, 1.35 mmol) were slowly added over 10 min, and the reaction mixture was let stir for 45 min. After that time, 1.6 equiv. of anhydrous DMF (0.15 mL, 1.97 mmol) were slowly added. The reaction was stirred for 2 h at $-78\text{ }^{\circ}\text{C}$, and the temperature was then raised up to $-15\text{ }^{\circ}\text{C}$. At this point, the reaction was quenched with 10 ml of H₂O and extracted with diethyl ether (3 x 10 mL). The combined organic layers were washed with 30 mL of brine, dried over MgSO₄, concentrated on a rotatory evaporator and purified by silica column chromatography eluting with petroleum ether:ethyl acetate (30:1) to yield the pure product as a yellow solid (97 mg, 0.32 mmol, 26% yield). ¹H NMR (400 MHz, CDCl₃) δ 10.13 (s, 1H), 8.30 (s, 1H), 7.44 (s, 1H), 2.99 (s, 6H), 1.49-1.38 (m, 3H), 1.10 (d, *J* = 7.5 Hz, 18 H); ¹³C NMR (101 MHz, CDCl₃) δ 191.85, 147.74, 145.32, 139.90, 136.17, 130.75, 43.80, 18.59, 10.88.

5-Triisopropylsilyl-2-Hydroxymethyl-4-dimethylaminopyridine (^{3-NMe2-5-TIPS}PyCH₂OH) The procedure followed is inspired by a method reported by Klein Gebbink and co-workers.⁷⁴ NaBH₄ (0.63 mmol, 24 mg, 2 equiv.) was dissolved in dry methanol (5 mL) under N₂ and the resulting mixture was stirred for 3 min. A solution of ^{3-NMe2-5-TIPS}PyCHO (97 mg, 0.32 mmol, 1 equiv.) in dry methanol was then added. The reaction was stirred at room temperature overnight. The solution was diluted with CH₂Cl₂, washed with saturated NaHCO₃, and the aqueous layer was extracted with CH₂Cl₂ (3 x 10 mL). The combined organics were dried with MgSO₄ and concentrated under reduced pressure to afford the desired product as a white solid (80 mg, 0.26 mmol, 81% yield). ¹H NMR (400 MHz, CDCl₃) δ 8.15 (s, 1H), 7.70 (s, 1H), 5.04 (s, 2H), 2.89 (s, 6H), 1.45-1.38 (m, 3H), 1.08 (d, *J* = 7.5 Hz, 18H).

2-Chloromethyl-5-triisopropylsilyl-3-dimethylaminopyridine hydrochloride (^{3-NMe2-5-TIPS}PyCH₂Cl·HCl): The procedure followed is inspired by a method reported by Costas and co-workers.⁶⁵ A solution of ^{3-NMe2-5-TIPS}PyCH₂OH (80 mg, 0.26 mmol, 1 equiv.) in dry CH₂Cl₂ (5 mL) was cooled to 0 °C. Thionyl chloride (28 μL, 0.39 mmol, 1.5 equiv.) was slowly added. After addition, the resulting mixture was stirred at rt overnight. Then, the solvent was removed at reduced pressure to yield the desired product as a brown solid (100 g, 0.28 mmol, >99% yield). ¹H NMR (400 MHz, CDCl₃) δ 8.15 (s, 1H), 7.81 (s, 1H), 5.21 (s, 2H), 3.05 (s, 6H), 1.47-1.37 (m, 3H), 1.07 (d, *J* = 7.5 Hz, 18H).

(*S,S*)-^{3-NMe2-5-TIPS}bpbp (L4): A 20 mL vial was charged with a stir bar, (*S,S*)-2,2'-bispyrrolidine tartrate (1 equiv., 45 mg, 0.131 mmol), H₂O (2 mL), and CH₂Cl₂ (2 mL). Solid NaOH pellets (6.4 equiv., 33.5 mg, 0.84 mmol) were added, followed by ^{3-NMe2-5-TIPS}PyCH₂Cl·HCl (2.1 equiv., 100 mg, 0.28 mmol). After 18 h stirring at room temperature, the reaction mixture was diluted with 1 M NaOH. The aqueous layer was extracted with CH₂Cl₂ (3x), and the organic extracts were combined, dried over MgSO₄, and concentrated in vacuo. The obtained crude ligand was purified by silica gel chromatography eluting with CH₂Cl₂:CH₃OH:NH₄OH (20 : 1 : 0.4) first, followed by CH₂Cl₂:CH₃OH:NH₄OH (10 : 1 : 0.4), and the collected fractions were combined, washed with 1 M NaOH, dried over MgSO₄, and concentrated in vacuo to provide the desired (*S,S*)-^{3-NMe2-5-TIPS}bpbp ligand as a light-brownish solid (78 mg, 0.108 mmol, 83% yield). ¹H NMR (400 MHz, C₆D₆) δ 8.59 (s, 2H), 7.46 (s, 2H), 4.64 (d, *J* = 11.3 Hz, 2H), 3.87 (d, *J* = 11.3 Hz, 2H), 3.34 – 3.29 (m, 2H), 3.18 – 3.14 (m, 2H), 2.76 (s, 12H), 2.74 – 2.72 (m, 2H), 1.84 – 1.80 (m, 4H), 1.64 – 1.60 (m, 4H), 1.32 – 1.24 (m, 6H), 1.06 (dd, *J* = 7.4, 3.8 Hz, 36H); ¹³C NMR (101 MHz, CDCl₃) δ 210.89, 148.76, 148.37, 132.94, 128.02, 56.99, 55.87, 45.30, 31.83, 29.37, 23.79, 18.60, 10.79; HRMS: *m/z* calculated for C₄₂H₇₇N₆Si₂, [L+H]⁺ 721.5748, found 721.5765.

4.4.3 Synthesis of Manganese Complexes

(*S,S'*)-[Mn(CF₃SO₃)₂(^{CF3}bpmcn)] (^{CF3}1): A suspension of Mn(CF₃SO₃)₂ (47.3 mg, 0.134 mmol) in anhydrous THF (1 mL) was added dropwise to a vigorously stirred solution of (*S,S*)-^{CF3}bpmcn (66 mg, 0.143 mmol) in THF (1 mL). The resulting mixture was stirred at rt overnight. Then, the solution was dried under vacuum, to provide a precipitate that was washed with diethyl ether several times. The resulting precipitate was dissolved in CH₂Cl₂, and slow diethyl ether diffusion over the resultant solution afforded, in a few days the desired complex as light-yellow crystals (34 mg, 0.042 mmol, yield 31%). HRMS: *m/z* calculated for C₂₃H₂₆F₆MnN₄O₃S, [M-OTf]⁺ 664.0962, found 664.0963.

(*S,S'*)-[Mn(CF₃SO₃)₂(^{Cl}bpmcn)] (^{Cl}1): A suspension of Mn(CF₃SO₃)₂ (84 mg, 0.238 mmol) in anhydrous THF (1 mL) was added dropwise to a vigorously stirred solution of (*S,S*)-^{Cl}bpmcn (100 mg, 0.254 mmol) in THF (1 mL). Following the previous conditions, slow diethyl ether diffusion over a CH₂Cl₂ solution afforded in a few days the desired complex as white crystals (118 mg, 0.158 mmol, yield 66%). HRMS: *m/z* calculated for C₂₁H₂₆Cl₂F₃MnN₄O₃S 596.0435, found 596.0431.

(*S,S'*)-[Mn(CF₃SO₃)₂(^{Pyr}bpmcn)] (^{Pyr}1): A suspension of Mn(CF₃SO₃)₂ (72 mg, 0.203 mmol) in anhydrous THF (1 mL) was added dropwise to a vigorously stirred solution of (*S,S*)-^{Pyr}bpmcn (100 mg, 0.216 mmol) in THF (1 mL). Following the previous conditions, slow diethyl ether diffusion over a CH₂Cl₂ solution afforded in a few days the desired complex as a light-brown solid (117 mg, 0.143 mmol, yield 71%). HRMS: *m/z* calculated for C₂₉H₄₂F₃MnN₆O₃S, [M-OTf]⁺ 666.2372, found 666.2378.

(*S,S'*)-[Mn(CF₃SO₃)₂(^{H-TIPS}bpmcn)] (2): A suspension of Mn(CF₃SO₃)₂ (69 mg, 0.195 mmol) in anhydrous THF (1 mL) was added dropwise to a vigorously stirred solution of (*S,S*)-^{H-TIPS}bpmcn (100 mg, 0.208 mmol) in THF (1 mL). Following the previous conditions, slow diethyl ether diffusion over the resultant solution afforded in a few days the desired complex as a white crystalline material (112 mg, 0.134 mmol, yield 69%). HRMS: *m/z* calculated for C₃₀H₄₈F₃MnN₄O₃SSi, [M-OTf]⁺ 684.2549, found 684.2548.

(*S,S'*)-[Mn(CF₃SO₃)₂(^{NMe2,TIPS}bpmcn)] (3): A suspension of Mn(CF₃SO₃)₂ (44 mg, 0.123 mmol) in anhydrous THF (1 mL) was added dropwise to a vigorously stirred solution of (*S,S*)-^{NMe2,TIPS}bpmcn (69 mg, 0.132 mmol) in THF (1 mL). Following the previous conditions, slow diethyl ether diffusion over the resultant solution afforded in a few days the desired complex as a white crystalline material (40 mg, 0.045 mmol, yield 37%). HRMS: *m/z* calculated for C₃₂H₅₃F₃MnN₅O₃SSi, [M-OTf]⁺ 727.2971, found 727.2965.

(*S,S'*)-[Mn(CF₃SO₃)₂(^{3-NMe2-5-TIPS}bpbp)] (4): A suspension of Mn(CF₃SO₃)₂ (30 mg, 0.086 mmol) in anhydrous THF (1 mL) was added dropwise to a vigorously stirred solution of (*S,S*)-^{3-NMe2-5-TIPS}bpbp (67 mg, 0.092 mmol) in THF (1 mL). Following the previous conditions, slow diethyl ether diffusion over the resultant solution afforded in a few days the desired complex as a white crystalline material (72 mg, 0.067 mmol, yield 78%). HRMS: *m/z* calculated for C₄₃H₇₆F₃MnN₆O₃SSi₂ [M-OTf]⁺ 924.4571, found 924.4568.

4.4.4 X-Ray Crystal Structure Determination of (*S,S*)-[Mn(OTf)₂(^{CF3}bpmcn)] (^{CF3}1) and (*S,S*)-[Mn(OTf)₂(^{Cl}bpmcn)] (^{Cl}1)

4.4.4.1 X-ray crystal structure determination of complex ^{CF3}1

C₂₄H₂₆F₁₂MnN₄O₆S₂, Fw = 813.55, colourless block, 0.37 × 0.37 × 0.25 mm³, orthorhombic, P2₁2₁2₁ (no. 19), a = 17.4091(4), b = 21.8591(4), c = 52.0015(10) Å, V = 19789.1(7) Å³, Z = 24, D_x = 1.638 g/cm³,

$\mu = 0.64 \text{ mm}^{-1}$. The diffraction experiment was performed on a Bruker Kappa ApexII diffractometer with sealed tube and Triumph monochromator ($\lambda = 0.71073 \text{ \AA}$) at a temperature of 150(2) K up to a resolution of $(\sin \theta/\lambda)_{\text{max}} = 0.61 \text{ \AA}^{-1}$. The crystal appeared to be twinned with a 90° rotation about the b-axis as twin operation. Consequently, two orientation matrices were used for the intensity integration with the Eval15 software.⁷⁹ A multi-scan absorption correction and scaling was performed with TWINABS⁸⁰ (correction range 0.61-0.75). A total of 313818 reflections was measured, 36502 reflections were unique ($R_{\text{int}} = 0.057$), 30552 reflections were observed [$I > 2\sigma(I)$]. The structure was solved with Patterson superposition methods using SHELXT.⁸¹ Structure refinement was performed with SHELXL-2018⁸² on F^2 of all reflections. Non-hydrogen atoms were refined freely with anisotropic displacement parameters. All hydrogen atoms were included in calculated positions and refined with a riding model. Some of the CF_3 groups and some of the triflate ligands were refined with disorder models. 2828 Parameters were refined with 7905 restraints (distance/angle restraints for the ordered parts, distance/angle/displacement restraints for the disordered parts). $R1/wR2 [I > 2\sigma(I)]: 0.0417 / 0.0920$. $R1/wR2 [\text{all refl.}]: 0.0563 / 0.0973$. $S = 1.034$. Twin fraction BASF = 0.4682(2). Based on the non-overlapping reflections, the absolute structure was determined by refinements as inversion twins, resulting in the Flack parameter⁸³ $x=0.012(18)$ for the first twin component and $x=0.016(19)$ for the second. Residual electron density between -0.39 and 0.57 e/\AA^3 . Geometry calculations and checking for higher symmetry was performed with the PLATON program.⁸⁴

4.4.4.2 X-ray crystal structure determination of complex **C1**

$\text{C}_{22}\text{H}_{26}\text{Cl}_2\text{F}_6\text{MnN}_4\text{O}_6\text{S}_2$, Fw = 746.43, colourless block, $0.45 \times 0.25 \times 0.13 \text{ mm}^3$. The structural results are described here in the 3-dimensional superstructure approximation.^[*] Triclinic, P1 (no. 1), $a = 11.6525(3)$, $b = 23.5064(9)$, $c = 25.3367(11) \text{ \AA}$, $\alpha = 62.385(3)$, $\beta = 84.988(2)$, $\gamma = 79.137(1)^\circ$, $V = 6039.2(4) \text{ \AA}^3$, $Z = 8$, $D_x = 1.642 \text{ g/cm}^3$, $\mu = 0.64 \text{ mm}^{-1}$. The diffraction experiment was performed on a Bruker Kappa ApexII diffractometer with sealed tube and Triumph monochromator ($\lambda = 0.71073 \text{ \AA}$) at a temperature of 150(2) K up to a resolution of $(\sin \theta/\lambda)_{\text{max}} = 0.65 \text{ \AA}^{-1}$. The Eval15 software⁷⁹ was used for the intensity integration. A multi-scan absorption correction and scaling was performed with SADABS⁸⁰ (correction range 0.68-0.75). A total of 150766 reflections was measured, 55361 reflections were unique ($R_{\text{int}} = 0.030$), 46244 reflections were observed [$I > 2\sigma(I)$]. The structure was solved with Patterson superposition methods using SHELXT.⁸¹ Structure refinement was performed with SHELXL-2018⁸² on F^2 of all reflections. Twinning by *pseudo*-merohedry was included by the matrix $(-1,0,0 / 0,-1,0 / 0,-1,1)$. Non-hydrogen atoms were refined freely with anisotropic displacement parameters. All hydrogen atoms were included in calculated positions and refined with a riding model. Potential disorder was not modeled in the refinement. 3114 Parameters were refined with 16267 restraints (distance/angle/displacement restraints for the independent molecules, flatness restraints for the aromatic moieties). $R1/wR2 [I > 2\sigma(I)]: 0.0457 / 0.1083$. $R1/wR2 [\text{all refl.}]: 0.0585 / 0.1194$. $S = 1.034$. Twin fraction BASF = 0.4992(15). Because of the twinning and the overlap of all reflections, no attempt for an absolute structure determination was undertaken. Residual electron density between -0.79 and 1.44 e/\AA^3 . Geometry calculations and checking for higher symmetry was performed with the PLATON program.⁸⁴

* Description as a modulated structure in 3+1 dimensional space is possible with the following unit cell parameters: $a = 11.65498(13)$, $b = 11.22862(10)$, $c = 11.75548(15) \text{ \AA}$, $\alpha = 90.014(1)$, $\beta = 100.867(1)$, $\gamma = 89.991(1)^\circ$, $V = 1510.85(3) \text{ \AA}^3$, $q = [0, 0.2269, 0]$.

4.4.5 General Procedure for Catalytic Hydroxylation Reaction

A 20 mL vial was charged with substrate (1 equiv.), catalyst (1 mol%) and the corresponding solvent (2 mL). The carboxylic acid was then added with indicated loading. The vial was cooled on an ice bath with stirring. Subsequently, a solution of H₂O₂ in the corresponding solvent (indicated loading, diluted from a 35% H₂O₂ aqueous solution) was delivered by syringe pump over 30 min. After the oxidant addition, the resulting mixture was brought to room temperature, and at this point, a 0.8 M biphenyl solution in CH₃CN (0.5 equiv) was added as internal standard. The solution was filtered through a silica plug, which was subsequently rinsed with 2 x 1 mL EtOAc. Then the sample was submitted to GC analysis to determine the mass balance, the conversion, and relative ratio of products by comparison with authentic samples. Yield for propyl-*p*-benzoquinone was calculated with the response factor of methyl-*p*-benzoquinone.

Author Contributions

E.M-R. and R.K.G. devised the project and designed experiments. M.C.1. provided complex **5**. M.L. performed X-ray analysis. M.C.2. provided comments on Chapter content. E.M-R. wrote the Chapter and R.K.G. provided comments on the experiments and Chapter content.

4.5 References

1. Genovino, J.; Sames, D.; Hamann, L. G.; Touré, B. B., Accessing Drug Metabolites via Transition-Metal Catalyzed C–H Oxidation: The Liver as Synthetic Inspiration. *Angew. Chem. Int. Ed.* **2016**, *55* (46), 14218-14238.
2. Börgel, J.; Tanwar, L.; Berger, F.; Ritter, T., Late-stage aromatic C–H oxygenation. *J. Am. Chem. Soc.* **2018**, *140* (47), 16026-16031.
3. Fukuzumi, S.; Ohkubo, K., One-Step Selective Hydroxylation of Benzene to Phenol. *Asian J. Org. Chem.* **2015**, *4* (9), 836-845.
4. Ottenbacher, R. V.; Talsi, E. P.; Bryliakov, K. P., Recent progress in catalytic oxygenation of aromatic C–H groups with the environmentally benign oxidants H₂O₂ and O₂. *Appl. Organomet. Chem.* **2020**, *34* (11), e5900.
5. Mancuso, A.; Sacco, O.; Sannino, D.; Venditto, V.; Vaiano, V., One-Step Catalytic or Photocatalytic Oxidation of Benzene to Phenol: Possible Alternative Routes for Phenol Synthesis? *Catalysts* **2020**, *10* (12), 1424.
6. Lyakin, O. Y.; Talsi, E. P., Direct C–H Oxidation of Aromatic Substrates in the Presence of Biomimetic Iron Complexes. In *Frontiers of Green Catalytic Selective Oxidations*, Springer: 2019; pp 253-276.
7. Enthaler, S.; Company, A., Palladium-catalysed hydroxylation and alkoxylation. *Chem. Soc. Rev.* **2011**, *40* (10), 4912-4924.
8. Lücke, B.; Narayana, K.; Martin, A.; Jähnisch, K., Oxidation and ammoxidation of aromatics. *Adv. Synth. Catal.* **2004**, *346* (12), 1407-1424.
9. Tanev, P. T.; Chibwe, M.; Pinnavaia, T. J., Titanium-containing mesoporous molecular sieves for catalytic oxidation of aromatic compounds. *Nature* **1994**, *368* (6469), 321-323.

10. Niwa, S.-i.; Eswaramoorthy, M.; Nair, J.; Raj, A.; Itoh, N.; Shoji, H.; Namba, T.; Mizukami, F., A one-step conversion of benzene to phenol with a palladium membrane. *Science* **2002**, *295* (5552), 105-107.
11. Kamata, K.; Yamaura, T.; Mizuno, N., Chemo- and Regioselective Direct Hydroxylation of Arenes with Hydrogen Peroxide Catalyzed by a Divanadium-Substituted Phosphotungstate. *Angew. Chem. Int. Ed.* **2012**, *51* (29), 7275-7278.
12. Morimoto, Y.; Bunno, S.; Fujieda, N.; Sugimoto, H.; Itoh, S., Direct hydroxylation of benzene to phenol using hydrogen peroxide catalyzed by nickel complexes supported by pyridylalkylamine ligands. *J. Am. Chem. Soc.* **2015**, *137* (18), 5867-5870.
13. Tsuji, T.; Zaoputra, A. A.; Hitomi, Y.; Mieda, K.; Ogura, T.; Shiota, Y.; Yoshizawa, K.; Sato, H.; Kodera, M., Specific enhancement of catalytic activity by a dicopper core: selective hydroxylation of benzene to phenol with hydrogen peroxide. *Angew. Chem. Int. Ed.* **2017**, *56* (27), 7779-7782.
14. Capocasa, G.; Olivo, G.; Barbieri, A.; Lanzalunga, O.; Di Stefano, S., Direct hydroxylation of benzene and aromatics with H₂O₂ catalyzed by a self-assembled iron complex: evidence for a metal-based mechanism. *Catal. Sci. Technol.* **2017**, *7* (23), 5677-5686.
15. Kwong, H. K.; Lo, P. K.; Yiu, S. M.; Hirao, H.; Lau, K. C.; Lau, T. C., Highly selective and efficient ring hydroxylation of alkylbenzenes with hydrogen peroxide and an osmium(VI) nitrido catalyst. *Angew. Chem. Int. Ed.* **2017**, *56* (40), 12260-12263.
16. Ticconi, B.; Colcerasa, A.; Di Stefano, S.; Lanzalunga, O.; Lapi, A.; Mazzonna, M.; Olivo, G., Oxidative functionalization of aliphatic and aromatic amino acid derivatives with H₂O₂ catalyzed by a nonheme imine based iron complex. *RSC Adv.* **2018**, *8* (34), 19144-19151.
17. Muthuramalingam, S.; Anandababu, K.; Velusamy, M.; Mayilmurugan, R., One step phenol synthesis from benzene catalysed by nickel(II) complexes. *Catal. Sci. Technol.* **2019**, *9* (21), 5991-6001.
18. Anandababu, K.; Muthuramalingam, S.; Velusamy, M.; Mayilmurugan, R., Single-step benzene hydroxylation by cobalt(II) catalysts via a cobalt(III)-hydroperoxo intermediate. *Catal. Sci. Technol.* **2020**, *10* (8), 2540-2548.
19. Kumari, S.; Muthuramalingam, S.; Dhara, A. K.; Singh, U.; Mayilmurugan, R.; Ghosh, K., Cu(I) complexes obtained via spontaneous reduction of Cu(II) complexes supported by designed bidentate ligands: bioinspired Cu(I) based catalysts for aromatic hydroxylation. *Dalton Trans.* **2020**, *49* (39), 13829-13839.
20. Muthuramalingam, S.; Anandababu, K.; Velusamy, M.; Mayilmurugan, R., Benzene Hydroxylation by Bioinspired Copper(II) Complexes: Coordination Geometry versus Reactivity. *Inorg. Chem.* **2020**, *59*, 5918-5928.
21. Masferrer-Rius, E.; Hopman, R. M.; van der Kleij, J.; Lutz, M.; Klein Gebbink, R. J. M., On the Ability of Nickel Complexes Derived from Tripodal Aminopyridine Ligands to Catalyze Arene Hydroxylations. *CHIMIA* **2020**, *74* (6), 489-494.
22. Ticconi, B.; Capocasa, G.; Cerrato, A.; Di Stefano, S.; Lapi, A.; Marincioni, B.; Olivo, G.; Lanzalunga, O., Insight into the chemoselective aromatic vs. side-chain hydroxylation of alkylaromatics with H₂O₂ catalyzed by a non-heme imine-based iron complex. *Catal. Sci. Technol.* **2021**, *11*, 171-178.
23. Li, Z.; Wang, Z.; Chekshin, N.; Qian, S.; Qiao, J. X.; Cheng, P. T.; Yeung, K.-S.; Ewing, W. R.; Yu, J.-Q., A tautomeric ligand enables directed C-H hydroxylation with molecular oxygen. *Science* **2021**, *372*, 1452-1457.

24. Masferrer-Rius, E.; Borrell, M.; Lutz, M.; Costas, M.; Klein Gebbink, R. J. M., Aromatic C–H Hydroxylation Reactions with Hydrogen Peroxide Catalyzed by Bulky Manganese Complexes. *Adv. Synth. Catal.* **2021**, *363* (15), 3783-3795.
25. Cheng, L.; Wang, H.; Cai, H.; Zhang, J.; Gong, X.; Han, W., Iron-catalyzed arene C–H hydroxylation. *Science* **2021**, *374* (6563), 77-81.
26. Que, L.; Tolman, W. B., Biologically inspired oxidation catalysis. *Nature* **2008**, *455* (7211), 333-340.
27. Vicens, L.; Olivo, G.; Costas, M., Rational Design of Bioinspired Catalysts for Selective Oxidations. *ACS Catal.* **2020**, *10* (15), 8611-8631.
28. Bartoli, J.-F.; Mouries-Mansuy, V.; Le Barch-Ozette, K.; Palacio, M.; Battioni, P.; Mansuy, D., New manganese β -polynitroporphyrins as particularly efficient catalysts for biomimetic hydroxylation of aromatic compounds with H₂O₂. *Chem. Commun.* **2000**, (10), 827-828.
29. Jensen, M. P.; Lange, S. J.; Mehn, M. P.; Que, E. L.; Que, L., Biomimetic Aryl Hydroxylation Derived from Alkyl Hydroperoxide at a Nonheme Iron Center. Evidence for an Fe^{IV}=O Oxidant. *J. Am. Chem. Soc.* **2003**, *125* (8), 2113-2128.
30. Jensen, M. P.; Mehn, M. P.; Que Jr, L., Intramolecular Aromatic Amination through Iron-Mediated Nitrene Transfer. *Angew. Chem. Int. Ed.* **2003**, *42* (36), 4357-4360.
31. Taktak, S.; Flook, M.; Foxman, B. M.; Que Jr, L.; Rybak-Akimova, E. V., *ortho*-Hydroxylation of benzoic acids with hydrogen peroxide at a non-heme iron center. *Chem. Commun.* **2005**, (42), 5301-5303.
32. de Visser, S. P.; Oh, K.; Han, A.-R.; Nam, W., Combined Experimental and Theoretical Study on Aromatic Hydroxylation by Mononuclear Nonheme Iron(IV)–Oxo Complexes. *Inorg. Chem.* **2007**, *46* (11), 4632-4641.
33. Kang, M.-J.; Song, W. J.; Han, A.-R.; Choi, Y. S.; Jang, H. G.; Nam, W., Mechanistic insight into the aromatic hydroxylation by high-valent iron(IV)-oxo porphyrin π -cation radical complexes. *J. Org. Chem.* **2007**, *72* (16), 6301-6304.
34. Kudrik, E. V.; Sorokin, A. B., N-Bridged Diiron Phthalocyanine Catalyzes Oxidation of Benzene with H₂O₂ via Benzene Oxide with NIH Shift Evidenced by Using 1,3,5-[D₃] Benzene as a Probe. *Chem. Eur. J.* **2008**, *14* (24), 7123-7126.
35. Kang, Y.; Chen, H.; Jeong, Y. J.; Lai, W.; Bae, E. H.; Shaik, S.; Nam, W., Enhanced Reactivities of Iron(IV)-Oxo Porphyrin π -Cation Radicals in Oxygenation Reactions by Electron-Donating Axial Ligands. *Chem. Eur. J.* **2009**, *15* (39), 10039-10046.
36. Makhlynets, O. V.; Das, P.; Taktak, S.; Flook, M.; Mas-Ballesté, R.; Rybak-Akimova, E. V.; Que Jr, L., Iron-Promoted *ortho*-and/or *ipso*-Hydroxylation of Benzoic Acids with H₂O₂. *Chem. Eur. J.* **2009**, *15* (47), 13171-13180.
37. Makhlynets, O. V.; Rybak-Akimova, E. V., Aromatic Hydroxylation at a Non-Heme Iron Center: Observed Intermediates and Insights into the Nature of the Active Species. *Chem. Eur. J.* **2010**, *16* (47), 13995-14006.
38. Thibon, A.; Jollet, V.; Ribal, C.; Sénéchal-David, K.; Billon, L.; Sorokin, A. B.; Banse, F., Hydroxylation of Aromatics with the Help of a Non-Haem FeOOH: A Mechanistic Study under Single-Turnover and Catalytic Conditions. *Chem. Eur. J.* **2012**, *18* (9), 2715-2724.

39. Carneiro, L.; Silva, A. R., Selective direct hydroxylation of benzene to phenol with hydrogen peroxide by iron and vanadyl based homogeneous and heterogeneous catalysts. *Catal. Sci. Technol.* **2016**, *6* (22), 8166-8176.
40. Kal, S.; Draksharapu, A.; Que Jr, L., Sc³⁺ (or HClO₄) activation of a nonheme Fe^{III}-OOH intermediate for the rapid hydroxylation of cyclohexane and benzene. *J. Am. Chem. Soc.* **2018**, *140* (17), 5798-5804.
41. Kal, S.; Que Jr, L., Activation of a Non-Heme Fe^{III}-OOH by a Second Fe^{III} to Hydroxylate Strong C-H Bonds: Possible Implications for Soluble Methane Monooxygenase. *Angew. Chem. Int. Ed.* **2019**, *58* (25), 8484-8488.
42. Rebilly, J. N.; Zhang, W.; Herrero, C.; Dridi, H.; Sénéchal-David, K.; Guillot, R.; Banse, F., Hydroxylation of aromatics by H₂O₂ catalyzed by mononuclear non-heme iron complexes: Role of triazole hemilability in substrate-induced bifurcation of the H₂O₂ activation mechanism. *Chem. Eur. J.* **2020**, *26*, 659-668.
43. Tkachenko, N. V.; Ottenbacher, R. V.; Lyakin, O. Y.; Zima, A. M.; Samsonenko, D. G.; Talsi, E. P.; Bryliakov, K. P., Highly Efficient Aromatic C-H Oxidation with H₂O₂ in the Presence of Iron Complexes of the PDP Family. *ChemCatChem* **2018**, *10* (18), 4052-4057.
44. Lyakin, O. Y.; Zima, A. M.; Tkachenko, N. V.; Bryliakov, K. P.; Talsi, E. P., Direct Evaluation of the Reactivity of Nonheme Iron(V)-Oxo Intermediates toward Arenes. *ACS Catal.* **2018**, *8* (6), 5255-5260.
45. Tkachenko, N. V.; Lyakin, O. Y.; Zima, A. M.; Talsi, E. P.; Bryliakov, K. P., Effect of different carboxylic acids on the aromatic hydroxylation with H₂O₂ in the presence of an iron aminopyridine complex. *J. Organomet. Chem.* **2018**, *871*, 130-134.
46. Zima, A. M.; Lyakin, O. Y.; Lubov, D. P.; Bryliakov, K. P.; Talsi, E. P., Aromatic C-H oxidation by non-heme iron(V)-oxo intermediates bearing aminopyridine ligands. *J. Mol. Catal.* **2020**, *483*, 110708.
47. Raba, A.; Cokoja, M.; Herrmann, W. A.; Kühn, F. E., Catalytic hydroxylation of benzene and toluene by an iron complex bearing a chelating di-pyridyl-di-NHC ligand. *Chem. Commun.* **2014**, *50* (78), 11454-11457.
48. Lindhorst, A. C.; Schütz, J.; Netscher, T.; Bonrath, W.; Kühn, F. E., Catalytic oxidation of aromatic hydrocarbons by a molecular iron-NHC complex. *Catal. Sci. Technol.* **2017**, *7* (9), 1902-1911.
49. Conde, A.; Diaz-Requejo, M. M.; Pérez, P. J., Direct, copper-catalyzed oxidation of aromatic C-H bonds with hydrogen peroxide under acid-free conditions. *Chem. Commun.* **2011**, *47* (28), 8154-8156.
50. Vilella, L.; Conde, A.; Balcells, D.; Díaz-Requejo, M. M.; Lledós, A.; Pérez, P. J., A competing, dual mechanism for catalytic direct benzene hydroxylation from combined experimental-DFT studies. *Chem. Sci.* **2017**, *8* (12), 8373-8383.
51. Kejriwal, A.; Bandyopadhyay, P.; Biswas, A. N., Aromatic hydroxylation using an oxo-bridged diiron(III) complex: a bio-inspired functional model of toluene monooxygenases. *Dalton Trans.* **2015**, *44* (39), 17261-17267.
52. Balland, V.; Mathieu, D.; Pons-Y-Moll, N.; Bartoli, J. F.; Banse, F.; Battioni, P.; Girerd, J.-J.; Mansuy, D., Non-heme iron polyazadentate complexes as catalysts for oxidations by H₂O₂: particular efficiency in aromatic hydroxylations and beneficial effects of a reducing agent. *J. Mol. Catal. A: Chem.* **2004**, *215* (1-2), 81-87.
53. Thibon, A.; Bartoli, J.-F.; Guillot, R.; Sainton, J.; Martinho, M.; Mansuy, D.; Banse, F., Non-heme iron polyazadentate complexes as catalysts for aromatic hydroxylation by H₂O₂: Particular efficiency of

- tetrakis(2-pyridylmethyl)ethylenediamine–iron(II) complexes. *J. Mol. Catal. A: Chem.* **2008**, 287 (1-2), 115-120.
54. Ottenbacher, R. V.; Talsi, E. P.; Bryliakov, K. P., Chiral Manganese Aminopyridine Complexes: the Versatile Catalysts of Chemo- and Stereoselective Oxidations with H₂O₂. *Chem. Rec* **2018**, 18 (1), 78-90.
55. Talsi, E. P.; Bryliakov, K. P., Chemo- and stereoselective C–H oxidations and epoxidations/*cis*-dihydroxylations with H₂O₂, catalyzed by non-heme iron and manganese complexes. *Coord. Chem. Rev.* **2012**, 256 (13-14), 1418-1434.
56. Bryliakov, K. P.; Talsi, E. P., Active sites and mechanisms of bioinspired oxidation with H₂O₂, catalyzed by non-heme Fe and related Mn complexes. *Coord. Chem. Rev.* **2014**, 276, 73-96.
57. Olivo, G.; Lanzalunga, O.; Mandolini, L.; Di Stefano, S., Substituent effects on the catalytic activity of bipyrrrolidine-based iron complexes. *J. Org. Chem.* **2013**, 78 (22), 11508-11512.
58. Cussó, O.; Garcia-Bosch, I.; Ribas, X.; Lloret-Fillol, J.; Costas, M., Asymmetric epoxidation with H₂O₂ by manipulating the electronic properties of non-heme iron catalysts. *J. Am. Chem. Soc.* **2013**, 135 (39), 14871-14878.
59. Cussó, O.; Garcia-Bosch, I.; Font, D.; Ribas, X.; Lloret-Fillol, J.; Costas, M., Highly stereoselective epoxidation with H₂O₂ catalyzed by electron-rich aminopyridine manganese catalysts. *Org. Lett.* **2013**, 15 (24), 6158-6161.
60. Cussó, O.; Cianfanelli, M.; Ribas, X.; Klein Gebbink, R. J. M.; Costas, M., Iron catalyzed highly enantioselective epoxidation of cyclic aliphatic enones with aqueous H₂O₂. *J. Am. Chem. Soc.* **2016**, 138 (8), 2732-2738.
61. Hansch, C.; Leo, A.; Taft, R., A survey of Hammett substituent constants and resonance and field parameters. *Chem. Rev.* **1991**, 91 (2), 165-195.
62. Murphy, A.; Dubois, G.; Stack, T. D. P., Efficient epoxidation of electron-deficient olefins with a cationic manganese complex. *J. Am. Chem. Soc.* **2003**, 125 (18), 5250-5251.
63. Urbanová, K.; Ramírez-Macías, I.; Martín-Escolano, R.; Rosales, M. J.; Cussó, O.; Serrano, J.; Sánchez-Moreno, M.; Costas, M.; Ribas, X.; Marín, C., Effective Tetradentate Compound Complexes against *Leishmania* spp. that Act on Critical Enzymatic Pathways of These Parasites. *Molecules* **2019**, 24 (1), 134.
64. Shen, D.; Qiu, B.; Xu, D.; Miao, C.; Xia, C.; Sun, W., Enantioselective epoxidation of olefins with H₂O₂ catalyzed by bioinspired aminopyridine manganese complexes. *Org. Lett.* **2016**, 18 (3), 372-375.
65. Milan, M.; Bietti, M.; Costas, M., Highly enantioselective oxidation of nonactivated aliphatic C–H bonds with hydrogen peroxide catalyzed by manganese complexes. *ACS Cent. Sci.* **2017**, 3 (3), 196-204.
66. Ottenbacher, R. V.; Talsi, E. P.; Bryliakov, K. P., Mechanism of Selective C–H Hydroxylation Mediated by Manganese Aminopyridine Enzyme Models. *ACS Catal.* **2015**, 5 (1), 39-44.
67. Dantignana, V.; Milan, M.; Cussó, O.; Company, A.; Bietti, M.; Costas, M., Chemoselective Aliphatic C–H Bond Oxidation Enabled by Polarity Reversal. *ACS Cent. Sci.* **2017**, 3 (12), 1350-1358.
68. Talsi, E. P.; Samsonenko, D. G.; Ottenbacher, R. V.; Bryliakov, K. P., Highly Enantioselective C–H Oxidation of Arylalkanes with H₂O₂ in the Presence of Chiral Mn-Aminopyridine Complexes. *ChemCatChem* **2017**, 9 (24), 4580-4586.

69. Ottenbacher, R. V.; Talsi, E. P.; Rybalova, T. V.; Bryliakov, K. P., Enantioselective Benzylic Hydroxylation of Arylalkanes with H₂O₂ in Fluorinated Alcohols in the Presence of Chiral Mn Aminopyridine Complexes. *ChemCatChem* **2018**, *10* (22), 5323-5330.
70. Ottenbacher, R. V.; Talsi, E. P.; Bryliakov, K. P., Highly enantioselective undirected catalytic hydroxylation of benzylic CH₂ groups with H₂O₂. *J. Catal.* **2020**, *390*, 170-177.
71. Zhao, J.; Nanjo, T.; de Lucca, E. C.; White, M. C., Chemoselective methylene oxidation in aromatic molecules. *Nat. Chem.* **2019**, *11* (3), 213-221.
72. Font, D.; Canta, M.; Milan, M.; Cussó, O.; Ribas, X.; Klein Gebbink, R. J. M.; Costas, M., Readily accessible bulky iron catalysts exhibiting site selectivity in the oxidation of steroidal substrates. *Angew. Chem. Int. Ed.* **2016**, *55* (19), 5776-5779.
73. Gormisky, P. E.; White, M. C., Catalyst-controlled aliphatic C–H oxidations with a predictive model for site-selectivity. *J. Am. Chem. Soc.* **2013**, *135* (38), 14052-14055.
74. Chen, J.; Lutz, M.; Milan, M.; Costas, M.; Otte, M.; Klein Gebbink, R. J., Non-Heme Iron Catalysts with a Rigid Bis-Isoindoline Backbone and Their Use in Selective Aliphatic C–H Oxidation. *Adv. Synth. Catal.* **2017**, *359* (15), 2590-2595.
75. Ribelli, T. G.; Fantin, M.; Daran, J.-C.; Augustine, K. F.; Poli, R.; Matyjaszewski, K., Synthesis and characterization of the most active copper ATRP catalyst based on tris[(4-dimethylaminopyridyl)methyl]amine. *J. Am. Chem. Soc.* **2018**, *140* (4), 1525-1534.
76. Comba, P.; Morgen, M.; Wadepohl, H., Tuning of the properties of transition-metal bispidine complexes by variation of the basicity of the aromatic donor groups. *Inorg. Chem.* **2013**, *52* (11), 6481-6501.
77. Codolà, Z.; Gamba, I.; Acuña-Parés, F.; Casadevall, C.; Clémancey, M.; Latour, J.-M.; Luis, J. M.; Lloret-Fillol, J.; Costas, M., Design of iron coordination sites as highly active homogenous water oxidation catalysts by deuteration of oxidation-sensitive sites. *J. Am. Chem. Soc.* **2018**, *141* (1), 323-333.
78. Kowol, C. R.; Miklos, W.; Pfaff, S.; Hager, S.; Kallus, S.; Pelivan, K.; Kubanik, M.; Enyedy, E. v. A.; Berger, W.; Heffeter, P., Impact of stepwise NH₂-methylation of triapine on the physicochemical properties, anticancer activity, and resistance circumvention. *J. Med. Chem.* **2016**, *59* (14), 6739-6752.
79. Schreurs, A. M. M.; Xian, X.; Kroon-Batenburg, L. M. J., EVAL15: a diffraction data integration method based on ab initio predicted profiles. *J. Appl. Cryst.* **2010**, *43* (1), 70-82.
80. Sheldrick, G. M., SADABS. Universität Göttingen, Germany. **2014**.
81. Sheldrick, G. M., SHELXT—Integrated space-group and crystal-structure determination. *Acta Cryst.* **2015**, *A71*, 3-8.
82. Sheldrick, G. M., Crystal structure refinement with SHELXL. *Acta Cryst.* **2015**, *C71* (1), 3-8.
83. Flack, H. D., On enantiomorph-polarity estimation. *Acta Cryst.* **1983**, *A39*, 876-881.
84. Spek, A. L., Structure validation in chemical crystallography. *Acta Cryst.* **2009**, *D65* (2), 148-155.

Chapter 5

Exploration of Highly Electron-Rich Manganese Complexes in Enantioselective Oxidation Catalysis; a Focus on Enantioselective Benzylic Oxidation

Abstract

The direct enantioselective hydroxylation of benzylic C–H bonds to form chiral benzylic alcohols represents a challenging transformation. Herein, we report on the exploration of new biologically inspired manganese and iron complexes bearing highly electron-rich aminopyridine ligands containing 4-pyrrolidinopyridine moieties ((*S,S*)-**1**, (*R,R*)-**1**, **2** and **5**) in combination with chiral bis-pyrrolidine and *N,N*-cyclohexanediamine backbones in enantioselective oxidation catalysis with aqueous H₂O₂. The current manganese complexes outperform the analogous manganese complexes containing 4-dimethylaminopyridine moieties (**3** and **4**) in benzylic oxidation reactions in terms of alcohol yield while keeping similar ee values (~ 60% ee), which is attributed to the higher basicity of the 4-pyrrolidinopyridine group. A detailed investigation of different carboxylic acid additives in enantioselective benzylic oxidation provides new insights into how to rationally enhance enantioselectivities by means of proper tuning of the environment around the catalytic active site, and has resulted in the selection of Boc-*L-tert*-leucine as the preferred additive. Using these optimized conditions, manganese complex **2** was shown to be effective in the enantioselective benzylic oxidation of a series of arylalkane substrates with up to 50% alcohol yield and 62% product ee. A final set of experiments also highlights the use of the new 4-pyrrolidinopyridine-based complexes in the asymmetric epoxidation of olefins (up to 98% epoxide yield and >99% ee).

This chapter is based on:

Masferrer-Rius, E.; Li, F.; Lutz, M.; Klein Gebbink, R. J. M. *Catal. Sci. Technol.* **2021**, *11*, 7751-7763

5.1 Introduction

The direct hydroxylation of C–H groups under catalytic conditions is an interesting strategy for late-stage functionalization.¹⁻³ In biological systems, metallo-enzymes utilize dioxygen as terminal oxidant to perform such challenging transformations.⁴ Inspired by these systems, chemists have focused on the design of molecular catalysts making use of transition metals and using H₂O₂ as the terminal oxidant. Of special interest are enantioselective hydroxylation reactions due to the importance of chiral oxygenated molecules in natural products as well as in synthetic chemicals (agrochemicals, pharmaceuticals, etc).

Several examples of enantioselective aliphatic C(sp³)–H oxidation catalysts exist, generally making use of manganese, iron or ruthenium as the transition-metal, often in combination with porphyrin, salen or aminopyridine ligands.⁵⁻³⁶ Among these systems, the ones based on manganese and iron supported by aminopyridine ligands have emerged as a very powerful family of catalysts.³⁷ It has been well established that such complexes activate H₂O₂, in most cases with the help of a carboxylic acid as an additive, to generate powerful and selective electrophilic metal-oxo species.^{22, 23, 38} On the one hand, the use of both non-heme iron and manganese complexes with aminopyridine ligands in asymmetric epoxidation reactions has been described extensively with high yields and enantioselectivities.³⁹⁻⁶² On the other hand, the enantioselective oxidation of aliphatic C(sp³)–H bonds remains amongst the most challenging reactions, in which aminopyridine-based manganese complexes have particularly appeared as effective catalysts in the last years.⁶³

The general mechanism of this latter oxidation reaction entails an initial HAT step from the substrate to the high valent manganese-oxo species, followed by a hydroxyl rebound step to generate the final alcohol product. The main challenges are based on the stereoselection of the C–H bond oxidation, which usually originates from enantio-discriminating HAT (Figure 1A) or OH rebound steps (Figure 1B),³⁶ and the undesired overoxidation of the initial alcohol product producing ketone products. Regarding the latter drawback, a useful approach has been developed that makes use of hydrogen bond donor solvents, such as fluorinated alcohol solvents, to strongly deactivate electron rich C–H bonds that are in *alpha*-position to a hydroxyl group toward reaction with electrophilic reagents, thereby disfavoring alcohol overoxidation and preventing the loss of chirality. Accordingly, the use of fluorinated alcohol solvents has been widely applied in different kinds of oxidation reactions.^{26, 31, 32, 64-71}

Examples of enantioselective aliphatic C(sp³)–H oxidation reactions catalyzed by biologically inspired manganese complexes bearing aminopyridine ligands include a system to generate enantiomerically enriched products, that was reported by Bietti, Costas and co-workers. These authors developed a catalytic approach for the oxidative desymmetrization of

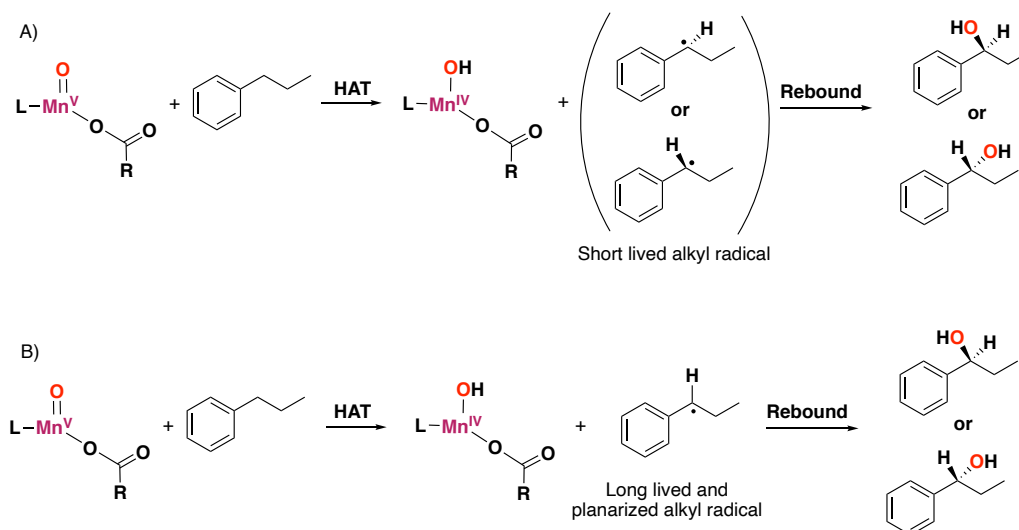


Figure 1. Enantioselective aliphatic (benzylic) C–H oxidation of propylbenzene catalyzed by aminopyridine-based manganese complexes. A) Mechanism in which the origin of the enantioselectivity is determined at the HAT step.³⁶ B) Mechanism in which the origin of the enantioselectivity is determined at the rebound step (OH transfer step).³⁶

mono-substituted cyclohexanes using bulky bioinspired manganese catalysts in combination with H₂O₂, generating γ -ketones with up to 85% yield and 96% ee.^{21, 25} More recently, the enantioselective C–H lactonization of unactivated methylenes directed by carboxylic acids has also been described using the same kind of catalysts to afford chiral γ -lactones with up to 88% yield and >99% ee.³⁰ Focusing on enantioselective benzylic oxidation, Sun and co-workers developed an oxidative desymmetrization approach for the enantioselective oxidation of benzylic methylene groups of spirocyclic hydrocarbons by the bioinspired manganese catalyst **Mn(S-PEB)** and H₂O₂, affording up to 94% yield and 98% ee of the resulting ketone products (Figure 2A).^{27, 29} Later on, the same authors used their manganese-catalyzed system also for the oxidation of oxindoles and dihydroquinolinones, with up to 67% yield and 99% ee; as well as for the oxidation of benzylic methylene C–H bonds of indane-based substrates using fluorinated alcohol solvents, with up to 78% yield and 95% ee for the alcohol product (Figure 2A).^{28, 31}

Company, Bietti, Costas and co-workers developed a manganese-catalyzed benzylic hydroxylation of simple aromatic substrates to the corresponding alcohol products using fluorinated alcohol solvents, which prevented the overoxidation of the alcohol to the ketone (*vide supra*). Particularly, they showed that the use of the electron-rich manganese catalysts **Mn(d^{MM}bpbp)** and **Mn(Me^{2N}bpbp)** (**4**) affords the alcohol products with up to 61% yield with respect to H₂O₂ and in 66% ee (Figure 2B).⁶⁸ Bryliakov and co-workers have employed the **Mn(dpf)** catalyst for the undirected enantioselective benzylic oxidation of simple arylalkanes with H₂O₂, first in acetonitrile as solvent. They could get up to 86% ee for the alcohol product

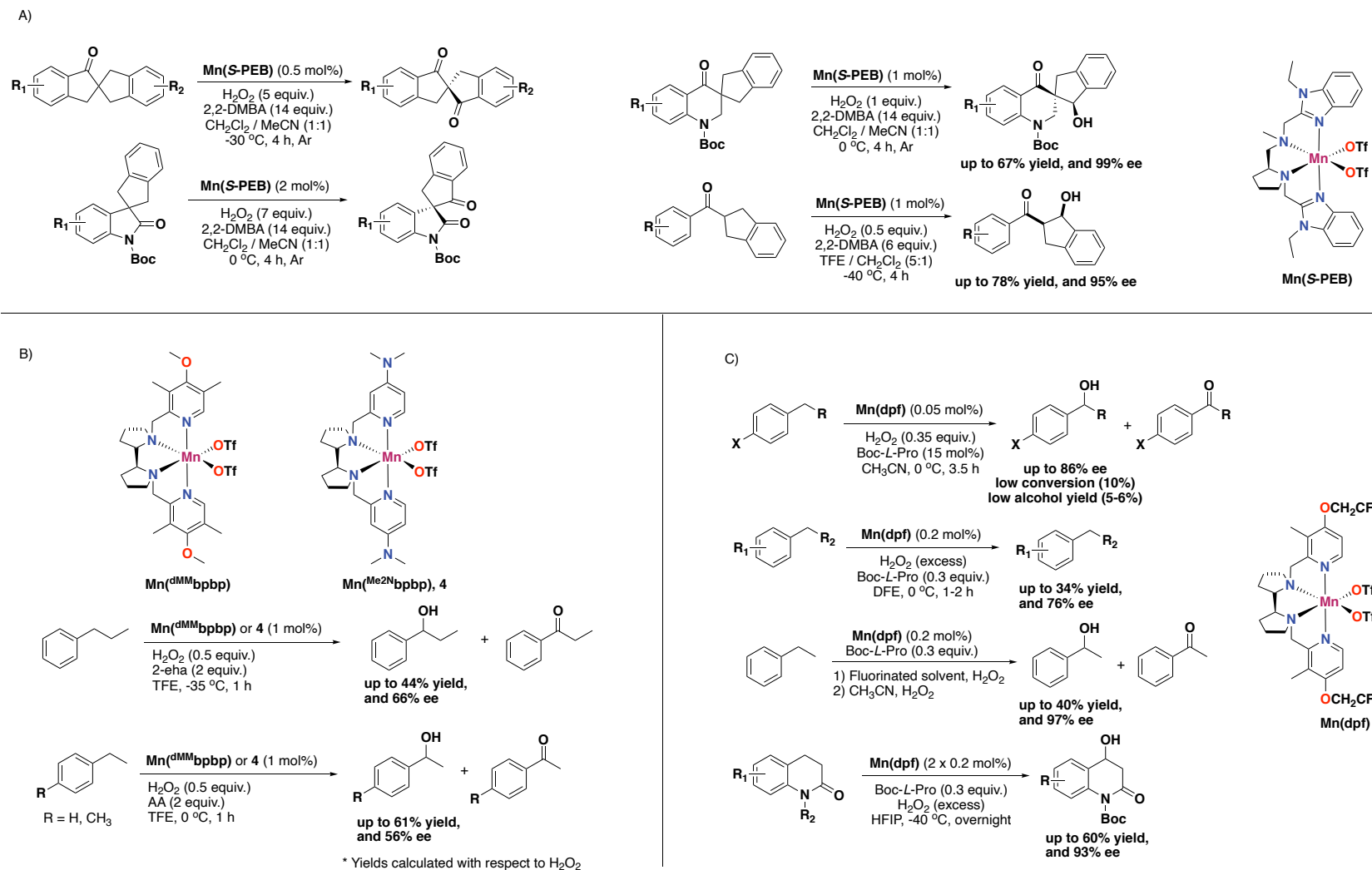


Figure 2. Selected examples of enantioselective benzylic oxidation reactions catalyzed by aminopyridine-based manganese complexes (TFE = 2,2,2-trifluoroethanol, HFIP = 1,1,1,3,3,3-hexafluoro-2-propanol, AA = acetic acid, 2,2-DMBA = 2,2-dimethylbutanoic acid, 2-eha = 2-ethylhexanoic acid).

in the oxidation of substituted-ethylbenzenes, despite the fact that the alcohol/ketone ratio, conversions and yields for the alcohol products were low (5-6% alcohol yield; Figure 2C).^{24,72} In a follow-up study, they could enhance oxidation towards the alcohol product by switching to fluorinated alcohol solvents, providing up to 34% yield and up to 76% ee for alcohol products in the oxidation of substituted-ethylbenzene substrates. To the best of our knowledge these are the highest ee values reported for the direct oxidation of simple arylalkanes towards alcohol products.²⁶ Much more recently, the same authors used a one-pot sequential oxidation and oxidative kinetic resolution approach to obtain 40% yield and 97% ee for the 1-phenylethanol product, as well as up to 60% yield and 93% ee for the oxidation of 3,4-dihydroquinolinone derivatives.³² Remarkably, the **Mn(dpf)** catalyst in these latter examples is used in combination with an enantiopure amino acid additive, namely Boc-*L*-proline (Figure 2C).

In Chapter 3 and 4, we have shown that bulky manganese complexes supported by aminopyridine ligands are highly selective in aromatic oxidation reactions towards phenol products, whereas the use of electron-rich manganese complexes switches the chemoselectivity of the reaction, favoring benzylic C(sp³)-H bond oxidation in substituted arene substrates. Based on these observations, we concluded that the electronic nature of the ligand is a key factor in controlling the chemoselectivity of these Mn-catalyzed C-H oxidations.⁷³ In addition, Bryliakov and co-workers have recently developed several electron-rich aminopyridine ligands based on *para*-substituted aminopyridines (NEt₂, NMeⁱPr, N(CH₂)₄ substituents). Particularly, they have shown that the corresponding diferric complexes supported by these ligands can generate high-spin oxoiron(V) intermediates upon reaction with H₂O₂, which are active in asymmetric epoxidation and aliphatic hydroxylation reactions.^{74,75} This strategy of including electron donating groups in the *para*-position of the pyridine ligand was first reported by Di Stefano *et al.*⁷⁶ and Costas *et al.*^{43,57}

Inspired by these findings, we have explored electron-rich N₂Py₂-type ligands bearing *para*-pyrrolidine substituted pyridine donors in enantioselective oxidation catalysis with manganese as the metal center. Since 4-pyrrolidinopyridine is a stronger N-heteroaromatic electron donor ligand compared to 4-dimethylaminopyridine, DMAP (pK_a = 18.33 and 17.95 for 4-pyrrolidinopyridine and DMAP, respectively)^{77,78}, we hypothesize that the greater electron-donating capacity of the 4-pyrrolidinopyridine donors might lead to a better stabilization of the active manganese-oxo species formed upon reaction with H₂O₂, and accordingly to a better catalytic performance. Herein, we report on the rational development of the new manganese complexes (***S,S***-**1**, (***R,R***)-**1** and **2** bearing 4-pyrrolidinopyridine moieties (Figure 3B) and their use in the undirected enantioselective catalytic oxidation of benzylic C-H groups using aqueous H₂O₂ as benign oxidant, carboxylic acids as co-ligands, and fluorinated alcohol solvents to provide good alcohol yields and ee's. Interestingly, the current complexes outperform the

analogous manganese complexes **3** and **4** containing 4-dimethylaminopyridine moieties in terms of benzylic alcohol product formation.⁶⁸ Furthermore, we have also explored manganese and iron complexes derived from the 4-pyrrolidinopyridine-modified ligands in the asymmetric epoxidation of olefin substrates.

5.2 Results and Discussion

5.2.1 Synthesis and Characterization of Ligands and Metal Complexes

The (*S,S*)-Pyr**bpmcn**, (*R,R*)-Pyr**bpmcn** and (*S,S*)-Pyr**bppb** ligands ((*S,S*)-**L1**, (*R,R*)-**L1** and **L2**, respectively) were prepared in good yields by the reaction of two equiv. of 2-chloromethyl-4-pyrrolidinopyridine hydrochloride with one equiv. of the corresponding amine backbone (Figure 3A). The ligands were characterized by ¹H NMR and ¹³C NMR spectroscopy, as well as high resolution mass spectrometry (see SI for further details). Characterization of ligand **L2** agrees with literature data.⁷⁴

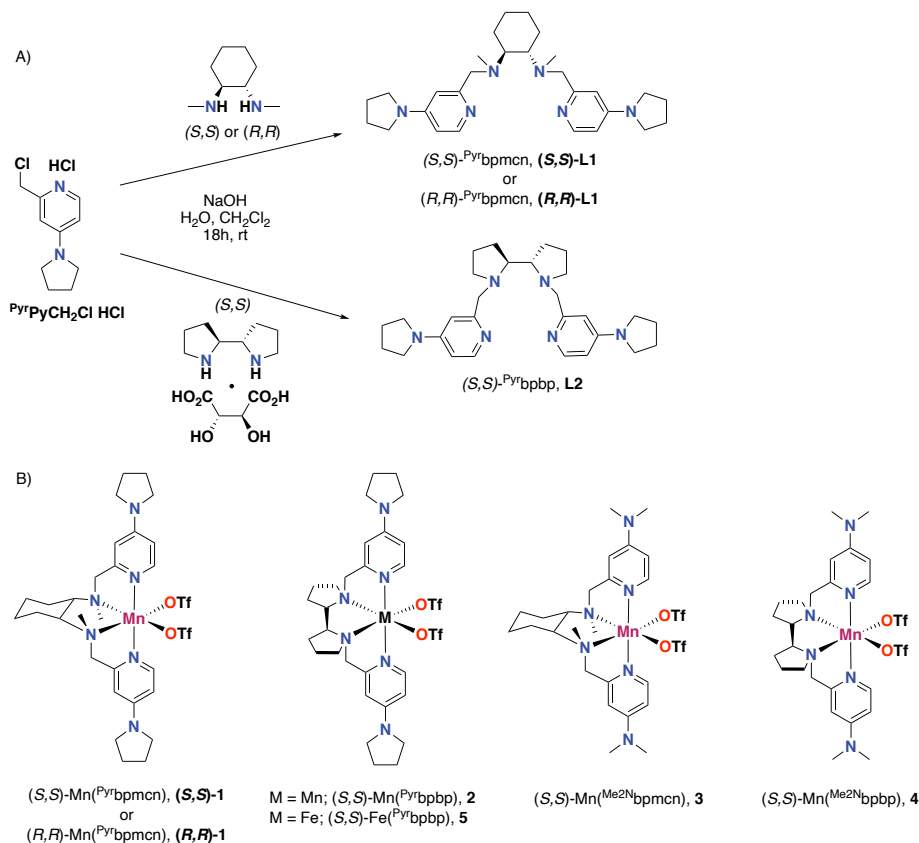


Figure 3. A) Synthesis of tetradentate aminopyridine ligands (*S,S*)-**L1**, (*R,R*)-**L1** and **L2**. B) Metal complexes used in this Chapter.

Complexation reactions were then performed by the reaction of equimolar amounts of the corresponding ligand with [Mn^{II}(CF₃SO₃)₂] in dry THF under an inert atmosphere to afford

manganese complexes (*S,S*)-[Mn^{II}(**L1**)(CF₃SO₃)₂] and (*R,R*)-[Mn^{II}(**L1**)(CF₃SO₃)₂] (**(*S,S*)-1** and **(*R,R*)-1**), and (*S,S*)-[Mn^{II}(**L2**)(CF₃SO₃)₂] (**2**) as microcrystalline solids (for further details see SI). Complexes **(*S,S*)-1** and **2** were characterized by high resolution mass spectrometry (HRMS). HRMS analysis of **(*S,S*)-1** showed a prominent mass peak at *m/z* 666.2378 corresponding to the [Mn^{II}(**L1**)(CF₃SO₃)₂]⁺ ion (calc. 666.2372). For complex **2** a prominent mass peak at *m/z* 664.2212 corresponding to the [Mn^{II}(**L2**)(CF₃SO₃)₂]⁺ ion (calc. 664.2215) was found. Manganese complexes (*S,S*)-[Mn^{II}(**L3**)(CF₃SO₃)₂] (**3**) and (*S,S*)-[Mn^{II}(**L4**)(CF₃SO₃)₂] (**4**) were also synthesized in order to compare the catalytic properties of the new complexes.⁴³ ⁴⁹Synthesis of non-heme iron complex **5** was performed using equimolar amounts of **L2** and [Fe^{II}(CF₃SO₃)₂(CH₃CN)₂] in dry THF under an inert atmosphere. HRMS analysis of the complex showed a prominent mass peak at *m/z* 665.2189 corresponding to the [Fe^{II}(**L2**)(CF₃SO₃)₂]⁺ ion (calc. 665.2184).

5.2.2 Crystal and Molecular Structure of Complexes 2 and 5

The solid state structures of complexes **2** and **5** were confirmed by X-ray crystallography (Figure 4).⁷⁹ Selected bond distances and bond angles for both complexes are listed in Table 1, and compared with the analogous manganese complex containing 4-dimethylaminopyridine

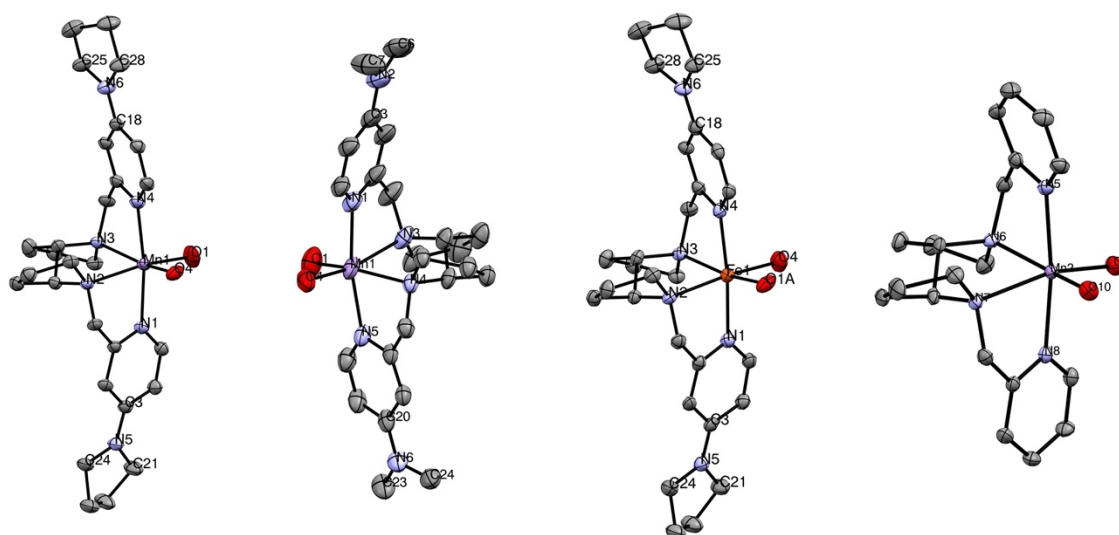


Figure 4. From left to right: ORTEP diagrams of the molecular structure of (*S,S*)-[Mn^{II}(CF₃SO₃)₂(Pyrbpbp)] (**2**), (*R,R*)-[Mn^{II}(CF₃SO₃)₂(Me₂Nbpbp)] (**(*R,R*)-4**), (*S,S*)-[Fe^{II}(CF₃SO₃)₂(Pyrbpbp)] (**5**), and (*S,S*)-[Mn^{II}(CF₃SO₃)₂(bpbp)] (**Mn(bpbp)**), showing the atom numbering scheme. Triflate anions are omitted except for the oxygen atoms directly bound to the metal center, and hydrogen atoms are omitted for clarity. The structure of complex **(*R,R*)-4** was reported by Costas and co-workers,⁴³ the structure of **Mn(bpbp)** by Bryliakov and co-workers.⁴⁰

moieties, (*R,R*)-[Mn(CF₃SO₃)₂(Me₂Nbpbp)] (**(*R,R*)-4**).⁴³ The molecular structure of **2** shows that the manganese ion adopts a distorted octahedral coordination geometry with a *cis-α*

conformation,⁸⁰ in which four coordination sites are occupied by nitrogen atoms of the tetradentate aminopyridine, while the remaining two sites are occupied by the oxygen atoms of the triflate anions in a *cis* orientation. The two pyridine moieties are placed above and below the plane containing the manganese center, whereas the two nitrogen of the (*S,S*)-bis-pyrrolidine backbone and the two oxygen atoms of the triflate ions are almost within the same plane, providing an overall C_2 -symmetric structure. In a similar way, the molecular structure of non-heme iron complex **5** shows a distorted octahedral coordination geometry with a *cis- α* conformation.

The Mn–N bond distances in complex **2** range from 2.222(3) to 2.300(3) Å and the Mn–O bond distances from 2.152(3) to 2.184(2) Å. These values compare quite well with the Mn–N and Mn–O bond distances of complex (***R,R***)-**4** (from 2.210(4) to 2.315(3) Å and 2.177(4) to 2.195(3) Å, respectively).⁴³ On the other hand, complex **2** displays a slightly smaller O–Mn–O angle (101.19(12)°) relative to the corresponding angle in complex (***R,R***)-**4** (104.08(14)°), which means that the 4-pyrrolidinopyridine moieties introduce some steric strain in the complex. The Fe–N bond distances in complex **5** range from 2.157(3) to 2.227(3) Å and the Fe–O bond distances are 2.153(3) Å, which are indicative of a high-spin iron complex.^{57,81}

Comparing complexes **2** and **5**, we find that their structures are very much alike, with slightly longer Mn–N distances and similar Mn/Fe–O distances. The O–Fe–O angle of complex **5** is much smaller (94.01(11)°) than the O–Mn–O angle in **2** and (***R,R***)-**4** though, which we attribute to the difference in the ionic radius of the two metal ions (the ionic radius of Mn(II) being larger than that of Fe(II)). This observation is a general trend that has been observed for other iron and manganese complexes bearing the same ligand, such as for Mn and Fe complexes with the parent bpbp ligand (O–M–O angle of 107.45(9) and 85.81(5), respectively)^{40,82} and with the (*S*-PEB) ligand (see Figure 2A for structure of the (*S*-PEB) ligand, O–M–O angle of 105.1(1) and 101.5(2), respectively).^{83,84}

Overall, the molecular structure of complexes **2** and **5** do not differ significantly from the structure of 4-dimethylamino-substituted complex (***R,R***)-**4**, nor from the non-substituted bis-pyrrolidine manganese complex (**Mn(bpbp)**).⁴⁰ This shows that the pyrrolidine and dimethylamino substituents provide similar structural properties to the complexes. Accordingly, the introduction of a pyrrolidine substituent in the para-position of each pyridine ring of the bpbp ligand does not produce significant changes in the structural geometry of the complex.

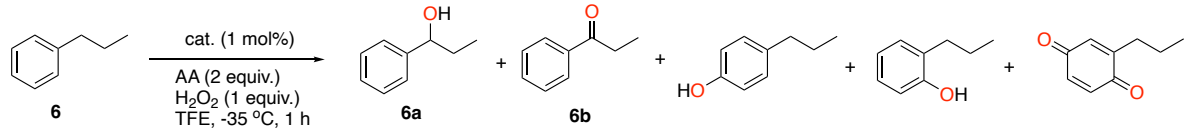
Table 1. Selected bond lengths (Å) and angles (°) for manganese complexes **2**, (*R,R*)-**4**, **5** and **Mn(bpbp)**.

2		<i>(R,R)</i> - 4 ⁴³		5		Mn(bpbp) ⁴⁰	
Mn1-N1	2.222(3)	Mn1-N1	2.210(4)	Fe1-N1	2.157(3)	Mn2-N8	2.250(2)
Mn1-N4	2.215(3)	Mn1-N5	2.210(3)	Fe1-N4	2.162(3)	Mn2-N5	2.239(2)
Mn1-N2	2.294(3)	Mn1-N3	2.301(4)	Fe1-N2	2.226(3)	Mn2-N7	2.273(2)
Mn1-N3	2.300(3)	Mn1-N4	2.315(3)	Fe1-N3	2.227(3)	Mn2-N6	2.300(2)
Mn1-O1	2.152(3)	Mn1-O1	2.177(4)	Fe1-O4	2.153(3)	Mn2-O7	2.145(2)
Mn1-O4	2.184(2)	Mn1-O4	2.195(3)	Fe1-O1	2.153(3)	Mn2-O10	2.152(2)
N6-C25	1.474(5)	N2-C6	1.450(6)	N6-C28	1.472(5)	-	-
N6-C28	1.462(5)	N2-C7	1.457(8)	N6-C25	1.463(5)	-	-
N6-C18	1.346(4)	N2-C3	1.344(7)	N6-C18	1.346(5)	-	-
N5-C24	1.466(4)	N6-C24	1.434(6)	N5-C24	1.462(5)	-	-
N5-C21	1.466(5)	N6-C23	1.469(6)	N5-C21	1.470(5)	-	-
N5-C3	1.346(4)	N6-C20	1.352(5)	N5-C3	1.348(5)	-	-
N1-Mn1-N2	76.26(10)	N4-Mn1-N5	75.45(11)	N1-Fe1-N2	77.76(11)	N8-Mn2-N7	74.80(8)
N3-Mn1-N4	75.87(10)	N3-Mn1-N1	74.80(13)	N3-Fe1-N4	77.37(11)	N6-Mn2-N5	76.03(9)
N2-Mn1-N3	77.1(1)	N3-Mn1-N4	77.3(1)	N2-Fe1-N3	79.4(1)	N7-Mn2-N6	78.68(9)
N2-Mn1-N4	95.5(1)	N1-Mn1-N4	91.9(1)	N2-Fe1-N4	96.5(1)	N7-Mn2-N5	101.02(9)
O1-Mn1-O4	101.2(1)	O1-Mn1-O4	104.1(1)	O4-Fe1-O1	94.0(1)	O7-Mn2-O10	103.51(7)
C25-N6-C28	112.3(3)	C6-N2-C7	117.3(5)	C28-N6-C25	111.7(3)	-	-
C18-N6-C28	123.9(3)	C3-N2-C7	120.7(5)	C18-N6-C25	124.5(3)	-	-
C21-N5-C24	112.3(3)	C23-N6-C24	117.8(4)	C21-N5-C24	112.2(3)	-	-
C3-N5-C21	124.1(3)	C20-N6-C23	120.4(4)	C3-N5-C21	124.5(3)	-	-

5.2.3 Pyrrolidine vs dimethylamino: amine-substituted pyridines in Mn-catalyzed benzylic oxidation

We rationalize that 4-pyrrolidinopyridine is a stronger N-heteroaromatic electron donor moiety compared to DMAP and pyridine ($pK_a = 18.33, 17.95$ and 12.53 for 4-pyrrolidinopyridine, DMAP and pyridine, respectively),^{77,78} and accordingly we believe that complex (**S,S**)-**1** and **2**, containing the tetradentate aminopyridine ligands with the pyrrolidine substituents, will better stabilize the active oxidant that is being formed upon reaction of the complex with H_2O_2 , that is the high-valent manganese-oxo species.^{29, 37, 38, 63, 85-87} Thus, we have tested manganese complexes (**S,S**)-**1** and **2** (1 mol%) in catalytic benzylic oxidation reactions in the presence of acetic acid as additive and 2,2,2-trifluoroethanol (TFE) as solvent, using propylbenzene (**6**, 0.2 mmol) as model substrate (Table 2). For comparison purposes, manganese complexes **3** and **4** were also tested for the same oxidation reaction. Aqueous hydrogen peroxide (1 equiv.) was delivered at -35 °C over a period of 30 min using a syringe pump (see Experimental Section for further details on catalytic conditions).

Table 2. Catalytic enantioselective benzylic oxidation of propylbenzene (**6**) with AA.



Catalyst	r.s.m ^a	Alcohol ^b	Ketone ^b	<i>p</i> -Phenol ^b	<i>o</i> -Phenol ^b	Quinone ^b	ee ^c	MB ^d
(S,S)- 1	26	35	4	1	<1	1	32	68
2	34	34	5	<1	n.d.	1	33	74
3	43	23	1	2	1	1	39	71
4	37	27	4	1	<1	1	36	70
5	25	<1	n.d.	<1	<1	<1	-	25

^a Remaining starting material (r.s.m) in %. ^b Yields in % with respect to substrate determined by GC against an internal standard. ^c Enantiomeric excess determined by HPLC on a chiral stationary phase. (*S*)-(-)-1-phenyl-1-propanol (**6a**) was obtained as the major enantiomer. ^d Mass balance (MB) was calculated considering remaining starting material and all products formed: MB = (r.s.m %) + (Product Yields %). n.d. = non-detected. AA = Acetic acid.

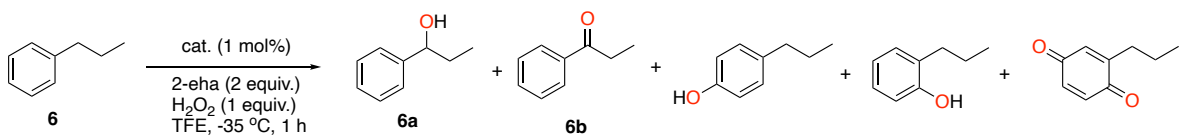
Crude mixtures were analyzed by GC to screen for benzylic oxidation products. The benzylic alcohol product **6a** was detected as the main oxidized product, together with the overoxidized ketone **6b** as a minor product, indicating that the first-formed alcohol product can engage in a second oxidation step even in the presence of a fluorinated alcohol solvent. Products deriving from oxidation at the aromatic ring (*para*-phenol, *ortho*-phenol and benzoquinone) were also

detected in small amounts, indicating that aromatic oxidation takes place to a small extent using the current manganese complexes. This finding agrees with our previous studies outlined in Chapter 3 and Chapter 4 of this thesis on the oxidation of aromatic substrates catalyzed by bioinspired manganese complexes, where electron-rich Mn complexes show the formation of benzylic alcohols as the main oxidized product, whereas aromatic oxidation toward phenols occurs to a lower extent.⁷³

Under these conditions, complexes (*S,S*)-**1** and **2** generate the alcohol product **6a** in 34 to 35% yield, together with the ketone product **6b** in 4 to 5% yield and trace amounts of the aromatic oxidation products. For both complexes the (*S*)-alcohol product formed in 32 and 33% ee, respectively, showing that a change in the amine backbone does not induce a significant change in enantioselectivity. Complexes **3** and **4** yield the benzylic alcohol product **6a** in 23 and 27%, respectively, in this reaction, whereas the ketone yield is low (1% and 4%, respectively). The ee value for the (*S*)-alcohol obtained for these latter manganese complexes ranges between 36% and 39%, showing a slight increase compared to complexes (*S,S*)-**1** and **2**. Overall, when acetic acid is used as additive, complexes (*S,S*)-**1** and **2** afford a higher catalytic activity than complexes **3** and **4** based on substrate conversion and combined alcohol and ketone yield, whereas ee values are slightly lower. Mass balances of these reactions are not excellent, which could indicate that overoxidation to non-detected products may occur.

Worthy of note is that use of non-heme iron complex **5** in this reaction resulted in the formation of only trace amounts of benzylic alcohol product **6a**, while substrate conversion was considerable (75%), indicating a poor mass balance for this reaction. This observation indicates that the use of iron as the metal is not optimal for this aliphatic (benzylic) hydroxylation reaction. Moreover, *para*-phenol, *ortho*-phenol and quinone products were also detected in trace amounts, indicating that complex **5** shows aromatic oxidation to some extent, which was also noted by Bryliakov and co-workers for related non-heme iron complexes supported by tetradentate aminopyridine ligands.⁸⁸⁻⁹¹ Accordingly, we focused our study on benzylic oxidation exclusively on the use of manganese complexes as catalysts.

Because of the importance of carboxylic acids in H₂O₂-mediated oxidation catalysis, we decided to investigate different carboxylic acid additives. One of the carboxylic acids that has shown promising results in aliphatic C–H hydroxylation, as well as in epoxidation reactions, is racemic 2-ethylhexanoic acid (2-eha). When using this acid, an increase in ee values of the alcohol product has been documented for several manganese-catalyzed and iron-catalyzed oxidations.^{42, 43, 45, 57, 59, 92} Therefore, here we have studied the oxidation of substrate **6** using 2-eha following the previously mentioned conditions (Table 3).

Table 3. Catalytic enantioselective benzylic oxidation of propylbenzene with 2-eha.


Catalyst	r.s.m. ^a	Alcohol ^b	Ketone ^b	<i>p</i> -Phenol ^b	<i>o</i> -Phenol ^b	Quinone ^b	ee ^c	MB ^d
(<i>S,S</i>)- 1	31	34	7	<1	1	n.d.	59	73
2	39	34	8	n.d.	n.d.	n.d.	58	81
3	44	26	3	<1	<1	n.d.	50	73
4	38	30	6	n.d.	n.d.	n.d.	58	74

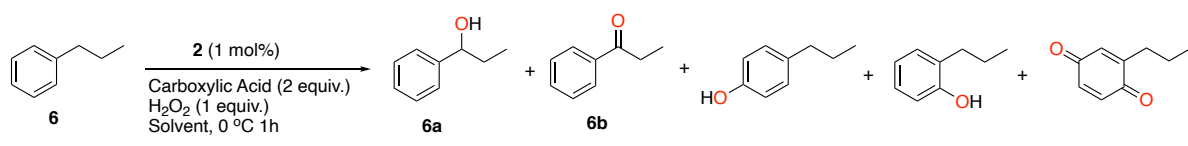
^aRemaining starting material (r.s.m) in %. ^bYields in % with respect to substrate determined by GC against an internal standard. ^cEnantiomeric excess determined by HPLC on a chiral stationary phase. (*S*)-(-)-1-phenyl-1-propanol (**6a**) was obtained as the main enantiomer. ^dMass balance (MB) was calculated considering remaining starting material and all products formed: MB = (r.s.m %) + (Product Yields %). n.d. = non-detected. 2-eha = 2-ethylhexanoic acid.

With 2-eha, complexes (*S,S*)-**1** and **2** showed similar benzylic alcohol yields as with the use of acetic acid (34% yield), whereas the formation of overoxidized ketone product slightly increased to 7-8% yield. Interestingly, ee values for the alcohol product increase for all complexes when 2-eha is employed. Complexes (*S,S*)-**1** and **2** showed ee values for the (*S*)-alcohol product up to 59%, which means a two-fold increase in comparison with the use of acetic acid as additive (compare Table 2 and Table 3). For the manganese complexes bearing 4-dimethylaminopyridine groups (**3** and **4**), the ee value increased in a similar way only in the case of complex **3** containing the bis-pyrrolidine backbone (58% ee), whereas complex **4** based on the *N,N*-cyclohexanediamine backbone showed a smaller increase (50% ee). Also under these conditions, complexes **3** and **4** showed lower conversions and alcohol and ketone yields compared to complexes (*S,S*)-**1** and **2**.

From these results, we concluded that manganese complexes (*S,S*)-**1** and **2** with either a bis-pyrrolidine or a *N,N*-cyclohexanediamine backbone are promising catalysts for benzylic oxidations, since they show high ee values for the alcohol product. Comparing our results to the systems previously described by Costas⁶⁸ and Bryliakov,^{24, 26, 32, 72} we can conclude that the current complexes perform the benzylic hydroxylation of an alkylbenzene with ee's commensurate to state-of-the-art homogeneous catalysts (see Figure 2B and 2C). In addition, complexes (*S,S*)-**1** and **2** show higher conversions and benzylic alcohol yields (34% yield) than complexes **3** and **4** bearing 4-dimethylaminopyridine moieties. We believe that the reason for the (slight) increase in alcohol yield is caused by the higher basicity of the ligands resulting from the pyrrolidine substituents, which provide the complex with a more electron-donating ligand and therefore might provide a better stabilization of the active oxidant.

Complex **2** was then chosen for further reaction optimization, since a better mass balance was observed compared to the use of complex (*S,S*)-**1**. Initially the use of another fluorinated solvent, *i.e.* 1,1,1,3,3,3-hexafluoro-2-propanol (HFIP), was explored using acetic acid and 2-eha as additives (Table 4). In these experiments, a high alcohol/ketone product ratio (A/K of 31 and 18, using AA and 2-eha, respectively) was observed with only trace amounts of overoxidized ketone product being formed. This observation agrees with the stronger hydrogen bond donor ability of HFIP compared with TFE (A/K = 4.25 for complex **2** in combination with 2-eha in TFE), providing an enhanced polarity reversal to alcohol groups and favoring the deactivation of proximal C–H bonds toward oxidation by high valent metal-oxo species.⁶⁸ However, due to the higher melting point of HFIP compared to TFE (−3.3 and −43.5 °C, respectively), the reaction in HFIP was performed at a higher reaction temperature of 0 °C, resulting in lower ee values of the alcohol product when 2-eha was employed (48% and 58% for HFIP and TFE, respectively). Using acetonitrile as the solvent in the current oxidation reaction provided a low alcohol/ketone ratio (A/K of 0.2 and 0.5, using AA and 2-eha, respectively), indicating that overoxidation of the primary alcohol product is highly favored in this solvent (Table 4). Thus, TFE was chosen as the solvent for further reaction optimization, because it provides good A/K product ratios and allows the reaction to be performed at a lower temperature (−35 °C), which has been shown to be crucial to obtain good enantioselectivities.

Table 4. Screening of different solvents in the oxidation of propylbenzene with complex **2**.



Solvent	CA ^a	r.s.m. ^b	A ^c	K ^c	<i>p</i> -Phenol ^c	<i>o</i> -Phenol ^c	Quinone ^c	ee ^d	A/K ^e	MB ^f
HFIP	AA	31	31	1	1	<1	1	29	31	65
HFIP	2-eha	60	18	<1	<1	1	n.d.	48	18	79
CH₃CN	AA	61	5	25	n.d.	n.d.	n.d.	-	0.2	91
CH₃CN	2-eha	73	5	10	n.d.	n.d.	n.d.	-	0.5	87

^a Carboxylic acid: AA = acetic acid, 2-eha = 2-ethylhexanoic acid. ^b Remaining starting material (r.s.m) in % . ^c Yields in % with respect to substrate determined by GC against an internal standard. ^d Enantiomeric excess determined by HPLC. For reactions in CH₃CN the ee value was not determined because of low alcohol formation. ^e Alcohol/Ketone ratio. ^f Mass balance (MB) was calculated considering remaining starting material and all products formed: MB = (r.s.m %) + (Product Yields %). n.d. = non-detected. HFIP = 1,1,1,3,3,3-hexafluoro-2-propanol. A = alcohol, K = ketone.

5.2.4 Carboxylic acid optimization

Since our data showed that the enantioselectivity of the manganese-catalyzed benzylic oxidation reaction changes upon variation of the carboxylic acid additive, we decided to look in more detail into different types of acids. It is well known that these H₂O₂-mediated aliphatic oxidation reactions proceed through a so-called “carboxylic acid-assisted” pathway, in which the acid is bound to the active oxidant after O–O bond cleavage of a manganese-hydroperoxo intermediate to form a high-valent manganese-oxo species.^{38, 42, 85, 93, 94} On basis of this mechanism, we believe that choosing a carboxylic acid with the optimal structure might be a key factor to engineer a proper chiral environment around the catalytic site to generate an oxidant capable of performing benzylic oxidations with high levels of enantioselectivity. Accordingly, we have screened several carboxylic acid additives for their impact on overall catalytic activity and more specifically on product enantioselectivity (Figure 5 shows the structures of the carboxylic acids used in this Chapter).

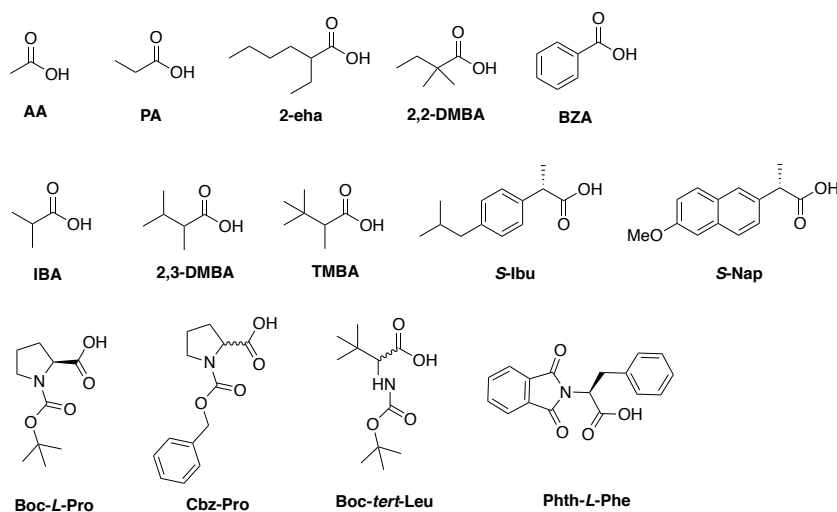
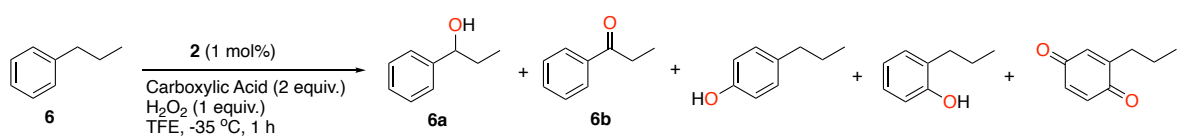


Figure 5. Structures and abbreviations of carboxylic acid additives used in this Chapter.

First, we decided to test a series of carboxylic acids with different types of alpha-carbons. We have considered an acid with a primary alpha-carbon (acetic acid, AA), a secondary (propionic acid, PA), a tertiary (2-ethylhexanoic acid, 2-eha), a quaternary (2,2-dimethylbutanoic acid, 2,2-DMBA), as well as an sp²-hybridized alpha-carbon (benzoic acid, BZA). Table 5 summarizes the catalytic data for the use of this set of additives in the oxidation of propylbenzene (**6**). Increasing the length of the alkyl chain of the carboxylic acid, by using propionic acid, did provide a slight increase in alcohol and ketone yield (38% and 7% yield, respectively) compared to the use of AA. However, the ee value for the alcohol product did not increase (Table 5, Entry 1 and 2). Interestingly, when acids with tertiary and quaternary alpha-carbons were used (2-eha and 2,2-DMBA), ee values for the benzylic alcohol significantly increased (58% ee), without deterioration of the alcohol yield (Table 5, Entry 3 and 4). Worthy

of note is the use of 2,2-DMBA, which provided a significant increase in ketone formation (14% yield), clearly favoring oxidation of the initial alcohol product compared to the other carboxylic acids tested. The use of this acid does also provide the alcohol with an increased ee. The use of a carboxylic acid with an sp^2 -hybridized alpha-carbon, such as benzoic acid, resulted in a decrease in alcohol ee (25% ee) compared to the use of AA, as well as in a lower alcohol yield (Table 5, Entry 5). Accordingly, this first data set indicated that the use of a carboxylic acid additive with a tertiary sp^3 -hybridized alpha-carbon provides the best results in terms of alcohol yield and ee value. In all these cases, aromatic oxidation is basically suppressed to a minimum.

Table 5. Screening of carboxylic acids with different types of alpha-carbons.



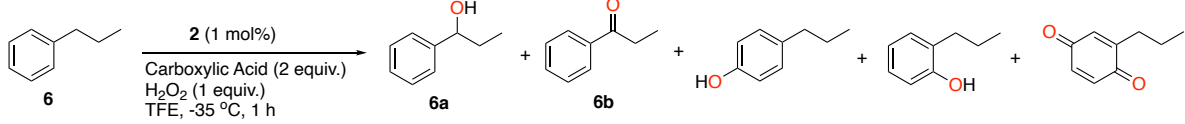
Entry	CA ^a	r.s.m ^b	A ^c	K ^c	<i>p</i> -Phenol ^c	<i>o</i> -Phenol ^c	Quinone ^c	ee ^d	MB ^e
1	AA	34	34	5	<1	n.d.	1	33	74
2	PA	29	38	7	1	n.d.	n.d.	34	75
3	2-eha	39	34	8	n.d.	n.d.	n.d.	58	81
4	2,2-DMBA	31	27	14	n.d.	n.d.	n.d.	58	72
5	BZA	37	23	7	n.d.	n.d.	n.d.	25	67

^a Carboxylic acid: AA = acetic acid, PA = propionic acid, 2-eha = 2-ethylhexanoic acid, 2,2-DMBA = 2,2-dimethylbutanoic acid, BZA = benzoic acid. ^b Remaining starting material (r.s.m) in %. ^c Yields in % with respect to substrate determined by GC against an internal standard. ^d Enantiomeric excess determined by HPLC on a chiral stationary phase. (*S*)-(-)-1-phenyl-1-propanol (**6a**) was obtained as the main enantiomer. ^e Mass balance (MB) was calculated considering remaining starting material and all products formed: MB = (r.s.m %) + (Product Yields %). n.d. = non-detected. A = alcohol, K = ketone.

Next, we decided to screen a set of carboxylic acids with tertiary alpha-carbons in which the substitution on one of the beta-carbons varies (Table 6). Accordingly, we considered an acid with a primary beta-carbon (isobutyric acid, IBA), a secondary (2-eha), a tertiary (2,3-dimethylbutanoic acid, 2,3-DMBA), a quaternary (2,3,3-trimethylbutanoic acid, TMBA), as well as an sp^2 -hybridized beta-carbon (*S*-ibuprofen, *S*-Ibu and *S*-Naproxen, *S*-Nap). The use of IBA, containing a tertiary alpha-carbon and a primary beta-carbon, provided similar results as for the use of 2-eha in terms of alcohol and ketone yield. However, the ee value for the benzylic alcohol product decreased to 40% (Table 6, Entry 1). Carboxylic acids with a tertiary and quaternary beta-carbon (2,3-DMBA and TMBA, respectively) showed decreased alcohol and ketone yields, as well as a lower ee value for the alcohol (Table 6, Entry 3 and 4). Finally, carboxylic acids with a tertiary alpha-carbon and an sp^2 -hybridized beta-carbon were also

considered (*S*-Ibu and *S*-Nap). Interestingly, these additives were enantiopure, whereas all other carboxylic acids tested either lack a chiral center or were used in their racemic form. Similar results to those obtained with 2-eha in terms of alcohol and ketone yield were obtained when *S*-Ibu was used (Table 6, Entry 5). Noteworthy is that *S*-Ibu provided the highest substrate conversion (*i.e.* activity) of all carboxylic acids tested in this series, however, a slight decrease in ee value was observed (53%). When *S*-Nap was employed, much lower yields and alcohol ee were obtained (Table 6, Entry 6), indicating that a carboxylic acid with a bulkier naphthalene group in its structure does not create an optimal surrounding around the catalytic active site. On basis of this analysis, we concluded that an acid additive containing a tertiary alpha-carbon and a secondary beta-carbon (such as 2-eha) provides the best performance in the H₂O₂-mediated benzylic oxidation of propylbenzene with manganese catalyst **2**. Interestingly, using this set of carboxylic acid additives led to a complete suppression of aromatic oxidation activity.

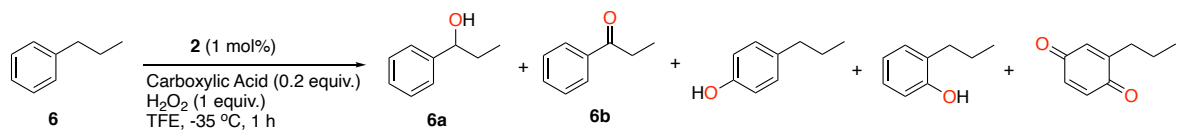
Table 6. Screening of carboxylic acids containing tertiary alpha-carbons with different types of beta-carbons.



Entry	CA ^a	r.s.m ^b	A ^c	K ^c	p-Phenol ^c	o-Phenol ^c	Quinone ^c	ee ^d	MB ^e
1	IBA	32	34	7	n.d.	n.d.	n.d.	40	73
2	2-eha	39	34	8	n.d.	n.d.	n.d.	58	81
3	2,3-DMBA	43	30	6	n.d.	n.d.	n.d.	51	79
4	TMBA	47	28	6	n.d.	n.d.	n.d.	51	81
5	S-Ibu	30	32	6	n.d.	n.d.	n.d.	53	68
6	S-Nap	48	20	3	n.d.	n.d.	n.d.	49	71

^aCarboxylic acid: IBA = isobutyric acid, 2-eha = 2-ethylhexanoic acid, 2,3-DMBA = 2,3-dimethylbutanoic acid, TMBA = 2,3,3-trimethylbutanoic acid, *S*-Ibu = *S*-ibuprofen, *S*-Nap = *S*-Naproxen. ^b Remaining starting material (r.s.m) in %. ^c Yields in % with respect to substrate determined by GC against an internal standard. ^d Enantiomeric excess determined by HPLC on a chiral stationary phase. (*S*)-(-)-1-phenyl-1-propanol (**6a**) was obtained as the main enantiomer. ^e Mass balance (MB) was calculated considering remaining starting material and all products formed: MB = (r.s.m %) + (Product Yields %). n.d. = non-detected. A = alcohol, K = ketone.

Finally, we considered the use of chiral amino acids as carboxylic acid additives. Recent studies have shown the advantageous use of these additives in other H₂O₂-mediated oxidations using bioinspired manganese complexes as catalysts.^{24, 26, 32, 72} Amino acids comprise a tertiary alpha-carbon, which seems optimal for enantioselective benzylic oxidation with catalyst **2** on the basis of our screening of carboxylic acids with different types of alpha-carbons (Table 7). Accordingly, we have tested *N*-protected prolines, leucines and phenylalanines containing different protecting groups (Boc, Cbz and Phth) and chiralities (*L* and *D*).

Table 7. Screening of N-protected amino acids as carboxylic acid additives containing tertiary alpha-carbons.


Entry	CA ^a	r.s.m ^b	A ^c	K ^c	p-Phenol ^c	o-Phenol ^c	Quinone ^c	ee ^d	MB ^e
1	Boc-<i>L</i>-Pro	46	31	7	<1	n.d.	n.d.	47	84
2	Cbz-<i>L</i>-Pro	27	38	6	1	n.d.	n.d.	52	72
3	Cbz-<i>D</i>-Pro	39	27	4	1	n.d.	n.d.	61	71
4	Boc-<i>L</i>-tert-Leu	29	42	9	<1	n.d.	n.d.	58	80
5	Boc-<i>D</i>-tert-Leu	37	30	16	n.d.	n.d.	n.d.	52	83
6	Phth-<i>L</i>-Phe	43	24	5	<1	n.d.	n.d.	46	72

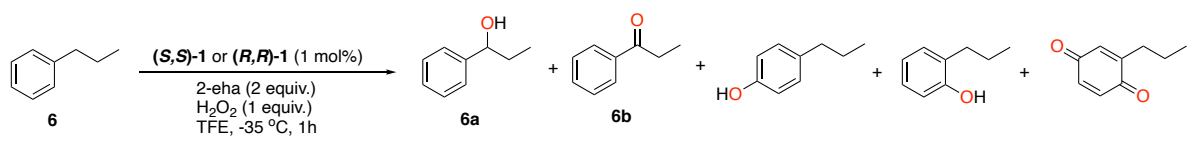
^a Carboxylic acid: Boc-*L*-Pro = *N*-tert-butylcarboxy-*L*-proline, Cbz-*L*-Pro = *N*-carbobenzyloxy-*L*-proline, Cbz-*D*-Pro = *N*-carbobenzyloxy-*D*-proline, Boc-*L*-tert-Leu = *N*-tert-butylcarboxy-*L*-leucine, Boc-*D*-tert-Leu = *N*-tert-butylcarboxy-*D*-leucine, Phth-*L*-Phe = Phthalimido-*L*-phenylalanine. ^b Remaining starting material (r.s.m) in %. ^c Yields in % with respect to substrate determined by GC against an internal standard. ^d Enantiomeric excess determined by HPLC on a chiral stationary phase. (*S*)-(-)-1-phenyl-1-propanol (**6a**) was obtained as the main enantiomer. ^e Mass balance (MB) was calculated considering remaining starting material and all products formed: MB = (r.s.m %) + (Product Yields %). n.d. = non-detected. A = alcohol, K = ketone.

Regarding the prolines employed, we have considered both Boc-*L*-proline and a Cbz-*L*-proline. For Boc-*L*-proline we obtained up to 31% alcohol yield in 47% ee and 7% ketone yield, (Table 7, Entry 1). For Cbz-*L*-proline we obtained a higher conversion and yields, with the alcohol product being formed in 38% yield, and the ketone in 6% yield. The ee value for the alcohol product in this case was 52%. Since the Cbz protecting group provided better conversion and yields, we decided to also test the Cbz-proline additive with opposite stereochemistry *D* (Table 7, compare entries 2 and 3). Interestingly, we found that the overall activity of the current system changes by switching the chirality of the amino acid additive, indicating that a proper engineering of the chiral environment around the catalytic active site is crucial, and that subtle modifications may translate into different performances. The experiment using Cbz-*D*-Pro provided a lower conversion and alcohol yield, whereas the alcohol ee increased to 61% (Table 7, Entry 3). Next, we have also considered leucines with different chiralities (Boc-*L*-tert-leucine and Boc-*D*-tert-leucine) as amino acid additives. Boc-*L*-tert-leucine provides the benzylic alcohol product in up to 42% yield, together with the ketone product in 9% yield. The ee value in this case was as high as 58%. The use of the opposite enantiomer, Boc-*D*-tert-leucine, again led to a different catalytic performance. The yield for the alcohol product decreased to 30%, whereas the ketone product was formed in a much higher amount (16%). The ee value for the alcohol product slightly decreased to 52%. Finally, we have also considered phthalamido-protected *L*-phenylalanine as additive. However, product yields were much lower with only

24% alcohol yield and 5% ketone yield, and an ee value of 46% was observed for the alcohol product (Table 7, Entry 6).

An important observation from these experiments is that by switching the chirality of the amino acid additive, the enantioselectivity in the alcohol product does not change for this catalytic system, *i.e.* the (*S*)-alcohol is observed as the major product in all cases. Therefore, we can conclude that the enantioselectivity of the reaction is dictated by the chirality of the starting Mn-complex and is not perturbed by (chiral) additives, as was previously described in other studies using similar manganese complexes for the oxidation of aliphatic C–H bonds.^{26, 32} Indeed, by using complex (*S,S*)-**1** in combination with 2-eha, the (*S*)-(-)-1-phenyl-1-propanol product was generated as the main enantiomer in 59% ee, while the (*R*)-(+)-1-phenyl-1-propanol product formed as the main enantiomer in 57% ee at a similar conversion and yield when using complex (*R,R*)-**1** of opposite chirality (Table 8).

Table 8. Investigation on the chirality of the complex for the enantioselective benzylic oxidation of propylbenzene as substrate.



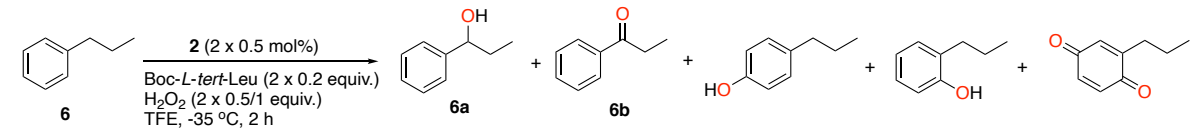
Chirality	r.s.m. ^a	A ^b	K ^b	<i>p</i> -Phenol ^b	<i>o</i> -Phenol ^b	Quinone ^b	ee ^c	Config.	MB ^d
(<i>R,R</i>)	43	27	4	n.d.	n.d.	n.d.	57	(<i>R</i>)	74
(<i>S,S</i>)	31	34	7	<1	1	n.d.	59	(<i>S</i>)	73

^a Remaining starting material (r.s.m) in %. ^b Yields in % with respect to substrate determined by GC against an internal standard. ^c Enantiomeric excess of the alcohol determined by HPLC on a chiral stationary phase. ^d Mass balance (MB) was calculated considering remaining starting material and all products formed: MB = (r.s.m %) + (Product Yields %). n.d. = non-detected. 2-eha = 2-ethylhexanoic acid. A = alcohol, K = ketone.

From the data compiled in Table 8, we concluded that the best carboxylic acid additive is Boc-*L*-*tert*-leucine, providing the highest benzylic alcohol yield (42%) and a good ee value (58%). These characteristics could be slightly increased by making use of an iterative addition protocol (see Experimental Section for further details). This methodology consists of adding a first portion of manganese complex (0.5 mol%) and carboxylic acid additive (0.2 equiv.) and adding H₂O₂ (0.5 equiv.) over a period of 1 h. Then, a new portion of complex (0.5 mol%) and carboxylic acid (0.2 equiv.) is added, and a second portion of H₂O₂ (0.5 equiv.) is added again over a period of 1 h. This procedure provided us with a slight increase in conversion and alcohol yield (up to 46%), keeping a similar ee value of 60% (Table 9, Entry 1). This observation could indicate that catalyst lifetime is an issue in these H₂O₂-mediated C–H oxidations, as it has been

previously described that oxidative degradation of the ligand occurs for related non-heme iron and manganese complexes.⁹⁵⁻⁹⁷ When the same iterative addition protocol was used but employing a total of 2 equiv. of H₂O₂, the overoxidized ketone product was obtained as the main product in 55% yield, together with the alcohol product in 23% yield, indicating that overoxidation is highly favored when a large excess of oxidant is used (Table 9, Entry 2).

Table 9. Iterative addition protocol for the oxidation of propylbenzene using complex **2** and Boc-*L*-tert-Leu as the additive.



Entry	H ₂ O ₂ ^a	r.s.m. ^b	A ^c	K ^c	<i>p</i> -Phenol ^c	<i>o</i> -Phenol ^c	Quinone ^c	ee ^d	MB ^e
1	2 x 0.5	23	46	9	n.d.	n.d.	n.d.	60	78
2	2 x 1	<1	23	55	<1	n.d.	n.d.	72	78

^a Total equivalents of H₂O₂ used in the oxidation reaction (added in two portions). ^b Remaining starting material (r.s.m) in %. ^c Yields in % with respect to substrate determined by GC against an internal standard. ^d Enantiomeric excess determined by HPLC on a chiral stationary phase. (*S*)-(-)-1-phenyl-1-propanol (**6a**) was obtained as the main enantiomer. ^e Mass balance (MB) was calculated considering remaining starting material and all products formed: MB = (r.s.m %) + (Product Yields %). n.d. = non-detected.

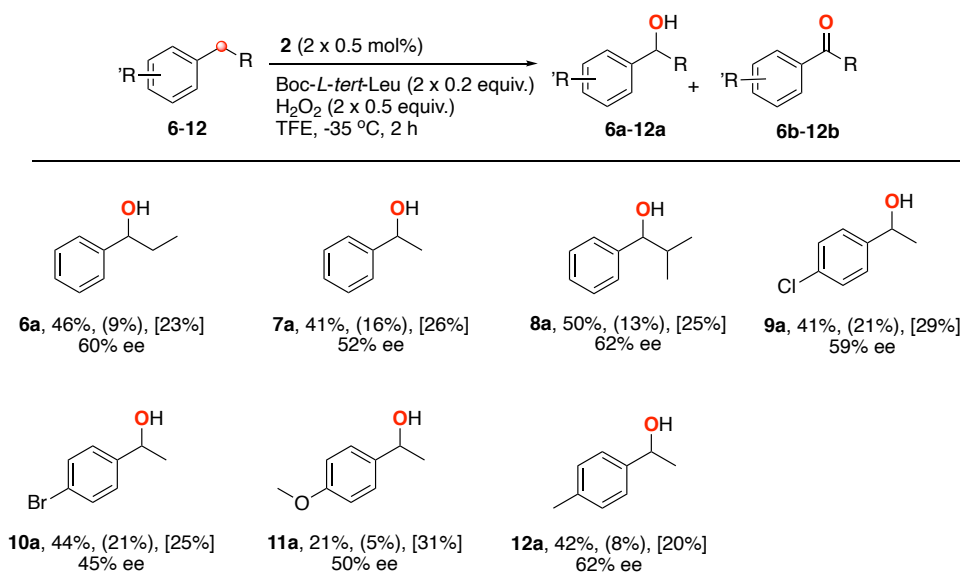
Interestingly, the ee value for the alcohol product increased to 72%, which can be explained by a kinetic resolution effect in the secondary oxidation step. This kinetic resolution methodology has been previously used to reach high alcohol ee values by Bryliakov et al..^{24,32,98} The iterative addition protocol using an overall 2.0 equiv. of oxidant also led to full substrate conversion. Overall, the catalytic system **2**/H₂O₂/Boc-*L*-tert-leucine performs the oxidation of monoalkylbenzene **6** with higher alcohol yields compared to the system developed by Bryliakov and co-workers.²⁶ Similar conversions were obtained for both systems (~ 75%), whereas alcohol yield was higher with the current complex (46% and 34% alcohol yield for the use of catalyst **2** and **Mn(dpf)**, respectively). However, ee values for the alcohol product were lower when **2** was used instead of **Mn(dpf)** (60% and 76% ee for the use of catalyst **2** and **Mn(dpf)**, respectively). Of note is that ee's have been considerably increased using a kinetic resolution approach with **Mn(dpf)**, obtaining up to 97% alcohol ee (Figure 2C).³²

5.2.5 Substrate Scope

Using the optimized reaction conditions, including Boc-*L*-tert-leucine as the carboxylic acid additive, we explored the enantioselective benzylic hydroxylation of different aromatic substrates by manganese complex **2** (Scheme 1). In general, our current catalytic system with the highly electron-rich manganese complex and an enantiopure amino acid additive affords a

high selectivity for aliphatic (benzylic) C–H bond oxidation over aromatic oxidation of these substrates.

Oxidation of ethylbenzene (**7**) leads to the benzylic alcohol product **7a** in 41% yield and 52% ee, along with the corresponding ketone **7b** in 16% yield. Interestingly, isobutylbenzene (**8**) was also considered, which bears a reactive tertiary aliphatic C–H bond. Benzylic alcohol product **8a** was obtained in 50% yield and 62% ee, together with the corresponding ketone product **8b** in 13% yield. The 2-methyl-1-phenyl-2-propanol product derived from oxidation at the tertiary position was only detected in trace amounts, which agrees with the favorable oxidation of a benzylic C–H bond (activated C–H bond, BDE = 85.4 kcal/mol) compared to a tertiary aliphatic C–H bond (non-activated C–H bond, BDE = 96 kcal/mol).⁹⁹ Next, we extended our study to the oxidation of *para*-substituted ethylbenzenes as substrates, containing electron-withdrawing and electron-donating substituents. Oxidized products were obtained in



Scheme 1. Asymmetric synthesis of benzylic alcohols by a manganese-catalyzed C–H oxidation. Reactions were performed on 0.2 mmol scale in 2.5 mL of TFE, 0.5 mol% of complex **2** and 0.2 equiv. of Boc-*L*-tert-Leu (complex **2**, carboxylic acid, and oxidant were all added in portionwise twice; for details, see the Experimental Section). Yields were determined by GC, and ee was determined by HPLC on a chiral stationary phase. Yields for the overoxidized ketone products are shown in parenthesis, whereas remaining starting material (r.s.m%) is shown in brackets.

good benzylic alcohol yields ranging from 21 to 50%, with overoxidized ketone products between 5 and 21% yield. Enantioselectivity values for the alcohol product range from 45 to 62%. Oxidation of 1-chloro-4-ethylbenzene (**9**), containing an electron-withdrawing substituent, provided the alcohol product **9a** in 41% yield and 59% ee, together with ketone byproduct **9b** in 21% yield. 1-bromo-4-ethylbenzene (**10**) was also considered, which yielded the desired benzylic alcohol product **10a** in 44% yield and 45% ee, generating the ketone

product **10b** in 21% yield. Oxidation of 4-ethylanisole (**11**), which bears an electron-donating substituent, provided lower activities, with the benzylic alcohol product **11a** in 21% yield and 50% ee, with the ketone **11b** being formed in only 5% yield. A dialkylbenzene was also considered in the current Chapter. Particularly, we explored the oxidation of 4-ethyltoluene (**12**), which contains two benzylic positions. Interestingly, reaction mainly occurred on the ethyl substituent, which bears the C–H bonds with the lower BDE (85.4 and 89.7 kcal/mol for the BDE of the benzylic C–H bond of ethylbenzene and toluene, respectively),⁹⁹ affording the benzylic alcohol product **12a** in 42% yield and 62% ee, with the ketone product **12b** in 10% yield. Oxidation at the other benzylic position occurred to a much lower extent, generating 4-ethylbenzyl alcohol in 5% yield. Other by-products were also detected, which might be assigned to products in which oxidation takes place at both alkyl substituents.

5.2.6 Asymmetric Epoxidation Reactions

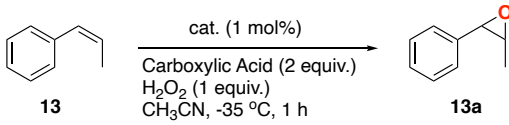
Finally, to provide an extended impression of their catalytic properties, the new manganese complexes (*S,S*)-**1** and **2** were also tested in the epoxidation reaction of *cis*- β -methylstyrene (**13**) as substrate (Table 10). The outcome of these experiments shows that these complexes are highly efficient epoxidation catalysts as well, with yields up to 98% for the epoxide product **13a** using only 1 equiv. of the H₂O₂ oxidant, and up to 97% ee for the epoxide product when 2-eha is employed as carboxylic acid additive. The use of 2-eha as the carboxylic acid additive instead of acetic acid leads to a significant increase in enantioselectivity, as was reported before for related non-heme iron and manganese complexes.⁴² 2-Cyclohexene-1-one (**14**) represents a much more challenging, electron-poor substrate for epoxidation reactions. Using manganese catalysts (*S,S*)-**1** and **2**, the epoxide product **14a** was obtained in poor yields, with values up to 28 and 19%, respectively, when acetic acid was used as additive (Table 11, Entries 1 and 3). Changing the carboxylic acid to 2-eha provided a significant decrease in epoxide yield (Table 11, Entries 2 and 4).

For these reactions we have not been able to determine the enantioselectivity due to low concentration of the epoxide product. Next, we tested the non-heme iron complex **5**, which provided much higher efficiencies for the epoxidation of **14**, with yields up to 67 and 56% when acetic acid and 2-eha were employed, respectively. This observation contrasts with the previous study on enantioselective benzylic oxidations, where catalyst **5** was not capable of performing the aliphatic C–H hydroxylation of propylbenzene towards the benzylic alcohol product, and it shows that a highly electron-rich iron complex performs better for the epoxidation of aliphatic olefins compared to the analogous manganese complexes. Remarkably, the enantioselectivity obtained when **5** is used in the presence of 2-eha was excellent (>99%), which represents an

increase compared with the related non-heme iron complex supported with the aminopyridine ligand containing dimethylamino substituents.⁵⁹

Overall, the current complexes containing 4-pyrrolidinopyridine moieties provide enhanced enantioselectivities for the epoxidation of olefins. This finding is in accordance with the increase in enantioselectivity reported in previous studies by the introduction of dimethylamino or other similar amine substituents into several manganese and iron complexes, compared to the use of complexes with non-substituted pyridines.^{37, 43, 45, 49, 52, 53, 61}

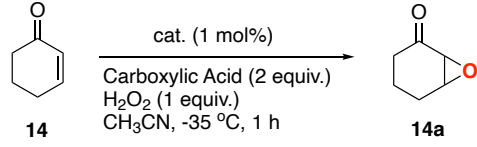
Table 10. Catalytic asymmetric epoxidation of *cis*- β -methylstyrene with manganese complexes.



Entry	Catalyst	CA ^a	r.s.m ^b	Epoxide ^c	ee ^d
1	(<i>S,S</i>)- 1	AA	<1	98	78
2	(<i>S,S</i>)- 1	2-eha	<1	98	93
3	2	AA	<1	98	84
4	2	2-eha	<1	98	97

^a Carboxylic acid: AA = acetic acid, 2-eha = 2-ethylhexanoic acid. ^b Remaining starting material (r.s.m) in % . ^c Yields in % with respect to substrate determined by GC against an internal standard. ^d Enantiomeric excess determined by chiral GC.

Table 11. Catalytic asymmetric epoxidation of 2-cyclohexene-1-one using manganese and iron complexes.



Entry	Catalyst	CA ^a	r.s.m ^b	Epoxide ^c	ee ^d
1	(<i>S,S</i>)- 1	AA	24	28	-
2	(<i>S,S</i>)- 1	2-eha	57	4	-
3	2	AA	35	19	-
4	2	2-eha	48	10	-
5	5	AA	13	67	53
6	5	2-eha	20	56	>99

^a Carboxylic acid: AA = acetic acid, 2-eha = 2-ethylhexanoic acid. ^b Remaining starting material (r.s.m) in % . ^c Yields in % with respect to substrate determined by GC against an internal standard. ^d Enantiomeric excess determined by HPLC on a chiral stationary phase. Ee values for Mn-catalyzed oxidations were not possible to determine due to low epoxide formation.

5.3 Conclusions

A new series of chiral manganese and iron complexes supported by highly electron-donating pyridylalkylamine ligands containing 4-pyrrolidinopyridine moieties (**(*S,S*)-1**, **(*R,R*)-1**, **2** and **5**) were synthesized and characterized. The manganese complexes were tested as efficient catalysts for enantioselective benzylic oxidations using H₂O₂ as terminal oxidant in the presence of fluorinated alcohol solvents and carboxylic acid additives for the controlled activation of H₂O₂. The current complexes afford improved benzylic alcohol yields compared with the analogous manganese complexes with 4-dimethylaminopyridine moieties (**3** and **4**), which we rationally assign to the higher basicity of the 4-pyrrolidinopyridine group. In addition, we have presented a systematic study on the modulation of the carboxylic acid additive for the proper engineering of the environment around the catalytic active site, which has allowed the formation of several benzylic alcohol products in moderate to good enantioselectivities. Finally, we have also shown that the current manganese and iron complexes are effective catalysts for the asymmetric epoxidation of olefins at low oxidant loadings, with special emphasis on the good yields and excellent enantioselectivities obtained for the epoxidation of a challenging olefin catalyzed by non-heme iron complex **5**.

Future efforts in our laboratory will focus on the further development of highly electron-rich manganese and iron complexes that make use of strong electron-donating ligands for a better stabilization of the metal-oxo active species. Improvement of enantioselectivities for benzylic alcohol products, as well as the understanding of the factors that govern product chemoselectivity (aliphatic vs aromatic oxidation) are currently being explored.

5.4 Experimental Section

5.4.1 General Remarks

The synthesis of manganese and iron complexes, and other air- and moisture-sensitive reactions was performed under an inert nitrogen atmosphere using standard Schlenk line and glovebox techniques. All catalytic oxidation reactions were run under air with no precautions taken to exclude moisture. The solvents diethyl ether, toluene, and acetonitrile were purified using an MBraun MB SPS-800 solvent purification system. Tetrahydrofuran and methanol were dried with sodium and magnesium turnings, respectively, and distilled under nitrogen prior to use. Ligands (*S,S*)-Me₂Nbpbp and (*S,S*)-Me₂Nbpmcn were synthesized according to literature procedures.^{49, 57} Mn(OTf)₂ was bought from Sigma-Aldrich. Manganese complexes (*S,S*)-[Mn(OTf)₂(^{NMe2}bpbp)] and (*S,S*)-[Mn(OTf)₂(^{NMe2}bpmcn)] were synthesized according to literature procedures.^{43, 49} All other reagents and compounds for independent oxidation reaction product identification were obtained commercially and used without further purification. GC quantification was done by using calibration lines for each compound employing an internal standard.

Column chromatography was performed using Merck silica gel (60-200 mesh). ¹H, ¹³C, and ¹⁹F NMR spectra were recorded with a 400 MHz Varian spectrometer at 25 °C, chemical shifts (δ) are given in

ppm referenced to the residual solvent peak. IR spectra were recorded with a Perkin-Elmer Spectrum One FTIR spectrometer. HRMS analysis was performed with a 6560 Ion Mobility LC/Q-TOF instrument from Agilent Technologies. GC analyses were performed on a Perkin-Elmer Clarus 500 Gas Chromatograph equipped with a PE Elite-5 column ((30m x 0.32 mm x 0.25 μ m), (5% phenyl)-(95% methyl)polysiloxane) and a flame-ionization detector; and on an Agilent Cyclodex B column ((60m x 0.25 mm x 0.25 μ m), Chiral column). HPLC analyses were performed on a Perkin-Elmer Flexar LC System equipped with a Chiralcel® OD column (250 mm x 4.6 mm x 10 μ m, Chiral Column). Single-crystal X-ray diffraction was carried out using a Bruker Kappa ApexII diffractometer.

Appendix D contains the supplementary information of this Chapter, which includes ¹H-NMR spectra for the newly synthesized ligands, and representative GC and HPLC chromatographs of the catalytic reactions.

5.4.2 Synthesis of Ligands and Manganese Complexes

5.4.2.1 Synthesis of Ligands

The procedures for the synthesis of (4-Pyrrolidinopyridin-2-yl)methanol (^{Pyr}PyCH₂OH), 2-Chloromethyl-4-pyrrolidinopyridine hydrochloride (^{Pyr}PyCH₂Cl·HCl) and (*S,S*)-^{Pyr}bpmcn ((*S,S*)-L1) are described in Chapter 4 of this thesis.

(*R,R*)-^{Pyr}bpmcn ((*R,R*)-L1) was synthesized following a procedure analogous to (*S,S*)-^{Pyr}bpmcn using (*R,R*)-*N,N*-dimethyl-1,2-cyclohexanediamine (130 mg, 0.9 mmol) and ^{Pyr}PyCH₂Cl·HCl (2.04 equiv., 430 mg, 1.84 mmol). After following the same purification protocol as for (*S,S*)-^{Pyr}bpmcn, the desired ligand was obtained as a light-brown solid (152 mg, 0.33 mmol, 37% yield). ¹H NMR (400 MHz, CD₃CN): δ 8.47 (d, 3 H), 7.70 (t, 3 H), 7.59 (d, 3 H), 7.18 (t, 3 H), 3.81 (s, 6 H).

(*S,S*)-^{Pyr}bpbp (L2): A 20 mL vial was charged with a stir bar, (*S,S*)-2,2'-bispyrrolidine tartrate (1 equiv., 334 mg, 0.97 mmol) and H₂O (2.5 mL), and CH₂Cl₂ (2.5 mL). Solid NaOH pellets (6.4 equiv., 250 mg, 6.2 mmol) were added, followed by ^{Pyr}PyCH₂Cl·HCl (2.2 equiv., 500 mg, 2.14 mmol). After 18 h stirring at room temperature, the reaction mixture was diluted with 1 M NaOH. The aqueous layer was extracted with CH₂Cl₂ (3x), and the organic extracts were combined, dried over MgSO₄, and concentrated in vacuo. The obtained crude ligand was purified by silica gel chromatography eluting with CH₂Cl₂:CH₃OH:NH₄OH (90 : 4.5 : 1.8) first, followed by CH₂Cl₂:CH₃OH:NH₄OH (90 : 9 : 1.8), and the collected fractions were combined, washed with 1 M NaOH, dried over MgSO₄, and concentrated in vacuo to provide the desired (*S,S*)-^{Pyr}bpbp ligand as a light-brown solid (203 mg, 0.44 mmol, 45% yield). ¹H NMR (400 MHz, CDCl₃) δ 7.74 (d, *J* = 6.7 Hz, 2H), 6.62 (d, *J* = 2.5 Hz, 2H), 6.23 (dd, *J* = 6.7, 2.5 Hz, 2H), 4.45 (d, *J* = 17.0 Hz, 2H), 3.84 (d, *J* = 17.0 Hz, 2H), 3.57 (s, 4H), 3.38 (s, 4H), 3.12 (dt, *J* = 9.9, 5.8 Hz, 2H), 2.93 - 2.83 (m, 2H), 2.41 (dt, *J* = 9.9, 7.3 Hz, 2H), 2.12 (s, 8H), 2.01 - 1.95 (m, 2H), 1.80 - 1.71 (m, 4H), 1.54 (dt, *J* = 12.6, 6.2 Hz, 2H); ¹³C NMR (101 MHz, CDCl₃) δ 154.39, 154.00, 139.81, 105.04, 104.75, 69.88, 58.16, 56.20, 48.55, 29.88, 25.32, 24.20; IR (ATR) ν , cm⁻¹: 2966, 2906, 2864, 2842, 2794, 2766, 1596, 1544, 1496, 1481, 1448, 1388, 1349, 1243, 1179, 1155, 1123, 1015, 980, 804; HRMS: *m/z* calculated for C₂₈H₄₁N₆, [M+H]⁺ 461.3393, found 461.3390.

(*S,S*)-^{Me2N}bpmcn (L3) and **(*S,S*)-^{Me2N}bpbp (L4)** were synthesized accordingly to literature procedures described by Sun *et al* and Costas *et al*.^{49,57}

5.4.2.3 Synthesis of Manganese and Iron Complexes

(*S,S'*)-[Mn(CF₃SO₃)₂(^{Pyrr}bpmcn)] ((*S,S*)-Mn(^{Pyrr}bpmcn), (*S,S*)-1): A suspension of Mn(CF₃SO₃)₂ (72 mg, 0.203 mmol) in anhydrous THF (1 mL) was added dropwise to a vigorously stirred solution of (*S,S*)-^{Pyrr}bpmcn (100 mg, 0.216 mmol) in THF (1 mL). The resulting mixture was stirred at rt overnight. Then, the solution was dried under vacuum, to provide a precipitate that was washed with diethyl ether several times. The resulting precipitate was dissolved in CH₂Cl₂, and slow diethyl ether diffusion into the resultant solution afforded, in a few days the desired complex as a brown microcrystalline material (117 mg, 0.143 mmol, yield 71%). HRMS: *m/z* calculated for C₂₉H₄₂F₃MnN₆O₃S, [M-OTf]⁺ 666.2372, found 666.2378. IR (ATR) ν , cm⁻¹: 2934, 1614, 1519, 1457, 1400, 1217, 1150, 1028, 1013, 635.

(*R,R'*)-[Mn(CF₃SO₃)₂(^{Pyrr}bpmcn)] ((*R,R*)-Mn(^{Pyrr}bpmcn), (*R,R*)-1): Following the procedure for the synthesis complex (*S,S*)-1 outlined above and starting from Mn(CF₃SO₃)₂ (38 mg, 0.109 mmol) and (*R,R*)-^{Pyrr}bpbp (54 mg, 0.116 mmol), complex (*R,R*)-1 was obtained as a brown microcrystalline material (60 mg, 0.073 mmol, yield 67%). HRMS: *m/z* calculated for C₂₉H₄₂F₃MnN₆O₃S, [M-OTf]⁺ 666.2372, found 666.2378. IR (ATR) ν , cm⁻¹: 2934, 1614, 1519, 1457, 1401, 1221, 1150, 1029, 1012, 809, 635, 514.

(*S,S'*)-[Mn(CF₃SO₃)₂(^{Pyrr}bpbp)] (Mn(^{Pyrr}bpbp), 2): A suspension of Mn(CF₃SO₃)₂ (88 mg, 0.25 mmol) in anhydrous THF (1 mL) was added dropwise to a vigorously stirred solution of (*S,S*)-^{Pyrr}bpbp (123 mg, 0.27 mmol) in THF (1 mL). After some minutes a white precipitate was formed. Following the procedure described for complex (*S,S*)-1, slow diethyl ether diffusion into a CH₂Cl₂ solution afforded in a few days the desired complex as a white microcrystalline material (130 mg, 0.16 mmol, yield 64%). HRMS: *m/z* calculated for C₂₉H₄₀F₃MnN₆O₃S, [M-OTf]⁺ 664.2215, found 664.2212. IR (ATR) ν , cm⁻¹: 2968, 1616, 1522, 1462, 1404, 1302, 1233, 1214, 1156, 1033, 1014, 807, 635, 513. Crystals suitable for X-ray diffraction were obtained by dissolving 10 mg of the complex in a 5 mL vial in a minimal amount of 1,2-difluorobenzene. This vial was put into a 20 mL vial filled with Et₂O. The larger vial was capped tightly. After 3 days, colourless crystals formed after slow diffusion of Et₂O into the smaller vial. Details on the structure determination are described in section 3.

(*S,S'*)-[Fe(CF₃SO₃)₂(^{Pyrr}bpbp)] (Fe(^{Pyrr}bpbp), 5): A suspension of Fe(CF₃SO₃)₂·(CH₃CN)₂ (95 mg, 0.218 mmol) in anhydrous THF (1 mL) was added dropwise to a vigorously stirred solution of (*S,S*)-^{Pyrr}bpbp (95 mg, 0.206 mmol) in THF (1 mL). Following the procedure described for complex (*S,S*)-1, slow diethyl ether diffusion into a CH₂Cl₂ solution afforded in a few days the desired complex as a yellow microcrystalline material (87 mg, 0.107 mmol, yield 55%). HRMS: *m/z* calculated for C₂₉H₄₀F₃FeN₆O₃S, [M-OTf]⁺ 665.2184, found 665.2189. IR (ATR) ν , cm⁻¹: 3252, 2971, 2879, 1650, 1615, 1557, 1538, 1520, 1483, 1460, 1404, 1353, 1220, 1152, 1026, 1012, 892, 809, 757, 633, 572, 515. Crystals suitable for X-ray diffraction were obtained by dissolving 10 mg of the complex in a 5 mL vial in a minimal amount of THF. After 3 days, colourless crystals formed after slow evaporation of the THF solution. Details on the structure determination are described in section 3.

(*S,S'*)-[Mn(CF₃SO₃)₂(^{Me2N}bpmcn)] (Mn(^{Me2N}bpmcn), 3), and (*S,S'*)-[Mn(CF₃SO₃)₂(^{Me2N}bpbp)] (Mn(^{Me2N}bpbp), 4) were prepared following reported procedures reported by Sun *et al* and Costas *et al*.^{43, 49}

5.4.3 X-Ray Crystal Structure Determination of Mn Complexes

5.4.3.1 X-Ray Crystal Structure Determination of complex 2

$C_{30}H_{40}F_6MnN_6O_6S_2 \cdot C_6H_4F_2$, Fw = 927.83, colourless block, $0.34 \times 0.20 \times 0.08$ mm³, orthorhombic, P2₁2₁2₁ (no. 19), a = 10.2605(2), b = 15.2842(3), c = 26.1552(5) Å, V = 4101.77(14) Å³, Z = 4, D_x = 1.502 g/cm³, μ = 0.51 mm⁻¹. The diffraction experiment was performed on a Bruker Kappa ApexII diffractometer with sealed tube and Triumph monochromator (λ = 0.71073 Å) at a temperature of 150(2) K up to a resolution of (sin θ/λ)_{max} = 0.65 Å⁻¹. The Eval15 software¹⁰¹ was used for the intensity integration. A multi-scan absorption correction and scaling was performed with SADABS¹⁰² (correction range 0.67-0.75). A total of 79976 reflections was measured, 9425 reflections were unique (R_{int} = 0.042), 8231 reflections were observed [I > 2σ(I)]. The structure was solved with Patterson superposition methods using SHELXT.¹⁰³ Structure refinement was performed with SHELXL-2018¹⁰⁴ on F² of all reflections. Non-hydrogen atoms were refined freely with anisotropic displacement parameters. The 1,2-difluorobenzene solvent molecule was refined with a disorder model. Minor disorder of the triflate CF₃ groups has not been resolved. Hydrogen atoms were introduced in calculated positions and refined with a riding model. 541 Parameters were refined with 9 restraints (C-F distances and molecular flatness of the solvent molecule). R1/wR2 [I > 2σ(I)]: 0.0380 / 0.0988. R1/wR2 [all refl.]: 0.0461 / 0.1031. Flack parameter¹⁰⁵ x = 0.011(5). S = 1.045. Residual electron density between -0.51 and 0.60 e/Å³. Geometry calculations and checking for higher symmetry was performed with the PLATON program.¹⁰⁶

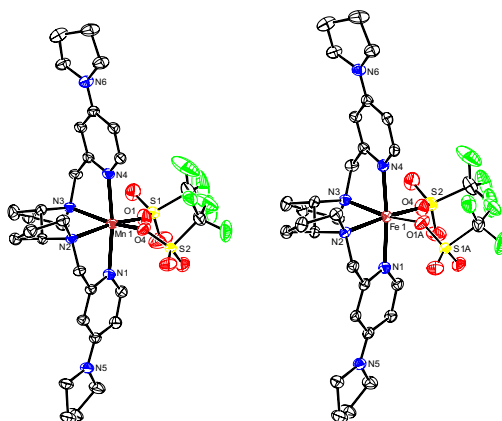


Figure 6. Left: Molecular structure of **2** in the crystal (50% probability level). Hydrogen atoms and disordered 1,2-difluorobenzene solvent molecule are omitted for clarity. Right: Molecular structure of **5** in the crystal (50% probability level). Only the major component of the disordered triflate is shown. Hydrogen atoms and disordered THF solvent molecule are omitted for clarity.

5.4.3.2 X-Ray Crystal Structure Determination of complex 5

$C_{30}H_{40}F_6FeN_6O_6S_2 \cdot C_4H_8O$, Fw = 886.75, light-purple block^{†*}, $0.21 \times 0.14 \times 0.08$ mm³, orthorhombic, P2₁2₁2₁ (no. 19), a = 10.2594(3), b = 15.1887(4), c = 25.5178(5) Å, V = 3976.38(16) Å³, Z = 4, D_x = 1.481 g/cm³, μ = 0.57 mm⁻¹. The diffraction experiment was performed on a Bruker Kappa ApexII diffractometer with sealed tube and Triumph monochromator (λ = 0.71073 Å) at a temperature of 150(2) K up to a resolution of (sin θ/λ)_{max} = 0.65 Å⁻¹. The Eval15 software¹⁰¹ was used for the intensity

* The crystal was obtained from an intense purple solution. It was not possible to determine the crystal colour reliably.

integration. A multi-scan absorption correction and scaling was performed with SADABS¹⁰² (correction range 0.63-0.75). A total of 59532 reflections was measured, 9137 reflections were unique ($R_{\text{int}} = 0.058$), 7530 reflections were observed [$I > 2\sigma(I)$]. The structure was solved with Patterson superposition methods using SHELXT.¹⁰³ Structure refinement was performed with SHELXL-2018¹⁰⁴ on F^2 of all reflections. One coordinated triflate ligand and the THF solvent molecule were refined with a disorder model. The minor disorder component of the triflate was refined isotropically. All other non-hydrogen atoms were refined freely with anisotropic displacement parameters. Hydrogen atoms of the metal complex were located in difference Fourier maps. Hydrogen atoms in the disordered THF were introduced in calculated positions. All hydrogen atoms were refined with a riding model. 580 Parameters were refined with 372 restraints (distances, angles and displacement parameters of the disordered moieties). $R1/wR2 [I > 2\sigma(I)]: 0.0397 / 0.0931$. $R1/wR2 [\text{all refl.}]: 0.0541 / 0.0981$. Flack parameter¹⁰⁵ $x = 0.003(7)$. $S = 1.059$. Residual electron density between -0.34 and $0.42 \text{ e}/\text{\AA}^3$. Geometry calculations and checking for higher symmetry was performed with the PLATON program.¹⁰⁶

5.4.4 Reaction Protocol for Catalytic Studies

General Procedure for Benzylic Hydroxylation Reactions. Catalytic reactions were performed open to air with no precautions taken to exclude moisture. A 20 mL vial was charged with: substrate (1 equiv.) and the indicated loading of catalyst and solvent (2 mL). The carboxylic acid was added in the indicated loading. The vial was cooled on an acetonitrile/dry ice bath ($-35 \text{ }^\circ\text{C}$), while stirring. Subsequently, a solution of H_2O_2 in the corresponding solvent (1 equiv., diluted from a 35% H_2O_2 aqueous solution) was delivered by syringe pump over 30 min. After addition of the oxidant, the resulting mixture was stirred at $-35 \text{ }^\circ\text{C}$ for another 30 min. Then, the solution was brought to room temperature, and at this point, a 0.8 M biphenyl solution in CH_3CN (0.5 equiv.) was added as internal standard. The solution was filtered through a silica plug, which was subsequently rinsed with $2 \times 1 \text{ mL}$ isopropanol. Then the sample was submitted to GC analysis to determine the remaining amount of starting material and the amounts of reaction products by comparison with authentic samples. For the determination of ee values the sample was submitted to HPLC analysis using a chiral column.

Iterative Addition Protocol for Benzylic Hydroxylation Reactions. These reactions were performed open to air with no precautions taken to exclude moisture. A 20 mL vial was charged with substrate (1 equiv.), carboxylic acid (0.2 equiv.), catalyst (0.5 mol%) in 2 mL of the corresponding solvent. The vial was cooled on an acetonitrile/dry ice bath ($-35 \text{ }^\circ\text{C}$), while stirring. Subsequently, a solution of H_2O_2 in the corresponding solvent (0.5 equiv. or 1 equiv., diluted from a 35% H_2O_2 aqueous solution) was delivered by syringe pump over 30 min. After addition of the oxidant, the resulting mixture was stirred at $-35 \text{ }^\circ\text{C}$ for 30 min more. Then, a solution of the catalyst (0.5 mol%) and carboxylic acid (0.2 equiv.) in the corresponding solvent (0.5 mL) was added to the stirring reaction, immediately followed by dropwise addition of a second solution of H_2O_2 (0.5 equiv. or 1 equiv., diluted from a 35% H_2O_2 aqueous solution) was delivered by syringe pump over 30 min. Finally, the solution was brought to room temperature, and at this point, a 0.8 M biphenyl solution in CH_3CN (0.5 equiv) was added as internal standard. The solution was filtered through a silica plug, which was subsequently rinsed with $2 \times 1 \text{ mL}$ isopropanol. Then the sample was submitted to GC analysis to determine the remaining amount of starting material and the amounts of reaction products by comparison with authentic samples. For the determination of ee values the sample was submitted to HPLC analysis using a chiral column.

General Procedure for Epoxidation Reactions. Epoxidation reactions were performed open to air with no precautions taken to exclude moisture. A 20 mL vial was charged with: substrate (1 equiv.) and the indicated loading of catalyst and solvent (2 mL). The carboxylic acid was added in the indicated

loading. The vial was cooled on an acetonitrile/dry ice bath ($-35\text{ }^{\circ}\text{C}$), while stirring. Subsequently, a solution of H_2O_2 in the corresponding solvent (1 equiv., diluted from a 35% H_2O_2 aqueous solution) was delivered by syringe pump over 30 min. After addition of the oxidant, the resulting mixture was stirred at $-35\text{ }^{\circ}\text{C}$ for 30 min more. Then, the solution was brought to room temperature, and at this point, a 1 M nitrobenzene solution in CH_3CN (0.5 equiv) was added as internal standard. The solution was filtered through a silica plug, which was subsequently rinsed with 2 x 1 mL EtOAc. Then the sample was submitted to GC analysis to determine the remaining amount of starting material and the amounts of reaction products by comparison with authentic samples. For the determination of ee values the sample was submitted to GC analysis using a chiral column.

Author Contributions

E.M-R. and R.K.G. devised the project and designed experiments. E.M-R. performed the experiments and analyzed the data. F.L. performed the synthesis of complex **5** and catalytic epoxidation reactions. M.L. performed X-ray analysis. E.M-R. wrote the Chapter and R.K.G. provided comments on the experiments and Chapter content.

5.5 References

1. White, M. C.; Zhao, J., Aliphatic C–H Oxidations for Late-Stage Functionalization. *J. Am. Chem. Soc.* **2018**, *140* (43), 13988-14009.
2. Hong, B.; Luo, T.; Lei, X., Late-Stage Diversification of Natural Products. *ACS Cent. Sci.* **2020**, *6* (5), 622-635.
3. Feng, K.; Quevedo, R. E.; Kohrt, J. T.; Oderinde, M. S.; Reilly, U.; White, M. C., Late-stage oxidative C(sp³)–H methylation. *Nature* **2020**, *580* (7805), 621-627.
4. Que, L.; Tolman, W. B., Biologically inspired oxidation catalysis. *Nature* **2008**, *455* (7211), 333-340.
5. Groves, J. T.; Viski, P., Asymmetric hydroxylation by a chiral iron porphyrin. *J. Am. Chem. Soc.* **1989**, *111* (22), 8537-8538.
6. Srinivasan, K.; Michaud, P.; Kochi, J. K., Epoxidation of olefins with cationic (salen)manganese (III) complexes. The modulation of catalytic activity by substituents. *J. Am. Chem. Soc.* **1986**, *108* (9), 2309-2320.
7. Groves, J. T.; Viski, P., Asymmetric hydroxylation, epoxidation, and sulfoxidation catalyzed by vaulted binaphthyl metalloporphyrins. *J. Org. Chem.* **1990**, *55* (11), 3628-3634.
8. Hamachi, K.; Irie, R.; Katsuki, T., Asymmetric benzylic oxidation using a Mn-SALEN complex as catalyst. *Tetrahedron Lett.* **1996**, *37* (28), 4979-4982.
9. Hamada, T.; Irie, R.; Mihara, J.; Hamachi, K.; Katsuki, T., Highly enantioselective benzylic hydroxylation with concave type of (salen)manganese(III) complex. *Tetrahedron* **1998**, *54* (34), 10017-10028.
10. Miyafuji, A.; Katsuki, T., Asymmetric desymmetrization of *meso*-tetrahydrofuran derivatives by highly enantiotopic selective C–H oxidation. *Tetrahedron* **1998**, *54* (35), 10339-10348.
11. Komiya, N.; Noji, S.; Murahashi, S.-I., Manganese catalyzed asymmetric oxidation of alkanes to optically active ketones bearing asymmetric center at the α -position. *Tetrahedron Lett.* **1998**, *39* (43), 7921-7924.

12. Zhang, R.; Yu, W.-Y.; Lai, T.-S.; Che, C.-M., Enantioselective hydroxylation of benzylic C–H bonds by D_4 -symmetric chiral oxoruthenium porphyrins. *Chem. Commun.* **1999**, (18), 1791-1792.
13. Murahashi, S. I.; Noji, S.; Komiya, N., Catalytic enantioselective oxidation of alkanes and alkenes using (salen)manganese complexes bearing a chiral binaphthyl strapping unit. *Adv. Synth. Catal.* **2004**, *346* (2-3), 195-198.
14. Zhang, R.; Yu, W.-Y.; Che, C.-M., Catalytic enantioselective oxidation of aromatic hydrocarbons with D_4 -symmetric chiral ruthenium porphyrin catalysts. *Tetrahedron: Asymmetry* **2005**, *16* (21), 3520-3526.
15. Murahashi, S.-I.; Noji, S.; Hirabayashi, T.; Komiya, N., Manganese-catalyzed enantioselective oxidation of C–H bonds of alkanes and silyl ethers to optically active ketones. *Tetrahedron: Asymmetry* **2005**, *16* (21), 3527-3535.
16. Le Maux, P.; Srouf, H. F.; Simonneaux, G., Enantioselective water-soluble iron–porphyrin-catalyzed epoxidation with aqueous hydrogen peroxide and hydroxylation with iodobenzene diacetate. *Tetrahedron* **2012**, *68* (29), 5824-5828.
17. Burg, F.; Gicquel, M.; Breitenlechner, S.; Pöthig, A.; Bach, T., Site- and Enantioselective C–H Oxygenation Catalyzed by a Chiral Manganese Porphyrin Complex with a Remote Binding Site. *Angew. Chem. Int. Ed.* **2018**, *57* (11), 2953-2957.
18. Burg, F.; Breitenlechner, S.; Jandl, C.; Bach, T., Enantioselective oxygenation of exocyclic methylene groups by a manganese porphyrin catalyst with a chiral recognition site. *Chem. Sci.* **2020**, *11* (8), 2121-2129.
19. Nagataki, T.; Tachi, Y.; Itoh, S., Synthesis, characterization, and catalytic oxygenation activity of dinuclear iron(III) complex supported by binaphthol-containing chiral ligand. *J. Mol. Catal. A: Chem.* **2005**, *225* (1), 103-109.
20. Mekmouche, Y.; Duboc-Toia, C.; Ménage, S.; Lambeaux, C.; Fontecave, M., Hydroxylation of alkanes catalysed by a chiral μ -oxo diferric complex: a metal-based mechanism. *J. Mol. Catal. A: Chem.* **2000**, *156* (1-2), 85-89.
21. Milan, M.; Bietti, M.; Costas, M., Highly enantioselective oxidation of nonactivated aliphatic C–H bonds with hydrogen peroxide catalyzed by manganese complexes. *ACS Cent. Sci.* **2017**, *3* (3), 196-204.
22. Olivo, G.; Cussó, O.; Costas, M., Biologically inspired C–H and C=C oxidations with hydrogen peroxide catalyzed by iron coordination complexes. *Chem. Asian J.* **2016**, *11* (22), 3148-3158.
23. Olivo, G.; Cussó, O.; Borrell, M.; Costas, M., Oxidation of alkane and alkene moieties with biologically inspired nonheme iron catalysts and hydrogen peroxide: from free radicals to stereoselective transformations. *J. Biol. Inorg. Chem.* **2017**, *22* (2), 425-452.
24. Talsi, E. P.; Samsonenko, D. G.; Bryliakov, K. P., Asymmetric autoamplification in the oxidative kinetic resolution of secondary benzylic alcohols catalyzed by manganese complexes. *ChemCatChem* **2017**, *9* (13), 2599-2607.
25. Milan, M.; Bietti, M.; Costas, M., Aliphatic C–H Bond Oxidation with Hydrogen Peroxide Catalyzed by Manganese Complexes: Directing Selectivity through Torsional Effects. *Org. Lett.* **2018**, *20* (9), 2720-2723.
26. Ottenbacher, R. V.; Talsi, E. P.; Rybalova, T. V.; Bryliakov, K. P., Enantioselective Benzylic Hydroxylation of Arylalkanes with H_2O_2 in Fluorinated Alcohols in the Presence of Chiral Mn Aminopyridine Complexes. *ChemCatChem* **2018**, *10* (22), 5323-5330.

27. Qiu, B.; Xu, D.; Sun, Q.; Miao, C.; Lee, Y.-M.; Li, X.-X.; Nam, W.; Sun, W., Highly enantioselective oxidation of spirocyclic hydrocarbons by bioinspired manganese catalysts and hydrogen peroxide. *ACS Catal.* **2018**, *8* (3), 2479-2487.
28. Qiu, B.; Xu, D.; Sun, Q.; Lin, J.; Sun, W., Manganese-catalyzed asymmetric oxidation of methylene C–H of spirocyclic oxindoles and dihydroquinolinones with hydrogen peroxide. *Org. Lett.* **2019**, *21* (3), 618-622.
29. Li, X.-X.; Guo, M.; Qiu, B.; Cho, K.-B.; Sun, W.; Nam, W., High-Spin Mn(V)-Oxo Intermediate in Nonheme Manganese Complex-Catalyzed Alkane Hydroxylation Reaction: Experimental and Theoretical Approach. *Inorg. Chem.* **2019**, *58* (21), 14842-14852.
30. Cianfanelli, M.; Olivo, G.; Milan, M.; Klein Gebbink, R. J. M.; Ribas, X.; Bietti, M.; Costas, M., Enantioselective C–H Lactonization of Unactivated Methylens Directed by Carboxylic Acids. *J. Am. Chem. Soc.* **2019**, *142* (3), 1584-1593.
31. Sun, Q.; Sun, W., Catalytic Enantioselective Methylene C(sp³)–H Hydroxylation Using a Chiral Manganese Complex/Carboxylic Acid System. *Org. Lett.* **2020**, *22*, 9529–9533.
32. Ottenbacher, R. V.; Talsi, E. P.; Bryliakov, K. P., Highly Enantioselective Undirected Catalytic Hydroxylation of Benzylic CH₂ Groups with H₂O₂. *J. Catal.* **2020**, *390*, 170-177.
33. Ottenbacher, R. V.; Bryliakova, A. A.; Shashkov, M. V.; Talsi, E. P.; Bryliakov, K. P., To Rebound or... Rebound? Evidence for the “Alternative Rebound” Mechanism in C–H Oxidations by the Systems Nonheme Mn Complex/H₂O₂/Carboxylic Acid. *ACS Catal.* **2021**, *11*, 5517-5524.
34. Vicens, L.; Bietti, M.; Costas, M., General Access to Modified α -Amino Acids by Bioinspired Stereoselective γ -C–H Bond Lactonization. *Angew. Chem. Int. Ed.* **2021**, *60* (9), 4740-4746.
35. Bryliakov, K. P., Catalytic asymmetric oxygenations with the environmentally benign oxidants H₂O₂ and O₂. *Chem. Rev.* **2017**, *117* (17), 11406-11459.
36. Milan, M.; Bietti, M.; Costas, M., Enantioselective aliphatic C–H bond oxidation catalyzed by bioinspired complexes. *Chem. Commun.* **2018**, *54* (69), 9559-9570.
37. Vicens, L.; Olivo, G.; Costas, M., Rational Design of Bioinspired Catalysts for Selective Oxidations. *ACS Catal.* **2020**, *10* (15), 8611-8631.
38. Ottenbacher, R. V.; Talsi, E. P.; Bryliakov, K. P., Chiral Manganese Aminopyridine Complexes: the Versatile Catalysts of Chemo- and Stereoselective Oxidations with H₂O₂. *Chem. Rec.* **2018**, *18* (1), 78-90.
39. Wu, M.; Wang, B.; Wang, S.; Xia, C.; Sun, W., Asymmetric epoxidation of olefins with chiral bioinspired manganese complexes. *Org. Lett.* **2009**, *11* (16), 3622-3625.
40. Ottenbacher, R. V.; Bryliakov, K. P.; Talsi, E. P., Non-Heme Manganese Complexes Catalyzed Asymmetric Epoxidation of Olefins by Peracetic Acid and Hydrogen Peroxide. *Adv. Synth. Catal.* **2011**, *353* (6), 885-889.
41. Garcia-Bosch, I.; Gomez, L.; Polo, A.; Ribas, X.; Costas, M., Stereoselective Epoxidation of Alkenes with Hydrogen Peroxide using a Bipyrrrolidine-Based Family of Manganese Complexes. *Adv. Synth. Catal.* **2012**, *354* (1), 65-70.
42. Lyakin, O. Y.; Ottenbacher, R. V.; Bryliakov, K. P.; Talsi, E. P., Asymmetric epoxidations with H₂O₂ on Fe and Mn aminopyridine catalysts: probing the nature of active species by combined electron paramagnetic resonance and enantioselectivity study. *ACS Catal.* **2012**, *2* (6), 1196-1202.

43. Cussó, O.; Garcia-Bosch, I.; Font, D.; Ribas, X.; Lloret-Fillol, J.; Costas, M., Highly stereoselective epoxidation with H₂O₂ catalyzed by electron-rich aminopyridine manganese catalysts. *Org. Lett.* **2013**, *15* (24), 6158-6161.
44. Maity, N. C.; Bera, P. K.; Ghosh, D.; Abdi, S. H.; Kureshy, R. I.; Noor-ul, H. K.; Bajaj, H. C.; Suresh, E., Manganese complexes with non-porphyrin N₄ ligands as recyclable catalyst for the asymmetric epoxidation of olefins. *Catal. Sci. Technol.* **2014**, *4* (1), 208-217.
45. Ottenbacher, R. V.; Samsonenko, D. G.; Talsi, E. P.; Bryliakov, K. P., Highly enantioselective bioinspired epoxidation of electron-deficient olefins with H₂O₂ on aminopyridine Mn catalysts. *ACS Catal.* **2014**, *4* (5), 1599-1606.
46. Shen, D.; Miao, C.; Wang, S.; Xia, C.; Sun, W., A mononuclear manganese complex of a tetradentate nitrogen ligand—synthesis, characterizations, and application in the asymmetric epoxidation of olefins. *Eur. J. Inorg. Chem.* **2014**, *2014* (33), 5777-5782.
47. Miao, C.; Wang, B.; Wang, Y.; Xia, C.; Lee, Y.-M.; Nam, W.; Sun, W., Proton-promoted and anion-enhanced epoxidation of olefins by hydrogen peroxide in the presence of nonheme manganese catalysts. *J. Am. Chem. Soc.* **2016**, *138* (3), 936-943.
48. Ottenbacher, R. V.; Samsonenko, D. G.; Talsi, E. P.; Bryliakov, K. P., Enantioselective epoxidations of olefins with various oxidants on bioinspired Mn complexes: evidence for different mechanisms and chiral additive amplification. *ACS Catal.* **2016**, *6* (2), 979-988.
49. Shen, D.; Qiu, B.; Xu, D.; Miao, C.; Xia, C.; Sun, W., Enantioselective epoxidation of olefins with H₂O₂ catalyzed by bioinspired aminopyridine manganese complexes. *Org. Lett.* **2016**, *18* (3), 372-375.
50. Chen, X.; Gao, B.; Su, Y.; Huang, H., Enantioselective Epoxidation of Electron-Deficient Alkenes Catalyzed by Manganese Complexes with Chiral N₄ Ligands Derived from Rigid Chiral Diamines. *Adv. Synth. Catal.* **2017**, *359* (15), 2535-2541.
51. Du, J.; Miao, C.; Xia, C.; Lee, Y.-M.; Nam, W.; Sun, W., Mechanistic insights into the enantioselective epoxidation of olefins by bioinspired manganese complexes: role of carboxylic acid and nature of active oxidant. *ACS Catal.* **2018**, *8* (5), 4528-4538.
52. Wang, W.; Sun, Q.; Xia, C.; Sun, W., Enantioselective epoxidation of olefins with hydrogen peroxide catalyzed by bioinspired aminopyridine manganese complexes derived from L-proline. *Chin. J. Chem.* **2018**, *39* (9), 1463-1469.
53. Clarasó, C.; Vicens, L.; Polo, A.; Costas, M., Enantioselective Epoxidation of β, β -Disubstituted Enamides with a Manganese Catalyst and Aqueous Hydrogen Peroxide. *Org. Lett.* **2019**, *21* (7), 2430-2435.
54. Xu, D.; Sun, Q.; Lin, J.; Sun, W., Ligand regulation for manganese-catalyzed enantioselective epoxidation of olefins without acid. *Chem. Commun.* **2020**, *56* (86), 13101-13104.
55. Ottenbacher, R.; Kurganskiy, V.; Talsi, E.; Bryliakov, K. P., Manganese Catalyzed Enantioselective Epoxidation of α, β -Unsaturated Amides with H₂O₂. *Adv. Synth. Catal.* **2021**, *363*, 2778-2782.
56. Wu, M.; Miao, C. X.; Wang, S.; Hu, X.; Xia, C.; Kuehn, F. E.; Sun, W., Chiral Bioinspired Non-Heme Iron Complexes for Enantioselective Epoxidation of α, β -Unsaturated Ketones. *Adv. Synth. Catal.* **2011**, *353* (16), 3014-3022.
57. Cussó, O.; Garcia-Bosch, I.; Ribas, X.; Lloret-Fillol, J.; Costas, M., Asymmetric epoxidation with H₂O₂ by manipulating the electronic properties of non-heme iron catalysts. *J. Am. Chem. Soc.* **2013**, *135* (39), 14871-14878.

58. Cussó, O.; Ribas, X.; Lloret-Fillol, J.; Costas, M., Synergistic Interplay of a Non-Heme Iron Catalyst and Amino Acid Coligands in H₂O₂ Activation for Asymmetric Epoxidation of α -Alkyl-Substituted Styrenes. *Angew. Chem. Int. Ed.* **2015**, *54* (9), 2729-2733.
59. Cussó, O.; Cianfanelli, M.; Ribas, X.; Klein Gebbink, R. J. M.; Costas, M., Iron catalyzed highly enantioselective epoxidation of cyclic aliphatic enones with aqueous H₂O₂. *J. Am. Chem. Soc.* **2016**, *138* (8), 2732-2738.
60. Zima, A. M.; Lyakin, O. Y.; Ottenbacher, R. V.; Bryliakov, K. P.; Talsi, E. P., Dramatic effect of carboxylic acid on the electronic structure of the active species in Fe(PDP)-catalyzed asymmetric epoxidation. *ACS Catal.* **2016**, *6* (8), 5399-5404.
61. Wang, W.; Sun, Q.; Xu, D.; Xia, C.; Sun, W., Asymmetric Epoxidation of Olefins with H₂O₂ Catalyzed by a Bioinspired Aminopyridine N₄ Iron Complex. *ChemCatChem* **2017**, *9* (3), 420-424.
62. Cussó, O.; Ribas, X.; Costas, M., Biologically inspired non-heme iron-catalysts for asymmetric epoxidation; design principles and perspectives. *Chem. Commun.* **2015**, *51* (76), 14285-14298.
63. Chen, J.; Jiang, Z.; Fukuzumi, S.; Nam, W.; Wang, B., Artificial nonheme iron and manganese oxygenases for enantioselective olefin epoxidation and alkane hydroxylation reactions. *Coord. Chem. Rev.* **2020**, *421*, 213443.
64. Roberts, B. P., Polarity-reversal catalysis of hydrogen-atom abstraction reactions: concepts and applications in organic chemistry. *Chem. Soc. Rev.* **1999**, *28* (1), 25-35.
65. Salamone, M.; Bietti, M., Tuning reactivity and selectivity in hydrogen atom transfer from aliphatic C-H bonds to alkoxy radicals: role of structural and medium effects. *Acc. Chem. Res.* **2015**, *48* (11), 2895-2903.
66. Wang, D.; Shuler, W. G.; Pierce, C. J.; Hilinski, M. K., An iminium salt organocatalyst for selective aliphatic C-H hydroxylation. *Org. Lett.* **2016**, *18* (15), 3826-3829.
67. Gaster, E.; Kozuch, S.; Pappo, D., Selective Aerobic Oxidation of Methylarenes to Benzaldehydes Catalyzed by N-Hydroxyphthalimide and Cobalt(II) Acetate in Hexafluoropropan-2-ol. *Angew. Chem. Int. Ed.* **2017**, *56* (21), 5912-5915.
68. Dantignana, V.; Milan, M.; Cussó, O.; Company, A.; Bietti, M.; Costas, M., Chemoselective Aliphatic C-H Bond Oxidation Enabled by Polarity Reversal. *ACS Cent. Sci.* **2017**, *3* (12), 1350-1358.
69. Lumb, J. P., Stopping aerobic oxidation in its tracks: chemoselective synthesis of benzaldehydes from methylarenes. *Angew. Chem. Int. Ed.* **2017**, *56* (32), 9276-9277.
70. Borrell, M.; Gil-Caballero, S.; Bietti, M.; Costas, M., Site-Selective and Product Chemoselective Aliphatic C-H Bond Hydroxylation of Polyhydroxylated Substrates. *ACS Catal.* **2020**, *10* (8), 4702-4709.
71. Masferrer-Rius, E.; Hopman, R. M.; van der Kleij, J.; Lutz, M.; Klein Gebbink, R. J. M., On the Ability of Nickel Complexes Derived from Tripodal Aminopyridine Ligands to Catalyze Arene Hydroxylations. *CHIMIA* **2020**, *74* (6), 489-494.
72. Talsi, E. P.; Samsonenko, D. G.; Ottenbacher, R. V.; Bryliakov, K. P., Highly Enantioselective C-H Oxidation of Arylalkanes with H₂O₂ in the Presence of Chiral Mn-Aminopyridine Complexes. *ChemCatChem* **2017**, *9* (24), 4580-4586.
73. Masferrer-Rius, E.; Borrell, M.; Lutz, M.; Costas, M.; Klein Gebbink, R. J. M., Aromatic C-H Hydroxylation Reactions with Hydrogen Peroxide Catalyzed by Bulky Manganese Complexes. *Adv. Synth. Catal.* **2021**, *363*, 3783-3795.

74. Zima, A. M.; Lyakin, O. Y.; Bushmin, D. S.; Soshnikov, I. E.; Bryliakov, K. P.; Talsi, E. P., Non-heme perferryl intermediates: Effect of spin state on the epoxidation enantioselectivity. *Molecular Catalysis* **2021**, *502*, 111403.
75. Zima, A. M.; Lyakin, O. Y.; Bryliakov, K. P.; Talsi, E. P., Low-Spin and High-Spin Perferryl Intermediates in Non-Heme Iron Catalyzed Oxidations of Aliphatic C–H Groups. *Chem. Eur. J.* **2021**, *27* (28), 7781-7788.
76. Olivo, G.; Lanzalunga, O.; Mandolini, L.; Di Stefano, S., Substituent effects on the catalytic activity of bipyrrrolidine-based iron complexes. *J. Org. Chem.* **2013**, *78* (22), 11508-11512.
77. Kaljurand, I.; Kütt, A.; Sooväli, L.; Rodima, T.; Mäemets, V.; Leito, I.; Koppel, I. A., Extension of the self-consistent spectrophotometric basicity scale in acetonitrile to a full span of 28pK_a units: unification of different basicity scales. *J. Org. Chem.* **2005**, *70* (3), 1019-1028.
78. Malecki, J. G.; Maroń, A., Chloride and pseudohalide hydride-carbonyl ruthenium(II) complexes with 4-pyrrolidinopyridine as co-ligand. *Transition Met. Chem.* **2013**, *38* (2), 133-142.
79. CCDC 2100950-2100951 contain the supplementary crystallographic data for this Chapter. These data can be obtained free of charge from The Cambridge Crystallographic Data Centre via www.ccdc.cam.ac.uk/data_request/cif.
80. Knof, U.; von Zelewsky, A., Predetermined chirality at metal centers. *Angew. Chem. Int. Ed.* **1999**, *38* (3), 302-322.
81. Zang, Y.; Kim, J.; Dong, Y.; Wilkinson, E. C.; Appelman, E. H.; Que, L., Models for nonheme iron intermediates: Structural basis for tuning the spin states of Fe(TPA) complexes. *J. Am. Chem. Soc.* **1997**, *119* (18), 4197-4205.
82. Yazerski, V. A.; Spannring, P.; Gatineau, D.; Woerde, C. H.; Wieclawska, S. M.; Lutz, M.; Kleijn, H.; Klein Gebbink, R. J. M., Making Fe(BPBP)-catalyzed C–H and C=C oxidations more affordable. *Org. Biomol. Chem.* **2014**, *12* (13), 2062-2070.
83. Wang, B.; Miao, C.; Wang, S.; Xia, C.; Sun, W., Manganese Catalysts with C₁-Symmetric N₄ Ligand for Enantioselective Epoxidation of Olefins. *Chem. Eur. J.* **2012**, *18* (22), 6750-6753.
84. Wang, B.; Wang, S.; Xia, C.; Sun, W., Highly Enantioselective Epoxidation of Multisubstituted Enones Catalyzed by Non-Heme Iron Catalysts. *Chem. Eur. J.* **2012**, *18* (24), 7332-7335.
85. Ottenbacher, R. V.; Talsi, E. P.; Bryliakov, K. P., Mechanism of selective C–H hydroxylation mediated by manganese aminopyridine enzyme models. *ACS Catal.* **2015**, *5* (1), 39-44.
86. Talsi, E. P.; Ottenbacher, R. V.; Bryliakov, K. P., Bioinspired oxidations of aliphatic C–H groups with H₂O₂ in the presence of manganese complexes. *J. Organomet. Chem.* **2015**, *793*, 102-107.
87. Sun, W.; Sun, Q., Bioinspired manganese and Iron complexes for enantioselective oxidation reactions: ligand design, catalytic activity, and beyond. *Acc. Chem. Res.* **2019**, *52* (8), 2370-2381.
88. Lyakin, O. Y.; Zima, A. M.; Tkachenko, N. V.; Bryliakov, K. P.; Talsi, E. P., Direct Evaluation of the Reactivity of Nonheme Iron(V)–Oxo Intermediates toward Arenes. *ACS Catal.* **2018**, *8* (6), 5255-5260.
89. Tkachenko, N. V.; Ottenbacher, R. V.; Lyakin, O. Y.; Zima, A. M.; Samsonenko, D. G.; Talsi, E. P.; Bryliakov, K. P., Highly Efficient Aromatic C–H Oxidation with H₂O₂ in the Presence of Iron Complexes of the PDP Family. *ChemCatChem* **2018**, *10* (18), 4052-4057.

90. Tkachenko, N. V.; Lyakin, O. Y.; Zima, A. M.; Talsi, E. P.; Bryliakov, K. P., Effect of different carboxylic acids on the aromatic hydroxylation with H₂O₂ in the presence of an iron aminopyridine complex. *J. Organomet. Chem.* **2018**, *871*, 130-134.
91. Zima, A. M.; Lyakin, O. Y.; Lubov, D. P.; Bryliakov, K. P.; Talsi, E. P., Aromatic C–H oxidation by non-heme iron(V)-oxo intermediates bearing aminopyridine ligands. *Molecular Catalysis* **2020**, *483*, 110708.
92. Mitra, M.; Cussó, O.; Bhat, S. S.; Sun, M.; Cianfanelli, M.; Costas, M.; Nordlander, E., Highly enantioselective epoxidation of olefins by H₂O₂ catalyzed by a non-heme Fe(II) catalyst of a chiral tetradentate ligand. *Dalton Trans.* **2019**, *48* (18), 6123-6131.
93. Talsi, E. P.; Bryliakov, K. P., Chemo- and stereoselective C–H oxidations and epoxidations/*cis*-dihydroxylations with H₂O₂, catalyzed by non-heme iron and manganese complexes. *Coord. Chem. Rev.* **2012**, *256* (13-14), 1418-1434.
94. Bryliakov, K. P.; Talsi, E. P., Active sites and mechanisms of bioinspired oxidation with H₂O₂, catalyzed by non-heme Fe and related Mn complexes. *Coord. Chem. Rev.* **2014**, *276*, 73-96.
95. Chen, J.; Klein Gebbink, R. J. M., Deuterated N₂Py₂ Ligands: Building More Robust Non-Heme Iron Oxidation Catalysts. *ACS Catal.* **2019**, *9* (4), 3564-3575.
96. Bukowski, M. R.; Zhu, S.; Koehntop, K. D.; Brennessel, W. W.; Que, L., Characterization of an Fe^{III}-OOH species and its decomposition product in a bleomycin model system. *JBIC, J. Biol. Inorg. Chem.* **2004**, *9* (1), 39-48.
97. Pijper, D.; Saisaha, P.; de Boer, J. W.; Hoen, R.; Smit, C.; Meetsma, A.; Hage, R.; van Summeren, R. P.; Alsters, P. L.; Feringa, B. L., The unexpected role of pyridine-2-carboxylic acid in manganese based oxidation catalysis with pyridin-2-yl based ligands. *Dalton Trans.* **2010**, *39* (43), 10375-10381.
98. Miao, C.; Li, X.-X.; Lee, Y.-M.; Xia, C.; Wang, Y.; Nam, W.; Sun, W., Manganese complex-catalyzed oxidation and oxidative kinetic resolution of secondary alcohols by hydrogen peroxide. *Chem. Sci.* **2017**, *8* (11), 7476-7482.
99. Luo, Y.-R., *Comprehensive Handbook of Chemical Bond Energies*. CRC press: Boca Raton, FL: 2007.
100. Comba, P.; Morgen, M.; Wadepohl, H., Tuning of the properties of transition-metal bispidine complexes by variation of the basicity of the aromatic donor groups. *Inorg. Chem.* **2013**, *52* (11), 6481-6501.
101. Schreurs, A. M. M.; Xian, X.; Kroon-Batenburg, L. M. J., EVAL15: a diffraction data integration method based on ab initio predicted profiles. *J. Appl. Cryst.* **2010**, *43* (1), 70-82.
102. Sheldrick, G. M., SADABS. Universität Göttingen, Germany. **2014**.
103. Sheldrick, G. M., SHELXT—Integrated space-group and crystal-structure determination. *Acta Cryst.* **2015**, *A71*, 3-8.
104. Sheldrick, G. M., Crystal structure refinement with SHELXL. *Acta Cryst.* **2015**, *C71* (1), 3-8.
105. Parsons, S.; Flack, H. D.; Wagner, T., Use of intensity quotients and differences in absolute structure refinement. *Acta Cryst.* **2013**, *B69* (3), 249-259.
106. Spek, A. L., Structure validation in chemical crystallography. *Acta Cryst.* **2009**, *D65* (2), 148-155.

Chapter 6

An Experimental and Computational Study on Tetradentate Imidazole-based Manganese Complexes for Oxidation Catalysis

Abstract

A novel family of tetradentate amino-imidazole ligands that comprise bulky diphenylimidazole moieties was synthesized and characterized. Complexation reactions of the ligands to manganese(II) and iron(II) ions have been explored experimentally and computationally. The study shows that C_2 -symmetric manganese complexes (*S,S*)-**1** and (*S,S*)-**2**, based on diphenylimidazole moieties, are not synthetically accessible, presumably due to an increased steric demand of the ligand. In contrast, C_1 -symmetric manganese complex, (*S,S*)-**3**, comprising a combination of a diphenylimidazole and a bulky pyridine moiety has been successfully synthesized. Imidazole-based manganese complex (*S,S*)-**3** did not show activity in arene oxidation catalysis using H_2O_2 as benign oxidant, whereas the previously reported complexes (*S,S*)-[Mn(^{Bz}bpmcn)] and (*S,S*)-[Mn(^{Bz}bpbp)] are active towards the generation of phenol products. This observation might be a stimulus to further explore imidazole-based ligands in non-heme oxidation catalysis.

This chapter is based on:

Masferrer-Rius, E.; Sansores-Paredes, M. L. G.; Klein Gebbink, R. J. M. *Manuscript in preparation*

6.1 Introduction

The development of bioinspired first-row transition metal complexes for oxidation catalysis has been an important research field in the past decades. In particular, chemists have focused their attention towards mimicking non-heme enzymes, which are usually based on iron, copper or manganese and often comprise histidine residues that coordinate to the central metal(s) in their active site.¹⁻³ In most of the cases, the final goal in these studies has been the application of the bioinspired metal complexes as effective catalysts for oxidation reactions making use of the benign oxidant H₂O₂, such as asymmetric epoxidation, enantioselective aliphatic C–H oxidation or aromatic oxidation.⁴⁻¹²

Within this context, tetradentate aminopyridine-based iron and manganese complexes have been extensively explored.¹³⁻¹⁶ Particularly, efforts have been devoted to the modification of the amine backbone¹⁷⁻²² or the pyridine heterocycle²³⁻³² of the ligand architecture, whereas the use of other *N*-coordinating heterocycles has been less explored. Along this vein, benzimidazole, quinoline or oxazoline groups have been reported as suitable moieties for the synthesis of tetradentate ligand structures that can coordinate to iron or manganese.^{7, 23, 33-36}

Benzimidazole-containing ligands have been, by far, the most explored alternative for the heterocyclic moiety in aminopyridine ligands within the framework of metal-based oxidation catalysis.⁷ In 2012, Sun and co-workers reported on *C*₁-symmetric iron and manganese complexes supported by tetradentate amino-benzimidazole ligands based on a chiral proline backbone, that catalyze asymmetric epoxidation reactions with aqueous H₂O₂ (see Figure 1, Mn(*S*-PEB) and Fe(*S*-PEB)).^{18, 37} The Mn(*S*-PEB) complex is also an effective catalyst for aliphatic oxidations to generate ketone products, as well as for the oxidation of alcohols to ketones.^{38, 39} In 2018, Sun and co-workers also reported on the catalytic activity of Mn(*S*-PEB) for the enantioselective benzylic oxidation of spirocyclic hydrocarbons, generating the ketone products with up to 94% yield and 98% ee.^{40, 41} In a later study, the substrate scope of these reactions was expanded to include the enantioselective oxidation of oxindoles and dihydroquinolinones, with up to 67% yield and 99% ee.⁴² The Mn(*S*-PEB) complex also catalyzes the enantioselective benzylic oxidation of methylene C–H bonds of indane-based substrates to reach up to 78% yield and 95% ee for the alcohol product, employing fluorinated alcohol solvents.⁴³ The same research group has described the synthesis of bpmcn- and bpbp-type ligands containing benzimidazole groups as well (bpmcn = *N,N'*-dimethyl-*N,N'*-bis(2-picolyl)-cyclohexane-*trans*-1,2-diamine; bpbp = *N,N'*-bis(2-pyridylmethyl)-2,2'-bipyrrrolidine), and reported that the corresponding iron and manganese complexes are catalytically active in the enantioselective epoxidation of alkenes with H₂O₂ (see Figure 1, (*R,R*)-[Mn(^{Bz}bpmcn)] and (*R,R*)-[Mn(^{Bz}bpbp)]).^{44, 45} Besides the PEB-based complexes, a number of other *C*₁-symmetric manganese and iron complexes derived from a tetradentate

ligand containing a benzimidazole ring have been described in the literature. For example, manganese complexes combining a benzimidazole and a pyridine moiety were described as active catalysts for aliphatic C–H oxidation reactions (see Figure 1, (R,R) -[Mn(^{Bz},Pybpmcn)] or (R,R) -[Mn(^{Bz},NMe₂bpmcn)]).⁴⁶ Remarkable, Costas, Klein Gebbink and co-workers described a non-symmetric iron complex comprising a benzimidazole moiety in combination with a bulky pyridine moiety, which was found to be an efficient catalyst for the challenging enantioselective epoxidation of cyclic aliphatic enones with H₂O₂ (see Figure 1, (S,S) -[Mn(^{Bz},TIPSBpbbp)]).³³ Nevertheless and to the best of our knowledge, no examples of reactivity of amino-benzimidazole-based complexes in the oxidation of aromatic substrates have ever been reported.

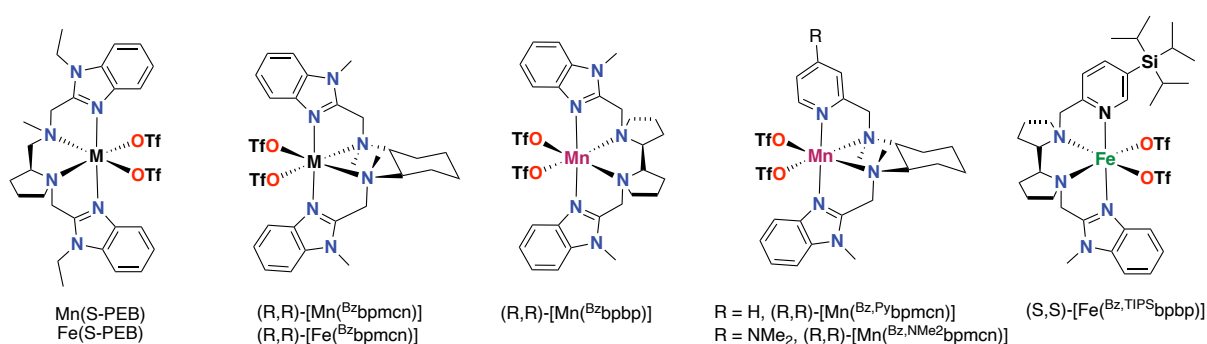


Figure 1. Examples of manganese and iron complexes supported by tetradentate amino-benzimidazole ligands.^{18, 33, 37, 44-46}

In Chapter 3 of this thesis, we have explored the use of bulky aminopyridine-based manganese complexes bearing triisopropylsilyl (TIPS) substituents on the pyridine moieties in aromatic oxidation reactions. These complexes were found to show a significant enhancement in catalytic activity and selectivity for the formation of phenol products (up to 37% yield) compared to the parent amino-pyridine complexes, by preventing product inhibition through phenolate binding.⁴⁷

Using the same concept of including steric bulk in the amino-pyridine ligand, we have set out to explore the development of bulky amino-imidazole ligands and their corresponding manganese and iron complexes. To this end, we have designed three modified versions of tetradentate amino-imidazole ligands that bear two phenyl substituents on each imidazole ring (see Figure 2, ligands **L1**, **L2** and **L3**). Most importantly, the idea was to create a set of ligands that are more bulky with respect to their parent benzimidazole-based ligands (*cf.*, ligands ^{Bz}bpmcn, ^{Bz}bpbbp, ^{Bz},TIPSBpbbp, resp.; Figure 1), which could serve as the starting point for more efficient arene oxidation catalysts that suffer less from product inhibition.⁴⁷ Accordingly, we describe the synthesis of ligands **L1-L3** in this chapter, along with experimental and computational studies on the complexation of these ligands to manganese and iron salts.

Moreover, the reactivity of the successfully synthesized complexes has been explored in the field of oxidation catalysis using H_2O_2 as benign oxidant.

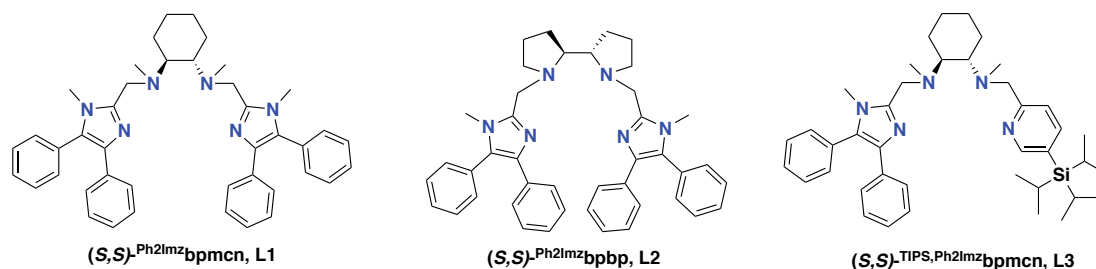


Figure 2. Overview of the amino-imidazole ligands explored in this chapter.

6.2. Results and Discussion

6.2.1 Synthesis and Characterization of Bulky Amino-Imidazole Ligands

For the synthesis of the new C_2 -symmetric ligands **L1** and **L2** it was necessary to first prepare the corresponding imidazole synthon **7**. For its preparation, a synthesis based on four reaction steps was followed (Figure 3a). The first reaction consisted of the methylation of 4,5-diphenylimidazole using iodomethane, which afforded the desired product **4** in 81% yield. Next, **4** was lithiated using *n*-BuLi, and subsequently reacted with DMF to generate the aldehyde product **5** in an excellent yield of 91%. Reduction of the aldehyde to alcohol product **6** was then performed using NaBH_4 , which proceeded in 72% yield. The final step was based on a reaction of the alcohol compound with SOCl_2 to form the desired imidazole synthon **7** in 70% yield.

Ligands **L1** and **L2** were then prepared by the reaction of two equiv. of the synthon **7** with one equiv. of the corresponding amine backbone (99% and 60% yield for **L1** and **L2**, respectively) (Figure 3b). Both ligands were characterized by ^1H NMR and ^{13}C NMR spectroscopy, and HRMS analysis (see Experimental Section for further details). A different synthetic strategy was followed for ligand **L3** (see Figure 3c). In this case amina **8** was synthesized first, by reaction of (S,S) -*N,N'*-dimethyl-1,2-diaminocyclohexane with TIPS-PyCHO ²⁸ following a protocol previously described by Costas and co-workers.⁴⁸ In the next step, **8** was reacted with sodium cyanoborohydride in the presence of trifluoroacetic acid to provide pyridyl diamine **9** in >99% yield. Finally, treatment of compound **11** with **7** in the presence of sodium triacetoxyborohydride resulted in the desired ligand **L3** in 65% yield. This ligand was also characterized by ^1H NMR and ^{13}C NMR spectroscopy, and HRMS analysis (see Experimental Section for further details).

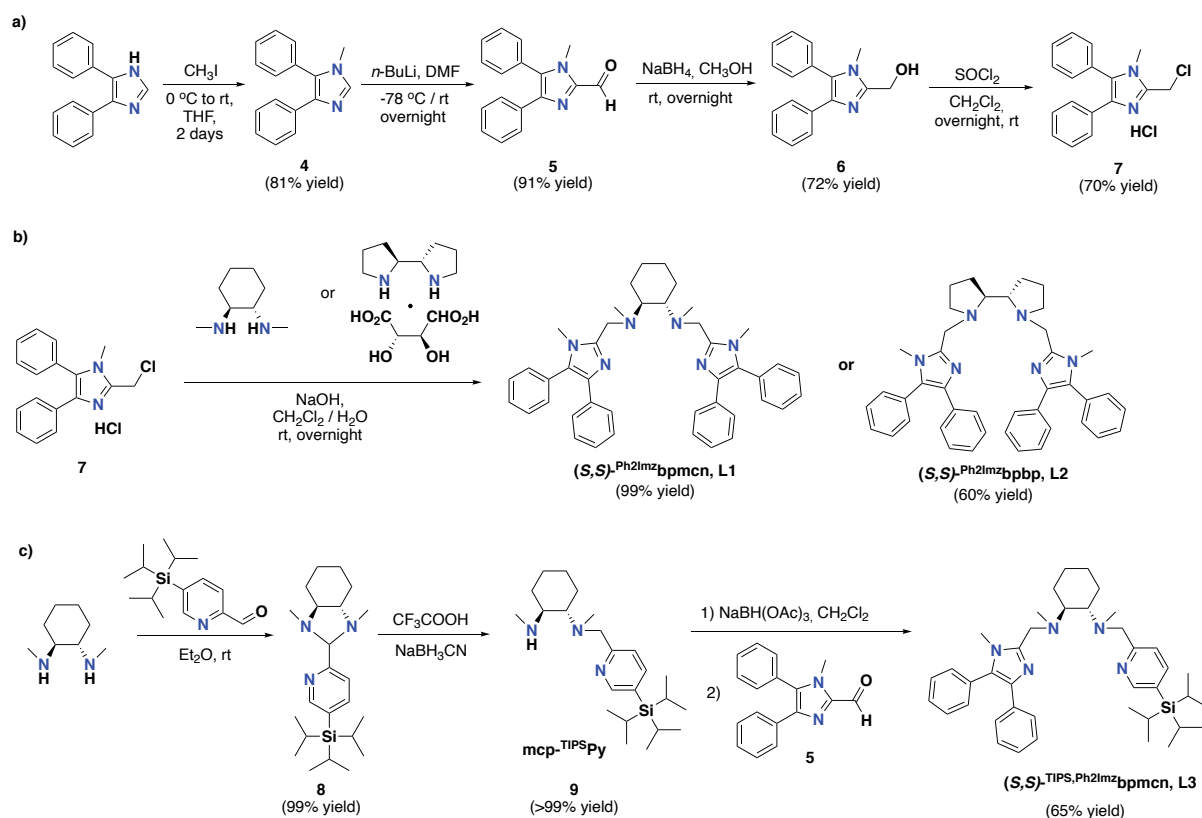


Figure 3. a) Synthesis of imidazole synthon **7**. b) Synthesis of tetradentate amino-imidazole ligands **L1** and **L2**. c) Synthesis of non-symmetric amino-imidazole ligand **L3**.

6.2.2 Complexation Reactions

Initial complexation reactions were performed by reacting equimolar amounts of the corresponding ligand with $[\text{Mn}^{\text{II}}(\text{OTf})_2]$ under an inert atmosphere at room temperature. The structure of the envisioned manganese complexes is represented in Figure 4. Literature complexes $(S,S)\text{-}[\text{Mn}(\text{B}^z\text{bpmcn})]$ and $(S,S)\text{-}[\text{Mn}(\text{B}^z\text{bpbp})]$, based on the non-bulky amino-benzimidazole ligands B^zbpmcn and B^zbpbp , can be synthesized according to these standard procedures in a rather straightforward manner, as previously reported in the literature.^{44, 45} However, complexation reactions using the new and bulky ligands **L1** and **L2** did not provide the desired manganese complexes $(S,S)\text{-1}$ and $(S,S)\text{-2}$, presumably due to the large steric bulk of the ligand, which possibly makes the complexation to manganese more difficult. HRMS analysis of the crude reaction mixtures showed that the ligand was still present, whereas no peak corresponding to a manganese species could be detected. In contrast, complexation of the bulky C_1 -symmetric ligand **L3** to $[\text{Mn}^{\text{II}}(\text{OTf})_2]$, following the standard procedure, provided the desired manganese complex $(S,S)\text{-3}$ in 42% yield. Characterization of this complex by HRMS showed a prominent mass peak at m/z 839.3298 corresponding to the $[\text{Mn}^{\text{II}}(\text{L3})(\text{OTf})]^+$ ion (calc. 839.3284; see Experimental Section for further details on the synthesis).

geometry optimization of all ligands and complexes studied in this chapter, this time considering the compounds with *R,R* stereochemistry (see Experimental Section for computational details). We have selected this chirality since X-ray crystallographic structures of the manganese complexes based on the benzimidazole ligands with *R,R* chirality are available in the literature.^{44, 45} This approach allowed us to build the starting geometries of all complexes in a more reasonable and representative way.

As the geometry of all complexes were successfully optimized using DFT, we assume that all of them might be synthetically accessible (Figure 5). All computed geometries showed almost fully C_2 -symmetric structures. Selected bond distances and angles are shown in Table 1 and Table 2 and are compared with X-ray crystallographic structures (R,R) -[Mn(**Bz**bp**mcn**)]^{X-ray} and (R,R) -[Mn(**Bz**bp**bp**)]^{X-ray}. From this comparison, it is clear that the experimental and computed data are similar (Table 1), which gives credit to the DFT calculations. Bond distances are similar for all structures considered, with Mn-N_{imidazole} bond distances ranging from 2.18 to 2.28 Å, Mn-N_{amine} bond distances from 2.29 to 2.39 Å, and the Mn-O bond distances from 2.08 to 2.19 Å. Selected angles are also very similar in all complexes studied, with the exception of the O-Mn-O angle which ranged from 98.2 ° for (R,R) -[Mn(**Bz**bp**bp**)], to 110.8 ° for (R,R) -[Mn(**Bz**bp**mcn**)], and 114.1 ° for (S,S) -[Mn(**Bz**bp**mcn**)]. This variation might be attributed to the different rigidity of the amine backbones.

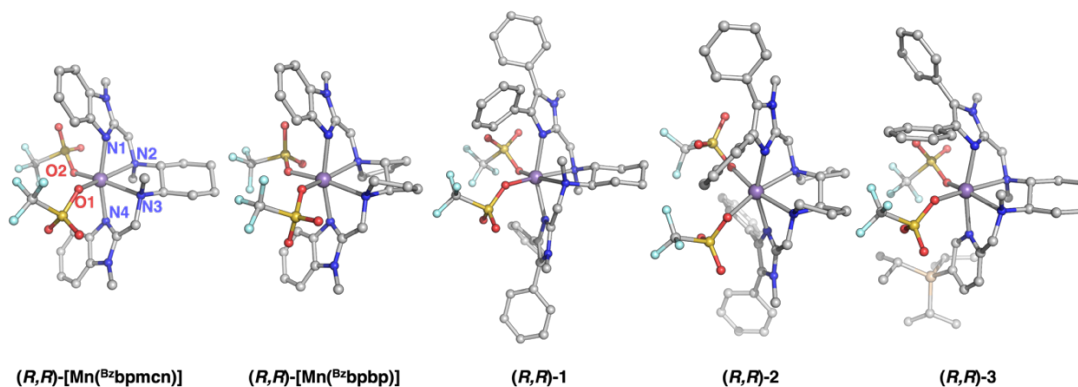


Figure 5. B3LYP-D3BJ/def2TZVP//B3LYP-D3BJ/6-31G(d,p) optimized geometries of complexes (R,R) -[Mn(**Bz**bp**mcn**)], (R,R) -[Mn(**Bz**bp**bp**)], (R,R) -1, (R,R) -2 and (R,R) -3. Structures are represented as sticks and spheres. Hydrogen atoms are omitted for clarity. Labelled atoms are shown for (R,R) -[Mn(**Bz**bp**mcn**)], and the same atom numbering is used for the rest of the complexes.

In order to obtain a more rational insight into the outcome of the complexation reactions, we analyzed the distances between the amino-imidazole ligand and the labile triflate co-ligands in each optimized structure (Figure 6a). In doing so, we have checked for close distances between the imidazole moieties and the triflate groups. For complexes (R,R) -[Mn(**Bz**bp**mcn**)] and (R,R) -[Mn(**Bz**bp**bp**)], we have checked the distance between the carbon atom of the aryl ring of the

Table 1. Selected bond distances (Å) for X-ray crystallographic complexes (R,R) -[Mn(^{Bz}bpmcn)]^{X-ray} ⁴⁴ and (R,R) -[Mn(^{Bz}bpbp)]^{X-ray} ⁴⁵ and computed complexes (R,R) -[Mn(^{Bz}bpmcn)], (S,S) -[Mn(^{Bz}bpmcn)], (R,R) -[Mn(^{Bz}bpbp)], (R,R) -1, (R,R) -2 and (R,R) -3.

	Distances					
	Mn-N1	Mn-N2	Mn-N3	Mn-N4	Mn-O1	Mn-O2
(R,R) -[Mn(^{Bz} bpmcn)] ^{X-ray}	2.244(4)	2.299(3)	2.346(3)	2.221(4)	2.160(3)	2.192(2)
(R,R) -[Mn(^{Bz} bpbp)] ^{X-ray}	2.216(4)	2.303(3)	2.325(3)	2.215(4)	2.155(4)	2.190(3)
(R,R) -[Mn(^{Bz} bpmcn)]	2.182	2.388	2.387	2.185	2.115	2.098
(S,S) -[Mn(^{Bz} bpmcn)]	2.175	2.393	2.392	2.175	2.105	2.105
(R,R) -[Mn(^{Bz} bpbp)]	2.199	2.374	2.348	2.193	2.115	2.113
(R,R) -1	2.281	2.350	2.349	2.282	2.112	2.112
(R,R) -2	2.288	2.330	2.330	2.289	2.109	2.109
(R,R) -3	2.210	2.399	2.328	2.219	2.083	2.120

Table 2. Selected bond angles (°) for X-ray crystallographic complexes (R,R) -[Mn(^{Bz}bpmcn)]^{X-ray} ⁴⁴ and (R,R) -[Mn(^{Bz}bpbp)]^{X-ray} ⁴⁵ and computed complexes (R,R) -[Mn(^{Bz}bpmcn)], (S,S) -[Mn(^{Bz}bpmcn)], (R,R) -[Mn(^{Bz}bpbp)], (R,R) -1, (R,R) -2 and (R,R) -3.

	Angles					
	N1-Mn-N2	N1-Mn-N3	N2-Mn-N3	N2-Mn-N4	N3-Mn-N4	O1-Mn-O2
(R,R) -[Mn(^{Bz} bpmcn)] ^{X-ray}	75.1(1)	98.0(1)	78.2(1)	94.7(1)	74.4(1)	100.3(1)
(R,R) -[Mn(^{Bz} bpbp)] ^{X-ray}	74.0(1)	93.9(1)	78.7(1)	98.0(1)	73.9(1)	100.5(1)
(R,R) -[Mn(^{Bz} bpmcn)]	73.8	94.0	76.8	95.0	73.9	110.8
(S,S) -[Mn(^{Bz} bpmcn)]	74.0	94.2	76.2	94.2	74.0	114.1
(R,R) -[Mn(^{Bz} bpbp)]	73.2	97.0	77.2	91.8	73.7	98.2
(R,R) -1	73.4	89.1	77.9	89.1	73.4	107.6
(R,R) -2	73.1	88.1	78.1	88.1	73.1	106.2
(R,R) -3	74.2	98.2	77.2	90.5	73.9	109.3

benzimidazole group that points towards the triflate groups and the oxygen atom of the triflate directly bound to the metal, which range from 3.23 to 3.37 Å in the computed structures (see Figure 6a). In the experimental structures (R,R) -[Mn(^{Bz}bpmcn)]^{X-ray} and (R,R) -[Mn(^{Bz}bpbp)]^{X-ray}, these distances are slightly longer, ranging from 3.34 to 3.44 Å. However, the closest distances in complexes (R,R) -[Mn(^{Bz}bpmcn)] and (R,R) -[Mn(^{Bz}bpbp)] were found between

one of the oxygens of the triflate that is not directly bound to the metal and the carbon atom located between the two nitrogen atoms of the imidazole ring; these distances are 3.03 and 3.07 Å, respectively (see Figure 6a). In the computed structures of complexes **(R,R)-1** and **(R,R)-2**, these same distances between a non-coordinated triflate oxygen atom and the carbon atom located between the two nitrogen atoms of the diphenylimidazole are also the closest distances between the triflate and imidazole moieties, and were found to be actually slightly shorter than for **(R,R)-[Mn(^{Bz}bpmcn)]** and **(R,R)-[Mn(^{Bz}bpbp)]**, with values of 3.02 and 3.06 Å, respectively. Moreover, the distance between the metal-bound oxygen atom of the triflate group and the ortho-carbon atom of the phenyl substituent of the imidazole group (3.09 Å) is closer than the closest distance between the metal-bound oxygen atom in the structures of **(R,R)-[Mn(^{Bz}bpmcn)]** and **(R,R)-[Mn(^{Bz}bpbp)]**. An additional close distance was found between the meta-carbon atom of a phenyl substituent on the imidazole and one the fluorine atoms of the triflate ligand (3.25 and 3.30 Å). From this analysis, we conclude that ligands **L1** and **L2** are positioned in closer proximity to the triflate groups compared to benzimidazole ligands ^{Bz}bpmcn and ^{Bz}bpbp, indicating the former ligands are bulkier than the latter. Note that all the above-mentioned distances are measured between carbons and heteroatoms, and thus shorter distances might be found when considering the hydrogen atoms directly bound to the carbon. For complex **(R,R)-3** longer proximity distances were found than for the other complexes. The meta-carbon atom of the phenyl substituent is positioned at a distance of 3.60 Å from the metal-bound oxygen atom of the triflate group, whereas a slightly shorter distance of 3.45 Å exists between the central carbon atom of the TIPS group and an oxygen atom of the triflate (see Figure 6a). Accordingly, C₁-symmetric ligand **L3** seems less sterically demanding than the other ligands considered in this study.

In order to further analyze the ability of the ligands to accommodate the manganese ion, superpositions of the calculated structures of the different manganese complexes were then made to compare the shape and occupied space of the ligands around the metal center (Figure 6b). These superpositions were generated using the PyMOL software by fixing the same position of the metal and the carbon and nitrogen atoms of the ligand backbone of two complexes. Superpositions of complexes **(R,R)-[Mn(^{Bz}bpmcn)]** and **(R,R)-1** and of complexes **(R,R)-[Mn(^{Bz}bpbp)]** and **(R,R)-2** corroborate that complexes based on diphenylimidazole moieties are bulkier than the ones based on benzimidazoles. These superpositions show how the phenyl substituents of the imidazoles in complexes **(R,R)-1** and **(R,R)-2** more closely approach the cavity that accommodates the Mn(OTf)₂ moiety. Some further differences are observed in the overall orientation of the azole ring. For instance, in the overlay between complexes **(R,R)-1** and **(R,R)-3**, the azole ring in complex **(R,R)-3** is more bend towards the manganese center than in complex **(R,R)-1**. On the other hand, between complexes **(R,R)-[Mn(^{Bz}bpmcn)]** and **(R,R)-3** there seems to be no real difference between the orientation of the

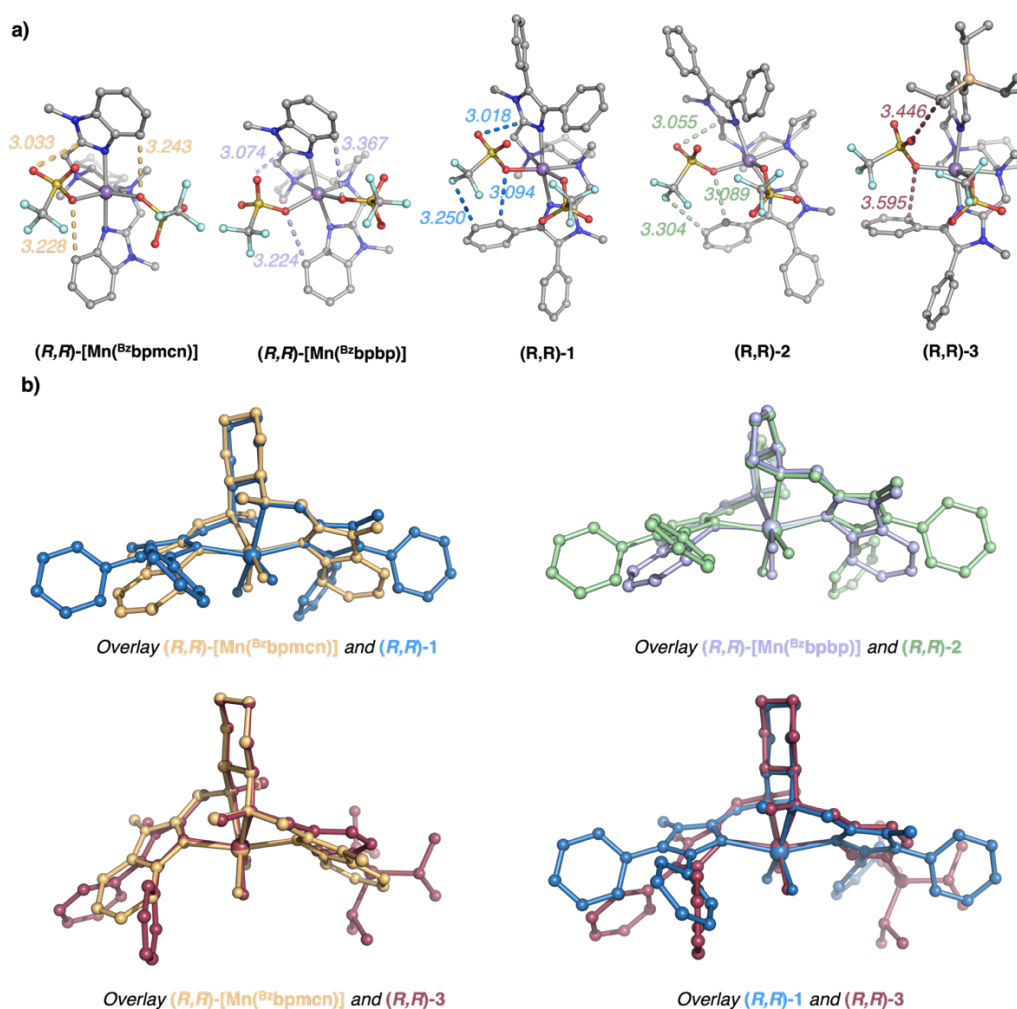


Figure 6. a) Representation of selected distances (Å) between the ligand and the triflate co-ligands in the DFT-optimized geometries of complexes (R,R) -[Mn(^{Bz}bpmcn)], (R,R) -[Mn(^{Bz}bpbp)], (R,R) -1, (R,R) -2 and (R,R) -3. b) Representation of the superposition of different manganese complexes. All optimized geometries are represented as sticks and spheres. Hydrogens are omitted for clarity, whereas only the oxygen atom of the triflate group bound to the metal is shown in b).

azole rings. This observations are corroborated in the overlay between complexes (R,R) -[Mn(^{Bz}bpmcn)] and (R,R) -1, in which the azole rings in (R,R) -[Mn(^{Bz}bpmcn)] are closer to manganese than in (R,R) -1. This comparison seems to imply greater steric stress in structures based on ligand **L1**. Despite the fact that the azole ring in complex (R,R) -1 is less bended towards the manganese, we can see shorter distances between the non-bound oxygens of the triflates and the azole ring in complex (R,R) -1 compared to (R,R) -[Mn(^{Bz}bpmcn)].

Finally, we looked at the thermochemistry of each complexation reaction. It is generally accepted that ligand complexation for high-spin first-row transition metals is fast, and thus one can assume that equilibrium will be reached rapidly. For this reason, transition states were not considered in the current study, and only the thermochemistry of the complexation was

considered (see Figure 7a), although exceptions can occur, and significant barriers might need to be overcome. For instance, in the situation where a multidentate ligand needs to undergo a conformational change during complexation, this can create a significant barrier.

Focusing on the thermodynamics, only the energies of the reactants and the products need to be considered. In this regard, it is worth to mention that we have considered a solvated $\text{Mn}(\text{OTf})_2 \cdot 4\text{CH}_3\text{CN}$ structure as reference (*i.e.* adding explicit solvent), since this is a reasonable solution structure of $\text{Mn}(\text{OTf})_2$. The complexation reaction energies (ΔE) were calculated by subtracting the energy of reactants to products (see Figure 7b). Worthy of note is that we cannot directly interpret the calculated value of a given complexation energy (ΔE), but we should be able to compare different ligands and predict for which ligand the complexation is most favorable. Following this approach, in Figure 7c a representation of the complexation reaction relative energies ($\Delta\Delta E$) for each ligand is shown and referenced to complex **(R,R)-3**. Regarding bpmcn-based complexes, we can see that complex **(R,R)-[Mn(^{Bz}bpmcn)]** is 1.15 kcal/mol less favorable to form than complex **(R,R)-3**. Moreover, complexation to form **(R,R)-1** is 4.30 kcal/mol less favorable than complexation to form **(R,R)-3**. This latter observation (*i.e.* the calculated complexation energy for **(R,R)-1** is higher than for **(R,R)-3**) tells us that computational studies might be in line with our experimental findings, in which we have not been able to form complex **(R,R)-1** using standard experimental conditions, whereas complex **(R,R)-3** is accessible. Calculated complexation energies for complexes based on the bpbp ligand family were found to be more favorable than those observed for bpmcn-based complexes, which might be due to the higher rigidity of the bis-pyrrolidine backbone of the ligand compared with that of the *N,N*-dimethylcyclohexanediamine backbone. Complexation of **(R,R)-[Mn(^{Bz}bpbp)]** is favored by 5.49 kcal/mol with respect to **(R,R)-3**. In a similar way, the complexation of **(R,R)-2** is 3.33 kcal/mol more favorable than that of **(R,R)-3**. Again, these calculations seem to be in line with the experimental data, since complexation of **(R,R)-[Mn(^{Bz}bpbp)]** is computed to be more favorable than that of **(R,R)-2**, and complex **(R,R)-[Mn(^{Bz}bpbp)]** has been successfully synthesized whereas complexation of **(R,R)-2** has not. Finally, we have also calculated the complexation energy for complex **(S,S)-[Mn(^{Bz}bpmcn)]**, which was found to be 1.54 kcal/mol less favorable than that for complex **(R,R)-3**. Based on this latter finding, we assume that calculated complexation reaction energies for complexes with *S,S* stereochemistry will have the same trend as that observed for complexes with *R,R* stereochemistry.

We have provided experimental and computational insights into why complexation reactions of **L1** and **L2** with a manganese(II) ion did not work. Nevertheless, our experiments showed that the complexation of ligand **L1** to an iron(II) salt does result in the anticipated iron complex.

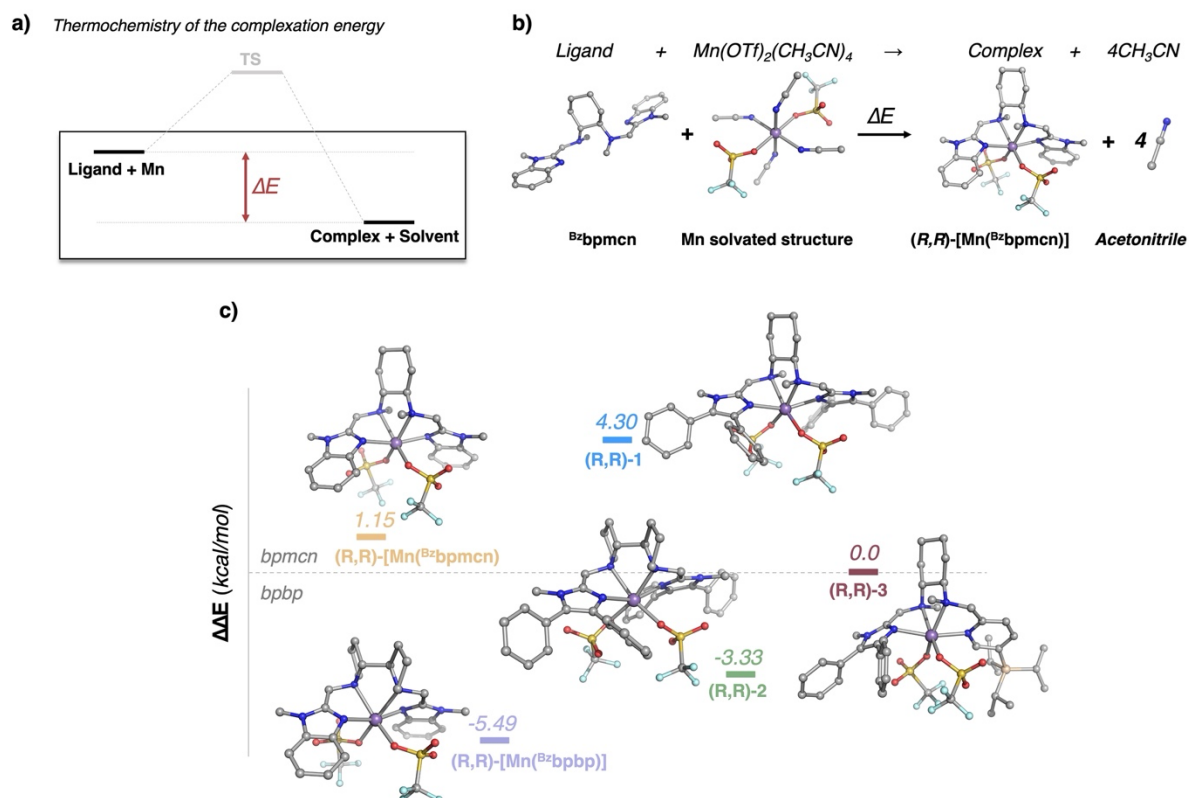


Figure 7. a) Representation of the strategy applied to get insight in the thermochemistry of the complexation reactions between ligands Bzbpmcn , Bzbpbp , **L1**, **L2** and **L3** and $\text{Mn}(\text{OTf})_2$. The complexation reaction energies (ΔE) have been calculated by subtracting the energy of reactants to products. b) Complexation reaction scheme and representation of the optimized geometries at the B3LYP-D3BJ/SMD/def2TZVP//B3LYP-D3BJ/6-31G(d,p) level of theory for (R,R) -[Mn(Bzbpmcn)]. Ligands and complexes have been built and optimized on the basis of available crystallographic structures, whereas a reasonable solvated structure has been constructed for $\text{Mn}(\text{OTf})_2$. c) Representation of the difference between the complexation reaction relative energies ($\Delta\Delta E$) for each ligand calculated at the same level of theory. All relative energies are in kcal/mol and referenced to the complexation energy of (R,R) -**3**. All optimized geometries are represented as sticks and spheres, and hydrogens are omitted for clarity.

Because typical Mn(II)–N bond distances are longer than Fe(II)–N bond distances, we would expect more steric strain to arise when arranging the bulky diphenylimidazole moieties of **L1** within in the iron complex. In addition, the ionic radius of Fe(II) is smaller than the one of Mn(II), again suggesting that the iron complex would suffer from more steric strain. At this point, we are not able to provide a rational explanation for the different behavior observed for **L1** in terms of its coordination to Mn(II) and Fe(II).

6.2.4 Catalytic Oxidation Experiments

Exploration of the reactivity of manganese complexes (S,S) -[Mn(Bzbpmcn)], (S,S) -[Mn(Bzbpbp)] and (S,S) -**3** has initially focused on their oxidation activity towards aromatic

substrates, whereas iron complexes (**(S,S)-10** and **(S,S)-11**) were not tested in the current study. Propylbenzene was selected as model substrate using the previously found optimized reaction conditions, *i.e.* 1 mol% catalyst, 1 equiv. of substrate, 0.5 equiv. of dichloroacetic acid and 1 equiv. of H₂O₂ (see Chapter 3 of this thesis).⁴⁷ Complex **(S,S)-[Mn(Bz**bpmcn**)]** was capable of converting 20% of the substrate and afforded 6% yield of *para*-phenol, together with *ortho*-phenol and benzoquinone in 2 and 1% yield, respectively. The benzylic alcohol product was also detected in 1% yield (Table 3, entry 1). The reactivity of complex **(S,S)-[Mn(Bz**bpbp**)]** towards propylbenzene was similar, with *para*-phenol, *ortho*-phenol, benzoquinone and benzylic alcohol products being formed in 5, 2, 1 and 1% yield, respectively (Table 3, entry 2). For both complexes good mass balances were observed. Complex **(S,S)-3**, on the other hand, did show a similar substrate conversion (22%), but did not yield the corresponding phenol products.

Table 3. Oxidation of propylbenzene using the manganese complexes synthesized in this study.

Entry	Catalyst	r.s.m. ^a	Yield 4-propylphenol ^b	Yield 2-propylphenol ^b	Yield BQ ^b	Yield A ^b	Yield K ^b	MB ^c
1	(S,S)-[Mn(Bzbpmcn)]	80	6	2	1	1	n.d.	92
2	(S,S)-[Mn(Bzbpbp)]	77	5	2	1	1	n.d.	88
3	(S,S)-3	78	n.d.	n.d.	n.d.	n.d.	n.d.	80

^aRemaining starting material in %. ^bYields in % with respect to substrate determined by GC against an internal standard. ^cMass balance was calculated considering remaining starting material and all products formed, plus a percentage of substrate loss calculated from blank experiments (an average of 2% of substrate is lost): MB = (100 – conversion %) + (Product Yields %) + (Substrate loss). n.d. = non-detected. BQ = benzoquinone.

Based on the poor results obtained, we decided to check for other oxidation reactions of less challenging substrates, such as the epoxidation of olefins. In this context, cyclooctene (1 equiv.) was selected as the substrate, and the catalytic experiment was performed using 1 mol% of catalyst, acetic acid (2 equiv.) as additive and H₂O₂ (1 equiv.) as benign oxidant in CH₃CN as the solvent (see Experimental Section for further details). These experiments showed that complex **(S,S)-3** is capable of carrying out catalytic epoxidation reactions, but displays poor yields for the desired epoxide product (7%).

Interestingly, complexes **(S,S)-[Mn(Bz**bpmcn**)]** and **(S,S)-[Mn(Bz**bpbp**)]** are excellent catalysts for enantioselective benzylic oxidation, as detailed in the Introduction section.⁴⁰⁻⁴³

Nevertheless, such complexes has never before been tested for the benzylic hydroxylation of simple arylalkanes, to the best of our knowledge. Along this vein, we have tested the enantioselective benzylic oxidation of the simple arylalkane propylbenzene, using these complexes under previously established reaction conditions, *i.e.* 1 mol% catalyst, 2 equiv. of racemic 2-ethylhexanoic acid, 1 equiv. of H₂O₂ and 1 equiv. of propylbenzene in 2,2,2-trifluoroethanol (TFE) at -35 °C. Under these conditions, complex (*S,S*)-[Mn(^{Bz}bpmcn)] afforded 57% substrate conversion with 16% yield of the benzylic alcohol product (69% ee for the (*S*)-alcohol), together with the overoxidized ketone product in 1% yield. Small amounts of aromatic oxidation products were also detected. Complex (*S,S*)-[Mn(^{Bz}bpbp)] provided a similar reactivity, with 52% substrate conversion, 16% yield of alcohol product (69% ee) and 2% yield of ketone. Again, small amounts of aromatic oxidation products were also detected. The mass balance in these experiments ranged from 61-69%.

The catalytic results show the sensitivity of the current class of manganese complexes towards changes in the experimental conditions. Of particular note is that these complexes preferentially perform benzylic oxidation reactions when 2-ethylhexanoic acid additive is used, whereas oxidation at the arene ring is preferred when dichloroacetic acid is employed as additive.

6.3 Conclusions

A new type of amino-imidazole ligand containing a diphenylimidazole moiety has been synthesized and characterized. Exploration of the complexation reaction between these ligands and metal salts, such as iron and manganese triflate, have been studied by means of experimental and computational techniques. C₂-symmetric complexes based on diphenylimidazole moieties were not synthetically accessible using the standard reaction conditions, which might be due to the large steric bulk of the ligand. DFT geometry optimization of the manganese complexes was performed to study the interaction and proximity between the amino-imidazole ligand and the metal-triflate moiety, and predicts that higher steric stress might occur in complexes containing two diphenylimidazole moieties. Moreover, studies on the thermodynamics of the metal complexation reactions have allowed a comparison between complexation reactions using different ligands. The outcome of this comparison indicates that complexation of diphenylimidazole-based ligands to Mn(OTf)₂ are less favorable than those using the less bulky benzimidazole-based ligands, which is in agreement with our experimental data. In contrast to the C₂-symmetric manganese complexes bearing diphenylimidazole moieties, we have been able to synthesize and characterize a C₁-symmetric manganese complex (*S,S*)-**3**, in which a diphenylimidazole and a bulky pyridine moiety are combined within the ligand framework. This indicated a lower steric demand for the non-

symmetric ligand in complex, which is corroborated by our computational studies. Complex (*S,S*)-**3** exhibits catalytic activity in olefin epoxidation with aqueous H₂O₂, whereas complexes (*S,S*)-[Mn(^{Bz}bpmcn)] and (*S,S*)-[Mn(^{Bz}bpbp)] exhibit catalytic activity towards arene oxidation. These combined observations raise a further interest in the development of imidazole-based metal complexes for oxidation catalysis.

6.4 Experimental Section

6.4.1 General Remarks

Air- and moisture-sensitive reactions were performed under an inert nitrogen atmosphere using standard Schlenk line and glovebox techniques. All catalytic oxidation reactions were run under air with no precautions taken to exclude moisture. The solvents diethyl ether and acetonitrile were purified using an MBraun MB SPS-800 solvent purification system. Tetrahydrofuran and methanol were dried with sodium and magnesium turnings, respectively, and distilled under nitrogen prior to use.

All other reagents and reaction products were obtained commercially from Across, Aldrich, Scharlab or Fluorochem, and used without further purification. Ligands (*S,S*)-^{Bz}bpmcn and (*S,S*)-^{Bz}bpbp were synthesized following reported procedures.^{44,45} Column chromatography was performed using Merck silica gel (60-200 mesh). ¹H and ¹³C NMR spectra were recorded with a 400 MHz Varian spectrometer at 25 °C, chemical shifts (δ) are given in ppm referenced to the residual solvent peak. IR spectra were recorded with a Perkin-Elmer Spectrum One FTIR spectrometer. ESI-MS measurements were recorded with a Walters LCT Premier XE KE317 machine. GC analyses were performed on a Perkin-Elmer Clarus 500 Gas Chromatograph equipped with a PE Elite-5 column ((30m x 0.23 mm x 0.25 μm), (50% phenyl)-(50% methyl)polysiloxane) and a flame-ionization detector. HPLC analyses were performed on a Perkin-Elmer Flexar LC System equipped with a Chiralcel® OD column (250 mm x 4.6 mm x 10 μm, Chiral Column).

Appendix E contains the supplementary information of this Chapter, which includes ¹H-NMR spectra for the newly synthesized ligands.

6.4.2 Synthesis of Imidazole/Pyridine Synthons and Ligands

1-methyl-4,5-diphenylimidazole (4): This compound was prepared following a modified procedure reported by Moret and co-workers.⁴⁹ Sodium hydride (0.66 g, 16.4 mmol, 60 wight% dispersion in mineral oil) was suspended in dry THF (50 mL) and cooled to 0 °C. 4,5-Diphenylimidazole (3 g, 13.62 mmol) was added in portions, keeping the temperature below 15 °C, and the reaction was then allowed to stir overnight at room temperature. Next, iodomethane (1 mL, 16.4 mmol) was added at room temperature, allowing the reaction to stir overnight. The reaction was quenched with an aqueous solution of NH₄Cl (10 mL), followed by extraction with CH₂Cl₂ (3 x 10 mL). Organic layers were combined and dried with MgSO₄. After filtration and evaporation of the solvents, a yellow powder was obtained, which was washed with cold toluene to yield the desired compound as a white powder (2.59 g, 11.1 mmol, 81% yield). ¹H NMR (400 MHz, CDCl₃) δ 8.66 (s, 1H), 7.54 – 7.45 (m, 5H), 7.37 – 7.32 (m, 2H), 7.25 – 7.20 (m, 3H), 3.66 (s, 3H); Spectral properties of the product agree with the literature data.

1-methyl-4,5-diphenyl-1H-imidazole-2-carboxaldehyde (5): This compound was prepared following a modified procedure reported by Sun and co-workers.⁵⁰ 1-Methyl-4,5-diphenylimidazole (1 g, 4.3

mmol, 1 equiv.) was dissolved in anhydrous THF (20 mL) under inert atmosphere and cooled to $-78\text{ }^{\circ}\text{C}$ in an acetone/dry ice bath. Then 1 equiv. of *n*-BuLi (1.6 M in hexanes, 4.3 mmol, 2.7 mL) was slowly added over 10 min, and the reaction mixture was let to stir for 30 min. At that point, 2 equiv. of anhydrous DMF (8.6 mmol, 0.67 mL) were slowly added. The reaction was stirred for 1 h, and the temperature was raised up to $-15\text{ }^{\circ}\text{C}$ after that time. At this point, the reaction was quenched with 1 M HCl solution (20 mL). Then, the pH was made basic by addition of a saturated NaHCO_3 solution (15 mL) and extracted with CH_2Cl_2 (3 x 20 mL). The combined organic layers were dried with MgSO_4 and concentrated on a rotatory evaporator after filtration to yield **5** as a light-yellow solid (1.03 g, 3.93 mmol, 91% yield). ^1H NMR (400 MHz, CDCl_3) δ 9.93 (s, 1H), 7.53 – 7.45 (m, 5H), 7.36 – 7.32 (m, 2H), 7.25 – 7.21 (m, 3H), 3.84 (s, 3H); ^{13}C NMR (101 MHz, CDCl_3) δ 182.28, 143.05, 141.28, 133.30, 130.46, 129.65, 129.28, 128.67, 128.34, 127.41, 127.10, 32.89; Spectral properties of the product agree with the literature data.

1-methyl-4,5-diphenyl-2-hydroxymethylimidazole (6): 5 (817 mg, 3.11 mmol) was dissolved in dry methanol (15 mL), and NaBH_4 (2 equiv., 236 mg, 6.23 mmol) was directly added as a solid in little portions at $0\text{ }^{\circ}\text{C}$. The reaction mixture was stirred overnight at room temperature, and then water (10 mL) and saturated NaHCO_3 solution (10 mL) were slowly added. After 10 min of stirring, the mixture was extracted with CH_2Cl_2 (3 x 20 mL), the combined organic phases were dried with anhydrous MgSO_4 and after filtration the solvent was removed under reduced pressure to yield **6** as a white solid (593 mg, 2.24 mmol, 72% yield). ^1H NMR (400 MHz, CDCl_3) δ 7.46 – 7.38 (m, 5H), 7.25 – 7.15 (m, 5H), 4.89 (s, 2H), 3.45 (s, 3H), 3.32 (s, 1H); ^{13}C NMR (101 MHz, CDCl_3) δ 147.04, 135.42, 133.57, 130.92, 130.34, 130.08, 129.18, 128.98, 128.35, 126.77, 126.74, 56.89, 31.21.

2-Chloromethyl-1-methyl-4,5-diphenylimidazole hydrochloride (7): The procedure followed is inspired by the method reported by Costas and co-workers. A solution of **6** (500 mg, 1.89 mmol, 1 equiv.) in dry CH_2Cl_2 (20 mL) was cooled to $0\text{ }^{\circ}\text{C}$. Thionyl chloride (0.1 mL, 2.84 mmol, 1.5 equiv.) was slowly added. After addition, the resulting mixture was stirred at rt overnight. Then, the solvent was removed at reduced pressure to yield the desired product **7** as a brown solid (423 mg, 1.33 mmol, 70% yield). ^1H NMR (400 MHz, CDCl_3) δ 7.61 – 7.48 (m, 3H), 7.42 (dd, $J = 7.9, 1.8\text{ Hz}$, 2H), 7.35 – 7.29 (m, 2H), 7.26 – 7.18 (m, 3H), 5.40 (s, 2H), 3.69 (s, 3H), 2.16 (s, 1H); ^{13}C NMR (101 MHz, CDCl_3) δ 141.35, 130.76, 130.66, 130.61, 129.52, 129.24, 129.03, 128.66, 126.93, 125.74, 125.48, 56.30, 31.74.

(*S,S*)-^{Ph2Imz}bpmcn (L1): A 20 mL vial was charged with a stir bar, (*S,S*)-*N,N*-Dimethyl-1,2-cyclohexanediamine (1 equiv., 92 mg, 0.65 mmol) and H_2O (2 mL), and CH_2Cl_2 (5 mL). Solid NaOH pellets (7.5 equiv., 196 mg, 4.89 mmol) were added, followed by **7** (2.05 equiv., 423 mg, 1.33 mmol). After 18 h stirring at room temperature, the reaction mixture was diluted with 4 M NaOH (10 mL). The aqueous layer was extracted with CH_2Cl_2 (3 x 15 mL), and the organic extracts were combined, dried over MgSO_4 , filtered, and concentrated *in vacuo*. The desired ligand L1 was obtained as a light-yellow solid (409 mg, 0.64 mmol, 99% yield). ^1H NMR (400 MHz, CDCl_3) δ 7.45 – 7.36 (m, 10H), 7.25 – 7.09 (m, 10H), 3.85 (d, $J = 5.3\text{ Hz}$, 4H), 3.52 (s, 6H), 2.71 (d, $J = 7.1\text{ Hz}$, 2H), 2.17 (s, 6H), 2.02 (d, $J = 11.3\text{ Hz}$, 2H), 1.83 – 1.76 (m, 2H), 1.31 – 1.19 (m, 4H); ^{13}C NMR (101 MHz, CDCl_3) δ 145.97, 136.25, 135.01, 131.41, 130.85, 129.98, 129.04, 128.45, 128.14, 126.84, 126.08, 62.35, 51.16, 35.82, 31.12, 25.78, 24.24; HRMS: m/z calculated for $\text{C}_{42}\text{H}_{47}\text{N}_6$, $[\text{L}+\text{H}]^+$ 635.3862, found 635.3872.

(*S,S*)-^{Ph2Imz}bpbp (L2): A 20 mL vial was charged with a stir bar, (*S,S*)-2,2'-bispyrrolidine tartrate (1 equiv., 343 mg, 0.1 mmol) and H_2O (16 mL), and CH_2Cl_2 (16 mL). Solid NaOH pellets (6.4 equiv., 255 mg, 6.37 mmol) were added, followed by **7** (2.2 equiv., 700 mg, 2.19 mmol). After 18 h stirring at room temperature, the reaction mixture was diluted with 1 M NaOH (20 mL). The aqueous layer was extracted

with CH_2Cl_2 (3 x 20 mL), and the organic extracts were combined, dried over MgSO_4 , filtered, and concentrated *in vacuo*. The obtained crude ligand was purified by silica gel chromatography eluting with $\text{CH}_2\text{Cl}_2:\text{CH}_3\text{OH}:\text{NH}_4\text{OH}$ (10 : 0.5 : 0.4 (v/v)), and the collected fractions were combined, washed with 1 M NaOH, dried over MgSO_4 , filtered, and concentrated *in vacuo* to provide the desired ligand **L2** as a light-yellow solid (380 mg, 0.6 mmol, 60% yield). ^1H NMR (400 MHz, CDCl_3) δ 7.48 – 7.38 (m, 10H), 7.33 – 7.30 (m, 4H), 7.20 – 7.07 (m, 6H), 4.04 (d, $J = 13.3$ Hz, 2H), 3.65 (d, $J = 13.3$ Hz, 2H), 3.48 (s, 6H), 2.98 – 2.94 (m, 2H), 2.72 – 2.70 (m, 2H), 2.46 – 2.39 (m, 2H), 1.76 – 1.65 (m, 8H); ^{13}C NMR (101 MHz, CDCl_3) δ 145.78, 136.42, 134.91, 131.30, 130.94, 129.80, 128.99, 128.46, 128.14, 126.95, 126.12, 64.99, 55.61, 52.25, 31.18, 26.33, 24.18; HRMS: m/z calculated for $\text{C}_{42}\text{H}_{45}\text{N}_6$, $[\text{L}+\text{H}]^+$ 633.3706, found 633.3712.

(*S,S*)-^{TIPS,Ph²Imz}bpmcn (L3): This compound was prepared following a modified procedure reported by Klein Gebbink, Costas, and co-workers.³³ **9*** (300 mg, 0.77 mmol, 1 equiv.) was dissolved in CH_2Cl_2 (10 mL) and cooled to 0 °C, and $\text{NaB}(\text{OAc})_3$ (320 mg, 1.5 mmol, 1.9 equiv.) were added to the reaction mixture, which was stirred for 30 min at 0 °C. **5** (202 mg, 0.77 mmol, 1 equiv.) was added at this point, and the crude mixture was stirred at rt overnight. Then, the mixture was extracted with aqueous NaHCO_3 (3 x 40 mL). The combined organic phase was dried over MgSO_4 , filtered, and the solvent was removed under reduced pressure. The product was then purified by alumina column chromatography eluting with $\text{EtOAc} : \text{petroleum ether} : \text{NEt}_3$ (9 : 1 : 0.1 (v/v)) and the collected fractions were combined, washed with saturated 4M NaOH solution, dried over MgSO_4 , filtered, and concentrated *in vacuo* to provide the title compound **L3** (316 mg, 0.5 mmol, 65% yield) as a white solid. ^1H NMR (400 MHz, CDCl_3) δ 8.53 (s, 1H), 7.72 – 7.32 (m, 8H), 7.21 – 7.07 (m, 4H), 3.96 – 3.71 (m, 4H), 3.48 (s, 3H), 2.69 (d, $J = 7.0$ Hz, 2H), 2.29 (s, 3H), 2.18 (s, 3H), 2.04 – 1.95 (m, 2H), 1.78 (s, 2H), 1.41 – 1.33 (m, 3H), 1.29 – 1.18 (m, 4H), 1.04 (d, $J = 7.5$ Hz, 18H); ^{13}C NMR (101 MHz, CDCl_3) δ 161.19, 154.56, 146.26, 143.37, 130.92, 130.88, 129.06, 128.97, 128.48, 128.39, 128.16, 126.92, 126.86, 126.07, 122.37, 64.36, 62.52, 62.41, 60.85, 51.42, 36.32, 31.27, 25.89, 25.55, 24.58, 24.28, 18.58, 10.74; HRMS: m/z calculated for $\text{C}_{40}\text{H}_{58}\text{N}_5\text{Si}$, $[\text{L}+\text{H}]^+$ 636.4461, found 636.4471.

6.4.3 Synthesis of Metal Complexes

General Procedure for Complexation with $\text{Mn}(\text{OTf})_2$:

A suspension of $\text{Mn}(\text{OTf})_2$ (1 equiv.) in anhydrous CH_3CN (1 mL) was added dropwise to a vigorously stirred solution of the ligand (1.07 equiv.) in CH_3CN (1 mL). The resulting mixture was stirred at rt overnight. Then, the solution was dried under vacuum, to provide a precipitate that is washed with diethyl ether several times. The resulting precipitate is then crystallized by slow diffusion to yield the desired complex.

(*S,S'*)- $[\text{Mn}(\text{OTf})_2(\text{TIPS,Ph}^2\text{Imz bpmcn})]$ ((*S,S*)-3): A suspension of $\text{Mn}(\text{OTf})_2$ (26 mg, 0.074 mmol) in anhydrous CH_3CN (1 mL) was added dropwise to a vigorously stirred solution of **L3** (50 mg, 0.079 mmol) in CH_3CN (1 mL). Following the previously described procedure, the desired complex was obtained after slow diffusion of pentane into a solution of the complex in CH_2Cl_2 as microcrystalline material (31 mg, 0.0313 mmol, yield 42%). HRMS: m/z calculated for $\text{C}_{41}\text{H}_{57}\text{F}_3\text{MnN}_5\text{O}_3\text{SSi}$, $[\text{M}-\text{OTf}]^+$ 839.3284, found 839.3298.

(*S,S'*)- $[\text{Fe}(\text{Cl})_2(\text{Ph}^2\text{Imz bpmcn})]$ ((*S,S*)-10): Under a N_2 atmosphere, FeCl_2 (10 mg, 0.078 mmol) was slowly added as a solid to a **L3** (50 mg, 0.079 mmol) solution in anhydrous CH_3CN (1 mL). After

* See Experimental Section of Chapter 4 for the synthesis of compound **9** (referred to as **mcp-TIPSPy**)

overnight reaction, the solvent was removed under vacuum, and the precipitate washed several times with Et₂O, to afford the desired complex as an orange solid (33 mg, 0.043 mmol, yield 55%). HRMS: *m/z* calculated for C₄₂H₄₆ClFeN₆, [M-Cl]⁺ 725.2822, found 725.2822.

(*S,S'*)-[Fe(CH₃CN)₂(^{Ph²Imz}bpmcn)](SbF₆)₂ ((*S,S*)-11): Under a N₂ atmosphere, **10** (33 mg, 0.043 mmol) was mixed with AgSbF₆ (30 mg, 0.086 mmol) in CH₃CN (2 mL) and stirred overnight at room temperature. Then, the reaction mixture was filtered through Celite® and evaporated to dryness to afford the desired complex as a brown solid (25 mg, 0.02 mmol, yield 47%). HRMS: *m/z* calculated for C₄₂H₄₆F₆FeN₆Sb, [M-(CH₃CN)₂(SbF₆)]⁺ 925.2076, found 925.2077.

6.4.4 Reaction Protocol for Catalytic Studies

6.4.4.1 General Procedure for Catalytic Aromatic Hydroxylation Reactions

A 20 mL vial was charged with: substrate (1 equiv.), catalyst (1 mol%) and HFIP (2 mL). Dichloroacetic acid was then added (0.5 equiv.). The vial was cooled on an ice bath with stirring. Subsequently, a solution of H₂O₂ in HFIP (1 equiv., diluted from a 35% H₂O₂ aqueous solution) was delivered by syringe pump over 30 min. After the oxidant addition, the resulting mixture was brought to room temperature, and at this point, a 0.8 M biphenyl solution in CH₃CN (0.5 equiv) was added as internal standard. The solution was filtered through a Celite®, silica and alumina plug, which was subsequently rinsed with EtOAc (2 x 1 mL). Then the sample was submitted to GC analysis to determine the mass balance, the conversion, and relative ratio of products by comparison with authentic samples.

6.4.4.2 General Procedure for Catalytic Epoxidation Reactions

A 20 mL vial was charged with: substrate (1 equiv.), catalyst (1 mol%) and CH₃CN (2 mL). Acetic acid was then added (2 equiv.). The vial was cooled on an ice bath with stirring. Subsequently, a solution of H₂O₂ in CH₃CN (1 equiv., diluted from a 35% H₂O₂ aqueous solution) was delivered by syringe pump over 30 min. After the oxidant addition, the resulting mixture was brought to room temperature, and at this point, a 1 M nitrobenzene solution in CH₃CN (0.5 equiv.) was added as internal standard. The solution was filtered through a silica plug, which was subsequently rinsed with EtOAc (2 x 1 mL). Then the sample was submitted to GC analysis to determine the mass balance, the conversion, and relative ratio of products by comparison with authentic samples.

6.4.4.3 General Procedure for Catalytic Benzylic Hydroxylation Reactions

A 20 mL vial was charged with: substrate (1 equiv.), catalyst (1 mol%) and TFE (2 mL). 2-Ethylhexanoic acid was then added (2 equiv.). The vial was cooled on an acetonitrile/dry ice bath with stirring. Subsequently, a solution of H₂O₂ in TFE (1 equiv., diluted from a 35% H₂O₂ aqueous solution) was delivered by syringe pump over 30 min. After the oxidant addition, the resulting mixture was stirred 30 min further, and then brought to room temperature. At this point, a 0.8 M biphenyl solution in CH₃CN (0.5 equiv.) was added as internal standard. The solution was filtered through a silica plug, which was subsequently rinsed with isopropanol (2 x 1 mL). Then the sample was submitted to GC analysis to determine the remaining amount of starting material and the amounts of reaction products by comparison with authentic samples. For the determination of ee values the sample was submitted to HPLC analysis using a chiral column.

6.4.5 Computational Methods

Full geometry optimizations were performed with the hybrid DFT B3LYP functional⁵¹ including the D3BJ dispersion correction and the 6-31G(d,p) basis set^{52,53} using Gaussian 16.⁵⁴ Analytical frequency calculations were performed at the same level of theory as the geometry optimizations. We have also checked that none of the frequencies was imaginary. More accurate energies were obtained by single-point calculations including the DFT hybrid B3LYP-D3BJ dispersion correction with the def2TZVP basis set. The effects of the acetonitrile solvent were implicitly included in these single-point energy calculations using the Polarizable Continuum Model (PCM) via the SMD option. All energies are ZPE-corrected.

Author Contributions

E.M-R. and R.K.G. devised the project and designed experiments. E.M-R. performed the experiments and analyzed the data. M.L.G.S-P. performed DFT calculations. E.M-R. wrote the Chapter and R.K.G. provided comments on the experiments and Chapter content.

6.5 References

1. Que, L.; Tolman, W. B., Biologically inspired oxidation catalysis. *Nature* **2008**, *455* (7211), 333-340.
2. Bruijninx, P. C.; van Koten, G.; Klein Gebbink, R. J. M., Mononuclear non-heme iron enzymes with the 2-His-1-carboxylate facial triad: recent developments in enzymology and modeling studies. *Chem. Soc. Rev.* **2008**, *37* (12), 2716-2744.
3. Porta, J.; Vahedi-Faridi, A.; Borgstahl, G. E. O., Structural analysis of peroxide-soaked MnSOD crystals reveals side-on binding of peroxide to active-site manganese. *J. Mol. Biol.* **2010**, *399* (3), 377-384.
4. Cussó, O.; Ribas, X.; Costas, M., Biologically inspired non-heme iron-catalysts for asymmetric epoxidation; design principles and perspectives. *Chem. Commun.* **2015**, *51* (76), 14285-14298.
5. Bryliakov, K. P., Catalytic asymmetric oxygenations with the environmentally benign oxidants H₂O₂ and O₂. *Chem. Rev.* **2017**, *117* (17), 11406-11459.
6. Milan, M.; Bietti, M.; Costas, M., Enantioselective aliphatic C–H bond oxidation catalyzed by bioinspired complexes. *Chem. Commun.* **2018**, *54* (69), 9559-9570.
7. Sun, W.; Sun, Q., Bioinspired manganese and iron complexes for enantioselective oxidation reactions: ligand design, catalytic activity, and beyond. *Acc. Chem. Res.* **2019**, *52* (8), 2370-2381.
8. Chen, J.; Jiang, Z.; Fukuzumi, S.; Nam, W.; Wang, B., Artificial nonheme iron and manganese oxygenases for enantioselective olefin epoxidation and alkane hydroxylation reactions. *Coord. Chem. Rev.* **2020**, *421*, 213443.
9. Costas, M., Site and Enantioselective Aliphatic C–H Oxidation with Bioinspired Chiral Complexes. *Chem. Rec.* **2021**, *21*, 4000-4014.
10. Radhika, S.; Aneja, T.; Philip, R. M.; Anilkumar, G., Recent advances and trends in the biomimetic iron-catalyzed asymmetric epoxidation. *Appl. Organomet. Chem.* **2021**, *35* (6), e6217.
11. Lyakin, O. Y.; Talsi, E. P., Direct C–H Oxidation of Aromatic Substrates in the Presence of Biomimetic Iron Complexes. In *Frontiers of Green Catalytic Selective Oxidations*, Springer: 2019; pp 253-276.

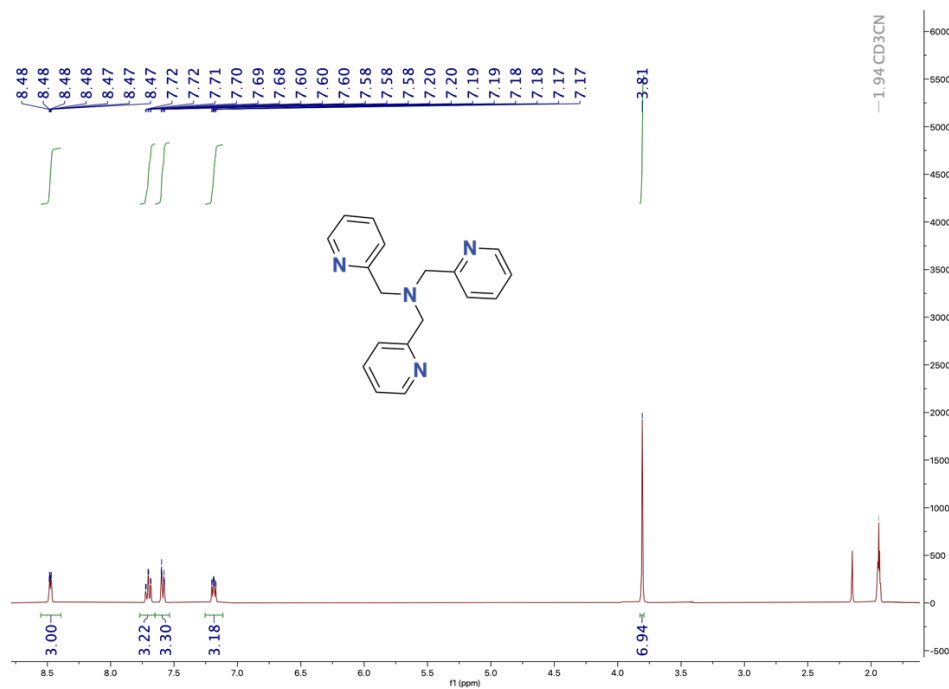
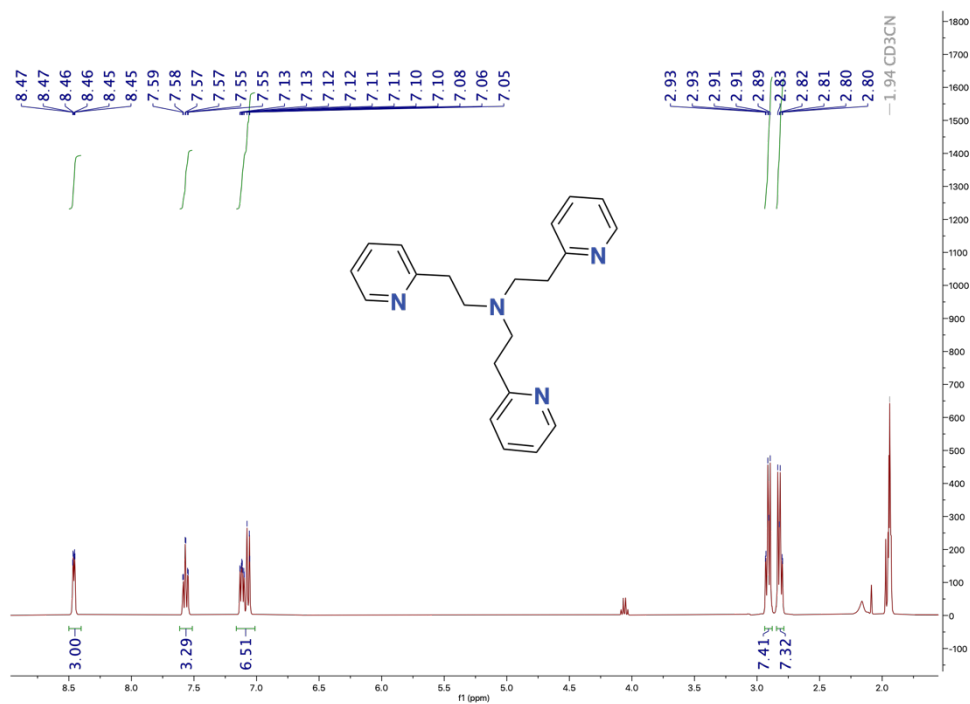
12. Ottenbacher, R. V.; Talsi, E. P.; Bryliakov, K. P., Recent progress in catalytic oxygenation of aromatic C–H groups with the environmentally benign oxidants H₂O₂ and O₂. *Appl. Organomet. Chem.* **2020**, *34* (11), e5900.
13. Codolà, Z.; Lloret-Fillol, J.; Costas, M., Aminopyridine iron and manganese complexes as molecular catalysts for challenging oxidative transformations. *Prog. Inorg. Chem.* **2014**, *59* (2016), 447-531.
14. Olivo, G.; Cussó, O.; Costas, M., Biologically inspired C–H and C=C oxidations with hydrogen peroxide catalyzed by iron coordination complexes. *Chem. Asian J.* **2016**, *11* (22), 3148-3158.
15. Olivo, G.; Cussó, O.; Borrell, M.; Costas, M., Oxidation of alkane and alkene moieties with biologically inspired nonheme iron catalysts and hydrogen peroxide: from free radicals to stereoselective transformations. *J. Biol. Inorg. Chem.* **2017**, *22* (2), 425-452.
16. Vicens, L.; Olivo, G.; Costas, M., Rational Design of Bioinspired Catalysts for Selective Oxidations. *ACS Catal.* **2020**, *10* (15), 8611-8631.
17. Chen, M. S.; White, M. C., A predictably selective aliphatic C–H oxidation reaction for complex molecule synthesis. *Science* **2007**, *318* (5851), 783-787.
18. Wang, B.; Wang, S.; Xia, C.; Sun, W., Highly Enantioselective Epoxidation of Multisubstituted Enones Catalyzed by Non-Heme Iron Catalysts. *Chem. Eur. J.* **2012**, *18* (24), 7332-7335.
19. Mikhalyova, E. A.; Makhlynets, O. V.; Palluccio, T. D.; Filatov, A. S.; Rybak-Akimova, E. V., A new efficient iron catalyst for olefin epoxidation with hydrogen peroxide. *Chem. Commun.* **2012**, *48* (5), 687-689.
20. Clarasó, C.; Vicens, L.; Polo, A.; Costas, M., Enantioselective Epoxidation of β,β -Disubstituted Enamides with a Manganese Catalyst and Aqueous Hydrogen Peroxide. *Org. Lett.* **2019**, *21* (7), 2430-2435.
21. Murphy, A.; Dubois, G.; Stack, T. D. P., Efficient epoxidation of electron-deficient olefins with a cationic manganese complex. *J. Am. Chem. Soc.* **2003**, *125* (18), 5250-5251.
22. Chen, J.; Lutz, M.; Milan, M.; Costas, M.; Otte, M.; Klein Gebbink, R. J. M., Non-Heme Iron Catalysts with a Rigid Bis-Isoindoline Backbone and Their Use in Selective Aliphatic C–H Oxidation. *Adv. Synth. Catal.* **2017**, *359* (15), 2590-2595.
23. Cussó, O.; Garcia-Bosch, I.; Ribas, X.; Lloret-Fillol, J.; Costas, M., Asymmetric epoxidation with H₂O₂ by manipulating the electronic properties of non-heme iron catalysts. *J. Am. Chem. Soc.* **2013**, *135* (39), 14871-14878.
24. Cussó, O.; Garcia-Bosch, I.; Font, D.; Ribas, X.; Lloret-Fillol, J.; Costas, M., Highly stereoselective epoxidation with H₂O₂ catalyzed by electron-rich aminopyridine manganese catalysts. *Org. Lett.* **2013**, *15* (24), 6158-6161.
25. Olivo, G.; Lanzalunga, O.; Mandolini, L.; Di Stefano, S., Substituent effects on the catalytic activity of bipyrrrolidine-based iron complexes. *J. Org. Chem.* **2013**, *78* (22), 11508-11512.
26. Talsi, E. P.; Samsonenko, D. G.; Bryliakov, K. P., Asymmetric autoamplification in the oxidative kinetic resolution of secondary benzylic alcohols catalyzed by manganese complexes. *ChemCatChem* **2017**, *9* (13), 2599-2607.
27. Talsi, E. P.; Bryliakov, K. P., Autoamplification-Enhanced Oxidative Kinetic Resolution of sec-Alcohols and Alkyl Mandelates, and its Kinetic Model. *ChemCatChem* **2018**, *10* (12), 2693-2699.

28. Font, D.; Canta, M.; Milan, M.; Cussó, O.; Ribas, X.; Klein Gebbink, R. J. M.; Costas, M., Readily accessible bulky iron catalysts exhibiting site selectivity in the oxidation of steroidal substrates. *Angew. Chem. Int. Ed.* **2016**, *55* (19), 5776-5779.
29. Milan, M.; Bietti, M.; Costas, M., Highly enantioselective oxidation of nonactivated aliphatic C–H bonds with hydrogen peroxide catalyzed by manganese complexes. *ACS Cent. Sci.* **2017**, *3* (3), 196-204.
30. Cianfanelli, M.; Olivo, G.; Milan, M.; Klein Gebbink, R. J. M.; Ribas, X.; Bietti, M.; Costas, M., Enantioselective C–H lactonization of unactivated methylenes directed by carboxylic acids. *J. Am. Chem. Soc.* **2019**, *142* (3), 1584-1593.
31. Gormisky, P. E.; White, M. C., Catalyst-controlled aliphatic C–H oxidations with a predictive model for site-selectivity. *J. Am. Chem. Soc.* **2013**, *135* (38), 14052-14055.
32. Zhao, J.; Nanjo, T.; de Lucca, E. C.; White, M. C., Chemoselective methylene oxidation in aromatic molecules. *Nat. Chem.* **2019**, *11* (3), 213-221.
33. Cussó, O.; Cianfanelli, M.; Ribas, X.; Klein Gebbink, R. J. M.; Costas, M., Iron catalyzed highly enantioselective epoxidation of cyclic aliphatic enones with aqueous H₂O₂. *J. Am. Chem. Soc.* **2016**, *138* (8), 2732-2738.
34. Guillemot, G.; Neuburger, M.; Pfaltz, A., Synthesis and Metal Complexes of Chiral C₂-Symmetric Diamino–Bisoxazoline Ligands. *Chem. Eur. J.* **2007**, *13* (32), 8960-8970.
35. Dai, W.; Li, G.; Chen, B.; Wang, L.; Gao, S., A porphyrin-inspired iron catalyst for asymmetric epoxidation of electron-deficient olefins. *Org. Lett.* **2015**, *17* (4), 904-907.
36. Dai, W.; Shang, S.; Chen, B.; Li, G.; Wang, L.; Ren, L.; Gao, S., Asymmetric epoxidation of olefins with hydrogen peroxide by an in situ-formed manganese complex. *J. Org. Chem.* **2014**, *79* (14), 6688-6694.
37. Wang, B.; Miao, C.; Wang, S.; Xia, C.; Sun, W., Manganese Catalysts with C₁-Symmetric N₄ Ligand for Enantioselective Epoxidation of Olefins. *Chem. Eur. J.* **2012**, *18* (22), 6750-6753.
38. Shen, D.; Miao, C.; Wang, S.; Xia, C.; Sun, W., Efficient benzylic and aliphatic C–H oxidation with selectivity for methylenic sites catalyzed by a bioinspired manganese complex. *Org. Lett.* **2014**, *16* (4), 1108-1111.
39. Shen, D.; Miao, C.; Xu, D.; Xia, C.; Sun, W., Highly efficient oxidation of secondary alcohols to ketones catalyzed by manganese complexes of N₄ ligands with H₂O₂. *Org. Lett.* **2015**, *17* (1), 54-57.
40. Qiu, B.; Xu, D.; Sun, Q.; Miao, C.; Lee, Y.-M.; Li, X.-X.; Nam, W.; Sun, W., Highly enantioselective oxidation of spirocyclic hydrocarbons by bioinspired manganese catalysts and hydrogen peroxide. *ACS Catal.* **2018**, *8* (3), 2479-2487.
41. Li, X.-X.; Guo, M.; Qiu, B.; Cho, K.-B.; Sun, W.; Nam, W., High-Spin Mn(V)-Oxo Intermediate in Nonheme Manganese Complex-Catalyzed Alkane Hydroxylation Reaction: Experimental and Theoretical Approach. *Inorg. Chem.* **2019**, *58* (21), 14842-14852.
42. Qiu, B.; Xu, D.; Sun, Q.; Lin, J.; Sun, W., Manganese-catalyzed asymmetric oxidation of methylene C–H of spirocyclic oxindoles and dihydroquinolinones with hydrogen peroxide. *Org. Lett.* **2019**, *21* (3), 618-622.
43. Sun, Q.; Sun, W., Catalytic Enantioselective Methylene C(sp³)–H Hydroxylation Using a Chiral Manganese Complex/Carboxylic Acid System. *Org. Lett.* **2020**, *22* (24), 9529-9533.

44. Wang, X.; Miao, C.; Wang, S.; Xia, C.; Sun, W., Bioinspired manganese and iron complexes with tetradentate N ligands for the asymmetric epoxidation of olefins. *ChemCatChem* **2013**, *5* (8), 2489-2494.
45. Shen, D.; Miao, C.; Wang, S.; Xia, C.; Sun, W., A mononuclear manganese complex of a tetradentate nitrogen ligand—synthesis, characterizations, and application in the asymmetric epoxidation of olefins. *Eur. J. Inorg. Chem.* **2014**, *2014* (33), 5777-5782.
46. Wang, W.; Xu, D.; Sun, Q.; Sun, W., Efficient Aliphatic C–H Bond Oxidation Catalyzed by Manganese Complexes with Hydrogen Peroxide. *Chem. Asian J.* **2018**, *13* (17), 2458-2464.
47. Masferrer-Rius, E.; Borrell, M.; Lutz, M.; Costas, M.; Klein Gebbink, R. J. M., Aromatic C–H Hydroxylation Reactions with Hydrogen Peroxide Catalyzed by Bulky Manganese Complexes. *Adv. Synth. Catal.* **2021**, *363* (15), 3783-3795.
48. Codolà, Z.; Gamba, I.; Acuña-Parés, F.; Casadevall, C.; Clémancey, M.; Latour, J.-M.; Luis, J. M.; Lloret-Fillol, J.; Costas, M., Design of iron coordination complexes as highly active homogenous water oxidation catalysts by deuteration of oxidation-sensitive sites. *J. Am. Chem. Soc.* **2018**, *141* (1), 323-333.
49. Folkertsma, E.; Benthem, S. H.; Witteman, L.; Van Slagmaat, C. A. M. R.; Lutz, M.; Klein Gebbink, R. J. M.; Moret, M.-E., Formation of exceptionally weak C–C bonds by metal-templated pinacol coupling. *Dalton Trans.* **2017**, *46* (19), 6177-6182.
50. Moore, T. W.; Sana, K.; Yan, D.; Krumm, S. A.; Thepchatrri, P.; Snyder, J. P.; Marengo, J.; Arrendale, R. F.; Prussia, A. J.; Natchus, M. G., Synthesis and Metabolic Studies of Host-Directed Inhibitors for Antiviral Therapy. *ACS Med. Chem. Lett.* **2013**, *4* (8), 762-767.
51. Lee, C.; Yang, W.; Parr, R. G., Development of the Colle-Salvetti correlation-energy formula into a functional of the electron density. *Phys. Rev. B: Condens. Matter* **1988**, *37* (2), 785.
52. Hariharan, P. C.; Pople, J. A., The influence of polarization functions on molecular orbital hydrogenation energies. *Theor. Chim. Acta* **1973**, *28* (3), 213-222.
53. Hehre, W. J.; Ditchfield, R.; Pople, J. A., Self-consistent molecular orbital methods. XII. Further extensions of Gaussian-type basis sets for use in molecular orbital studies of organic molecules. *J. Chem. Phys.* **1972**, *56* (5), 2257-2261.
54. Gaussian 16, Revision C.01, Frisch, M. J.; Trucks, G. W.; Schlegel, H. B.; Scuseria, G. E.; Robb, M. A.; Cheeseman, J. R.; Scalmani, G.; Barone, V.; Petersson, G. A.; Nakatsuji, H.; Li, X.; Caricato, M.; Marenich, A. V.; Bloino, J.; Janesko, B. G.; Gomperts, R.; Mennucci, B.; Hratchian, H. P.; Ortiz, J. V.; Izmaylov, A. F.; Sonnenberg, J. L.; Williams-Young, D.; Ding, F.; Lipparini, F.; Egidi, F.; Goings, J.; Peng, B.; Petrone, A.; Henderson, T.; Ranasinghe, D.; Zakrzewski, V. G.; Gao, J.; Rega, N.; Zheng, G.; Liang, W.; Hada, M.; Ehara, M.; Toyota, K.; Fukuda, R.; Hasegawa, J.; Ishida, M.; Nakajima, T.; Honda, Y.; Kitao, O.; Nakai, H.; Vreven, T.; Throssell, K.; Montgomery, J. A., Jr.; Peralta, J. E.; Ogliaro, F.; Bearpark, M. J.; Heyd, J. J.; Brothers, E. N.; Kudin, K. N.; Staroverov, V. N.; Keith, T. A.; Kobayashi, R.; Normand, J.; Raghavachari, K.; Rendell, A. P.; Burant, J. C.; Iyengar, S. S.; Tomasi, J.; Cossi, M.; Millam, J. M.; Klene, M.; Adamo, C.; Cammi, R.; Ochterski, J. W.; Martin, R. L.; Morokuma, K.; Farkas, O.; Foresman, J. B.; Fox, D. J. Gaussian, Inc., Wallingford CT, 2016.

Appendix A – Supplementary Information to Chapter 2

NMR spectra

Figure A1. ¹H NMR spectra of tpa ligand.Figure A2. ¹H NMR spectra of tpea ligand.

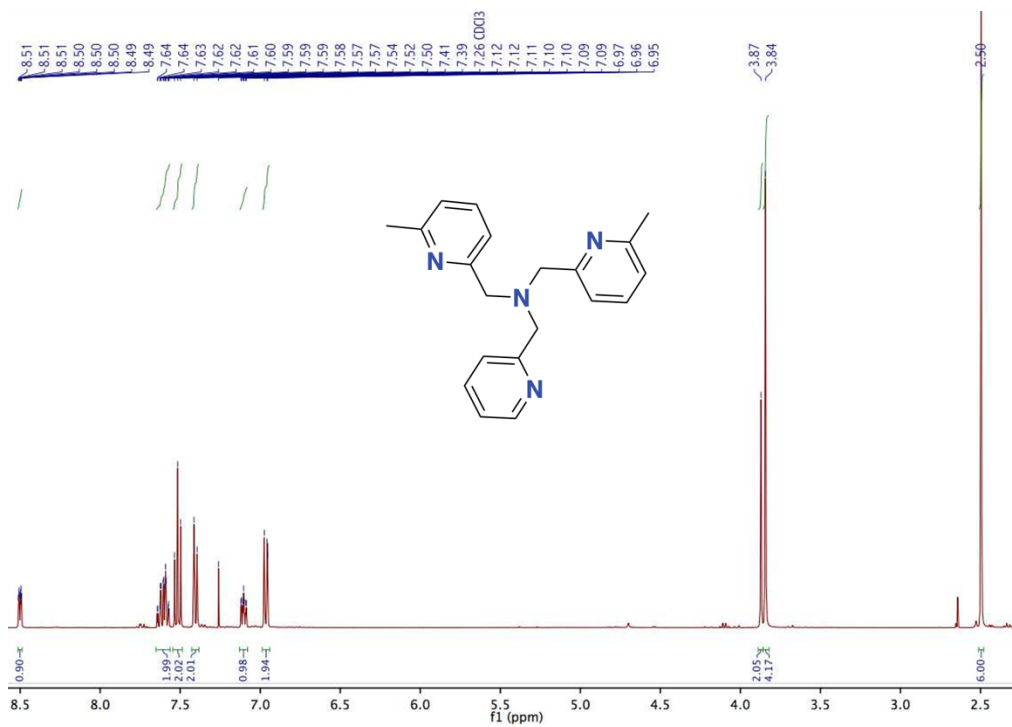


Figure A5. ¹H NMR spectra of 6-Me₂-tpa ligand.

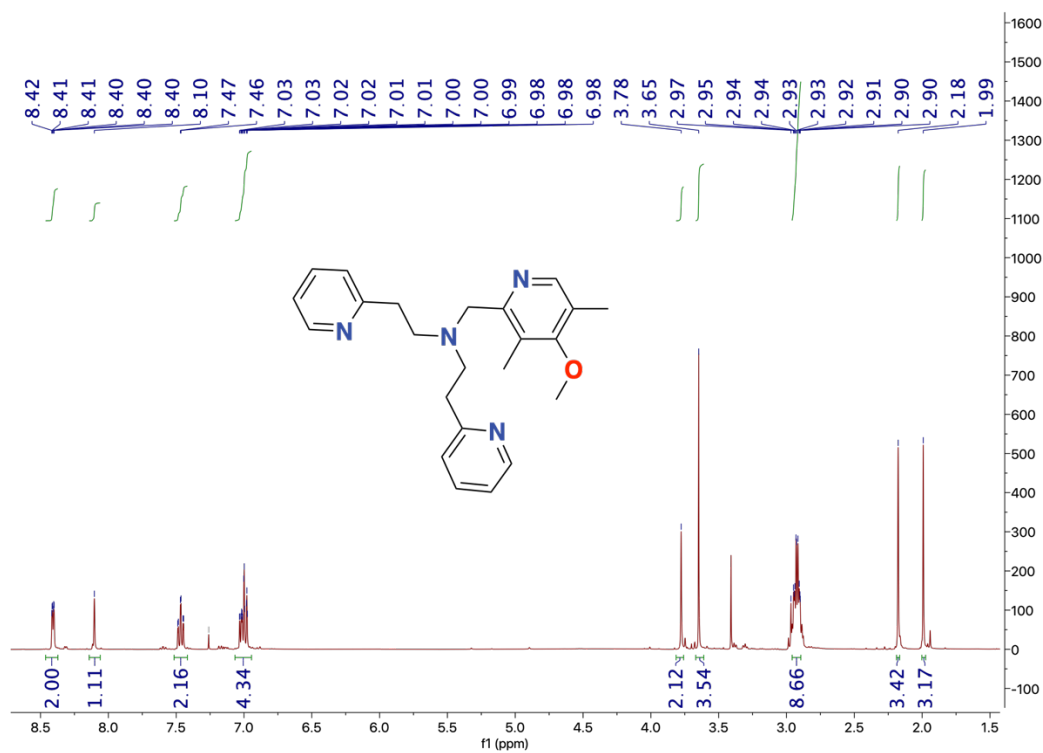


Figure A6. ¹H NMR spectra of 4-OMe-3,5-Me-pmap ligand.

Appendix B – Supplementary Information to Chapter 3

Investigation on Catalyst Inhibition: MS Data

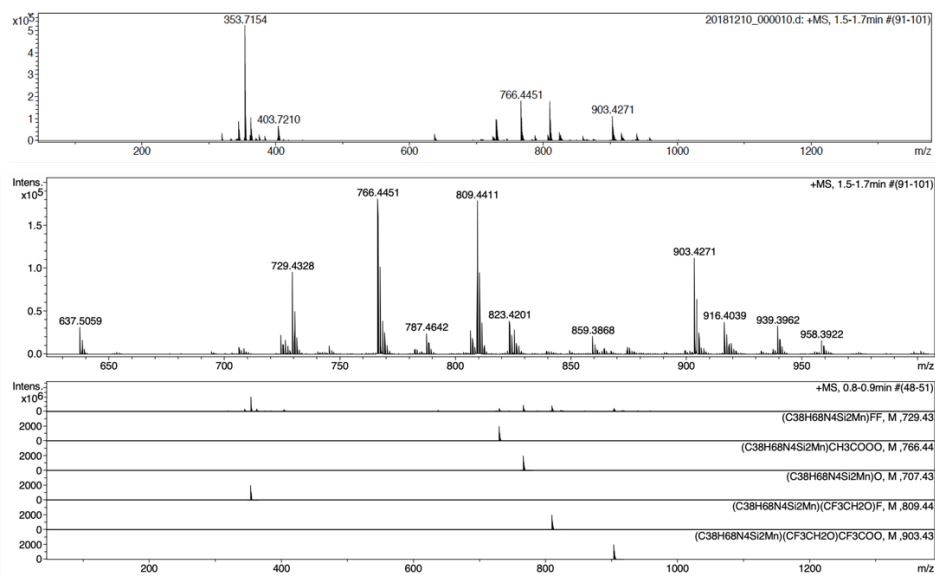


Figure B1. ESI-MS experiment of a catalytic experiment using catalyst **Mn**(^{tips}**bpmcn**) (1 mol%), HOAc (2 equiv) and H₂O₂ (1 equiv) in TFE at 0 °C. Top: full spectrum. Bottom: zoom of the left part of the spectrum with values of theoretical peaks.

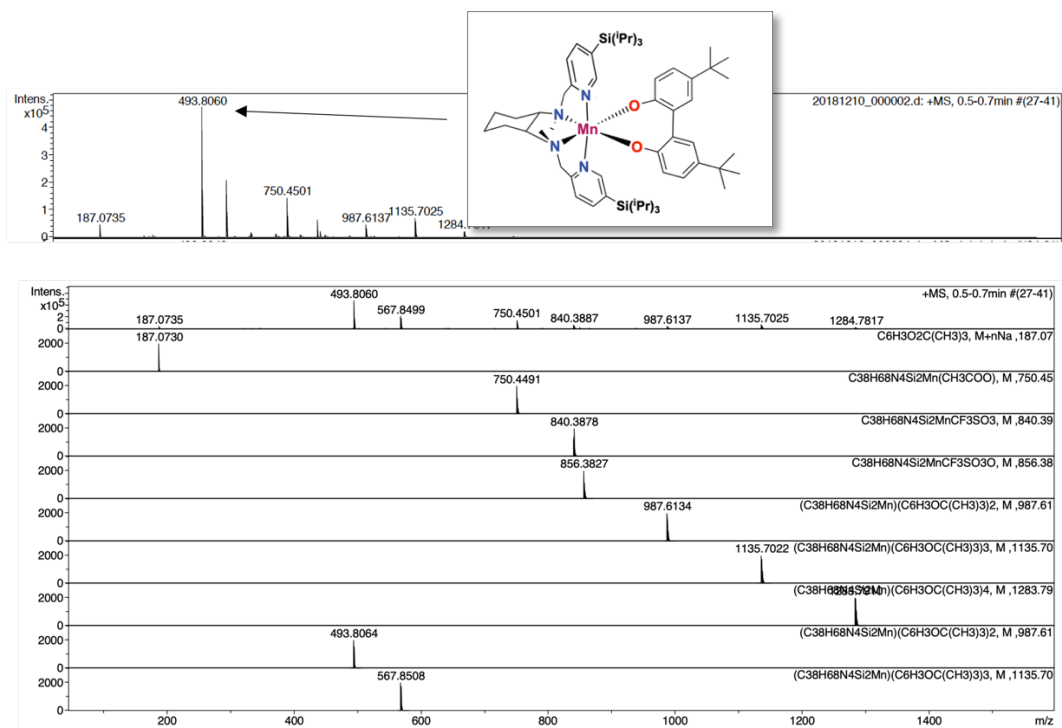
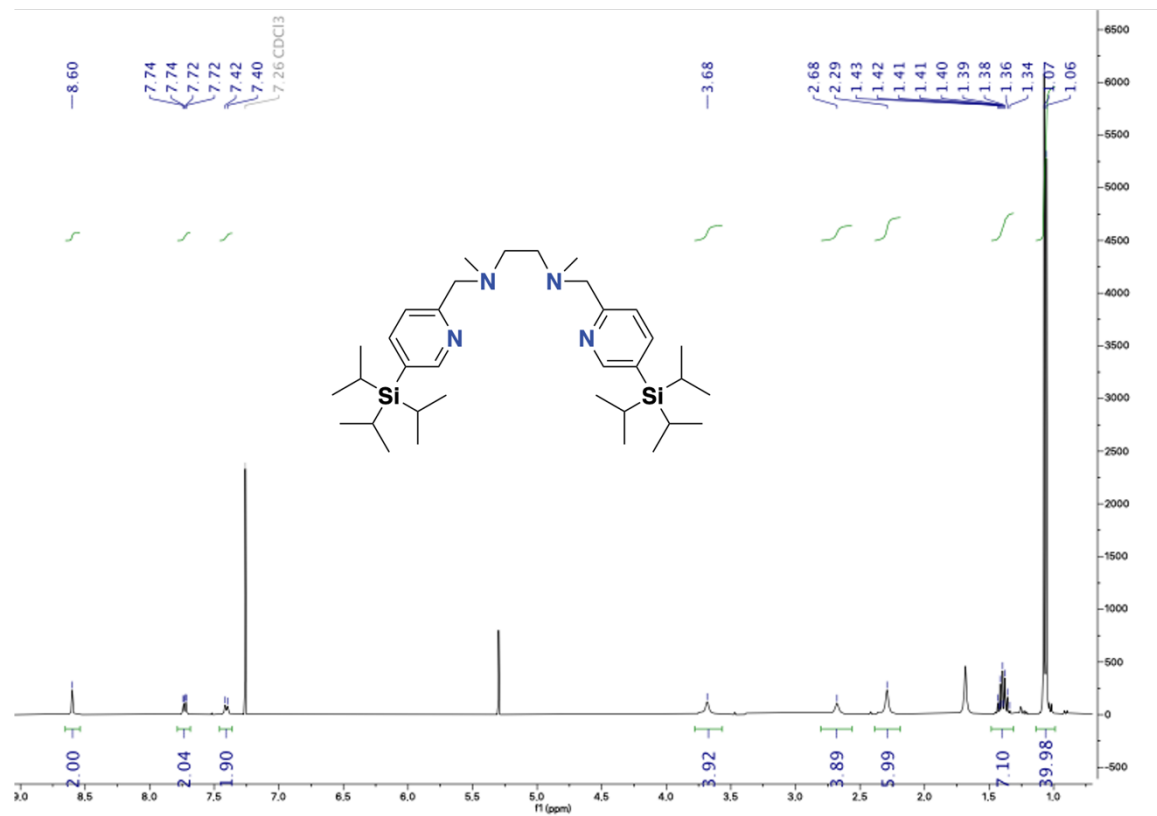
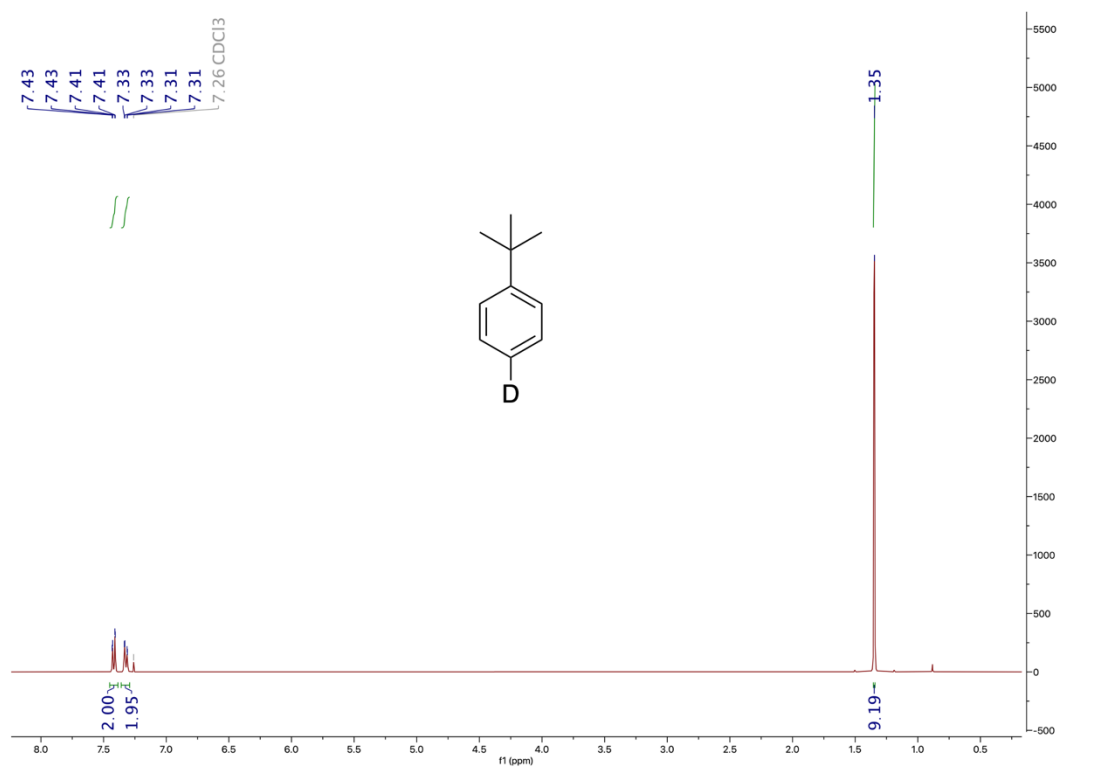


Figure B2. ESI-MS experiment of a catalytic experiment using catalyst **Mn**(^{tips}**bpmcn**) (1 mol%), HOAc (2 equiv), H₂O₂ (1 equiv) and *tert*-butylbenzene (1 equiv) in TFE at 0 °C. a) full spectrum, b) calculated theoretical peaks.

NMR Spectra

Figure B3. ^1H NMR spectra of *tipsbpmen* ligand.Figure B4. ^1H NMR spectra of *tert*-butylbenzene-4- d_1 .

Representative GC Chromatographs of Crude Reactions

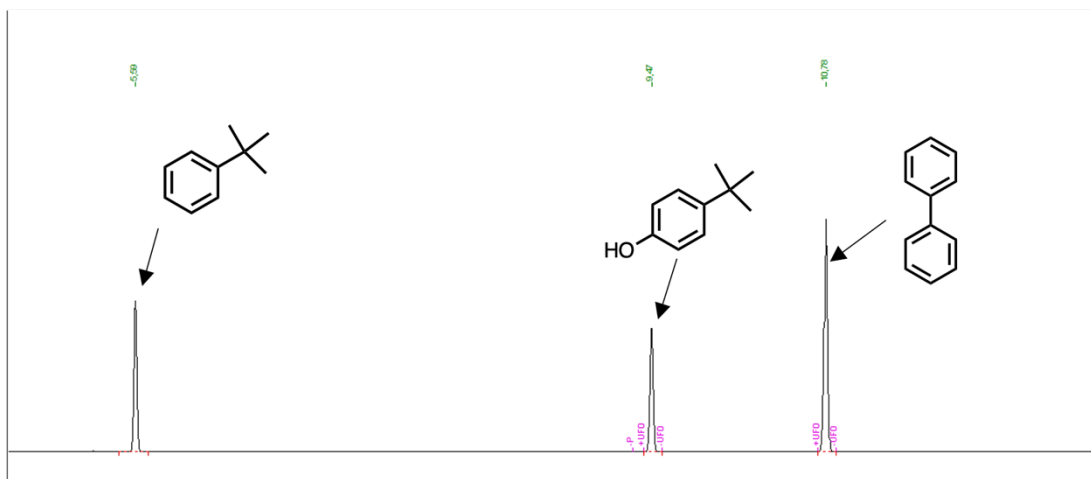


Figure B5. Representative GC chromatograph of a catalytic experiment with *tert*-butylbenzene as substrate.

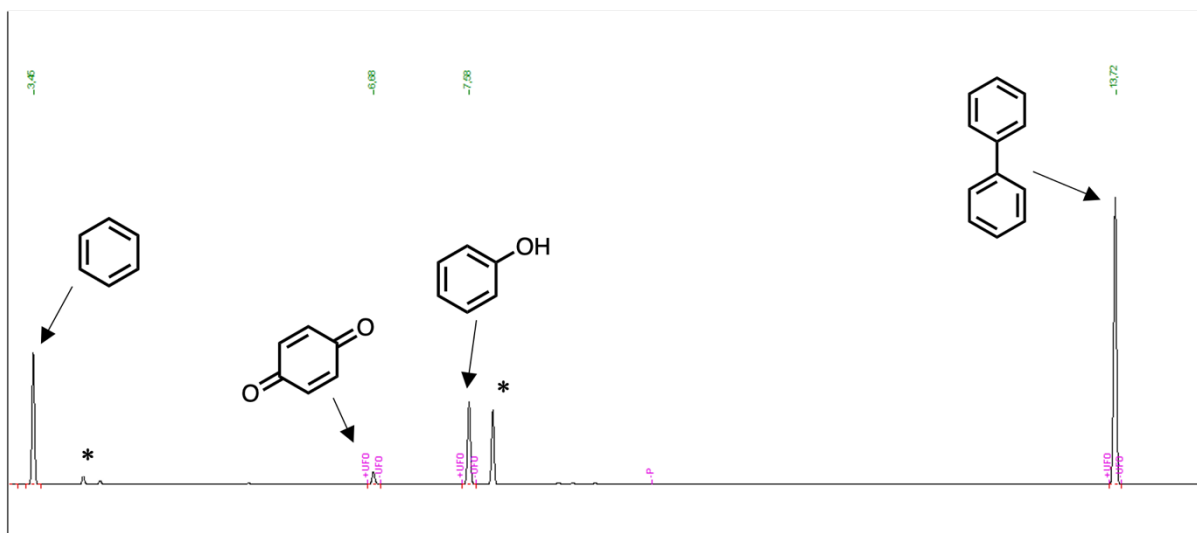


Figure B6. Representative GC chromatograph of a catalytic experiment with benzene as substrate. Peaks with the asterisk are impurities from the methyl acetate used in the experiments for the oxidation of benzene. Methyl acetate was used instead of ethyl acetate in order to flush the crude reaction mixture through a Celite®, silica and alumina plug; the reason being that the peak of benzene and ethyl acetate overlap in the GC chromatograph.

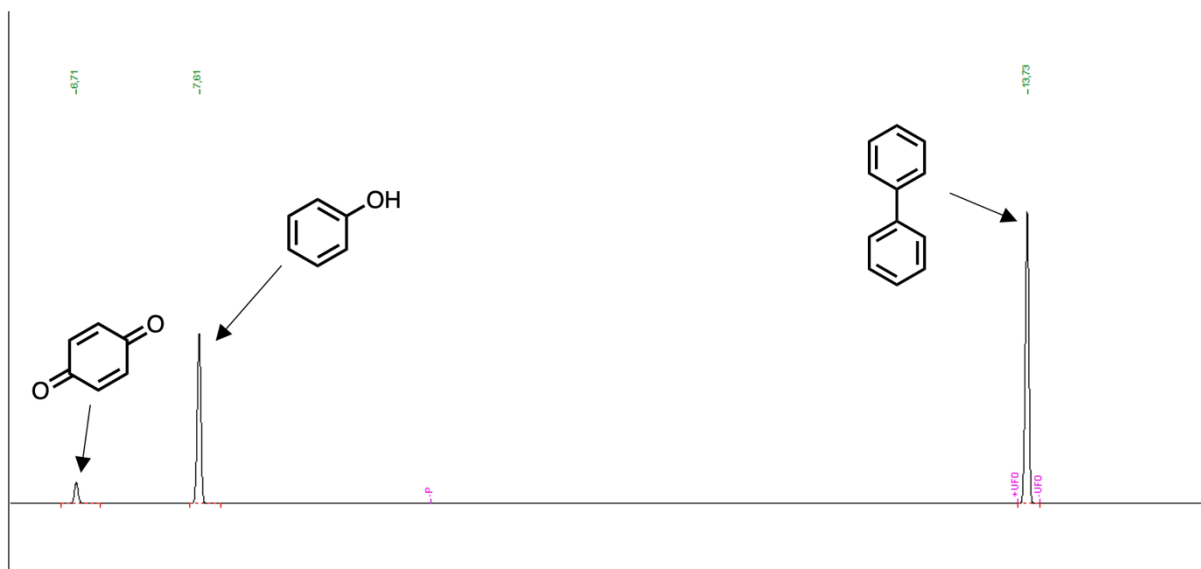


Figure B7. Representative GC chromatograph of a catalytic experiment with phenol as substrate.

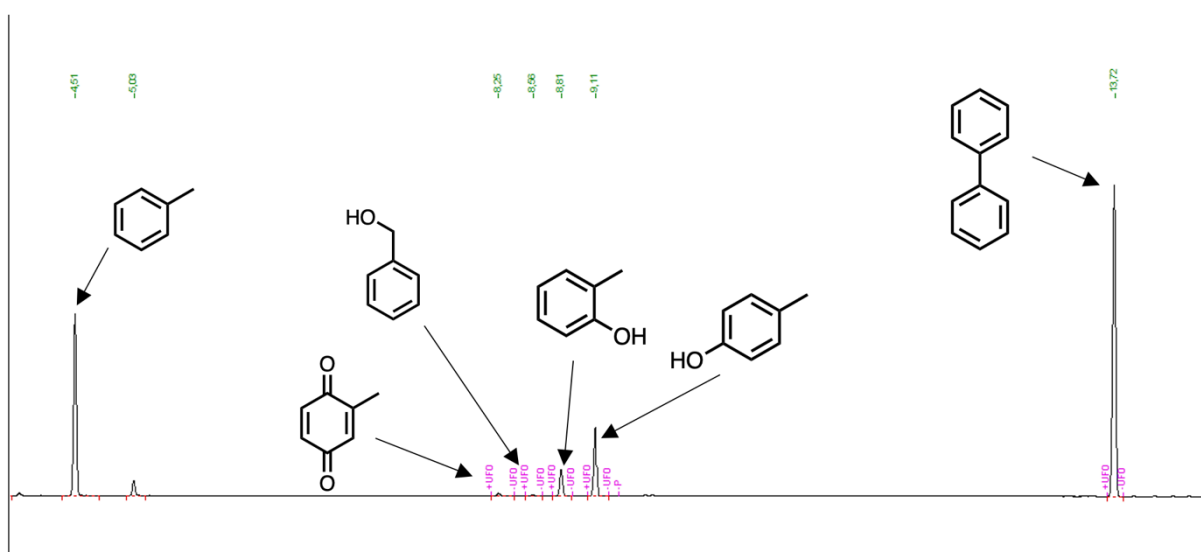


Figure B8. Representative GC chromatograph of a catalytic experiment with toluene as substrate (benzaldehyde was not detected).

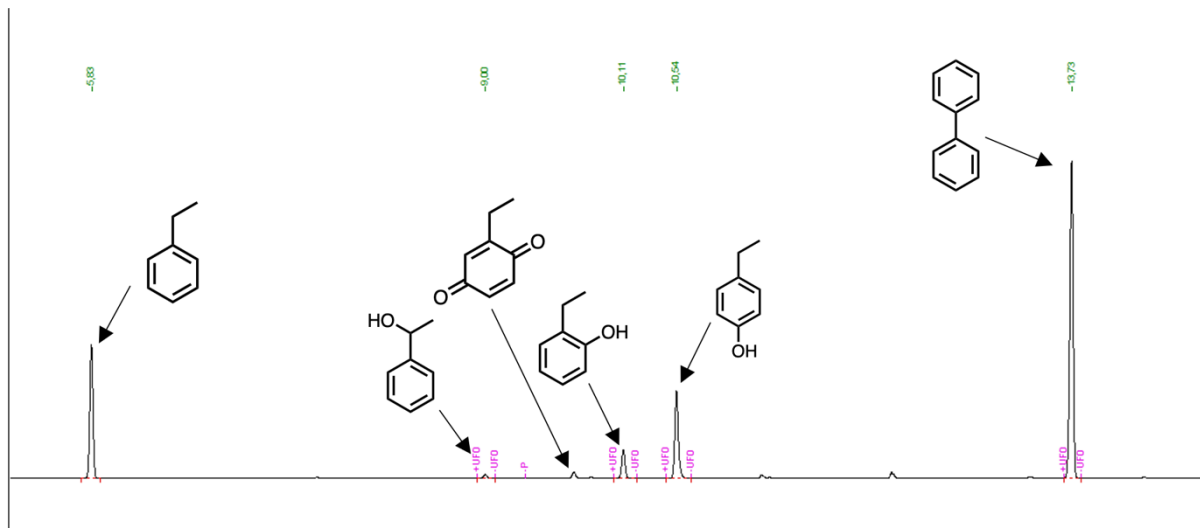


Figure B9. Representative GC chromatograph of a catalytic experiment with ethylbenzene as substrate (ketone product was not detected).

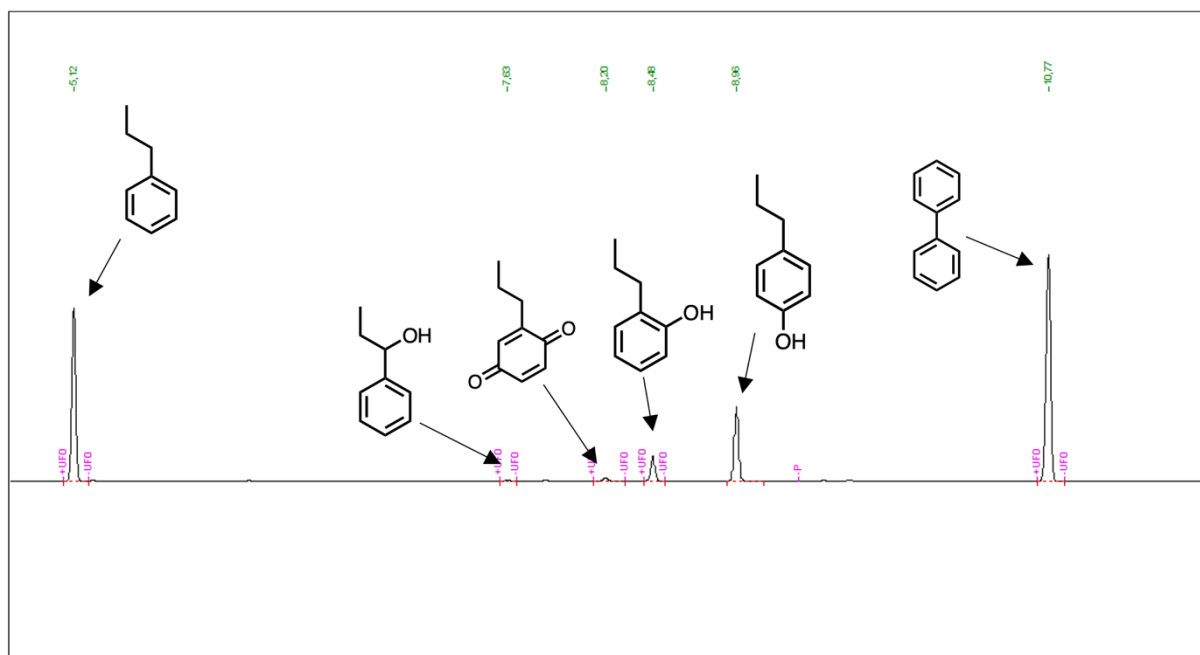


Figure B10. Representative GC chromatograph of a catalytic experiment with propylbenzene as substrate (ketone product was not detected).

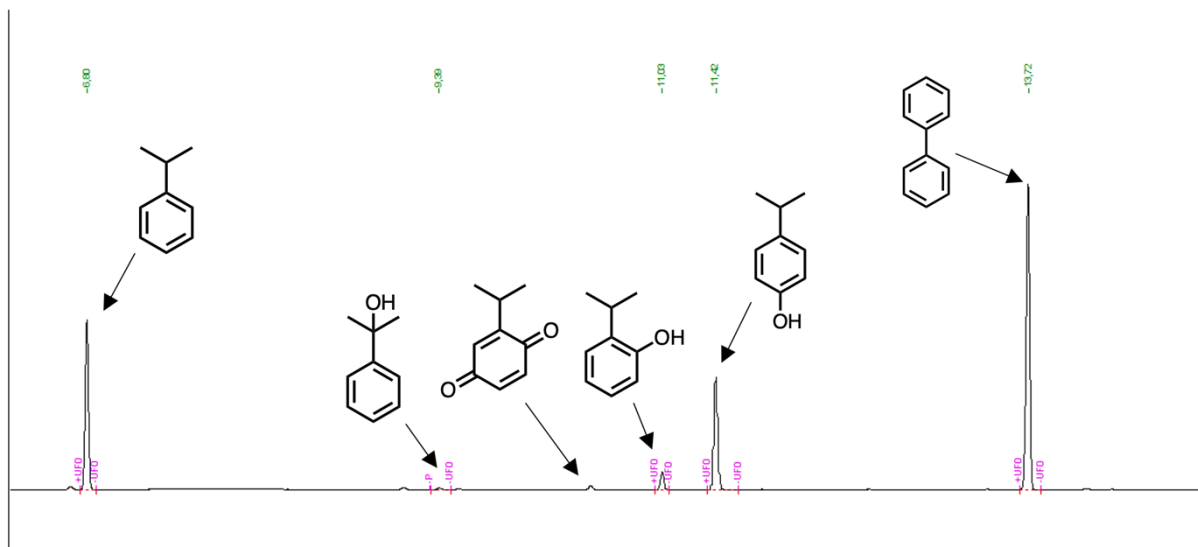


Figure B11. Representative GC chromatograph of a catalytic experiment with cumene as substrate.

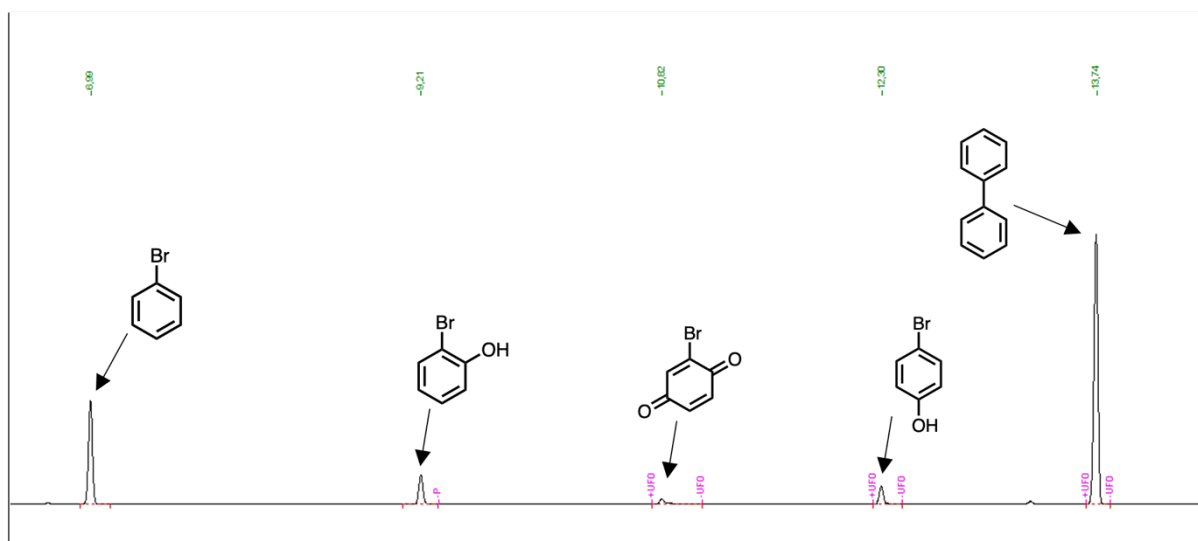


Figure B12. Representative GC chromatograph of a catalytic experiment with bromobenzene as substrate.

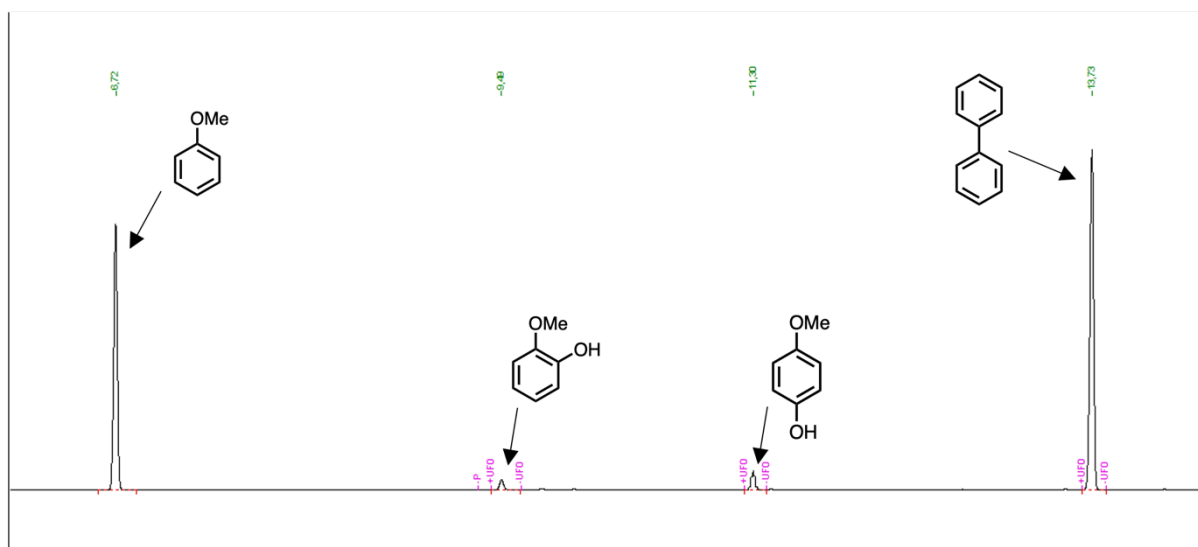


Figure B13. Representative GC chromatograph of a catalytic experiment with anisole as substrate (benzoquinone product was not detected).

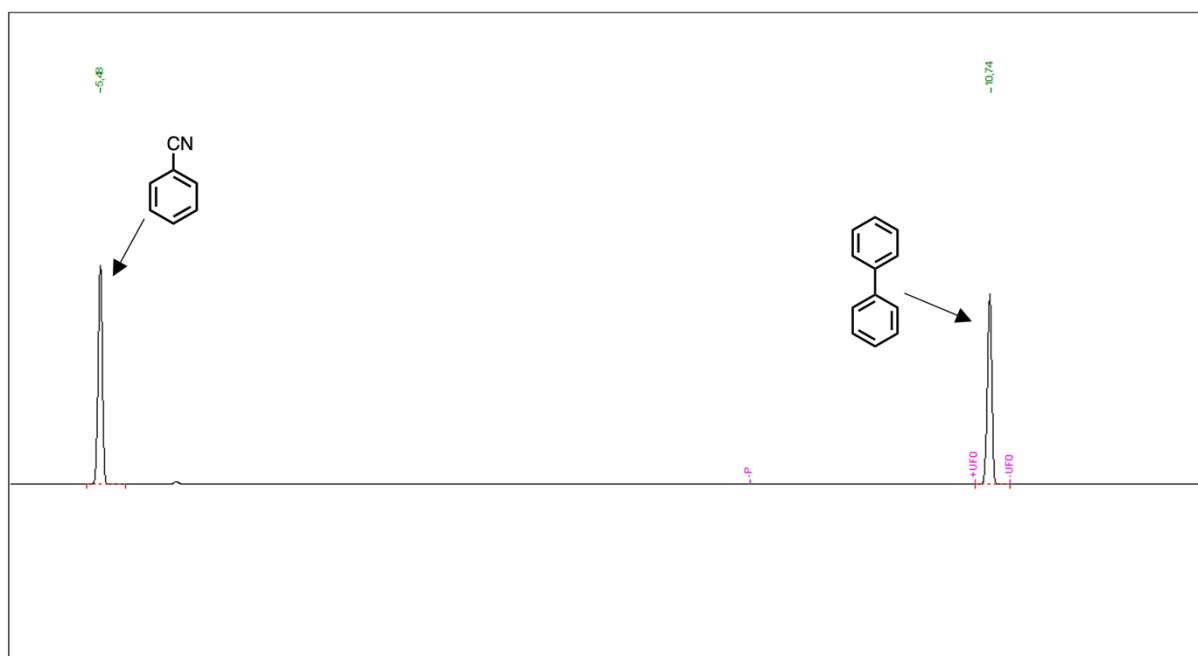
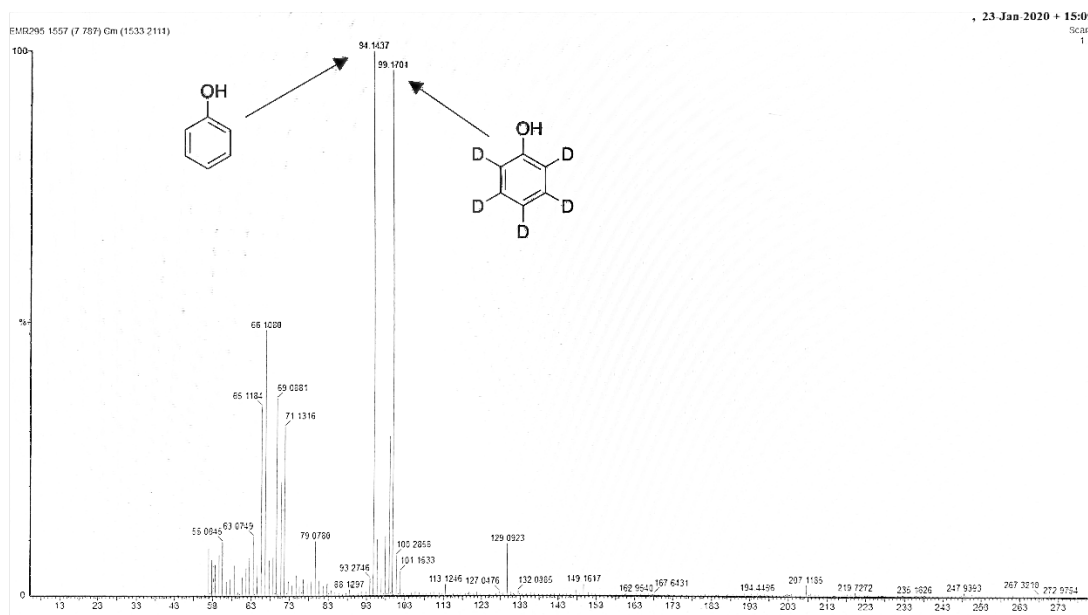
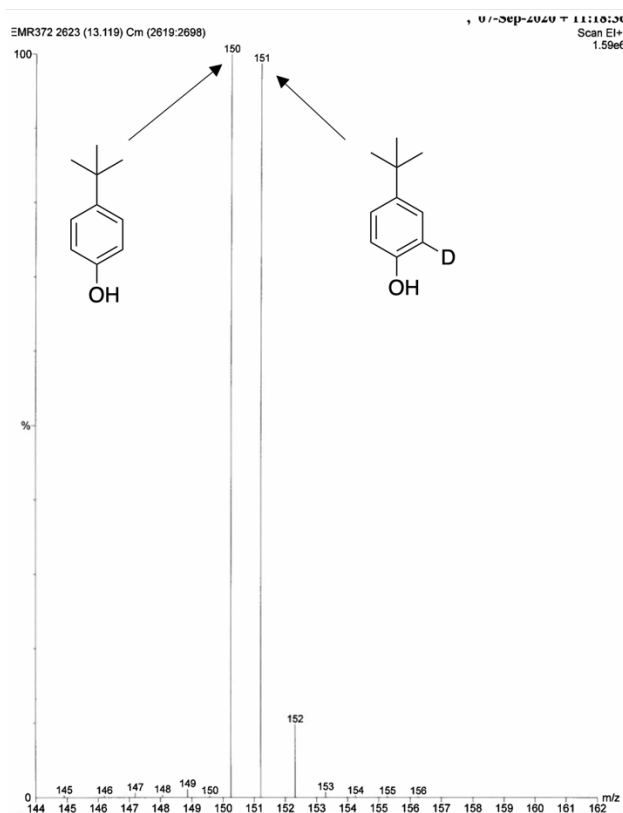


Figure B14. Representative GC chromatograph of a catalytic experiment with benzonitrile as substrate.

GC-MS Data

Figure B15. GC-MS spectrum from competitive oxidation between benzene and benzene-d₆.Figure B16. GC-MS spectrum from oxidation of *tert*-butyl-4-deuterobenzene.

Appendix C – Supplementary Information to Chapter 4

NMR spectra

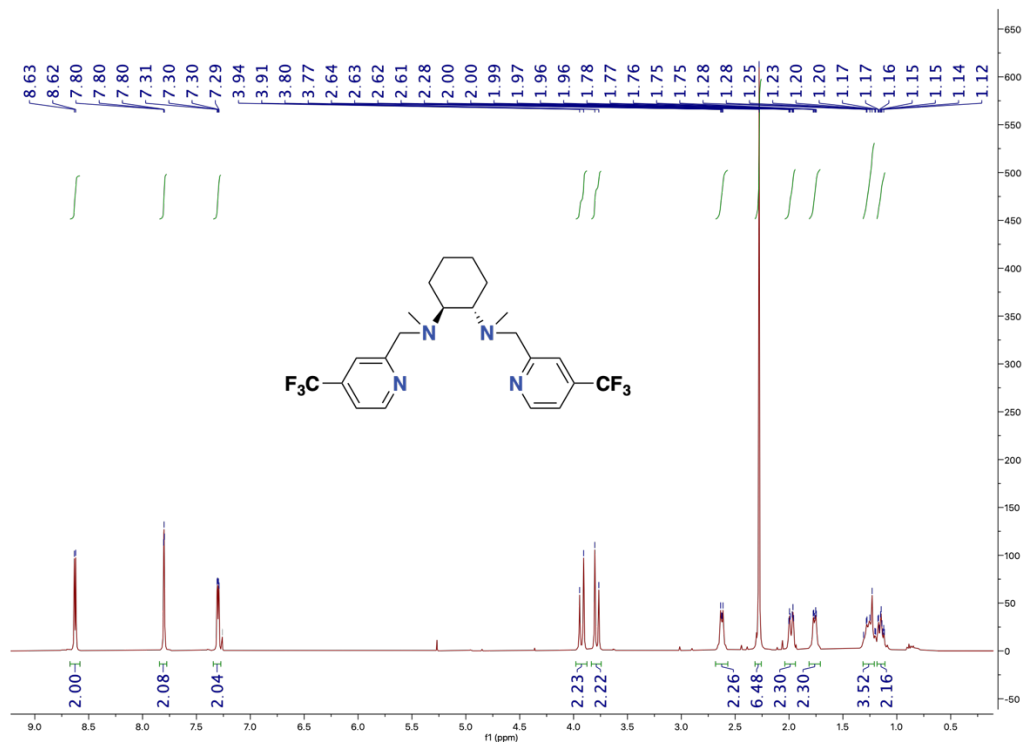


Figure C1. $^1\text{H-NMR}$ of $(S,S)\text{-CF}_3\text{bpmcn}$ in CDCl_3

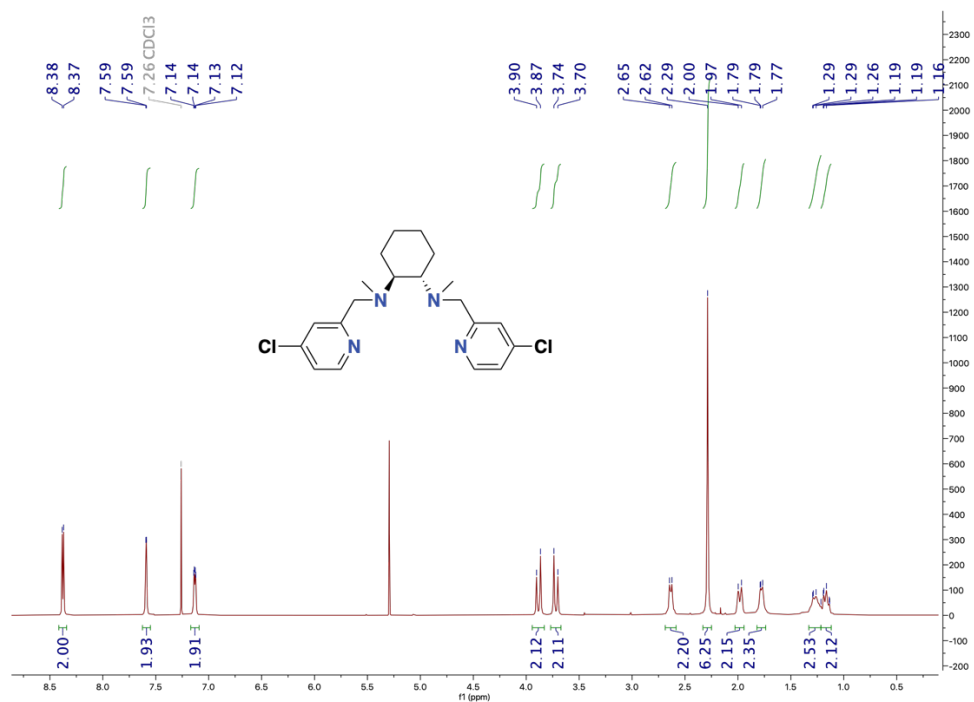
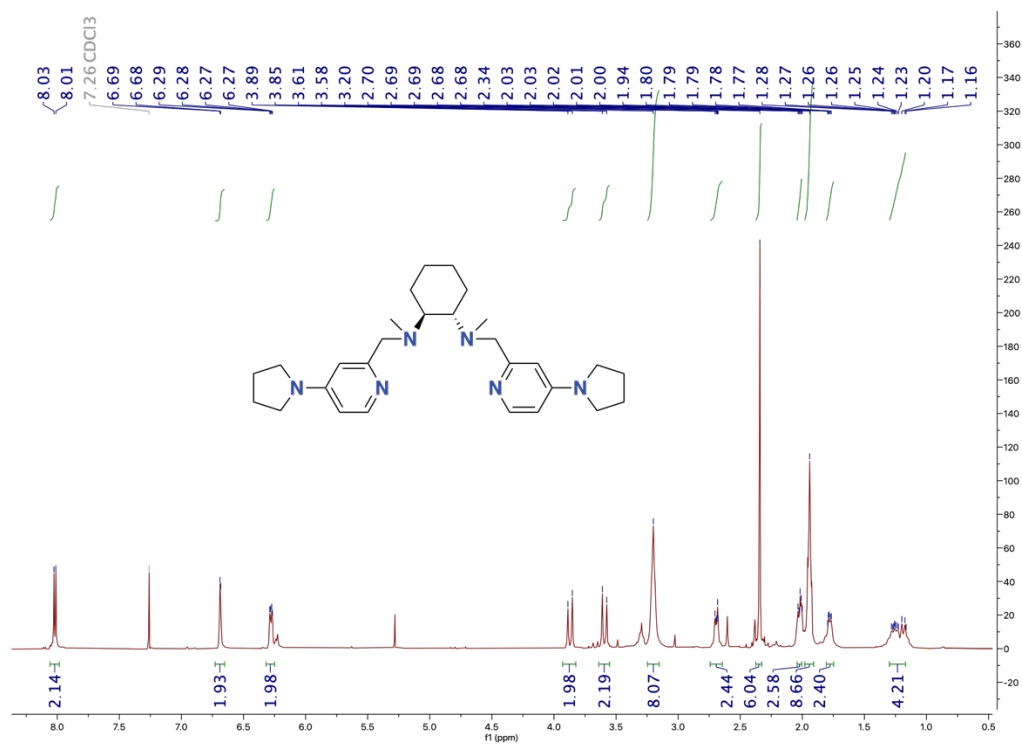
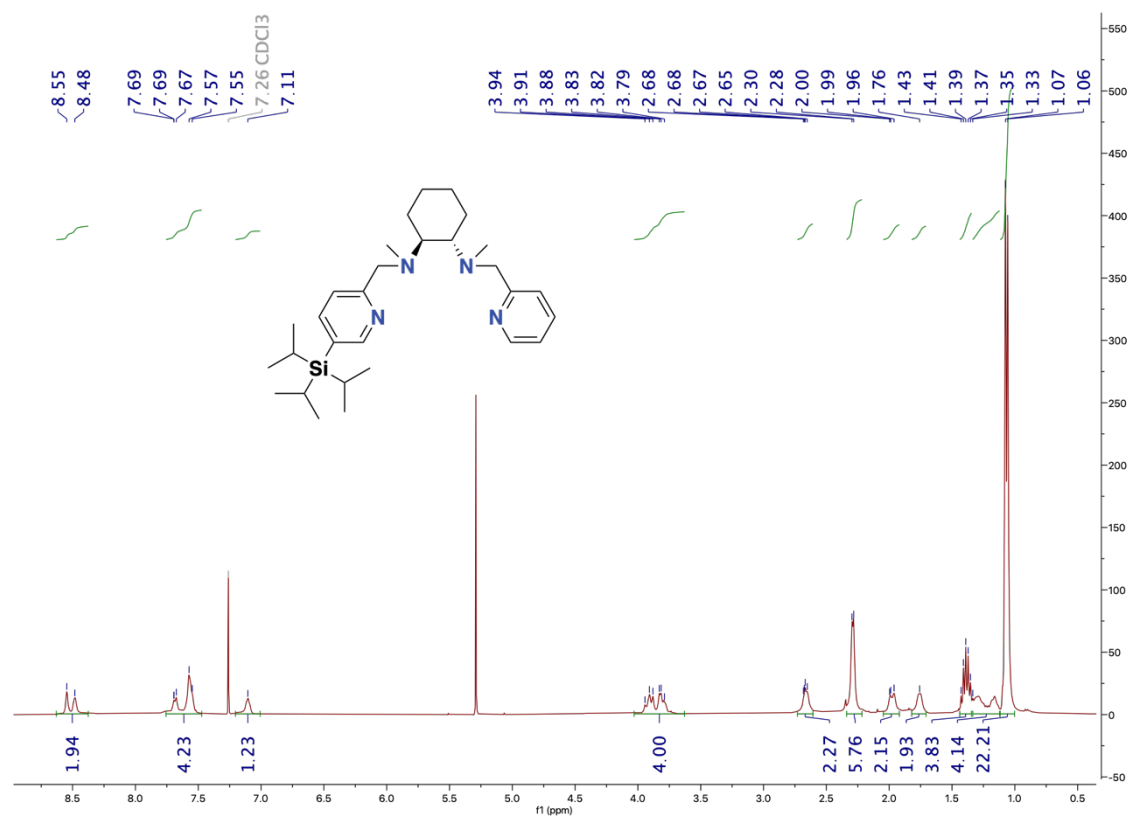


Figure C2. $^1\text{H-NMR}$ of $(S,S)\text{-Clbpmcn}$ in CDCl_3

Figure C3. ¹H-NMR of (S,S)-Pyrbpmcn in CDCl₃Figure C4. ¹H-NMR of (S,S)-H,tipsbpmcn in CDCl₃

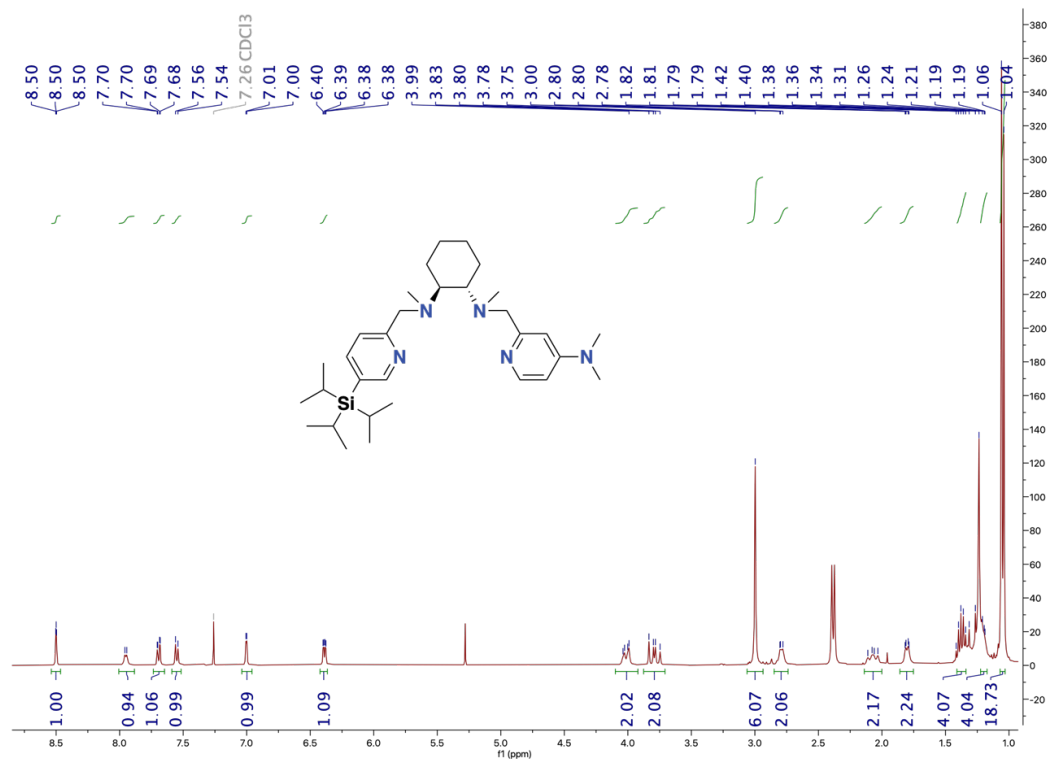


Figure C5. ¹H-NMR of (S,S)-NMe₂,TiPS₁bpmcn in CDCl₃

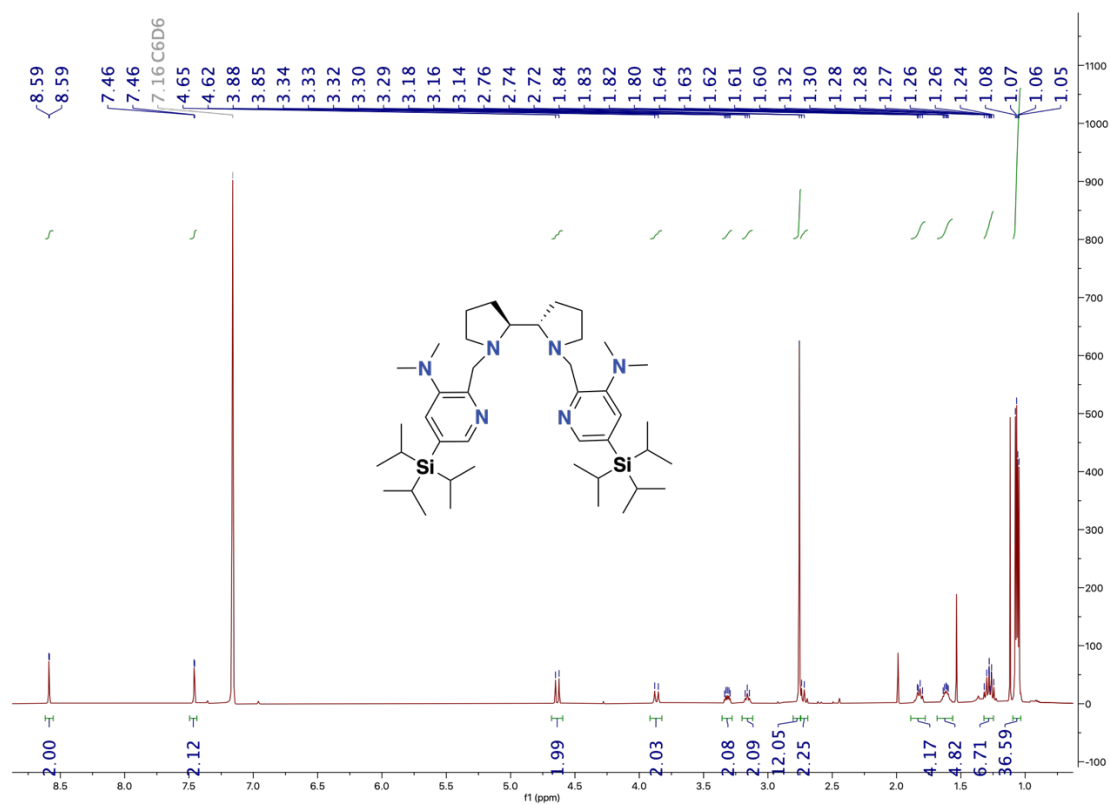


Figure C6. ¹H-NMR of 3-NMe₂-5-TiPS₁bpbp ligand in C₆D₆

Appendix D – Supplementary Information to Chapter 5

NMR spectra

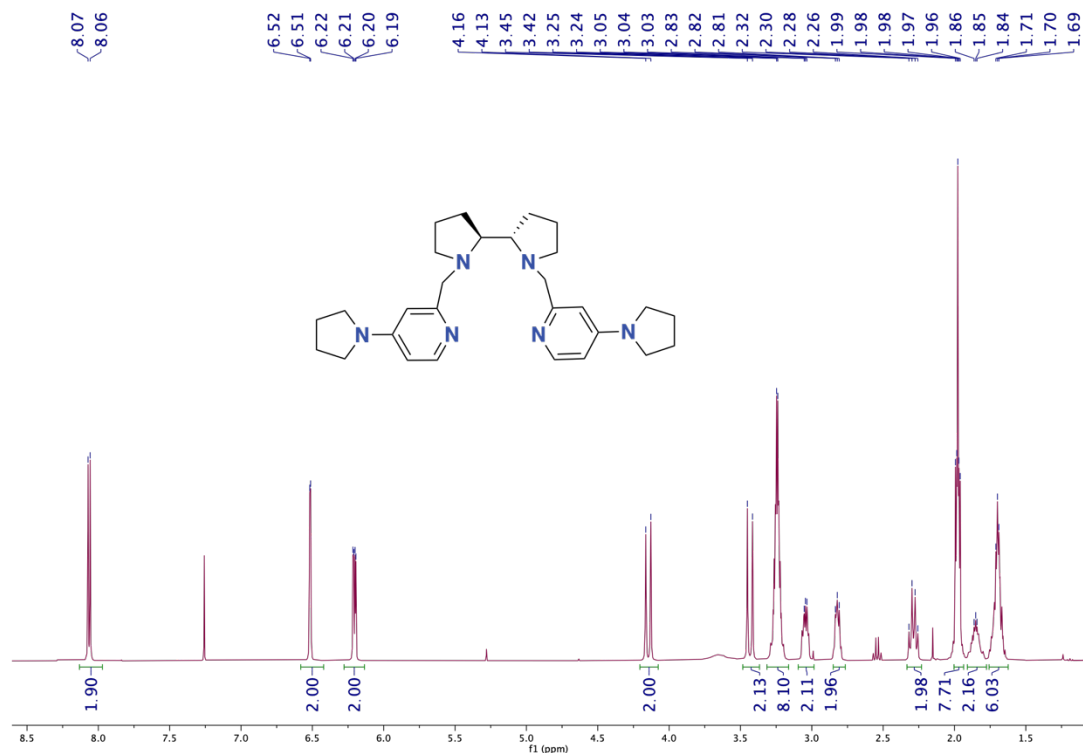


Figure D1. $^1\text{H-NMR}$ of (S,S) -Pyr'bbpb in CDCl_3

Representative GC and HPLC Chromatograms of Crude Reactions

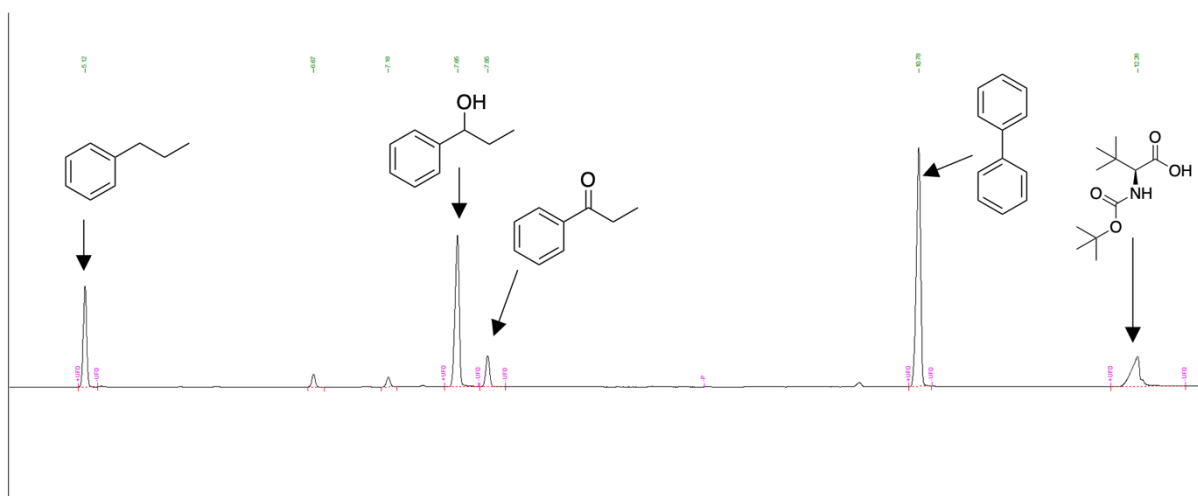
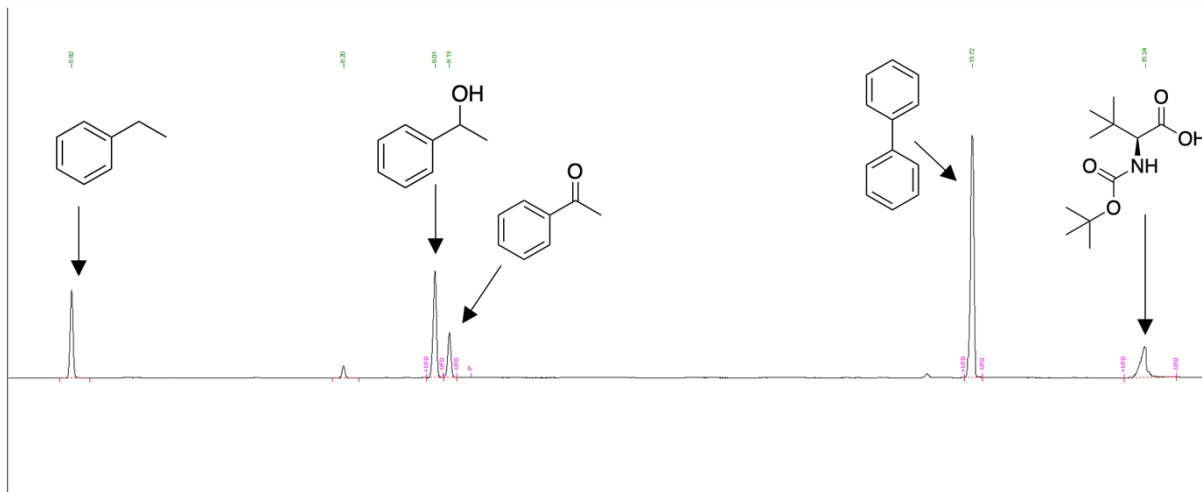


Figure D2. Representative GC chromatogram for the oxidation of propylbenzene.



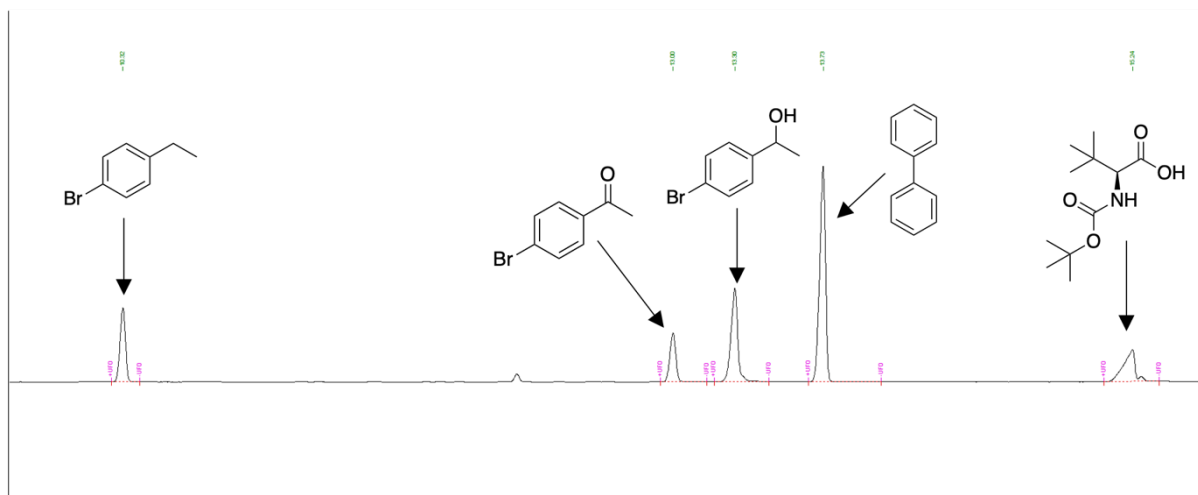


Figure D6. Representative GC chromatograph for the oxidation of 1-bromo-1-ethylbenzene.



Figure D7. Representative GC chromatograph for the oxidation of 4-ethylanisole.

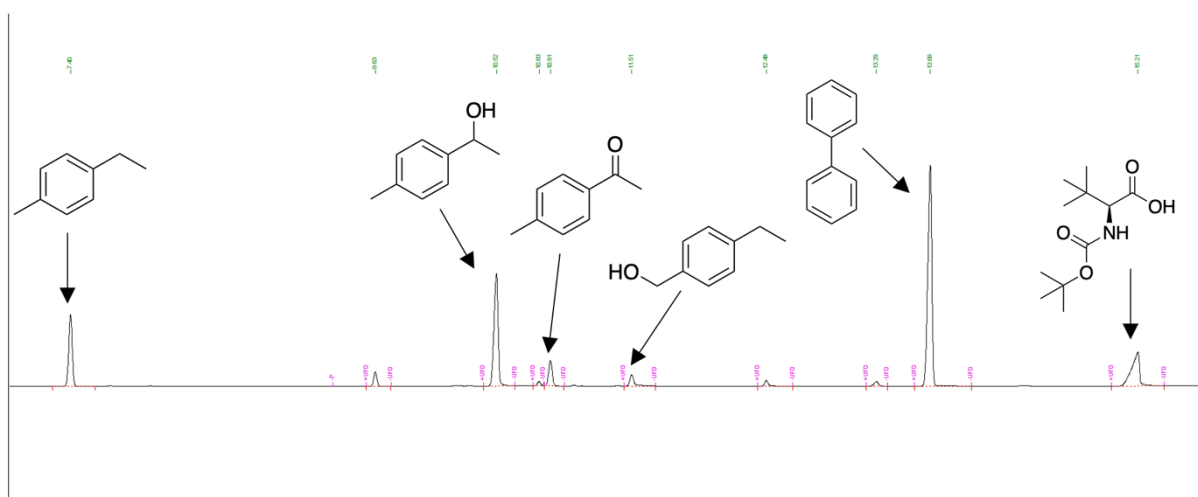


Figure D8. Representative GC chromatograph for the oxidation of 4-ethyltoluene.

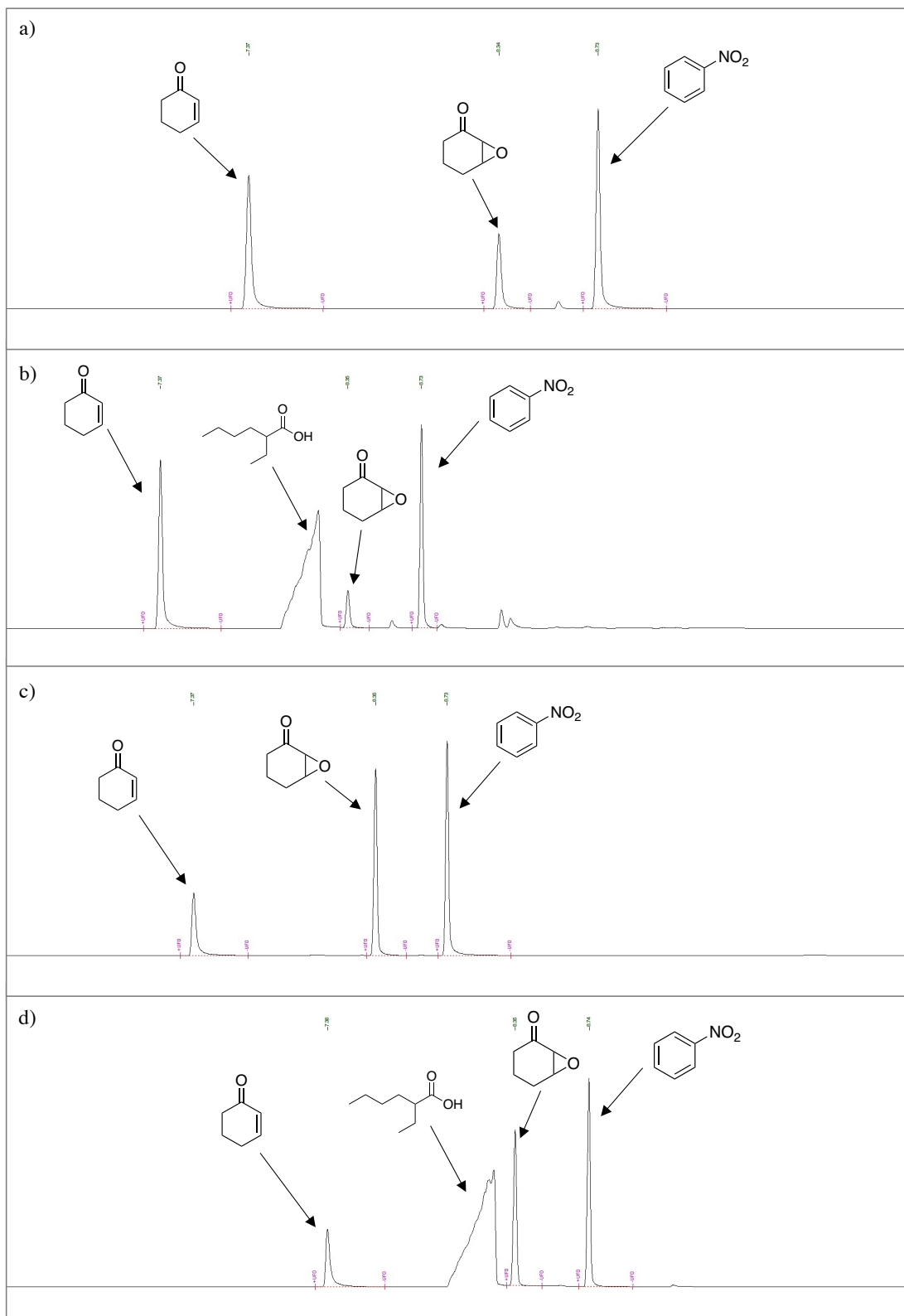


Figure D9. Representative GC chromatographs for the epoxidation of 2-cyclohexenone. a) GC chromatograph corresponding to a catalytic experiment using $\text{Mn}(\text{Pyrbppp})$ and AA. b) GC chromatograph corresponding to a catalytic experiment using $\text{Mn}(\text{Pyrbppp})$ and 2-eha. c) GC chromatograph corresponding to a catalytic experiment using $\text{Fe}(\text{Pyrbppp})$ and AA. d) GC chromatograph corresponding to a catalytic experiment using $\text{Fe}(\text{Pyrbppp})$ and 2-eha.

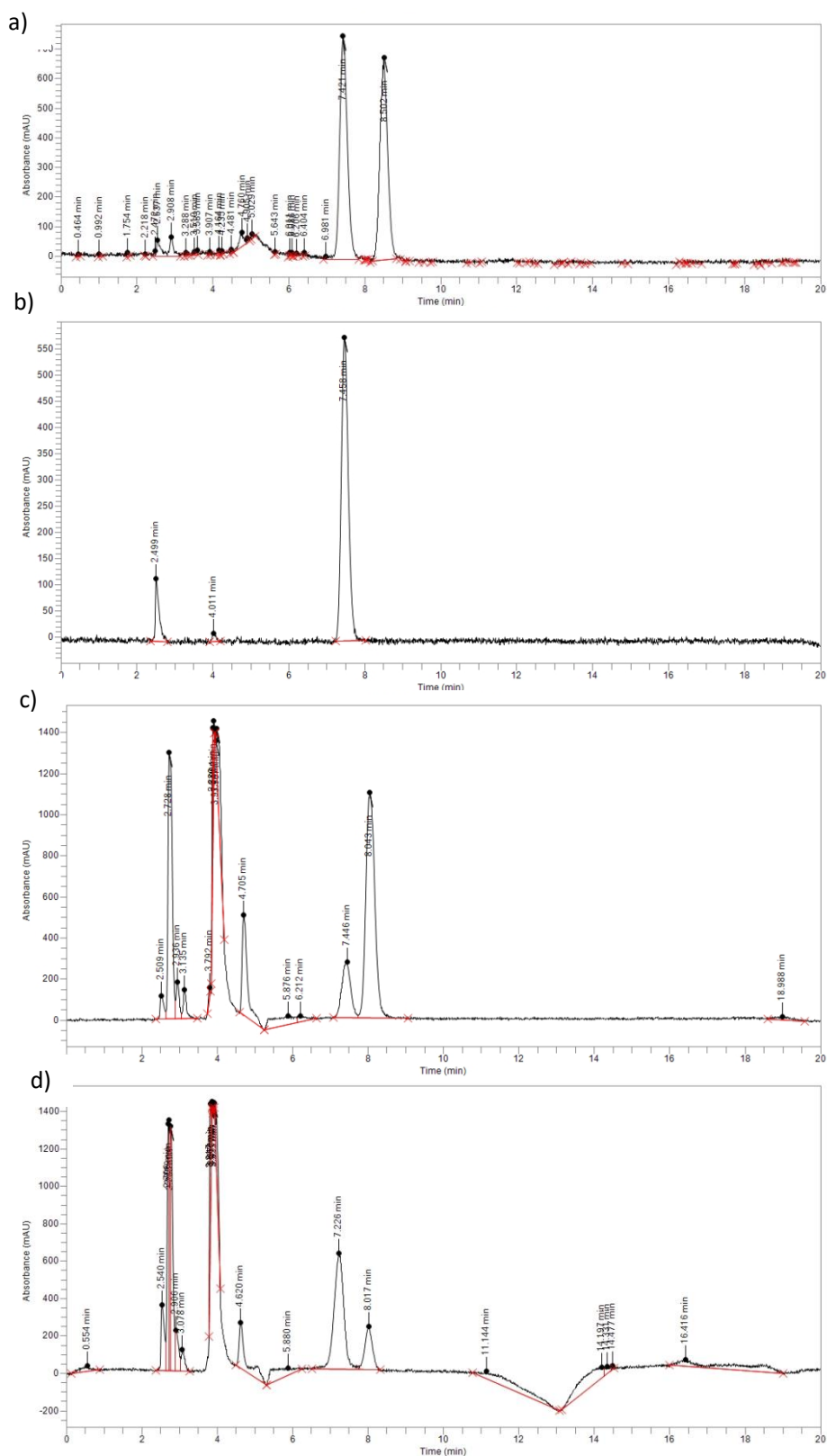


Figure D10. Representative HPLC chromatographs for the oxidation of propylbenzene. a) Chromatograph corresponding to the racemic mixture of 1-phenyl-1-propanol. b) Chromatograph corresponding to (*R*)-(+)-1-phenyl-1-propanol. c) Chromatograph corresponding to the catalytic experiment using (*S,S*)-Mn(*P*^{yr}bpbp). d) Chromatograph corresponding to the catalytic experiment using (*R,R*)-Mn(*P*^{yr}bpbp).

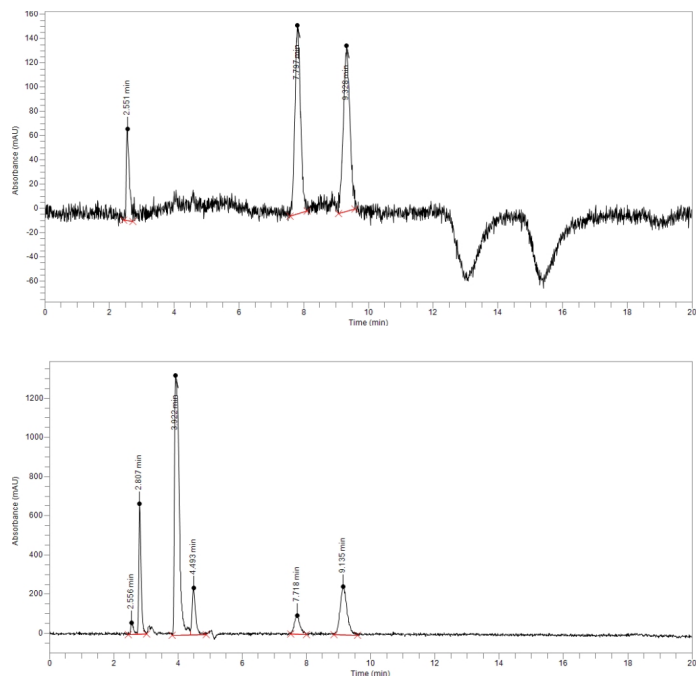


Figure D11. Representative HPLC chromatographs for the oxidation of ethylbenzene. Top: Chromatograph corresponding to the racemic mixture of 1-phenylethanol. Bottom: Chromatograph corresponding to the catalytic experiment.

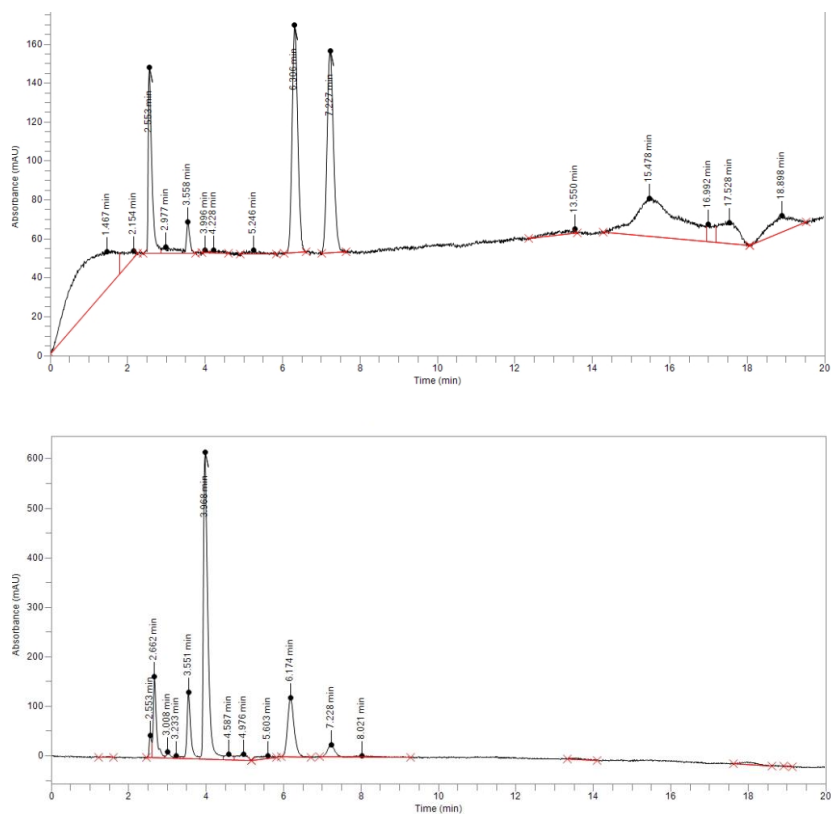


Figure D12. Representative HPLC chromatographs for the oxidation of isobutylbenzene. Top: Chromatograph corresponding to the racemic mixture of 2-methyl-1-phenyl-1-propanol. Bottom: Chromatograph corresponding to the catalytic experiment.

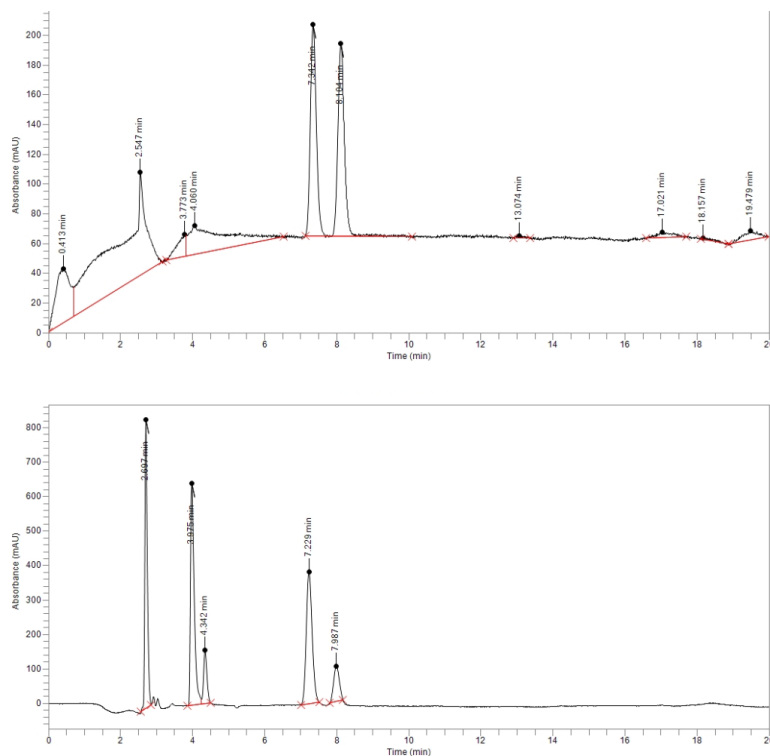


Figure D13. Representative HPLC chromatographs for the oxidation of 1-chloro-4-ethylbenzene. Top: Chromatograph corresponding to the racemic mixture of 1-(4-chlorophenyl)ethanol. Bottom: Chromatograph corresponding to the catalytic experiment.

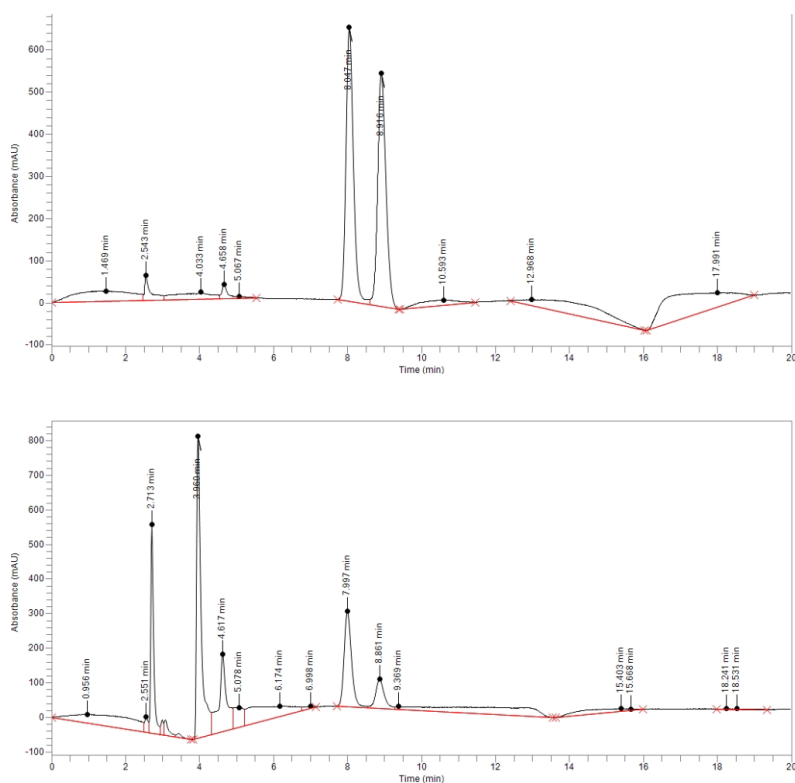


Figure D14. Representative HPLC chromatographs for the oxidation of 1-bromo-4-ethylbenzene. Top: Chromatograph corresponding to the racemic mixture of 4-bromo-alpha-methylbenzyl alcohol. Bottom: Chromatograph corresponding to the catalytic experiment.

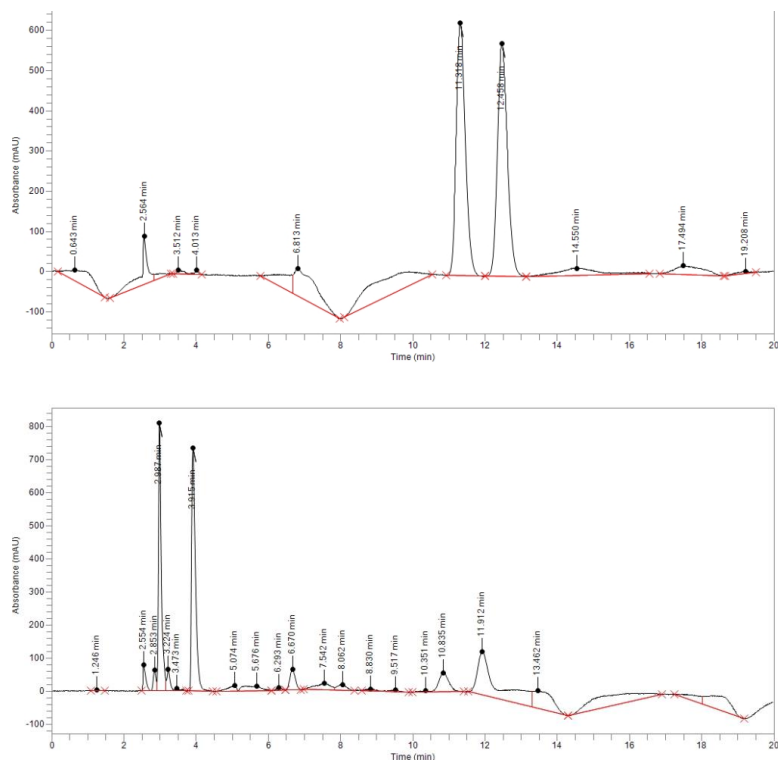


Figure D15. Representative HPLC chromatographs for the oxidation of 4-ethylanisole. Top: Chromatograph corresponding to the racemic mixture of 4-methoxyphenyl methyl carbinol. Bottom: Chromatograph corresponding to the catalytic experiment.

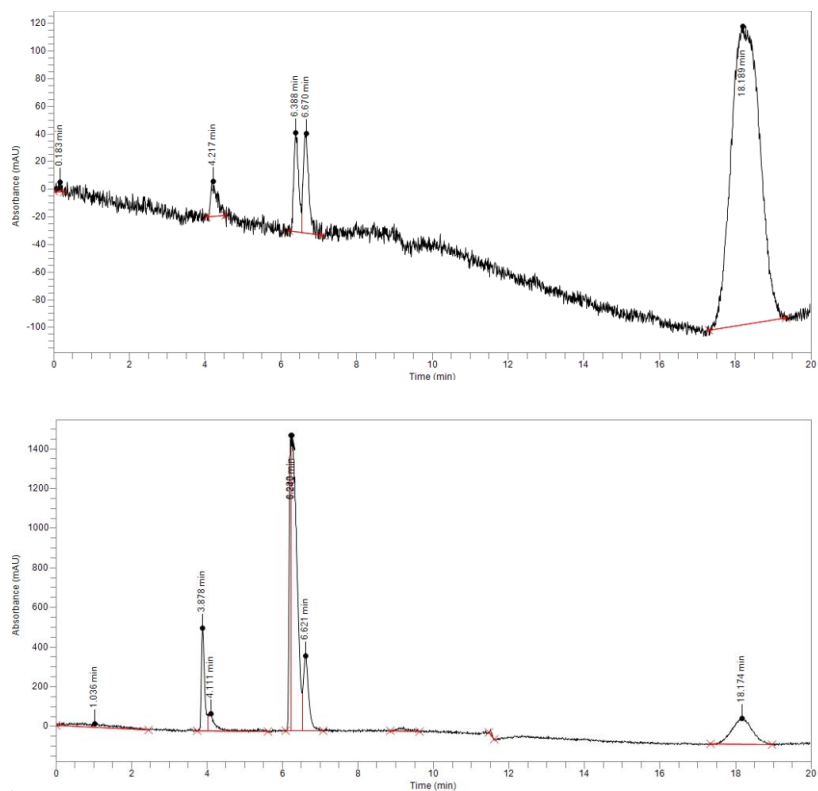
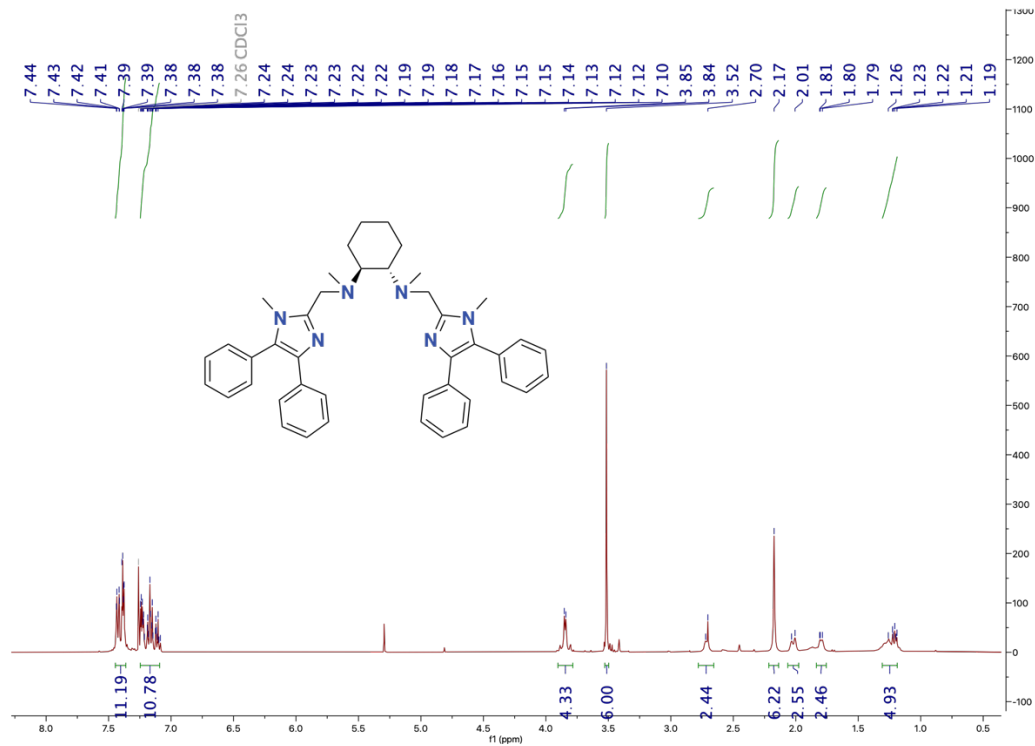
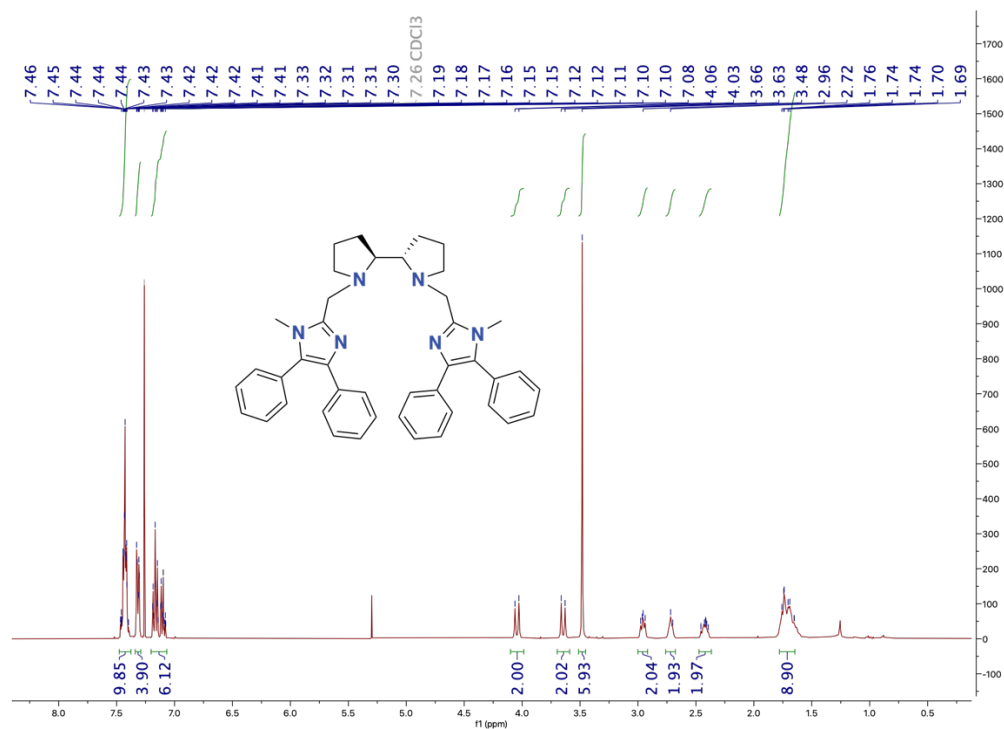


Figure D16. Representative HPLC chromatographs for the oxidation of 4-ethyltoluene. Top: Chromatograph corresponding to the racemic mixture of alpha,4-dimethylbenzyl alcohol. Bottom: Chromatograph corresponding to the catalytic experiment.

Appendix E – Supplementary Information to Chapter 6

NMR spectra

Figure D1. ^1H NMR of (S,S) -Ph₂Imzbpmcn (L1) in CDCl₃Figure D2. ^1H NMR of (S,S) -Ph₂Imzbpbp (L2) in CDCl₃

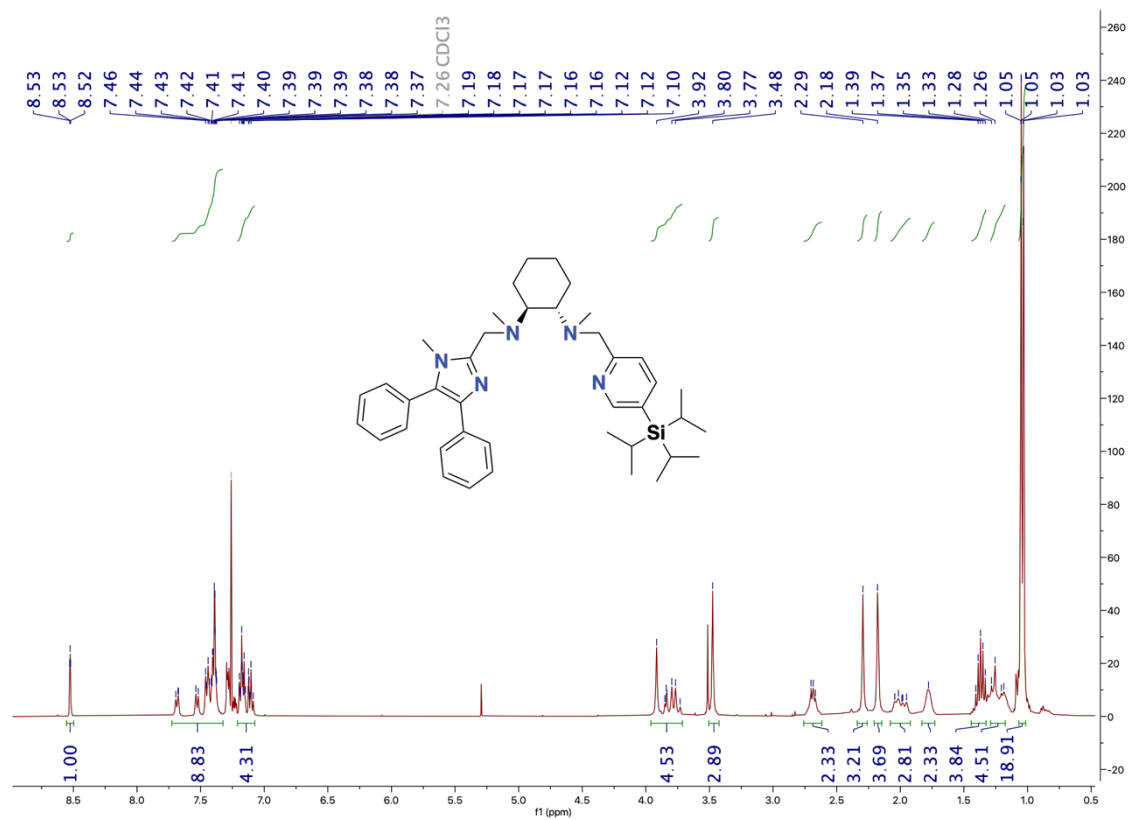


Figure D3. ¹H NMR of **(S,S)-TIPS,Ph₂Imz]bpmcn (L3)** in CDCl₃

Summary

Because of the low availability, toxicity and high price of noble metals, the development of new coordination complexes based on first-row transition metals (*i.e.* non-noble metals) as catalysts is highly desirable and required. Nowadays, we can see how this transition is materializing in the field of homogeneous catalysis, and particularly in oxidation chemistry. Along the same line, the present thesis focuses on the development of new first-row transition metal complexes as catalysts for aromatic oxidation reactions, using aqueous hydrogen peroxide as a benign oxidant. The interest in these reactions relies on the phenol products, which are highly desirable as intermediates for the generation of pharmaceuticals and functional polymers. Particularly challenging is the development of catalytic reactions that directly yield phenol products through the direct oxidation of aromatic C–H bonds of an arene substrate, and concomitantly avoid overoxidation of the phenol product and display a high regioselectivity amongst the C–H bonds present within the arene substrate.

Chapter 1 of this thesis presents an extensive review on aromatic oxidation reactions catalyzed by metalloenzymes and by synthetic first-row transition-metal complexes as homogeneous catalysts. The chapter is classified on basis of the transition-metal employed (*i.e.* iron, copper, nickel and manganese), as well as on the type of system (*i.e.* metalloenzymes or synthetic metal complexes). On the one hand, iron and copper containing metalloenzymes have been widely studied and many of these show catalytic activity for the oxidation of aromatic substrates using dioxygen. On the other hand, there are no nickel and manganese containing metalloenzymes known to perform aromatic oxidations in nature, despite several of them being active in other types of oxidation processes. Regarding synthetic metal complexes, in the past years many studies have focused on the investigation of bio-inspired iron catalysts and, consequently, a huge number of iron-based catalytic systems have been reported to perform arene oxidation reactions using benign sacrificial oxidants. In the same vein, bio-inspired copper complexes have also been investigated in detail for aromatic oxidation reactions, but most of the examples display stoichiometric reactions, and only in recent years have catalytic systems been described. Finally, synthetic nickel and manganese complexes have been much less explored in the field of arene oxidation, and only few examples have been reported to date. Overall, this chapter shows the currently known metalloenzymes found in nature to perform arene oxidations, as well as the development of first-row transition metal complexes able to carry out these reactions and the corresponding mechanistic studies.

In **Chapter 2** of this thesis, an investigation is presented on the ability of nickel(II) complexes supported by tripodal tetradentate aminopyridine ligands to catalyze the direct

hydroxylation of benzene to phenol using aqueous H_2O_2 as oxidant. A set of tripodal tetradentate aminopyridine ligands and their corresponding nickel(II) complexes have been synthesized and characterized (Figure 1). Catalytic tests were carried out using benzene as substrate, triethylamine as a base, and H_2O_2 in acetonitrile as solvent, while employing 10 mol% of catalyst loading. Catalytic reactions run under air, at 60 °C, and for 5 h using a closed reaction vessel resulted in phenol yields ranging from 9-10 % (*i.e.* no more than one turnover number per nickel). These findings showed that the use of different aminopyridine ligands in the nickel complexes does not lead to different reactivity in arene oxidation, therefore suggesting that the ligands do not play an important role in catalysis. Moreover, a screening of different reaction solvents showed that the fluorinated alcohol 1,1,1,3,3,3-hexafluoro-2-propanol (HFIP) is the best solvent to perform the oxidation of benzene to phenol. In addition, several nickel(II) salts, including nickel nitrate hexahydrate and nickel chloride hexahydrate, led to 7 and 3 % phenol yield, respectively, showing that aromatic oxidation can also be achieved using simple commercial nickel(II) salts with high chemoselectivity. Overall, the involvement of a putative dinickel(III) bis(μ -oxo) species as intermediate was questioned in this chapter, and it is suggested that decomposition of the nickel complex occurs under the experimental conditions, possibly leading to the formation of nickel-based nanoparticles that are involved in catalysis.

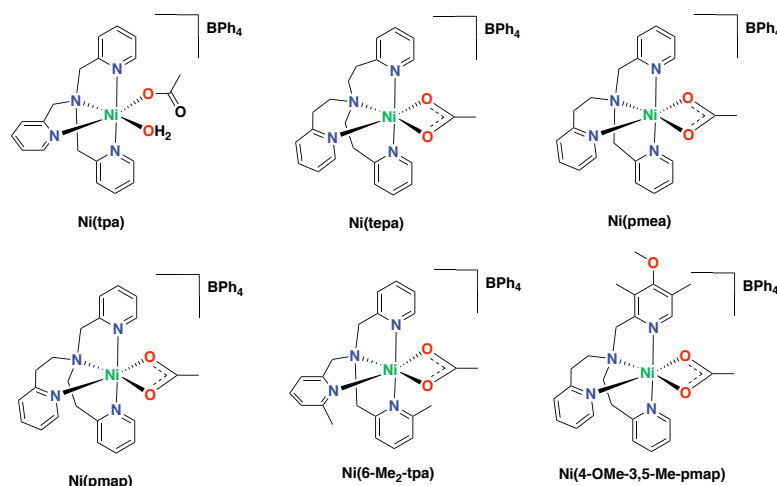


Figure 1. Nickel(II) complexes supported by tetradentate aminopyridine ligands studied in **Chapter 2**.

Next, **Chapter 3** reveals the catalytic capacity of bulky manganese complexes in aromatic oxidation reactions. In the past, manganese complexes supported by aminopyridine ligands have been shown to act as excellent catalysts for different kinds of oxidation reactions, such as aliphatic C–H oxidations and epoxidation of alkenes. In addition, the introduction of bulky triisopropylsilyl (TIPS) groups in tetradentate aminopyridine ligands has been reported to efficiently modulate the regioselectivity of aliphatic C–H oxidations. Along the same line, bioinspired manganese(II) complexes containing bulky tetradentate aminopyridine ligands were investigated in Chapter 3 as catalysts for the direct hydroxylation of aromatic substrates

to the corresponding phenol products with aqueous H_2O_2 . Particularly, it was found that the combination of a bulky manganese complex, a halogenated carboxylic acid additive, a fluorinated alcohol solvent, and H_2O_2 allows for the oxidation of alkylbenzenes towards phenol products with product yields that are amongst the highest reported for homogeneous arene oxidation catalysts, *i.e.* 29 – 37% yield for aromatic oxidation products with the *para*-phenol as the main product in all cases (Figure 2). The observed reactivity is reminiscent to reactions proceeding via an electrophilic aromatic substitution type of mechanism. Interestingly, it was found that the chemoselectivity of the oxidation reaction depends on the ligand used. While complexes with bulky aminopyridine ligands favor oxidation of the aromatic ring, complexes containing electron-rich aminopyridine ligands oxidize the more activated aliphatic (benzylic) position (Figure 2).

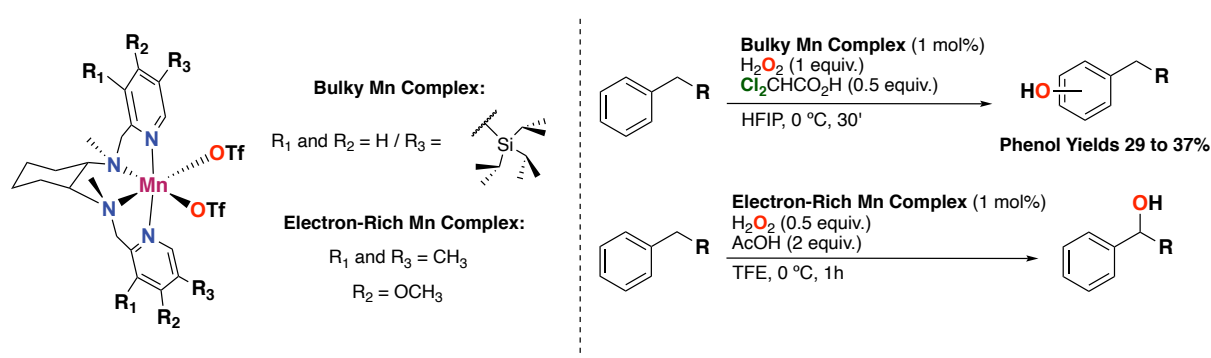


Figure 2. Left: General structure of manganese(II) complexes studied in **Chapter 3**. Right: Manganese-catalyzed oxidation of aromatic substrates with a carboxylic acid additive and aqueous H_2O_2 , yielding phenols or benzylic alcohol products depending on the catalyst and carboxylic acid employed.

Remarkably, halogenated carboxylic acids additives were found to produce a dramatical increase in catalytic activity compared to aliphatic carboxylic acids, generating phenol products in high yields. Dichloroacetic acid was selected as the additive of choice and a twofold role in catalysis was proposed. First, the acid additive keeps the phenol products protonated, which avoids product inhibition by phenolate binding to the catalyst, which is a common issue that has been described in the literature. Second, the electron-deficient character of the acid makes the metal oxo intermediate responsible for oxidation more electrophilic, which results in a more reactive oxidant towards arenes. Further insight into the mechanism of the aromatic oxidation reactions was also obtained and several experimental observations, such as the product profile observed in alkylbenzene oxidations, a negligible C–H/C–D kinetic isotope effect and the effectiveness of using $^t\text{BuOOH}$ as oxidant, suggest that the oxidation reaction proceeds through a metal-based mechanism, with no significant involvement of hydroxyl radicals.

As described in Chapter 3, one of the main challenges in aromatic oxidation reactions is to avoid phenolate binding to the metal center of the complex, which prevents efficient catalytic

turnover. This issue has been prevented to some extent by using electron-deficient carboxylic acids, *i.e.* halogenated carboxylic acids, which also enhance the electrophilicity of the active oxidant. To further investigate this aspect, **Chapter 4** provides an investigation into the electronic properties of the aminopyridine ligand of the manganese catalyst. It is hypothesized that electron-withdrawing substituents on the ligand could enhance the electrophilicity of the manganese-oxo species, and therefore, also improve the efficiency of the complex towards the reaction with arene substrates. In order to explore the electronic properties of the manganese catalyst, a set of complexes of the general formula $[\text{Mn}^{\text{II}}(\text{CF}_3\text{SO}_3)(^x\text{bpmcn})]$ ($X = \text{CF}_3, \text{Cl}, \text{H}, \text{dMM}, \text{Me}_2\text{N}, \text{Pyr}, \text{TIPS}$ and $\text{Ph}(\text{CF}_3)_2$), with different electron-withdrawing and electron-donating substituents on each of the pyridine moieties were synthesized (Figure 3).

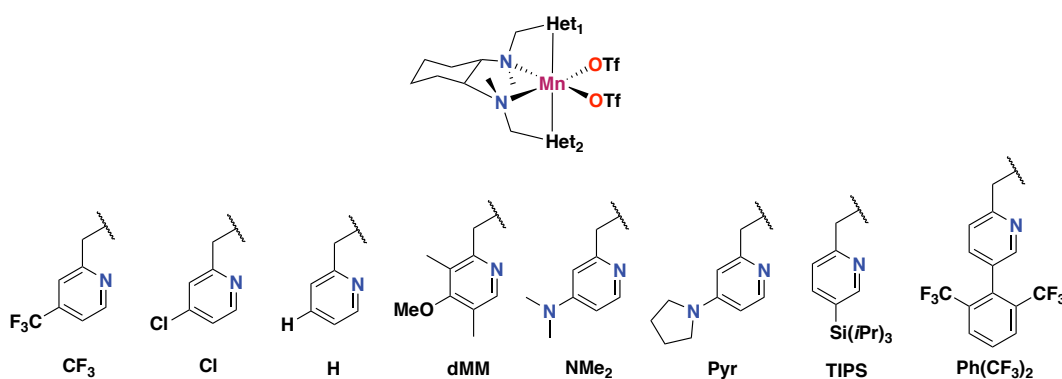


Figure 3. General structure of the different manganese complexes studied in **Chapter 4**.

In addition, C_1 -symmetric complexes were also considered and, consequently, complexes containing one bulky pyridine and a substituted pyridine were synthesized. Interestingly, the most electron-poor manganese complex of the series (*i.e.* containing CF_3 groups) were found inactive for the oxidation of an alkylbenzene, showing only trace amounts of phenol products. The explanation of this result is related to the ability of the ligand to stabilize the active oxidant formed upon activation of H_2O_2 , *i.e.* a ligand with significant electron-donating abilities seems necessary for the formation and stabilization of the high-valent manganese-oxo species. In contrast, electron-rich manganese complexes (*i.e.* containing dimethylmethoxy, dimethylamino or pyrrolidine groups) afforded a significant increase in catalytic activity, with up to 69% substrate conversion for the oxidation of propylbenzene. Next to the formation of aromatic oxidation products in a total yield of 15%, these complexes also displayed aliphatic (benzylic) oxidation reactivity towards the alcohol product in up to 16% alcohol yield. Combining the observations in this chapter and the previous one, manganese complexes bearing bulky substituents in combination with electron-rich substituents were considered as the next candidates for the development of aromatic oxidation catalysts. Accordingly, a set of manganese complexes containing both a bulky TIPS group and a dimethylamino group on the same pyridine moiety were synthesized. Surprisingly, none of these complexes were active in

the aromatic oxidation of alkylbenzenes towards phenol products. Overall, this chapter illustrates the sensitivity of manganese-catalyzed aromatic oxidations to modulation of the electronic and steric properties of the supporting aminopyridine ligand, and how C_2 -symmetric manganese complexes with bulky TIPS groups outperform all other complexes tested in this study for the oxidation of aromatic substrates to yield phenol products.

In the previous chapter electron-rich manganese complexes were found to be active in the aliphatic (benzylic) oxidation reaction of alkylbenzene substrates. This kind of complexes were further studied in **Chapter 5** by exploring new manganese and iron complexes bearing highly electron-rich aminopyridine ligands containing 4-pyrrolidinopyridine moieties in enantioselective oxidation catalysis employing aqueous H_2O_2 (Figure 4). Since 4-pyrrolidinopyridine groups are stronger *N*-heteroaromatic electron donor ligands compared to typically used 4-dimethylaminopyridine ($pK_a = 18.33$ and 17.95 , respectively), it was hypothesized that the greater electron-donating capacity of the former groups might lead to a better stabilization of the active manganese-oxo species formed upon reaction with H_2O_2 , and accordingly to a better catalytic performance. Indeed, new manganese complexes containing *para*-pyrrolidine substituted pyridine donors lead to higher alcohol yields in benzylic oxidation reactions, while providing similar ee's (60%). A detailed screening of different carboxylic acid additives with the pyrrolidine-substituted complexes revealed chiral Boc-*L*-tert-leucine as the preferred additive, with up to 50% alcohol yields and 62% ee for the oxidation of alkylbenzenes, while aromatic oxidation products were not detected. Finally, these complexes were also tested for asymmetric epoxidation reactions, and it was found that the corresponding iron complex was the best catalyst for the epoxidation of olefins, with up to 98% epoxide yield and >99% ee.

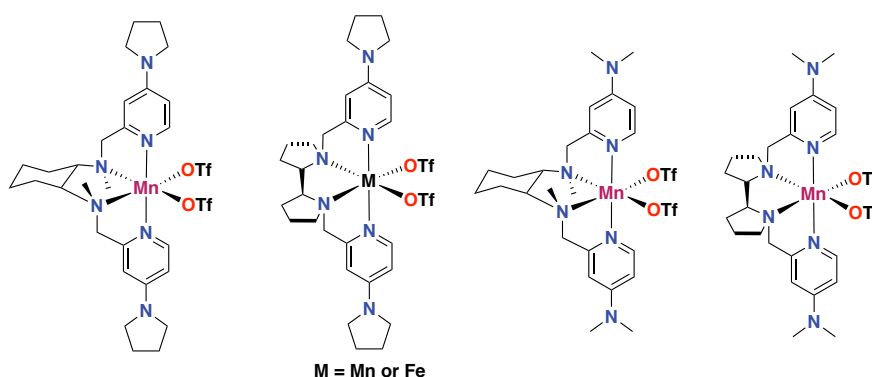


Figure 4. Manganese(II) and iron(II) complexes supported by electron-rich aminopyridine ligands studied in **Chapter 5**.

Finally, **Chapter 6** explores a new type of manganese complex based on bulky amino-imidazole ligands for oxidation catalysis. The synthesis of bulky amino-imidazole ligands bearing two phenyl substituents on each imidazole ring was accomplished (Figure 5), and their complexation to manganese(II) and iron(II) salts explored. The idea was to create a set of

ligands that are bulkier with respect to the parent benzimidazole-based ligands, so that the corresponding complexes would show enhance reactivity towards arene oxidation because of diminished product inhibition (cf. Chapter 3).

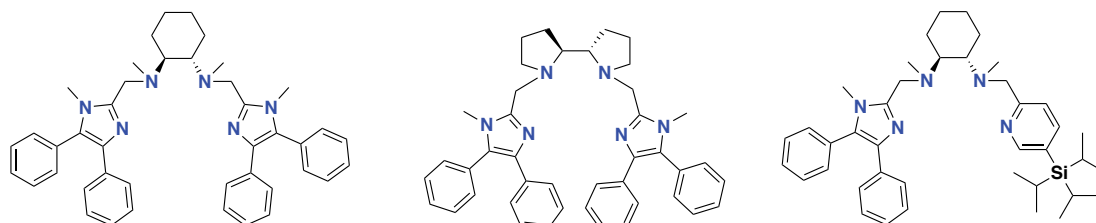


Figure 5. Bulky amino-imidazole ligands explored in **Chapter 6**.

C_2 -symmetric Mn-complexes based on diphenylimidazole moieties deemed not synthetically accessible, which was intuitively explained by the bulky character of the ligand. On the other hand, a C_1 -symmetric complex bearing a diphenylimidazole and a bulky pyridine moiety was successfully synthesized. Further insights into the coordination behavior of these ligands to manganese(II) ions was obtained by DFT geometry optimizations and calculations on the thermochemistry of the complexation reactions. The outcome of this computational study indicates that complexation of diphenylimidazole-based ligands to $Mn(OTf)_2$ are less favorable than those using less bulky benzimidazole-based ligands, which is in agreement with the experimental data. Finally, exploration of the catalytic properties of the successfully obtained C_1 -symmetric complex showed its activity in olefin epoxidation reactions, whereas it turned out to be inactive the aromatic oxidation of an alkylbenzene substrate to phenol products. The study presented in this chapter opens the door for the further exploration of imidazole-based complexes in the field of oxidation catalysis.

Concluding Remarks

In conclusion, this thesis describes the utility of amino-pyridine ligands in Mn-catalyzed and Ni-catalyzed arene oxidation reactions, *i.e.* the direct oxidation of aromatic C–H bonds to the corresponding phenol product. The presented results are supported by the synthesis and characterization of the ligands and the corresponding metal complexes, and a deep analysis of the catalytic tests is provided.

First, the use of coordination complexes based on manganese outperform those based on nickel in arene oxidation. We believe that manganese compounds can efficiently activate H_2O_2 to generate metal-based oxidants that are capable of hydroxylating arene substrates, whereas it might be that catalytic systems based on nickel complexes in combination with H_2O_2 involve the generation of non-selective hydroxyl radicals. Thus, the promising results obtained with

manganese complexes have prompted us to investigate these in more detail in this thesis. The introduction of steric bulk into a manganese complex can be used as a promising strategy in aromatic oxidation catalysis, improving the reactivity and chemoselectivity of these particular transformations by retarding product inhibition. These promising results warrant the future investigation of coordination complexes based on manganese and supported by bulky aminopyridine ligands.

Second, the modulation of the electronic properties of the manganese-based complexes has been shown to dramatically affect their reactivity in oxidation catalysis. In this regard, a key point for obtaining an effective catalyst system is the use of a metal complex bearing a highly electron-rich ligand, which assures the effective activation of H_2O_2 , or in other words, the proper stabilization of the high-valent manganese-oxo species.

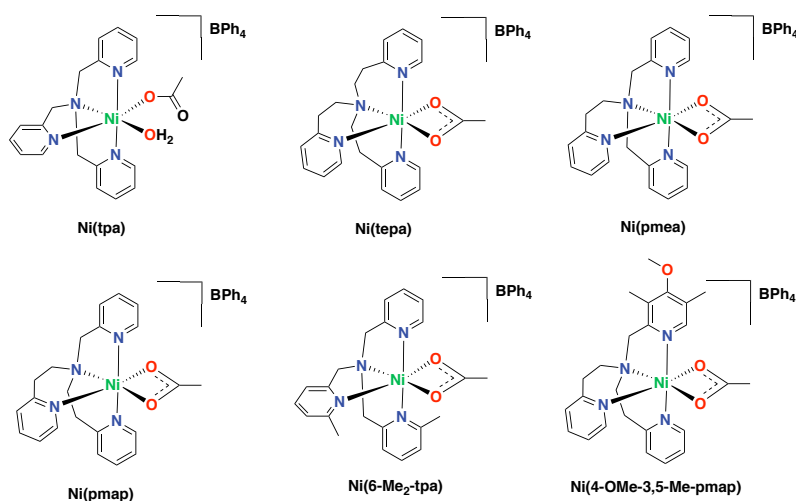
In a broader context, this thesis has shown that the use of bulky ligands and electron-donating ligands in bio-inspired manganese catalysis both play important roles in catalytic aromatic oxidation processes, which can open up opportunities for the further development of transition metal complexes as homogeneous oxidation catalysts in a more general sense. Other key features for the design of such catalyst systems include the proper choice of additives that may have an activating or (product) selecting role, as was shown for the use of carboxylic acid additives and fluorinated alcohol solvents for the catalysts developed in this thesis. Noteworthy, the current thesis presents new catalytic systems based on first-row transition metal complexes and adds into the transition from noble metal to non-noble metal catalysis.

Samenvatting

Vanwege de lage beschikbaarheid, toxiciteit en hoge prijs van edelmetalen is de ontwikkeling van nieuwe katalysatoren op basis van 3d-overgangsmetalen (d.w.z. niet-edelmetalen) zeer wenselijk en vereist. Deze overgang in de ontwikkeling van nieuwe katalysatoren komt o.a. tot uiting in de homogene katalyse, en met name bij de ontwikkeling van coördinatiecomplexen als katalysatoren voor oxidatiereacties. Dit proefschrift richt zich op de ontwikkeling van homogene katalysatoren op basis van de 3d-overgangsmetalen mangaan en nikkel voor aromatische oxidatiereacties, waarbij waterige waterstofperoxide als mild oxidatiemiddel wordt gebruikt. Dergelijke reacties zijn van groot belang aangezien er fenolen geproduceerd worden; deze zijn zeer gewild als tussenproducten voor het maken van o.a. farmaceutische producten en functionele polymeren. Bijzonder uitdagend is de ontwikkeling van katalytische reacties die in een enkele stap fenolproducten opleveren door de directe oxidatie van aromatische C–H-bindingen, en tegelijkertijd zowel overoxidatie van het fenolproduct vermijden als een hoge regioselectiviteit vertonen tussen de verschillende C–H-bindingen in het areensubstraat.

Hoofdstuk 1 van dit proefschrift beschrijft een uitgebreid overzicht van aromatische oxidatiereacties die worden gekatalyseerd door metallo-enzymen of synthetische metaalcomplexen waarin het actieve centrum bestaat uit een (laat) 3d-overgangsmetaal. Het hoofdstuk is ingedeeld per 3d-overgangsmetaal, nl. ijzer, koper, nikkel en mangaan, waarbij voor elk metaal telkens voorbeelden van metallo-enzymen en synthetische metaalcomplexen in detail beschreven worden. IJzer- en koper-bevattende metallo-enzymen zijn uitgebreid bestudeerd in de literatuur en veel van deze metallo-enzymen zijn in staat aromatische substraten te oxideren tot het overeenkomstige fenolproduct met behulp van moleculaire zuurstof. Er zijn daarentegen geen nikkel- en mangaan-bevattende metallo-enzymen bekend die aromatische oxidaties kunnen uitvoeren, ondanks dat dergelijke metallo-enzymen actief zijn in andere oxidatiereacties. Veel recente studies aan homogene katalysatoren voor aromatische oxidatiereacties hebben zich gericht op de ontwikkeling van bio-geïnspireerde ijzerkatalysatoren en meerdere ijzer-complexen zijn in staat aromatische oxidatiereacties op katalytische wijze uit te voeren met behulp van milde oxidatiemiddelen. Soortgelijk onderzoek aan bio-geïnspireerde kopercomplexen kent een lange historie; echter, de meeste van deze complexen zijn in staat stoichiometrische aromatische oxidatiereacties uit te voeren en pas meer recent zijn enkele katalytische systemen beschreven. Nikkel- en mangaancomplexen zijn tot zover veel minder onderzocht voor aromatische oxidatiereacties en er zijn slechts enkele katalytische voorbeelden bekend.

In **Hoofdstuk 2** van dit proefschrift is onderzocht in hoeverre nikkel(II)-complexen gebaseerd op tripodale, tetradentate aminopyridine-liganden de directe hydroxylering van benzeen tot fenol kunnen katalyseren met waterige H_2O_2 als oxidatiemiddel (zie Figuur 1). Katalytische testen werden in aanwezigheid van 10 mol% katalysator uitgevoerd met benzeen als substraat, triethylamine als base en H_2O_2 in acetonitril als oplosmiddel. Katalytische reacties, uitgevoerd aan de lucht, bij 60 °C, gedurende 5 uur en in een gesloten reactievat, resulteerden in fenolopbrengsten variërend van 9-10% (d.w.z. niet meer dan één omzetting per nikkel). Deze bevindingen toonden aan dat het variëren van het aminopyridine-ligand in de nikkelcomplexen niet leidt tot een veranderde reactiviteit in aromatische oxidatiereacties, wat suggereert dat de liganden geen belangrijke rol spelen in de reactie. Tevens toonde een screening van verschillende oplosmiddelen aan dat de gefluoreerde alcohol 1,1,1,3,3,3-hexafluor-2-propanol (HFIP) het beste oplosmiddel is voor de oxidatie van benzeen tot fenol. Bovendien leidde het gebruik van verschillende nikkel(II)-zouten, waaronder nikkelnitraat en nikkelchloride (beide als hexahydraat), tot respectievelijk 7% en 3% fenolopbrengst. Dit toont aan dat aromatische oxidatie met een hoge chemoselectiviteit ook kan worden bereikt met behulp van eenvoudige, commercieel verkrijgbare nikkel(II)-zouten.

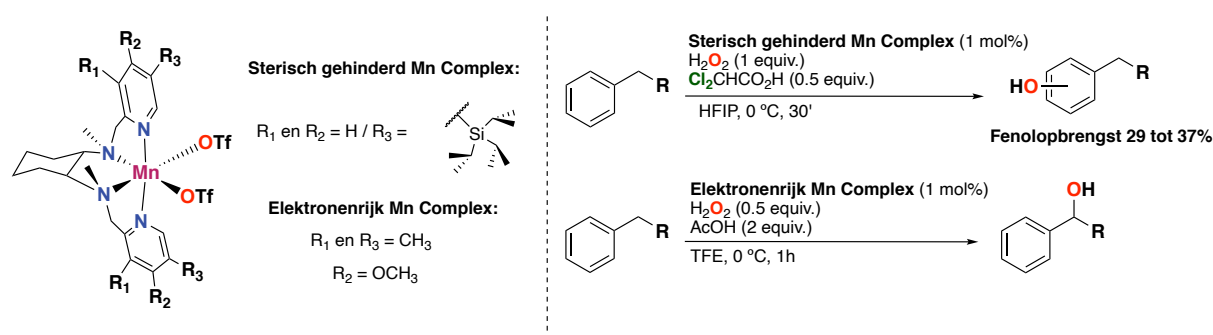


Figuur 1. De in **Hoofdstuk 2** bestudeerde nikkel(II)-complexen, gebaseerd op tripodale, tetradentate aminopyridine-liganden.

Al met al trekt dit hoofdstuk de betrokkenheid van een vermeend dinikkel(III)bis(μ -oxo)-intermediair, zoals gepostuleerd in de literatuur, in twijfel. In plaats daarvan wordt de ontleding van de nikkelcomplexen onder de experimentele omstandigheden gesuggereerd, mogelijk leidend tot de vorming van nikkel-nanodeeltjes die vervolgens betrokken zijn bij de katalyse.

Hoofdstuk 3 beschrijft de katalytische eigenschappen van sterisch gehinderde, bio-geïnspireerde mangaancomplexen in aromatische oxidatiereacties. Mangaancomplexen afgeleid van aminopyridine-liganden zijn eerder beschreven als uitstekende katalysatoren voor

verschillende soorten oxidatiereacties, zoals alifatische C–H-oxidaties en de epoxidatie van alkenen. Daarnaast is bekend dat de introductie van grote (sterische) triisopropylsilyl-substituenten (TIPS) op de aminopyridine-liganden de efficiëntie en de regioselectiviteit van alifatische C–H-oxidaties kan verhogen. De studie beschreven in Hoofdstuk 3 laat zien dat het gebruik van een dergelijk sterisch gehinderd mangaancomplex, in combinatie met een gehalogeneerd carbonzuur-additief, een gefluoreerd alcoholoplosmiddel en H₂O₂, de directe oxidatie van alkylbenzenen tot fenolproducten mogelijk maakt. De behaalde opbrengsten van deze reacties behoren tot de hoogste die zijn gerapporteerd voor homogene oxidatiekatalysatoren: 29% – 37% opbrengst voor aromatische oxidatieproducten, met in alle gevallen het *para*-fenol als hoofdproduct (Figuur 2). De waargenomen reactiviteit doet denken aan reacties die verlopen via een mechanisme van een elektrofiële aromatische substitutie. Interessant is dat de chemoselectiviteit van de oxidatiereactie afhangt van het gebruikte ligand. Terwijl complexen met sterisch gehinderde aminopyridine-liganden de oxidatie van de aromatische ring prefereren, oxideren complexen die elektronenrijke aminopyridine-liganden bevatten juist de meer geactiveerde alifatische (benzylic) positie (Figuur 2).

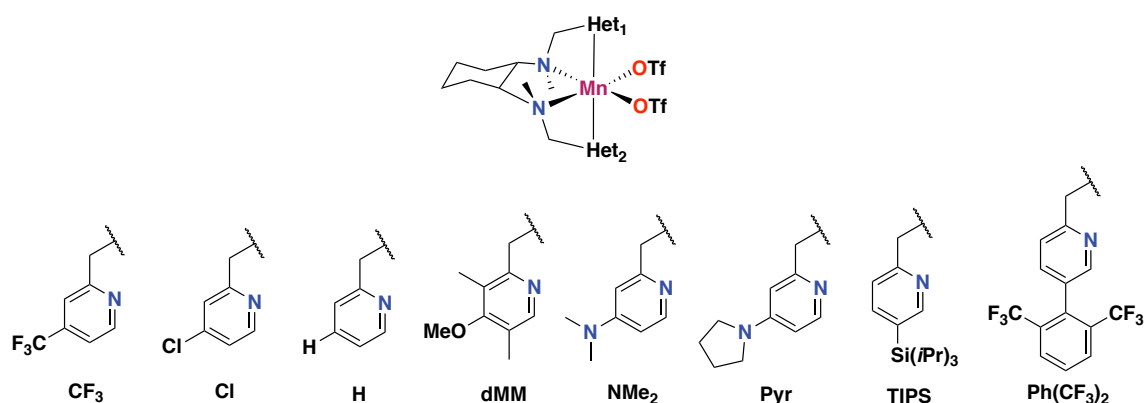


Figuur 2. Links: De algemene structuur van de in **Hoofdstuk 3** bestudeerde mangaan(II)-complexen. Rechts: Mangaan-gekatalyseerde oxidatie van aromatische substraten met waterige H₂O₂ levert fenolen of benzylic alcoholproducten op, afhankelijk van de gebruikte katalysator en het gekozen carbonzuur-additief.

In vergelijking met alifatische carbonzuur-addities veroorzaakt het gebruik van gehalogeneerde carbonzuur-addities een dramatische toename van de katalytische activiteit, waardoor de fenolproducten in hoge opbrengsten verkregen worden. Dichloorazijnzuur werd geselecteerd als het beste additief en er werd een dubbele functie voor het additief in de katalytische reactie voorgesteld. Ten eerste blijven de fenolproducten geprotoneerd in aanwezigheid van het zure additief. Hierdoor wordt productinhibitie in de vorm van fenolaatbinding aan de katalysator vermeden, hetgeen een veelbeschreven probleem is bij aromatische oxidatiereacties. Ten tweede wordt het metaal-oxo-intermediair, dat verantwoordelijk is voor de oxidatiereactie, elektrofieler door het elektron-deficiënte karakter van het additief; resulterend in een reactiever oxidant. Meer inzicht in het mechanisme van de aromatische oxidatiereacties werd verkregen door verschillende experimentele observaties,

zoals het productprofiel waargenomen in alkylbenzeenoxidatiereacties, een verwaarloosbaar C–H/C–D-kinetisch isotoopeffect en de effectiviteit van ^tBuOOH als oxidatiemiddel. De combinatie van deze observaties suggereert dat de mangaan-gekatalyseerde aromatische oxidatiereactie verloopt via een metaal-gebaseerd mechanisme en zonder significante betrokkenheid van hydroxylradicalen.

Eén van de belangrijkste uitdagingen bij aromatische oxidatiereacties is het vermijden van de fenolaatbinding aan het metaalcentrum van het complex (productinhibitie), zoals beschreven in Hoofdstuk 3. Dit probleem is tot op zekere hoogte voorkomen door gebruik te maken van elektron-deficiënte carbozuren, d.w.z. gehalogeneerde carbozuren, die ook de elektrofiliciteit van het metaal-oxo-intermediair verhogen. In **Hoofdstuk 4** is dit laatste aspect verder onderzocht door de elektronische eigenschappen van het aminopyridine-ligand te variëren. Daarbij werd verondersteld dat elektronenzuigende substituenten op het ligand de elektrofiliciteit van het mangaan-oxo-intermediair verhogen en daarom ook de efficiëntie van de aromatische oxidatiereactie verbeteren. Om de elektronische eigenschappen van de mangaankatalysator te onderzoeken werd een reeks complexen met de algemene formule $[\text{Mn}^{\text{II}}(\text{CF}_3\text{SO}_3)(\text{Xbpmcn})]$ ($\text{X} = \text{CF}_3, \text{Cl}, \text{H}, \text{dMM}, \text{Me}_2\text{N}, \text{Pyr}, \text{TIPS}$ en $\text{Ph}(\text{CF}_3)_2$) en met verschillende elektronenzuigende en elektronendonorende substituenten op elk van de pyridinegroepen gesynthetiseerd (Figuur 3). Daarnaast zijn C_1 -symmetrische complexen gesynthetiseerd, die één sterisch gehinderd pyridine en één gesubstitueerde pyridine bevatten.



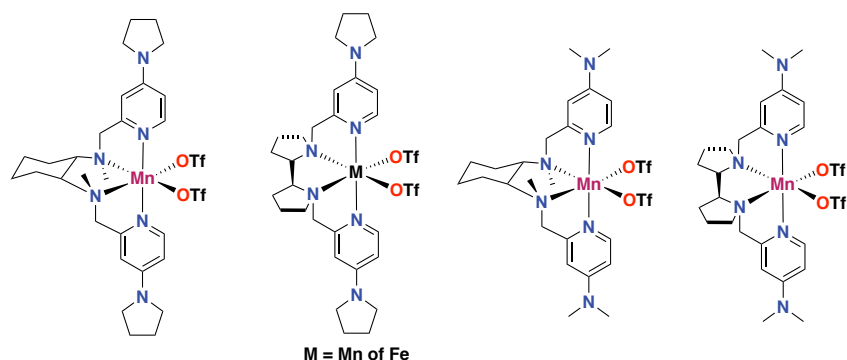
Figuur 3. De algemene structuur van de mangaancomplexen bestudeerd in **Hoofdstuk 4**.

Interessant is dat het meest elektronenarme mangaancomplex van de reeks (d.w.z. met de CF_3 -groepen) inactief blijkt te zijn in de oxidatie van een alkylbenzeen, aangezien er slechts sporen van fenolproducten gevormd werden. Dit resultaat is mogelijk gerelateerd aan het vermogen van het ligand om het metaal-oxo-intermediair gevormd na de activering van H_2O_2 te stabiliseren, d.w.z. een significant elektronendonorend vermogen van het ligand lijkt noodzakelijk voor de vorming en stabilisatie van dit hoogvalente intermediair. Het gebruik van elektronenrijke mangaancomplexen (d.w.z. met de dimethylmethoxy-, dimethylamino- of

pyrrolidinegroepen) leidt daarentegen tot een significante toename van de katalytische activiteit met tot 69% substraatconversie voor de oxidatie van propylbenzeen. Deze complexen vertonen naast de vorming van aromatische oxidatieproducten (15%) ook reactiviteit in de oxidatie van alifatische (benzylicke) C–H-bindingen, met een alcoholopbrengst van maximaal 16%; m.a.w. de verhoogde reactiviteit gaat ten koste van de regioselectiviteit.

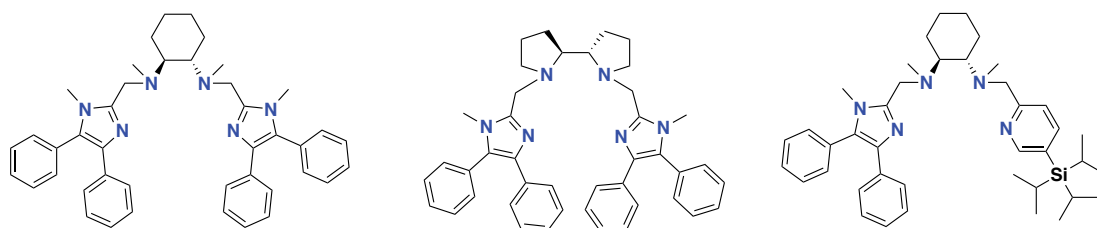
De combinatie van waarnemingen in Hoofdstukken 3 en 4 maken C₂-symmetrische mangaancomplexen met een combinatie van sterisch gehinderde en elektronenrijke substituenten tot de volgende kandidaten voor de ontwikkeling van aromatische oxidatiekatalysatoren. Verrassend genoeg bleek een reeks mangaancomplexen, die zowel een sterisch gehinderde TIPS-groep als een elektronrijke dimethylaminogroep op beide pyridinegroepen bevatten, inactief in de aromatische oxidatie van alkylbenzenen tot fenolproducten. Kortom, dit hoofdstuk illustreert de gevoeligheid van mangaan-gekatalyseerde aromatische oxidatiereacties voor de elektronische en sterische eigenschappen van het aminopyridine-ligand. C₂-symmetrische mangaancomplexen met TIPS-substituenten overtreffen daarbij alle andere complexen die in dit onderzoek zijn getest.

Hoofdstuk 5 bestudeert elektronenrijke mangaancomplexen met zeer elektronenrijke aminopyridine-liganden, die 4-pyrrolidinopyridine-eenheden bevatten, in enantioselectieve alifatische (benzylicke) oxidatiereacties van alkylbenzeensubstraten met behulp van waterige H₂O₂ (Figuur 4). Aangezien 4-pyrrolidinopyridine-groepen sterkere elektronendonorende N-heteroaromatische liganden zijn in vergelijking met de veelgebruikte 4-dimethylaminopyridine-groepen (pK_a = 18.33 en 17.95, respectievelijk), werd verondersteld dat de verhoogde elektronendonorende eigenschappen zouden kunnen leiden tot een betere stabilisatie van de actieve mangaan-oxo-intermediair en daarmee tot een verhoogde katalytische efficiëntie. De pyrrolidine-gesubstitueerde mangaancomplexen leveren inderdaad hogere alcoholopbrengsten op in een benzylicke oxidatiereactie, terwijl ze vergelijkbare ee's (60%) geven als de dimethylamino-gesubstitueerde complexen. Uit een screening van verschillende carbonzuur-additieven in combinatie met de pyrrolidine-gesubstitueerde complexen bleek het chirale Boc-*L-tert*-leucine het beste additief voor de oxidatie van alkylbenzenen, leidend tot een maximale alcoholopbrengst van 50% in 62% ee. In deze reactie werden geen aromatische oxidatieproducten gedetecteerd. Ten slotte werden deze mangaancomplexen en een overeenkomstig ijzercomplex ook op asymmetrische epoxidatiereacties getest. Daarbij bleek het ijzercomplex een zeer efficiënte katalysator voor de epoxidatie van olefines met een maximale epoxide-opbrengst van 98% en >99% ee.



Figuur 4. De in **Hoofdstuk 5** bestudeerde mangaan(II)- en ijzer(II)-complexen gebaseerd op elektronenrijke aminopyridineliganden.

Ten slotte is in **Hoofdstuk 6** een nieuwe type mangaancomplex met sterisch gehinderde amino-imidazoolliganden onderzocht in oxidatiekatalyse (Figuur 5). De intentie was om een reeks liganden te creëren die nog sterisch gehinderder zijn dan de oorspronkelijke liganden met benzimidazoolgroepen. Op basis van de resultaten met de TIPS-gefunctionaliseerde liganden, zijn de resulterende complexen interessante kandidaten voor de ontwikkeling van nieuwe katalysatoren voor aromatische oxidatiereacties waarbij productinhibitie zou kunnen optreden (zie Hoofdstuk 3).



Figuur 5. De sterisch gehinderde amino-imidazoolliganden die in **Hoofdstuk 6** onderzocht zijn.

De C_2 -symmetrische Mn-complexen op basis van de nieuwe difenylimidazoolliganden bleken synthetisch niet toegankelijk; dit werd intuïtief verklaard door het sterisch-gehinderde karakter van de liganden. Daarentegen werd met succes een C_1 -symmetrisch complex van een ligand met een difenylimidazool- en een sterisch gehinderde pyridine-groep gesynthetiseerd. Verder inzicht in het coördinatiegedrag van deze liganden met mangaan(II)-ionen werd verkregen met behulp van DFT-geometrie-optimalisaties en berekeningen aan de thermochemie van de complexatie-reacties. Deze computationele studie geeft aan dat complexatie van de difenylimidazool-gebaseerde liganden met $Mn(OTf)_2$ minder gunstig is dan complexatie van minder sterisch-gehinderde benzimidazool-gebaseerde liganden. Ten slotte bleek het verkregen C_1 -symmetrische complex een actieve katalysator voor de epoxidatie van olefinen, terwijl het inactief bleek te zijn in de aromatische oxidatie van een alkylbenzeensubstraat. De in dit hoofdstuk gepresenteerde studie is de aanzet tot een verdere verkenning van op imidazool-gebaseerde complexen als katalysatoren voor oxidatiereacties.

Conclusies

Samengevat beschrijft dit proefschrift het gebruik van aminopyridine-liganden in Mn-gekatalyseerde en Ni-gekatalyseerde aromatische oxidatiereacties, d.w.z. de directe oxidatie van aromatische C–H-bindingen tot de overeenkomstige fenolen. Naast de synthese en karakterisering van de liganden en de overeenkomstige metaalcomplexen, wordt een gedetailleerde analyse van de katalytische karakteristieken van de verschillende complexen gegeven.

Ten eerste presteren coördinatiecomplexen op basis van mangaan beter in aromatische oxidaties dan nikkelcomplexen. De mangaancomplexen zijn in staat om H_2O_2 op efficiënte wijze te activeren en metaal-gebaseerde oxidanten te genereren, die vervolgens aromatische substraten kunnen hydroxyleren. Daarentegen lijken katalytische systemen op basis van nikkelcomplexen niet-selectieve hydroxylradicalen te vormen in aanwezigheid van H_2O_2 . De veelbelovende resultaten die zijn verkregen met de mangaancomplexen hebben ons ertoe aangezet om deze in meer detail te onderzoeken in dit proefschrift. Voor de katalyse van aromatische oxidatiereacties kan de introductie van sterische bulk in een mangaancomplex worden gebruikt als een veelbelovende strategie, aangezien op deze manier de activiteit en chemoselectiviteit van de reacties worden verbeterd door productinhibitie te verminderen. Deze veelbelovende resultaten rechtvaardigen toekomstig onderzoek naar coördinatiecomplexen op basis van mangaan in combinatie met sterisch-gehinderde aminopyridine-liganden.

Ten tweede is aangetoond dat de modulatie van de elektronische eigenschappen van de mangaan-complexen hun reactiviteit in oxidatiekatalyse dramatisch beïnvloedt. Belangrijk voor het verkrijgen van een effectief katalysatorsysteem is in dit opzicht het gebruik van een metaalcomplex met een zeer elektronenrijk ligand. Hierdoor kan H_2O_2 effectief geactiveerd worden of, anders gezegd, wordt de juiste stabilisatie van het hoogvalente mangaan-oxo intermediair bereikt.

In een bredere context heeft dit proefschrift aangetoond dat het gebruik van sterisch gehinderde liganden en van elektronen-donerende liganden in bio-geïnspireerde mangaankatalyse beide een belangrijke rol spelen in aromatische oxidatiereacties. Dit biedt in meer algemene zin kansen voor de verdere ontwikkeling van overgangsmetaalcomplexen als homogene oxidatiekatalysatoren. Andere belangrijke overwegingen bij het ontwerp van dit soort katalysatoren zijn de juiste keuze van additieven, die een activerende of (product-) selecterende rol kunnen hebben. Zo werd in dit proefschrift het belang van carbonzuuradditieven en gefluoreerde alcoholoplosmiddelen aangetoond. De katalysatoren ontwikkeld in dit proefschrift maken gebruik van 3d-overgangsmetalen en de hierbij opgedane kennis draagt bij aan de algemene overgang van edelmetaal- naar niet-edelmetaalkatalyse.

Acknowledgements

During my stay in Utrecht, I have received a lot of help and contributions from many people, which have made this thesis possible. Thus, it is a great moment for me to look back at my PhD journey, and it is a pleasure for me to give my sincere acknowledgements to these people.

First and foremost, I would like to give my deepest gratitude to my promoter, prof. dr. Klein Gebbink. Dear **Bert**, thank you very much for giving me this opportunity to perform my PhD thesis at the OCC group in Utrecht. I remember how uncertain the beginning was, it was planned that I would perform my thesis at the company DSM, but at the end it turned out to not be possible anymore, and you then offered me the opportunity to do it at Utrecht, under your supervision. I remember the beginning of my project as a tough period, since I was new in the project, and I needed to get experienced in the lab. My first project was not easy, and I remember how you helped, trained, and motivated me to achieve my goals. I feel that after my first project I learned a lot, which allowed me to then create new ideas and projects. Overall, you have trained me to become an independent junior scientist, motivating me to come up with my own ideas, and allowing me to carry out these ideas in the laboratory. I benefitted a lot from our meetings and discussions, since you shared all your chemical experience and knowledge with me, which allowed me to take the right direction during all the projects I have worked with. Moreover, you have always taken care of my personal life in The Netherlands, especially at the beginning, when I was new in the country, and then also during the difficult time of the covid, when we had to work from home, and I was far away from my own country. I feel you always gave me support during all these times. Thank you for everything!

Marc-Etienne, your wide knowledge in chemistry and especially, your critical thinking has helped me a lot during my PhD. We have always had nice discussions, and your suggestions during the group meetings and work discussions were very useful for me. We have also spent very nice times during the NoNoMeCat meetings we had in different places around Europe. Overall, your help was of very important to me. Thank you! **Pieter**, thank you for your discussions, and for being one of the reading committee members of my thesis. I specially remember being your assistant during the catalysis course that you gave to 3rd year bachelor students. I remember it as a nice time, where we could have some nice discussions, and I could learn a lot from you. **Danny**, you joined the group at the middle of my PhD journey. You always showed your passion for chemistry and provided me with very insightful ideas. Thank you very much for the nice discussions and suggestions you gave me about my projects during the work discussions and group meetings. **Arnaud**, you just joined the group, and we only had the

opportunity to discuss briefly about my research. I wish you good luck with your new position in the group.

Johann, thank you for your discussions and your help, especially with NMR measurements and computer issues. It was fun to share a lot of moments with you during the annual meetings we had with the NoNoMeCat network. I also would like to thank the technicians of our group. First, **Jord**, you were the first technician I met when I arrived at the group. Although we only spent few months together in the group, I could learn from you, and you helped me a lot. **Thomas**, thank you very much for your help during most of my time as a PhD student. We shared a lot of fun moments, especially during the borrels that you organized! **Léon**, thank you a lot for your help as a technician as well, especially your help setting up the HPLC analysis. **Milka**, you were the secretary of the group during the first part of my PhD journey, when I arrived in The Netherlands. You helped me a lot arranging the important things during my start, which I appreciate a lot. **Barbara**, thank you as well for all your help during your stay in the group. Finally, **Silvia**, you are the current secretary of the group and you have helped me a lot during my last stages of my PhD, which I appreciate it a lot. Thank you!

Most of the chapters included in this thesis are supported by XRD structures. And this could not have been possible without the collaboration with **Martin Lutz**. Thank you very much for all your help solving my crystal structures, and all your discussions analyzing them. I appreciate it a lot!

I would like to highlight here that most parts of this thesis could not have been possible without the help of the students I have been supervising. I would like to give a huge thanks to each one of them. **Raoul**, you were the first bachelor student I supervised during my PhD journey. I learned a lot from this first experience, since it was something new to me. You helped me a lot for my thesis, and your contribution is reflected in *Chapter 2* of this thesis. It was fun sharing this time with you, thank you! **Jishai**, you were my second bachelor student, and you helped me to increase my library of nickel compounds. Your contribution is also reflected in *Chapter 2* of this thesis. **Jasper** and **Errikos**, you arrived together in the group as bachelor students, and you both worked under my supervision in two different projects. I remember this time as challenging, having to supervise you both, but it was much fun, and I have very good memories from this experience. Thank you very much to both of you! **Laurens**, you were the first master student I had to supervise. You know well that the project you were involved in was very challenging and though, but despite the difficulties you were able to always stay positive and you were able to come with new ideas. You proved to me to be an excellent scientist, and I enjoyed your time in the group a lot. Thank you very much for all your help and for the sweatshirt you gave me as a gift! **Jelle**, you arrived in the group as a master student, and you were also involved in another challenging project. It was a tough project, but you were able to

obtain some good results. Thank you for your help. **Xiaoyu**, you were the last master student I had to supervise during my stay at the OCC group. I remember you as a very good and experienced chemist, able to work independent in the lab. Your stay at the group allowed me to get some very nice results for my project. Thank you for everything! Finally, I also supervised some literature projects during my PhD. Therefore, I would like to give a huge thanks to **Joost, Sanne** and **Sam**. Your contributions were very helpful for me to learn about new topics and get new ideas for my projects.

A very important aspect that I would like to highlight from my PhD has been my involvement in the NoNoMeCat network. This has allowed me to learn from a lot of different scientists around Europe, being able to meet and discover new places and people. Here I would like to give a huge thanks to all the PhD students that, like me, have been part of this network: **Emily, Serhii, Pamela, Marco, Valeria, Andrea Darù, Simone, Andrea Mele, Runze, Marten, Christoph, Wei** and **Maxime**. I will remember all our meetings and shared experiences as very nice memories.

Being involved with the NoNoMeCat network allowed me to perform several secondments in different countries. The first one was in Bern, where I was able to learn directly from **Martin Albrecht**. Thanks for allowing me to stay at your group during a period of two months, and for being able to learn from your chemistry. I will always remember this period in Switzerland. Also, special thanks to **Nathalie**. I worked directly with you in the lab, and I remember you as an excellent chemist. Thanks for everything! **Albert**, you were Catalan, so we shared a lot of common things. I would like to thank you for all your help during my stay there. We shared a lot of fun experiences, especially during the travels that we did with your friends around Switzerland, where we were able to discover a lot of new places. During my stay in Bern, I was able to meet some more people, who helped me a lot during my stay in the country, and with who I shared a lot of experiences in and outside the lab. I will always remember the group outing that we did, where I played curling for the first time, as well as the football match that we watched in the stadium between Young Boys and Basel, where the temperature was $-13\text{ }^{\circ}\text{C}$. I would like to thank all the people that I met there: **Simone, Karst, Philipp, Matteo, Marta, Kevin, Pamela, Rachael, Chloë** and **Joe**.

My second secondment was in Girona, in the group of Miquel Costas. **Miquel**, thanks for allowing me to join your group for a period of 1 month. It was nice to spend some time at my home town, and to being able to learn from the chemistry that was performed in Girona. I would also like to thank you for everything you did for me. I will always remember the day that you informed me in one of your classes that there was the opportunity of doing a PhD within the NoNoMeCat network, and how you encouraged me in taking this step. Overall, your help has been very important for me and for my PhD journey. **Margarida**, you taught me a lot of things

within the lab, and our collaboration is reflected in *Chapter 3* of this thesis. Thanks a lot for your help! I would also like to thank all the people with whom I shared my stay in Girona: **Laura, Xavi, Anna, Giorgio, Michela, Mònica, Carles, Brenda, Raquel, Carla, Ernest, Lorena, Pau** and **Laia**.

Of course, I do not forget the former and current PhD students and PostDocs from the OCC group for all the help received, and for the friendship.

To the former OCC PhD candidates and PostDocs: **Jianming**, from the beginning we built a good friendship. We shared a lot of moments together, and since you also worked with oxidation chemistry, I was able to learn a lot from you. Thanks for all your help, for all the things that you taught me about our projects, and for always willing to help me outside the lab as well. **Alessio**, you were the funny guy of the group, always making jokes about everything. I will always remember you hiding me things, such as my posters, around the lab! We built a strong friendship from the beginning, since we shared a lot of common hobbies, especially football. I will always remember watching football matches at the bar, playing tennis together at Olympos, or all the parties that we did at your place or around the city. It was a pleasure being your paranymph during your PhD defense ceremony! **Jing**, you have become a nice friend, and we have shared a lot of moments together. We both had our ups and downs, but we had each other. During my PhD we have shared the office area, and we have been able to discuss a lot about our chemistry and projects. Thanks for all your help, and for teaching me a lot of things. **Dide**, you were almost finished with your PhD when I started in the group, but I was able to learn a lot from you. It was nice to share a lot of moments with you. **Manuel**, even though you had already finished your PhD in the group when I started, we were able to meet each other, and you were a good friend. I will remember the nice time we spend together, and how you guided me around Amsterdam. **Pradip**, I could see from the beginning that you were an excellent chemist. I learned a lot from you within the lab, and we shared a lot of good moments together. Thank you very much for giving me the opportunity of living in your apartment when you were moving. It has been a very nice place to spend most of my time in The Netherlands. **Bas**, you were almost done with your PhD when I started in the group, but we have been able to spend very nice moments together during some of the trips we organized with the group. **Peter**, you are an excellent scientist and a very funny guy. Thanks for all the shared moments. **Léon**, thanks for all the things you have taught me during the time we shared in the lab. **Sipeng**, we shared lab isle when I started working in the lab, and I received a lot of help from you. Thanks for all your insights and techniques you showed me. **Jacco**, we shared a lot of nice moments together during my stay in The Netherlands. You were an experienced guy, a person who I could ask everything I needed, and you were always willing to help. Thanks a lot for everything, and especially for checking my final version of the Dutch summary!

Tharun, you have become a very nice friend, and from the beginning we shared a lot of common hobbies, such as our support for Barça. I will always remember the times that we shared in the bar watching football games and playing tennis together. I wish you a very good future career! **Fuqiang**, **Carolien** and **Wirawan**, it was a pleasure meeting you, I wish you all the best for your future.

To the current PhD students and PostDocs of the group: **María**, when you arrived in the group, we soon became very good friends, you were the first person which who I could speak Spanish. During all these years we have spent very nice moments together, I always enjoy listening to your stories and experiences. Regarding our chemistry projects, those differ a lot from each other, but despite that we were able to discuss about our chemistry and learn from each other. Good luck with the final steps of your thesis, you will be very successful! And thanks for accepting being my paranymph! **Pamela**, you have become one of my best friends during my stay in The Netherlands. You arrived when I was in the middle of my PhD, and we soon established a strong friendship. We later came to live together in the same building, and being neighbors allowed us to know each other even more. I will always remember all the support you provided me, helping me when I had a problem with Word files and giving me nice ideas about how to solve problems in the lab. I always enjoyed eating together at your place, your “ragú” that was excellent, your sense of humor and you coming to my place and showing your dance choreography to Eila and me. We shared some common hobbies, such as the “Lord of the Rings”, and I was able to learn a little bit of Italian, such as “fuggite sciocchi”. **Pablo**, you have been a very good friend, and a person who I can trust. You were always willing to help me with my projects and the problems I had to face, and you have also helped me outside the lab. We have a lot of shared experiences together, borrels, dinners, being both the paranymphs of Alessio, and many more. I hope you are spending a nice time at my old apartment there, and I hope to spend more experiences together in the future. **Emily**, you have been a very good friend to me, always willing to help everybody else in the group. I will always remember our trips for the NoNoMeCat annual meetings around Europe, and the parties we did during my time in The Netherlands. You have always helped me within the lab, as well as in my personal life. I will always remember your help bringing me to the hospital one time when I was feeling sick, or the trip that we did together to Rostock by car. Thanks for this time, and I wish you the best with your future! We will defend our PhD thesis almost at the same time! **Fanshi**, you are a very good friend, and from the beginning we started talking about our own chemistry, and about life in general. Our projects were very close, both being involved in oxidation chemistry, and we have even collaborated and published together. It was a very good experience! You have also shared a lot about your life in China and about your family, which allowed me to know you a little bit more, and I have also shared some of my culture with you. I hope you enjoy your final steps of your PhD and hope to visit you soon in China. **Martine**, I have always

enjoyed the time I have spent with you. You are funny and I loved talking with you about football, tennis, geography, and the travels we have made in the past. Thank you very much for the help you have given me during my time in Utrecht, and specially writing my summary in Dutch. It was helpful, and I appreciate it a lot! I wish you the best with the final stage of your PhD, and I hope to stay in contact for the future. **Sander**, thanks for the nice time we have spent during these past years, and for the great atmosphere and professionalism you bring to the group. **Serhii**, we almost started our PhD at the same time, and we both were involved in the NoNoMeCat network. I really enjoyed the time we shared during this time, and all your stories and help in the lab. **Razvan**, you have just finished your time at the OCC group, and I can say I really enjoyed being your colleague. I wish you the best for your future. **Cody**, you are a very friendly person, I have enjoyed a lot having you as a colleague. I wish you the best for the rest of your PhD. **Errikos**, I met you during your bachelor project at OCC, where you were involved in one of my projects. Since that moment I could see you were an excellent chemist, willing to learn and improve. You also did your master project at OCC, and afterwards you joined as a PhD. Thus, I have known you for a long time. I have really enjoyed the borrels together, and watching Champions League matches at the pub. I wish you the best for your future! **Roel, Jochem, Luke, Joel, Maartje, Lars, Angshuk** and **Arjan**, thank you for the great atmosphere and for your help. I hope you all will enjoy the rest of your time in the OCC group!

I would also like to thank all the visitors that came by the OCC group during these 5 years: **Federica, Marco, Valeria, Marten, Andrea Darù, Zahra, Tsz** and **Josh**.

I would also like to acknowledge all the current and former students of the group for the good time spent together: **Stella, Maxime, Sofie, Lucas, Daniël, Noortje, Oscar, Jan, Yuri, Rohald, Cody** (student), **Sam Huizing, Jitse, Hidde, Marc, Isabelle, Rinske, Tom, Mirte, Abdullah, Storm, Lars** (student), **Camille, Arthur, Bram, Yoni, Elena, Roel** (student), **Erkay, Marijn, Ivo, Yang, Chick, Max, Sam de Loo, Lada, Jesse, Annemiek, Marije, Dylan, Janneke, Marieke, Pascale, Kasper, Koen, Alexandra, Bauke, Jasmijn, Tu, Thomas, Maartje** (student), **Vito, Andrea, Eva, Sjoerd** and all other students that I met during my time here at the OCC group.

Finally, I would like to thank my **family** and **friends** for the huge support and encouragements during my whole stay in The Netherlands. **Eila**, et vull donar unes gràcies infinites per tota l'ajuda i suport durant aquest temps. Ets la persona més especial, i sempre m'has donat la força necessària per superar qualsevol impediment. Sé que no va ser fàcil estar separats durant molt d'aquest temps, però sempre em quedaré amb el record de l'últim any vivint junts a Holanda. Ha estat el nostre primer lloc. T'estimo! Moltes gràcies a la **Gemma**, començant per la visita que ens vas fer a Holanda fins els dies d'estudi al teu pis de Girona o a altes hores de la matinada a la biblioteca. També per totes les experiències compartides, des de convertir anar a "la

cooperativa de Garriguella” com una tradició quan venia jo de visita, com aprendre de tu sobre mapes i muntanyes. Gràcies per haver estat sempre un suport i una bona amiga. També vull donar les gràcies “als amics de sempre”, especialment des de que vaig tornar finalment a casa. Per últim, però no menys importants, m’agradaria donar un especial gràcies als meus pares, en **Carles** i la **Neus**, i al meu germà **Carles** i la família Masferrer i Rius, per tot el suport que m’heu aportat tot i haver estat vivint en països diferents, per haver fet d’aquests últims Nadals i Estius moments tan especials. Moltes gràcies també a en **Manel**, la **Montse**, l’**Eloy**, la **Pepi** i en **Jesús** per el suport. En definitiva, moltes gràcies a totes les persones que m’han ajudat durant aquesta etapa de la meva vida!

Eduard

About the Author

The author of this thesis was born on August 20, 1993, in Arbúcies (Girona), Spain. He was raised up, and received primary and secondary education in Arbúcies. After graduating from high school in 2011, he started to study chemistry at University of Girona (UdG) in the same year, his major was chemistry. After four years of study, he obtained his BSc degree in 2015. Later on, he started his MSc program in Advanced Catalysis and Molecular Modelling at University of Girona (UdG), and he performed his MSc thesis at Concentrol under the supervision of Joaquim Serra Pica and prof. dr. Miquel Costas Salgueiro. The title of his MSc thesis was “Formulation of New Tin-Free Release Agents as an Alternative to Organotin-based Catalysts for Molded Polyurethane Foams”. He obtained his MSc degree in 2016. In December 2016, he moved to The Netherlands and started as a PhD student in the Organic Chemistry and Catalysis group at Utrecht University, under the supervision of prof. dr. R. J. M. Klein Gebbink. His project was financially supported by the Marie Skłodowska- Curie ITN Action (NoNoMeCat project) and the most important results of this project are presented in this thesis. Parts of this thesis have been presented at national and international conferences including the Netherlands’ Catalysis and Chemistry Conference (NCCC), Girona Seminar (2018, Girona, Spain), and the 21st International Symposium on Homogeneous Catalysis (ISHC-21, 2018, Amsterdam, The Netherlands).

List of Publications

Nickel is a Different Pickle: Trends in Water Oxidation Catalysis for Molecular Nickel Complexes

J. Hessels, **E. Masferrer-Rius**, F. Yu, R. J. Detz, R. J. M. Klein Gebbink, J. N. H. Reek. *ChemSusChem*, **2020**, *13*, 6629-6634.

On the Ability of Nickel Complexes Derived from Tripodal Aminopyridine Ligands to Catalyze Arene Hydroxylations

E. Masferrer-Rius, R. M. Hopman, J. van der Kleij, M. Lutz, R. J. M. Klein Gebbink. *CHIMIA*, **2020**, *74*, 489-494. (Chapter 2)

Aromatic C–H Hydroxylation Reactions with Hydrogen Peroxide Catalyzed by Bulky Manganese Complexes

E. Masferrer-Rius, M. Borrell, M. Lutz, M. Costas, R. J. M. Klein Gebbink. *Adv. Synth. Catal.*, **2021**, *363*, 3783-3795. (Chapter 3)

Exploration of Highly Electron-Rich Manganese Complexes in Enantioselective Oxidation Catalysis: a Focus on Enantioselective Benzylic Oxidation

E. Masferrer-Rius, F. Li, M. Lutz, R. J. M. Klein Gebbink. *Catal. Sci. Technol.*, **2021**, *11*, 7751-7763. (Chapter 5)

Electronic and Steric Ligand Effects on Catalytic Arene Oxidation by Aminopyridine-based Manganese Complexes

E. Masferrer-Rius, M. Cianfanelli, M. Lutz, M. Costas, R. J. M. Klein Gebbink., *in preparation*. (Chapter 4)

An Experimental and Computational Study on Tetradentate Imidazole-based Manganese Complexes for Oxidation Catalysis

E. Masferrer-Rius, M. L. G. Sansores-Paredes, R. J. M. Klein Gebbink., *in preparation*. (Chapter 6)

